MHD free-forced convection and mass transfer flow through temperature stratified high-porosity medium from a vertical plate with power-law variation wall temperature in the presence of hall and ion-slip currents

Thesis Submitted in Fulfillment of the Requirements for the Award of the Degree

of

Doctor of Philosophy

in

Applied Mathematics

by

Md. Delowar Hossain

Under the Supervision of

Professor Dr. Md. Abdus Samad

and

Professor Dr. Md. Mahmud Alam

Department of Applied Mathematics, University of Dhaka

Bangladesh

June, 2017 Registration No. 66/2014-15(Re-registration)

Certificate

This is to certify that the thesis entitled ‘MHD free-forced convection and mass transfer flow through temperature stratified high-porosity medium from a vertical plate with power-law variation wall temperature in the presence of hall and ion-slip currents’ submitted by Md. Delowar Hossain to Universty of Dhaka, Dhaka, is a record of bonafide research work carried out by him under our supervision and guidance in the Department of Applied Mathematics, University of Dhaka. Mr. Md. Delowar Hossain has worked for three years starting from November 2013 for preparing his thesis at this Department as a full time candidate and the thesis is, in our opinion, worthy of consideration for the award of Degree of Doctor of Philosophy in Applied Mathematics in accordance with the rules and regulations of this University. The results embodied in this thesis have not been submitted elsewhere for the award of any other degree.

Professor Dr. Md. Abdus Samad
Chairman & Supervisor
Department of Applied Mathematics
University of Dhaka
Dhaka-1000, Bangladesh

Professor Dr. Md. Mahmud Alam
Joint-Supervisor
Mathematics Discipline
Khulna University
Khulna-9208, Bangladesh

Table of contents

			Page
		Abstract	v-vi
		Acknowledgement	vii
		Nomenclature	viii-xi
		List of Published and Submitted Papers from this Thesis	xii
		Introduction	xiii-xv
Chapter 1		Available Information on MHD Heat and Mass Transfer flow	1-20
1.1		Magnetohydrodynamics(MHD)	
1.2		Electromagnetic Equations and MHD Approximations	
1.3.		The important Dimensionless Parameters of Fluid Dynamics and Magnetohydrodynamics	
1.4		Suction and Injection	
1.5		MHD Boundary Layer Phenomena	
	1.5.1.	MHD and Heat Transfer	
	1.5.2	Convection	
	1.5.3	Heat and Mass transfer	
	1.5.4	Effects of Rotation	
	1.5.5	Hall and Ion-Slip Currents	
	1.5.6	Soret (Thermal-diffusion) and Dufour (Diffusion thermo) numbers	
	1.5.7	Porosity Medium	
	1.5.8	Stratification	
Chapter 2		The Basic Equations	21-22
2.1		Equation of Continuity	
2.2		Momentum Equation	
2.3		Energy Equation	
2.4		Concentration Equation	
Chapter 3		The Calculation Technique	23-29
3.1		Nachtsheim-Swigert Shooting Iteration Technique	
3.2		Finite Difference Technique	

Chapter 4

4.1		Unsteady MHD free convection and mass transfer flow along a vertical oscillatory porous plate in a rotating system with Hall, ion-slip currents and heat source	30-57
4.1.1		Governing Equations	
4.1.2		Mathematical Formulation	
4.1.3		Solution Technique	
	4.1.3.1	Case I: Analytical Solution	
	4.1.3.2	Case II: Numerical Solution	
4.1.4.		Stability and Convergence Analysis	
4.1.5		Shear Stress, Nusselt number and Sherwood number	
4.1.6		Results and Discussion	
	4.1.6.1	Justification of Grid Space	
	4.1.6.2	Steady-State Solution	
4.1.7		Appendix	
		References	
4.2.		MHD free convection and mass transfer flow through a vertical oscillatory porous plate with Hall, ion-slip currents and heat source in a rotating system	58-81
4.2.1		Governing Equations	
4.2.2		Mathematical Formulation	
4.2.3		Solution Technique	
4.2.4		Stability and Convergence Analysis	
4.2.5		Shear Stress, Nusselt number and Sherwood number	
4.2.6		Results and Discussion	
	4.2.6.1	Justification of Grid Space	
	4.2.6.2	Steady-State Solution	
		References	

Chapter 5

5.1		Effect of Hall and ion-slip currents on MHD heat and mass transfer flow past a vertical plate with high porosity medium in a rotating system	82-109
5.1.1		Governing Equations	
5.1.2		Mathematical Formulation	
5.1.3		Solution Technique	

5.1.4		Stability and Convergence Analysis	
5.1.5		Shear Stress, Nusselt number and Sherwood number	
5.1.6		Results and Discussion	
	5.1.6.1	Justification of Grid Space	
	5.1.6.2	Steady- Tate Solution	
		References	
5.2		MHD free convection flow and mass transfer over a vertical plate with high porosity medium in presence of Hall and ion-slip currents in a rotating system	110-137
5.2.1		Governing Equations	
5.2.2		Mathematical Formulation	
5.2.3		Solution Technique	
5.2.4		Stability and Convergence Analysis	
5.2.5		Shear Stress, Nusselt number and Sherwood number	
5.2.6		Results and Discussion	
	5.2.6.1	Justification of Grid Space	
	5.2.6.2	Steady-State Solution	
		References	
Chapter 6			
		Effects of ion-slip current on MHD free convection flow in a temperature stratified porous medium in a rotating system	138-150
6.1		Governing Equations	
6.2		Mathematical Formulation	
6.3		Solution Technique	
6.4		Shear Stress and Nusselt number	
6.5		Results and Discussion	
		References	
Chapter 7			
		Effects of stratification on MHD free convection flow past a vertical plate in a porous medium with Hall and ion-slip currents in a rotating system	151-169
7.1		Governing Equations	
7.2		Mathematical Formulation	

7.3 Solution Technique
7.4 Shear Stress, Nusselt number and Sherwood number
7.5 Results and Discussion
References

Chapter 8

Effect of Hall and ion-slip currents on MHD boundary layer flow past along a vertical plate in porous medium with power-law variation wall temperature in a rotating system 170-182

8.1 Governing Equations
8.2 Mathematical Formulation
8.3 Solution Technique
8.4 Shear Stress and Nusselt number
8.5 Results and Discussion
References

Chapter 9

General Discussion 183-184
References 185-199

Abstract

Considerable research efforts have been devoted to the study of MHD free-force convection and mass transfer flow through temperature stratified high porosity medium from a vertical plate with power-law variation wall temperature in the presence of Hall and ion-slip currents under various flow conditions. A magnetic field is applied perpendicular to the plates. Various configurations have been considered for the plates. The whole system is rotated with a constant angular velocity Ω. The Hall and ion-slip currents effect has also been put into consideration. The effects of changing various parameters on the velocity, temperature and concentration distributions have been discussed. However, finding exact solutions of nonlinear problems is very difficult. In particular, obtaining an exact analytic solution of a given nonlinear problem is often more complicated as compared to that of a numerical solution, despite the availability of high performance supercomputers and software which provide efficient ways to perform high quality symbolic computations. In our analysis, the primary focus has been shown on the study of the physical and mathematical structure of fluid models. Method of explicit and implicit finite difference method, Nachtsheim-Swigert iteration technique are used as main tools for numerical approach while the perturbation technique is used for the analytical approach. The studies of the flow feature mentioned above are made in different sections taking different aspects of the flow that are of practical importance. The non-dimensional coupled partial differential equations of the momentum, energy and concentration equations are derived by considering suitable usual transformation and similarity variables. Also stability analysis has been derived for conversed solutions.

In **section 4.1 of chapter 4**, the similarity solutions have been obtained for one dimensional unsteady MHD free convection and mass transfer flow through a vertical oscillatory porous plate in a rotating porous medium with Hall, ion-slip currents and heat source. Two cases are considered, (a) analytical solution with perturbation technique, (b) numerical solution by implicit finite difference method.

In **section 4.2 of chapter 4** and **section 5.1, 5.2 of chapter 5**, similarity solutions have been obtained by finite difference method (implicit and explicit). The numerical solutions for the velocity profiles, temperature distributions as well as concentration distributions are obtained using implicit finite difference method for the effects of the various important parameters entering into the problem in case of the one dimensional problem. Also the shear stress, Nusselt number as well as Sherwood number have been computed by implicit finite difference method in case of one dimensional flow. Further the above mentioned flow problem has been considered for two dimensional case, unsteady MHD free convective flow. The local and average shear stresses as well as Nusselt number and Sherwood number have been computed by explicit finite difference technique in case of two dimensional flows. In both cases the stability conditions and convergence criteria of the explicit finite difference scheme have been analyzed for finding the restriction of the values of various parameters to get more accuracy.

In **chapter 6**, similarity equations of the corresponding momentum and energy equations are derived by introducing a time dependent length scale which in fact plays the role of a

similarity parameter. The suction velocity is taken to be inversely proportional to this parameter.

In **Chapter 7**, the flow structures of stratification fluid models are investigated in detail and some new exact solutions have been obtained. The ambient temperature has been assumed to be an increasing function with the distance along the plate. The heat transfer changes significantly with the stratification and magnetic parameters.

In **Chapter 8**, power-law variation wall temperature along vertical plate, in the presence of Hall and ion-slip currents are discussed. The plate surface has a power-law variation wall temperature and is permeable to allow for possible fluid with wall suction or blowing, velocity varied according to a power-law.

The Nachtsheim-Swigert iteration technique has been used **Chapter6, Chapter 7 and Chapter 8**.

The effects on the velocities, temperature, concentration, local and average shear stresses, Nusselt and Sherwood numbers of the various important parameters entering into the problems separately are discussed for each problem with the help of graphs and tables.

Finally, in **Chapter 9,** a general discussion on the overall results of the problems considered in the dissertation is sorted out.

Acknowledgement

I would like to express my deepest gratitude and appreciation to my supervisor Dr. Md. Abdus Samad, Professor and Chairman, Department of Applied Mathematics, University of Dhaka, Bangladesh for his willingness to accept me as a PhD student. Also I would like to thank Dr. Md. Abdus Samad for his guidance and all the useful discussions and brainstorming sessions, especially during the difficult conceptual development stage. His deep insights helped me at various steps of my research.

Special thanks to my co-supervisor Dr. Md. Mahmud Alam, Professor, Mathematics Discipline, Khulna University, Khulna, Bangladesh. He is considered me as a researcher in the Third World Academy Science (TWAS) research project in the first place. He taught me how to ask questions and express my ideas. He taught me how to write research papers, made me a better programmer, had confidence. His constructive criticisms, stimulating discussion and discipline and quality in research have been instrumental in the completion of my thesis.

Besides my supervisors, I am thankful to all teachers of this Department who helped me in one way or the other to carry out my work successfully. Especially Dr. Mohammad Ferdwos, Mr. Md. Rakib Hosen and Mr. Kajal Chandra Saha, for their help, support, encouragement and unique to endure the stressful and mostly lonely PhD journey.

I wish to express my sincerest gratitude to colleagues, Associate Professor Md. Nazrul Islam, Mohammad Shah Alam and Assistant Professor Mohammad Ali, Md Golam Hafez, Department of Mathematics, Chittagong University of Engineering & Technology, Chittagong, Bangladesh for sharing their research experience and for their helpful suggestions throughout my research.

I wish to further extend my thanks to all teachers and staffs of Applied Mathematics Department, University of Dhaka, Bangladesh for their help.

Finally, words cannot express the feelings I have for my parents for their constant unconditional support-both emotionally and financially.

Nomenclature

a	Wall temperature power index
$\mathbf{B}$	magnetic vector field
B_0	uniform magnetic field of strength
C	fluid concentration
$\overline{C}$	dimensionless concentration
c	Forcheimmer (inertial) coefficient
c_p	specific heat at constant pressure
c_s	concentration susceptibility
C_w	concentration at the plate
C_∞	species concentration at infinity
$C_\infty(x)$	the concentration of the ambient fluid
$C_{\infty, x=0}$	ambient concentration at the leading edge of the plate
D_m	mass diffusivity
D_f	Dufour number
$\overline{D}$	Diffusion coefficient
$\mathbf{D}$	Electric displacement
E_c	Eckert number
$\mathbf{E}$	Electric field
f'	dimensionless primary velocity
f_w	suction parameter(large)
g'	dimensionless secondary velocity
F_x	body force along x-axis
F	body force
g_0	acceleration due to gravity
G_m	modified Grashof Number
G_r	Grashof Number
$\mathbf{H}$	magnetic field strength
h	convective heat transfer coefficient
i	complex number
$\mathbf{J}$	current density
J_x, J_y, J_z	components of the current density $\mathbf{J}$
k	permeability of the porous medium
k_T	thermal diffusion ratio
k_f	thermal conductivity

$\bar{k}$	mass transfer coefficient
L	characteristic length
M	magnetic Parameter
$\bar{\bar{n}}$	zero or integer
$\bar{n}$	frequency
N_u	Nusselt number
N_{uL}, N_{uA}	local and average Nusselt numbers
P_r	Prandtl number
P	pressure of fluid
$\overline{Q}$	heat source quantity
Q	Fluid velocity in complex form
$\mathbf{q}$	vector velocity
$\mathbf{q_p}$	velocity of the charge
R	rotation parameter
S_1	stratification rate of the gradient of ambient temperature profiles
S_2	stratification rate of the gradient of ambient concentration profiles
S_{hL}, S_{hA}	local and average Sherwood numbers
S_0	Soret number
S_c	Schmidt number
S_T	thermal Stratification parameter
S_T^*	mass Stratification parameter
S_h	Sherwood number
t, n	time
T	temperature of the fluid in the boundary layer
$\overline{T}$	dimensionless temperature
T_m	mean fluid temperature
T_w	temperature at the wall
T_∞	temperature of the fluid at infinity
$T_\infty(x)$	the temperature of the ambient fluid
$T_{\infty,t=0}$	ambient temperature at any arbitrary reference point in the medium
$T_{\infty,x=0}$	ambient temperature at the leading edge of the plate
u, v, w	components of the velocity field $\mathbf{q}$
U, V, W	components of the dimensionless velocity field
U_0	free stream velocity
v_0	suction velocity at the wall
v_w	uniform blowing/suction at the plate

X, Y	dimensionless coordinates
x, y, z	cartesian coordinates

Greek Symbols

~	heat source parameter
	coefficient of volumetric thermal expansion of the fluid
*	volumetric coefficient of expansion with concentration
$_{e}$	Hall parameter
$_{i}$	ion-slip parameter
¥	permeability parameter
Γ	dimensionless Forcheimmer (inertial) parameter
«	viscosity of the fluid
$«_{e}$	magnetic permeability of the medium
³	kinematic viscosity
¤	dimensionless concentration
$\bar{¤}$	viscous dissipation
·	stream function
a	suction parameter
¦	similarity variable
—	dimensionless temperature
±	time dependent length scale
$±_{e}, ±'$	electrical conductivity of the fluid
Ω	angular velocity about the y-axis
$°_{e}$	charge density
°	fluid density
µ	oscillation frequency in non-dimension form
²	dimensionless time
$²_{U}$	shear stress in x-axis
$²_{W}$	shear stress in z-axis
$²_{x}, ²_{z}$	x and z components of shear stress
$²_{LU}, ²_{LW}$	x and z components of local shear stress
$²_{AU}, ²_{AW}$	x and z components of average shear stress
$µ_{e}$	electron cyclotron frequency
$²_{e}$	collision time of electrons
$µ_{i}$	ion cyclotron frequency
$²_{i}$	collision time of ions

©	thermal conductivity
£	porosity porous medium
£′	small number which is less than unity
£″	electrical permeability of the medium

Subscripts

w	conditions at the wall
∞	conditions at infinity
$(\infty, x = 0)$	at some reference point in the medium and at the outer edge of the boundary layer

Superscript

/	differentiation with respect ¦

List of Published and Submitted Papers from this Thesis

1. Md. Delowar Hossain, Md. Abdus Samad and Md. Mahmud Alam (2015), MHD free convection and mass transfer flow through a vertical oscillatory porous plate with Hall, ion-slip currents and heat source in a rotating system, Elsevier, Science Direct, Procedia engineering, vol.**105**, p56 – 63.
2. Md. Delowar Hossain, Md. Abdus Samad and Md. Mahmud Alam (2016), MHD free convection and mass transfer flow through a vertical oscillatory porous plate in a rotating porous medium with Hall, ion-slip currents and heat source, AMSE Journal-2016-Series: Modeling B, vol.**85**, N^{o} 1, p28-42, France.
3. Md. Delowar Hossain, Md. Abdus Samad and Md. Mahmud Alam (2016), Unsteady MHD free convection and mass transfer flow through a vertical oscillatory porous plate in a rotating porous medium with hall, ion-slip currents and heat source, Dhaka University Journal of Science,vol. vol.**64**(2), p91-98.
4. Md. Delowar Hossain, Md. Abdus Samad and Md. Mahmud Alam (2016), MHD free convection flow and mass transfer over a vertical plate with high porosity medium in presence of Hall and ion-slip currents in a rotating system, Applications and Applied mathematics (Accepted), USA.
5. Md. Delowar Hossain, Md. Abdus Samad and Md. Mahmud Alam (2016), Effect of Hall and ion-slip currents on MHD heat and mass transfer flow past a vertical plate with high porosity medium in a rotating system, Sylwan Journal, (submitted), Poland.
6. Md. Delowar Hossain, Md. Abdus Samad and Md. Mahmud Alam (2017), Effects of ion-slip current on MHD free convection flow in a temperature stratified porous medium in a rotating system, American Institute of Physics(AIP) Proceedings(Accepted).

Introduction

Fluid dynamics is an area of study that deals with the flow of fluids. The fluids in consideration include gases, liquids and ionized gases also called plasma. Electromagnetism studies the interaction between the electric and magnetic fields. Magnetohydrodynamics (MHD) combines the two areas of study of flow of liquids called hydrodynamics and the study of electromagnetism. Efficient, accurate and stable numerical methods for solving fluid flow problems, heat and mass transfer processes, chemical reactions and turbulent phenomena are of great importance in many industrial applications. It is nowadays generally recognized that computer based computation of complex problems may provide a cost-effective, quick and sufficiently reliable method in many cases. Sometimes, the computational methods may also be an alternative or a complement to experimental investigations.

The aim of this dissertation is to make some calculations, both analytical and numerical, on MHD heat and mass transfer flows to the investigators dealing with the problems in geophysics and astrophysics. The analyses so produced in fact arouse out of the natural tendency to investigate a subject that may be said to relate to some academic types of problems of solving the equations of the fluid mechanics with a new body force and some other source of dissipation in the energy equation. The results of these investigations may not have direct practical applications but are relevant to the problems mentioned above. It is however, to be mentioned that the thermal instability investigations of natural convection MHD flows have direct application to problems in geophysics and astrophysics. The largest on MHD and heat transfer flows was aroused in the field of aerodynamic heating. *Rossow* (1957) presented the first research paper on this subject for incompressible constant property flat plate boundary layer flow. His results indicated that the skin frictions and the heat transfer were reduced substantially when a transverse magnetic field was applied to the fluid.

In our analyses the combined buoyancy effects arising from the simultaneous diffusion of thermal energy and chemical species are considered on the MHD flow of electrically conducting fluid under the action of a transversely applied magnetic field. Other applications of MHD heat transfer include MHD generators, plasma propulsion in astronautics, nuclear reactor thermal dynamics and ionized-geothermal energy systems.

Further in studying the different aspects of astrophysical and geophysical problems the Coriolis force is necessary to include to the momentum equations. Considering its significance as compared to viscous and inertia forces, it is generally admitted that the Coriolis force due to the Earth's rotation has a strong effect on the hydromagnetic flow in the Earth's liquid core.

In most cases the Hall and ion-slip terms were ignored in applying Ohm's law, as they have no marked effect for small and moderate values of the magnetic field. However, the current trend for the application of MHD is towards a strong magnetic field, so that the influence of the electromagnetic force is noticeable (*Cramer and Pai*, 1973). Under these conditions, the Hall current and ion slip current are important and they have a marked effect on the magnitude and direction of the current density and consequently on the magnetic force

term. *Tani* (1962) studied the Hall effect on the steady motion of electrically conducting and viscous fluids in channels.

Stratification is a formation/deposition of layers which occur due to temperature variations, concentration differences, or the presence of different fluids. Effect of stratification is an important aspect in heat and mass transfer analyses. In practical situations where the heat and mass transfer mechanisms run simultaneously, it is interesting and important to analyze the influence of double stratification (stratification of medium with respect to thermal and concentration fields) on the convective transport in nanofluid. The analysis of natural and mixed convection in a doubly stratified medium is a fundamentally interesting and important problem, because of its broad range of engineering applications. These applications include heat rejection into the environment such as lakes, rivers, and seas, thermal energy storage systems such as solar ponds and heat transfer from thermal sources such as the condensers of power plants. Also thermal stratification is very important for solar engineering because higher energy efficiency can be achieved with better stratification and already has been shown by researchers that the thermal stratification in energy storage may significantly increase system performance.

The effects of diffusion-thermo and thermal-diffusion of heat and mass transfer have been examined by *Chapman and Cowling* (1952) and *Hirshfelder et al.* (1954) from the kinetic theory of gases. The heat and mass transfer simultaneously affecting each other that will cause the cross-diffusion effect. The heat transfer caused by concentration gradient is called the diffusion-thermo or Dufour effect. On the other hand, mass transfer caused by temperature gradients is called Soret or thermal-diffusion effect. Thus Soret effect is referred to species differentiation developing in an initial homogenous mixture submitted to a thermal gradient and the Dufour effect referred to the heat flux produced by a concentration gradient. The Soret effect, for instance has been utilized for isotope separation and in mixture between gases with very light molecular weight (H_2, H_e) and of medium molecular weight (N_2, air). Thus due to importance of Soret and Dufour effects for the fluids with very light molecular weight as well as medium molecular weight.

In **chapter 1**, available informations regarding MHD heat and mass transfer flows along with various effects is summarized and discussed from both analytical and numerical point of view.

In **chapter 2**, the basic governing equations related to the problems considered thereafter are shown in standard vector form.

In **chapter 3**, the calculation approach for different problems is discussed.

In **section 4.1 of chapter 4**, a specific one dimension unsteady problem of the MHD free convection and mass transfer flow through a vertical oscillatory porous plate in a rotating porous medium with Hall, ion-slip currents and heat source are considered and are solved analytically as well as numerically. The two dimension unsteady problem has been considered in **section 4.2 of chapter 4**.

In **section 5.1 of chapter 5**, a specific one dimension unsteady problem of the effect of Hall and ion-slip currents on MHD heat and mass transfer flow past a vertical plate with high

porosity medium in a rotating system is considered. The two dimension unsteady problem has been considered in **section 5.2** of **chapter 5**.

In **chapter 6**, the effects of ion-slip current on MHD free convection flow in a temperature stratified porous medium in a rotating system are considered.

In **chapter 7**, the effects of stratification on MHD free convection flow past a vertical plate in a porous medium with Hall and ion-slip currents in a rotating system are considered.

In **chapter 8**, effect of Hall and ion-slip currents on MHD boundary layer flow past a vertical plate in porous medium with power-law variation wall temperature in a rotating system is considered.

As problems mentioned above have been solved by employing an analytical method, explicit and implicit finite difference method, Nachtsheim-Swigert shooting iteration technique together with sixth order Runge-Kutta integration scheme.

Finally, a general discussion all the problems is produced in **chapter 9** with conclusive remarks.

Chapter 1

Available Information on MHD Heat and Mass transfer flow

1.1 Magnetohydrodynamics(MHD)

Magnetohydrodynamics (MHD) is the branch of continuum mechanics which deals with the flow of electrically conducting fluids in electric and magnetic fields. The largest advancement towards understanding of such phenomena comes from the field of astrophysics. It has long been suspected that most of the matter in the universe is in the plasma or highly ionized gaseous state, and much of the basic knowledge in the area of electromagnetic fluid dynamics has been evolved from these studies.

As a branch of plasma physics, the field of magnetohydrodynamics (MHD) consists of the study of a continuous electrically conducting fluid under the influence of electromagnetic fields. MHD included only the study of strictly incompressible fluid, but today the terminology is applied to studies of partially ionized gases as well. The essential requirements for problems to be analyzed under the laws of MHD are that the continuum approach be applicable.

Many natural phenomena and engineering problems are susceptible to MHD analysis. It is useful in astrophysics. Geophysics encounters MHD phenomena in the interactions of conducting fluids and magnetic fields that are present in and around heavenly bodies. Engineers employ MHD principles in the design of heat of exchangers, pumps and flow meters, in space vehicle propulsion, control and re-entry, in creating novel power generating system and in developing confinement schemes for controlled fusion.

The most important application of MHD is in the generation of electrical power with the flow of an electrically conducting fluid through a transverse magnetic field. Recently, experiments with ionized gases have been performed with the hope of producing power on a large scale in stationary plants with large magnetic fields. Cryogenic and superconducting magnets are required to produce these very large magnetic fields. Generation of MHD power on a smaller scale is of interest for space applications. The increasing number of technical applications using MHD effects has made it desirable to extend many of the available hydrodynamic solutions to include the effects of magnetic fields for those cases when the fluid is electrically conducting.

In most cases the Hall and ion-slip terms were ignored in applying Ohm’s law as they have no effect for small and moderate values of the magnetic field. However, the current trend for the application of magnetohydrodynamics is towards a strong magnetic field, so that the influence of electromagnetic force is noticeable.

It is generally known that, to convert the heat energy into electricity, several intermediate

transformations are necessary. Each of these steps means a loss of energy. This naturally limits the overall efficiency, reliability and compactness of the conversion process. Methods for direct conversion to energy are now increasingly receiving attention. Of these, the fuel cell converts the chemical energy of fuel directly into electrical energy; fusion energy utilizes the energy released when two hydrogen nuclei fuse into a heavier one and thermoelectrical power generating uses a thermocouple. Magnetohydrodynamic power generation is another important new process that is receiving worldwide attention.

Faraday (1832) carried out experiments with the flow of mercury in glass tubes placed between poles of a magnet and discovered that a voltage was induced across the tube due to the motion of the mercury across the magnetic fields, perpendicular to the direction of flow and to the magnetic field. He observed that the current generated by this induced voltage interacted with the magnetic filed to show down the motion of the fluid and this current produced its own magnetic field that obeyed Ampere's right hand rule and thus, in turn distorted the magnetic field.

The phenomena of MHD electrical power generation was first recognized when Michael *Faraday*(1832) experimented with the generation of electricity by moving an electrical conductor through a stationary magnetic field. In January 1832 he set up a rudimentary open-circuit MHD generator or flow meter on waterlo Bridge in London. On 13th August 1940 B. Karlovitz, a Hungarian engineer prposed a gaseous MHD system, he had from 1938 conducted experiments on the products of combustion of natural gas as a working fluid using the annular Hall-type MHD generator. Faraday also suggested that electrical power could be generated in a load circuit by the interaction of a flowing conducting fluid and a magnetic field.

The first astronomical application of the MHD theory occurred in 1899 when Bigalow suggested that the sun was gigantic magnetic system. *Hartmann and Lazarus* (1937) studied the influence of a transverse uniform magnetic field on the flow of a conducting fluid between two infinite parallel, stationary and insulated plates. *Alfven* (1942) discovered MHD waves in the sun. The waves are produced by disturbances which propagate simultaneously in the conducting fluid and the magnetic field. The American engineer *Richard* (1959) operated the first truly successful MHD generator producing about 10 kw of electric power. Further research by Rosa established the practicality of MHD for fossil-fuelled systems in 1990. MHD devices have been in use the early of the 20th century. More recently, MHD devices have been used for stirring, levitating and otherwise controlling flows of liquid metals for metallurgical processing and other application by *Kolesnichenko* (1990). Gas-phse MHD is probably best known in MHD power generation. *Sporn and Kantrouitz* (1959), *Steg and Sutton* (1960), major efforts have been carried out around the worked to develop this technology in order to improve electric conversion efficiency, increase reliability by eliminating moving parts and reduce emission from coal and gas plants. Closed-cycle liquid metal MHD system using both single-phase and two-phase flows also has been explored. Also MHD principle is utilized in stabilizing a flow against the transition from laminar to turbulent flow. The word magnetohydrodynmics (MHD) is derived from magnetic field,

liquid and movement. The field of MHD was initiated by *Alfven* (1942) for which he received the Nobel Prize in Physic in 1970. Disturbance in either the magnetic field or the fluid can propagate in both to produce MHD waves as well as upstream and downstream wave phenomena.

The fundamental concept behind MHD is that magnetic field can induce currents in moving conducting fluid, which in turn creates forces on the fluid and also changes the magnetic field itself.

1.2 Electromagnetic Equations and MHD Approximations

Magnetohydrodynamic equations are the ordinary electromagnetic and hydrodynamic equations modified to take account of the interaction between the motion of the fluid and electromagnetic field. Formulation of the electromagnetic theory in mathematical form is known as Maxwell's equations. Maxwell's basic equations show the relation of basic field quantities and their production. The basic laws of electromagnetic theory are all contained in special theory of relativity. But here we will always assume that all velocities are small in comparison with the speed of light. Before writing down the MHD equations, first of all know the ordinary electromagnetic equations and hydromagnetic equations(*Cramer and Pai,* 1973).

First, the electromagnetic equations are as follows;

Charge continuity

$$\nabla'.\mathbf{D} = \rho_e \tag{1.2.1}$$

Current continuity

$$\nabla'.\mathbf{J} = -\frac{\partial \rho_e}{\partial t} \tag{1.2.2}$$

Magnetic field continuity

$$\nabla'.\mathbf{B} = 0 \tag{1.2.3}$$

Ampere's Law

$$\nabla' \wedge \mathbf{H} = \mathbf{J} + \frac{\partial \mathbf{D}}{\partial \mathbf{t}} \tag{1.2.4}$$

Fraaday's Law

$$\nabla' \wedge \mathbf{E} = -\frac{\partial \mathbf{B}}{\partial \mathbf{t}} \tag{1.2.5}$$

Constitutive equations for $\mathbf{D}$ and $\mathbf{B}$

$$\mathbf{D} = \varepsilon'' \mathbf{E} \tag{1.2.6}$$

$$\mathbf{B} = \mu_e \mathbf{H} \tag{1.2.7}$$

Lorentz force on a charge

$$\mathbf{F_p} = q'\left(\mathbf{E} + \mathbf{q_p} \wedge \mathbf{B}\right) \tag{1.2.8}$$

Total current density flow

$$\mathbf{J} = \sigma'\left(\mathbf{E} + \mathbf{q} \wedge \mathbf{B}\right) + \rho_e \mathbf{q} \tag{1.2.9}$$

The equations (1.2.1)-(1.2.5) are the Maxwell's equations where $\mathbf{D}$ is the electric displacement, ρ_e is the charge density, $\mathbf{E}$ is the electric field, $\mathbf{B}$ is the magnetic field, $\mathbf{H}$ is the magnetic field strength, $\mathbf{J}$ is the current density, $\frac{\partial \mathbf{D}}{\partial t}$ is displacement current density, ε' is the electrical permeability of the medium, μ_e is the magnetic permeability of the medium, $\rho_e\mathbf{q}$ is the convection current due to charges moving with the fluid, $\mathbf{q}_p$ is the velocity of the charge, $\mathbf{q}$ is the velocity field, σ' is the electrical conductivity.

The electromagnetic equations as shown above are not usually applied in their present form and required interpretation and several assumptions to provide the set to be used in MHD. The charge density ρ_e in Maxwell's equations must then be interpreted as an excess charge density which is generally not large. In most problems the displacement current, the excess charge density and the current due to convection of the excess charge are small. The electromagnetic equations to be used are as follows;

$$\nabla'.\mathbf{D} = 0 \tag{1.2.10}$$

$$\nabla'.\mathbf{J} = 0 \tag{1.2.11}$$

$$\nabla'.\mathbf{B} = 0 \tag{1.2.12}$$

$$\nabla' \wedge \mathbf{H} = \mathbf{J} \tag{1.2.13}$$

$$\nabla' \wedge \mathbf{E} = -\frac{\partial \mathbf{B}}{\partial t} \tag{1.2.14}$$

$$\mathbf{D} = \varepsilon' \mathbf{E} \tag{1.2.15}$$

$$\mathbf{B} = \mu_e \mathbf{H} \tag{1.2.16}$$

$$\mathbf{J} = \sigma'(\mathbf{E} + \mathbf{q} \wedge \mathbf{B}) \tag{1.2.17}$$

Suitably represent the equations of fluid dynamics to take account of the electromagnetic phenomena;

(i) the MHD equation of continuity for viscous incompressible electrically conducting fluid remains the same as that of usual continuity equation

$$\nabla' \wedge \mathbf{q} = 0 \tag{1.2.18}$$

(ii) the MHD momentum equation for a viscous incompressible and electrically conducting fluid is

$$\rho \frac{\partial \mathbf{q}}{\partial t} = \rho \mathbf{F} - \nabla' p' + \mu \nabla^2 \mathbf{q} + \mathbf{J} \wedge \mathbf{B} \tag{1.2.19}$$

where $\mathbf{F}$ is the body force term per unit volume corresponding to the usual viscous fluid dynamics equations and the new term $\mathbf{J} \wedge \mathbf{B}$ is the force on the fluid per unit volume produced by the interaction of the current and magnetic field (called a $\mathbf{J} \wedge \mathbf{B}$ force or Loyrentz force);

(iii) the MHD energy equation for a viscous incompressible electrically conducting fluid is

$$\rho C_p \frac{DT}{Dt} = k \nabla^2 T + \bar{\Phi} + \frac{\mathrm{J}^2}{\sigma'} \tag{1.2.20}$$

In relation to the energy equation of the thermal boundary layer the term ¤ is the viscous dissipation term and the new term $\frac{J^2}{\pm'}$ is the Joule heating term and due to the resistance of the fluid to the flow of current;

(iv) the MHD equation of concentration for viscous incompressible electrically conducting fluid remains the same as $\frac{DC}{Dt} = D_M \nabla^2 C$ (1.2.21)

1.3 The important Dimensionless Parameters of Fluid Dynamics and Magnetohydrodynamics

Magnetic Parameter (M)

It is a dimensionless number which is used in magnetofluid dynamics and it is defined by the product of electron conductivity $\pm_e$, the square of the magnetic field strength and a characteristic length L divided by product of the mass density and the fluid velocity. i.e. Magnetic parameter $M = \frac{\pm_e B_0^2 L}{\circ U_0}$ which gives a measure of the relative importance of drag forces resulting from magnetic function and viscous forces in Hartmann flow and determines the velocity profile for such flow. This is the ratio of the magnetic force to the inertia force.

Heat Source parameter $(\sim)$

The heat source parameter is defined as, $\sim = \frac{\overline{Q}^3}{\circ c_p U_0^2}$. Here $\overline{Q}$ is the heating capacity of the medium, ³ is the kinematic viscosity, U_0 is the uniform velocity, ° is the density, c_p is the specific heat at constant pressure.

Prandtl Number (P_r)

Prandtl number is one of the characteristical numbers in fluid dynamics and heat transfer. It is the ratio between momentum diffusivity (kinematic viscosity) and thermal diffusivity. The Prandtl number is named after the German physicist Ludwig Prandtl.

It is defined as follows;

$$P_r = \frac{\text{Kinematic viscosity}}{\text{Thermal diffusivity}} = \frac{3}{\frac{©}{\circ c_p}} = \frac{\circ 3 c_p}{©}$$

where ³ is the kinetic viscosity, © is the thermal conductivity, c_p is specific heat at constant pressure, ° is the density of the fluid.

The Prandtl number is a grouping of the properties of the fluid. It can be related to the thickness of the thermal and velocity boundary layers. In particular sense, when $P_r = 1.0$, the velocity boundary layer and thermal boundary layer coincide. If the P_r values be small, then heat diffuses very quickly compared to the velocity (momentum) i.e. the thickness of the thermal boundary layer is such bigger than the velocity boundary layer for liquid metals. Conversely, P_r values be larger, then the momentum boundary layer is thicker than the thermal momentum boundary layer. It is used in heat transfer, free and forced convection calculations. For most gases over a wide range of temperature and pressure, Prandtl number is approximately constant. Therefore, it can be used to determine the thermal conductivity of gases at high temperatures, where it is difficult to measure experimentally due to the formation of convection currents. It depends on the fluid properties. It is evident that P_r various from fluid to fluid. Typical values for Prandtl number are, for air at 20^0C $P_r = 0.71$ (Approx.), at 20^0C for water $P_r = 7.0$ (Approx.),for electrolyte solution such as salt water, $P_r = 1.0$, for sea water (at 0^0C and 20^0C) $P_r = 13.4$ and $P_r = 7.2$ for mercury $P_r = 0.05$, but for high viscous fluid it may be very large, viz, for glycerin $P_r = 7250$.

Eckert number (E_c)

The Eckert number, first named in the early 1950s after Ernst R. G. Eckert. It is useful in determining the relative importance in a heat transfer situation of the kinetic energy of a flow. It is the ratio of the kinematic energy to the enthalpy(or the dynamic temperature to the temperature) driving force for heat transfer. It is defined as follows;

$$E_c = \frac{\text{kinematic energy}}{\text{Enthalpy}} = \frac{U_0^2}{c_p(T_w - T_\infty)}$$

where U_0 is a characteristic velocity of the flow, c_p is the specific heat at constant pressure and $(T_w - T_\infty)$ is the driving force for heat transfer e.g. difference between wall temperature and free stream temperature. For small Eckert number ($E_c << 1.0$) the terms in the energy equation describing the effects of pressure changes, viscous dissipation and body forces on the energy balance can be neglected and the equation reduces to a balance between conduction and convection.

The Eckert number phenomenon was investigated theoretically by Geropp in 1969 and describes a reversal in heat transfer from a moving wall at an Eckert number $E_c \approx 1$. In this report the Eckert number phenomenon is confirmed experimentally for the first time. Moreover, maximum heat transfer occurs at an Eckert number $E_c \approx 0.3$, which is of great importance for the cooling of hot surface in a gas-flow.

Grashof number (G_r)

The Grashof number is a dimensionless number in fluid dynamics and heat transfer. It arises frequently in the study of situations involving natural convection. It is used in analyzing the

velocity distribution in free convection systems. The Grashof number is used in the correlation of heat and mass transfer due to thermally induced natural convection at a solid surface immersed in a fluid. The significance of the Grashof number is that it represents the ratio between the buoyancy forces due to spatial variation in fluid density (caused by temperature differences) to the resulting force due to the viscosity of the fluid. It is named after the German engineer Franz Grashof,

$$G_r = \frac{g_0 \quad (T_w - T_\infty)^3}{U_0^3}$$

where $G_r >> 1$,the viscous force is negligible compared to the buoyancy force and inertia force. When buoyant forces overcome the viscous forces, the flow starts a transition to the turbulent regime. In natural convection the Grashof number plays the same role that the Reynolds number plays in forced convection.

Modified Grashof Number (G_m)

The modified number Grashof number is defined by

$$G_m = \frac{g_0 \quad ^*(C_w - C_\infty)^3}{U_0^3}$$

where, g_0 is the local acceleration due to gravity, * is the volumetric coefficient of concentration expansion and $(C_w - C_\infty)$ be the concentration difference. It is used in case of natural convection mass transfer problems.

Suction Parameter (a)

The suction parameter is defined as, $a = \frac{v_0}{U_0}$.

This is a ratio of the suction velocity to the wall and the free stream velocity.

Permeability Parameter $(¥)$

The permeability parameter is defined as $¥ = \frac{3^2}{kU_0^2}$

where k is the permeability of the porous medium, 3 is the kinematic viscosity, U_0 is the uniform velocity.

Rotational Parameter (R)

The rotational parameter is defined as

$$R = \frac{\Omega 3}{U_0^2}$$

where Ω is the angular velocity, 3 is the kinematic viscosity, U_0 is the free stream velocity

Forcheimmer (Inertial) Parameter (Γ)

The inertial parameter is defined as, $\Gamma = \frac{c^3}{U_0}$

where c is the Forcheimmer (inertial) coefficient, ^{3} is the kinematic viscosity, U_0 is the uniform velocity.

Hall Parameter $(\ _e)$

The Hall parameter is defined as, $_e = \mu_e{}^2{}_e$

where μ_e is the electron cyclotron frequency, $^2{}_e$ is the electron mean free time.

Ion-slip Parameter $(\ _i)$

The ion-slip parameter is defined as, $_i = \mu_i{}^2{}_i$

where μ_i is the ion cyclotron frequency, $^2{}_i$ is the ion mean free time.

Schmidt Number (S_c)

Schmidt number is the ratio of the viscous diffusivity to the mass diffusivity. It physically relates the relative thickness of the hydrodynamic layer and concentration boundary layer.
It is defined as follows:

$$S_c = \frac{\text{Viscous diffusion rate}}{\text{Molecular(mass) diffusion rate}} = \frac{^3}{D_m} = \frac{«}{°D_m}$$

where ^{3} is the kinematic viscosity , D_m is the mass diffusivity, « is the dynamic viscosity of the fluid. The Schmidt number is important in problems involving both momentum and convection mass transfer. This provides a measure of the relative effectiveness of the momentum and mass transport by diffusion in the velocity and concentration boundary layers respectively. For convection mass transfer in laminar flows, it determines the relative velocity and concentration boundary layer thickness.

Soret Number (S_0)

The Soret number is defined as, $S_0 = \frac{D_m k_T (T_w - T_\infty)}{^3 T_m (C_w - C_\infty)}$

where ^{3} is the kinematic viscosity, T_w and T_∞ are the temperature of the fluid at the wall and far away from the plate respectively as well as C_w and C_∞ are the concentration of the species at the wall and far away from the plate , D_m is the coefficient of mass diffusivity, k_T is the thermal diffusion ratio, T_m is the mean fluid temperature respectively.

Dufour Number (D_f)

The Dufour number is defined as, $D_f = \frac{D_m k_T}{c_s c_p \nu} \frac{(C_w - C_\infty)}{(T_w - T_{\infty,})}$

where, D_m is the coefficient of mass diffusivity, ν is the kinematic viscosity, T_w and T_∞ are the temperature of the fluid at the wall and far away from the plate respectively as well as C_w and C_∞ are the concentration of the species at the wall and far away from the plate, c_s is the concentration susceptibility, k_T is thermal diffusion ratio, c_p is the specific heat at constant pressure respectively.

Thermal Stratification Parameter (S_T)

The thermal stratification parameter is defined as, $S_T = \frac{2x}{(T_w - T_{\infty,x=0})} \frac{d}{dx}\{T_\infty(x)\}$

where x is the characteristic length, T_w is the temperature at the wall, $T_{\infty,x=0}$ is the ambient temperature at the leading edge of the plate, $\frac{d}{dx}\{T_\infty(x)\}$ is constant.

Mass Stratification Parameter (S_T^*)

whether mass stratification parameter is defined as; $S_T^* = \frac{2x}{(C_w - C_{\infty,x=0})} \frac{d}{dx}\{C_\infty(x)\}$

where x is the characteristic length, C_w is the concentration of the species at the wall, $C_{\infty,x=0}$ is the ambient concentration at the leading edge of the plate, $\frac{d}{dx}\{C_\infty(x)\}$ is constant.

Nusselt Number (N_u)

The Nusselt number is used to measure the enhancement of heat transfer when convection takes place and is defined as follows

$N_u = \frac{\text{convective heat transfer coefficient}}{\text{conduction heat transfer coefficient}} = \frac{hL}{k_f}$ is perpendicular to the flow direction.

where $L =$ characteristic length which is simply volume of the body divided by surface area of the body (useful for more complex shape), k_f thermal conductivity of the fluid, $h =$ convective heat transfer coefficient. A Nusselt number close to one, namely convection and conduction of similar magnitude, is characteristic of “slug flow” or laminar flow. A larger Nusselt number corresponds to more active convection, with turbulent flow typically in the 100-1000 range.

Sherwood number (S_h)

The Sherwood number is a dimensionless number used in masstransfer operation. It represents the ratio of length scale to the diffusive boundary layer thickness and is named in honor of Thomas Kilgore Sherwood and is defined as follows:

$$S_h = \frac{\text{Convective mass transfer coefficient}}{\text{Diffusive mass transfer coefficient}} = \frac{\bar{k}L}{\overline{D}}$$

It is the mass transfer equivalent of the Nusselt number where, $\bar{k}$ is the overall mass transfer coefficient, L is the characteristic length, $\overline{D}$ is the component diffusion coefficient.

1.4 Suction and Injection

Suction or injection on the boundary layer control played significant role in the field of aerodynamics and space sciences. The effect of suction on hydromagnetic boundary layer is of great interest in astrophysics. It is often necessary to prevent separation of the boundary layer to reduce the drag and attain high lift values. Many authors have made mathematical studies on these problems, especially in the case of steady flow.

On the other hand, one of the important problems facing the engineers engaged in high speed flow is the cooling of the surface to avoid the structural failures as a result of frictional heating and other factors. In these respect the possibility of using injection at the surface is a measure to cool the body in the high temperature fluid. Injection of secondary fluid through porous walls is of practical importance in flim cooling of turbine blades combustion chambers. In such applications injection usually occurs normal to the surface and the injected fluid may be similar to or different from the primary fluid. In some recent applications, however, it has been recognized that the cooling efficiency can be enhanced by vectored injection at an angle other than 90^0 to the surface. *Inger and Swearn* (1975) have theoretically proved this feature for a linear boundary layer. In addition, most previous calculations have been limited to injection rates ranging from small to moderate. *Shojaefard et al.* (2005) used suction/injection to control fluid flow on the surface of subsonic aircraft.. Many interests have been built in the study of flow of heat and mass transfer with suction or injection because of its extensive engineering applications. In the area of steady flow of viscous incompressible fluid over infinite porous plates subject to suction or injection, various aspects of the problem have been investigated by many authors. *Griith and Meredith* (1936) invstigated the possible improvement in Aircrat performance due to use of boundary layer suction. *Das* (2009) studied the effect of suction and injection on MHD three dimensional couette flow and heat transfer through a porous medium.

Prasanna et al. (2012) studied MHD boundary layer flow of heat and mass transfer over a moving vertical plate in a porous medium with suction and viscous dissipation. *Mutua et al.* (2013) was studied magnetohydrodynamic free convection flow of a heat generating fluid past a semi-infinite vertical porous plate with variable suction. Numerical investigation of buoyancy effects on hydromagnetic unsteady flow through a porous channel considering suction and injection is to be found in the study by *Makinde and Chinyoka* (2013).

The unsteady MHD free-convection flow governed by the impact of suction or injection is one of the distinguished present-day themes. For instance the process of suction or blowing has also its importance in many engineering activities such as in the design of thrust bearing and radial diffusers and thermal oil recovery. Suction is applied to chemical processes to remove reactants and injection is used to add reactants, cool the surface, prevent corrosion or scaling and reduce the drag (*Labropulu et al.* (1996)). *Ahmed and Khatun* (2013) carried out a theoretical analysis on Magneto-hydrodynamic oscillatory flow in a planer porous channel with suction and injection. They reported that suction/injection shifts the region of maximum velocity away from the centerline and leads to non-symmetry in the velocity and temperature.

1.5 MHD Boundary Layer Phenomena

Boundary layer phenomena occur when the influence of a physical quantity is restricted to small regions near confining boundaries. This phenomena occurs when the non-dimensional diffusion parameters the Reynolds number and the Peclet number or the magnetic Reynolds number are large. The fundamental concept of boundary layer was suggested by Prandtl (1904), it defines the boundary layers as a layer of fluid developing in flows with relatively low viscosity as compare with inertial force. The boundary layer is characterized by an abrupt change in the transverse direction of velocity (a hydrodynamic boundary layer), temperature (a thermal boundary layer) or concentration of individual chemical components (a diffusion boundary layer). The viscosity, thermal conductivity and diffusivity of the fluid are the principal influences on the formation of the flow in a boundary layer.

Prandtl fathered classical fluid dynamic boundary theory by observing, from experimental flows that for large Reynolds number, the viscosity and thermal conductivity appreciably influenced the flow only near a wall. When distant measurements in the flow direction are compared with a characteristic dimension in that direction, transverse measurements compared with the boundary layer thickness and velocities compared with the free stream velocity, the Navier-Stoks and energy equation can be considerably simplified by neglecting small quantities. The number of component equations is reduced to those in the flow direction and pressure changes across the boundary layer are negligible. The pressure is then only a function of the flow direction and can be determined from the inviscied flow solution. Also the number of viscous term is reduced to the dominant term and the heat conduction in the flow direction is negligible.

MHD boundary layer flows are separated into two types by considering the limiting cases of a very large or a negligible small magnetic Reynolds number. When the magnetic field is oriented in an arbitrary direction relative to a confining surface and the magnetic Reynolds number is very small, the flow direction component of the magnetic interaction and the corresponding Joule heating is only a function of the transverse magnetic field component and local velocity in the flow direction. Changes in the transverse magnetic field component and pressure across the boundary layer are negligible. The thickness of the magnetic boundary layer is very large and the induced magnetic field is negligible. However, when the magnetic Reynolds number is very large, the magnetic boundary layer thickness is small and

is of nearly the same size as the viscous and thermal boundary layers and then the MHD boundary layer equations must be solved simultaneously. In this case, the magnetic field moves with the flow and is called frozen mass. When a fluid is electrically conducting and a uniform steady magnetic field acts perpendicular to the channel walls, the structure of the flow changes drastically. The profile becomes flat in the so-called core as a result of the electromagnetic breaking effect, this breaking is due to the intraction of the induced electric current with applied magnetic field.

Moreover, two boundary layers develop in the vicinity of the walls. This layer has been theoretically predicted and experimentally characterized by *Julius* (1937) that present one of the most important characteristic features of MHD flows. This layer is one of the few flows that are amenable to rigorous analytic treatment. MHD boundary layer is a parading of MHD flow and develops when a liquid metal flows under the influence of a steady magnetic field. The book of *Schilchting* (1968) is an excellent collection of the boundary layer analysis.

1.5.1 MHD and Heat Transfer

With the advent of hypersonic flight, the field of MHD, as define above, which has attracted the interest of aero dynamists and associated largely with liquid metal pumping. It is possible to alter the flow and the heat transfer around high velocity vehicles provided that the air is sufficiently ionized. Further more, the invention of high temperature facilities such as the shock tube plasma jet have provided laboratory sources of following ionized gas, which provide an incentive for the study of plasma accelerators and generators. As a result of this, many of the classical problems of fluid mechanics have been reinvestigated. Some of these analyses awake out of the natural tendency of scientists to search a new subject. In this case it was the academic problem of solving the equations of fluid mechanics with a new body force and another source of dissipation in the energy equation. Some time there were no practical applications for these results. As for example, natural convection MHD flows have been of interest to the engineering community only since the investigations, directly applicable to the problems in geophysics and astrophysics. But it was in the field of aerodynamic heating that the largest interest was awaked.

Rossow (1957) presented the first paper on this subject. His result for incompressible constant property flat plate boundary layer flow indicated that the skin friction and heat transfer were reduced substantially when a transverse magnetic field was applied to the fluid. This encouraged a multitude analysis for every imaginable type of aerodynamic flow, and most of the research centered on the stagnation point, where in hypersonic flight, the highest degree of ionization could be expected. The results of these studies were sometimes contradictory concerning the amount by which the heat transfer would be reduced (some of this was due to misinterpretations and invalid comparison). Eventually, however, it was concluded that the field strength, necessary to provide sufficient shielding against heat fluxes during atmospheric flight, where not competitive (in terms of weight) with other method of cooling (*Sutton and Gloersen* (1961)). Comprehensive reviews of convective

heat transfer in porous medium can be found in the books by *Neild and Bejan* (2013), *Patankar and Spalding* (1970), *Rohsenow* (1998) and *Gosman et al*.(1969).

1.5.2 Convection

In the studies related to heat transfer, considerable effort has been directed towards the convective mode, in which the relative motion of the fluid provides an additional mechanism for the transfer of energy and material, the latter a more important consideration in cases where mass transfer, due to concentration difference, occurs. Convection is the collective movement of ensembles of molecules within fluid (e.g. liquids, gases), since, although the fluid motion modifies the transport process, the eventual transfer of energy from one fluid element to another in its neighborhood is through conduction. Also, at the surface, the process is predominantly that of conduction because the relative fluid motion is brought to zero at the surface. A study of the convective heat transfer therefore involves the mechanisms of conduction and sometimes, those of radiative processes as well, coupled with those of fluid flow. Convection plays a major role in transporting energy from the centre of the Sun to the surface and movements of the hot magma beneath the surface of the earth. In context of heat and mass transfer, the term "convection" is used to refer to the sum of advective and diffusive transfer. Note that in common use the term convection may refer loosely to heat transfer by convection, as opposed to mass transfer by convection, or the convection process in general.

Natural convection/Free convection

Natural convection is a mechanism or type of heat transport, in which the fluid motion is not generated by any external source (like a pump, fan, suction device, etc) but only by density differences in the fluid occurring due to temperature gradients. In natural convection, fluid surrounding a heat source receives heat, becomes less dens and rises. The presence of a proper acceleration such as the rising from resistance to gravity, or an equivalent force (arising from acceleration, centrifugal force or Coriolis effect), is essential for natural convection. Natural convection has attracted a great deal of attention from researchers because of its presence both in nature and engineering applications. Convection is also seen in the rising plum of hot air from fire, oceanic currents and sea-wind formation (where upward convection is also modified by Coriolis forces). Natural or free convection has attracted a great deal of attention from researchers because of its presence of both in nature and engineering application. In engineering applications, convection is commonly visualized in the formation of microstructures during the cooling of molten metals and fluid flows around shrouded heat-dissipation fins and solar ponds. A very common industrial application of natural convection is free air cooling without the aid of fans, this can happen on small scales (computer chips) to large scale process equipment. Free convection flows are studied because of their wide applications and hence it has attracted the attention of numerous investigators.

Osborne Reynolds was first to make use of the mathematical similarity between the moment-

um equation and energy equation in convection in 1874. The effects of magnetic filed on natural convection heat transfer studied by *Sparrow and Cess* (1961). The transient free convection flow past a semi-infinite vertical plate by integral method was first studied by *Siegel* (1958). Many researchers studied MHD free convection boundary layer flow on heat and mass transfer, some of them, *Jaluria, Y.* (1980), *Bejan* (1994), *Alam and Sattar* (2000). *Hady et al.* (2006), *Reddy et al.* (2012), *Asek and Benu* (2013), *Paraven and Rudraman* (2014), *Sharma et al.* (2014), *Ahmmed et al.* (2015), *Reddy* (2016).

1.5.3 Heat and Mass Transfer Flow

Heat and mass transfer are kinetic processes that may occur and be studied separately or jointly. Studying them apart is simpler but both processes are modeled by similar mathematical equations in the case of diffusion and convection (there is no mass transfer similarity to heat radiation) and it is thus more efficient to consider them jointly.

Mass transfer is the net movement of mass from one location, usually meaning stream, phase, fraction or component, to another. Mass transfer occurs in many processes, such as absorption, evaporation, adsorption, drying, precipitation, membrane filtration, and distillation. It is that involve diffusive and convective transport of chemical species within physical system. In industrial processes, mass transfer operations include separation of chemical components in distillation columns, absorber such as scrubbers, absorbers such as activated carbon beds and liquid-liquid extraction. Mass transfer is often coupled to additional transport process for instant in industrial cooling towers. In astrophysics mass transfer is the process by which matter gravitationally bound to a body, usually a star, fills its Roche lobe and becomes gravitationally bound to a second body, usually compact object. Mass transfer finds extensive application in chemical engineering problems. Mass transfer is used by different scientific disciplines for different processes and mechanisms. It is used in reaction engineering, separation engineering, heat transfer engineering and many other sub-disciplines of chemical engineering. Some common examples of mass transfer processes are the evaporation of water from a pond to the atmosphere, the purification of blood in the kidneys and liver, and the distillation of alcohol.

Heat transfer is a discipline of thermal engineering that concerns the generation, use convection and exchange of thermal energy and heat between physical systems. Transfer of heat is normally from a high temperature object to a lower temperature object. Heat transfer changes the internal energy of both systems involved according to the First Law of Thermodynamics. Additionally, subsidiary laws relating to fluid flow and rate equations for different moods of heat transfer are also required for a complete solution. It has applications in diverse fields of engineering, such as mechanical engineering, metallurgical engineering, electrical engineering, chemical engineering, nuclear engineering, aerospace engineering and space technology, cryogenic engineering, civil engineering. In industries and nature many transport process exist in which heat and mass transfer take place simultaneously as a result of combined buoyancy effect of thermal diffusion and diffusion of chemical species. The phenomenon of heat and mass

transfer is observed in buoyancy induced motions in the atmosphere, in bodies of water, quasi-solid bodies, such as earth and so on. In the past decades an intensive research effort had been devoted to problems on heat and mass transfer in view of their application to astrophysics, geophysics and engineering. In addition, the phenomenon of heat and mass transfer is also encountered in chemical process industries. The combined effect of heat and mass transfer can result in significant temperature changes and increased energy transfer rates at a wet surface. The majority of heat transfers used in the plastic molding industry is manufactured by the screen printing process. Screen printed heat transfers were introduced in the early 1960's. These additional effects have also been considered in several investigators, for example, the work of *Groots and Mozur* (1962), *Eckert and Drake* (1972), *Hurly and Jakeman* (1971), *Caldwel* (1974).

The natural convection boundary layer flow generated in a fluid adjacent to a heated, vertical semi-infinite plate is one of the fundamental flows in heat and mass transfer. Most studies have examined the fully developed flow with relatively few investigations of the transient response to impulsive heating. *Georgantopoulos et al.*(1979) have studied the effects of mass transfer on free convection problem in the Stokes problem for an infinite vertical limiting surface. *Georgantopolous and Nanousis* (1980) have consider the effects the mass transfer on free convection flow of an electrically conducting viscous fluid (e.g. of a stellar atmosphere) past an impulsively started infinite vertical limiting surface (e.g. of star) in the presence of transverse magnetic field.

Recently, the heat and mass transfer problem associated with the boundary layer saturated fluid under different physical conditions has been studied by several authors, some of them are *Das and Jana* (2010), *Farhad Ali et al.* (2013), *Alizadeh et al.* (2015), *Emad et al*. (2011), *Mangathai, et al.* (2015).

1.5.4 Effect of Rotation

The study of flow in rotating porous media is motivated by its practical applications in geophysics and engineering. Hydromagnetic convection flow in a rotating medium is of considerable importance due to its application in various areas of geophysics, astrophysics and fluid engineering viz. maintenance and secular variations in Earth's magnetic field due to motion of Earth's liquid core, internal rotation rate of the Sun, structure of the magnetic stars, solar and planetary dynamo problems, turbo machines, rotating MHD generators, rotating drum separators for liquid metal MHD applications, chemical process industry, ion propulsion, MHD bearings and rotating machinery etc. It may be noted that Coriolis and magnetic forces are comparable in magnitude and Coriolis force induces secondary flow in the flow-field.

In numerous hydromagnetic flows, rotation may also take place and the centrifugal forces can exert a significant effect on flow dynamics and heat transfer processes. Magnetic field and Hall current effect on MHD free convection flow past a vertical rotating flat plate was analyzed by *Kirimi Jacob et al.* (2012). *Yantovskiy and Tolmach* (1963) investigated

centrifugal force effects on rotating hydromagnetic generator configurations. *Michiyoshi and Numano* (1967) investigated the performance characteristics of the vortex MHD power generator using a partially ionized gas as a working fluid, showing that compressibility of the working fluid causes a much sharper decline of the radial velocity in the radial direction than in the case of an incompressible fluid at subsonic speeds. Further interesting studies of transient rotating hydromagnetic flow were reported by *Katsurai* (1972) and *Oliver* (1974).

The steady and unsteady Eckman layers of an incompressible fluid have been investigated as basic boundary layers in a rotating fluid appearing in oceanic, atmospheric, cosmic fluid dynamics and solar Physics or geophysical problems. It is well known that, in a rotating fluid near a flat plate, an Eckman layer exists where the viscous and Coriolis forces are of the same order of magnitude. Rotating flows are of considerable interest to engineers and metrologists. An extensive survey of this type of flows and their various applications have been given by *Thamizhsudar and Pandurangan* (2015), *Veera Krishna et al.* (2013), *Hannington Situma et al.* (2015), *Khaled* (2015).

1.5.5 Hall and Ion-Slip Currents

The Hall effect has deep roots in the history of electricity and magnetism. In 1879 U.S. Physicist Edwin H. Hall (Hall, 1879) made the momentous discovery that, when a current-caring conductor is placed in a magnetic filed, the electromagnetic force “presses” its electrons against one side of the conductor. One year later, He reported that his “pressing electricity” effect was ten times larger in ferromagnetic iron (Hall, 1881) than in non-magnetic conductors. Both discoveries were remarkable, given how little was known at the time about how charge moves through conductors. For this role, the Hall effect was frequently called the queen of solid-state transport experiments. If the magnetic field is perpendicular to electric field, there will be an electromagnetic force which is perpendicular to both magnetic and electric field. Such a force will cause the charged particles to move in the direction perpendicular to both magnetic and electric field. Then a new component of electric current density in the direction perpendicular to both magnetic and electric field which is known as Hall current. The Hall effect can be used to measure certain properties of current carries as well as to detect the presence of a current on a magnetic field.

The electric field or Hall field is a result of the force that the magnetic field exerts on the moving positive or negative particles that constitute the electric current as well as ion-slip current. This current always has a tendency to move from positive to negative. The electric current density $\mathbf{J}$ represents the relative motion of charged particles in a fluid. The equation of the electric current density may be derived from the diffusion velocities of the charge particles *Hughes and Young* (1966), *Pai* (1962), *Shercliff* (1965)). If the Hall and ion-slip terms are retained in generalized Ohm’s law, then the current density is given by (*Sutton and Sherman,*1965)

$$\mathbf{J} = \pm\left(\mathbf{E} + \mathbf{q} \wedge \mathbf{B}\right) - \frac{\mu_e{}^2{}_e}{B_0}\mathbf{J} \wedge \mathbf{B} + \frac{\mu_e{}^2{}_e \mu_i{}^2{}_i}{B_0^2}\left[\left(\mathbf{J} \wedge \mathbf{B}\right) \wedge \mathbf{B}\right] \qquad (1.5.5.1)$$

where **q** is the velocity vector, **E** is the intensity vector of the electric field, **J** is the electric current density, **B** is the magnetic induction vector, μ_e and μ_i are the electron and ion cyclotron frequencies, τ_e and τ_i are the collision times of electrons and ions. In the generalized Ohm's law (1.5.5.1), the second term on the right side gives rise to the Hall effect and the last term introduces ion-slip. Hall coefficient defines the ratio of the induced electric field to the product of the current density and the applied magnetic field. Under these conditions, the Hall and ion-slip are important and they have market effect on the magnitude and direction of the current density and consequently on the magnetic force term. Several investigators have studied the effects of magnetic fields on the convection heat and mass transfer by ignoring the Hall and Ion-slip terms in Ohms law were ignored. However, in the presence of strong magnetic field, the influence of Hall current and ion-slip are important.

The heat transfer aspect of MHD channel flow, on taking into account Hall current, was studied by *Cowling* (1957). The combined effects of the Hall and ion-slip currents on heat transfer have been studied by *Mital and Bhat* (1980). An analysis of the MHD couette flow, taking into account the Hall and ion-slip effects, has been carried out by *Soundalgeker et al.* (1979) for fully developed flow. The effects Hall and ion-slip currents on free convective heat generating flow in a rotating fluid have studied by *Ram* (1995). The transient Hartmann flow with heat transfer considering the ion-slip has been investigated by *Attia* (2005, 2006). *Attia* (2009) has studied the ion-slip effect on unsteady coquette flow with heat transfer under exponential decaying pressure gradient. The combined effects of Hall and ion-slip currents on unsteady MHD coquette flows in rotating system have been investigated by *Basant K Jha and Apere* (2010). *Mark et. al.* (2014) investigated Hall current effects on a flow in a variable magnetic field past an infinite vertical, porous flat plate. *Dileep and Priyanka* (2012) studied heat transfer effects on rotating MHD couette flow in a channel partially filled by a porous medium with Hall current. *Singh et al.* (2016) studied the effects of Hall current and ion-slip on unsteady hydromagnetic generalized couette flow in a rotating Darcian channel. MHD free convection heat and mass transfer flow through a porous medium bounded by a vertical surface in presence of Hall current were analyzed by *Tavva et al.* (2012).

1.5.6 Soret (Thermal-diffusion) and Dufour (Diffusion-thermo) numbers

Soret and Dufour effects are interesting physical phenomenon in fluid mechanics, when heat and mass transfer occur simultaneously, the relations between the fluxes and the driving potentials are of a more intricate nature. It has been found that energy flux can be generated not only by temperature gradients but also by concentration gradients. The heat transfer caused by a concentration gradient is termed as diffusion thermo (Dufour) effect. On the other hand, mass transfer created by temperature gradients is called as thermal-diffusion (Soret) effect. Generally, in heat transfer process, the Soret and Dufour effects are neglected because they are smaller order of magnitude than the effects described by Fouriers and Ficks laws. The thermal-diffusion(Soret) effect, for instance, has been utilized for isotope

separation, and in mixture between gasses with very light molecular weight (H_2, H_e) and of medium molecular weight (N_2, air), the diffusion-thermo (Dufour) effect was found to be of a considerable magnitude such that it cannot be ignored. In view of the importance of these above mentioned effects, *Dursukanya and Worek* (1992) studied diffusion-thermo and thermal-diffusion effects in transient and steady natural convection from a vertical surface. *Panneerselvi and Kowsalya* (2015) analyzed ion-Slip and Dufour effect on unsteady free convection flow past an infinite vertical plate with oscillatory suction velocity and variable permeability. *Venkata et al.* (2014) investigated Dufour and Soret effects on unsteady MHD free convection flow past a semi-infinite moving vertical plate in a porous medium with viscous dissipation. *Kafoussias* (1992) studied the MHD free convection and mass transfer flow past an infinite vertical plate moving on its own plane taken into account the thermal diffusion effect. *Nanousis* (1992) extended the work of *Kafoussias* (1992) to the case of rotating fluid taken into account the Soret effect. *Emmanuel et al.* (2008) studied numerically the effect of thermal-diffusion and diffusion thermo on combined heat and mass transfer of a steady MHD convective and slip flow due to a rotating disk with viscous dissipation and Ohmic heating. *Ahmed* (2009) considered free convective heat and mass transfer of an incompressible, electrically conducting fluid over a stretching sheet in the presence of suction and injection with thermal-diffusion and diffusion-thermo effects Many researchers studied MHD free convection flow with Soret and Dufour effect, some them, *Srinivasa et al.* (2014), *Govardhan et al.* (2012), *Bishwa and Animesh* (2016).

1.5.7 Porosity Medium

Porosity is the ratio of pore volume to its total volume. Porosity or void fraction is a measure of the void (i.e. empty) spaces in a material, and is a fraction of the volume of voids over the total volume. The term porosity is used in multiple fields including pharmaceutics, ceramics, metallurgy, materials, manufacturing, earth sciences, soil mechanics and engineering. Porosity is controlled by: rock type, pore distribution, cementation, diagenetic history and composition. Porosity is related properties of any rock or loose sediment. Most oil and gas has been produced from sandstones. These rocks usually have high porosity. Porosity is absolutely necessary to make a productive oil or gas well. The petroleum geologist must stay focused on the porosity of the prospective reservoir. Porosity consists of the tiny spaces in the rock that holds the oil or gas. Mathematically, porosity is the open space in a rock divided by the total rock volume (solid + space or holes). The holes in sandstone are called porosity (from the word “porous”). The skeletal portion of the material is often called the “matrix” or “frame”. The pores are typically filled with a fluid (liquid or gas). The skeletal material is usually a solid, but structures like foams are often also usefully analyzed using concept of porous media. Properties for any porous media of interest may also be specied. The following properties are required:

1. Porosity
2. Viscous resistance

3. Inertial resistance

A porous medium is most often characterized by its porosity. Other properties of the medium (e.g., permeability, tensile strength, electrical conductivity) can sometimes be derived from the respective properties of its contituents (solid matrix and fluid) and the media porosity and pores structure, but such a derivation is usually complex. Even the concept of porosity is only straight forward for a poroelastic medium.

Many natural substances such as rocks and soil (e.g. aquifers, petroleum reservoirs), zeolites, biological tissues (e.g. bones, wood, cork) and made materials such as cements and ceramics can be considered as porous media. Many of their important properties can only be rationalized by considering them to be porous media. The concept of porous media is used in many areas of applied science and engineering, filtration, mechanics (acoustics, geomechanics, soil mechanics, rock mechanics), engineering (petroleum engineering, bio-remediation, construction engineering), geosciences (hydrogeology, petroleum geology, geophysics), biology and biophysics, material science etc. Fluid flow through media is a subject of most common interest and has emerged a separate field of study. The study of more general behavior of porous media involving deformation of the solid frame is called poromechanics.

The literature is rich with references dealing with MHD free convection flows in presence of porous medium for instance *Pop and Watanabe* (1994). Before 1996 , the effects of the presence of a transverse magnetic field on the natural convection of an electrically conducting fluid boundary layer flow in a high porosity and thermally stratified medium have not been considered. Hydromagnetic natural convection from an isothermal inclined surface adjacent to a thermally stratified porous medium was studied by *Chamkha* (1997). Many researchers studied MHD free convection boundary layer flow heat and mass transfer high-porosity medium, some of them are *Al-Humoud and Chamkha* (2006), *Takhar et al.* (2003). *Anwar* (2005).

1.5.8 Stratification

Stratification is a characteristic of all porous media surrounded by differentially heated and salted side walls and enclosed regions of porous structures. The dynamics of flows in a thermally stratified fluid are also important and arise in many contexts, ranging from industrial settings to the oceanic and atmospheric environments. Influence of stratification is an important aspect in heat and mass transfer analysis. Stratification is a formation/deposition of layers which occur due to temperature variations, concentration differences, or the presence of different fluids. In practical situations where the heat and mass transfer mechanisms run parallel, it is interesting to analyze the effect of double stratification (stratification of medium with respect to thermal and concentration fields) on the convective transport in micro polar fluid. The analysis of free convection in a doubly stratified medium is a fundamentally interesting and important problem because of its broad range of engineering applications. These applications include heat rejection into the environment such as lakes, rivers, seas, thermal energy storage systems such as solar

ponds and heat transfer from thermal sources such as the condensers of power plants. Although the effect of stratification of the medium on the heat removal process in a fluid is important, very little work has been reported in literature. The effect of stratification is an important aspect in heat and mass transfer and has been studied by several researches. In real-world situations where heat and mass transfer run simultaneously, it is significant to investigate the effect of double stratification on the convective transport. A stratified fluid consisting of fluid parcels of various densities will tend under gravity to arrange itself so that the higher densities are found below lower densities. The vertical layering introduces an obvious gradient of properties in the vertical direction, which affects the velocity. Stratified fluids are universal in nature, present in almost any heterogeneous fluid body such that heterogeneous mixture in industries, salinity stratification in estuaries, density stratification of the atmosphere. Thermal stratification is the scientific term that describes the layering of bodies of water based on their temperature. As water heats and cools, it expands and contracts, changing in density. Thermal stratification is a natural occurrence, in any static body of water and occurs when the surface layer of water, warmed by the sun, becomes less dense than the water lower it. Analysis of thermal stratification is very important for solar engineering because higher energy efficiency can be achieved with better stratification and already shown by researchers that the thermal stratification in energy storage may significantly increase system performance. Several studies have been found to analyze the influence of the combined heat and mass transfer process by natural convection in a thermal and /or mass stratified porous medium, owing to its wide applications, such as development of advanced technologies for nuclear waste management, hot dike complexes in volcanic regions for heating of ground water, separation process in chemical engineering, etc. Here stratified porous medium means that the ambient concentration of dissolved constituent and/or ambient temperature is not uniform and varies as a linear function of vertical distance from the origin. *Chen and Eichorn* (1976) have been analyzed that natural convective flow over a heated vertical surface in a thermal stratified medium using the local non similarity method for the solution of the governing equations. When the heat and mass transfer is present simultaneously then it is important to analyze the effect of double stratifications on the convective flows, such flows involve in the rivers, lakes and seas, thermal energy storage systems and solar ponds etc.

Although the effect of stratification of the medium on the heat removal process in a fluid is important, very little work has been reported in the literature. The science of magneto hydrodynamics (MHD) was concerned with geophysical and astrophysical problems for a number of years. In recent years, the possible use of MHD is to affect a flow stream of an electrically conducting fluid for the purpose of thermal protection, braking, propulsion and control. More recent and relevant studies are also due to *Akira Nakayama and Hitoshi Koyama* (1987), *Narayana and Murthy* (2006), *Srinivas and Kishan* (2014).

Chapter 2

The Basic Equations

The equations governing the MHD convective flow of electrically conducting fluid in a rotating vertical porous plate with porous medium in the presence of Hall and ion-slip currents are;

2.1 Equation of Continuity

The mass conservation equation also called the continuity equation is derived from the law of conservation of mass. Considering a section of the fluid flow region, the mass entering the section equals the mass leaving this section such that there is no mass being created or destroyed. For an unsteady fluid flow, the vector form of the continuity equation is derived in many fluid mechanics text books such as (Curie, 1974).

$$\frac{\partial \circ}{\partial t} + \frac{\partial}{\partial x_i}\left(\circ u_i\right) = 0 \tag{2.1.1}$$

where $i = 1,2,3$ along the x, y and z directions respectively. Since we are considering a fluid flow that is incompressible, the density of the fluid is assumed to be constant and in this case the continuity equation takes the form

$$\frac{\partial u_i}{\partial x_i} = 0 \tag{2.1.2}$$

2.2 Momentum Equation

The conservation of momentum states that within some problem domain, the momentum remains constant. Momentum is neither created nor destroyed but only changed through the action of forces as described by Newton's laws of motion. Newton's second law of motion states that the rate of change of momentum of a body is equal to the net sum of resultant forces acting on the body. Considering a rotating frame of reference with a uniform angular velocity Ω, the equation of momentum becomes:

$$\frac{\partial \mathbf{q}}{\partial t} + (\mathbf{q}.\text{ď})\mathbf{q} + 2\,\text{t} \wedge \mathbf{q} = \mathbf{F} - \frac{1}{\circ}\text{ď}p + {}^{3}\nabla^{2}\mathbf{q} - \frac{{}^{3}}{k}\mathbf{q} + \frac{1}{\circ}\mathbf{J} \wedge \mathbf{B} \tag{2.2.1}$$

where the MHD body force and Coriolis terms are included in the Navier-Stokes equations to model the momentum equation.

Note that the pressure gradient and body force term are given by $\frac{\partial P}{\partial x} = -\circ_{\infty} g_0$ and $F_x = -g_0$

. Combining the pressure and the body force term then introduce the volumetric coefficient of thermal expansion and the concentration expansion co-efficient, then,

$$F_x - \frac{1}{\circ}\frac{\partial P}{\partial x} = g_0 \left(T - T_{\infty}\right) + g_0 \,{}^{*}\left(C - C_{\infty}\right)$$

If the Hall and ion-slip terms are retained in generalized Ohm's law, then the current density

is given by (Sherma and Sutton, 1965)

$$\mathbf{J} = \pm\left(\mathbf{E} + \mathbf{q} \wedge \mathbf{B}\right) - \frac{\mu_e^2{}_e}{B_0}\mathbf{J} \wedge \mathbf{B} + \frac{\mu_e^2{}_e \mu_i^2{}_i}{B_0^2}\left[\left(\mathbf{J} \wedge \mathbf{B}\right) \wedge \mathbf{B}\right] \tag{2.2.2}$$

where $_e = \mu_e^2{}_e$ Hall parameter and $_i = \mu_i^2{}_i$ ion-slip parameter.

In light of discussion in section 1.2, the basic electromagnetic equations of Maxwell's & Ohm's law (with Hall and ion-slip currents) are:

$$\text{d}'.\mathbf{D} = 0 \tag{2.1.3}$$

$$\text{d}'.\mathbf{J} = 0 \tag{2.2.4}$$

$$\text{d}'.\mathbf{B} = 0 \tag{2.2.5}$$

$$\text{d}' \wedge \mathbf{H} = \mathbf{J} \tag{2.1.6}$$

$$\text{d}' \wedge \mathbf{E} = -\frac{\partial \mathbf{B}}{\partial t} \tag{2.2.7}$$

$$\mathbf{D} = £''\mathbf{E} \tag{2.2.8}$$

$$\mathbf{B} = «_{\mathbf{e}}\mathbf{H} \tag{2.2.9}$$

$$\mathbf{J} = \pm\left(\mathbf{E} + \mathbf{q} \wedge \mathbf{B}\right) - \frac{\mu_e^2{}_e}{B_0}\mathbf{J} \wedge \mathbf{B} + \frac{\mu_e^2{}_e \mu_i^2{}_i}{B_0^2}\left[\left(\mathbf{J} \wedge \mathbf{B}\right) \wedge \mathbf{B}\right] \tag{2.2.10}$$

2.3 Energy equation

The equation is based on conservation of energy which states that energy is neither created nor destroyed but can be transformed from one form to another. It is derived from the first law of thermodynamics.

$$\frac{\partial T}{\partial t} + (\mathbf{q}.\text{d}')T = \frac{©}{°\,c_p}\nabla^2 T + \frac{³}{c_p}\left(\frac{\partial q_i}{\partial x_k} + \frac{\partial q_k}{\partial x_i}\right)^2 + \frac{J^2}{°\,c_p\pm} + \frac{\overline{Q}\left(T_\infty - T\right)}{°\,c_p} \tag{2.3.1}$$

where $i, k = 1, 2, 3$. The electrical dissipation which is the heat energy produced by the work done by electrical current. This dissipative heat due to electric currents is $\frac{J^2}{\pm}$,which is the Joule heating.

2.4 Concentration Equation

The concentration equation is also called the diffusion equation and is based on the principle of mass conservation for each component or constituent in a fluid mixture. In the absence of chemical reactions, the rate at which the mass of some species enters a control volume minus the rate at which the species mass leaves the control volume is equal to the rate at which the species mass is stored in the control volume. In this case, the concentration equation given as

$$\frac{\partial C}{\partial t} + (\mathbf{q}.\text{d}')C = D_M \nabla^2 C + D_T \nabla^2 T \tag{2.4.1}$$

The problems which will be dealt henceforth will fall into the categories that will be specified by the above mentioned equations and hence they (above equations) would serve as the basic governing equations.

Chapter 3

The Calculation Techniques

Many physical phenomena in applied science and engineering when formulated into mathematical models fall into a category of system known as non-linear coupled partial differential equations. Most of these problems can be formulated as second order partial differential equations. A system of non-linear coupled partial differential equations with the boundary conditions is very difficult to solve analytically. No analytical solution is available, the numerical method can be used. Nowadays there are several methods that enable us to solve numerically the governing equations of heat transfer problems. These include: the finite difference method, finite element method, finite volume method, boundary element method, the sixth order Rung-Kutta method along with Nachtsheim-Swigert shooting iteration technique etc. The numerical approce of partial differential equations is a broad subject. Partial differential equations play one of the most important role of computer analyzes or simulations of continuous physical systems, such as heat conduction, mechanics, fluids, electromagnetic etc.

Hence two numerical procedures have been adopted to obtain solutions. A standard initial value solver namely the sixth order Rung-Kutta method along with Nachtsheim-Swigert Shooting iteration technique have been used as a first numerical technique. After that, the governing equations are transformed by usual transformation into a non-dimensional system of non-linear coupled partial differential equations with initial and boundary conditions. Hence the solution of our problem be based on advanced numerical methods. The explicit as well as implicit finite differential method has been used for solving the obtained non-linear coupled partial differential equations, initially one problem of this thesis has been solved analytically based on the work of *Ganapathy* (1994).

3.1 Nachtsheim-Swigert Shooting Iteration Technique

To solve boundary layer equations by using Shooting method technique, there are three asymptotic boundary conditions $f''(0), g'(0)$ and$^{-}{}'(0)$.

Within the context of initial value method and Nachtsheim-Swigert iteration technique the outer boundary conditions can be functionally represented as;

$$f'(\text{¦}_{\max}) = f'(f''(0), g'(0), ^{-}{}'(0)) = ¢_1 \tag{3.1.1}$$

$$g(\text{¦}_{\max}) = g(f''(0), g'(0), ^{-}{}'(0)) = ¢_2 \tag{3.1.2}$$

$$^{-}(\text{¦}_{\max}) = ^{-}(f''(0), g'(0), ^{-}{}'(0)) = ¢_3 \tag{3.1.3}$$

with asymptotic convergences criteria are given by

$$f''(\text{¦}_{\max}) = f''(f''(0), g'(0), ^{-}{}'(0)) = ¢_4 \tag{3.1.4}$$

$$g'(\text{¦}_{\max}) = g'(f''(0), g'(0), ^{-}{}'(0)) = ¢_5 \tag{3.1.5}$$

$$\bar{}'(\dagger_{\max}) = \bar{}'(f''(0), g'(0), \bar{}'(0)) = ¢_6 \tag{3.1.6}$$

Now choosing,

$$\left.\begin{array}{l} f''(0) = g_1 \\ g'(0) = g_2 \\ \bar{}'(0) = g_3 \end{array}\right\} \tag{3.1.7}$$

Expanding first order Taylor series expansion after using the above equations (3.1.1)-(3.1.6) yields;

$$f'(\dagger_{\max}) = f_c'(\dagger_{\max}) + \frac{\partial f'}{\partial g_1}\Delta g_1 + \frac{\partial f'}{\partial g_2}\Delta g_2 + \frac{\partial f'}{\partial g_3}\Delta g_3 = ¢_1 \tag{3.1.8}$$

$$g(\dagger_{\max}) = g_c(\dagger_{\max}) + \frac{\partial g}{\partial g_1}\Delta g_1 + \frac{\partial g}{\partial g_2}\Delta g_2 + \frac{\partial g}{\partial g_3}\Delta g_3 = ¢_2 \tag{3.1.9}$$

$$\bar{}(\dagger_{\max}) = \bar{}_c(\dagger_{\max}) + \frac{\partial \bar{}}{\partial g_1}\Delta g_1 + \frac{\partial \bar{}}{\partial g_2}\Delta g_2 + \frac{\partial \bar{}}{\partial g_3}\Delta g_3 = ¢_3 \tag{3.1.10}$$

$$f''(\dagger_{\max}) = f_c''(\dagger_{\max}) + \frac{\partial f''}{\partial g_1}\Delta g_1 + \frac{\partial f''}{\partial g_2}\Delta g_2 + \frac{\partial f''}{\partial g_3}\Delta g_3 = ¢_4 \tag{3.1.11}$$

$$g'(\dagger_{\max}) = g_c'(\dagger_{\max}) + \frac{\partial g'}{\partial g_1}\Delta g_1 + \frac{\partial g'}{\partial g_2}\Delta g_2 + \frac{\partial g'}{\partial g_3}\Delta g_3 = ¢_5 \tag{3.1.12}$$

$$\bar{}'(\dagger_{\max}) = \bar{}_c'(\dagger_{\max}) + \frac{\partial \bar{}'}{\partial g_1}\Delta g_1 + \frac{\partial \bar{}'}{\partial g_2}\Delta g_2 + \frac{\partial \bar{}'}{\partial g_3}\Delta g_3 = ¢_6 \tag{3.1.13}$$

The subscript ‘c’ indicates the value of the function at $\dagger_{\max}$ determine from the trial integration. Solution of these equations in a least squares sense requires determining the minimum value of the error as;

$$E = ¢_1^{\,2} + ¢_2^{\,2} + ¢_3^{\,2} + ¢_4^{\,2} + ¢_5^{\,2} + ¢_6^{\,2} \tag{3.1.14}$$

Now differentiating E with respect to g_1, g_2 and g_3 yields

$$¢_1\frac{\partial ¢_1}{\partial g_1} + ¢_2\frac{\partial ¢_2}{\partial g_1} + ¢_3\frac{\partial ¢_3}{\partial g_1} + ¢_4\frac{\partial ¢_4}{\partial g_1} + ¢_5\frac{\partial ¢_5}{\partial g_1} + ¢_6\frac{\partial ¢_6}{\partial g_1} = 0 \tag{3.1.15}$$

$$¢_1\frac{\partial ¢_1}{\partial g_2} + ¢_2\frac{\partial ¢_2}{\partial g_2} + ¢_3\frac{\partial ¢_3}{\partial g_2} + ¢_4\frac{\partial ¢_4}{\partial g_2} + ¢_5\frac{\partial ¢_5}{\partial g_2} + ¢_6\frac{\partial ¢_6}{\partial g_2} = 0 \tag{3.1.16}$$

$$¢_1\frac{\partial ¢_1}{\partial g_3} + ¢_2\frac{\partial ¢_2}{\partial g_3} + ¢_3\frac{\partial ¢_3}{\partial g_3} + ¢_4\frac{\partial ¢_4}{\partial g_3} + ¢_5\frac{\partial ¢_5}{\partial g_3} + ¢_6\frac{\partial ¢_6}{\partial g_3} = 0 \tag{3.1.17}$$

Applying equations (3.1.8) -(3.1.13) in equations (3.1.15)-(3.1.17), then obtained equation as follows,

$$\left[\left(\frac{\partial f'}{\partial g_1}\right)^2 + \left(\frac{\partial g}{\partial g_1}\right)^2 + \left(\frac{\partial \bar{}}{\partial g_1}\right)^2 + \left(\frac{\partial f''}{\partial g_1}\right)^2 + \left(\frac{\partial g'}{\partial g_1}\right)^2 + \left(\frac{\partial \bar{}'}{\partial g_1}\right)^2\right]\Delta g_1$$

$$+\left[\frac{\partial f'}{\partial g_2}\frac{\partial f'}{\partial g_1} + \frac{\partial g}{\partial g_2}\frac{\partial g}{\partial g_1} + \frac{\partial \bar{}}{\partial g_2}\frac{\partial \bar{}}{\partial g_1} + \frac{\partial f''}{\partial g_2}\frac{\partial f''}{\partial g_1} + \frac{\partial g'}{\partial g_2}\frac{\partial g'}{\partial g_1} + \frac{\partial \bar{}'}{\partial g_2}\frac{\partial \bar{}'}{\partial g_1}\right]\Delta g_2$$

$$+\left[\frac{\partial f'}{\partial g_3}\frac{\partial f'}{\partial g_1} + \frac{\partial g}{\partial g_3}\frac{\partial g}{\partial g_1} + \frac{\partial \bar{}}{\partial g_3}\frac{\partial \bar{}}{\partial g_1} + \frac{\partial f''}{\partial g_3}\frac{\partial f''}{\partial g_1} + \frac{\partial g'}{\partial g_3}\frac{\partial g'}{\partial g_1} + \frac{\partial \bar{}'}{\partial g_3}\frac{\partial \bar{}'}{\partial g_1}\right]\Delta g_3$$

$$= -\left[f_c' \frac{\partial f'}{\partial g_1} + g_c \frac{\partial g}{\partial g_1} + \bar{}_c \frac{\partial \bar{}}{\partial g_1} + f_c'' \frac{\partial f''}{\partial g_1} + g_c' \frac{\partial g'}{\partial g_1} + \bar{}_c' \frac{\partial \bar{}'}{\partial g_1} \right] \tag{3.1.18}$$

$$\left[\frac{\partial f'}{\partial g_1}\frac{\partial f'}{\partial g_2} + \frac{\partial g}{\partial g_1}\frac{\partial g}{\partial g_2} + \frac{\partial \bar{}}{\partial g_1}\frac{\partial \bar{}}{\partial g_2} + \frac{\partial f''}{\partial g_1}\frac{\partial f''}{\partial g_2} + \frac{\partial g'}{\partial g_1}\frac{\partial g'}{\partial g_2} + \frac{\partial \bar{}'}{\partial g_1}\frac{\partial \bar{}'}{\partial g_2} \right] \Delta g_1$$

$$+ \left[\left(\frac{\partial f'}{\partial g_2}\right)^2 + \left(\frac{\partial g}{\partial g_2}\right)^2 + \left(\frac{\partial \bar{}}{\partial g_2}\right)^2 + \left(\frac{\partial f''}{\partial g_2}\right)^2 + \left(\frac{\partial g'}{\partial g_2}\right)^2 + \left(\frac{\partial \bar{}'}{\partial g_2}\right)^2 \right] \Delta g_2$$

$$+ \left[\frac{\partial f'}{\partial g_3}\frac{\partial f'}{\partial g_2} + \frac{\partial g}{\partial g_3}\frac{\partial g}{\partial g_2} + \frac{\partial \bar{}}{\partial g_3}\frac{\partial \bar{}}{\partial g_2} + \frac{\partial f''}{\partial g_3}\frac{\partial f''}{\partial g_2} + \frac{\partial g'}{\partial g_3}\frac{\partial g'}{\partial g_2} + \frac{\partial \bar{}'}{\partial g_3}\frac{\partial \bar{}'}{\partial g_2} \right] \Delta g_3$$

$$= -\left[f_c' \frac{\partial f'}{\partial g_2} + g_c \frac{\partial g}{\partial g_2} + \bar{}_c \frac{\partial \bar{}}{\partial g_2} + f_c'' \frac{\partial f''}{\partial g_2} + g_c' \frac{\partial g'}{\partial g_2} + \bar{}_c \frac{\partial \bar{}'}{\partial g_2} \right] \tag{3.1.19}$$

$$\left[\frac{\partial f'}{\partial g_1}\frac{\partial f'}{\partial g_3} + \frac{\partial g}{\partial g_1}\frac{\partial g}{\partial g_3} + \frac{\partial \bar{}}{\partial g_1}\frac{\partial \bar{}}{\partial g_3} + \frac{\partial f''}{\partial g_1}\frac{\partial f''}{\partial g_3} + \frac{\partial g'}{\partial g_1}\frac{\partial g'}{\partial g_3} + \frac{\partial \bar{}'}{\partial g_1}\frac{\partial \bar{}'}{\partial g_3} \right] \Delta g_1$$

$$+ \left[\frac{\partial f'}{\partial g_2}\frac{\partial f'}{\partial g_3} + \frac{\partial g}{\partial g_2}\frac{\partial g}{\partial g_3} + \frac{\partial \bar{}}{\partial g_2}\frac{\partial \bar{}}{\partial g_3} + \frac{\partial f''}{\partial g_2}\frac{\partial f''}{\partial g_3} + \frac{\partial g'}{\partial g_2}\frac{\partial g'}{\partial g_3} + \frac{\partial \bar{}'}{\partial g_2}\frac{\partial \bar{}'}{\partial g_3} \right] \Delta g_2$$

$$+ \left[\left(\frac{\partial f'}{\partial g_3}\right)^2 + \left(\frac{\partial g}{\partial g_3}\right)^2 + \left(\frac{\partial \bar{}}{\partial g_3}\right)^2 + \left(\frac{\partial f''}{\partial g_3}\right)^2 + \left(\frac{\partial g'}{\partial g_3}\right)^2 + \left(\frac{\partial \bar{}'}{\partial g_3}\right)^2 \right] \Delta g_3$$

$$= -\left[f_c' \frac{\partial f'}{\partial g_3} + g_c \frac{\partial g}{\partial g_3} + \bar{}_c \frac{\partial \bar{}}{\partial g_3} + f_c'' \frac{\partial f''}{\partial g_3} + g_c' \frac{\partial g'}{\partial g_3} + \bar{}_c' \frac{\partial \bar{}'}{\partial g_3} \right] \tag{3.1.20}$$

From equations (3.1.18) to (3.1.20), the following equations obtained as follows;

$$a_{11}\Delta g_1 + a_{12}\Delta g_2 + a_{13}\Delta g_3 = b_1 \tag{3.1.21}$$

$$a_{21}\Delta g_1 + a_{22}\Delta g_2 + a_{23}\Delta g_3 = b_2 \tag{3.1.22}$$

$$a_{31}\Delta g_1 + a_{32}\Delta g_2 + a_{33}\Delta g_3 = b_3 \tag{3.1.23}$$

where

$$a_{11} = \left[\left(\frac{\partial f'}{\partial g_1}\right)^2 + \left(\frac{\partial g}{\partial g_1}\right)^2 + \left(\frac{\partial \bar{}}{\partial g_1}\right)^2 + \left(\frac{\partial f''}{\partial g_1}\right)^2 + \left(\frac{\partial g'}{\partial g_1}\right)^2 + \left(\frac{\partial \bar{}'}{\partial g_1}\right)^2 \right] \tag{3.1.24}$$

$$a_{22} = \left[\left(\frac{\partial f'}{\partial g_2}\right)^2 + \left(\frac{\partial g}{\partial g_2}\right)^2 + \left(\frac{\partial \bar{}}{\partial g_2}\right)^2 + \left(\frac{\partial f''}{\partial g_2}\right)^2 + \left(\frac{\partial g'}{\partial g_2}\right)^2 + \left(\frac{\partial \bar{}'}{\partial g_2}\right)^2 \right] \tag{3.1.25}$$

$$a_{33} = \left[\left(\frac{\partial f'}{\partial g_3}\right)^2 + \left(\frac{\partial g}{\partial g_3}\right)^2 + \left(\frac{\partial \bar{}}{\partial g_3}\right)^2 + \left(\frac{\partial f''}{\partial g_3}\right)^2 + \left(\frac{\partial g'}{\partial g_3}\right)^2 + \left(\frac{\partial \bar{}'}{\partial g_3}\right)^2 \right] \tag{3.1.26}$$

$$a_{12} = a_{21} = \left(\frac{\partial f'}{\partial g_2}\frac{\partial f'}{\partial g_1} + \frac{\partial g}{\partial g_2}\frac{\partial g}{\partial g_1} + \frac{\partial \bar{}}{\partial g_2}\frac{\partial \bar{}}{\partial g_1} + \frac{\partial f''}{\partial g_2}\frac{\partial f''}{\partial g_1} + \frac{\partial g'}{\partial g_2}\frac{\partial g'}{\partial g_1} + \frac{\partial \bar{}'}{\partial g_2}\frac{\partial \bar{}'}{\partial g_1} \right) \tag{3.1.27}$$

$$a_{13} = a_{31} = \left(\frac{\partial f'}{\partial g_3}\frac{\partial f'}{\partial g_1} + \frac{\partial g}{\partial g_3}\frac{\partial g}{\partial g_1} + \frac{\partial \bar{}}{\partial g_3}\frac{\partial \bar{}}{\partial g_1} + \frac{\partial f'''}{\partial g_3}\frac{\partial f''}{\partial g_1} + \frac{\partial g'}{\partial g_3}\frac{\partial g'}{\partial g_1} + \frac{\partial \bar{}'}{\partial g_3}\frac{\partial \bar{}'}{\partial g_1} \right) \tag{3.1.28}$$

$$a_{23} = a_{32} = \left(\frac{\partial f'}{\partial g_3}\frac{\partial f'}{\partial g_2} + \frac{\partial g}{\partial g_3}\frac{\partial g}{\partial g_2} + \frac{\partial \bar{}}{\partial g_3}\frac{\partial \bar{}}{\partial g_2} + \frac{\partial f''}{\partial g_3}\frac{\partial f''}{\partial g_2} + \frac{\partial g'}{\partial g_3}\frac{\partial g'}{\partial g_2} + \frac{\partial \bar{}'}{\partial g_3}\frac{\partial \bar{}'}{\partial g_2} \right) \tag{3.1.29}$$

$$b_1 = -\left[f_c' \frac{\partial f'}{\partial g_1} + g_c \frac{\partial g}{\partial g_1} + \bar{}_c \frac{\partial \bar{}}{\partial g_1} + f_c'' \frac{\partial f''}{\partial g_1} + g_c' \frac{\partial g'}{\partial g_1} + \bar{}_c' \frac{\partial \bar{}'}{\partial g_1} \right] \tag{3.1.30}$$

$$b_2 = -\left[f_c' \frac{\partial f'}{\partial g_2} + g_c \frac{\partial g}{\partial g_2} + \bar{}_c \frac{\partial \bar{}}{\partial g_2} + f_c'' \frac{\partial f''}{\partial g_2} + g_c' \frac{\partial g'}{\partial g_2} + \bar{}_c' \frac{\partial \bar{}'}{\partial g_2} \right] \tag{3.1.31}$$

$$b_3 = -\left[f_c' \frac{\partial f'}{\partial g_3} + g_c \frac{\partial g}{\partial g_3} + \bar{}_c \frac{\partial \bar{}}{\partial g_3} + f_c'' \frac{\partial f''}{\partial g_3} + g_c' \frac{\partial g'}{\partial g_3} + \bar{}_c' \frac{\partial \bar{}'}{\partial g_3} \right] \tag{3.1.32}$$

In matrix form, equations (3.1.21)- (3.1.23) can be written as follows;

$$\begin{pmatrix} a_{11} & a_{12} & a_{13} \\ a_{21} & a_{22} & a_{23} \\ a_{31} & a_{32} & a_{33} \end{pmatrix} \begin{pmatrix} \Delta g_1 \\ \Delta g_2 \\ \Delta g_3 \end{pmatrix} = \begin{pmatrix} b_1 \\ b_2 \\ b_3 \end{pmatrix} \tag{3.1.33}$$

Now solve the system of linear equations (3.1.33) by Cramers rule and obtained as follows;

$$\left.\begin{aligned} \Delta g_1 &= \frac{\det A_1}{\det A} \\ \Delta g_2 &= \frac{\det A_2}{\det A} \\ \Delta g_3 &= \frac{\det A_3}{\det A} \end{aligned}\right\} \tag{3.1.34}$$

where,

$$\det A = \begin{vmatrix} a_{11} & a_{12} & a_{13} \\ a_{21} & a_{22} & a_{23} \\ a_{31} & a_{32} & a_{33} \end{vmatrix} \tag{3.1.35}$$

$$\det A_1 = \begin{vmatrix} b_1 & a_{12} & a_{13} \\ b_2 & a_{22} & a_{23} \\ b_3 & a_{32} & a_{33} \end{vmatrix} \tag{3.1.36}$$

$$\det A_2 = \begin{vmatrix} a_{11} & b_1 & a_{13} \\ a_{21} & b_2 & a_{23} \\ a_{31} & b_3 & a_{33} \end{vmatrix} \tag{3.1.37}$$

$$\det A_3 = \begin{vmatrix} a_{11} & a_{12} & b_1 \\ a_{21} & a_{22} & b_2 \\ a_{31} & a_{32} & b_3 \end{vmatrix} \tag{3.1.38}$$

Then the (unspecified) missing values g_1, g_2 and g_3 are as follows;

$$g_1 \equiv g_1 + \Delta g_1 \tag{3.1.39}$$

$$g_2 \equiv g_2 + \mathrm{a} g_2 \tag{3.1.40}$$

$$g_3 \equiv g_3 + \Delta g_3 \tag{3.1.41}$$

Thus adopting the Nachtsheim-Swigert iteration technique numerical described, a computer

program will be setup for the solution of the basic coupled non-linear ordinary differential equations of present problem where the integration technique will be adopted as the six order Rung-Kutta method of integration. Based on the integrations done with the above numerical technique, the obtained results will be presented in the appropriate section.

3.2 Finite Difference Technique

The finite difference method is the popular method and also the easiest one to apply to problems with simple geometries. The computational domain is covered by a grid. Taylor series expansion or polynomial fitting are used to approximate the derivatives of the variables with respect to coordinates. Algebraic equations are achieved at each grid point and the resulting set of equations can be solved simultaneously at each node.

In order to solve the governing partial differential equations by finite difference method, a two-dimensional region as shown in Fig.3.2.1 is considered. It is covered by a rectangular grid formed by two sets of lines drawn parallel to the coordinate axes with grid spacing Δx and Δy in x and y directions respectively.

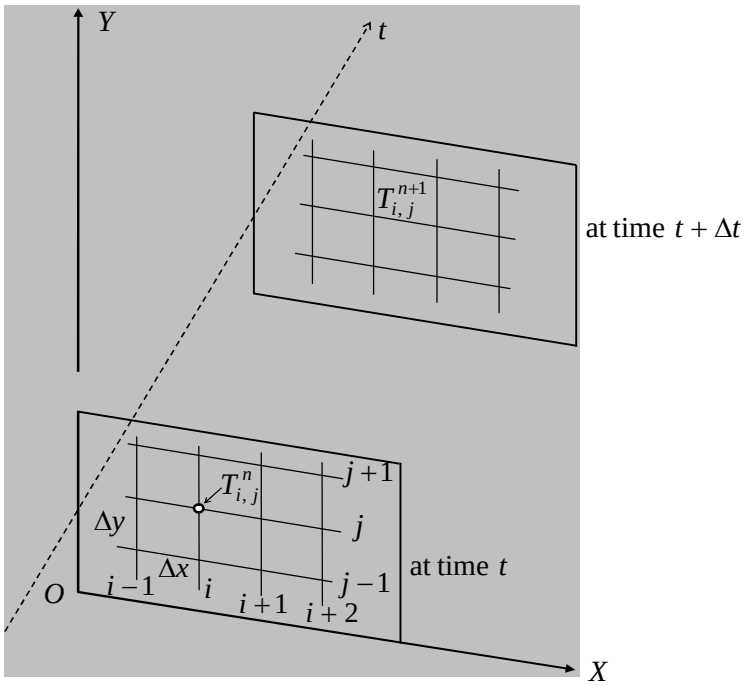

Fig.3.2.1 Space-Time index notation

The numerical values of the dependent variables are obtained at the points of intersection of the parallel lines, called *mesh* points, *lattice* points or *nodal* points. These values are obtained by discrediting the governing partial differential equations over the region of intersect to derive approxi-mately equivalent algebraic equations. The discretization consists of replacing each derivative of the partial differential equation at a mesh point by a finite difference approximation in terms of the values of the dependent variable at the mesh point and at the immediate neighboring mesh points and boundary points. In doing so, a set of algebraic equation arise.

Let the temperature T at a representative point be a function of two special coordinates x, y and time t. We adopt the following notation. The subscripts i and j represent x and y coordinates and superscript n represent time. Let the mesh spacing in x and y directions are denoted by Δx and Δy also the time step by Δt. Thus $T(x, y, t)$ can be represented by $T(i\Delta x, j\Delta y, n\Delta t) = T_{i,j}^{n}$. With this notation let us assume that the function T and its derivatives are continuous. Then from Taylor's series expansions, the finite difference

approximations to derivatives can be obtained. For example, the Taylor's series expansion of $T_{i+1,j}$ about the grid point (i, j) gives

$$T_{i+1,j} = T_{i,j} + \left[\Delta x \frac{\partial T}{\partial x} + \frac{(\Delta x)^2}{2!} \frac{\partial^2 T}{\partial x^2} + \frac{(\Delta x)^3}{3!} \frac{\partial^3 T}{\partial x^3} + \frac{(\Delta x)^4}{4!} \frac{\partial^4 T}{\partial x^4} + \text{higher order terms} \right]_{i,j} \quad (3.2.1)$$

or, $\left(\frac{\partial T}{\partial x} \right)_{i,j} = \frac{T_{i+1,j} - T_{i,j}}{\Delta x} + O(\Delta x)$ is the forward difference approximation to the derivative $\frac{\partial T}{\partial x}$ with a truncation error of order Δx.

Similarly,

$$T_{i-1,j} = T_{i,j} - \left[\Delta x \frac{\partial T}{\partial x} - \frac{(\Delta x)^2}{2!} \frac{\partial^2 T}{\partial x^2} + \frac{(\Delta x)^3}{3!} \frac{\partial^3 T}{\partial x^3} - \frac{(\Delta x)^4}{4!} \frac{\partial^4 T}{\partial x^4} + \text{higher order terms} \right]_{i,j} \quad (3.2.2)$$

or, $\left(\frac{\partial T}{\partial x} \right)_{i,j} = \frac{T_{i,j} - T_{i-1,j}}{\Delta x} + O(\Delta x)$ is the backward difference approximation to the derivative $\frac{\partial T}{\partial x}$ with a truncation error of order Δx.

Both approximations are first order accurate.

Subtracting equation (3.2.2) from (3.2.1), we obtain

$$\left(\frac{\partial T}{\partial x} \right)_{i,j} = \frac{T_{i+1,j} - T_{i-1,j}}{2\Delta x} + \left[O(\Delta x)^2 \right].$$

This is a central difference approximation to the derivative $\frac{\partial T}{\partial x}$ with a truncation error of order $(\Delta x)^2$, which is second order accurate.

The central difference approximation to a second order partial derivative $\frac{\partial^2 T}{\partial x^2}$ can be similarly obtained by adding the equations (3.2.1) and (3.2.2).

Thus $\left(\frac{\partial^2 T}{\partial x^2} \right)_{i,j} = \frac{T_{i+1,j} - 2T_{i,j} + T_{i-1,j}}{(\Delta x)^2} + \left[O(\Delta x)^2 \right]$

Similar expressions can be written for y derivative

$$\left(\frac{\partial T}{\partial y} \right)_{i,j} = \frac{T_{i,j+1} - T_{i,j-1}}{2\Delta y} + \left[O(\Delta y)^2 \right]$$

$$\left(\frac{\partial^2 T}{\partial y^2} \right)_{i,j} = \frac{T_{i,j+1} - 2T_{i,j} + T_{i,j-1}}{(\Delta y)^2} + \left[O(\Delta y)^2 \right]$$

which are also second order accurate.

The expressions for mixed derivatives can be obtained by differentiating with respect to each variable in turn. Thus for example,

$$\left(\frac{\partial^2 T}{\partial x \partial y}\right)_{i,j} = \frac{\partial}{\partial x}\left(\frac{\partial T}{\partial y}\right)_{i,j} = \frac{\left(\frac{\partial T}{\partial y}\right)_{i+1,j} - \left(\frac{\partial T}{\partial y}\right)_{i-1,j}}{2\Delta x} = \frac{\left(\frac{T_{i+1,j+1} - T_{i+1,j-1}}{2\Delta y}\right) - \left(\frac{T_{i-1,j+1} - T_{i-1,j-1}}{2\Delta y}\right)}{2\Delta x}$$

$$\therefore \left(\frac{\partial^2 T}{\partial x \partial y}\right)_{i,j} = \frac{T_{i+1,j+1} - T_{i+1,j-1} - T_{i-1,j+1} - T_{i-1,j-1}}{4\Delta x \Delta y}$$

Proceeding in a similar manner, the central difference approximation to the third derivative is found to be

$$\left(\frac{\partial^3 T}{\partial x^3}\right)_{i,j} = \frac{T_{i+2,j} - 2T_{i+1,j} + 2T_{i-1,j} - T_{i-2,j}}{2\Delta x^3}$$

Similar approximations can be obtained even to higher order derivatives.

Chapter 4

4.1 Unsteady MHD free convection and mass transfer flow along a vertical oscillatory porous plate in a rotating system with Hall, ion-slip currents and heat source

The MHD mass transfer flow under the action of strong magnetic field plays a decisive role in astrophysical and geophysical problems. Hall and ion-slip currents are likely to be important in flows of laboratory plasma. In the study of magneto hydrodynamic fluid flow in a rotating system has been motivated by several important problems, such as maintenance and secular variations of earth's magnetic field, the internal rotation rate of sun, the structure of rotating stars, the planetary and solar dynamo problem, centrifugal machines etc.

Convection in porous medium has applications in geothermal energy recovery, oil extraction, thermal energy storage and flow through filtering devices. The study of effects of magnetic field on free convection flow is important in liquid-metals, electrolytes and ionized gases. The thermal physics of hydro magnetic problems with mass transfer is of interest in power engineering and metallurgy. The study of MHD viscous flows with Hall currents has important engineering applications in problems of MHD generators and of Hall accelerators. In recent years the theoretical study of MHD channel flows has been a subject of great interest due to its widespread applications in designing cooling systems with liquid metals, petroleum industry, and purification of crude oil, polymer technology, and centrifugal separation of matter from fluid, MHD generators, pumps, accelerators and flow meters. The first exact solution of Navier-Stokes equation with flow of viscous incompressible fluid past a horizontal plate was oscillating in its own plane was investigated by *Stokes* (1851). *Turbatu et al.* (1998) investigated the flow of an incompressible viscous fluid past an infinite plate oscillating with increasing or decreasing velocity amplitude of oscillation. Combined effects of Hall and ion-slip currents on free convective heat generating flow past a semi-infinite vertical flat plate have been investigated by *Abo-Eldahab et al.* (2000). *Ramana et al.* (2011) analyzed an unsteady MHD free convective mass transfer flow past an infinite vertical porous plate with variable suction and Soret effect. *Das et al.*(2011) analyzed the eeffect of heat source on MHD free convection flow past an oscillating porous plate in the slip regime. *Maji et al.* (2009) investigated the Hall effects on hydromagnetic flow on an oscillating porous plate. *Jha and Apere* (2012) investigated time-dependent MHD couette flow of rotating fluid with Hall and ion-slip currents. The study of heat generation or absorption effects in moving fluids is important in view of several physical problems, such as fluids undergoing exothermic or endothermic chemical reactions. *Chaudhary and Arpita* (2007) studied combined heat and mass transfer effects on MHD free convection flow past an oscillating plate embedded in porous medium. *Joaquin et al.* (2011) studied the combined heat and mass transfer by natural convection from a semi-infinite plate submitted to a

magnetic field with Hall currents. *Okedoye* (2013) investigated heat and Hall effect of an oscillating plate in a porous medium. *Ahmed et al.* (2010) has studied the unsteady MHD free convective flow past a vertical porous plate immersed in a porous medium with Hall current, thermal diffusion and heat source. *Muthucumaraswamy and Vijayalakshmi* (2008) studied the effects of heat and mass transfer on flow past an oscillating vertical plate with variable temperature. *Rajput and Gaurav* (2016) investigated Soret effect on unsteady MHD flow through porous medium past an oscillating inclined plate with variable wall temperature and mass diffusion. *Das et al.* (2008) studied unsteady viscous incompressible flow due to an oscillating plate in a rotating fluid. *Revankar* (2000) studied free convection effect on flow past an impulsively started or oscillating infinite vertical plate.

Hence our aim is to investigate the unsteady MHD free convection and mass transfer flow along a vertical oscillatory porous plate in a rotating system with Hall, ion-slip currents and heat source. Also the effects of different flow parameters encountered in the equations are studied. The problem is governed by system of coupled nonlinear partial differential equations. The problem is solved by analytically in Case I and numerically in Case II. The effects of various parameters on the velocity, temperature, concentration, shear stresses (in x and z -axes), Nusselt number and Sherwood number are discussed and presented graphically.

4.1.1 Governing Equations

Consider the unsteady flow of an electrically conducting incompressible viscous fluid past an infinite vertical porous plate $y = 0$. When the plate velocity $U(t)$ oscillates in time t with a frequency $\bar{n}$ and is given as $U(t) = U_0(1 + \cos \bar{n} t)$. The flow is assumed to be in the $x-$direction and which is taken along the plate in the upward direction and $y-$axis is normal to it. Initially the fluids as well as the plate are at rest but for time $t > 0$, the whole system is allowed to rotate with a constant angular velocity Ω about the $y-$axis. Initially, it is considered that the plate as well as the fluid is at the same temperature. Also it is assumed that the temperature of the plate and spices concentration are raised to $\mathrm{T_w}(> \mathrm{T_\infty})$ and $\mathrm{C_w}(> \mathrm{C_\infty})$ respectively, which are there after maintained constant, where T_w, C_w are temperature and spices concentration at the wall and T_∞, C_∞ are the temperature and the concentration of the spices outside the boundary layer respectively, the physical configuration of the problem is shown in Fig.4.1A. A uniform magnetic field $\mathbf{B}$ is acting transverse to the plate. Using the relation $\overline{\nabla} \cdot \mathbf{B} = 0$ for the magnetic field $\mathbf{B} = (B_x, B_y, B_z)$, $B_y = B_0$ has been considered everywhere in the fluid (B_0 is a constant). However, for such a fluid, the hall and ion-slip currents will significantly affected the flow in presence of large magnetic fields. The induced magnetic field is neglected since the magnetic Reynolds

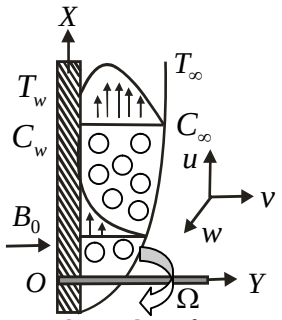

Fig.4.1A Physical configuration and coordinate system

number of a partially-ionized fluid is very small. If $\mathbf{J} = (J_x, J_y, J_z)$ is the current density, from the relation $\nabla \cdot \mathbf{J} = 0$, $J_y =$ constant has been obtained. Since the plate is electrically non-conducting, $J_y = 0$ at the plate and hence zero everywhere. Since the plate is infinite in extent, all physical quantities, except pressure, are functions of y and t only. The governing equations for the problems are as follows;

Continuity equation; $$\frac{\partial v}{\partial y} = 0 \tag{4.1.1}$$

Momentum equation;

$$\frac{\partial u}{\partial t} + v\frac{\partial u}{\partial y} = \nu \frac{\partial^2 u}{\partial y^2} + g_0 \beta (T - T_\infty) + g_0 \beta^* (C - C_\infty) + 2\Omega w - \frac{\nu}{k} u - \frac{\sigma_e B_0^2}{\rho(\omega_e^2 + \tau_e^2)}(\omega_e u + \tau_e w) \tag{4.1.2}$$

$$\frac{\partial w}{\partial t} + v\frac{\partial w}{\partial y} = \nu \frac{\partial^2 w}{\partial y^2} - 2\Omega u - \frac{\nu}{k} w + \frac{\sigma_e B_0^2}{\rho(\omega_e^2 + \tau_e^2)}(\tau_e u - \omega_e w) \tag{4.1.3}$$

Energy equation;

$$\frac{\partial T}{\partial t} + v\frac{\partial T}{\partial y} = \frac{\kappa}{\rho c_p}\frac{\partial^2 T}{\partial y^2} + \frac{\overline{Q}(T_\infty - T)}{\rho c_p} \tag{4.1.4}$$

Concentration equation;

$$\frac{\partial C}{\partial t} + v\frac{\partial C}{\partial y} = D_m \frac{\partial^2 C}{\partial y^2} + \frac{D_m k_T}{T_m}\frac{\partial^2 T}{\partial y^2} \tag{4.1.5}$$

where the variables and related quantities are defined in the Nomenclature.

The initial and boundary conditions for the model are;

$$u = 0,\ w = 0,\ T = T_\infty,\ C = C_\infty \quad \text{for } t \le 0 \tag{4.1.6}$$

$$u = U_0\left[1 + \frac{\varepsilon'}{2}\left(e^{i\omega t} + e^{-i\omega t}\right)\right],\ w = 0,\ T = T_w,\ C = C_w \quad \text{at} \quad y = 0, \quad t > 0 \tag{4.1.7}$$

$$u = 0,\ w = 0,\ T = T_\infty,\ C = C_\infty \quad \text{as} \quad y \to \infty$$

4.1.2 Mathematical Formulation

Now a convenient solution of equation (1) is

$$v = -v_0 \text{ (constant)} \tag{4.1.8}$$

where the constant velocity v_0 acting normal to the plate which is positive or negative for suction or blowing. Using equation (4.1.8), the equations (4.1.2)-(4.1.5) become

Momentum equation;

$$\frac{\partial u}{\partial t} - v_0\frac{\partial u}{\partial y} = \nu \frac{\partial^2 u}{\partial y^2} + g_0 \beta (T - T_\infty) + g_0 \beta^* (C - C_\infty) + 2\Omega w - \frac{\nu}{k} u - \frac{\sigma_e B_0^2}{\rho(\omega_e^2 + \tau_e^2)}(\omega_e u + \tau_e w) \tag{4.1.9}$$

$$\frac{\partial w}{\partial t} - v_0 \frac{\partial w}{\partial y} = \text{³} \frac{\partial^2 w}{\partial y^2} - 2\Omega u - \frac{\text{³}}{k} w + \frac{\pm_e B_0^2}{\circ\left(\sim_e^2 + \ _e^2\right)}\left(\ _e u - \sim_e w\right) \tag{4.1.10}$$

Energy equation;

$$\frac{\partial T}{\partial t} - v_0 \frac{\partial T}{\partial y} = \frac{\copyright}{\circ c_p} \frac{\partial^2 T}{\partial y^2} + \frac{\overline{Q}\left(T_\infty - T\right)}{\circ c_p} \tag{4.1.11}$$

Concentration equation;

$$\frac{\partial C}{\partial t} - v_0 \frac{\partial C}{\partial y} = D_m \frac{\partial^2 C}{\partial y^2} + \frac{D_m k_T}{T_m} \frac{\partial^2 T}{\partial y^2} \tag{4.1.12}$$

The initial and boundary conditions for the model are;

$$u = 0,\ w = 0,\ T = T_\infty,\ C = C_\infty \quad \text{for } t \le 0 \tag{4.1.13}$$

$$u = U_0\left[1 + \frac{£'}{2}\left(e^{it\overline{n}} + e^{-it\overline{n}}\right)\right],\ w = 0,\ T = T_w,\ C = C_w \quad \text{at} \quad \text{y} = 0, \quad t > 0 \tag{4.1.14}$$

$$u = 0,\ w = 0,\ T = T_\infty,\ C = C_\infty \quad \text{as} \quad \text{y} \to \infty$$

Equations (4.1.9)-(4.1.12) reduce to non-dimensional form, introducing the following non-dimensional quantities;

$$Y = \frac{yU_0}{\text{³}}, U = \frac{u}{U_0}, W = \frac{w}{U_0}, \text{²} = \frac{tU_0^2}{\text{³}}, \mu = \frac{\overline{n}\,\text{³}}{U_0^2}, \overline{T} = \frac{T - T_\infty}{T_w - T_\infty}, \overline{C} = \frac{C - C_\infty}{C_w - C_\infty} \tag{4.1.15}$$

The non-dimensional system of coupled equations have been obtained by using the above mentioned non-dimensional quantities in equations (4.1.9)-(4.1.12),

Momentum equation;

$$\frac{\partial U}{\partial \text{²}} - \text{ª} \frac{\partial U}{\partial Y} = \frac{\partial^2 U}{\partial Y^2} + G_r \overline{T} + G_m \overline{C} + 2RW - ¥U - \frac{M\left(\sim_e U + \ _e W\right)}{\sim_e^2 + \ _e^2} \tag{4.1.16}$$

$$\frac{\partial W}{\partial \text{²}} - \text{ª} \frac{\partial W}{\partial Y} = \frac{\partial^2 W}{\partial Y^2} - 2RU - ¥W + \frac{M\left(\ _e U - \sim_e W\right)}{\sim_e^2 + \ _e^2} \tag{4.1.17}$$

Energy equation;

$$\frac{\partial \overline{T}}{\partial \text{²}} - \text{ª} \frac{\partial \overline{T}}{\partial Y} = \frac{1}{P_r} \frac{\partial^2 \overline{T}}{\partial Y^2} - \sim \overline{T} \tag{4.1.18}$$

Concentration equation;

$$\frac{\partial \overline{C}}{\partial \text{²}} - \text{ª} \frac{\partial \overline{C}}{\partial Y} = \frac{1}{S_c} \frac{\partial^2 \overline{T}}{\partial Y^2} + S_0 \frac{\partial^2 \overline{T}}{\partial Y^2} \tag{4.1.19}$$

The corresponding boundary conditions are as follows;

$$U = 0,\ W = 0,\ \overline{T} = 0,\ \overline{C} = 0 \qquad \text{for } \text{²} \le 0 \tag{4.1.20}$$

$$U = 1 + \frac{£'}{2}\left(e^{i\mu \text{²}} + e^{-i\mu \text{²}}\right),\ W = 0,\ \overline{T} = 1,\ \overline{C} = 1 \qquad \text{at} \quad Y = 0, \quad \text{²} > 0$$
$$U = 0,\ W = 0,\ \overline{T} = 0,\ \overline{C} = 0 \qquad \text{as} \quad Y \to \infty \tag{4.1.21}$$

where $a\left(=\frac{\nu_0}{U_0}\right)$, $R\left(=\frac{\Omega^3}{U_0^2}\right)$, $M\left(=\frac{\pm_e B_0^{2}3}{°U_0^2}\right)$, $P_r\left(=\frac{°c_p{}^3}{©}\right)$, $S_c\left(=\frac{^3}{D_m}\right)$, $\sim\left(=\frac{\overline{Q}^3}{°c_pU_0^2}\right)$

$G_r\left(=\frac{g_0\ \ (T_w-T_\infty)^3}{U_0^3}\right), G_m\ \left(=\frac{g_0\ \ ^*(C_w-C_\infty)^3}{U_0^3}\right),\qquad S_0\left(=\frac{D_m k_T(T_w-T_\infty)}{^3T_m(C_w-C_\infty)}\right),\quad ¥\left(=\frac{^{3\ 2}}{kU_0^2}\right)$

4.1.3 Solution Technique

4.1.3.1 Case I: Analytical Solution

The equations (4.1.16)-(4.1.17) have been further simplified by putting the fluid velocity in complex form; $Q(Y,²)=(U+iW)$. Then the system of coupled ordinary differential equations become;

$$\frac{\partial Q}{\partial ²}-a\frac{\partial Q}{\partial Y}=\frac{\partial^2 Q}{\partial Y^2}+G_r\overline{T}+G_m\overline{C}-¶Q \tag{4.1.22}$$

$$\frac{\partial \overline{T}}{\partial ²}-a\frac{\partial \overline{T}}{\partial Y}=\frac{1}{P_r}\frac{\partial^2\overline{T}}{\partial Y^2}-\sim\overline{T} \tag{4.1.23}$$

$$\frac{\partial \overline{C}}{\partial ²}-a\frac{\partial \overline{C}}{\partial Y}=\frac{1}{S_c}\frac{\partial^2\overline{C}}{\partial Y^2}+S_0\frac{\partial^2\overline{T}}{\partial Y^2} \tag{4.1.24}$$

where $Q=(U+iW),\ ¶=¥+2iR+\frac{M(\sim_e-\ _e)}{\sim_e^{\ 2}+\ _e^{\ 2}}$

The corresponding boundary conditions (4.1.20) and (4.1.21) are now transformed in the following form;

$$Q=0,\ \overline{T}=0,\ \overline{C}=0\qquad \text{for}\ \ ²\le 0 \tag{4.1.25}$$

$$\begin{aligned} ²>0,\quad & Q=1+\frac{£'}{2}\left(e^{iμ²}+e^{-iμ²}\right),\ \overline{T}=1,\ \overline{C}=1 \quad \text{at}\ \ Y=0\\ & Q=0,\ \overline{T}=0,\ \overline{C}=0 \qquad\qquad\qquad\ \ \text{as}\ \ Y\to\infty \end{aligned} \tag{4.1.26}$$

In order to solve the equation (4.1.22)-(4.1.24) with the boundary condition (4.1.26) in the neighborhood of the plate, the unsteady flow is superimposed on the mean steady flow. In fact owing to the appearance of i in the ensuing differential equations, the solution must be a linear combination of $e^{μ²}$ and $e^{-μ²}$ where μ the frequency of oscillation, following equations is have been considered by *Ganapathy* (1994);

$$Q(Y,²)=Q_0(Y)+\frac{£'}{2}\left[e^{iμ²}Q_1(Y)+e^{-iμ²}Q_2(Y)\right] \tag{4.1.27}$$

$$\overline{T}(Y,²)=\overline{T}_0(Y)+\frac{£'}{2}\left[e^{iμ²}\overline{T}_1(Y)+e^{-iμ²}\overline{T}_2(Y)\right] \tag{4.1.28}$$

$$\overline{C}(Y,²)=\overline{C}_0(Y)+\frac{£'}{2}\left[e^{iμ²}\overline{C}_1(Y)+e^{-iμ²}\overline{C}_2(Y)\right] \tag{4.1.29}$$

where $Q_0=U_0+W_0,\quad Q_1+Q_2=U_1+iW_1$

The equations (4.1.22)-(4.1.24) become by equation (4.1.27)-(4.1.29) are as follows;

$$\left.\begin{aligned}
&\frac{\partial^2 Q_0}{\partial Y^2}+\text{a}\frac{\partial Q_0}{\partial Y}-\P Q_0+G_r\overline{T}_0+G_m\overline{C}_0=0\\
&\frac{\partial^2 Q_1}{\partial Y^2}+\text{a}\frac{\partial Q_1}{\partial Y}+G_r\overline{T}_1+G_m\overline{C}_1-(\P+i\mu)Q_1=0\\
&\frac{\partial^2 Q_2}{\partial Y^2}+\text{a}\frac{\partial Q_2}{\partial Y}+G_r\overline{T}_2+G_m\overline{C}_2-(\P-i\mu)Q_2=0
\end{aligned}\right\} \quad (4.1.30)$$

$$\left.\begin{aligned}
&\frac{\partial^2 \overline{T}_0}{\partial Y^2}+\text{a}P_r\frac{\partial \overline{T}_0}{\partial Y}-\sim P_r\overline{T}_0=0\\
&\frac{\partial^2 \overline{T}_1}{\partial Y^2}+\text{a}P_r\frac{\partial \overline{T}_1}{\partial Y}-(\sim P_r+i\mu P_r)\overline{T}_1=0\\
&\frac{\partial^2 \overline{T}_2}{\partial Y^2}+\text{a}P_r\frac{\partial \overline{T}_2}{\partial Y}-(\sim P_r-i\mu P_r)\overline{T}_2=0
\end{aligned}\right\} \quad (4.1.31)$$

$$\left.\begin{aligned}
&\frac{\partial^2 \overline{C}_0}{\partial Y^2}+\text{a}S_c\frac{\partial \overline{C}_0}{\partial Y}+S_0S_c\frac{\partial^2 \overline{T}_0}{\partial Y^2}=0\\
&\frac{\partial^2 \overline{C}_1}{\partial Y^2}+\text{a}S_c\frac{\partial \overline{C}_1}{\partial Y}-i\mu S_c\overline{C}_1+S_0S_c\frac{\partial^2 \overline{T}_1}{\partial Y^2}=0\\
&\frac{\partial^2 \overline{C}_2}{\partial Y^2}+\text{a}S_c\frac{\partial \overline{C}_2}{\partial Y}+i\mu S_c\overline{C}_2+S_0S_c\frac{\partial^2 \overline{T}_2}{\partial Y^2}=0
\end{aligned}\right\} \quad (4.1.32)$$

The appropriate boundary conditions for the equations (4.1.25)-(4.1.26) are as follows;

$$\begin{aligned}
&Q_0=1,\ \overline{T}_0=1,\ \overline{C}_0=1 \qquad \text{at } Y=0\\
&Q_0=0,\overline{T}_0=0,\overline{C}_0=0 \qquad \text{as } Y\to\infty
\end{aligned} \quad (4.1.33)$$

$$\begin{aligned}
&Q_1=1,\ \overline{T}_1=0,\ \overline{C}_1=0 \qquad \text{at } Y=0\\
&Q_1=0,\ \overline{T}_1=0,\overline{C}_1=0 \qquad \text{as } Y\to\infty
\end{aligned} \quad (4.1.34)$$

$$\begin{aligned}
&Q_2=1,\ \overline{T}_2=0,\ \overline{C}_2=0 \qquad \text{at } Y=0\\
&Q_2=0,\ \overline{T}_2=0,\ \overline{C}_2=0 \qquad \text{as } Y\to\infty
\end{aligned} \quad (4.1.35)$$

Solving equation (4.1.30)-(4.1.32) by using boundary conditions (4.1.33)-(4.1.35), the following equations have been obtained;

$$Q_0=B_5e^{-A_7Y}-B_3e^{-A_2Y}-B_4e^{-A_3Y}$$

$$\overline{}_0=e^{-A_2Y}$$

$$\text{¤}_0=A_4e^{-A_2Y}+A_5e^{-A_3Y}$$

$$Q_1=e^{-A_{13}Y}$$

$$\overline{T}_1=0$$

$$\overline{C}_1=0$$

$$Q_2=e^{-A_{19}Y}$$

$$\overline{T}_2=0$$

$$\overline{C}_2=0$$

Now putting the values of $Q_0,\overline{}_0,\text{¤}_0,Q_1,\overline{}_1,\text{¤}_1,Q_2,\overline{}_2,\text{¤}_2$ in equation (4.1.27)-(4.1.29) then the following equations are as follows;

$$Q=B_5e^{-A_7Y}-B_3e^{-A_2Y}-B_4e^{-A_3Y}+\frac{\text{£}}{2}e^{i\mu^2}e^{-A_{13}Y}+\frac{\text{£}}{2}e^{-i\mu^2}e^{-A_{19}Y}$$

$$\bar{T} = e^{-A_2 Y}$$

$$\bar{C} = A_4 e^{-A_2 Y} + A_5 e^{-A_3 Y}$$

where the values of $A_2, A_3, A_4, A_5, A_7, A_{13}, A_{19}, B_1, B_2, B_3, B_4, B_8, B_{10}, B_5$ and other constants are defined in appendix.

4.1.3.2 Case II: Numerical Solution

The governing second order non-linear coupled partial differential equations have been solved with the associated initial and boundary conditions. For solving a transient free convection flow with mass transfer past an infinite plate, the implicit finite difference method has been used by *Callahan and Marner* (1976) which is conditional stable. On the contrary, the same problem has been studied by *Soundalgekar and Ganesan* (1980) by an implicit finite difference method which is fast convergent and unconditional stable. But Callahan and Marner (1976), *Soundalgekar and Ganesan* (1980) have been found same result using different methods on the same problem. The implicit finite difference method has been used to solve the equations (4.1.16)-(4.1.19) with boundary conditions (4.1.20). For the purpose, a rectangular region is considered where Y varies from 0 to 25. This value $Y_{\max}$ is supposed to represent ∞ and lies well outside the momentum, energy and concentration boundary layers. In this case, the region within the boundary layer is divided by some perpendicular lines of Y-axis, where Y-axis is normal to the medium as shown Fig.4.1.B. Number of grid spacing in Y-direction is $m(=400)$, hence the constant mesh size along Y-axis become $\Delta Y = 0.06(0 \le Y \le 25)$ with a smaller time step $\Delta t = 0.001$.

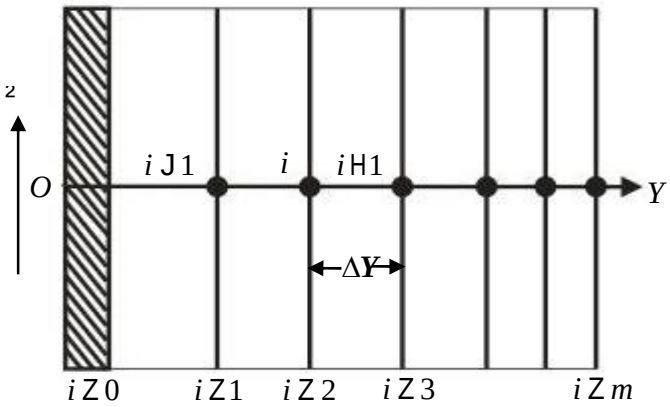

Fig.4.1.B Finite difference grid space

Let $U^n, W^n, \bar{T}^n$ and $\bar{C}^n$ denoted the values of $U, W, \bar{T}$ and $\bar{C}$ at the end of a time-step. Then an appropriate set of finite difference equations corresponding to the equations (4.1.16)-(4.1.19) are as follows;

$$\frac{U_i^{n+1} - U_i^n}{\Delta t} - a\frac{U_{i+1}^n - U_i^n}{\Delta Y} = G_r \bar{T}_i^n + G_m \bar{C}_i^n + \frac{U_{i+1}^n - 2U_i^n + U_{i-1}^n}{(\Delta Y)^2} + 2RW_i^n - \phi U_i^n - \frac{M}{\sigma_e^2 + \beta_e^2}\left(\sigma_e U_i^n + \beta_e W_i^n\right) \tag{4.1.36}$$

$$\frac{W_i^{n+1} - W_i^n}{\Delta t} - a\frac{W_{i+1}^n - W_i^n}{\Delta Y} = \frac{W_{i+1}^n - 2W_i^n + W_{i-1}^n}{(\Delta Y)^2} - 2RU_i^n - \phi W_i^n + \frac{M}{\sigma_e^2 + \beta_e^2}\left(\beta_e U_i^n - \sigma_e W_i^n\right) \tag{4.1.37}$$

$$\frac{\overline{T}_i^{n+1}-\overline{T}_i^{n}}{\Delta²}-\text{a}\,\frac{\overline{T}_{i+1}^{n}-\overline{T}_i^{n}}{\Delta Y}=\frac{1}{P_r}\frac{\overline{T}_{i+1}^{n}-2\overline{T}_i^{n}+\overline{T}_{i-1}^{n}}{(\Delta Y)^2}-\sim\overline{T}_i^{n} \tag{4.1.38}$$

$$\frac{\overline{C}_i^{n+1}-\overline{C}_i^{n}}{\Delta²}-\text{a}\,\frac{\overline{C}_{i+1}^{n}-\overline{C}_i^{n}}{\Delta Y}=\frac{1}{S_c}\frac{\overline{C}_{i+1}^{n}-2\overline{C}_i^{n}+\overline{C}_{i-1}^{n}}{(\Delta Y)^2}+S_0\frac{\overline{T}_{i+1}^{n}-2\overline{T}_i^{n}+\overline{T}_{i-1}^{n}}{(\Delta Y)^2} \tag{4.1.39}$$

The initial and boundary conditions are obtained as

$$U_i^0=0,\ W_i^0=0,\ \overline{T}_i^0=1,\ \overline{C}_i^0=1 \tag{4.1.40}$$

$$\left.\begin{aligned}&U_0^n=1,\ W_0^n=0,\ \overline{T}_0^n=1,\ \overline{C}_0^n=1\\&U_L^n=1,\ W_L^n=0,\ \overline{T}_L^n=1,\ \overline{C}_L^n=1\quad \textit{where } L\to\infty\end{aligned}\right\} \tag{4.1.41}$$

Here the subscripts i designate the grid points with Y coordinates and the superscript n represents a value of time, $²=\overline{\overline{n}}\Delta²$ where $\overline{\overline{n}}=0,1,2,3,....$ The primary velocity U, secondary velocity W, temperature $\overline{T}$ and concentration $\overline{C}$ distributions at all interior nodal points may be computed by successive applications of the above finite difference equations. The obtained values are discussed graphically.

4.1.4 Stability and Convergence Analysis

The analysis will remain incomplete unless discussion the stability and convergence of the finite different scheme. For the constant mesh sizes, the stability criteria of the scheme may be established as follows. The general terms of the Fourier expansion for $U, W, \overline{T}, \overline{C}$ at a time arbitrarily called $²=0$ are $e^{i\sim Y}$ apart from a constant, where $i=\sqrt{-1}$. At a time $²$ later, these terms become

$$\begin{aligned}&U:\ \cdot(²)e^{i\sim Y}\\&W:\ ¶(²)e^{i\sim Y}\\&\overline{T}:\ \overline{\ }(²)e^{i\sim Y}\\&\overline{C}:\ ¤(²)e^{i\sim Y}\end{aligned} \tag{4.1.42}$$

Substituting (4.1.42) into equations (4.1.36) - (4.1.39), over any one time step and denoting the values after the time step by $\cdot',¶',\overline{\ }'$ and $¤'$ gives after simplifications

$$\cdot'=\grave{a}(²)\,\text{Z}\,D\cdot(²)\,\text{H}\,E¶(²)\,\text{H}\,F\overline{\ }(²)\,\text{H}\,G¤(²) \tag{4.1.43}$$

$$¶'=\grave{a}(²)\,\text{Z}\,H\cdot(²)\,\text{H}\,I¶(²) \tag{4.1.44}$$

$$\overline{\ }'=\grave{a}(²)\,\text{Z}\,J\overline{\ }(²) \tag{4.1.45}$$

$$¤'=\grave{a}(²)\,\text{Z}\,K\overline{\ }(²)\,\text{H}\,L¤(²) \tag{4.1.46}$$

where

$$D=1-¥\Delta²+\text{a}\,\frac{\Delta²}{\Delta Y}\left(e^{i\sim\Delta Y}-1\right)+\frac{2\Delta²}{(\Delta Y)^2}\left[\cos\sim\Delta Y-1\right]-\frac{M\sim_e\Delta²}{\sim_e^2+\ _e^2}$$

$$I=1+\text{a}\,\frac{\Delta²}{\Delta Y}\left(e^{i\sim\Delta Y}-1\right)+\frac{2\Delta²}{(\Delta Y)^2}\left(\cos\sim\Delta Y-1\right)-¥\Delta²-\frac{M\sim_e\Delta²}{\sim_e^2+\ _e^2}$$

$$J=1+\text{a}\,\frac{\Delta²}{\Delta Y}\left(e^{i\sim\Delta Y}-1\right)+\frac{1}{P_r}\frac{2\Delta²}{(\Delta Y)^2}\left(\cos\sim\Delta Y-1\right)-\sim\Delta²$$

$$L = 1 + \text{a}\frac{\Delta^2}{\Delta Y}\left(e^{i\sim\Delta Y} - 1\right) + \frac{1}{S_c}\frac{2\Delta^2}{(\Delta Y)^2}\left(\cos\sim\Delta Y - 1\right) \quad , \quad E = \left[2R - \frac{M_{\ e}}{\sim_e^2 + \ _e^2}\right]\Delta^2$$

$$F = G_r\Delta^2 \qquad G = G_m\Delta^2 \qquad H = \frac{M_{\ e}\Delta^2}{\sim_e^2 + \ _e^2} - 2R\Delta^2 \qquad K = S_0\frac{2\Delta^2}{(\Delta Y)^2}\left(\cos\sim\Delta Y - 1\right)$$

The equations (4.2.50) to (4.2.53) are written in matrix form;

$$\begin{pmatrix} \cdot' \\ \P' \\ -' \\ \text{¤}' \end{pmatrix} = \begin{pmatrix} D & E & F & G \\ H & I & 0 & 0 \\ 0 & 0 & J & 0 \\ 0 & 0 & K & L \end{pmatrix}\begin{pmatrix} \cdot \\ \P \\ - \\ \text{¤} \end{pmatrix} \tag{4.1.47}$$

i.e. $\text{¦}' = T\text{¦}$ where i.e. ¦ is the column vector with element $\cdot, \P, \bar{}$ and ¤. For stability, the modulus of each eigenvalue of the amplication matrix T must not exceed unity. Let

$$a = \frac{\Delta^2}{\Delta Y},\ b = \frac{2\Delta^2}{(\Delta Y)^2}$$

Then $D = 1 - \text{a}a - b - \text{¥}\Delta^2 + \text{a}ae^{i\sim\Delta Y} + b\cos\sim\Delta Y$

$I = 1 - \text{a}a - b - \text{¥}\Delta^2 + \text{a}ae^{i\sim\Delta Y} + b\cos\sim\Delta Y$

$$J = 1 - \text{a}a - \frac{b}{P_r} - \sim\Delta^2 + \text{a}ae^{i\sim\Delta Y} + \frac{b}{P_r}\cos\sim\Delta Y$$

$$L = 1 - \text{a}a - \frac{b}{S_c} + \text{a}ae^{i\sim\Delta Y} + \frac{b}{S_c}\cos\sim\Delta Y$$

The coefficients a and b are all real and non-negative. We can demonstrate that the maximum modulus of D, I, J and L occur when $\sim\Delta Y = m\text{®}$, where m is an integer and hence D, I, J and L are real. For sufficiently large, the value of $|J|, |L|, |D|$ and $|I|$ are greater when m is an odd integer, in which case

$$D = (1 - \text{a}a - b) + (-\text{a}a - b - \text{¥}\Delta^2)$$

$$I = (1 - \text{a}a - b) + (-\text{a}a - b - \text{¥}\Delta^2)$$

$$J = \left(1 - \text{a}a - \frac{b}{P_r}\right) + \left(-\text{a}a - \frac{b}{P_r} - \sim\Delta^2\right)$$

$$L = \left(1 - \text{a}a - \frac{b}{S_c}\right) + \left(-\text{a}a - \frac{b}{S_c}\right)$$

To satisfy the condition $|J| \le 1, |L| \le 1, |D| \le 1$ and $|I| \le 1$ the most negative allowable value is

$J = -1,\ L = -1, D = -1,\ I = -1$

Hence the stability conditions are

$$\text{a}a + b + \frac{1}{2}\text{¥}\Delta^2 \le 1$$

$$\text{a}a + b + \frac{1}{2}\text{¥}\Delta^2 \le 1$$

$$^{a}a+\frac{b}{P_r}+\frac{1}{2}\sim\Delta^{2}\le 1$$

$$^{a}a+\frac{b}{S_c}\le 1$$

4.1.5 Shear Stress, Nusselt number and Sherwood number

The quantities of chief physical interest are shear stress, Nusselt number and Sherwood number. The following equations represent the shear stress at the plate. The shear stress in x and z components are as follows;

$^{2}_{U}=\left(\frac{\partial u}{\partial y}\right)_{y=0}$ and $^{2}_{W}=\left(\frac{\partial w}{\partial y}\right)_{y=0}$ which are proportion to $\left(\frac{\partial U}{\partial Y}\right)_{Y=0}$ and $\left(\frac{\partial W}{\partial Y}\right)_{Y=0}$.

From the temperature field, the effect of various parameters on the local heat transfer coefficients has been studied. The following relation represents the heat transfer rate that is well known Nusselt number. Nusselt number $N_u=-k\left(\frac{\partial T}{\partial y}\right)_{y=0}$ which is proportional to

$\left(\frac{\partial \overline{T}}{\partial Y}\right)_{Y=0}$.

And from the concentration field, the effect of various parameters on the mass transfer coefficients has been analyzed. The following relation represents the mass transfer rate that is well known Sherwood. Sherwood number $S_h=-D_m\left(\frac{\partial C}{\partial y}\right)_{y=0}$ which is proportional to

$\left(\frac{\partial \overline{C}}{\partial Y}\right)_{Y=0}$.

The numerical values of the shear stress, Nusselt number and Sherwood number are evaluated by Five-point approximation formula for the derivatives. The obtained values are discussed graphically.

4.1.6 Results and Discussion

4.1.6.1 Justification of Grid Space

The code is conversed with three different grid space $m=350,400,450$ where m is the grid number. It is seen that there is a little change for the above mentioned grid points which are shown in Fig.4.1C. For saving power and time, the computation for results of velocity, temperature and concentration have been carried out for $m=400$.

4.1.6.2 Steady-State Solution

The numerical solutions of the non-linear differential equation (4.1.9)-(4.1.12) under the boundary conditions (4.1.13)-(4.1.14) have been performed by applying implicit finite difference method. In order to verify the effects of time step size Δ^{2}, the programming code is run our model with different step sizes such as $^{2}=10,40,80,90,100,110,120$. To get

Steady-State solutions, the computations have been carried out up to ² =120. It is observed that, the result of computations for $U, W, \bar{T}$ and $\bar{C}$, however shows little changes after ² =80. Thus the solutions of all variables for ² =90 are essentially steady-state. Grid space and steady state solution are shown for rotational parameter R in Fig.4.1C and Fig. 4.1D for primary velocity.

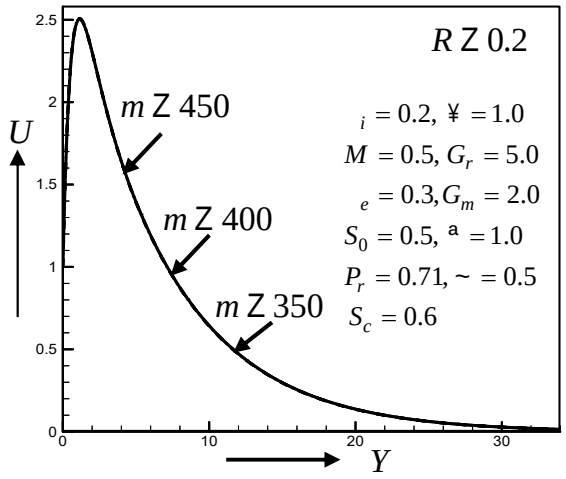

Fig.4.1C Primary velocity for different grid space of rotational parameter *R*

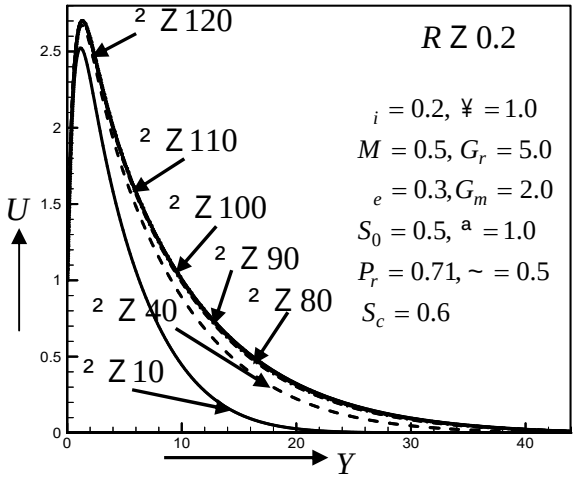

Fig.4.1D Primary velocity for different time step rotational parameter *R*

Unsteady MHD free convection and mass transfer flow along a vertical oscillatory porous plate in a rotating system with Hall, ion-slip currents and heat source have been investigated using analytically as well as numerically. To study the physical situation of this problem, the primary velocity, secondary velocity, temperature and concentration distribution within the boundary layer have been computed and also find the Shear stress, Nusselt number and Sherwood number at the plate. The velocity in x-direction is called primary velocity and that of in z-direction is called secondary velocity. For the purpose of discussing the effects of various parameters on the flow behaviors in the boundary layer. Numerical calculations have been carried out for different values of Hall parameter($_e$), ion-slip parameter($_i$), magnetic parameter(M), rotation parameter(R), Prandtl number(P_r), suction parameter(ª), Schmidt number (S_c), Grashof number(G_r), modified Grashof number(G_m), Soret number (S_0), permeability parameter(¥) and heat source parameter(~). It is observed that these parameters affect the velocity, temperature and concentration fields. The values for the parameters are chosen arbitrarily. Some standard values for the Prandtl number (P_r) and Schmidt number (S_c) are considered because of the physical importance. These are $P_r = 0.71$ corresponds to air, $P_r = 1.00$ corresponds to electrolyte solution such as salt water and $P_r = 7.0$ corresponds to water $20^0 C$ and Schmidt number S_c the values 0.60, 0.78,1.0 are considered, which represent specific condition of flow (0.60 for water vapor, 0.78 for ammonia, 1.0 for carbondioxid). The importance of cooling problem in nuclear engineering in connection with the cooling of reactors, the values of G_r and G_m are taken to be positive.

For the purpose of computation, $\mu t = ® / 2, £' = 0.001$ have been chosen arbitrarily. For brevity negligible effects on velocity, temperature and concentration distributions are not shown.

Discussion of Analytic solution (figures of 1st column) and Numerical Solution (figures of 2nd and 3rd columns)

To observe the physical situations of the problem, the primary velocity, secondary velocity, temperature and concentration distribution have been displayed in Figs.4.1.1-4.1.29 and Fig.4.1.30(a)-4.1.58(a) in case of analytical(case I) and numerical(case II) solutions. Also in numerical solution, the physical importance of the problem with the above mentioned parameters, the shear stresses (in x and z-axes), Nusselt number and Sherwood number have been displayed in Figs. 4.1.30(b)-4.1.58(b).

Figs. 4.1.1, Fig. 4.1.3, Figs. 4.1.30(a) and Fig. 4.1.32(a) depict the variation in the primary velocity profiles for different values of Hall parameter ($_e$) and ion-slip parameter ($_i$) in case of analytic and numerical solutions of the problem. These figures indicate that, the primary velocity increase with the increase of Hall and ion-slip parameters. This is because the effective conductivity decreases with increasing $_e$ and $_i$ which reduces the magnetic damping force on primary velocity. Due to analytical and numerical solutions of the problem theses figures are qualitatively identical but quantitatively different. Similar trend arises in secondary velocity profiles with the increase of $_e$ which can be found in Fig.4.1.2 and Fig.4.1.31 (a) in case of analytic and numerical solutions respectively. These two figures are qualitatively identical but quantitatively different. But the secondary velocity profiles have decreasing effect with the increase of $_i$ which are shown in Fig.4.1.4 and Fig.4.1.33 (a). Also these two figures are qualitatively identical but quantitatively different. In numerical solution, the shear stresses in x-axis increases with the increase of $_e$ and $_i$ which are shown in Fig. 4.1.30(b) and Fig. 4.1.32(b). The shear stress in z-axis increases with the increase of $_e$ while the opposite behavior is shown for increasing $_i$ which are shown in Fig. 4.1.31(b) and Fig. 4.1.33(b) for numerical solution. The Hall effect accelerated the fluid flow along secondary direction, as a result rate of flow along z-axis increases, so the shear stress along z - axis is increased.

From Fig.4.1.5 and Fig. 4.1.34(a) it is seen that the primary velocity decrease with the increase of permeability parameter (¥) in case of analytic and numerical solutions. It is expected physically also because the resistance posed by the porous medium to the decelerated flow due to the rotation reduces with increasing ¥ which leads to decrease in the primary velocity. From these two figures, it is indicated that the qualitative behavior are

same but quantitatively different. The variations of secondary velocity for various values of ¥ in case of analytic and numerical solutions are plotted in Fig. 4.1.6 and Fig. 4.1.35(a) respectively. From these figures it is observed that secondary velocity increases with the increase of ¥. From these two figures it is seen that the qualitatively identical but quantitatively different. In numerical solution, the shear stress in x-axis decreases whereas in z- axis has reverse effect with the increase of ¥ which are found in Fig. 4.1.34(b) and Fig. 4.1.35(b).

It is observed that there is rise in the primary velocity with the increase of modified Grashof number (G_m) in Fig. 4.1.7 and Fig. 4.1.36(a) in case of analytic and numerical solutions respectively. This expected, increase in the values of G_m has the tendency to increase the mass buoyancy effect, which gives rise to an increase in the induced flow. These two figures are qualitatively identical but quantitatively different. From Fig. 4.1.8 and Fig. 4.1.37(a) it is found that the modified Grashof number has reverse effect on secondary velocity field in case of analytic and numerical solutions. From these two figures it is seen that the qualitative nature of the flow is identically same but quantitatively different. In numerical solution the shear stress in x- axis increases with the increase of G_m which is shown in Fig. 4.1.36(b). The modified Grashof number has the tendency to increase mass buoyancy force, as a result the rate of the flow of the fluid increases. Thus shear stress in x- axis increases in numerical solution. Whereas the shear stress in z- axis decreases with the increase of G_m which is shown in Fig.4.1.37(b).

Fig.4.1.9, Fig.4.1.10, Fig 4.1.38(a) and Fig 4.1.39(a) show the variation of primary and secondary velocity profiles for various values of Grashof number (G_r) in case of analytic and numerical solutions respectively. Fig.4.1.9 and Fig 4.1.38(a) reveal the primary velocity variation with (G_r) correspond to cooling of the plate. It is observed that greater cooling of the plate i.e. increase in G_r results an increase in primary velocity in case of analytic and numerical solutions respectively. It is expected, that the increase in the values of thermal Grashof number has the tendency to enhancement of thermal buoyancy force. This gives rise to an increase in the induced flow. These two figures are qualitatively same but quantitatively different. Opposite behavior are found in case of secondary profiles for increasing values of G_r which are shown in Fig.4.1.10 and Fig. 4.1.39(a) in both cases. Due to analytic and numerical solutions Fig.4.1.10 and Fig. 4.1.39(a) are qualitatively identical but quantitatively different. In numerical solution, the shear stress in x- axis increases whereas shear stress in z- axis decreases with the increase of G_r which are shown in Fig. 4.1.38(b) and Fig. 4.1.39(b).

Fig.4.1.11- Fig.4.1.14 and Fig.4.1.40 (a)- Fig.4.1.43 (a) illustrate the influence of suction parameter (a) on the velocity (primary and secondary), temperature and concentration distribution in case of analytic and numerical solutions respectively. It is seen that the primary velocity decreases with the increase of suction parameter for both analytic and numerical solutions which are shown in Fig.4.1.11 and Fig.4.1.40 (a). Since the effect of

suction is to suck away the fluid near the wall, the momentum boundary layer is reduced due to suction. These two figures are qualitatively same but quantitatively different. But opposite behavior is found on secondary velocity which are shown in Fig. 4.1.12 and Fig.4.1.41 (a) in case of analytic and numerical solutions. These two figures are qualitatively identical but quantitatively different. In Fig. 4.1.13, Fig. 4.1.14, Fig.4.1.42 (a) and Fig. 4.1.43(a), it is found that increasing a decreases temperature and concentration distributions in case of analytic and numerical solutions. Sucking decelerated fluid particles through the porous wall reduces the growth of thermal and concentration boundary layers. These four figures are qualitatively identical but quantitatively different. In numerical solution, the shear stress in x - axis decreases whereas shear stress in z - axis increases with the increases of a which are found in Fig. 1.4.40(b) and Fig. 4.1.41(b). In Fig. 4.1.42(b) and Fig.4.1.43 (b), the Nusselt and Sherwood numbers increase with the increase of a for numerical solution.

From Fig. 4.1.15 and Fig.4.1.44 (a), it is found that the primary velocity decreases with an increase of magnetic parameter (M) in case of analytic and numerical solutions respectively. The presence of magnetic field in an electrically conducting fluid introduces a force called Lorentz force. This force has tendency to slow down the motion of the fluid. These two figures are qualitatively same but quantitatively different. Whereas reverse effects are found in case of secondary profiles for increasing values of M which are shown in Fig.4.1.16 and Fig. 4.1.45(a) in both cases. The result indicates that the resulting Lorentzian body force will not act as a drag force. Due to analytical and numerical solutions Fig.4.1.16 and Fig. 4.1.45(a) are qualitatively identical but quantitatively different. In numerical solution the shear stress in x - axis decreases whereas shear stress in z - axis increases with the increases of M , which are found in Fig. 4.1.44(b) and Fig. 4.1.45(b).

In Fig. 4.1.17 and Fig.4.1.46 (a) illustrate that the primary velocity profiles decrease with the increase of Prandtl number P_r in case of analytic and numerical solutions. This is because in the free convection the plate velocity is higher than the adjacent fluid velocity and the momentum boundary layer thickness decreases. These two figures are qualitatively identical but quantitatively different. The secondary velocity has reverse effects which is shown in Fig.4.1.18 and Fig.4.1.47 (a) in case of analytic and numerical solutions. These two figures are qualitatively same but quantitatively different. From Fig.4.1.19 and Fig. 4.1.48 (a), it is found that the temperature profiles decrease with an increase of P_r in case of analytic and numerical solutions. Because if P_r increases, the thermal diffusivity decreases and these phenomena lead to the decreasing of energy ability that reduces the thermal boundary layer. These two figures are qualitatively identical but quantitatively different. The shear stress in x - axis decreases while shear stress in z - axis has opposite behavior which is shown in Fig. 4.1.46(b) and Fig.4.1.47 (b) in case of numerical solution. The Nusselt number does not show approximately any change with an increase of P_r which is shown in Fig. 4.1.48(b) for numerical solution.

It is clear that Fig.4.1.20, Fig.4.1.21, Fig.4.1.49 (a) and & Fig.4.1.50 (a) display the effects of rotational parameter (R) on the velocity (primary and secondary) in case of analytic and numerical solutions. The primary and secondary velocities decrease with the increase of R .

This implies that rotational retards fluid flow in the primary and secondary flow directions. These four figures are qualitatively same but quantitatively different in case of analytic and numerical solutions. The shear stress in x - axis and z - axis decrease with the increase of R which are shown in Fig. 4.1.49(b) and Fig.4.1.50 (b) for numerical solution.

It is clearly shown in Figs.4.1.22 and Fig.4.1.51 (a) the effects of Schmidt number (S_c) on primary velocity profiles for both analytic and numerical solutions. The primary velocity and concentration distributions decrease with the increase of S_c. This is due to a decrease in the molecular diffusivity, which results in a decrease in the velocity and concentration boundary layer thickness. These four figures are qualitatively identical but quantitatively different in case of analytic and numerical solutions. But opposite behaviors are shown on secondary velocity in Fig. 4.1.23 and Fig.4.1.52 (a) in case of analytic and numerical solutions. These two figures are qualitatively same but quantitatively different. The shear stress in x - axis decreases whereas shear stress in z - axis increases with the increase of S_c which are shown in Fig.4.1.51 (b) and Fig.4.1.52 (b) for numerical solution.

Figs.4.1.24, Fig. 4.1.26, Fig. 4.1.53(a) and Fig.4.1.55 (a) depict the velocity and concentration profiles for different values of the Soret number (S_0) in case of analytic and numerical solutions. The primary velocity and concentration distributions increase with the increase of S_0. The Soret number defines the effect of the temperature gradients inducing significant mass diffusion effects. It is noticed that an increase in S_0 results in an increase in the velocity and concentration within the boundary layer. These four figures are qualitatively identical but quantitatively different for analytical and numerical solutions. Whereas decreasing effects on secondary velocity which are shown in Fig.4.1.25 and Fig.4.1.54 (a) in case of analytic and numerical solutions. These two figures are qualitatively identical but quantitatively different. The shear stress in x - axis increases whereas shear stress in z - axis has reverse effect with the increase of S_0 which are shown in Fig.4.1.53 (b) and Fig.4.1.54 (b) in case of numerical solution. Also the Sherwood number has decreasing effect with increasing S_0 which is seen in Fig.4.1.55 (b) in case of numerical solution.

The effects of increasing the value of the heat source parameter (~) is to decrease the primary velocity and temperature distribution which are shown in Fig. 4.1.27, Fig.4.1.29, Fig.4.1.56 (a) and Fig.4.1.58 (a) for both analytic and numerical solutions respectively. This is expected due to the fact that when heat is absorbed, the buoyancy force decreases the velocity and temperature distribution. These four figures are qualitatively identical but quantitatively different. But secondary velocity has reverse effects with increasing ~ which are shown in Fig.4.1.28 and Fig.4.1.57 (a) in case of analytic and numerical solutions. These two figures are qualitatively identical but quantitatively different. The shear stress in x -axis, decrease while shear stress in z -axis, Nusselt number increases with the increase of ~ which are shown Fig.4.1.56 (b) and Fig.4.1.57 (b), Fig.4.1.58 (b) for numerical solution.

From these figures it is observed that for the effect of corresponding parameter in case of analytic and numerical solutions the qualitative characters of the flows are identically same but quantitatively behavior are different.

Case I (Analytic solution)

Case II (Numerical solution)

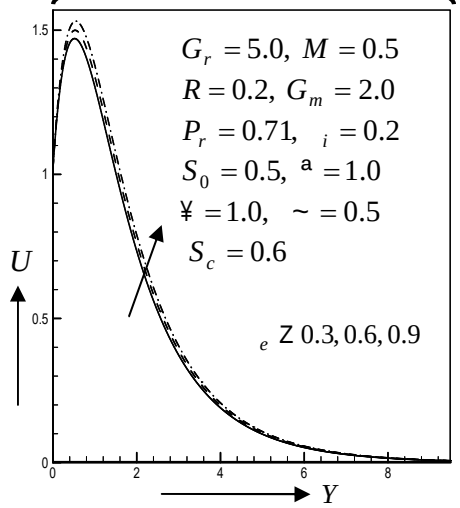

Fig.4.1.1 Primary velocity profile for different values of hall parameter $_e$

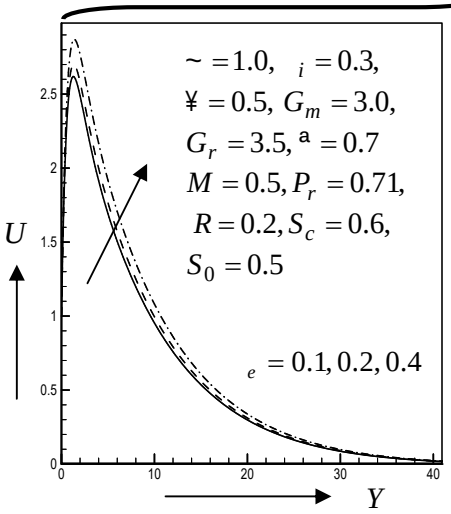

Fig. 4.1.30(a) Primary velocity profile for different values of Hall parameter $_e$

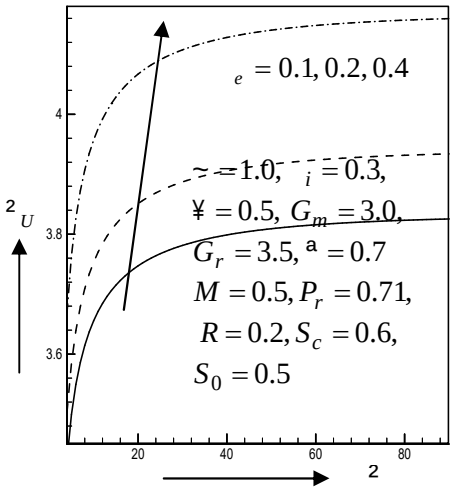

Fig. 4.1.30(b) Shear stress in x -axis for different values of Hall parameter $_e$

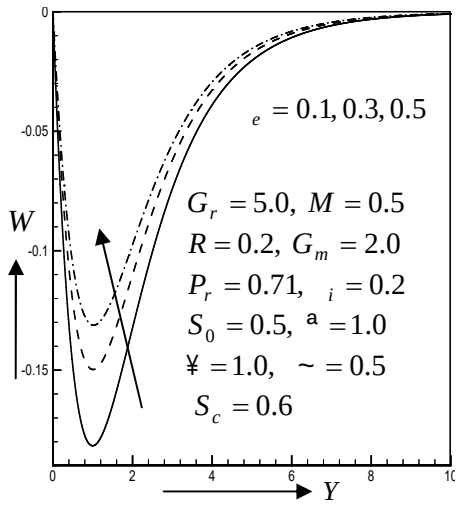

Fig.4.1.2 Secondary velocity profile for different values of Hall parameter $_e$

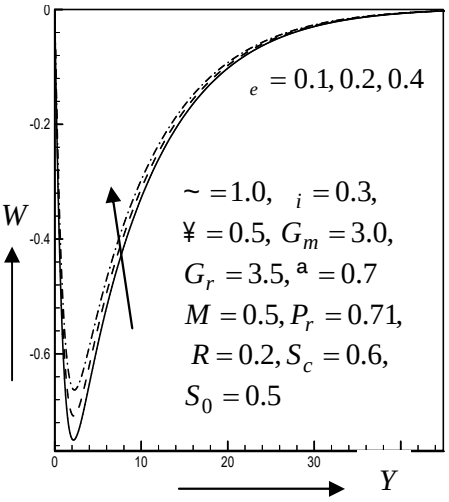

Fig. 4.1.31(a) Secondary velocity profile for different values of Hall parameter $_e$

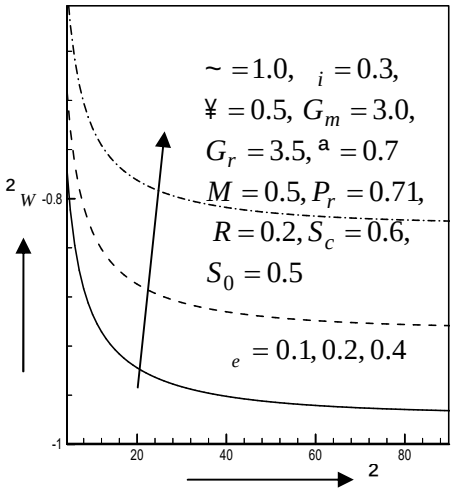

Fig. 4.1.31(b) Shear stress in z - axis for different values of Hall parameter $_e$

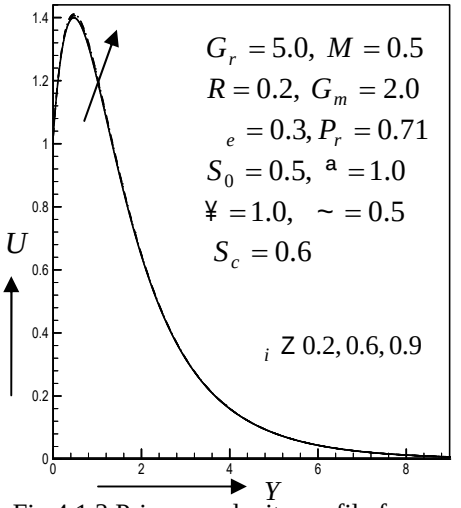

Fig.4.1.3 Primary velocity profile for different values of ion-slip parameter $_i$

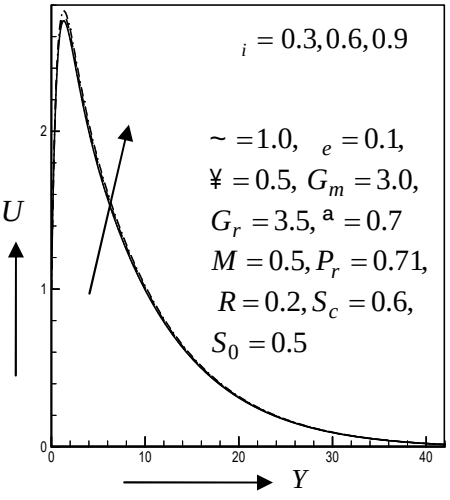

Fig. 4.1.32(a) Primary velocity profile for different values of ion-slip parameter $_i$

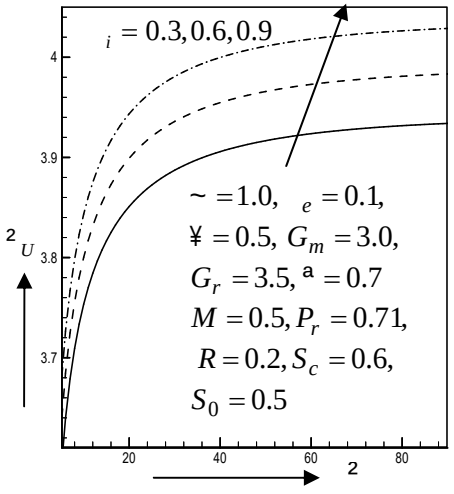

Fig. 4.1.32(b) Shear stress in x - axis for different values of ion-slip parameter $_i$

Case I (Analytic solution)

Case II (Numerical solution)

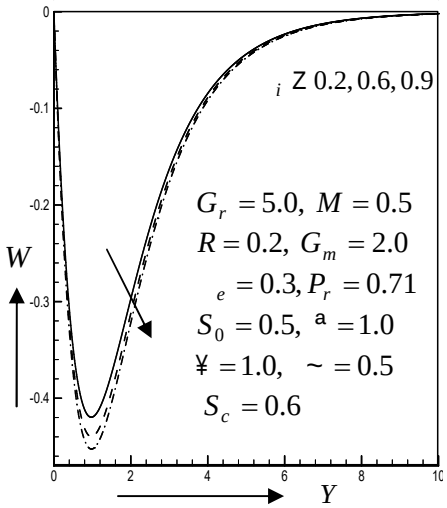

Fig.4.1.4 Secondary velocity profile for different values of ion- slip parameter $_i$

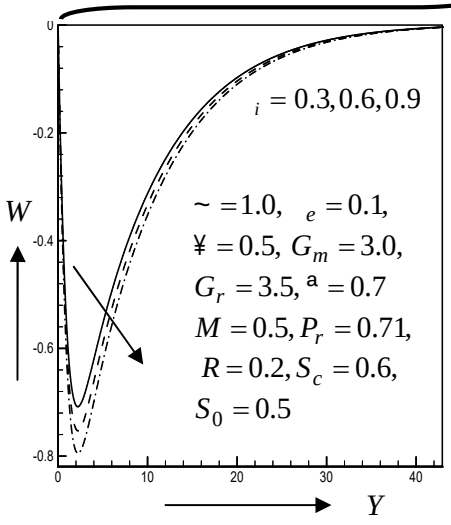

Fig.4.1.33(a) Secondary velocity profile for different values of ion-slip parameter $_i$

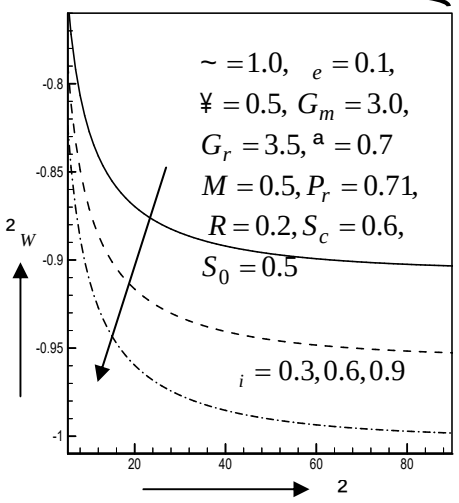

Fig.4.1.33(b) Shear stress in z - axis for different values of ion-slip parameter $_i$

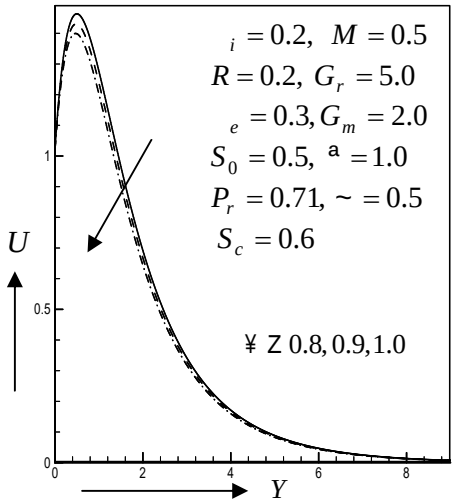

Fig.4.1.5 Primary velocity profile for different values of permeability parameter ¥

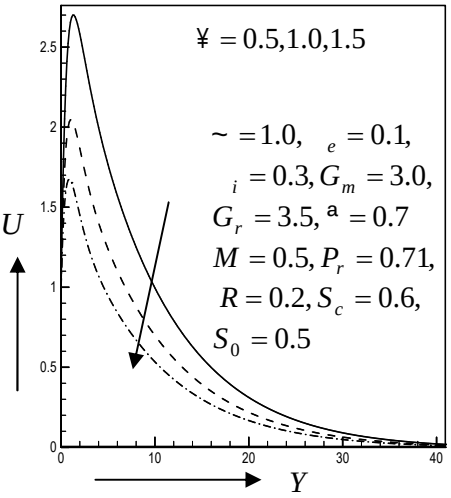

Fig. 4.1.34(a) Primary velocity profile for different values of permeability parameter ¥

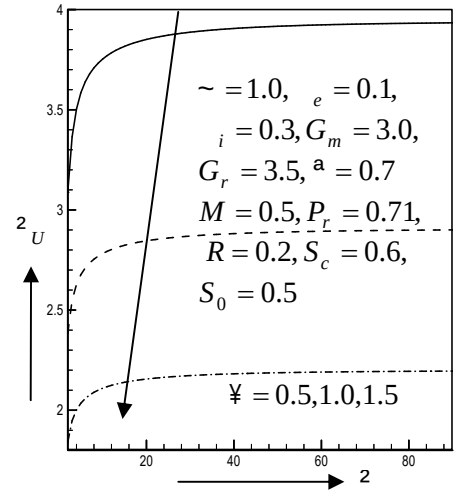

Fig.4.1.34(b) Shear stress in x - axis for different values of permeability parameter ¥

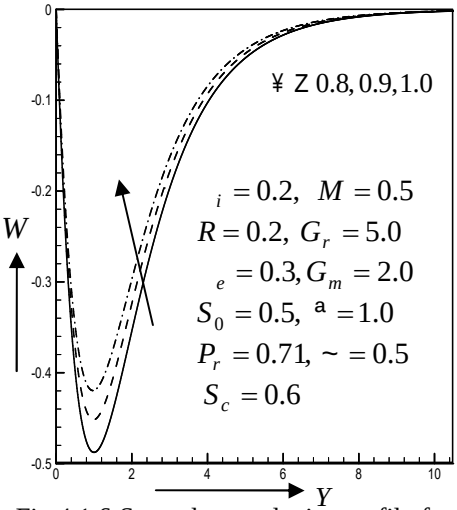

Fig.4.1.6 Secondary velocity profile for different values of permeability parameter ¥

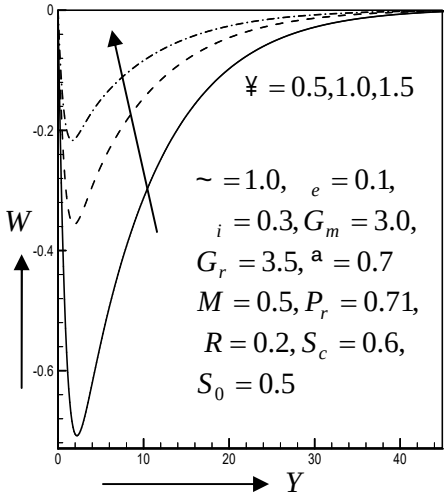

Fig.4.1.35(a) Secondary velocity profile for different values of permeability parameter ¥

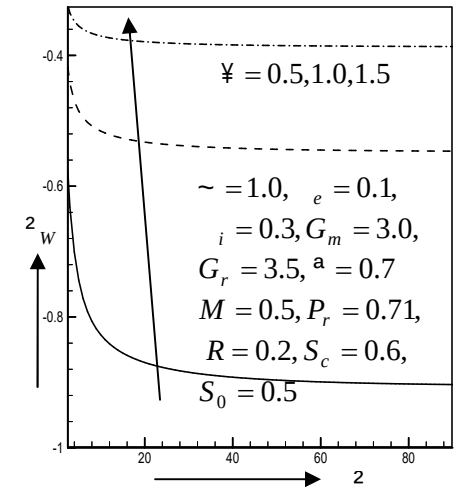

Fig. 4.1.35(b) Shear stress in z - axis for different values of permeability parameter ¥

Case I (Analytic solution)

Case II (Numerical solution)

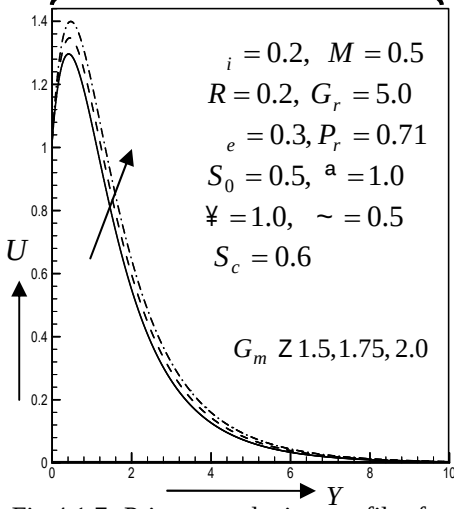

Fig.4.1.7 Primary velocity profile for different values of modified Grashof number G_m

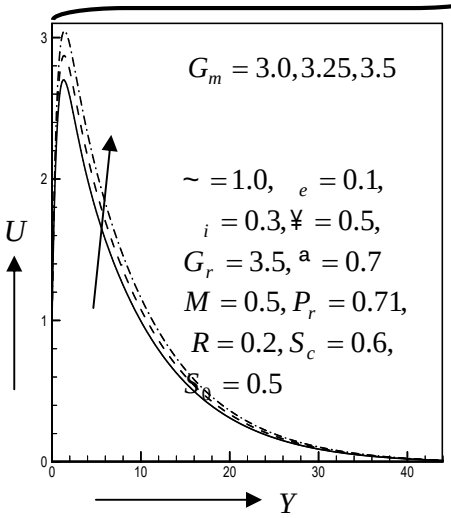

Fig. 4.1.36(a) Primary velocity profile for different values of modified Grashof number G_m

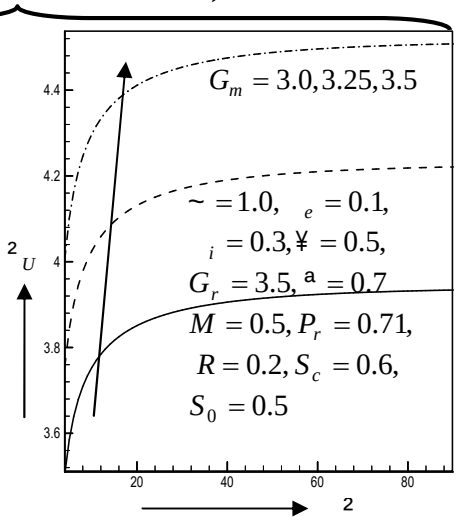

Fig.4.1.36(b) Shear stress in x - axis for different values of modified Grashof number G_m

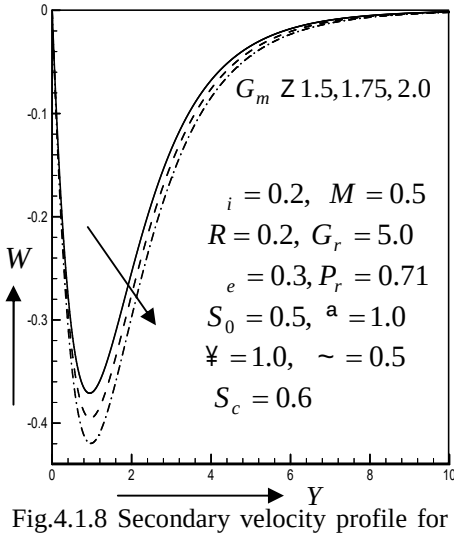

Fig.4.1.8 Secondary velocity profile for different values of modified Grashof number G_m

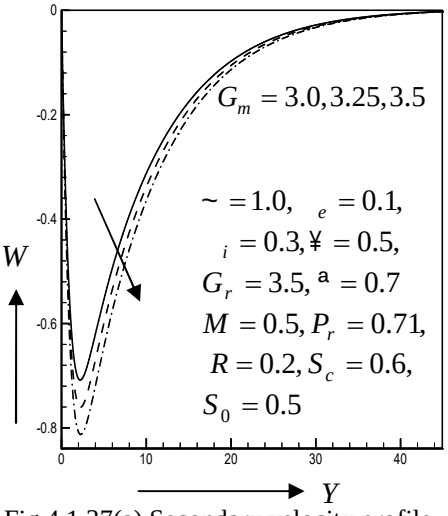

Fig.4.1.37(a) Secondary velocity profile for different values of modified Grashof number G_m

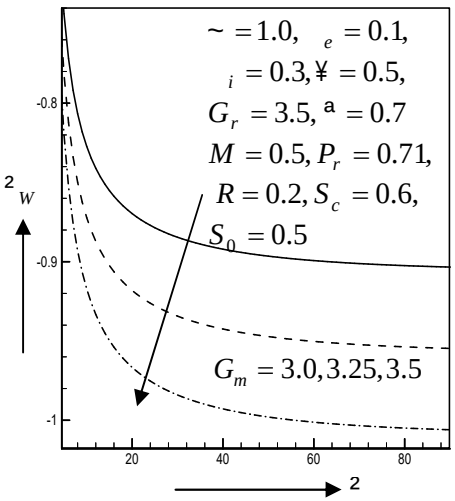

Fig. 4.1.37(b) Shear stress in z - axis for different values of modified Grashof number G_m

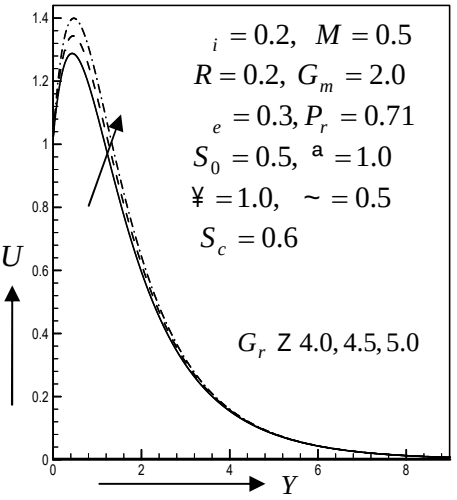

Fig.4.1.9 Primary velocity profile for different values of Grashof number G_r

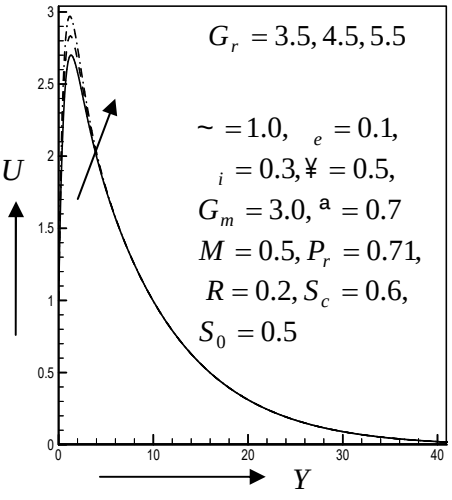

Fig. 4.1.38(a) Primary velocity profile for different values of Grashof number G_r

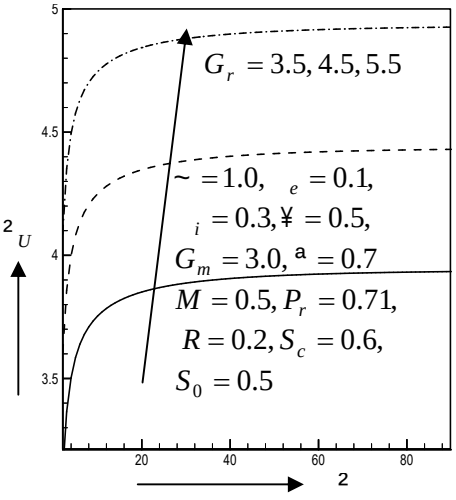

Fig.4.1.38(b) Shear stress in x - axis for different values of Grashof number G_r

Case I (Analytic solution)

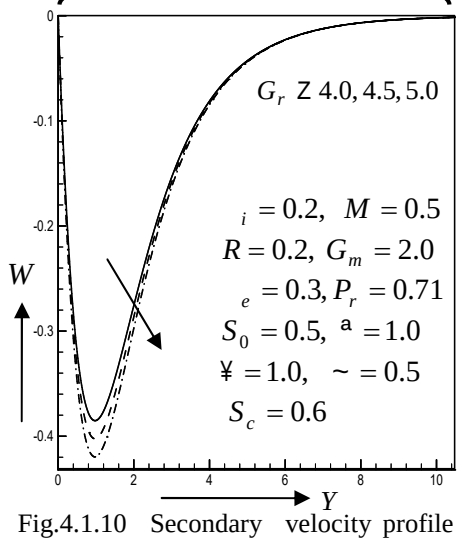

Fig.4.1.10 Secondary velocity profile for different values of Grashof number G_r

Case II (Numerical solution)

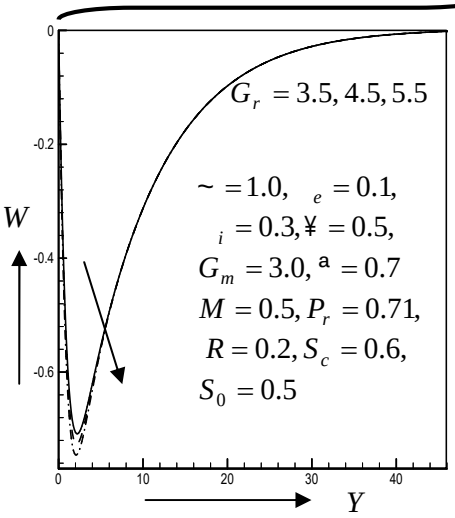

Fig.4.1.39(a) Secondary velocity profile for different values of Grashof number G_r

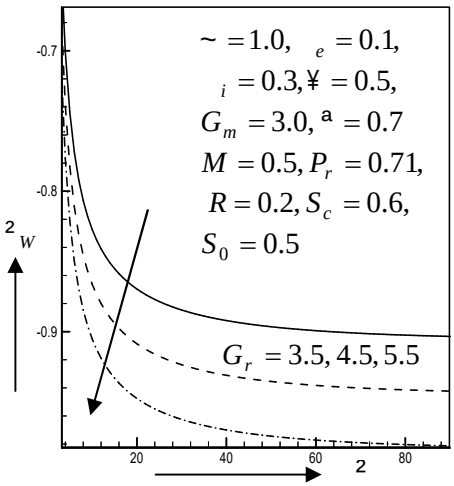

Fig4.1.39(b) Shear stress in z - axis for different values of Grashof number G_r

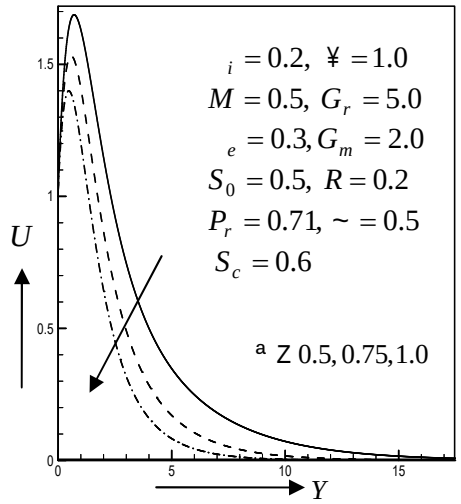

Fig.4.1.11 Primary velocity profile for different values suction parameter ^{a}

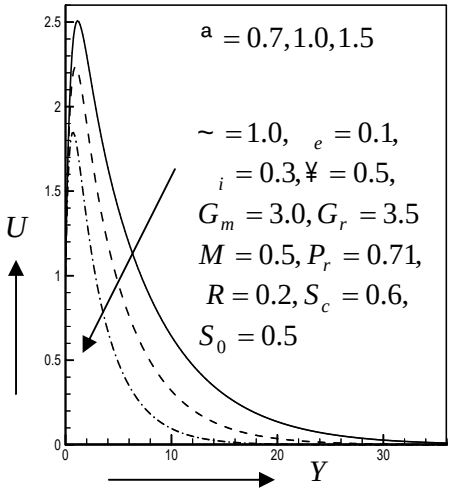

Fig. 4.1.40(a) Primary velocity profile for different values of suction parameter ^{a}

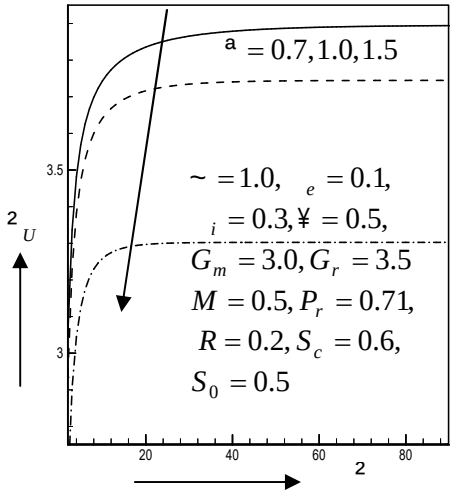

Fig 4.1.40(b) Shear stress in x - axis for different values of suction parameter ^{a}

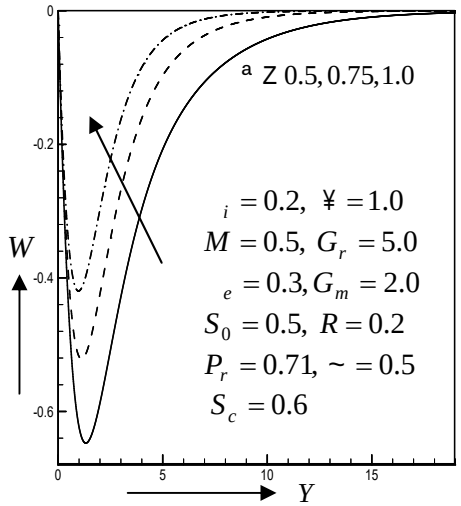

Fig.4.1.12 Secondary velocity profile for different values suction parameter ^{a}

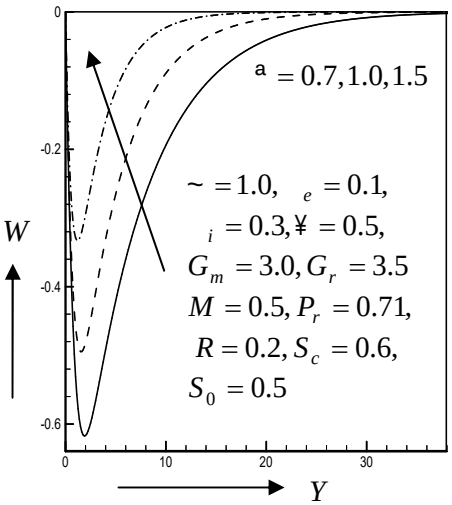

Fig.4.1.41(a) Secondary velocity profile for different values of suction parameter ^{a}

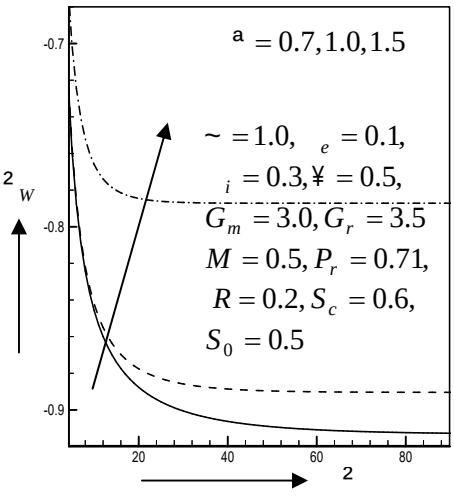

Fig 4.1.41(b) Shear stress in z - axis for different values of suction parameter ^{a}

Case I (Analytic solution)

Case II (Numerical solution)

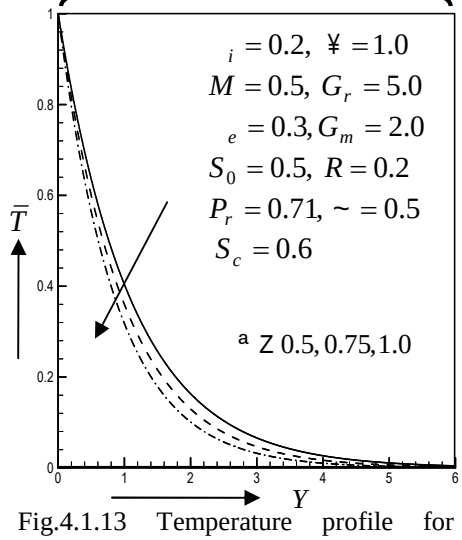

Fig.4.1.13 Temperature profile for different values suction parameter a

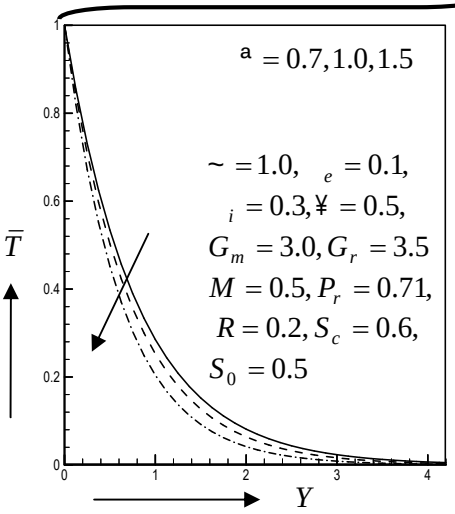

Fig. 4.1.42(a) Temperature profile for different values of suction parameter a

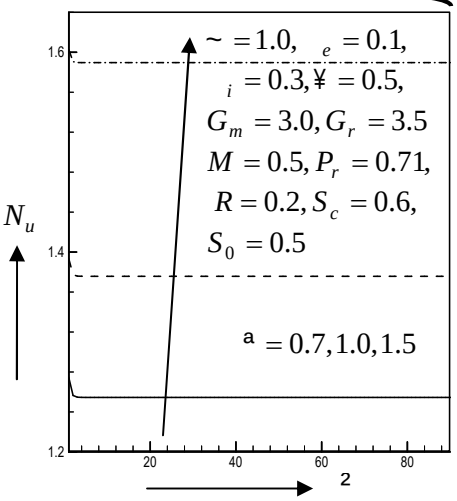

Fig 4.1.42(b) Nusselt number for different values of suction parameter a

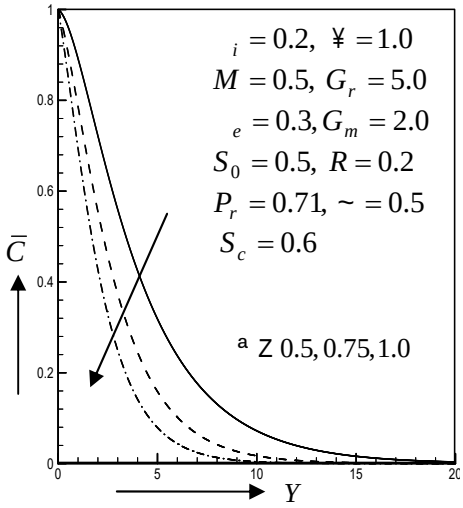

Fig.4.1.14 Concentration profile for different values suction parameter a

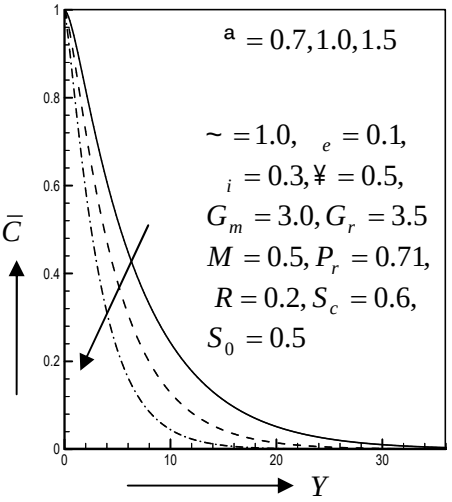

Fig. 4.1.43(a) Concentration profile for different values of suction parameter a

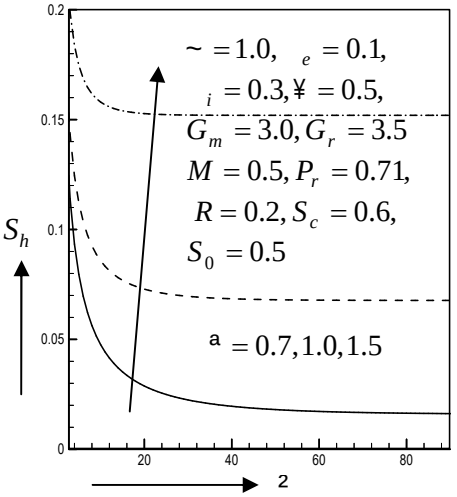

Fig 4.1.43(b) Sherwood number for different values of suction parameter a

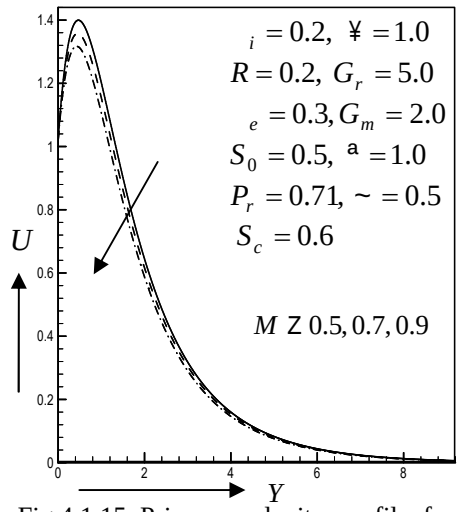

Fig.4.1.15 Primary velocity profile for different values of magnetic parameter M

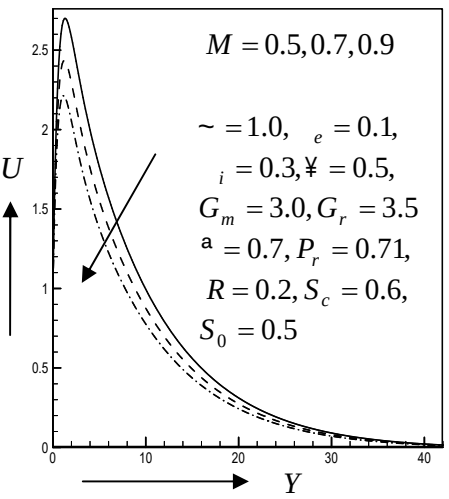

Fig4.1.44(a) Primary velocity profile for different values of magnetic parameter M

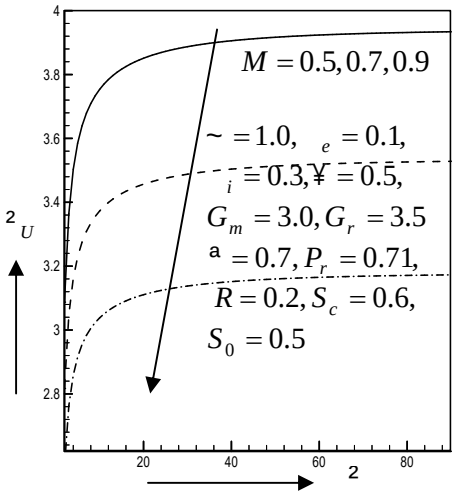

Fig. 4.1.44(b) Shear stress in x - axis for different values of magnetic parameter M

Case I (Analytic solution)

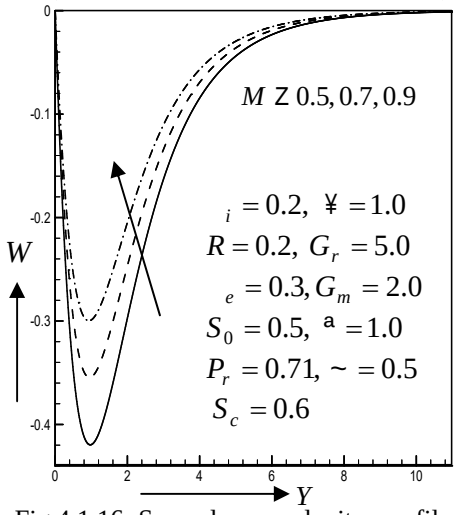

Fig.4.1.16 Secondary velocity profile for different values of magnetic parameter M

Case II (Numerical solution)

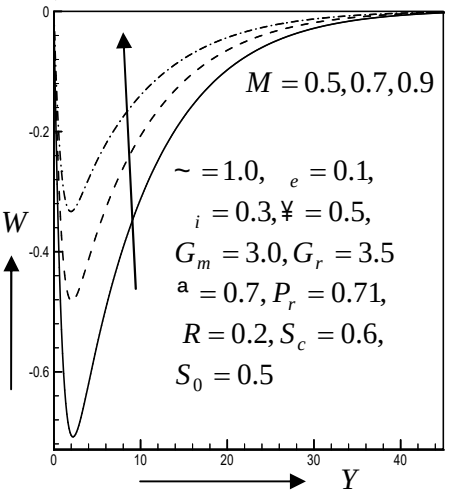

Fig.4.1.45(a) Secondary velocity profile for different values of magnetic parameter M

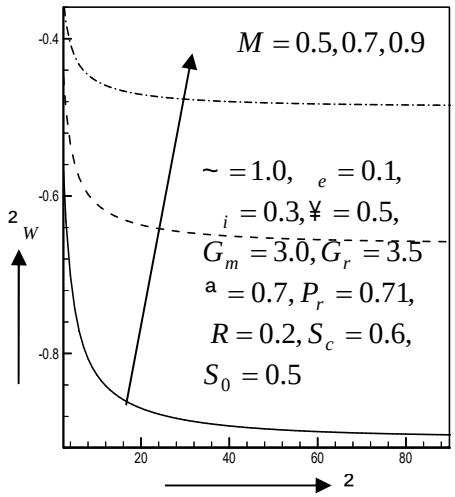

Fig. 4.1.45(b) Shear stress in z - axis for different values of magnetic parameter M

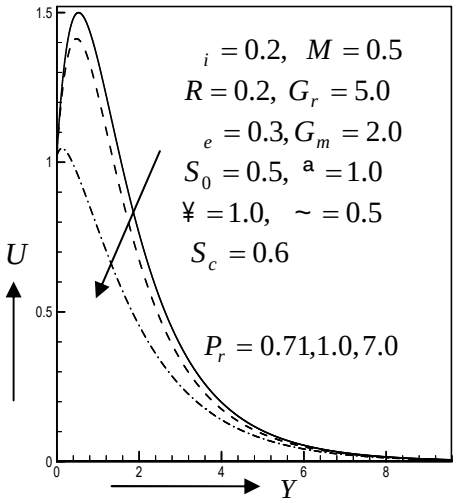

Fig.4.1.17 Primary velocity profile for different values of Prandtl number P_r

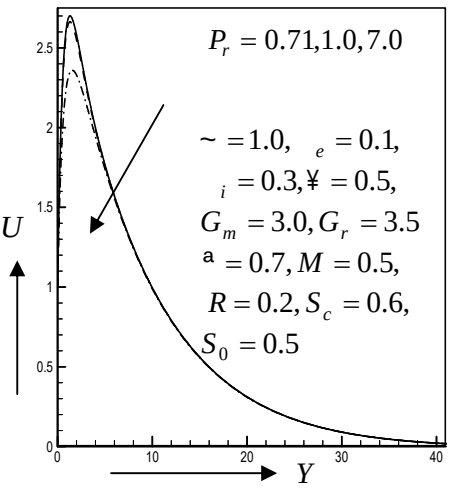

Fig. 4.1.46 (a) Primary velocity profile for different values of Prandtl number P_r

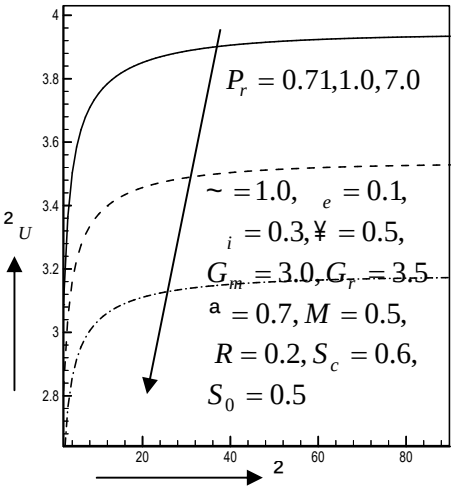

Fig. 4.1.46(b) Shear stress in x - axis for different values of Prandtl number P_r

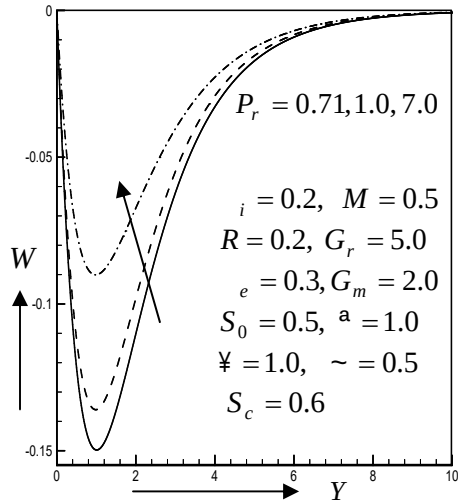

Fig.4.1.18 Secondary velocity profile for different values of P_r

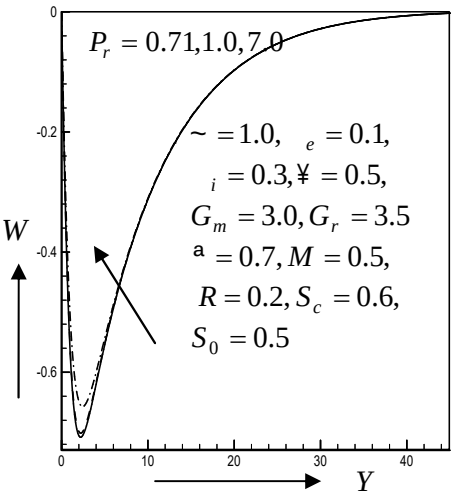

Fig.4.1.47(a) Secondary velocity profile for different values of Prandtl number P_r

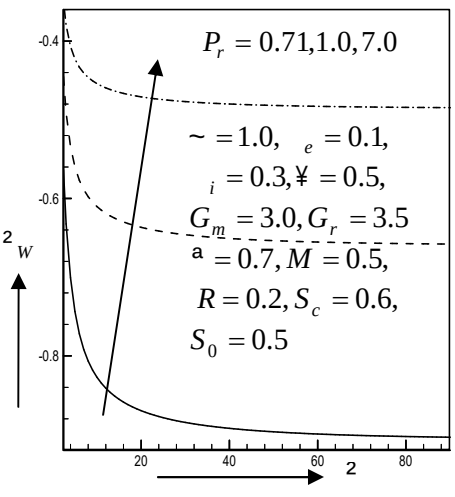

Fig. 4.1.47(b) Shear stress in z - axis for different values of P_r

Case I (Analytic solution)

Case II (Numerical solution)

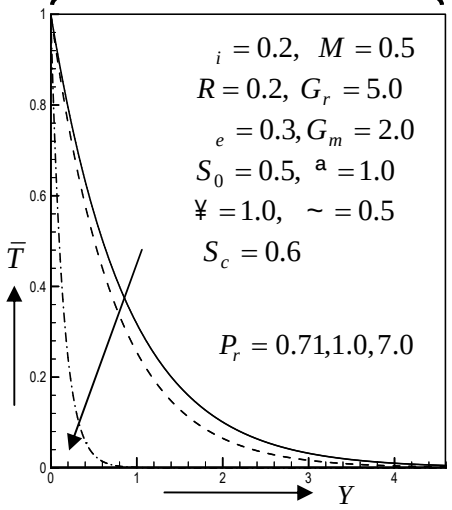

Fig.4.1.19 Temperature profile for different values of Prandtl number P_r

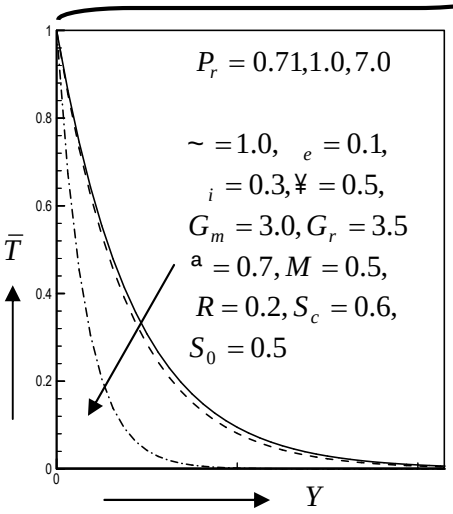

Fig. 4.1.48(a) Temperature profile for different values of Prandtl number P_r

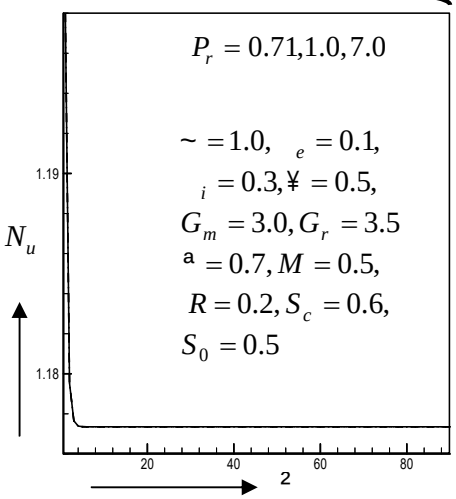

Fig. 4.1.48(b) Nusselt number for different values of Prandtl number P_r

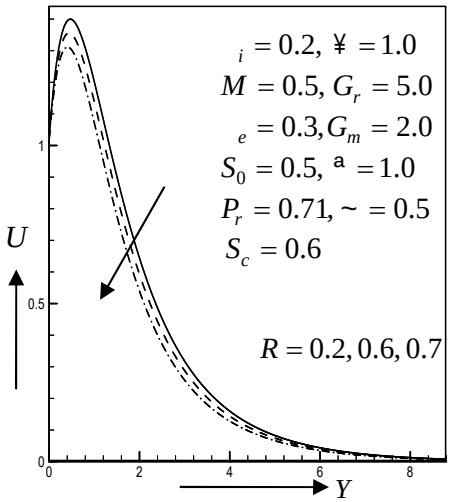

Fig.4.1.20 Primary velocity profile for different values of rotation parameter R

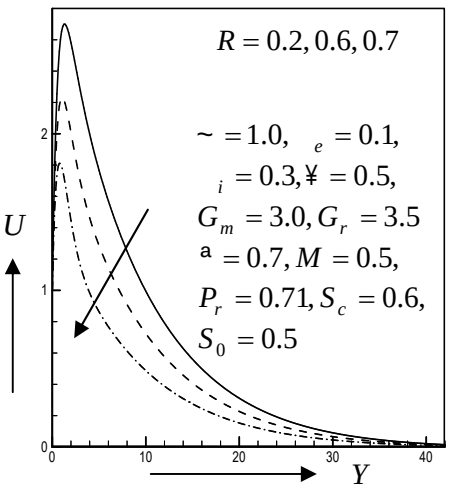

Fig. 4.1.49(a) Primary velocity profile for different values of rotation parameter R

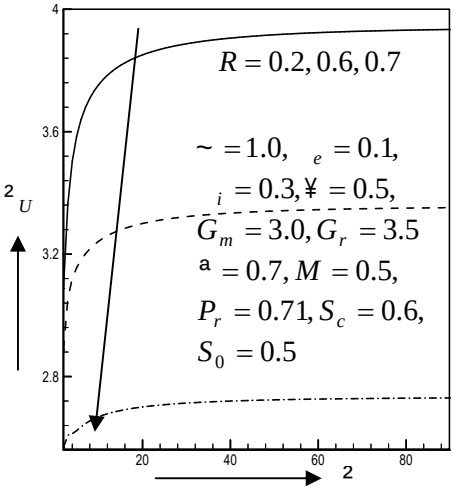

Fig. 4.1.49(b) Shear stress in *x*- axis for different values of rotation parameter R

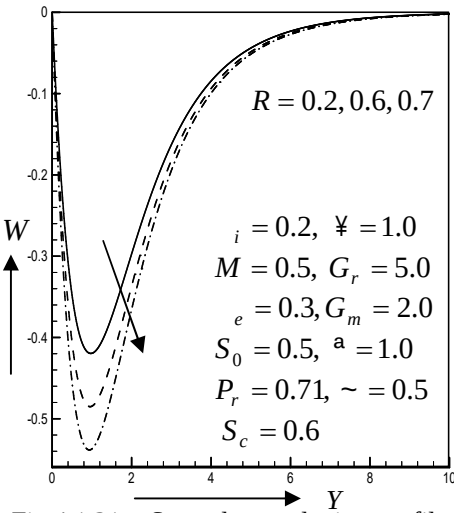

Fig.4.1.21 Secondary velocity profile for different values of rotation parameter R

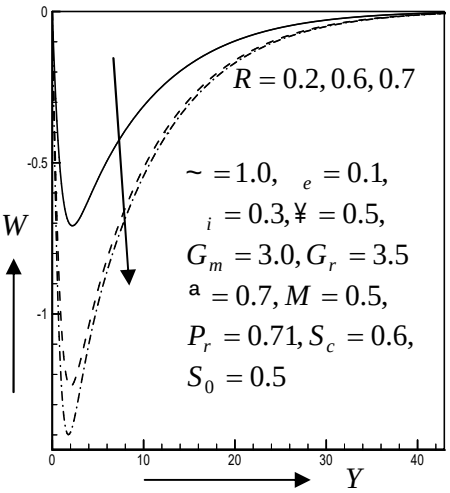

Fig.4.1.50(a) Secondary velocity profile for different values of rotation parameter R

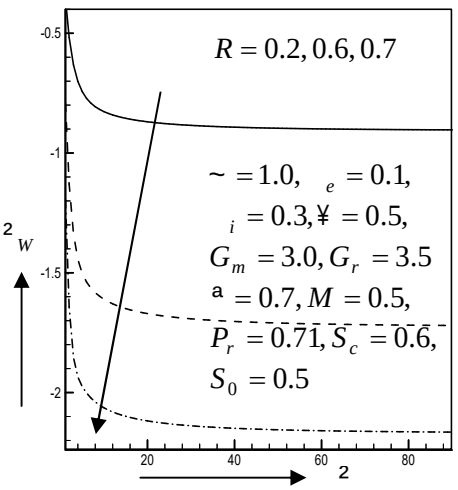

Fig. 4.1.50(b) Shear stress in *z* - axis for different values of rotation parameter R

Case I (Analytic solution)

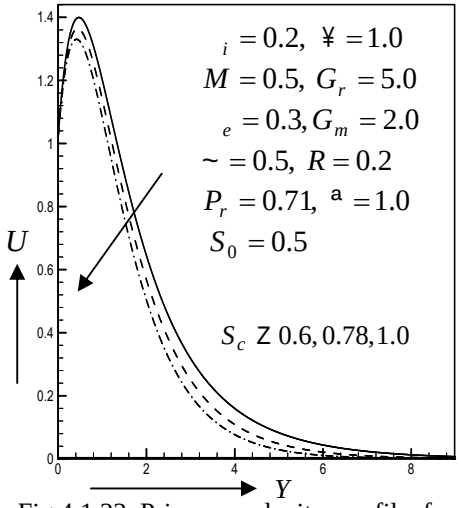

Fig.4.1.22 Primary velocity profile for different values of Schmidt parameter S_c

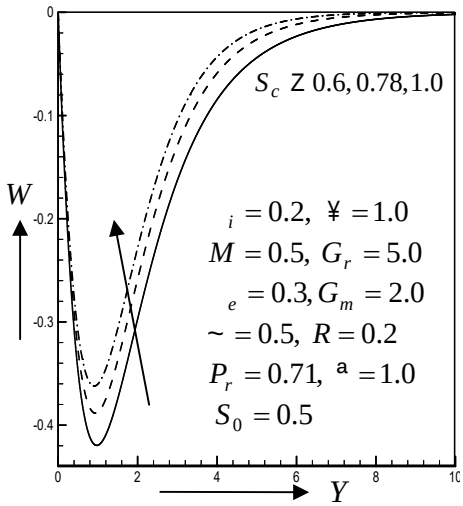

Fig.4.1.23 secondary velocity profile for different values of Schmidt parameter S_c

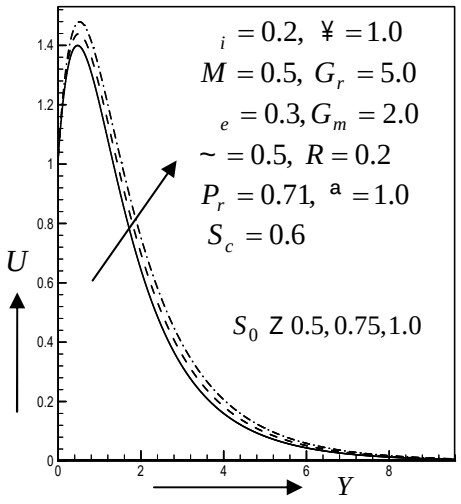

Fig.4.1.24 Primary velocity profile for different values of Soret parameter S_0

Case II (Numerical solution)

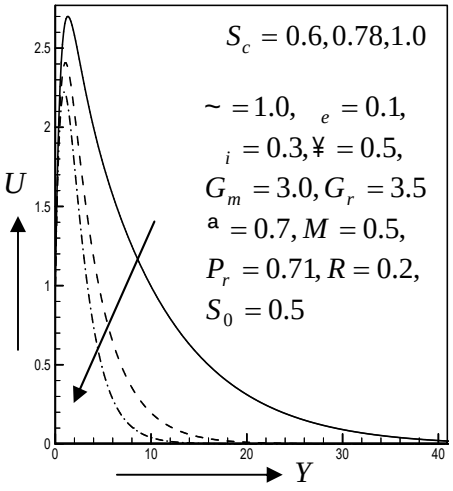

Fig. 4.1.51(a) Primary velocity profile for different values of Schmidt number S_c

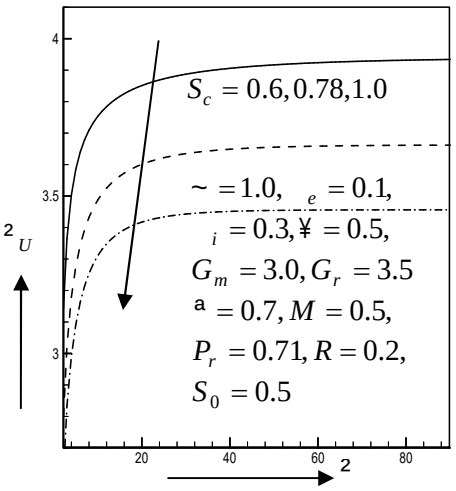

Fig. 4.1.51(b) Shear stress in x - axis for different values of Schmidt number S_c

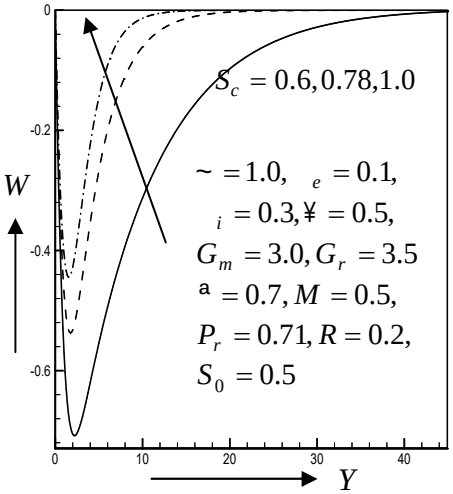

Fig. 4.1.52(a) Secondary velocity profile for different values of Schmidt number S_c

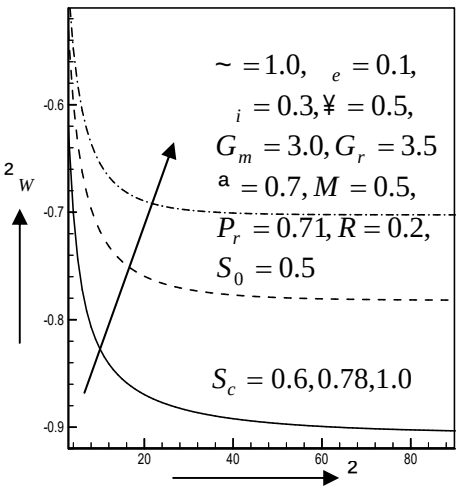

Fig. 4.1.52(b) Shear stress in z - axis for different values of Schmidt number S_c

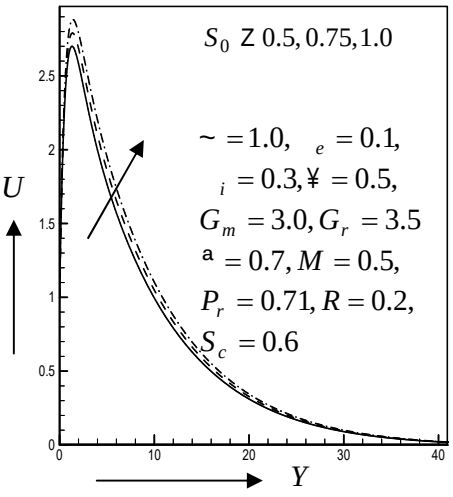

Fig. 4.1.53(a) Primary velocity profile for different values of Soret number S_0

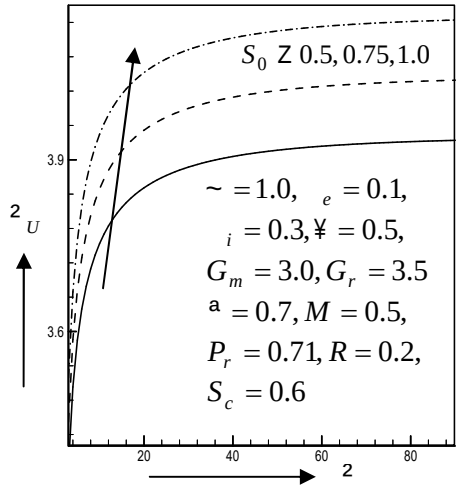

Fig. 4.1.53(b) Shear stress in x - axis for different values of Soret number S_0

Case I (Analytic solution)

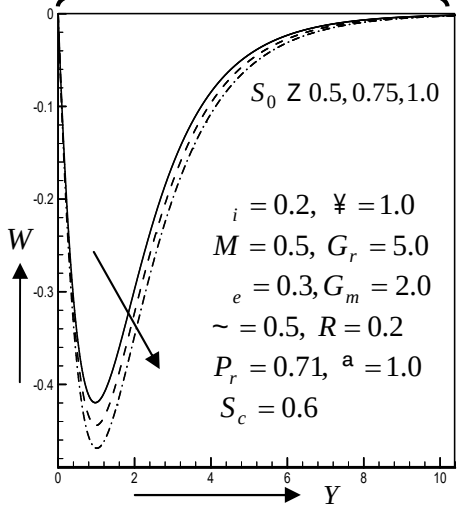

Fig.4.1.25 Secondary velocity profile for different values Soret number S_0

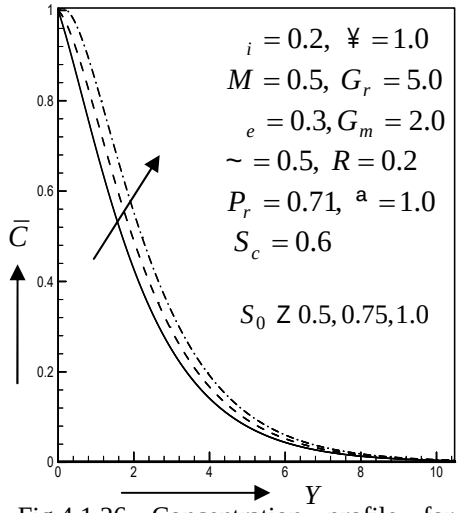

Fig.4.1.26 Concentration profile for different values of Soret parameter S_0

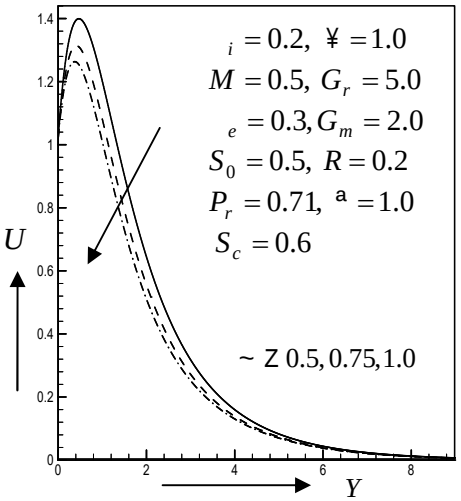

Fig.4.1.27 Primary velocity profile for different values heat source parameter $\sim$

Case II (Numerical solution)

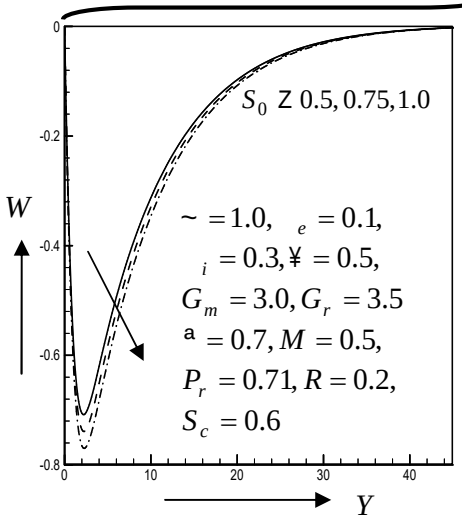

Fig.4.1.54(a) Secondary velocity profile for different values of Soret number S_0

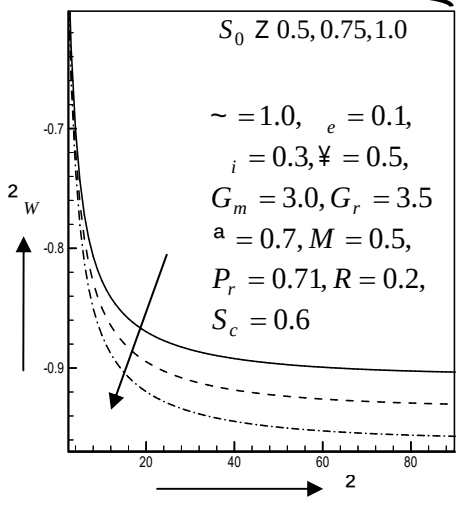

Fig. 4..54(b) Shear stress in z - axis for different values of Soret number S_0

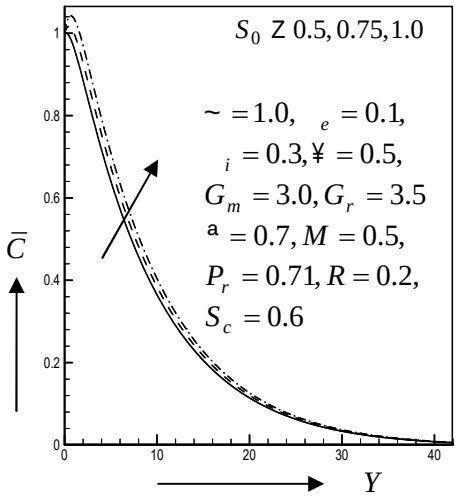

Fig. 4.1.55(a) Concentration profile for different values of Soret number S_0

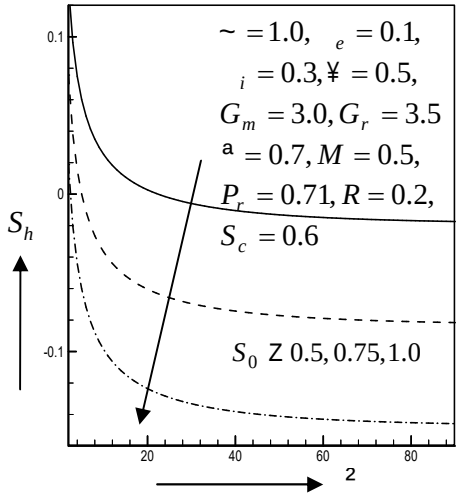

Fig. 4.1.55(b) Sherwood number for different values of Soret number S_0

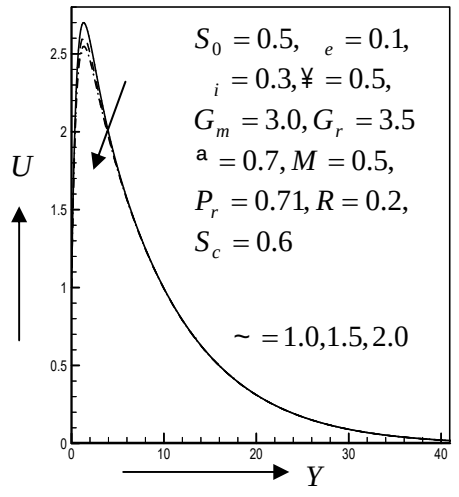

Fig. 4.1.56(a) Primary velocity profile for different values of heat source parameter $\sim$

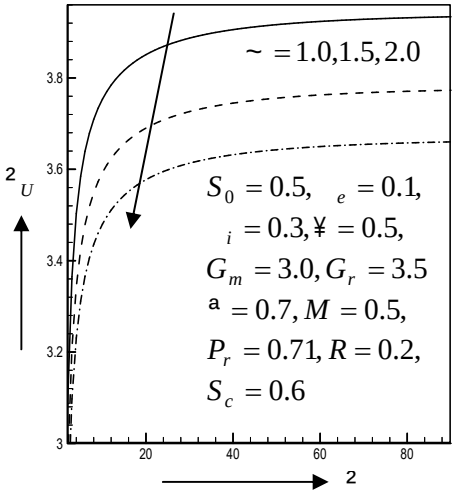

Fig. 4.1.56(b) Shear stress in x - axis for different values of heat source parameter $\sim$

Case I (Analytic solution)

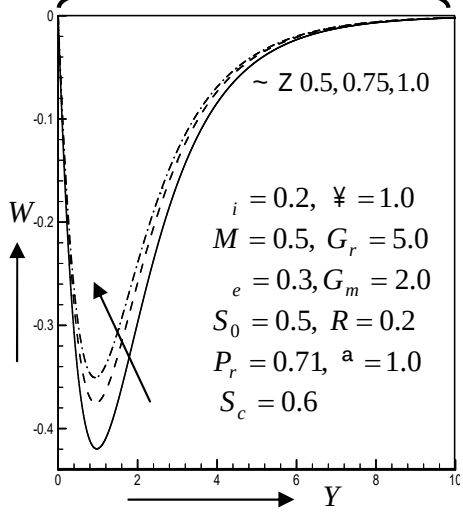

Fig.4.1.28 Secondary velocity profile for different values heat source parameter ~

Case II (Numerical solution)

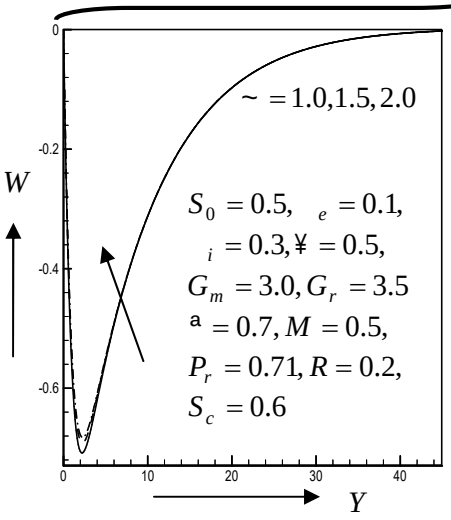

Fig. 4.1.57(a) Secondary velocity profile for different values of heat source parameter ~

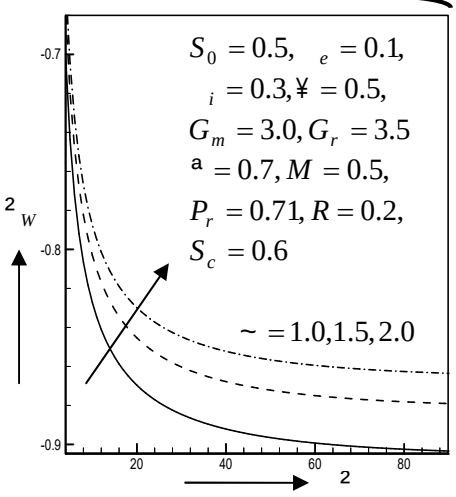

Fig. 4.1.57(b) Shear stress in z - axis for different values of heat source parameter ~

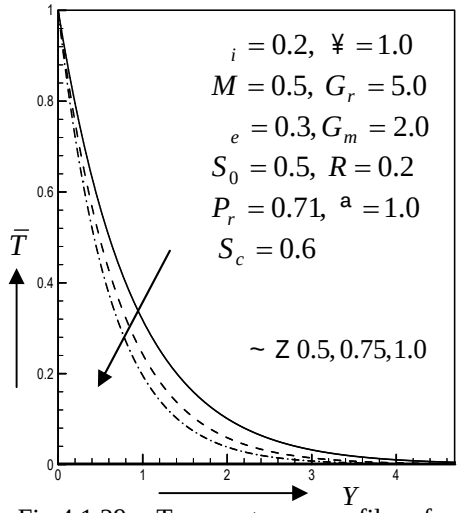

Fig.4.1.29 Temperature profile for different values heat source parameter ~

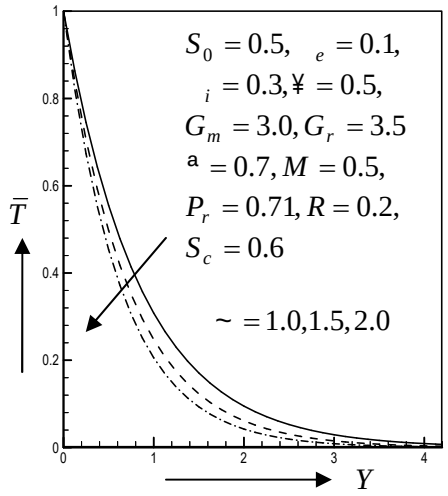

Fig. 4.1.58(a) Temperature profile for different values of heat source parameter ~

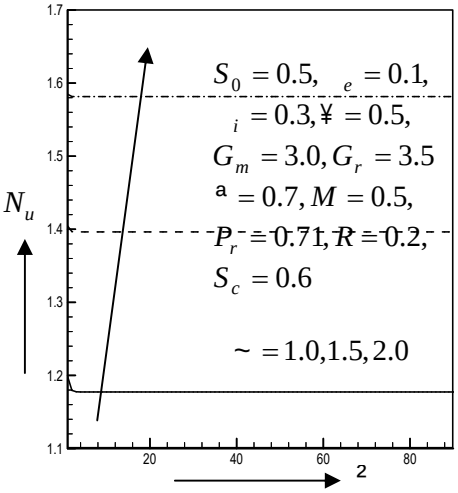

Fig. 4.1.58(b) Nusselt number for different values of heat source parameter ~

4.1.7 Appendix

$$A_2 = \frac{\mathrm{a}P_r + \sqrt{(\mathrm{a}P_r)^2 + 4P_r\sim}}{2},\ A_3 = \mathrm{a}S_c,\ A_4 = \frac{S_0 S_c A_2}{\mathrm{a}S_c - A_2},\ A_5 = (1 - A_4),\quad A_7 = \frac{\mathrm{a} + \sqrt{\mathrm{a}^2 + 4\P}}{2},$$

$$\P = ¥ + 2iR + \frac{M(\sim_e - \ _e)}{\sim_e^2 + \ _e^2},\ A_{13} = \frac{\mathrm{a} + \sqrt{\mathrm{a}^2 + 4B_8}}{2},\ A_{19} = \frac{\mathrm{a} + \sqrt{\mathrm{a}^2 + 4B_{10}}}{2},\ B_1 = G_r + A_4 G_m,$$

$$B_2 = A_5 G_m,\ B_3 = \frac{B_1}{A_2^2 - \mathrm{a}A_2 - \P},\ B_4 = \frac{B_2}{A_3^2 - \mathrm{a}A_3 - \P},\ B_5 = 1 + B_3 + B_4,$$

$$B_8 = \P + i\mu,\ B_{10} = \P - i\mu$$

References

Abo-Eldahab, E.M. and Aziz, M. A. (2000), Hall and ion-slip effects on MHD free convective heat generating flow past a semi-infinite vertical plate flat plate, 'Physica Scripta', vol.**61**, p344-348.

Ahmed, N., Kalita, H. and Barua, D. P. (2010), Unsteady MHD free convective flow past a vertical porous plate immersed in a porous medium with Hall current, thermal diffusion and heat source, 'International Journal of Engineering, Science and Technology', vol.**2**, No. 6, p59-74.

Callahan, G. D. and Marner, W. J. (1976), Transient free convection flow with mass transfer on an isothermal vertical flat plate, 'International Journal of Heat and Mass Transfer', vol.**19**(2), p165-174.

Chaudhary, R. C and Arpita Jain (2007), Combined heat and mass transfer, effects, on MHD free convection flow past an oscillating plate embedded in porous medium, 'Romanian Journal of Physics', vol.**52**, Nos. 5-7, p505-524.

Das, S., Jana, M., Guria, M. and Jana, R. N. (2008), Unsteady viscous incompressible flow due to an oscillating plate in a rotating fluid, 'Journal of Physical Sciences', vol.**12**, p51-64.

Das, S. S., Mishra, L. K. and Mishra, P. K. (2011), Effect of heat source on MHD free convection flow past an oscillating porous plate in the slip regime, 'International Journal of Energy and environment', vol.**2**(5), p945-951.

Ganapathy, R. (1994), A note on oscillatory couette flow in a rotating system, 'ASME Journal of Applied Mechanics', vol.**61**, p208-209.

Jha, B. K. and Apere, C. A. (2012), Time-dependent MHD couette flow of rotating fluid with Hall and ion-slip currents, 'Applied Mathematics and Mechanics'. -Engl. Ed., vol.**33**(4), p399–410.

Joaquin Zueco, Luis Ma Lopez-Ochoa, Pablo Eguia and Joaquin Collazo (2011), Combined

heat and mass transfer by natural convection from a semi-infinite plate submitted to a magnetic field with hall currents, 'Engineering Applications of Computational Fluid Mechanics', vol.**5**, No. 2, p188-200.

Maji, S.L., Kanch, A.K., Guria, M., Jana, R.N. (2009), Hall effects on hydromagnetic flow on an oscillating porous plate, 'Applied Mathematics and Mechanics', –Engl. Ed. **30**(4), p503-512.

Muthucumaraswamy, R. and Vijayalakshmi, A. (2008), Effects of heat and mass transfer on flow past an oscillating vertical plate with variable temperature, 'International Journal of Applied Mathematics and Mechanics', vol.**4**(1), p59-65.

Okedoye, A. M. (2013), Heat and Hall effect of an oscillating plate in a porous medium, 'Advances in Agriculture, Sciences and Engineering Research', vol.**3**(7), p972-983.

Ramana Reddy, G. V., Ramana Murthy, Ch. V. and Bhaskar Reddy, N. (2011), Unsteady MHD free convective mass transfer flow past an infinite vertical porous plate with variable suction and Soret effect, 'International Journal of Applied Mathematics and Mechanics', vol.**7**(21), p70-84.

Rajput, U. S. and Gaurav Kumar (2016), Soret effect on unsteady MHD flow through porous medium past an oscillating inclined plate with variable wall temperature and mass diffusion, 'International Research Journal of Engineering and Technology', vol.**3**(5), p2353-2358.

Revankar, S. T. (2000), Free convection effect on flow past an impulsively started or oscillating infinite vertical plate, 'Mechanics Research Communications', vol.**27**, p241–246.

Sondalgekar, V. M. and Ganesan, P. (1980), Transient free convection flow past a semi-infinite vertical plate with mass transfer, 'Regional Journal of Energy, Heat and Mass Transfer', vol.**2**, p83-91.

Stokes, G. (1851), On the effect of the internal friction of fluid on the motion of pendulum, 'Transactions Cambridge Philosophical Society', vol.**9**, p8.

Turbatu, S., Bühler K. and Zierep, J. (1998), New solutions of the II Stokes problem for an oscillating flat plate, ' Acta Mechanica', vol.**129**, p25-30.

4.2 MHD free convection and mass transfer flow through a vertical oscillatory porous plate with Hall, ion-slip currents and heat source in a rotating system

The study of a magnetohydrodynamics (MHD) free convection flow, with Hall and ion-slip currents, has important engineering applications in power generators, MHD accelerators, refrigeration coils, transmission lines, electric transformers and heating elements. The phenomenon of rotation is always encountered and is very often observed in cosmic and geophysical sciences. In present years, a considerable attention has been given to the study of hydrodynamic and hydromagnetic boundary layer flows in a viscous incompressible fluid in a rotating system. There are several engineering situations where in combined heat and mass transfer arise, such as dehumidifiers, humidifiers, desert coolers, chemical reactors; the interest in the new problems generates from their importance in liquid metals, electrolytes and ionized gases. On account of their varied importance, the flows have been studied by several authors are *Seth et al.* (2011), they investigated the effect of rotation on unsteady hydromagnetic natural convection flow past an impulsively moving vertical plate with ramped temperature in a porous medium with thermal diffusion and heat absorption. *Murali* (2015) investigated unsteady MHD free convection viscous dissipative flow past an infinite vertical plate with constant suction and heat source/sink. Effect of viscous dissipation on flow over a stretching porous sheet subjected to power law heat flux in presence of heat source was investigated by *Khaled* (2016). *Alam et al* (2014). Unsteady MHD free convective heat transfer flow along a vertical porous flat plate with internal heat generation. Effects of Hall current and heat transfer on the flow in a porous medium with slip condition have been described by *Hayat and Abbas* (2007). *Ghara et al.* (2012) have discussed Hall effects on oscillating flow due to electrically rotating porous disk and a fluid at infinity. *Smita et al.* (2015) investigated the effects of Hall current on transient convective MHD flow through porous medium past an infinite vertical oscillating plate with temperature gradient dependent heat source. The numerical solutions of heat and mass transfer effects of an unsteady MHD free convective flow past an infinite vertical plate with constant suction and heat source or sink were studied by *Ambethkar* (2009). *Nazibuddin and Sujit* (2012) studied MHD couette flow with heat transfer in presence of constant heat source. *Bhavana et al.* (2013) investigated the Soret effect on free convective unsteady MHD flow over a vertical plate with heat source. *Anjali and Wilfred* (2011) studied thermo diffusion effects on unsteady hydromagnetic free convection flow with heat and mass transfer past a moving vertical plate with time dependent suction and heat source in a slip flow regime. *Seth et al.* (2012) investigated the effects of Hall current and rotation on unsteady MHD couette flow in the presence of an inclined magnetic field. Hall current effect on magnetohydrodynamic free convection flow past a semi infinite vertical plate with mass transfer was studied by *Emad and Elsayed* (2001). *Ram*(1991) studied MHD convective flow in a rotating fluid with Hall and ion-slip currents. Hall and ion-slip effects on MHD free convective heat generating flow past a semi-infinite vertical flat plate were studied by *Emad and Mohaned*

(2000).

In this study the MHD free convection and mass transfer flow through a vertical oscillatory porous plate with hall, ion-slip currents and heat source in a rotating system have been considered. The problem is governed by system of coupled nonlinear partial differential equations whose exact solutions are difficult to obtain. The problem is solved by finite difference method. The effects of the various parameters entering into the problem are discussed and are illustrated graphically. The numerical values of local and average shear stress, local and average Nusselt number, local and average Sherwood number at the plate are discussed for various values of physical parameters and presented graphically.

4.2.1 Governing Equations

Consider a unsteady, laminar, incompressible, free convection boundary layer flow of an electrically conducting fluid along a semi-infinite vertical porous plate with the origin at the leading age. When the plate velocity $U(t)$ oscillates in time t with a frequency $\bar{n}$ and is given as $U(t) = U_0(1+\cos \bar{n} t)$. In this problem the temperature and concentration of the fluid at initially T_∞, C_∞ everywhere and the temperature and concentration at the plate T_w, C_w in the presence of a strong magnetic field normal to the plate. A rectangular Cartesian coordinates (x, y, z) taking x and y as the coordinates parallel and normal to the plate. Let the z-axis be coincident with the leading age of the plate. An external strong magnetic field **B** is applied in the y-direction. The induced magnetic field is neglected, since the magnetic Reynolds number is assumed to be very small. Due to Hall current, there is a force in *z*-direction which induces a cross flow in that direction and hence flow becomes three dimensional. The physical configuration and coordinate system is shown in Fig.4.2A. The governing equations within the boundary layer and Boussnesq's approximations may be written as follows;

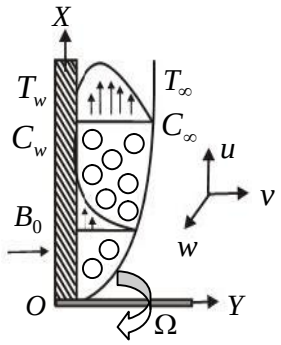

Fig.4.2A Physical configuration and coordinate system

Continuity equation; $\frac{\partial u}{\partial x} + \frac{\partial v}{\partial y} = 0$ (4.2.1)

Momentum equation;

$$\frac{\partial u}{\partial t} + u\frac{\partial u}{\partial x} + v\frac{\partial u}{\partial y} = \nu \frac{\partial^2 u}{\partial y^2} + g_0 \beta (T - T_\infty) + g_0 \beta^* (C - C_\infty) + 2\Omega w - \frac{\nu}{k} u - \frac{\sigma_e B_0^2}{\rho(\omega_e^2 + \tau_e^2)}(\omega_e u + \tau_e w) \quad (4.2.2)$$

$$\frac{\partial w}{\partial t} + u\frac{\partial w}{\partial x} + v\frac{\partial w}{\partial y} = \nu \frac{\partial^2 w}{\partial y^2} - 2\Omega u - \frac{\nu}{k} w + \frac{\sigma_e B_0^2}{\rho(\omega_e^2 + \tau_e^2)}(\tau_e u - \omega_e w) \quad (4.2.3)$$

Energy equation;

$$\frac{\partial T}{\partial t}+u\frac{\partial T}{\partial x}+v\frac{\partial T}{\partial y}=\frac{\text{©}}{\text{°}c_p}\frac{\partial^2 T}{\partial y^2}+\frac{\overline{Q}\left(T_\infty-T\right)}{\text{°}c_p} \tag{4.2.4}$$

Concentration equation;

$$\frac{\partial C}{\partial t}+u\frac{\partial C}{\partial x}+v\frac{\partial C}{\partial y}=D_m\frac{\partial^2 C}{\partial y^2}+\frac{D_m k_T}{T_m}\frac{\partial^2 T}{\partial y^2} \tag{4.2.5}$$

where all physical quantities are defined in the Nomenclature.

The initial and boundary conditions are as follows;

$$t\le 0,\quad u=0,v=0,w=0,T=T_\infty,C=C_\infty \quad \text{everywhere} \tag{4.2.6}$$

$$\begin{aligned} &t>0,\ \ u=0,v=0,w=0,T=T_\infty,C=C_\infty \ \text{ at } x=0\\ &u=U_0\left[1+\frac{\text{£}'}{2}\left(e^{it\overline{n}}+e^{-it\overline{n}}\right)\right],v=0,w=0,T=T_w,C=C_w \quad \text{at } y=0\\ &u=0,\ v=0,\ w=0,\ T=T_\infty,C=C_\infty \qquad\qquad \text{as } y\to\infty \end{aligned} \tag{4.2.7}$$

4.2.2 Mathematical Formulation

The problem is simplified by writing the equations in the non-dimensional form. Now introduce the following non-dimensional quantities are as follows;

$$\begin{aligned} &X=\frac{xU_0}{\text{з}},Y=\frac{yU_0}{\text{з}},U=\frac{u}{U_0},V=\frac{v}{U_0},W=\frac{w}{U_0},\text{²}=\frac{tU_0^2}{\text{з}},\text{µ}=\frac{\overline{n}^{\text{з}}}{U_0^2},\\ &\overline{T}=\frac{T-T_\infty}{T_w-T_\infty},\overline{C}=\frac{C-C_\infty}{C_w-C_\infty} \end{aligned} \tag{4.2.8}$$

Then introducing the dimensionless quantities (4.2.8) in equations (4.2.1)-(4.2.5) respectively, the following dimensionless equations have been obtained as;

$$\frac{\partial U}{\partial X}+\frac{\partial V}{\partial Y}=0 \tag{4.2.9}$$

$$\frac{\partial U}{\partial \text{²}}+U\frac{\partial U}{\partial X}+V\frac{\partial U}{\partial Y}=\frac{\partial^2 U}{\partial Y^2}+G_r\overline{T}+G_m\overline{C}+2RW-\text{¥}U-\frac{M\left(\sim_e U+{}_eW\right)}{\left(\sim_e^2+{}_e^2\right)} \tag{4.2.10}$$

$$\frac{\partial W}{\partial \text{²}}+U\frac{\partial W}{\partial X}+V\frac{\partial W}{\partial Y}=\frac{\partial^2 W}{\partial Y^2}-2RU-\text{¥}W+\frac{M\left({}_eU-\sim_e W\right)}{\left(\sim_e^2+{}_e^2\right)} \tag{4.2.11}$$

$$\frac{\partial \overline{T}}{\partial \text{²}}+U\frac{\partial \overline{T}}{\partial X}+V\frac{\partial \overline{T}}{\partial Y}=\frac{1}{P_r}\frac{\partial^2 \overline{T}}{\partial Y^2}-\sim\overline{T} \tag{4.2.12}$$

$$\frac{\partial \overline{C}}{\partial \text{²}}+U\frac{\partial \overline{C}}{\partial X}+V\frac{\partial \overline{C}}{\partial Y}=\frac{1}{S_c}\frac{\partial^2 \overline{C}}{\partial Y^2}+S_0\frac{\partial^2 \overline{T}}{\partial Y^2} \tag{4.2.13}$$

The corresponding boundary conditions are as follows;

$$\text{²}\le 0,\ \ U=0,V=0,\ W=0,\ \ \overline{T}=0,\ \ \overline{C}=0 \tag{4.2.14}$$

$$U = 1 + \frac{£'}{2}\left(e^{i\mu^2} + e^{-i\mu^2}\right),\ W = 0,\ \overline{T} = 1,\ \overline{C} = 1 \qquad \text{at} \quad Y = 0,\ ^2 > 0$$
$$U = 0,\ W = 0,\ \overline{T} = 0,\ \overline{C} = 0 \qquad \text{as} \quad Y \to \infty \tag{4.2.15}$$

where, $G_r\left(= \frac{g_0\ (T_w - T_\infty)^3}{U_0^3}\right)$, $G_m\left(= \frac{g_0\ ^*(C_w - C_\infty)^3}{U_0^3}\right)$, $M\left(= \frac{\pm_e B_0^{2\,3}}{^\circ U_0^2}\right)$, $P_r\left(= \frac{^\circ c_p\ ^3}{\pm}\right)$,

$S_c\left(= \frac{^3}{D_m}\right)$, $S_0\left(= \frac{D_m k_T (T_w - T_\infty)}{^3 T_m (C_w - C_\infty)}\right)$, $R\left(= \frac{\Omega^3}{U_0^2}\right)$, $\sim\left(= \frac{\overline{Q}^3}{^\circ c_p U_0^2}\right)$, $¥\left(= \frac{^{3\ 2}}{kU_0^2}\right)$.

4.2.3 Solution Technique

The governing second order nonlinear coupled dimensionless partial differential equations have been solved with the associated initial and boundary conditions. For simplicity the explicit finite difference method has been used to solve the equations (4.2.9)-(4.2.13) with initial and boundary conditions (4.2.14)-(4.2.15). To obtain the finite difference equations the region of the flow is divided into a grid or mesh of lines parallel to X and Y axes where X-axis is taken along the plate and Y-axis is normal to the plate. Here the plate of height $X_{\max}(=100)$ is considered i.e. X varies form 0 to 100 and assumed $Y_{\max}(=25)$ as corresponding to Y ì ã i.e. Y varies from 0 to 25. There are m Z 150 and n Z 150 grid spacing in the X and Y directions respectively as shown in Fig.4.2B. It is assumed that ΔX and ΔY are constant mesh sizes along X and Y directions respectively and taken as follows, $\Delta X = 0.67 (0 \le X \le 100$, $\Delta Y = 0.17 (0 \le Y \le 25$ with the smaller time step $\Delta^2 = 0.001$.

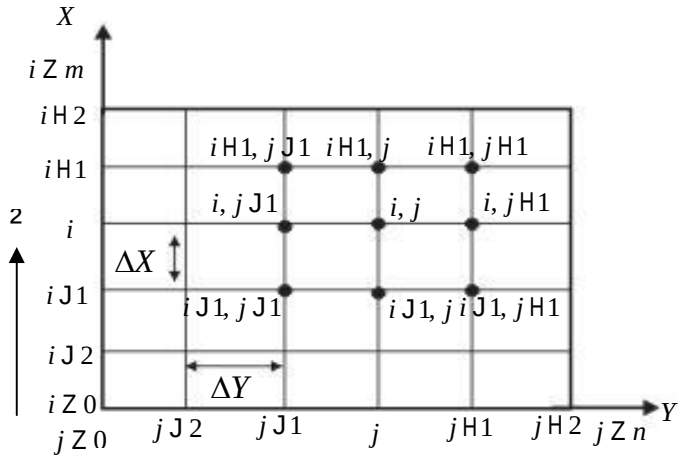

Fig.4.2.B Finite difference grid space

Let $U', W', \overline{T}'$ and $\overline{C}$à denote the values of $U, W, \overline{T}$ and $\overline{C}$ at the end of time-step respectively. Using the explicit finite difference approximation in to partial differential equations (4.2.9)-(4.2.13) then obtained an appropriate set of finite difference equations are as follows;

$$\frac{U'_{i,j} - U'_{i-1,j}}{\Delta X} + \frac{V_{i,j-1} - V_{i,j}}{\Delta Y} = 0 \tag{4.2.16}$$

$$\frac{U'_{i,j} - U_{i,j}}{\Delta^2} + U_{i,j}\frac{U_{i,j} - U_{i-1,j}}{\Delta X} + V_{i,j}\frac{U_{i,j+1} - U_{i,j}}{\Delta Y} = \frac{U_{i,j+1} - 2U_{i,j} + U_{i,j-1}}{(\Delta Y)^2} + G_r T'_{i,j} + G_m C'_{i,j}$$
$$+ 2RW_{i,j} - ¥U_{i,j} - \frac{M}{\sim_e^2 + {}_e^2}\left(\sim_e U_{i,j} + {}_e W_{i,j}\right) \tag{4.2.17}$$

$$\frac{W'_{i,j}-W_{i,j}}{\Delta²}+U_{i,j}\frac{W_{i,j}-W_{i-1,j}}{\Delta X}+V_{i,j}\frac{W_{i,j+1}-W_{i,j}}{\Delta Y}=\frac{W_{i,j+1}-2W_{i,j}+W_{i,j-1}}{(\Delta Y)^2}-2RU_{i,j}-¥W_{i,j}+\frac{M}{\sim_e^2+\ _e^2}\left(\ _eU_{i,j}-\sim_eW_{i,j}\right) \tag{4.2.18}$$

$$\frac{\overline{T}'_{i,j}-\overline{T}_{i,j}}{\Delta²}+U_{i,j}\frac{\overline{T}_{i,j}-\overline{T}_{i-1,j}}{\Delta X}+V_{i,j}\frac{\overline{T}_{i,j+1}-\overline{T}_{i,j}}{\Delta Y}=\frac{1}{P_r}\frac{\overline{T}_{i,j+1}-2\overline{T}_{i,j}+\overline{T}_{i,j-1}}{(\Delta Y)^2}-\sim\overline{T}_{i,j} \tag{4.2.19}$$

$$\frac{\overline{C}'_{i,j}-\overline{C}_{i,j}}{\Delta²}+U_{i,j}\frac{\overline{C}_{i,j}-\overline{C}_{i-1,j}}{\Delta X}+V_{i,j}\frac{\overline{C}_{i,j+1}-\overline{C}_{i,j}}{\Delta Y}=\frac{1}{S_c}\frac{\overline{C}_{i,j+1}-2\overline{C}_{i,j}+\overline{C}_{i,j-1}}{(\Delta Y)^2}+S_0\frac{\overline{T}_{i,j+1}-2\overline{T}_{i,j}+\overline{T}_{i,j-1}}{(\Delta Y)^2} \tag{4.2.20}$$

The initial and boundary conditions are obtained as follows;

$$U^0_{i,j}=0, V^0_{i,j}=0,\ W^0_{i,j}=0,\ \overline{T}^0_{i,j}=0,\ \overline{C}^0_{i,j}=0 \tag{4.2.21}$$

$$U^n_{0,j}=0, V^n_{0,j}=0,\ W^n_{0,j}=0,\ \overline{T}^n_{0,j}=0,\ \overline{C}^n_{0,j}=0$$

$$U^n_{i,0}=1,\ V^n_{i,0}=0,\ W^n_{i,0}=0,\ \overline{T}^n_{i,0}=1,\ \overline{C}^n_{i,0}=1 \tag{4.2.22}$$

$$U^n_{i,L}=0,\ V^n_{i,L}=0,\ W^n_{i,L}=0, \overline{T}^n_{i,L}=0, \overline{C}^n_{i,L}=0 \text{ where } L\to\infty$$

Here the subscripts i and j denote the grid points with X and Y-coordinates respectively and superscript n represents a value of time, $² = \overline{\overline{n}}\Delta²$ where $\overline{\overline{n}}=0,1,2,3,\ldots.$ From these conditions, the value of $\overline{T},\overline{C},U$ and w are known at $² = 0$. During any one time step, the coefficients $U_{i,j}$ and $V_{i,j}$ appearing in equations (4.2.17)-(4.2.20) are treated constants. Then at the end of any time step $\Delta²$, the new temperature $\overline{T'}$, the new concentration $\overline{C'}$, the new primary velocity U', the new secondary velocity W' and V at all grid points may be obtained by successive applications of equations (4.2.17)-(4.2.20) respectively. This process is repeated in time and provided the time is sufficiently small, $U,W,\overline{T}$ and $\overline{C}$ should eventually converge to values which approximate the steady-state solutions of equations (4.2.9)-(4.2.13). The converged solutions are shown graphically in Fig. 4.2.3(a-c)- Fig. 4.2.38(a-c).

4.2.4 Stability and Convergence Analysis

The analysis will remain incomplete unless the discussion of the stability and convergence of the finite difference method. For the constant mesh sizes, the stability criteria of the scheme can be established as follows. The general terms of the Fourier expansion for $U,W,\overline{T}$ and $\overline{C'}$ at a time arbitrarily called $² = 0$ are $e^{i\sim X}, e^{i\ Y}$ apart from a constant, where $i=\sqrt{-1}$. At time $²$ latter, these terms will become

$$\begin{aligned} U &: \cdot\ (²)e^{i\sim X}e^{i\ Y}\\ W &: ¶\,(²)e^{i\sim X}e^{i\ Y}\\ \overline{T} &: ¯\,(²)e^{i\sim X}e^{i\ Y}\\ \overline{C} &: ¤(²)e^{i\sim X}e^{i\ Y} \end{aligned} \tag{4.2.23}$$

Substituting (4.2.23) into equations (4.2.17) to (4.2.20), regarding the coefficients U and V as constants, over any one time step and denoting the values after the time step by $\cdot\,',\P\,',{}^{-}{}'$ and $\¤'$ gives after simplifications

$$\cdot\,' = A\cdot + B_1{}^{-} + C_1\¤ + D\P \tag{4.2.24}$$

$$\P' = E\P + F\cdot \tag{4.2.25}$$

$${}^{-}{}' = G^{-} \tag{4.2.26}$$

$$\¤' = H\¤ + I^{-} \tag{4.2.27}$$

where

$$A = 1 - U\frac{\Delta^2}{\Delta X}\left(1 - e^{-i\sim\Delta X}\right) - V\frac{\Delta^2}{\Delta Y}\left(e^{i\sim\Delta Y} - 1\right) + \frac{2\Delta^2}{(\Delta Y)^2}(\cos\ \Delta Y - 1) - ¥\Delta^2 - \frac{M\sim_e\Delta^2}{\sim_e^2 + \ {}_e^2}$$

$$E = 1 - U\frac{\Delta^2}{\Delta X}\left(1 - e^{-i\sim\Delta X}\right) - V\frac{\Delta^2}{\Delta Y}\left(e^{i\ \Delta Y} - 1\right) + \frac{2\Delta^2}{(\Delta Y)^2}(\cos\ \Delta Y - 1) - ¥\Delta^2 - \frac{M\sim_e\Delta^2}{\sim_e^2 + \ {}_e^2}$$

$$G = 1 - \frac{\Delta^2}{\Delta X}U\left(1 - e^{-i\sim\Delta X}\right) - \frac{\Delta^2}{\Delta Y}V\left(e^{i\ \Delta Y} - 1\right) + \frac{1}{P_r}\frac{2\Delta^2}{(\Delta Y)^2}(\cos\ \Delta Y - 1) - \sim\Delta^2$$

$$H = 1 - \frac{\Delta^2}{\Delta X}U\left(1 - e^{-i\sim\Delta X}\right) - \frac{\Delta^2}{\Delta Y}V\left(e^{i\ \Delta Y} - 1\right) + \frac{2}{S_c}\frac{\Delta^2}{(\Delta Y)^2}(\cos\ \Delta Y - 1)$$

$$B_1 = BG + CI$$

$$C_1 = CH$$

$$D = 2R\Delta^2 - \frac{M\ {}_e\Delta^2}{\sim_e^2 + \ {}_e^2}$$

$$I = \frac{2S_0\Delta^2(\cos\ \Delta Y - 1)}{(\Delta Y)^2}$$

These equations (4.2.24)-(4.2.27) can be written in the following matrix form;

$$\begin{bmatrix} \cdot\,' \\ \P\,' \\ {}^{-}{}' \\ \¤' \end{bmatrix} = \begin{bmatrix} A & D & B_1 & C_1 \\ F & E & 0 & 0 \\ 0 & 0 & G & 0 \\ 0 & 0 & I & H \end{bmatrix} \begin{bmatrix} \cdot \\ \P \\ {}^{-} \\ \¤ \end{bmatrix} \tag{4.2.28}$$

i.e. $¦' = T¦$ where $¦$ is the column vector with element $\cdot, \P, {}^{-}$ and $\¤$. For stability, the modulus of each eigenvalue of the amplification matrix T must not exceed unity. Assume that U is everywhere no-negative and V is everywhere non-positive, let

$$a = \frac{U\Delta^2}{\Delta X},\quad b = \frac{|-V|\Delta^2}{\Delta Y},\quad c = \frac{\Delta^2}{(\Delta Y)^2}$$

Hence

$$A = 1 - a - b - 2c + ae^{-i\sim\Delta X} + be^{i\ \Delta Y} + 2c\cos\ \Delta Y - ¥\Delta^2$$

$$E = 1 - a - b - 2c + ae^{-i\sim\Delta X} + be^{i\ \Delta Y} + 2c\cos\ \Delta Y - ¥\Delta^2 - \frac{M\sim_e\Delta^2}{\sim_e^2 + \ {}_e^2}$$

$$G = 1 - a - b - \frac{1}{P_r}2c + ae^{-i\sim\Delta X} + be^{i\ \Delta Y} + \frac{1}{P_r}2c\cos\ \Delta Y - \sim\Delta^2$$

$$H = 1 - a - b - \frac{1}{S_c} 2c + ae^{-i\sim\Delta X} + be^{i\ \Delta Y} + \frac{1}{S_c} 2c \cos\ \ \Delta Y$$

The coefficients a, b and c are all real and nonnegative. So that the maximum modulus of A, E, G and H occur when $\sim \Delta X = m®$ and $\Delta Y = n®$, where *m* and *n* are integer and hence A, E, G and H are real. For $\Delta²$ sufficiently large, the value $|A|, |E|, |G|$ and $|H|$ are greater when both *m* and *n* are odd integer, in which case;

$$A = 1 - a - b - 2c + (-a - b - 2c) - ¥\Delta²$$

$$E = 1 - a - b - 2c + (-a - b - 2c) - ¥\Delta² - \frac{M\sim_e \Delta²}{\sim_e^2 + \ _e^2}$$

$$G = 1 - a - b - \frac{1}{P_r} 2c + \left(-a - b - 2c \frac{1}{P_r} \right) - \sim\Delta²$$

$$H = 1 - a - b - \frac{1}{S_c} 2c + \left(-a - b - 2c \frac{1}{S_c} \right)$$

To satisfy $|A| \le 1, |E| \le 1, |G| \le 1$ and $|H| \le 1$ the most negative allowable values are $A = -1,\ E = -1,\ G = -1$ and $H = -1$.

Hence the stability conditions are as follows;

$$a + b + 2c + \frac{1}{2}\Delta² \le 1$$

$$a + b + 2c + \frac{1}{2}¥\Delta² + \frac{1}{2}\frac{M\sim_e \Delta²}{\sim_e^2 + \ _e^2} \le 1$$

$$a + b + \frac{2c}{P_r} + \frac{1}{2}\sim\Delta² \le 1$$

$$a + b + \frac{2c}{S_c} \le 1$$

4.2.5 Shear Stress, Nusselt number and Sherwood number

The quantities of chief physical interest are shear stress, Nusselt number and Sherwood number. The following equations represent the local and average shear stress at the plate. Local shear stress in x and z -axes are as follows;

$²_{LU} = «\left(\frac{\partial u}{\partial y}\right)_{y=0}$ and $²_{LW} = «\left(\frac{\partial w}{\partial y}\right)_{y=0}$ which are proportion to $\left(\frac{\partial U}{\partial Y}\right)_{Y=0}$ and $\left(\frac{\partial W}{\partial Y}\right)_{Y=0}$.

The average shear in x and z components are as follows;

$²_{AU} = «\int_0^{100}\left(\frac{\partial u}{\partial y}\right)_{y=0} dx$ and $²_{AW} = «\int_0^{100}\left(\frac{\partial w}{\partial y}\right)_{y=0} dx$ which are proportional to $\int_0^{100}\left(\frac{\partial U}{\partial Y}\right)_{Y=0} dX$ and $\int_0^{100}\left(\frac{\partial W}{\partial Y}\right)_{Y=0} dX$.

From the temperature field, the effects of various parameters on the local and average heat transfer coefficients have been studied. The following relations represent the local and average heat transfer rate that is well known as Nusselt number. Local and average Nusselt number are

$N_{uL} = -k\left(\frac{\partial T}{\partial y}\right)_{y=0}$, $N_{uA} = k\int_0^{100}\left(\frac{\partial T}{\partial y}\right)_{y=0} dx$ which are proportional to $\left(\frac{\partial \overline{T}}{\partial Y}\right)_{Y=0}$ and

$\int_0^{100}\left(\frac{\partial \overline{T}}{\partial Y}\right)_{Y=0} dX$

And from the concentration field, the effects of various parameters on the local and average mass transfer coefficients have been studied. The following relations represent the local and average mass transfer rate that is well known Sherwood number. Local and average Sherwood number are $S_{hL} = -D_m\left(\frac{\partial C}{\partial y}\right)_{y=0}$, $S_{hA} = -D_m\int_0^{100}\left(\frac{\partial C}{\partial y}\right)_{y=0} dx$ which are proportional to $\left(\frac{\partial \overline{C}}{\partial Y}\right)_{Y=0}$ and $\int_0^{100}\left(\frac{\partial \overline{C}}{\partial Y}\right)_{Y=0} dX$.

The numerical values of the local shear stress, local Nusselt number and local Sherwood number are evaluated by five point approximate formula for the derivatives and then the average shear stress, Nusselt and Sherwood number are calculated by the use of the Simpson's $\frac{1}{3}$ integration formula. The obtained values are shown graphically.

4.2.6. Results and Discussion

4.2.6.1 Justification of Grid Space

To verify the effects of space grid for m and n, the code is run with three different space grid such as $m \times n \times 100, m \times n \times 150$, $m \times n \times 200$. It is seen that there is a little change of results between them which are shown in Fig.4.2.1. According to this situation the result of velocity, temperature and concentration has been carried out for $m \times n \times 150$.

4.2.6.2 Steady-State Solution

The numerical solutions of the non-linear differential equation (4.2.10)-(4.2.13) under the boundary conditions (4.2.14)-(4.2.15) have been performed by applying explicit finite difference method. In order to verify the effects of time step size Δ², the programming code is run our model with three different step as ² = 05,50,60,70,80,100. To get steady –state solutions, the computations have been carried out up to ² = 80. It is observed that, the result of computations for $U, W, \overline{T}$ and $\overline{C}'$, however show little changes after ² = 50. Hence the velocity, temperature and concentration profiles are drawn for ² = 80. Grid space and steady state solution are shown in Fig.4.2.1 and Fig. 2.2.2 only for primary velocity for heat source parameter.

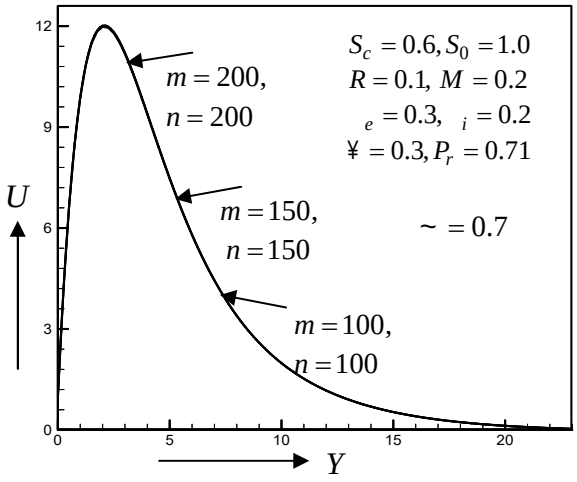

Fig.4.2.1 Primary velocity profiles for different grid space values of heat sorce parameter ~

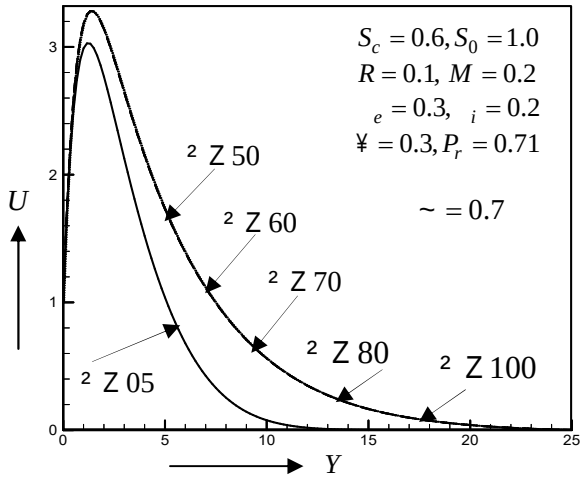

4.2.2 Primary velocity profiles for different time step of heat source parameter ~

The system of coupled nonlinear partial differential equations (4.2.10)- (4.2.13) governed by the boundary condition of equation (4.2.15) is solved numerically by explicit finite difference method. Numerical simulations were carried out for various values of parameters in order to discuss the influence on the fluid flow profiles. The velocity components in x and z-axes are commonly known as the primary and secondary velocities. The numerical calculation has been carried out for dimensionless primary velocity(U), secondary velocity(W), temperature($\overline{T}$), concentration($\overline{C}$), local shear stress in x-direction($^2_{LU}$), average shear stress in x-axis ($^2_{AU}$), local shear stress in z-axis ($^2_{LW}$), average shear stress in z-axis ($^2_{AW}$), local Nusselt number(N_{uL}), average Nusselt number(N_{uA}), local Sherwood number(S_{hL}) and average Sherwood number(S_{hA}) for various values of the parameters such as Hall parameter ($_e$), ion-slip parameter($_i$), magnetic parameter(M), rotational parameter (R), Prandtl number(P_r), Schmidt number (S_c), Grashof number(G_r), modified Grashof number(G_m), Soret number(S_0), permeability parameter(¥)and heat source(~). The values of the parameters are chosen arbitrarily in most cases. Throughout the calculations the values G_r and G_m are taken to be very large($G_r = 10.0$ and $G_m = 4.0$). Some standard values for the Prandtl number (P_r) and Schmidt number (S_c) are also considered because of the physical importance. Physically $P_r = 0.71$ corresponds to air at 20^0C, $P_r = 7.0$ corresponds to water at 20^0C, $P_r = 2.6$.corresponds to water at 67^0C and and $S_c = 0.6$.corresponds to water vapor, $S_c = 0.78, S_c = 1.0$ corresponds to methanol respectively at 25^0C and 1 atmosphere. For the purpose of computation, $\mu t = ® / 2, £ = 0.001$ has been chosen arbitrarily.

Form Figs.4.2.3 (a-c), it is seen that the primary velocity (U), the local and average shear stress in x-axis ($^2_{LU}, ^2_{AU}$,) decrease with the increase of ~. To increase the value of the heat source parameter ~ is to decrease the boundary layer which is expected when heat is

absorbed by the buoyancy force. But opposite behavior has been seen for secondary velocity (W), local and average shear stress in z - axis ($²_{LW}$, $²_{AW}$) in Figs.4.2.4 (a-c).

It is seen that from Fig.4.2.5 (a), the temperature $(\overline{T})$ distribution decreases with an increase of ~ . Because when heat is absorbed, the buoyancy force decreases the temperature profiles whereas local and average Nusselt number $\left[N_{uL} \propto -\left(\frac{\partial \overline{T}}{\partial Y}\right)_{Y=0} \text{ and } N_{uA} \propto -\int_0^{100}\left(\frac{\partial \overline{T}}{\partial Y}\right)_{Y=0} dX\right]$ have opposite behavior which have been illustrate in Figs.4.2.5(b,c). The Concentration $(\overline{C})$ distribution has an increasing effect is shown in Fig.4.2.6 (a) while the local and average Sherwood number $\left[S_{hL} \propto -\left(\frac{\partial \overline{C}}{\partial Y}\right)_{Y=0} \text{ and } S_{hA} \propto -\int_0^{100}\left(\frac{\partial \overline{C}}{\partial Y}\right)_{Y=0} dX\right]$ have opposite behavior which are shown in Figs. 4.2.6(b,c).

It is observed that in Figs.4.2.7 (a-c), the primary velocity (U), local and average shear stresses in x-axis ($²_{LU}$, $²_{AU}$) and increase with the increases of Hall parameter $_e$. The inclusion of Hall parameter decreases the resistive force imposed by the magnetic field due to its effect in reducing the effective conductivity.

Fig.4.2.8(a) depict that $_e$ increases, firstly the secondary velocity (W) decreases up to $Y = 0.6$ but after that (W) show increasing trend as Y increases further, thus there is a cross flow near $Y = 0.6$. Since secondary velocity is a result of Hall effect. The Local and average shear stresses in z-axis ($²_{LW}$, $²_{AW}$) have been decreased with an increase of $_e$ which are depicted in Figs.4.2.8 (b,c). The Hall parameter has a minor decreasing effect on the temperature $(\overline{T})$ profiles while local and average Nusselt number (N_{uL}, N_{uA}) increase which has been shown Figs.4.2.9 (a-c). It is observed from Figs.4.2.10 (a-c) that the Hall parameter has decreasing effect on concentration $(\overline{C})$ whereas opposite behavior have been seen for local and average Sherwood number (S_{hL}, S_{hA}).

The effect of ion-slip parameter $_i$ on primary velocity (U) has negligible effect in Fig. 4.2.11(a) whereas on local and average shear stresses in x-axis ($²_{LU}$, $²_{AU}$) have increasing effect are shown in Figs.4.2.11 (b,c). As $_i$ increases the effective conductivity, which in turn decreases the damping force on the velocity component in the direction of the flow and hence the (U), $²_{LU}$ and($²_{AU}$) increase in the flow direction. It is seen from Figs.4.2.12 (a-c), increasing $_i$, increase secondary velocity (W), local, average shear stress in z-axis ($²_{LW}$, $²_{AW}$). The effect of $_i$ on the temperature profiles $(\overline{T})$ has negligible effect and increasing effect on local and average Nusselt number (N_{uL}, N_{uA}) has been shown in Figs. 4.2.13(a-c). When $_i$ increase then thermal boundary layer thickness decreases. The effect of the $_i$ on the concentration profiles has negligible effect and increasing effect on local and average Sherwood number (S_{hL}, S_{hA}) which have been depicted in Figs. 4.2.14(a-c).

In Fig.4.2.15(a), it is seen that permeability parameter ¥ increases, firstly the primary velocity (U) decrease up to $Y = 0.9$ but after that (U) show increasing trend as Y increases

further, thus there is a cross flow is obtained near $Y = 0.9$. This indicates that the permeability of porous medium exerts retarding force on the primary flow. Local and average shear stress in x- axis (τ_{LU}, (τ_{AU}) are decreased which is seen in Figs.4.2.15 (b,c). It is seen from Figs.4.2.16 (a-c), the secondary velocity (W), local, average shear stress in z- axis (τ_{LW},τ_{AW}) are increased with an increase of ¥. From Figs. 4.2.17(a-c) and Figs. 4.2.18(a-c) it is observed that the temperature $(\overline{T})$ and concentration $(\overline{C})$ profiles increase whereas local and average Nusselt number (N_{uL}, N_{uA}), local and average Sherwood number (S_{hL}, S_{hA}) decrease with increasing ¥. This is due to the fact that increasing the value of permeability parameter has tendency to increase the thermal boundary layer and concentration species.

In Figs. 4.2.19(a-c), primary velocity (U), local and average shear stress in x- axis (τ_{LU}, τ_{AU}) profiles are plotted respectively for different values of magnetic parameter (M). The primary velocity (U) profiles decreases firstly, then start to increase with the increase of (M). So there is a cross flow near $Y = 11.0$. Similar behaviors are found for (τ_{LU},τ_{AU}). This is due to the fact, the transverse magnetic field normal to the flow direction has a tendency to create the drag known as the Lorentz force which tends to resist the flow. Similar behaviors are found in secondary velocity (W), local and average shear stress in z-axis (τ_{LW},τ_{AW}) which are shown in Figs. 4.2.20(a-c). Figs. 4.2.21(a-c) and Figs. 4.2.22(a-c) are illustrated that the temperature $(\overline{T})$ and concentration $(\overline{C})$ profiles increase whereas local and average Nusselt numbers (N_{uL}, N_{uA}), local and average Sherwood numbers (S_{hL}, S_{hA}) decrease with increasing M. The effects of a transverse magnetic field to an electrically conducting fluid give rise to a resistive-type force called the Lorentz force. This force has the tendency to increase its temperature and concentration distributions.

It is seen that in Fig. 4.2.23(a) the primary velocity (U) profiles decrease firstly, then start to increase with the increase of rotational parameter (R). So there is a cross flow near $Y = 11.0$. But local and average shear stress in x- axis (τ_{LU}, τ_{AU}) decrease with the increase of R which are shown in Figs.4.2.23 (b-c). In fact rotation parameter defines the relative magnitude of the Coriolis force and the viscous force, thus rotation retards primary flow in the boundary layer. The secondary velocity (W), local and average shear stress in z- axis (τ_{LW},τ_{AW}) have decreasing effect with the increase of effect of R are shown in Figs.4.2.24 (a-c). Figs. 4.2.25(a-c) and Figs. 4.2.26(a-c) are illustrated that the temperature $(\overline{T})$ and concentration $(\overline{C})$ profiles increases whereas local and average Nusselt numbers (N_{uL}, N_{uA}), local and average Sherwood numbers (S_{hL}, S_{hA}) are decreased.

From Figs.4.2.27 (a-c) it is found that the primary velocity (U), local and average shear stress in x-axis (τ_{LU},τ_{AU}) profiles increase with an increase in Soret number S_0. That is the momentum boundary layer increases as Soret number increases. But opposite behaviors are found on secondary velocity (W), local and average shear stress in z-axis (τ_{LW},τ_{AW}) which are shown in Figs.4.2.28 (a-c). It has been observed that there are small decreasing effects on the temperature $(\overline{T})$ profiles in Fig.4.2.29 (a) of increasing values of S_0. But local and

average Nusselt numbers (N_{uL} , N_{uA}) are increased with an increase in S_0 in Figs.4.2.29 (b,c). Fig.4.2.30 (a) illustrates the effect of S_0 on concentration $(\overline{C})$ profiles increases with an increase of S_0 . The concentration boundary layer increases rapidly and the concentration boundary layer increases with increase of S_0 that signifies that S_0 can control concentration boundary layer. Figs.4.2.30 (b,c) have been ploted that the local and average Sherwood numbers (S_{hL} , S_{hA}) have decreasing effect with an increase of S_0 . For buoyancy assisting and buoyancy opposing flows, an increase in the Soret parameter tends to thicken concentration boundary layer, thus (S_{hL} , S_{hA}) are decreasing at the wall.

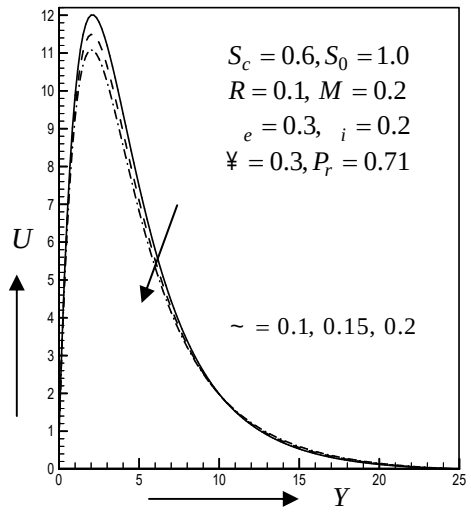

Fig.4.2.3(a) Primary velocity profiles for different values of ~

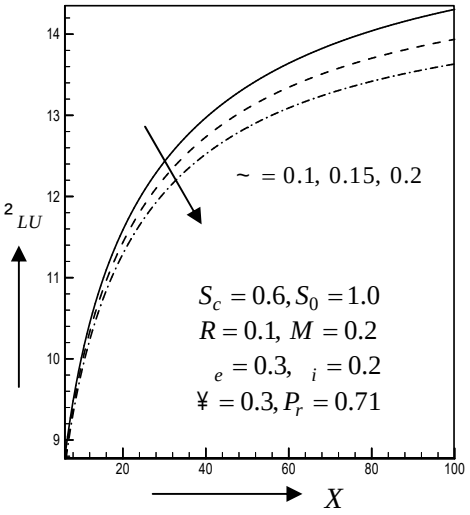

Fig.4.2.3 (b) Local shear stress in x -axis for different values of ~

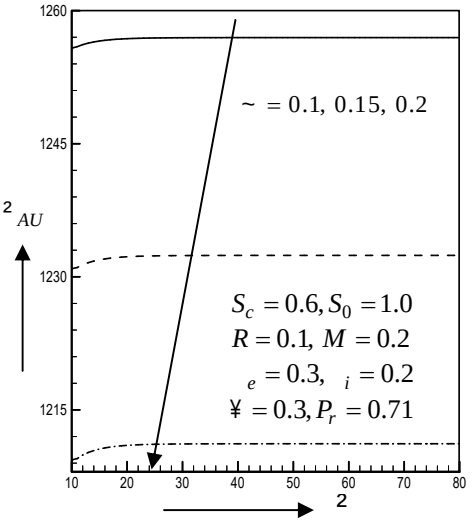

Fig.4.2.3(c) Average shear stress in x -axis for different values of ~

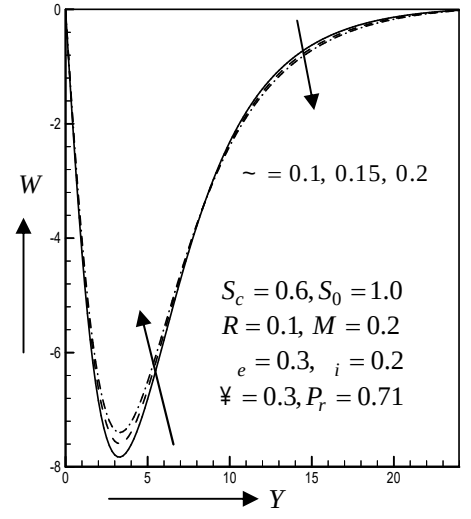

Fig.4.2.4 (a) Secondary velocity profiles for different values of ~

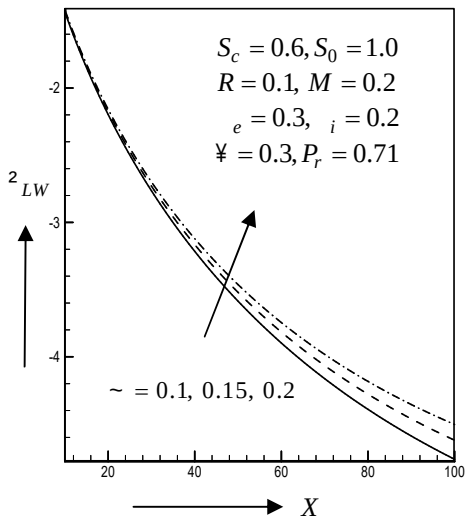

Fig.4.2.4(b) Local shear stress in z -axis for different values of ~

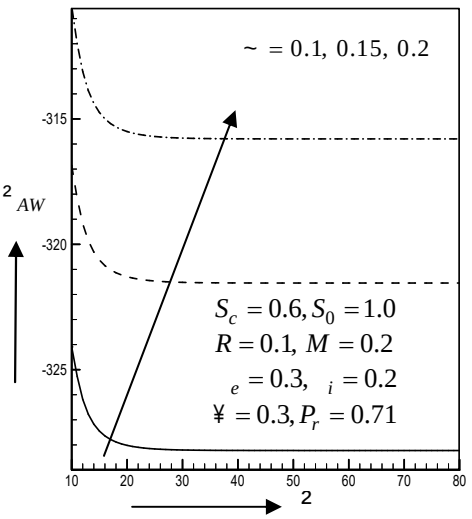

Fig.4.2.4(c) Average shear stress in z -axis for different values of ~

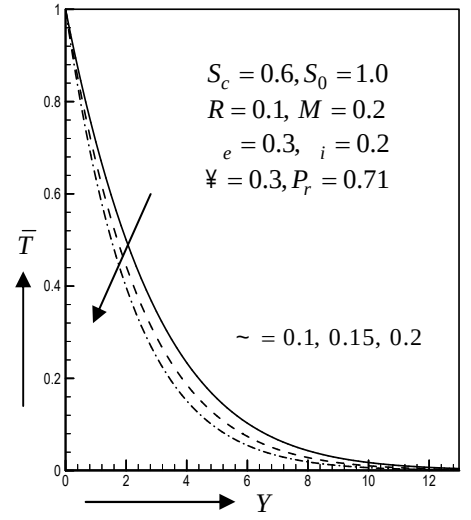

Fig.4.2.5(a) Temperature profiles for different values of ~

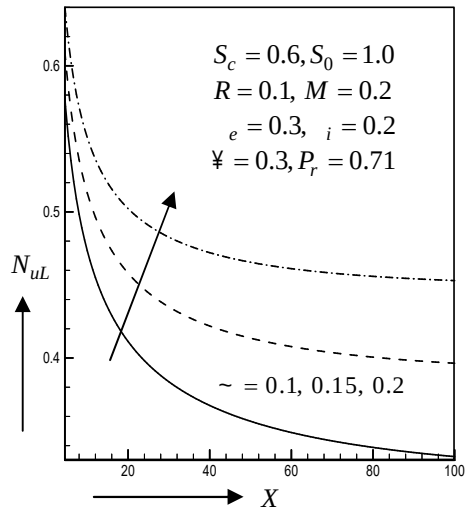

Fig.4.2.5(b) Local Nusselt number for different values of ~

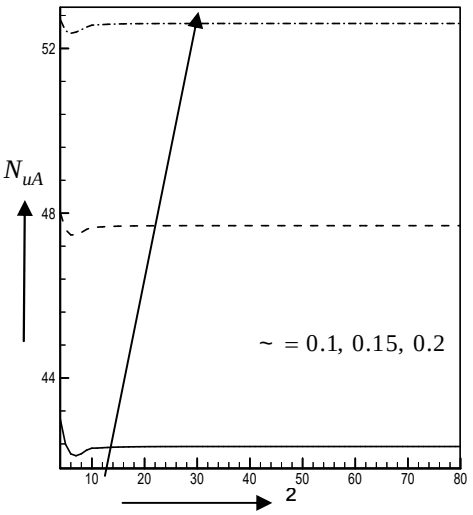

Fig. 4.2.5(c) Average Nusselt number for different values of ~

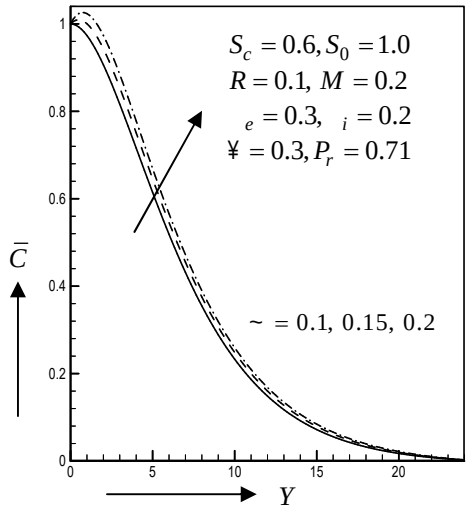

Fig. 4.2.6(a) Concentration profiles for different values of ~

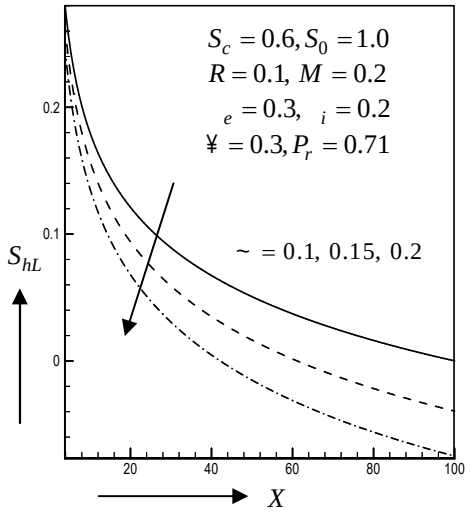

Fig. 4.2.6(b) Local Sherwood number for different values of ~

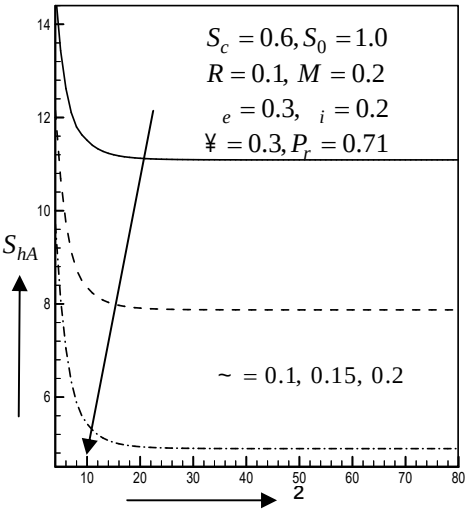

Fig. 4.2.6(c) Average Sherwood number for different values of ~

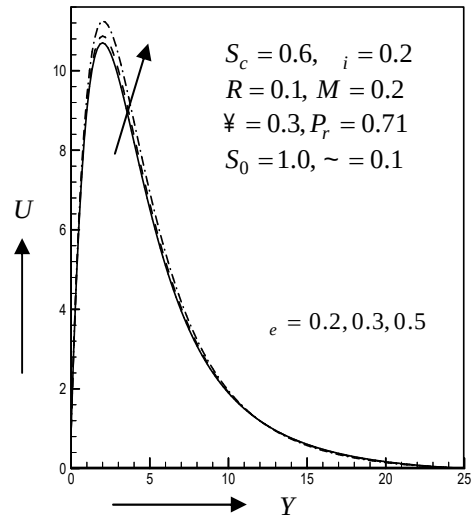

Fig. 4.2.7(a) Primary velocity profiles for different values of $_e$

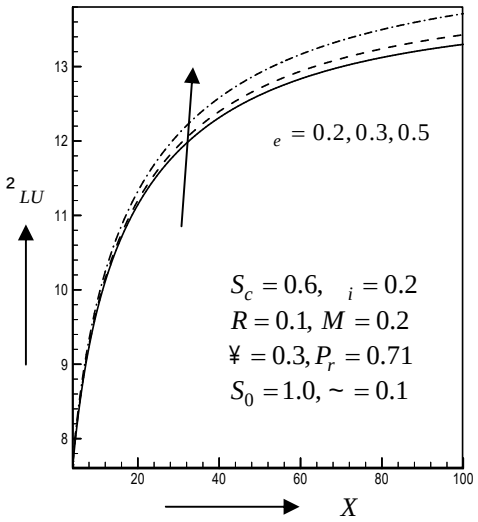

Fig. 4.2.7(b) Local shear stress in x -axis for different values of $_e$

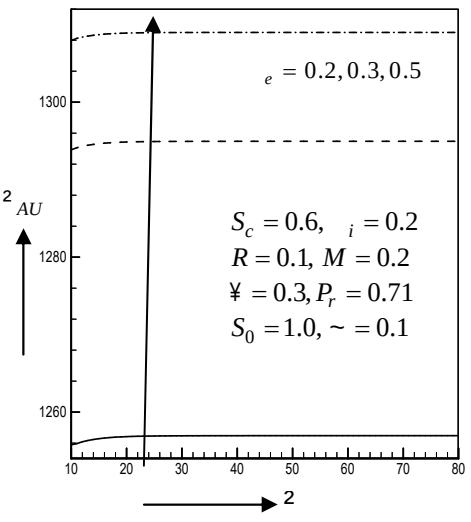

Fig.4.2.7(c) Average shear stress in x -axis for different values of $_e$

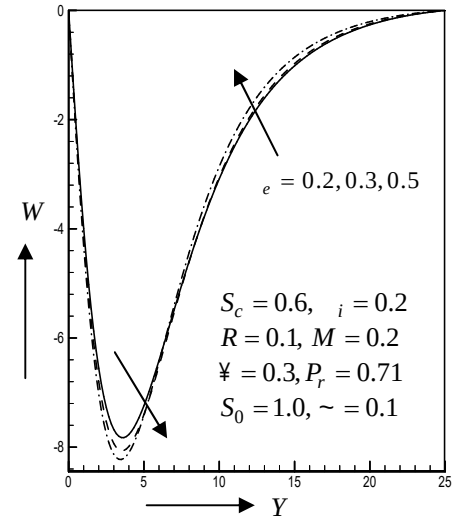

Fig. 4.2.8(a) Secondary velocity profiles for different values of $_e$

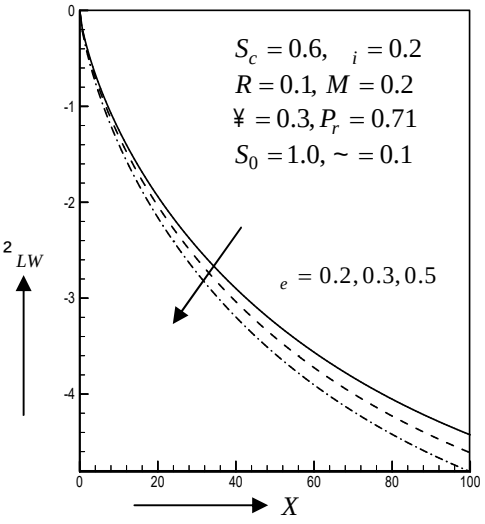

Fig. 4.2.8(b) Local shear stress in z -axis for different values of $_e$

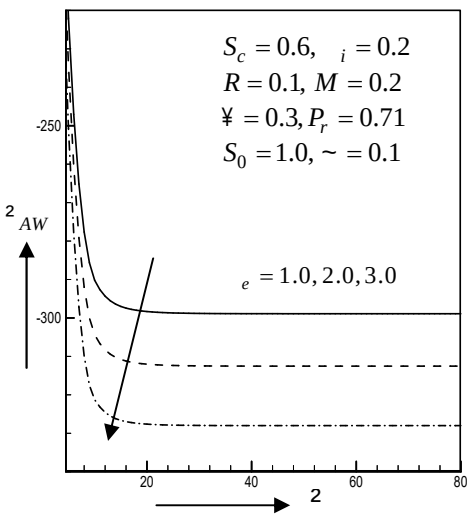

Fig. 4.2.8(c) Average shear stress in z – axis for different values of $_e$

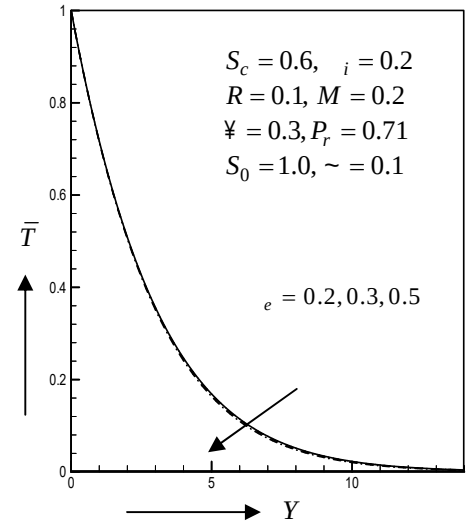

Fig.4.2.9(a) Temperature profiles for different values of $_e$

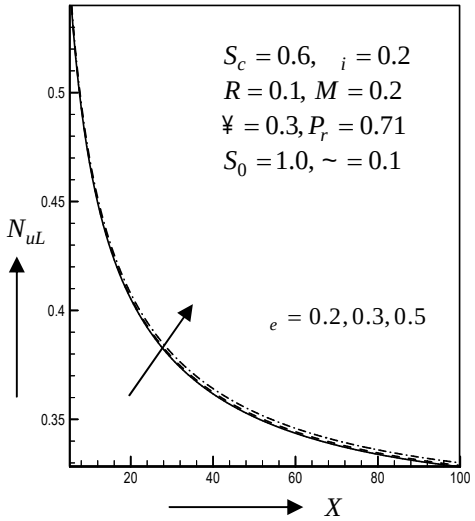

Fig. 4.2.9(b) Local Nusselt number for different values of $_e$

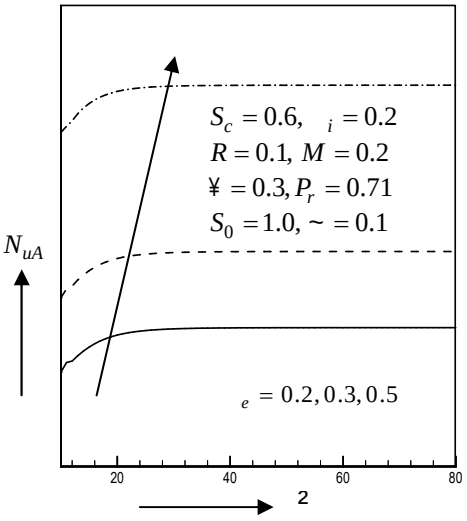

Fig. 4.2.9(c) Average Nusselt number for different values of $_e$

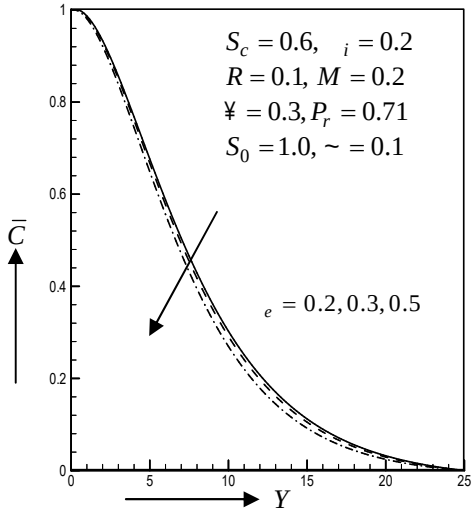

Fig. 4.2.10(a) Concentration profiles for different values of $_e$

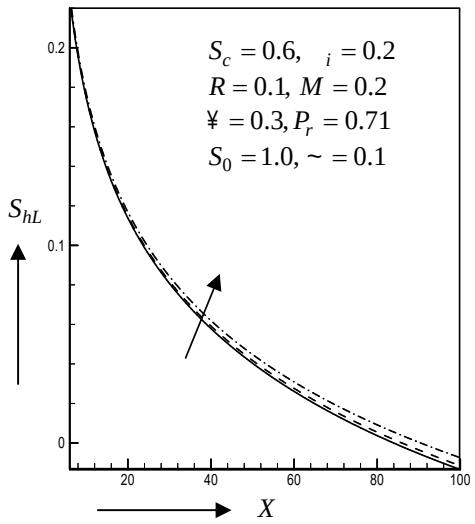

Fig. 4.2.10(b) Local Sherwood number for different values of $_e$

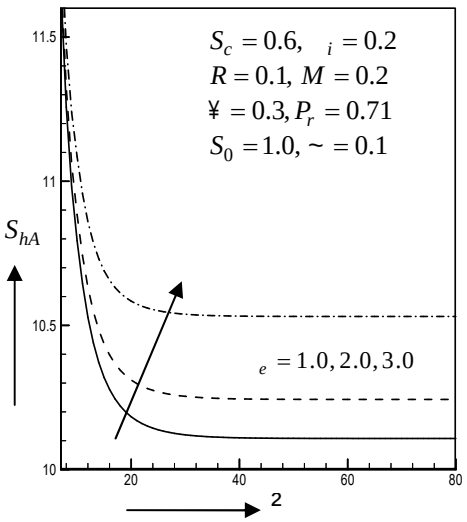

Fig.4.2.10(c) Average Sherwood number for different values of $_e$

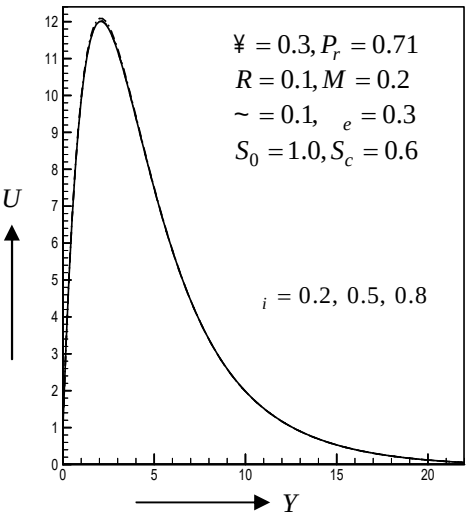

Fig. 4.2.11(a) Primary velocity profiles for different values of $_i$

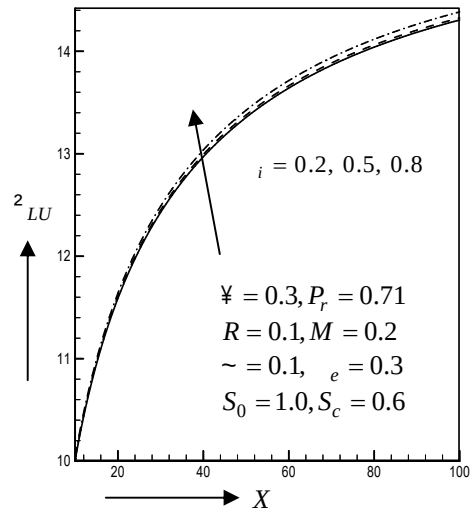

Fig.4.2.11(b) Local shear stress in x -axis for different values of $_i$

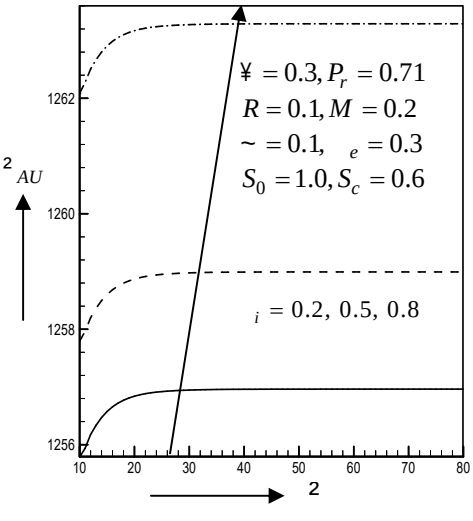

Fig. 4.2.11(c) Average shear stress in x -axis for different values of $_i$

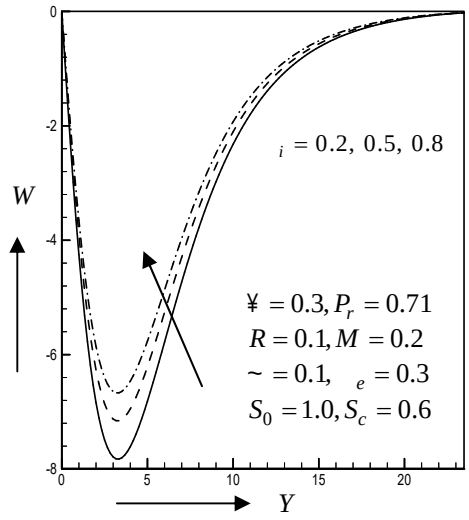

Fig. 4.2.12(a) Secondary velocity profiles for different values of $_i$

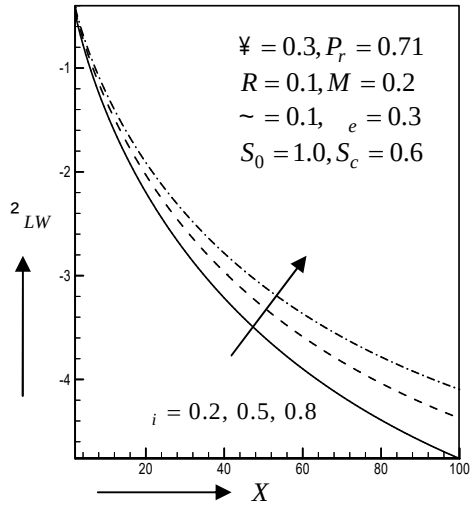

Fig. 4.2.12(b) Local shear stress in z -axis for different values of $_i$

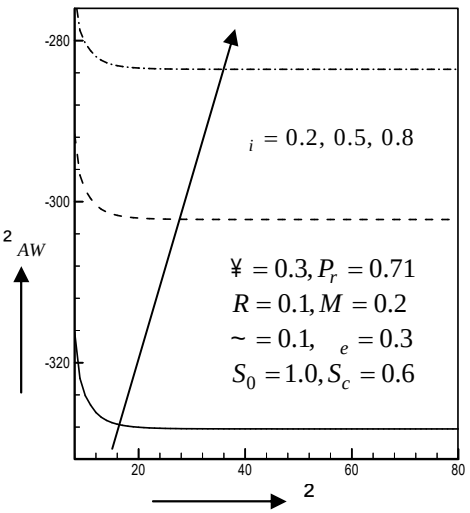

Fig. 4.2.12(c) Average shear stress in z -axis for different values of $_i$

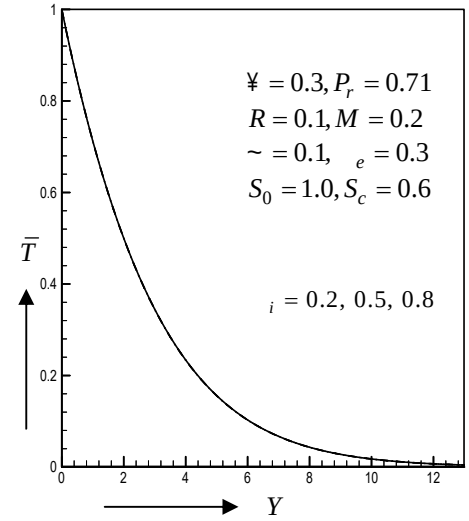

Fig.4.2.13(a) Temperature profiles for different values of $_i$

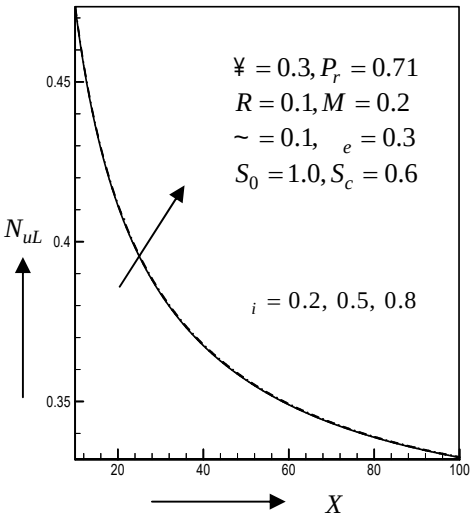

Fig. 4.2.13(b) Local Nusselt number for different values of $_i$

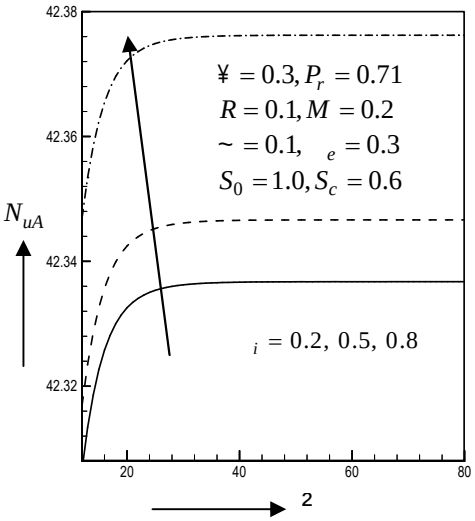

Fig. 4.2.13(c) Average Nusselt number for different values of $_i$

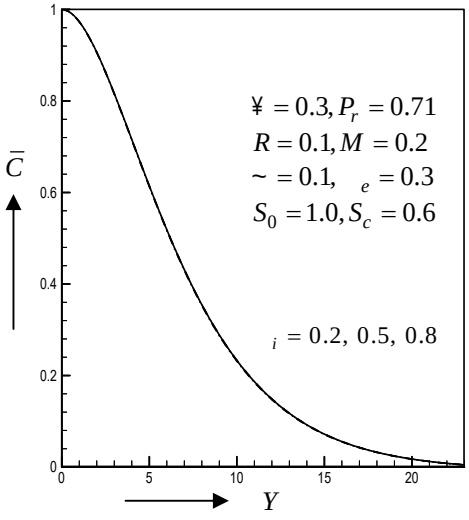

Fig. 4.2.14(a) Concentration profiles for different values of $_i$

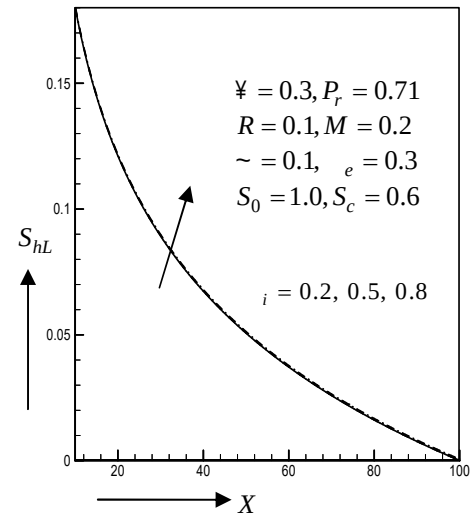

Fig. 4.2.14(b) Local Sherwood number for different values of $_i$

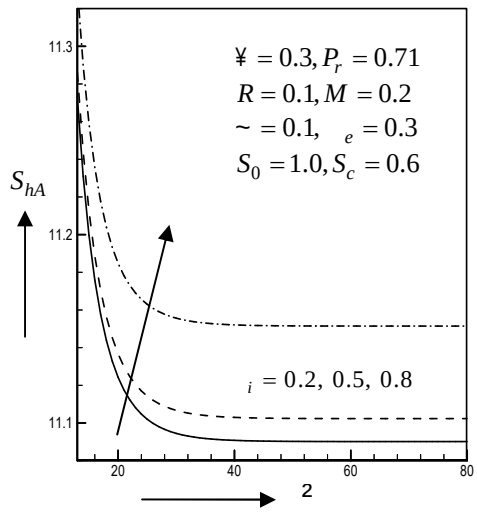

Fig. 4.2.14(c) Average Sherwood number for different values of $_i$

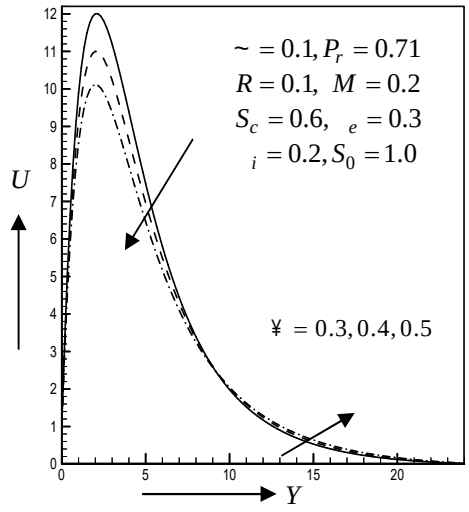

Fig.4.2.15(a) Primary velocity profiles for different values of ¥

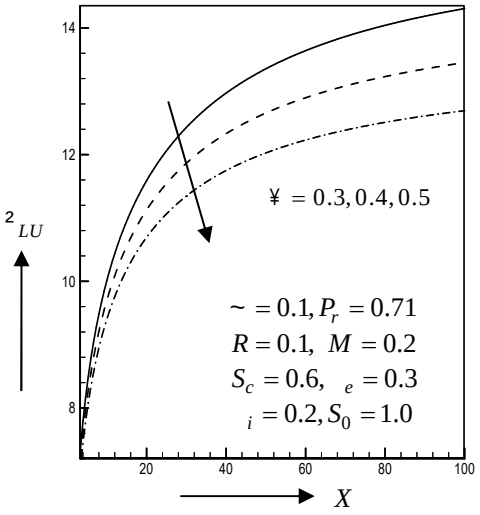

Fig. 4.2.15(b) Local shear stress in x -axis for different values of ¥

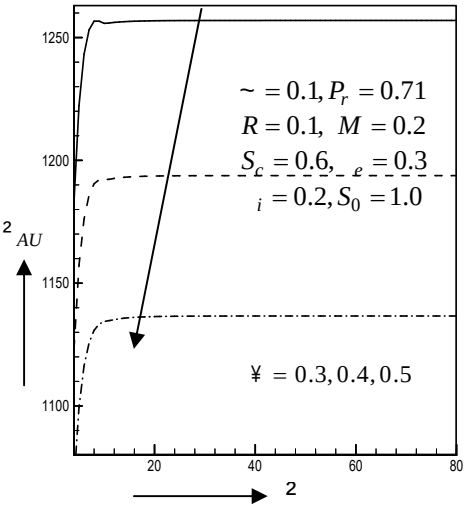

Fig. 4.2.15(c) Average shear stress in x -axis for different values of ¥

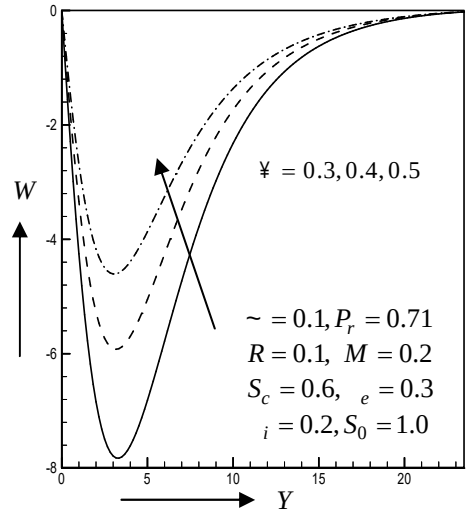

Fig. 4.2.16(a) Secondary velocity profiles for different values of ¥

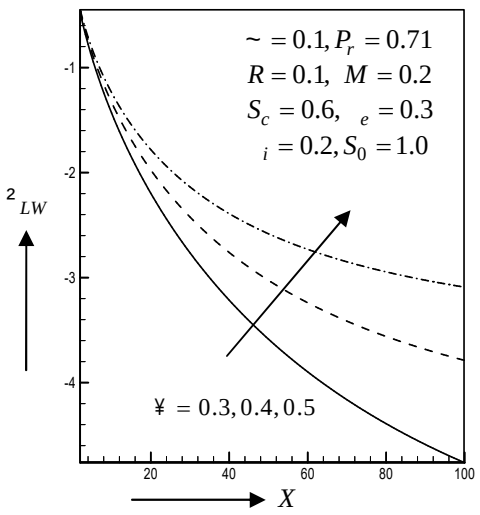

Fig. 4.2.16(b) Local shear stress in z -axis for different values of ¥

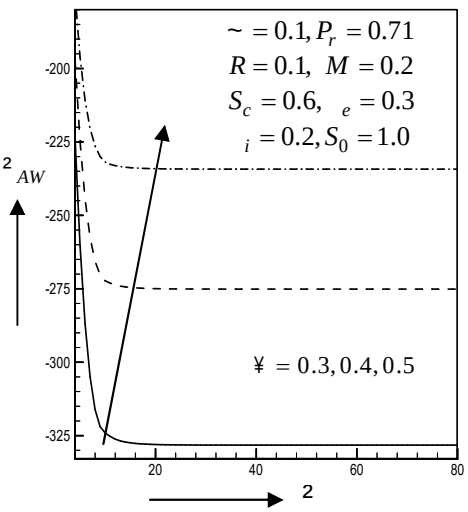

Fig. 4.2.16(c) Average shears stress in z -axis values of ¥

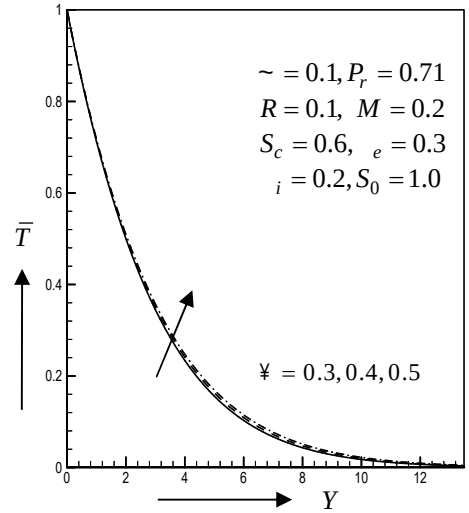

Fig.4.2.17(a) Temperature profiles for different values of ¥

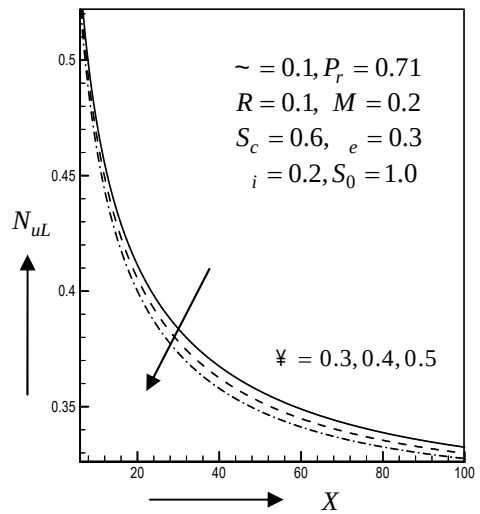

Fig.4.2.17(b) Local Nusselt number for different values of ¥

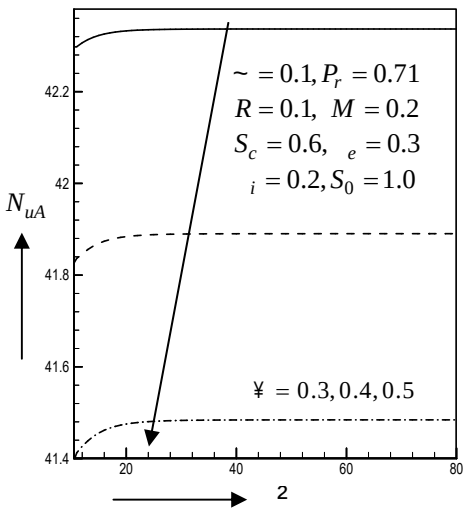

Fig.4.2.17(c) Average Nusselt number for different values of ¥

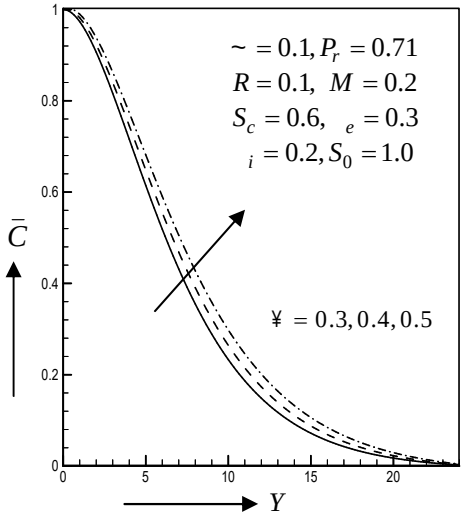

Fig. 4.2.18(a) Concentration profiles for different values of ¥

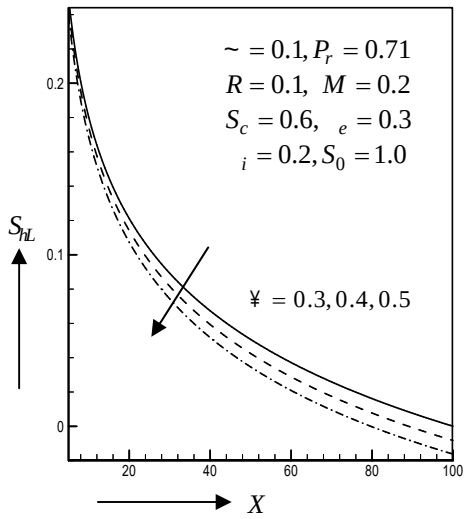

Fig. 4.2.18(b) Local Sherwood number for different values of ¥

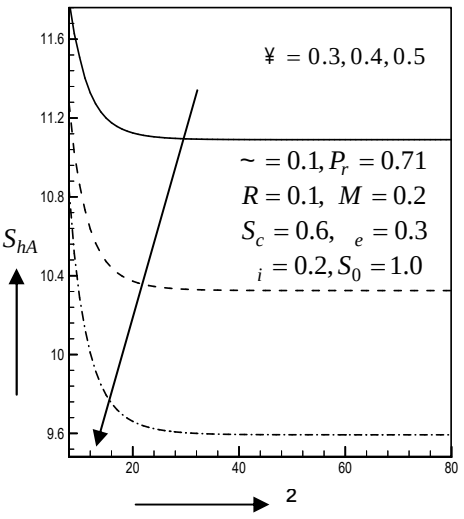

Fig. 4.2.18(c) Average Sherwood number for different values of ¥

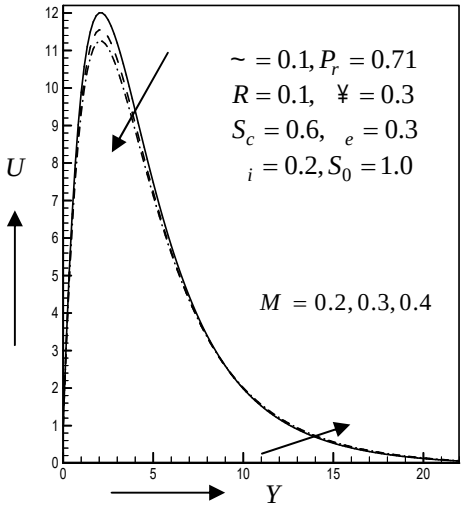

Fig. 4.2.19(a) Primary velocity profiles for different values of M

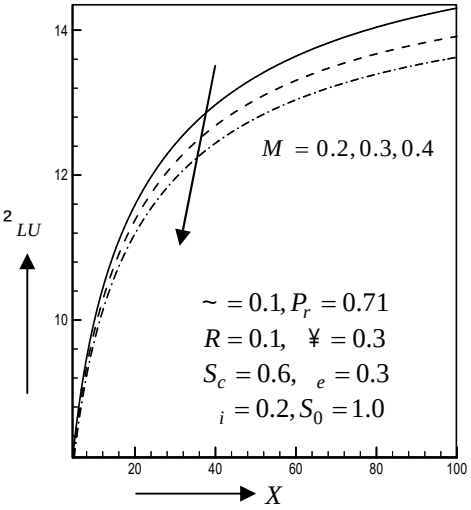

Fig. 4.2.19(b) Local shear stress in x-axis for different values of M

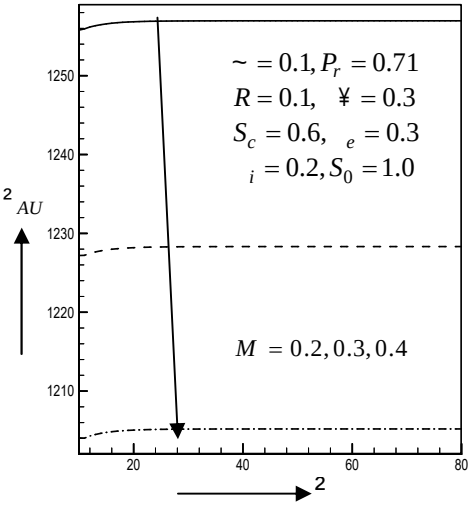

Fig. 4.2.19(c) Average shears stress in x-axis for different values M

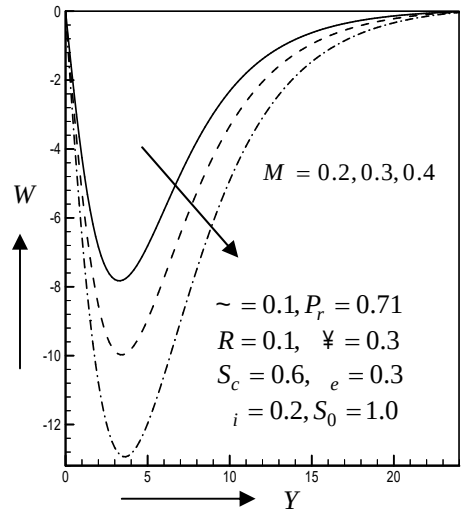

Fig. 4.2.20(a) Secondary velocity profiles for different values of M

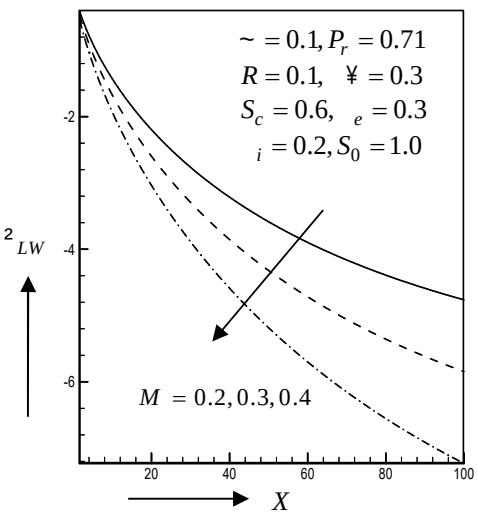

Fig. 4.2.20(b) Local shear stress in z-axis for different values of M

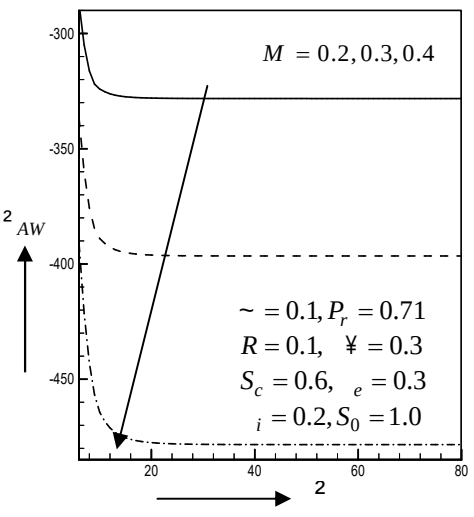

Fig. 4.2.20(c) Average shears stress in z-axis for different values of M

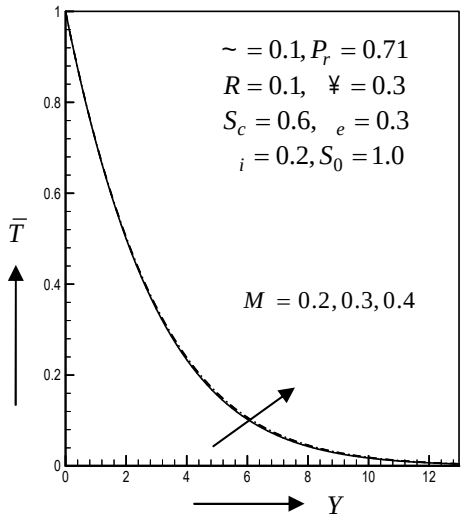

Fig.4.2.21(a) Temperature profiles for different values of M

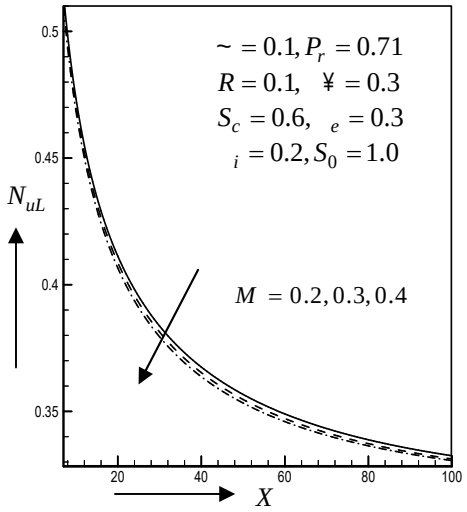

Fig. 4.2.21(b) Local Nusselt number for different values of M

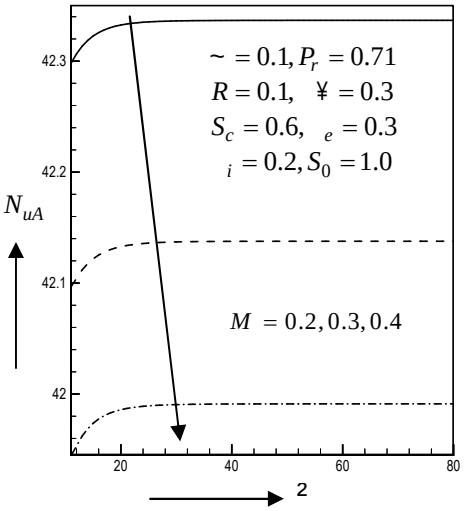

Fig. 4.2.21(c) Average Nusselt number for different values of M

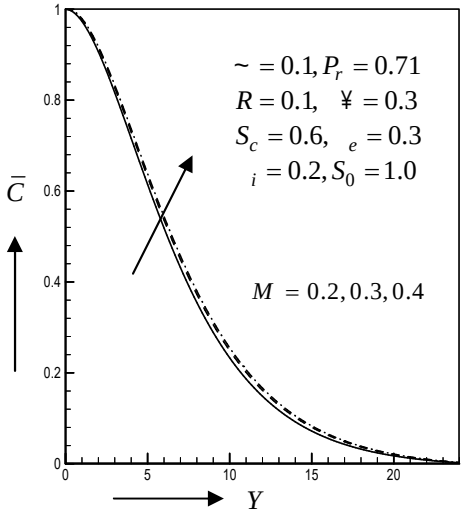

Fig. 4.2.22(a) Concentration profiles for different values of M

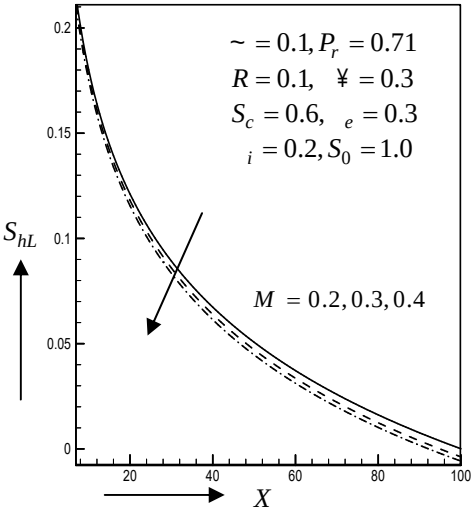

Fig. 4.2.22(b) Local Sherwood for different values of M

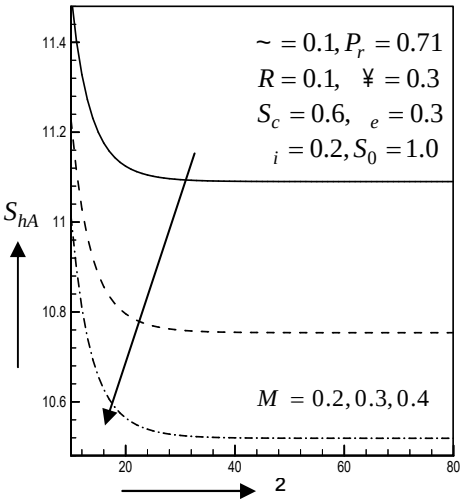

Fig. 4.2.22(c) Average Sherwood for different values of M

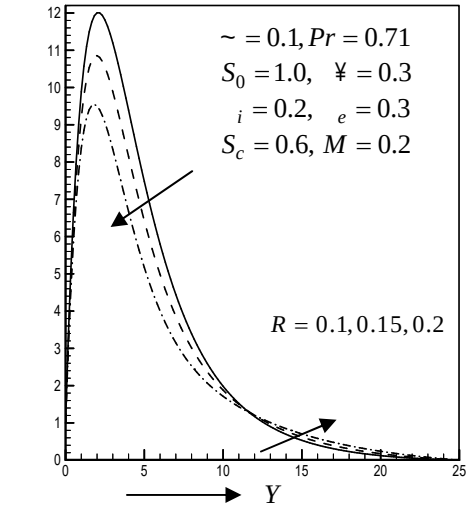

Fig. 4.2.23(a) Primary velocity profiles for different values of R

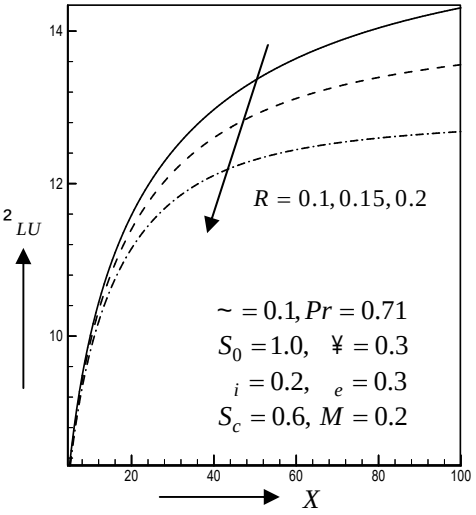

Fig. 4.2.23(b) Local shear stress in x-axis for different values of R

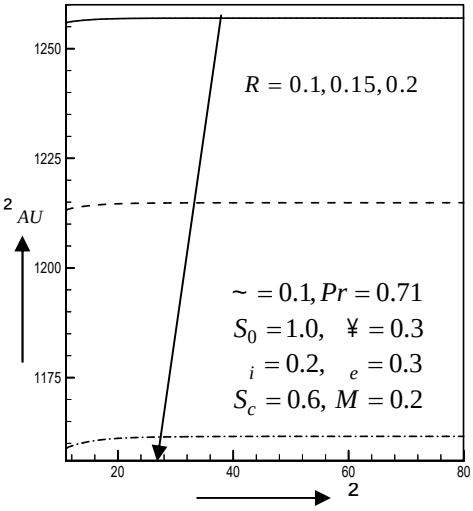

Fig. 4.2.23(c) Average shear stress in x-axis for different values of R

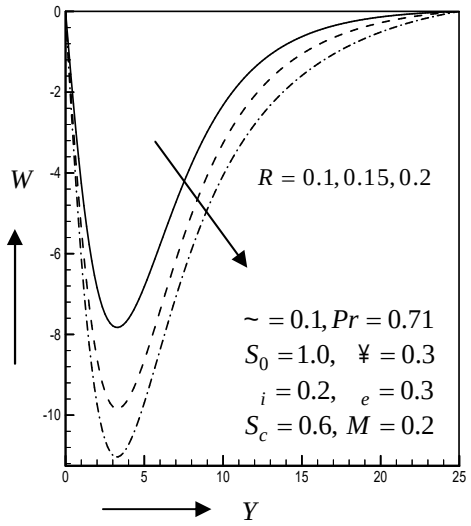

Fig. 4.2.24(a) Secondary velocity profiles for different values of R

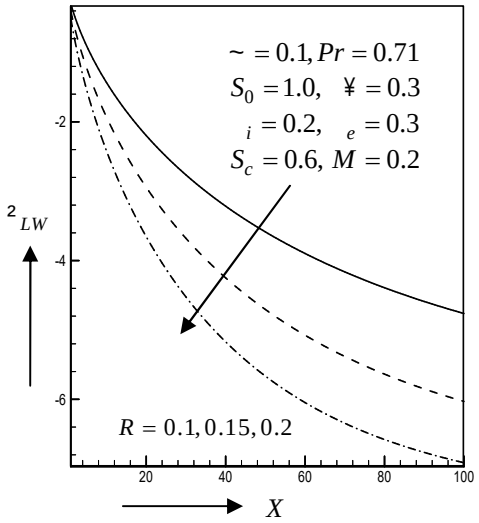

Fig. 4.2.24(b) Local shear stress in z -axis for different values of R

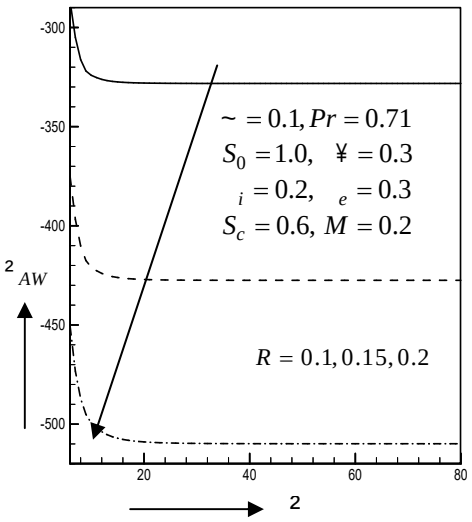

Fig. 4.2.24(c) Average shears stress in z -axis for different values of R

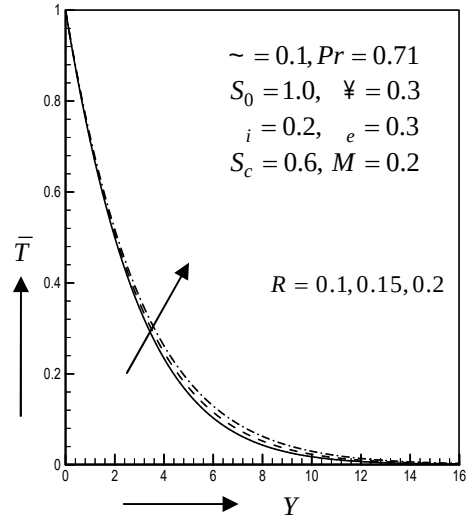

Fig.4.2.25(a) Temperature profiles for different values of R

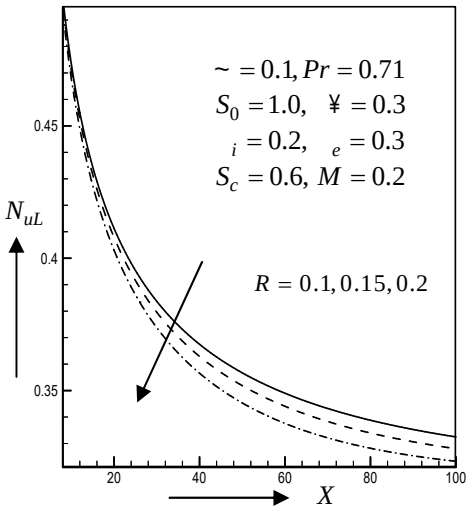

Fig. 4.2.25(b) Local Nusselt number for different values of R

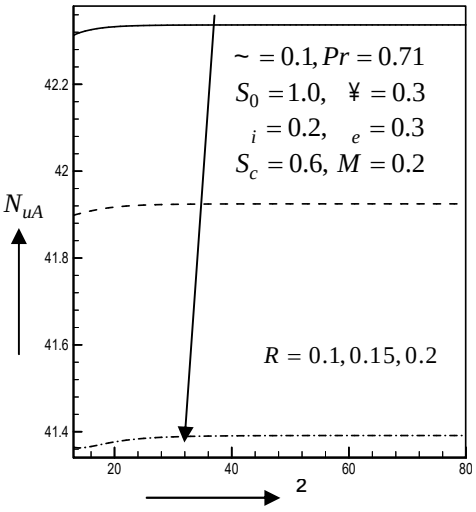

Fig. 4.2.25(c) Average Nusselt number for different values of R

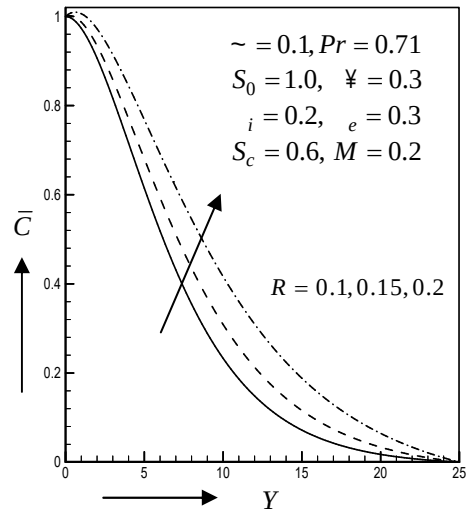

Fig. 4.2.26(a) Concentration profiles for different values of R

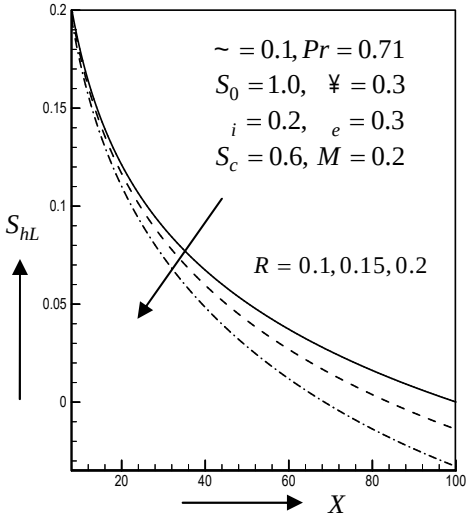

Fig. 4.2.26(b) Local Sherwood number for different values of R

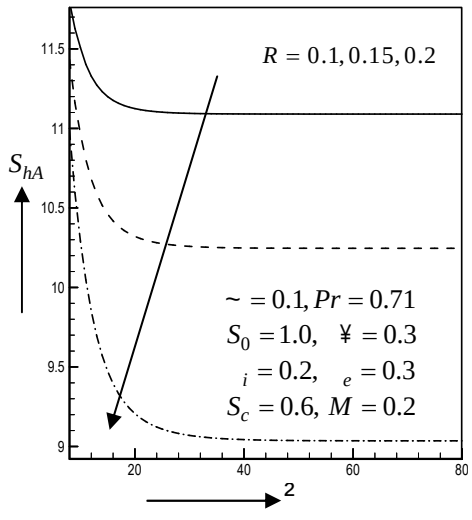

Fig. 4.2.26(c) Average Sherwood number for different values of R

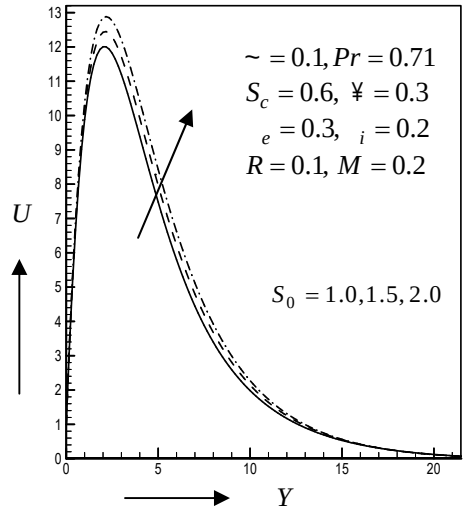

Fig. 4.2.27(a) Primary velocity profiles for different values of S_0

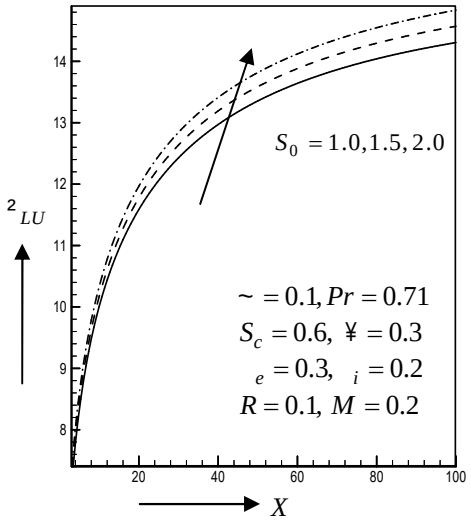

Fig. 4.2.27(b) Local shear stress in x-axis for different values of S_0

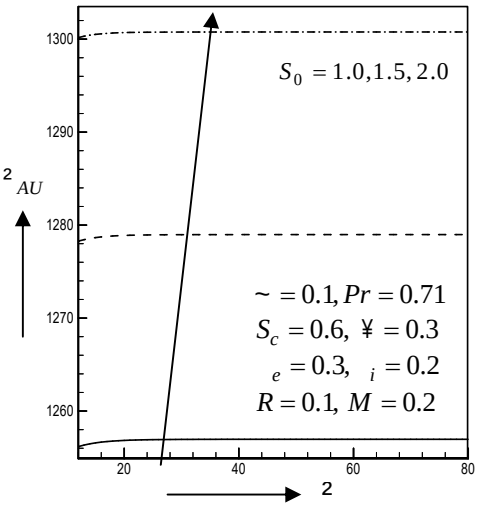

Fig. 4.2.27(c) Average shear stress in x-axis for different values of S_0

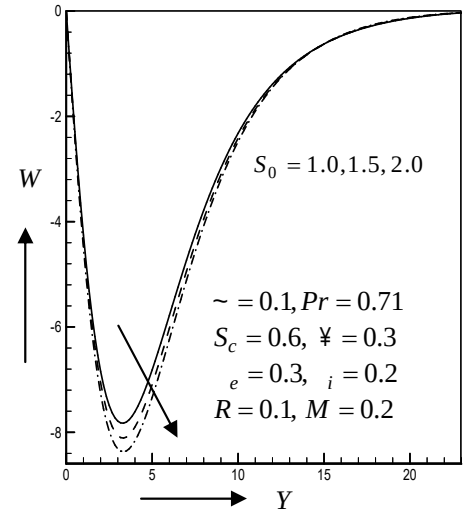

Fig. 4.2.28(a) Secondary velocity profiles for different values of S_0

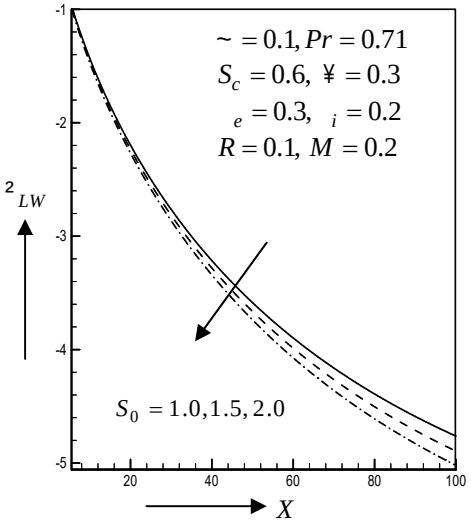

Fig. 4.2.28(b) Local shear stress in z-axis for different values of S_0

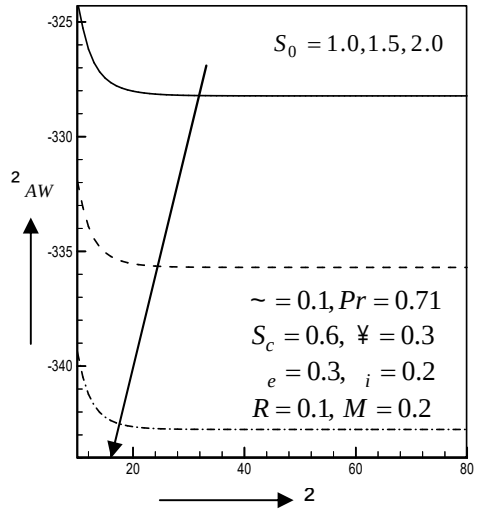

Fig. 4.2.28(c) Average shear stress in z-axis for different values of S_0

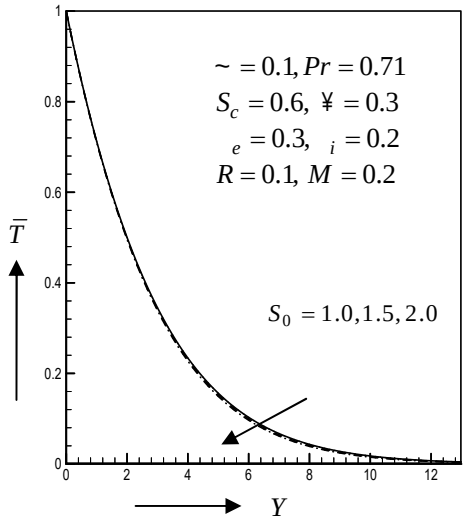

Fig.4.2.29(a) Temperature profile for different values of S_0

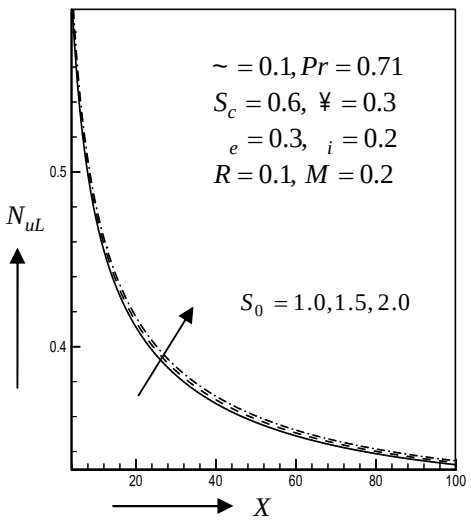

Fig. 4.2.29(b) Local Nusselt number for different values of S_0

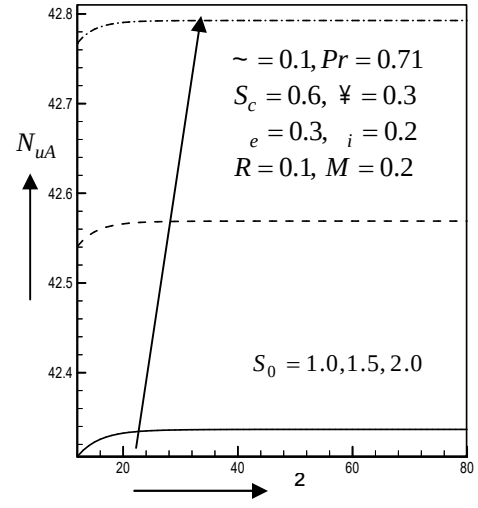

Fig. 4.2.29(c) Average Nusselt number for different values of S_0

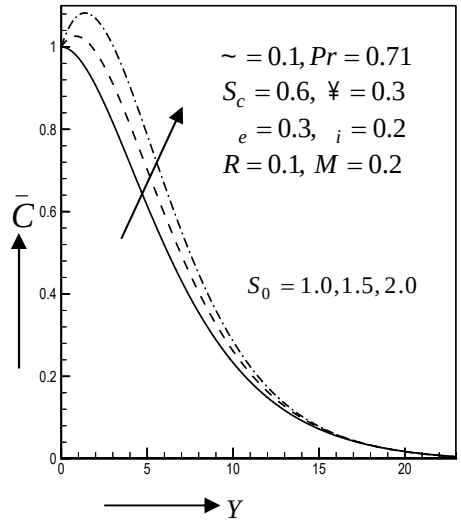

Fig. 4.2.30(a) Concentration profiles for different values of S_0

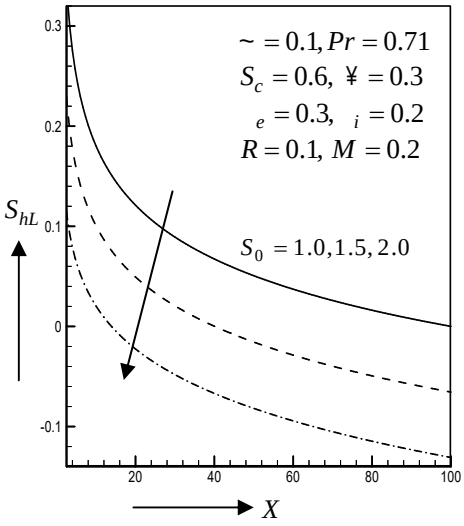

Fig. 4.2.30(b) Local Sherwood number for different values of S_0

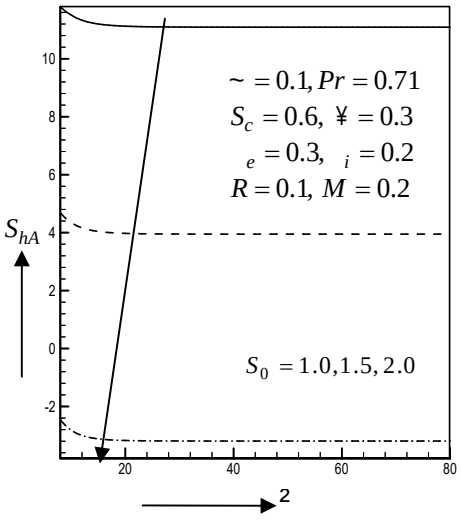

Fig. 4.2.30(c) Average Sherwood number for different values of S_0

References

Alam, M. S., Haque, M. M. and Uddin, M. J. (2014), Unsteady MHD free convective heat transfer flow along a vertical porous flat plate with internal heat generation, 'International Journal of Advances in Applied Mathematics and Mechanics', vol. **2**(2), p52 – 61.

Ambethkar, V. (2009), Numerical solutions of heat and mass transfer effects of an unsteady MHD free convective flow past an infinite vertical plate with constant suction and heat source or sink, 'International Journal of Applied Mathematics and Mechanics', vol.**5**(3), p96-115.

Anjali Devi, S. P. and Wilfred Samuel Raj, J. (2011), Thermo diffusion effects on unsteady hydromagnetic free convection flow with heat and mass transfer past a moving vertical plate with time dependent suction and heat source in a slip flow regime, 'International Journal of Applied Mathematics and Mechanics', vol.**7**(21), p20-51.

Bhavana, M. , Chenna Kesavaiah, D. and Sudhakaraiah, A. (2013), The soret effect on free convective unsteady MHD flow over a vertical plate with heat source, 'International Journnal of Innovative Research in Science, Engineering and Technology', vol.**2**(5), p1617-1628.

Emad M Abo-Eldahab and Mohaned A ElAziz (2000), Hall and ion-slip effects on MHD free convective heat generating flow past a semi-infinite vertical flat plate, 'Physica Scripta', vol.**61**, No. 3, p344.

Emad M. Aboeldahab and Elsayed M.E. Elbarbary (2001), Hall current effect on magnetohydrodynamic free convection flow past a semi infinite vertical plate with mass transfer, 'International Journal of Engineering Science', vol.**39**, p1641-1652.

Ghara, N., Guria, M. and Jana, R. N. (2012), Hall Effect on oscillating flow due to eccentrically rotating porous disk and a fluid at infinity, 'Meccanica', vol.**47**, p557–571.

Hayat, T. and Abbas, Z. (2007), Effects of Hall current and heat transfer on the flow in a porous medium with slip condition, 'Journal of Porous Media', vol.**10**, No. 1, p35–50.

Khaled K. Jaber (2016), Effect of viscous dissipation on flow over a stretching porous sheet subjected to power law heat flux in presence of heat source, 'International Journal of Modern Mathematical Sciences', vol.**14**(3), p212-220.

Murali Gundagani (2015), Unsteady MHD free convection viscous dissipative flow past an infinite vertical plate with constant suction and heat source/sink, 'Journal of Science and Arts', No.1(**30)**, p89-98.

Nazibuddin Ahmed and Sujit Talukdar (2012), MHD couette flow with heat transfer in presence of constant heat source, 'International Journal of Engineering Science and Technology, vol.**4**, No.06, p2887-2897.

Ram, P.C.(1991), MHD convective flow in a rotating fluid with Hall and ion-slip current , 'Wfirme- und Stofffibertragung', vol.**26**, p203-205.

Seth, G. S., Nandkeolyar, R. and Ansari, M. S. (2011), Effect of rotation on unsteady hydromagnetic natural convection flow past an impulsively moving vertical plate with ramped temperature in a porous medium with thermal diffusion and heat absorption, 'International Journal of Applied Mathematics and Mechanics,vol.**7**(21), p52-69.

Seth, G. S., Nandkeolyar, R. and Ansari, Md. S. (2012), Effects of Hall current and rotation on unsteady MHD couette flow in the presence of an inclined magnetic field, 'Journal of Applied Fluid Mechanics', vol.**5**, No. 2, p67-74.

Smita Sharma, Jitendra Singh and Singh, B. B. (2015), Effects of Hall current on transient convective MHD flow through porous medium past an infinite vertical oscillating plate with temperature gradient dependent heat source, 'IOSR Journal of Mathematics', vol.**11**(4), p42-47.

Chapter 5

5.1 Effect of Hall and ion-slip currents on MHD heat and mass transfer flow past a vertical plate with high porosity medium in a rotating system

The convection flow on a vertical surface embedded in porous media occurs in many important engineering problems such as in the design of pebble-bed nuclear reactors, catalytic reactors and compact heat exchangers, in geothermal energy convection, in petroleum reservoirs, in use of fibrous materials in the thermal insulation of buildings, in the heat transfer from a storage of agricultural products. It was shown by *Gebhart* (1962) that the viscous dissipation effect plays an important role in natural convection in viscous devices that are subjected to large deceleration or which operate at high rotative speeds and also in strong gravitational field processes on large scales (on large planets) and geological process. Hall and ion-slip currents are important and they have a marked effect on the magnitude and direction of the current density and consequently on the magnetic force term. The problem of MHD free convection flow with Hall and ion-slip currents has many important engineering applications, e.g. in power generators, Hall accelerators and flows in channels and ducts. *Jasem et al.* (2006) analyzed double diffusive convection of a rotating fluid over a surface embedded in a thermally stratified high porosity medium. *Ajay and Rama* (2009) studied the free convection heat and mass transfer with Hall current, Joule heating and thermal diffusion. *Hemant and Chaudhary* (2010) have studied MHD free convection and mass transfer flow over an infinite vertical plate with viscous dissipation. *Bhuvannvijaya and Mallikarjuna* (2014) investigated the effect of variable thermal conductivity on convective heat and mass transfer over a vertical plate in a rotating system with variable porosity regime. *Rachna* (2013) studied the heat and mass transfer along an accelerated vertical porous plate in the influence of various dissipation, heat source and variable suction. *Foisal and Alam* (2016) studied unsteady free convection fluid flow over an inclined plate in the presence of a magnetic field with thermally stratified high porosity medium. *Mahender and Srikanth* (2015) analyzed unsteady MHD free convection and mass transfer flow past a porous plate in presence of viscous dissipation. *Ferdows et al.* (2010) studied Dufour, Soret and viscous dissipation effects on heat and mass transfer in porous media with high porosities. The effects of variable properties and Hall current on steady MHD laminar convective fluid due to a porous rotating disk was studied by *Maleque and Sattar* (2005). *Das et al.* (2013) studied Hall effect on MHD free convection boundary layer flow past a vertical flat plate. *Khaled* (2014) discussed the effects of viscous dissipation and joule heating on MHD flow of a fluid with variable properties past a stretching vertical plate. Hydromagnetic rotating flow in a porous medium with slip condition and Hall current was investigated by *Farhad et al.* (2012). Viscous dissipation, Soret and Dufour effect on free convection heat and mass transfer from vertical surface in a porous

medium was studied by *Srinivas et al.* (2015). *Ali et al.* (2005) investigated natural convection flow in a rotating fluid over a vertical plate embedded in a thermally stratified high porosity medium. *Chen et al.* (1987) investigated transient natural convection on a vertical flat plate embedded in a high porosity medium.

Hence our aim is to investigate the effect of Hall and ion-slip currents on MHD heat and mass transfer flow past a vertical plate with high porous medium in a rotating system have been considered. Also the effects of different flow parameters encountered in the equations are investigated. The problem is governed by system of coupled nonlinear partial differential equations whose exact solution is difficult to obtain. Hence the problem is solved by finite difference method and is presented graphically.

5.1.1 Governing Equations

Consider the unsteady MHD free convection flow of an electrically conducting incompressible viscous fluid past an infinite vertical porous plate $y = 0$ has been considered. The flow is assumed to be in the $x-$axis which is taken along the plate in the upward direction. Let the fluid and the plate be in a rotation with uniform angular velocity Ω about the $y-$axis normal to the plate. A strong magnetic field $\mathbf{B}$ is imposed along $y-$axis and the plate is taken electrically non-conducting. Since the plate is infinite in extent, all physical quantities are functions of y and t only. Using the relation $\overline{\nabla}\cdot\mathbf{B}=0$ for the magnetic field $\mathbf{B}=(B_x,B_y,B_z)$, then obtain $B_y = B_0$ everywhere in the fluid (B_0 is a constant). The induced magnetic field is neglected, since the magnetic Reynolds number of a partially-ionised fluid is very small. If $\mathbf{J}=(J_x,J_y,J_z)$ is the current density, from the relation $\overline{\nabla}.\mathbf{J}=0$ gives $J_y =$ constant. Since the plate is electrically non-conducting, $J_y = 0$ at the plate and hence zero everywhere. The physical configuration of the problem is shown in Fig.5.1A. However, for such a fluid, the hall and ion-slip currents will significantly affected the flow in presence of large magnetic fields. The equations which govern the flow under the above consideration and Boussinesq's approximation are as follows:

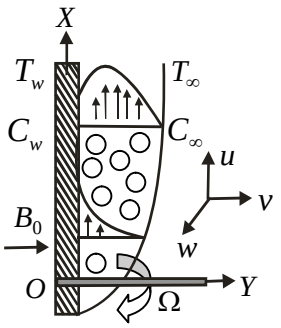

Fig.5.1A Physical configuration and coordinate system

Continuity equation; $\dfrac{\partial v}{\partial y} = 0$ (5.1.1)

Momentum equation;

$$\frac{1}{£^2}\left(\frac{\partial u}{\partial t}+v\frac{\partial u}{\partial y}\right)=\frac{¾}{£}\frac{\partial^2 u}{\partial y^2}+g_0\ \ (T-T_\infty)+g_0\ \ ^*(C-C_\infty)+2\Omega w-\frac{¾}{k}u-cu^2 - \frac{±_e B_0^2}{°\left(~_e^2+\ \ _e^2\right)}\left(~_e u+\ \ _e w\right) \tag{5.1.2}$$

$$\frac{1}{£^2}\left(\frac{\partial w}{\partial t}+v\frac{\partial w}{\partial y}\right)=\frac{³}{£}\frac{\partial^2 w}{\partial y^2}-2\Omega u-\frac{³}{k}w-cw^2+\frac{±_e B_0^2}{°\left(\sim_e^2+\ _e^2\right)}\left(\ _e u-\sim_e w\right) \tag{5.1.3}$$

Energy equation;

$$\frac{\partial T}{\partial t}+v\frac{\partial T}{\partial y}=\frac{©}{°c_p}\frac{\partial^2 T}{\partial y^2}+\frac{³}{c_p}\left[\left(\frac{\partial u}{\partial y}\right)^2+\left(\frac{\partial w}{\partial y}\right)^2\right]+\frac{±_e B_0^2}{°c_p\left(\sim_e^2+\ _e^2\right)}\left(u^2+w^2\right) \tag{5.1.4}$$

Concentration equation;

$$\frac{\partial C}{\partial t}+v\frac{\partial C}{\partial y}=D_m\frac{\partial^2 C}{\partial y^2}+\frac{D_m k_T}{T_m}\frac{\partial^2 T}{\partial y^2} \tag{5.1.5}$$

where the variables and related quantities are defined in the Nomenclature.

The initial and boundary conditions for the model are as follows;

$$t\le 0,\ \ u(y,t)=0, w(y,t)=0, T(y,t)=T_\infty, C(y,t)=C_\infty \qquad \text{everywhere} \tag{5.1.6}$$

$$\begin{aligned} &t>0,\ u(y,t)=U_0, w(y,t)=0, T(y,t)=T_w, C(y,t)=C_w \ \ at\ \ y=0\\ &u(y,t)=0, w(y,t)=0, T(y,t)=T_\infty, C(y,t)=C_\infty \quad at\ \ y\to\infty \end{aligned} \tag{5.1.7}$$

5.1.2 Mathematical Formulation

Now a convenient solution of equation (1) is

$$v=-v_0 \text{ (constant)} \tag{5.1.8}$$

where the constant v_0 represents the normal velocity at the plate which is positive or negative for suction or blowing.

Using equation (5.1.8), the equations (5.1.2)-(5.1.5) become

Momentum Equation:

$$\begin{aligned} \frac{1}{£^2}\left(\frac{\partial u}{\partial t}-v_0\frac{\partial u}{\partial y}\right)=&\frac{³}{£}\frac{\partial^2 u}{\partial y^2}+g_0\ \ \left(T-T_\infty\right)++g_0\ \ ^*\left(C-C_\infty\right)+2\Omega w-\frac{³}{k}u-cu^2\\ &-\frac{±_e B_0^2}{°\left(\sim_e^2+\ _e^2\right)}\left(\sim_e u+\ \ _e w\right) \end{aligned} \tag{5.1.9}$$

$$\frac{1}{£^2}\left(\frac{\partial w}{\partial t}-v_0\frac{\partial w}{\partial y}\right)=\frac{³}{£}\frac{\partial^2 w}{\partial y^2}-2\Omega u-\frac{³}{k}w-cw^2+\frac{±_e B_0^2}{°\left(\sim_e^2+\ _e^2\right)}\left(\ _e u-\sim_e w\right) \tag{5.1.10}$$

Energy equation:

$$\frac{\partial T}{\partial t}-v_0\frac{\partial T}{\partial y}=\frac{©}{°c_p}\frac{\partial^2 T}{\partial y^2}+\frac{³}{c_p}\left[\left(\frac{\partial u}{\partial y}\right)^2+\left(\frac{\partial w}{\partial y}\right)^2\right]+\frac{±_e B_0^2}{°c_p}\left(u^2+w^2\right) \tag{5.1.11}$$

Concentration equation:

$$\frac{\partial C}{\partial t}-v_0\frac{\partial C}{\partial y}=D_m\frac{\partial^2 C}{\partial y^2}+\frac{D_m k_T}{T_m}\frac{\partial^2 T}{\partial y^2} \tag{5.1.12}$$

The initial and boundary conditions for the model are as follows;

$$t\le 0,\ \ u(y,t)=0, w(y,t)=0, T(y,t)=T_\infty, C(y,t)=C_\infty \qquad \text{everywhere} \tag{5.1.13}$$

$$\begin{aligned} &t>0,\ u(y,t)=U_0, w(y,t)=0, T(y,t)=T_w, C(y,t)=C_w \ \ at\ \ y=0\\ &u(y,t)=0, w(y,t)=0, T(y,t)=T_\infty, C(y,t)=C_\infty \quad at\ \ y\to\infty \end{aligned} \tag{5.1.14}$$

For the purpose of solving the system of equation numerically, the transformation of governing equations into non-dimensional variables is introduced as follows;

$$Y = \frac{yU_0}{\text{3}}, U = \frac{u}{U_0}, W = \frac{w}{U_0}, \text{²} = \frac{tU_0^2}{\text{3}}, \overline{T} = \frac{T - T_\infty}{T_w - T_\infty}, \overline{C} = \frac{C - C_\infty}{C_w - C_\infty} \tag{5.1.15}$$

Thus introducing the relation (5.1.15) in equations (5.1.9)-(5.1.12), the following dimensionless differential equations have been obtained as follows;

$$\frac{\partial U}{\partial \text{²}} - \text{a}\frac{\partial U}{\partial Y} = \text{£}\frac{\partial^2 U}{\partial Y^2} + \text{£}^2 G_r \overline{T} + \text{£}^2 G_m \overline{C} + 2\text{£}^2 RW - \text{£}^2 \text{¥} U - \text{£}^2 \Gamma\left(U^2 + W^2\right) - \frac{M\text{£}^2\left(\sim_e U + \ _e W\right)}{\left(\sim_e^2 + \ _e^2\right)} \tag{5.1.16}$$

$$\frac{\partial W}{\partial \text{²}} - \text{a}\frac{\partial W}{\partial Y} = \text{£}\frac{\partial^2 W}{\partial Y^2} - 2\text{£}^2 RU - \text{£}^2 \text{¥} W - \text{£}^2 \Gamma\left(U^2 + W^2\right) + \frac{M\text{£}^2\left(\ _e U - \sim_e W\right)}{\left(\sim_e^2 + \ _e^2\right)} \tag{5.1.17}$$

$$\frac{\partial \overline{T}}{\partial \text{²}} - \text{a}\frac{\partial \overline{T}}{\partial Y} = \frac{1}{P_r}\frac{\partial^2 \overline{T}}{\partial Y^2} + E_c\left[\left(\frac{\partial U}{\partial Y}\right)^2 + \left(\frac{\partial W}{\partial Y}\right)^2\right] + \frac{ME_c\left(U^2 + W^2\right)}{\left(\sim_e^2 + \ _e^2\right)} \tag{5.1.18}$$

$$\frac{\partial \overline{C}}{\partial \text{²}} - \text{a}\frac{\partial \overline{C}}{\partial Y} = \frac{1}{S_c}\frac{\partial^2 \overline{C}}{\partial Y^2} + S_0\frac{\partial^2 \overline{T}}{\partial Y^2} \tag{5.1.19}$$

where $\text{a}\left(= \frac{v_0}{U_0}\right)$, $G_r\left(= \frac{g_0\ \ (T_w - T_\infty)\text{³}}{U_0^2}\right)$, $G_m\left(= \frac{g_0\ \ ^*(C_w - C_\infty)\text{³}}{U_0^2}\right), M\left(= \frac{\pm_e B_0^2 \text{³}}{\text{°}U_0^2}\right)$,

$P_r\left(= \frac{\text{°}\,\text{³}c_p}{\text{©}}\right)$, $S_c\left(= \frac{\text{³}}{D_m}\right)$, $S_0\left(= \frac{D_m k_T\left(T_w - T_\infty\right)}{\text{³}T_m\left(C_w - C_\infty\right)}\right)$, $R\left(= \frac{\Omega\text{³}}{U_0^2}\right)$, $\text{¥}\left(= \frac{\text{³}\ ^2}{kU_0^2}\right)$, $\Gamma\left(= \frac{c\text{³}}{U_0}\right)$,

$E_c\left(= \frac{U_0^2}{c_p\left(T_w - T_\infty\right)}\right)$.

The corresponding initial and boundary conditions are as follows;

$$\text{²} \le 0,\ U = 0,\ W = 0,\ \overline{T} = 0,\ \overline{C} = 0 \qquad \text{everywhere} \tag{5.1.20}$$

$$\begin{aligned} \text{²} > 0,\ \ & U(Y,\text{²}) = 1, W(Y,\text{²}) = 0, \overline{T}(Y,\text{²}) = 1,\ \overline{C}(Y,\text{²}) = 1 \ \ at\ Y = 0 \\ & U(Y,\text{²}) = 0, W(Y,\text{²}) = 0, \overline{T}(Y,\text{²}) = 0, \overline{C}(Y,\text{²}) = 0 \ \ at\ Y \to \infty \end{aligned} \tag{5.1.21}$$

5.1.3 Solution Technique

The governing second order non-linear coupled partial differential equations have been solved with the associated initial and boundary conditions. For solving a transient free convection flow with mass transfer past an infinite plate, the implicit finite difference method has been used by *Callahan and Marner* (1976) which is conditional stable. On the contrary, the same problem has been studied by *Soundalgekar and Ganesan* (1980) by an implicit finite difference method which is fast convergent and unconditional stable. But *Callahan and Marner* (1976), *Soundalgekar and Ganesan* (1980) have been found same result using different methods on the same problem.

From the concept of the above discussion, for simplicity the implicit finite difference method has been used to solve the equations (5.1.16)-(5.1.19) with boundary conditions (5.1.20)-(5.1.21). To solve the non-dimensional system of equations by implicit finite

difference technique, a set of finite difference equations is required. In this case, the region within the boundary layer is divided by some perpendicular lines of Y-axis, where Y-axis is normal to the medium is shown Fig.5.1.B. It is assumed that the maximum length of boundary layer is $Y_{\max}(=50)$ as corresponds to $Y \to \infty$ i.e. Y varies from 0 to 50 and number of grid spacing in Y-direction is $m(=400)$, hence the constant mesh size along Y-axis becomes $\Delta Y = 0.13(0 \le Y \le 50)$ with a smaller time step $\Delta t = 0.001$.

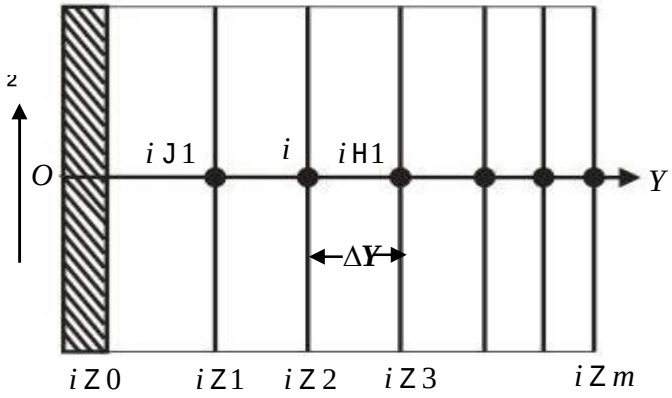

Fig.5.1B Finite difference grid space

Let $U^n, W^n, \bar{T}^n$ and $\bar{C}^n$ denoted the values of $U, W, \bar{T}$ and $\bar{C}$ at the end of a time-step respectively. Using the implicit finite difference approximation into the partial differential equations (5.1.16)-(5.1.19), the following set of difference equations are as follows;

$$\frac{U_i^{n+1}-U_i^n}{\Delta t} - a\frac{U_{i+1}^n - U_i^n}{\Delta Y} = \frac{U_{i+1}^n - 2U_i^n + U_{i-1}^n}{(\Delta Y)^2} + G_r \bar{T}_i^n + G_m \bar{C}_i^n + 2RW_i^n - \phi^2 U_i^n - \phi^2 (U_i^n)^2 \Gamma - \frac{\phi^2 M}{\sigma_e^2 + m_e^2}(\sigma_e U_i^n + m_e W_i^n) \tag{5.1.22}$$

$$\frac{W_i^{n+1}-W_i^n}{\Delta t} - a\frac{W_{i+1}^n - W_i^n}{\Delta Y} = \frac{W_{i+1}^n - 2W_i^n + W_{i-1}^n}{(\Delta Y)^2} - 2RU_i^n - \phi^2 W_i^n - \phi^2 (W_i^n)^2 \Gamma + \frac{\phi^2 M}{\sigma_e^2 + m_e^2}(m_e U_i^n - \sigma_e W_i^n) \tag{5.1.23}$$

$$\frac{\bar{T}_i^{n+1}-\bar{T}_i^n}{\Delta t} - a\frac{\bar{T}_{i+1}^n - \bar{T}_i^n}{\Delta Y} = \frac{1}{P_r}\frac{\bar{T}_{i+1}^n - 2\bar{T}_i^n + \bar{T}_{i-1}^n}{(\Delta Y)^2} + E_c\left[\left(\frac{U_{i+1}^n - U_i^n}{\Delta Y}\right)^2 + \left(\frac{W_{i+1}^n - W_i^n}{\Delta Y}\right)^2\right] + \frac{ME_c\left(U_i^{n2} + W_i^{n2}\right)}{\left(\sigma_e^2 + m_e^2\right)} \tag{5.1.24}$$

$$\frac{\bar{C}_i^{n+1}-\bar{C}_i^n}{\Delta t} - a\frac{\bar{C}_{i+1}^n - \bar{C}_i^n}{\Delta Y} = \frac{1}{S_c}\frac{\bar{C}_{i+1}^n - 2\bar{C}_i^n + \bar{C}_{i-1}^n}{(\Delta Y)^2} + S_0\frac{\bar{T}_{i+1}^n - 2\bar{T}_i^n + \bar{T}_{i-1}^n}{(\Delta Y)^2} \tag{5.1.25}$$

The initial and boundary conditions with the finite difference scheme are as follows;

$$U_i^0 = 0,\ W_i^0 = 0,\ \bar{T}_i^0 = 1,\ \bar{C}_i^0 = 1 \tag{5.1.26}$$

$$U_0^n = 1, W_0^n = 0, \bar{T}_0^n = 1,\ \bar{C}_0^n = 1$$
$$U_L^n = 0, W_L^n = 0, \bar{T}_L^n = 0, \bar{C}_L^n = 0 \text{ where } L \to \infty \tag{5.1.27}$$

Here the subscripts i designate the grid points with Y-coordinates and superscript n represents a value of time, $t = \bar{n}\Delta t$ where $\bar{n} = 0,1,2,3,\ldots$. The primary velocity (U), secondary velocity (W), temperature $(\bar{T})$ and concentration $(\bar{C})$ distributions at all interior nodal points

may be computed by successive applications of the above finite difference equations. The obtained values are discussed graphically which are shown in Figs. 5.1.3(a) to 5.1.44(a) respectively for various parameters.

5.1.4 Stability and Convergence Analysis

The analysis will remain incomplete unless discussion the stability and convergence of the finite different scheme. For the constant mesh sizes, the stability criteria of the scheme may be established as follows. The general terms of the Fourier expansion for $U, W, \overline{T}, \overline{C}$ at a time are all arbitrarily called $² = 0$ are $e^{i\sim Y}$ apart from a constant, where $i = \sqrt{-1}$. At a time ² later, these terms become

$$\begin{aligned} U &: \cdot(²)e^{i\sim Y} \\ W &: ¶(²)e^{i\sim Y} \\ \overline{T} &: \overline{\ }(²)e^{i\sim Y} \\ \overline{C} &: ¤(²)e^{i\sim Y} \end{aligned} \tag{5.1.28}$$

Substituting (5.1.28) into equations (5.1.22)-(5.1.25), over any one time step and denoting the values after the time step by $\cdot', ¶', \overline{\ }'$ and $¤'$ gives after simplifications

$$\cdot' = A\cdot + B¶ + C\overline{\ } + D¤ \tag{5.1.29}$$

$$¶' = E¶ + F\cdot \tag{5.1.30}$$

$$\overline{\ }' = G\overline{\ } + H\cdot + I¶ \tag{5.1.31}$$

$$¤' = J\overline{\ } + K¤ \tag{5.1.32}$$

where

$$A = 1 + \frac{ª\left(e^{\sim i\Delta Y} - 1\right)\Delta²}{\Delta Y} + \frac{2£\left(\cos\sim\Delta Y - 1\right)}{\left(\Delta Y\right)^2} - £^2¥\,\Delta² - £^2\Gamma U\Delta² - \frac{£^2 M\sim_e \Delta²}{\sim_e^2 + \ _e^2},$$

$$B = 2£^2 R\Delta² - \frac{£^2 M\ _e\Delta²}{\sim_e^2 + \ _e^2},$$

$$C = £^2 G_r\Delta²\ ,$$

$$D = £^2 G_m\Delta²\ ,$$

$$E = 1 + ª\Delta²\,\frac{\left(e^{i\sim\Delta Y} - 1\right)}{\Delta Y} + £\Delta²\,\frac{2\left(\cos\sim\Delta Y - 1\right)}{\left(\Delta Y\right)^2} - £^2¥\Delta² - \Delta²£^2\Gamma W - \frac{\Delta² M£^2\sim_e}{\sim_e^2 + \ _e^2},$$

$$F = 2£^2 R\Delta² + \frac{£^2 M\ _e\Delta²}{\sim_e^2 + \ _e^2}$$

$$G = 1 + ª\Delta²\,\frac{e^{i\sim\Delta Y} - 1}{\Delta Y} + \frac{1}{P_r}\frac{2\left(\cos\sim\Delta Y - 1\right)}{\left(\Delta Y\right)^2},$$

$$H = E_c U\left(\frac{e^{\sim Y} - 1}{\Delta Y}\right)^2 + \frac{ME_c U}{\sim_e^2 + \ _e^2},$$

$$I = E_c W\left(\frac{e^{\sim Y} - 1}{\Delta Y}\right)^2 + \frac{ME_c W}{\left(\sim_e^2 + \ _e^2\right)},\ J = S_0\,\frac{2\Delta²}{\left(\Delta Y\right)^2}\left(\cos\sim\Delta Y - 1\right),$$

$$K = 1 + \text{ª}\,\frac{\Delta^2}{\Delta Y}\left(e^{i\sim\Delta Y} - 1\right) + \frac{1}{S_c}\frac{2\Delta^2}{(\Delta Y)^2}\left(\cos\sim\Delta Y - 1\right)$$

The equations (5.1.29) -(5.1.32) can be written in the following matrix form;

$$\begin{pmatrix} \cdot' \\ \P' \\ \bar{} \\ \text{¤}' \end{pmatrix} = \begin{pmatrix} A & B & C & D \\ F & E & 0 & 0 \\ H & I & G & 0 \\ 0 & 0 & J & K \end{pmatrix} \begin{pmatrix} \cdot \\ \P \\ \bar{} \\ \text{¤} \end{pmatrix}$$

i.e. $\text{¦}' = T\text{¦}$ where ¦ is the column vector with element $\cdot, \P, \bar{}$ and ¤. For stability, the modulus of each eigenvalue of the amplification matrix T must be unity.

Let $a = \dfrac{\Delta^2}{\Delta Y}$ and $b = \dfrac{\Delta^2}{(\Delta Y)^2}$ then

$$A = 1 - a\text{ª} - 2b\text{£} + \text{ª}ae^{i\sim\Delta Y} + 2b\text{£}\cos\sim\Delta Y - \text{£}^2\text{¥}\Delta^2 - \text{£}^2\Gamma U\Delta^2 - \frac{\text{£}^2 M\sim_e \Delta^2}{\sim_e^2 + \ _e^2}$$

$$E = 1 - a\text{ª} - 2b\text{£} + \text{ª}ae^{i\sim\Delta Y} + 2b\text{£}\cos\sim\Delta Y - \text{£}^2\text{¥}\Delta^2 - \text{£}^2\Gamma W\Delta^2 - \frac{\text{£}^2 M\sim_e \Delta^2}{\sim_e^2 + \ _e^2}$$

$$G = 1 - \text{ª}a - \frac{2b}{P_r} + \text{ª}ae^{i\sim\Delta Y} + \frac{2b\cos\sim\Delta Y}{P_r},$$

$$K = 1 - \text{ª}a - \frac{2b}{S_c} + \text{ª}ae^{i\sim\Delta Y} + \frac{2b\cos\sim\Delta Y}{S_c},$$

The coefficients a and b are all real and nonnegative. Then demonstrate that the maximum modulus of A, E, G and K occur when $\sim\Delta Y = m\text{®}$, where m is an integers and hence A, E, G and K are real. For Δ^2 sufficiently large, the value of $|A|, |E|, |G|$ and $|K|$ are greatest when m is odd integer, in which case

$$A = (1 - a\text{ª} - 2b\text{£}) + (-\text{ª}a - 2b\text{£} - \text{£}^2\text{¥}\Delta^2 - \text{£}^2\Gamma U\Delta^2 - \frac{\text{£}^2 M\sim_e \Delta^2}{\sim_e^2 + \ _e^2}),$$

$$E = (1 - a\text{ª} - 2b\text{£}) + (-\text{ª}a - 2b\text{£} - \text{£}^2\text{¥}\Delta^2 - \text{£}^2\Gamma W\Delta^2 - \frac{\text{£}^2 M\sim_e \Delta^2}{\sim_e^2 + \ _e^2}),$$

$$G = (1 - \text{ª}a - \frac{2b}{P_r}) + (-\text{ª}a - \frac{2b}{P_r}),$$

$$K = (1 - \text{ª}a - \frac{2b}{S_c}) + (-\text{ª}a - \frac{2b}{S_c}).$$

To satisfy $|A| \le 1, |E| \le 1, |G| \le 1$ and $|K| \le 1$ the most negative allowable values are $A = -1, E = -1, G = -1, K = -1$.

Hence the stability conditions are

$$\text{ª}a + \frac{2b}{P_r} \le 1$$

$$\text{ª}a + \frac{2b}{S_c} \le 1$$

$$^{a}a + 2b£ + \frac{1}{2}£^{2}¥\Delta^{2} + \frac{1}{2}£^{2}\Gamma U\Delta^{2} + \frac{1}{2}\frac{£^{2}M\sim_{e}\Delta^{2}}{\sim_{e}^{2} + \ _{e}^{2}} \le 1$$

$$^{a}a + 2b£ + \frac{1}{2}£^{2}¥\Delta^{2} + \frac{1}{2}£^{2}\Gamma W\Delta^{2} + \frac{1}{2}\frac{£^{2}M\sim_{e}\Delta^{2}}{\sim_{e}^{2} + \ _{e}^{2}} \le 1$$

5.1.5 Shear Stress, Nusselt number and Sherwood number

The quantities of chief physical interest are shear stress, Nusselt number and Sherwood number. The shear stress is generally known as the Skin friction, the following equations represent the shear stress at the plate. Shear stresses in x and z axes are as follows;

$^{2}_{U} = «\left(\frac{\partial u}{\partial y}\right)_{y=0}$ and $^{2}_{W} = «\left(\frac{\partial w}{\partial y}\right)_{y=0}$ which are proportional to $\left(\frac{\partial U}{\partial Y}\right)_{Y=0}$ and $\left(\frac{\partial W}{\partial Y}\right)_{Y=0}$.

From the temperature field, the effects of various parameters on the heat transfer coefficients have been studied. The following relations represent the heat transfer rate that is well known Nusselt number. Nusselt number is $N_u = -k\left(\frac{\partial T}{\partial y}\right)_{y=0}$ which is proportional to $\left(\frac{\partial \overline{T}}{\partial Y}\right)_{Y=0}$.

Also from the concentration field, the effects of various parameters on the mass transfer coefficients have been studied. The following relation represents the mass transfer rate that is well known as Sherwood number. The Sherwood number is $S_h = -D_m\left(\frac{\partial C}{\partial y}\right)_{y=0}$ which is proportional to $\left(\frac{\partial \overline{C}}{\partial Y}\right)_{Y=0}$.

The numerical values of the shear stress, Nusselt number and Sherwood number are calculated by five point approximate formula for the derivatives. Values of $^{2}_{U}$, $^{2}_{W}$, N_u and S_h are shown graphically in Figs. 5.1.3(b) to 5.1.44(b) respectively for various parameters.

5.1.6 Results and Discussion

5.1.6.1 Justification of Grid Space

The code is conversed with three different grid space, such as m Z 250,300,400 where m is the grid number. It is seen that there is a little change for the above mentioned grid points which are shown in Fig.5.1.1. For same power and time, the results of velocity, temperature and concentration distributions have been carried out for m Z 300.

5.1.6.2 Steady- State Solution

The numerical solutions of the non-linear differential equation (5.1.9)-(5.1.12) under the boundary conditions (5.1.14) have been performed by applying implicit finite difference method. In order to verify the effects of time step size Δ^{2}, the programming code is run our model with eight different step sizes as ^{2} Z 20,60,70,80,90,100,110,120. To get steady–state solutions, the computations have been carried out up to ^{2} Z 120. It is observed that, the result

of computations for $U, W, \overline{T}$ and $\overline{C}$, however show little changes after ² Z 100. Thus the solutions of all variables for ² Z 100 are essentially steady-state. Grid space and steady state solution are shown in Fig. 5.1.1 and Fig. 5.1.2 only for primary velocity for rotation parameter.

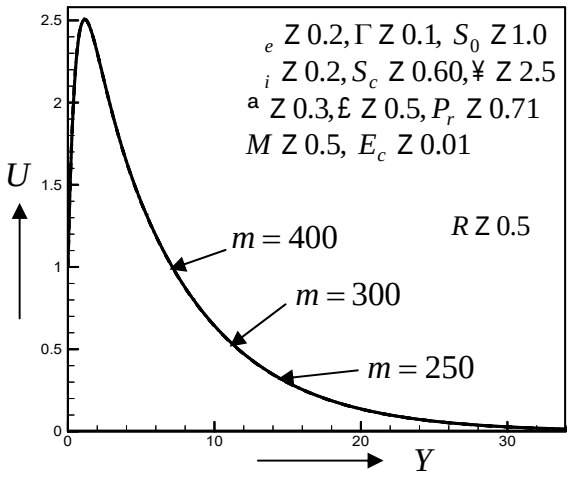

Fig.5.1.1 Primary velocity for different grid space of rotational parameter *R*

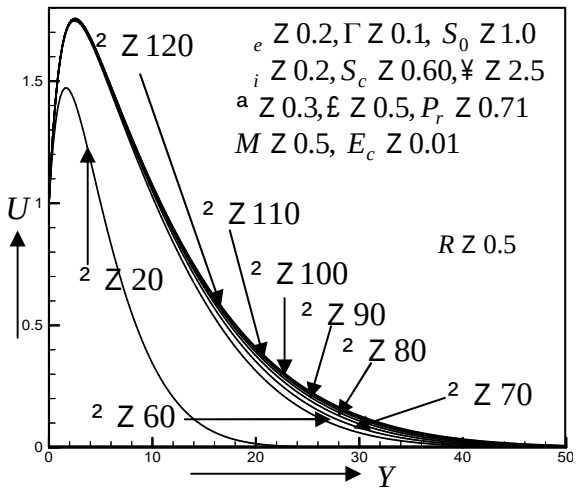

Fig.5.1.2 Primary velocity for different time step of rotation parameter *R*

The numerical solution was obtained for distributions of the dimensionless primary velocity (U), secondary velocity (W), temperature ($\overline{T}$), concentration ($\overline{C}$) as well as the shear stress in x-axis (²$_U$), shear stress in z-axis (²$_W$), Nusselt number (N_u) and Sherwood number (S_h). To study the behavior of these profiles are drawn for various values of the parameters that describe the flow, e.g. Hall parameter ($_e$), ion-slip parameter ($_i$), magnetic parameter (M), suction parameter (ª), permeability parameter (¥), prosity(£), inertial parameter (Γ), rotational parameter (R), Pramdtl number (P_r), Schmidt number(S_c), Soret numbrt (S_0), Grashof number(G_r)and modified Grashof number (G_m). The values of the Prandtl number are chosen $P_r = 0.71$ (Prandtl number for air at 20^0C), to $P_r = 1.0$ (Prandtl number for salt water at 20^0C), $P_r = 1.63$ (corresponds glycerin at 50^0C), which represent the specific condition of the flow. The values of the Schmidt number are chosen to represent the presence of species by $S_c = 0.6$ correspond to water vapor. In the calculation G_r and G_m are taken both positive. Throughout the calculations the values of G_r and G_m are taken to be large ($G_r = 5.0$ and $G_m = 2.0$). The values for the parameters are chosen arbitrarily in most cases.

It is observed that in Fig.5.1.3 (a,b) and Fig.5.1. 7(a,b), primary velocity (U) and shear stress in x-axis (²$_U$) are increased with an increase of Hall parameter $_e$ and ion-slip parameter $_i$. The effective conductivity decreases with the increase of $_e$ and $_i$ which reduces the magnetic damping force on primary velocity. Similar trend arises in secondary velocity W and shear stress in z-axis (²$_W$) with increasing $_e$ which is found in Fig. 5.1.4 (a,b). It is found that $_i$ has decreasing effect on W and ²$_W$ which is shown in Fig. 5.1.8 (a,b).

It is noted from Fig.5.1.5(a) and Fig. 5.1.9(a) that the temperature ($\overline{T}$) distribution decreases when $_e$ and $_i$ are increased and also thermal boundary layer thickness decreases whereas Nusselt number $\left[N_u \propto -\left(\frac{\partial \overline{T}}{\partial Y}\right)_{Y=0}\right]$ has opposite behavior which is shown in Fig.5.1.5(b) and Fig. 5.1.9(b). This is due to decrease in the thermal boundary layer thickness. Fig. 5.1. 6(a) and Fig. 5.1.10(a) illustrated that concentration increase near the plate and decrease far away from the plate with the increase of $_e$ and $_i$. So there is a cross flow in the boundary layer. While Sherwood number $\left[S_h \propto -\left(\frac{\partial \overline{C}}{\partial Y}\right)_{Y=0}\right]$ decreases which is shown in Fig. 5.1.6(b) and Fig. 5.1.10(b).

In Figs. 5.1.11(a,b), 5.1.12(a,b) and 5.1.13(a), it has been illustrated that primary velocity (U), shear stress in x-axis (^2_U), secondary velocity W , shear stress in z-axis (^2_W) and temperature distribution decrease with an increase of inertial parameter (Γ). The inertial parameter increases the resistance to the flow increases, causing the fluid flow in the porous medium to slow down. This results in reducing the net velocity and therefore, all its components as well as the wall friction. The temperature distribution decreases whereas Nusselt number increases with the increase of Γ which are found in Fig.5.1.13 (a,b). The concentration profiles has increasing effects near the plate while Sherwood number(S_h) decreases with an increase of Γ which are found in Fig. 5.1.14(a,b).

By analyzing the Fig. 5.1.15(a,b) it is clearly seen that the primary velocity (U), shear stress in x-axis (^2_U) profiles increase with increasing values of Eckert number (E_c).This is due to the heat energy stored in the liquid because of the frictional heating. But secondary velocity W , shear stress in z-axis (^2_W) profiles have reverse effect which are found in Fig. 5.1.16 (a,b). It is observed that increasing values of E_c is to increase the temperature distribution in flow region in Fig. 5.1.17(a). The viscous dissipation will lead to a heat generation inside the fluid. This is due to the fact that heat energy is stored in the fluid due to the frictional heating. Thus the effect of increasing E_c, is to enhance the temperature distribution inside the boundary layer. Nusselt number (N_u) has reverse effect which is shown in Fig. 5.1.17(b). From Fig. 5.1.18(a) it has been seen that the concentration profiles firstly decreases in the interval $0 \le Y \le 10$ and secondly increases $Y > 10$ with an increase (E_c). So there is obtained a cross flow inside the boundary layer. But Sherwood number (S_h) profiles increases with an increase of E_c which is found in Fig. 5.1.18(b).

Fig. 5.1.19(a,b) illustrate that the primary velocity (U), shear stress in x-axis (^2_U) increase with increasing values of porosity (£). Increasing porosity clearly serves to enhance the flow velocity i.e. accelerates the flow. Whereas secondary velocity W , shear stress in z-axis (^2_W) profiles have reverse effect which are found in Fig. 5.1.20 (a,b). It is found that temperature profile increases with increasing£ whereas Nusselt number decreases which are shown in Fig. 5.1.21(a,b). Also concentration profiles have minor

decreasing effects with an increase of £ which is found in Fig. 5.1.22(a). But Sherwood number (S_h) has increasing effect which is shown in Fig. 5.1.22(b).

From Fig. 5.1.23(a,b), it has been seen that the primary velocity U and shear stress in x-axis ($²_U$) decreases with an increase in magnetic parameter M. This is due to the fact that, the transverse magnetic field normal to the flow direction, has a tendency to create the drag known as the Lorentz force which tends to resist the flow. The secondary velocity W and the shear stress ($²_W$) increase with increase in M which has been illustrated in Fig. 5.1.24 (a,b). The result indicates that the resulting Lorentzian body force will not act as a drag force as in conventional MHD flows, but as an aiding body force. This will serve to accelerate the secondary fluid velocity. Temperature distributions increases with an increase in M in Fig. 5.1.25(a) whereas Nusselt number (N_u) has reverse effect which is shown in Fig. 5.1.25(b). As the magnetic parameter increases, all of the fluid thermal characteristics increase. It is also seen that the concentration profiles decrease firstly, and then start to increase with the increase of M. So there is a cross flow near $Y = 11.0$ (approximately) which is found in Fig. 5.1.26(a). The effects of a transverse magnetic field to an electrically conducting fluid gives rise to a resistive-type force called the Lorentz force. This force has the tendency to increase its concentration distributions. But Sherwood number (S_h) has increasing effect with increasing M which is shown in Fig. 5.1.26(b).

In Fig. 5.1.27 (a,b) illustrate that the primary velocity (U) and shear stress in x-axis ($²_U$) profiles decrease with the increase of Prandtl number(P_r). This is because in the free convection the plate velocity is higher than the adjacent fluid velocity and the momentum boundary layer thickness decreases. In Fig. 5.1.28 (a,b), the secondary velocity W and the shear stress $²_W$ are increased with an increase of P_r. In Fig.5.1.29 (a), the temperature profiles $\overline{T}$ decrease with an increase of P_r. If P_r increases, the thermal diffusivity decreases and these phenomena lead to the decreasing of energy ability that reduces the thermal boundary layer. The Nusselt number (N_u) has opposite behavior is shown in Fig.5.1.29 (b). The increase of Prandtl number means slow rate of thermal-diffusion. In Fig. 5.1.30(a) the concentration profiles increases firstly, then start to decrease with an increase P_r. So there is a cross flow near $Y = 10.0$. Whereas Sherwood number decreases with the increase of P_r which is shown in Fig.5.1.30 (b)

Fig. 5.1.31 (a,b) are displaying the effect of rotational parameter R on primary velocity U and shear stress in x-axis ($²_U$) are decreased with increase of R. In fact rotation parameter defines the relative magnitude of the Coriolis force and the viscous force, thus rotation retards primary flow and induces reverse flow in the boundary layer. Similar behaviors are found on secondary velocity W and shear stress in z-axis ($²_W$) which are shown in Fig.5.1.32 (a,b).

Fig.5.1.33 (a,b) shows that the primary velocity (U) and shear stress in x-axis ($²_U$) decrease with an increase of permeability parameter(¥). This is due to the fact that increasing the value of ¥ has tendency to resist the flow causing to reduce the thickness of the boundary layer whereas secondary velocity W and shear stress in z-axis ($²_W$) increase in magnitude

with increase of ¥ which is shown in Fig.5.1.34(a,b). The behavior of temperature distributions is clearly observed from Fig.5.1.35 (a), which shows that the temperature distributions decrease with increasing ¥ while Nusselt number has reverse effect which is found in Fig. 5.1.35(b). It is seen from Fig.5.1.36 (a) that the concentration distribution increases firstly, then start to decrease with an increase of ¥. So there is a cross flow near $Y = 11.0$ (approximately). This is due to the fact that increases in the concentration boundary layer thickness. But Sherwood number has opposite behavior which is shown in Fig.5.1.36 (b).

Fig.5.1.37 (a,b) are displaying that the primary velocity (U) and shear stress in x-axis ($²_U$) decrease with the increase of suction parameter (ª), expressing the fact that suction stabilized the boundary layer growth. But opposite behavior are found on secondary velocity W and shear stress in z-axis ($²_W$) with an increase of ª which are shown in Fig. 5.1.38(a,b). In Figs. 5.1.39(a), 5.1.40(a), it is seen that increasing ª decrease temperature and concentration distributions, which indicates that the thermal and concentration boundary layer thickness reduces while Nusselt and Sherwood numbers (N_u and S_h) increase which are shown in Figs. 5.1.39(b), 5.1.40(b).

From Fig. 5.1.41(a,b) it is found that the primary velocity(U) and shear stress in x-axis($²_U$) increase with an increase in Soret number S_0. This is because either a decrease in concentration difference or an increase in temperature difference leads to an increase in the value of S_0. Hence, increasing the S_0 increases the velocity of the fluid. But opposite behavior are found on secondary velocity (W)and shear stress in z-axis ($²_W$) which are shown in Fig.5.1.42 (a,b). It has been observed that there is increasing effects on the temperature ($\overline{T}$) distribution in Fig.5.1.43 (a) of increasing values of S_0. But Nusselt number (N_u) has decreased with an increase of S_0 in Fig. 5.1.43(b). Fig.5.1.44 (a) illustrates that the concentration ($\overline{C}$) distribution increases with an increase of S_0. The concentration boundary layer increases rapidly with increase of S_0 that signifies that S_0 can control concentration boundary layer. It has been seen that the Sherwood number has opposite behavior which is found in Fig.5.1.44 (b). This due to the fact that an increase in S_0 tends to thicken concentration boundary layer, thus decreasing the mass transfer rate at the wall.

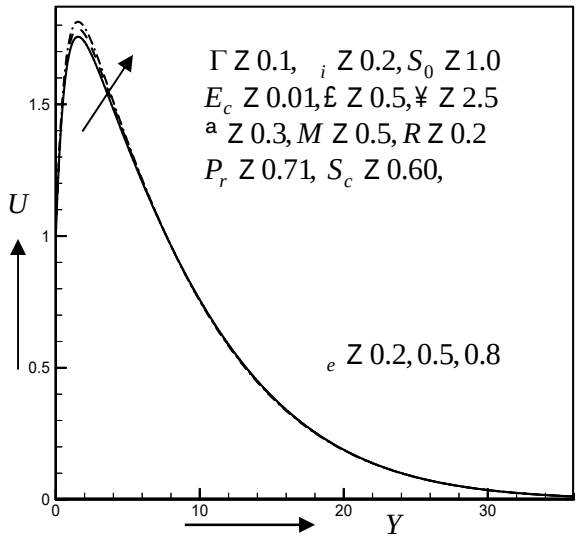

Fig. 5.1.3(a) Primary velocity profiles for different values of Hall parameter $_e$

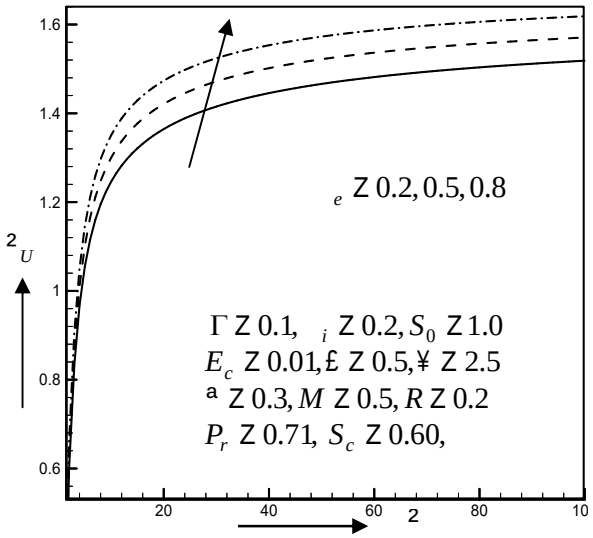

Fig. 5.1. 3(b) Shear stress in x-axis for different values of Hall parameter $_e$

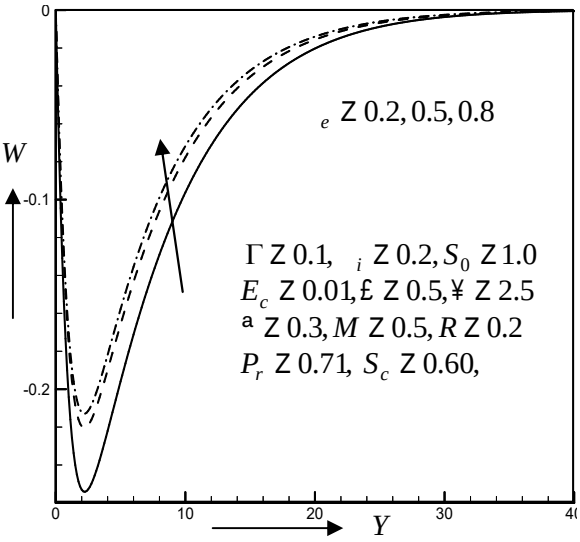

Fig. 5.1.4(a) Secondary velocity profiles for different values of Hall parameter $_e$

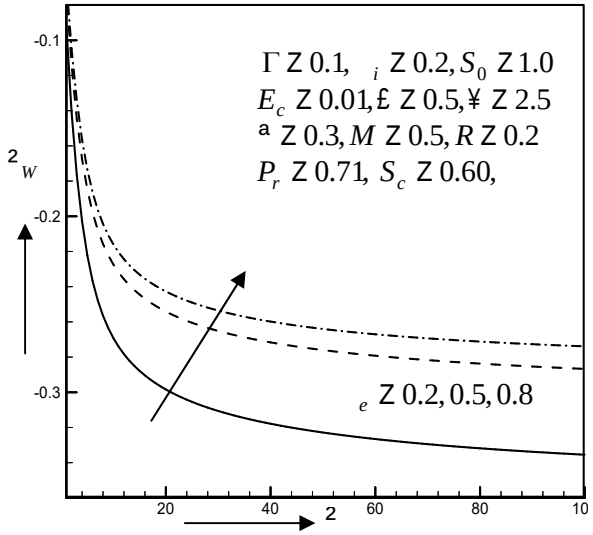

Fig. 5.1.4(b) Shear stress in z-axis for different values of Hall parameter $_e$

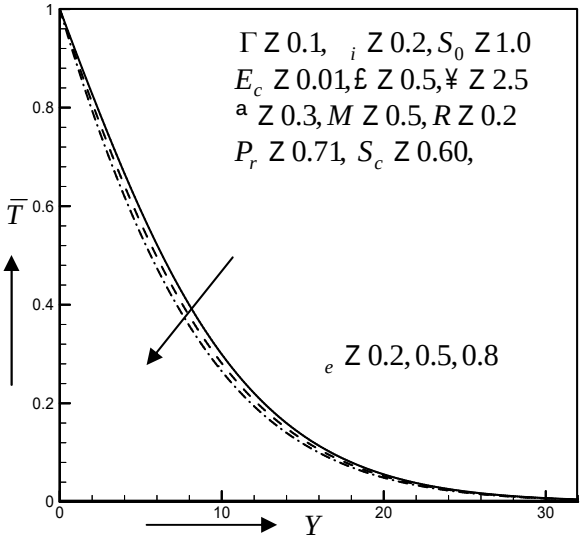

Fig. 5.1.5(a) Temperature velocity profiles for different values of Hall parameter $_e$

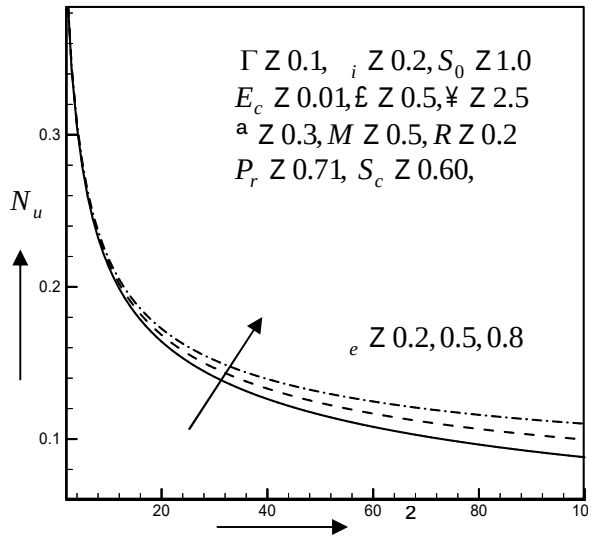

Fig. 5.1.5(b) Nusselt number profiles for different values of Hall parameter $_e$

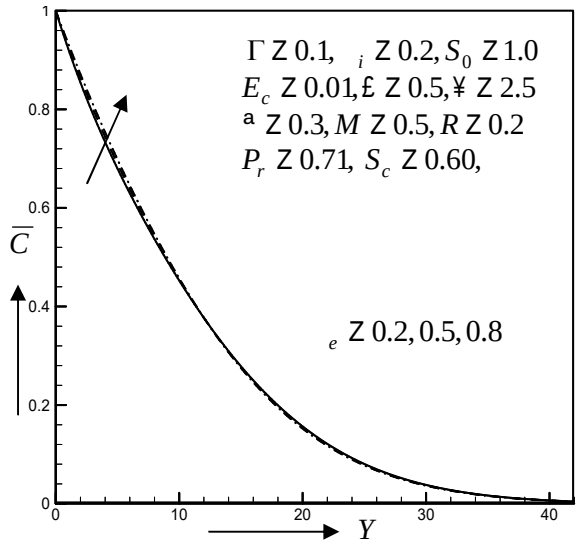

Fig. 5.1.6(a) Concentration profiles for different values of Hall parameter $_e$

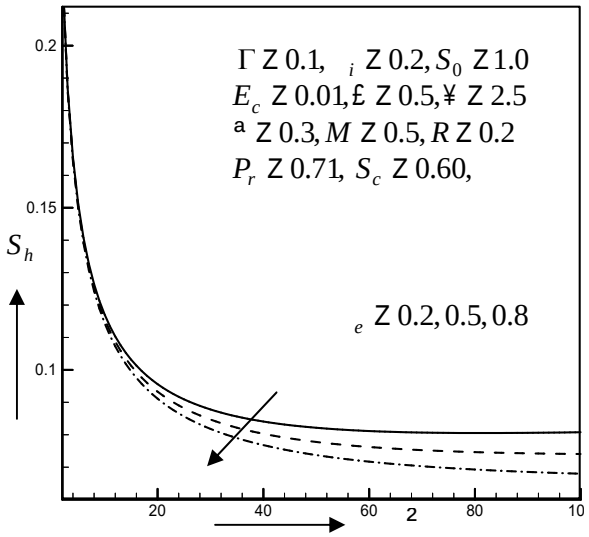

Fig. 5.1.6(b) Sherwood number profiles for different values of Hall parameter $_e$

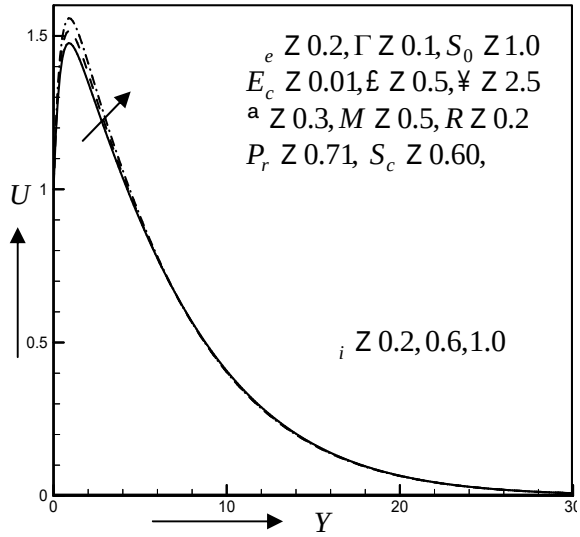

Fig. 5.1.7(a) Primary velocity profiles for different values of ion-slip parameter $_i$

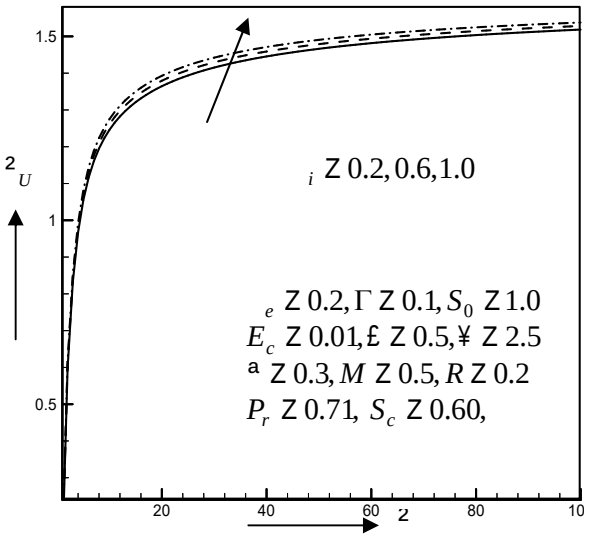

Fig. 5.1.7(b) Shear stress in x-axis for different values of ion-slip parameter $_i$

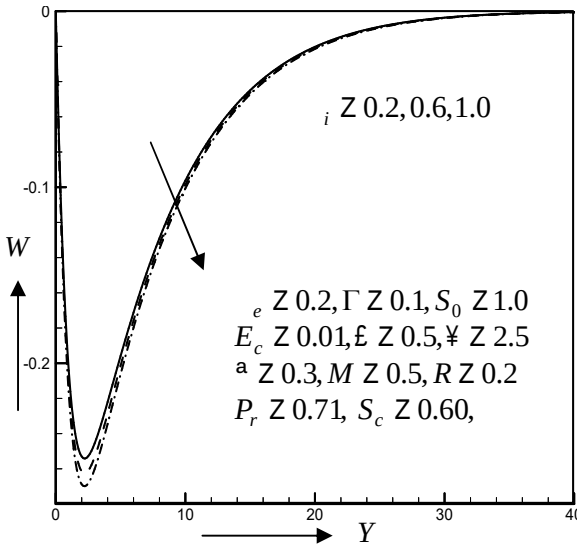

Fig. 5.1.8(a) Secondary velocity profiles for different values of ion-slip parameter $_i$

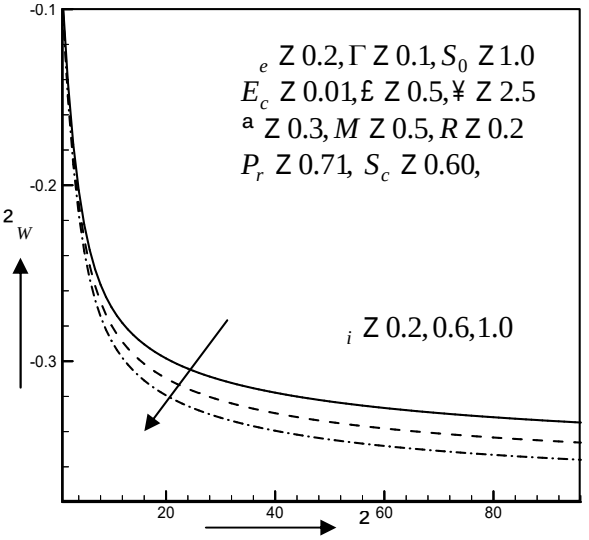

Fig. 5.1.8(b) Shear stress in z-axis for different values of ion-slip parameter $_i$

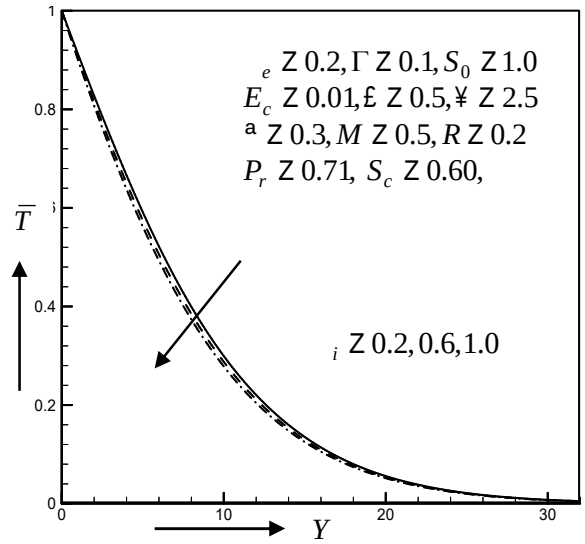

Fig. 5.1.9(a) Temperature profiles for different values of ion-slip parameter $_i$

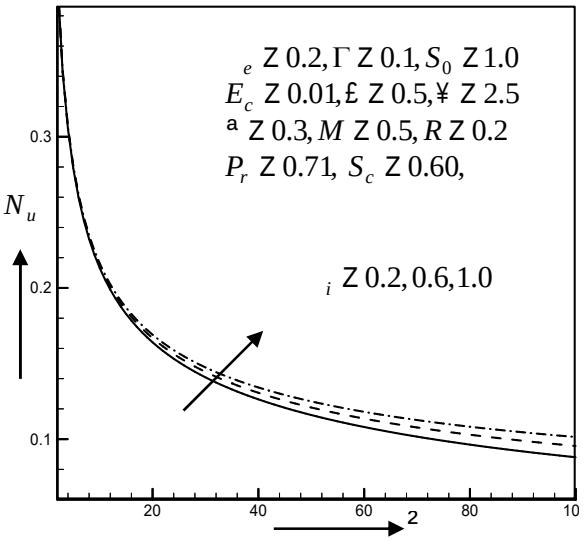

Fig. 5.1.9(b) Nusselt number profiles for different values of ion-slip parameter $_i$

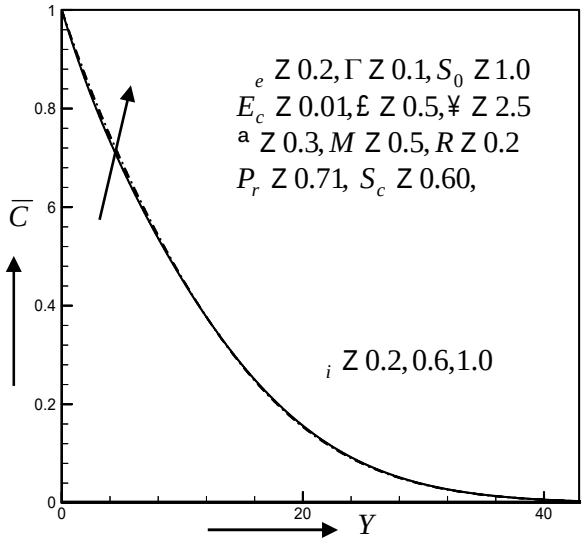

Fig. 5.1.10(a) Concentration profiles for different values of ion-slip parameter $_i$

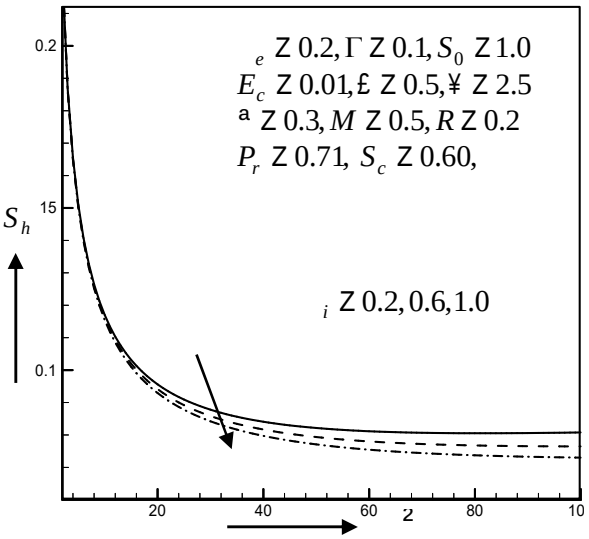

Fig. 5.1.10(b) Sherwood number profiles for different values of ion-slip parameter $_i$

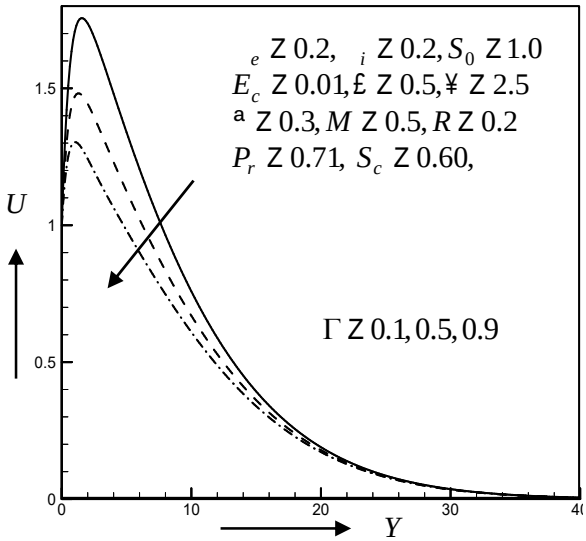

Fig. 5.1. 11(a) Primary velocity profiles for different values of inertial parameter Γ

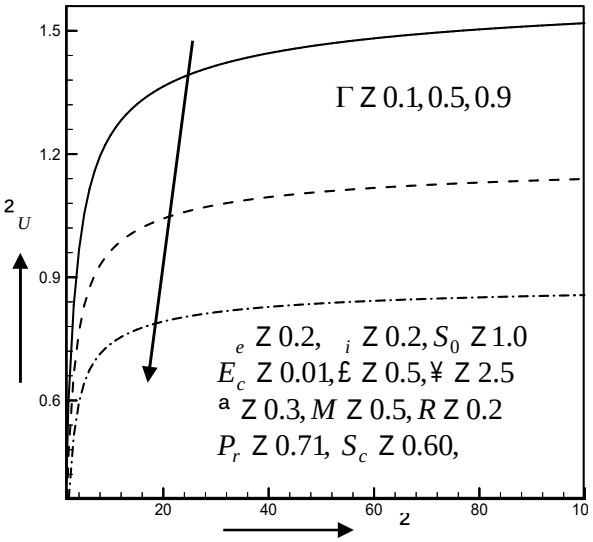

Fig. 5.1.11(b) Shear stress in x-axis for different values of inertial parameter Γ

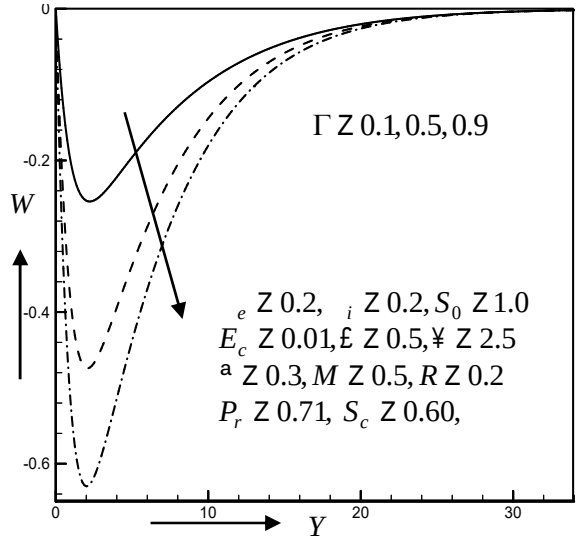

Fig. 5.1. 12(a) Secondary velocity profiles for different values of inertial parameter Γ

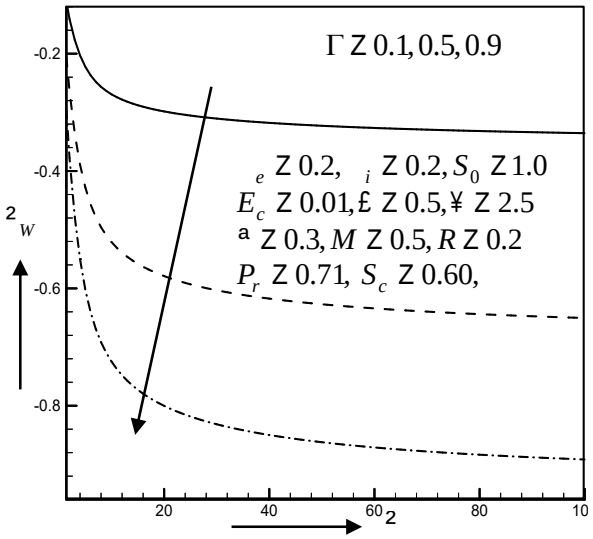

Fig. 5.1.12(b) Shear stress in z - axis for different values of inertial parameter Γ

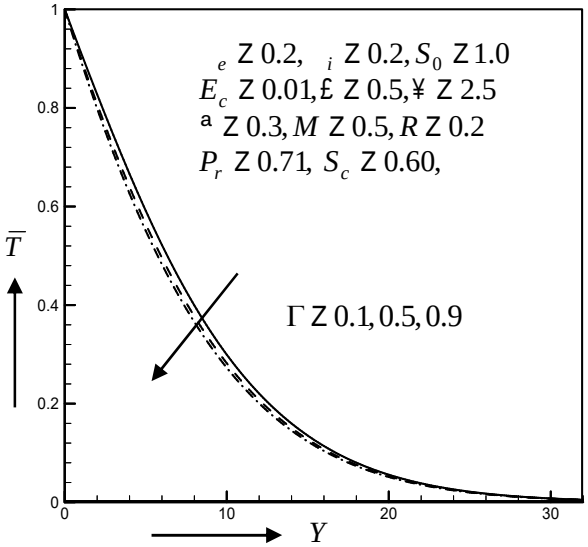

Fig. 5.1.13(a) Temperature profiles for different values of inertial parameter Γ

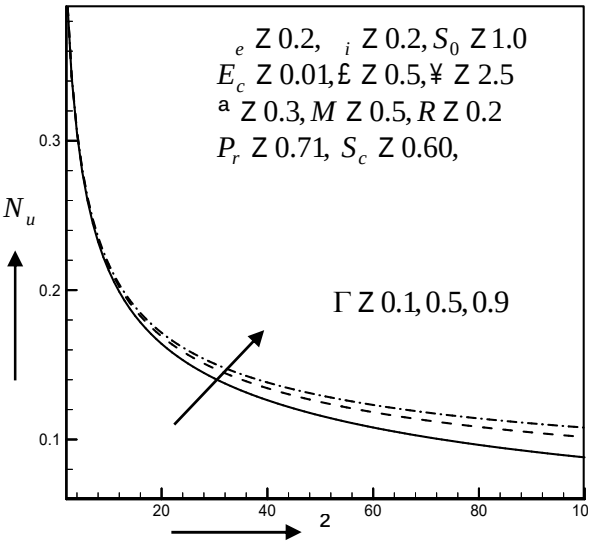

Fig. 5.1.13(b) Nusselt number profiles for different values of inertial parameter Γ

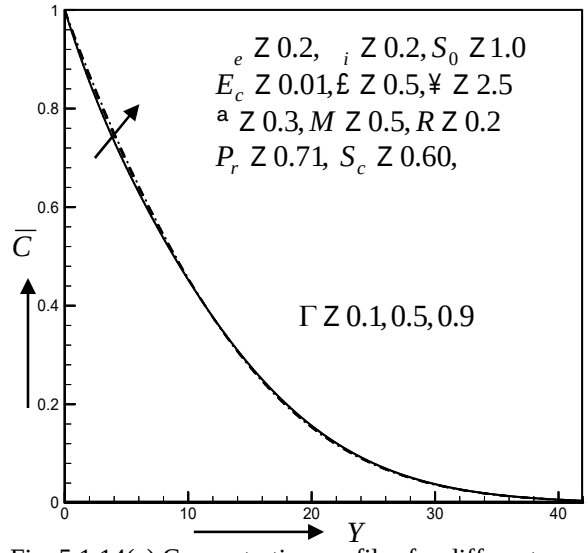

Fig. 5.1.14(a) Concentration profiles for different values of inertial parameter Γ

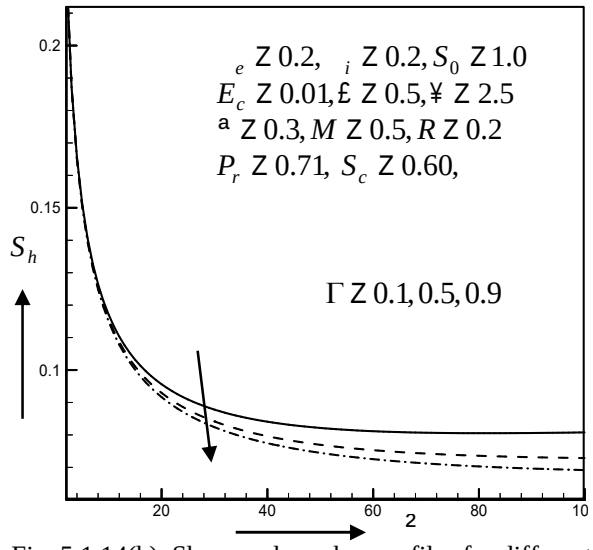

Fig. 5.1.14(b) Sherwood number profiles for different values of inertial parameter Γ

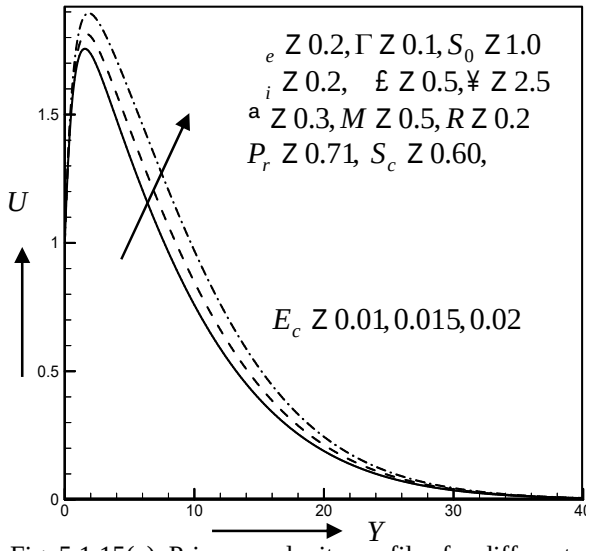

Fig. 5.1.15(a) Primary velocity profiles for different values of Eckert number E_c

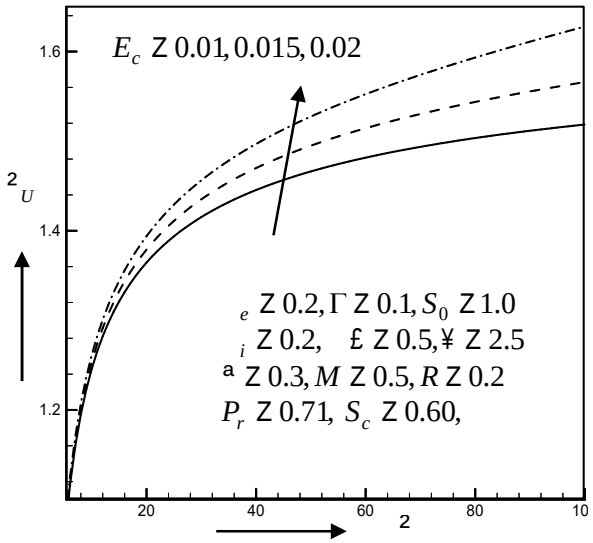

Fig. 5.1.15(b) Shear stress in x - axis for different values of Eckert number E_c

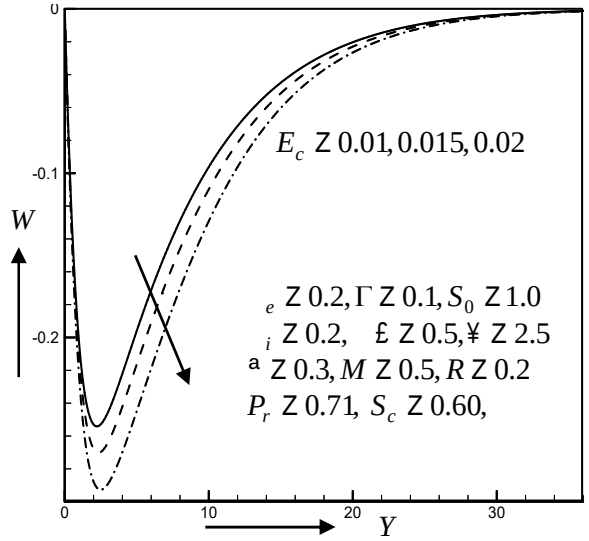

Fig. 5.1.16(a) Secondary velocity profiles for different values of Eckert number E_c

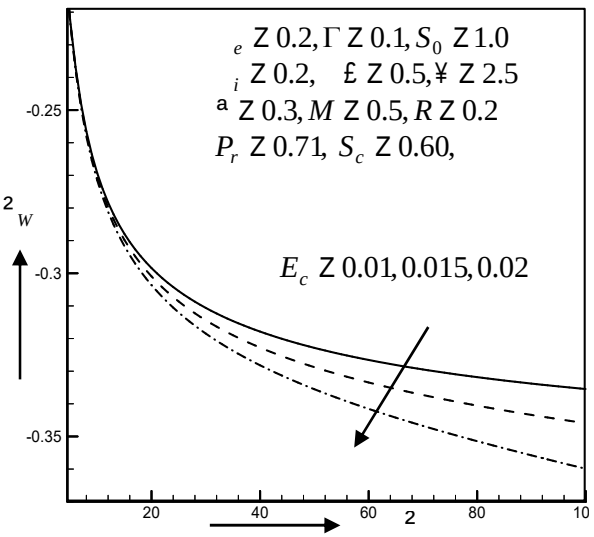

Fig. 5.1.16(b) Shear stress in z - axis for different values of Eckert number E_c

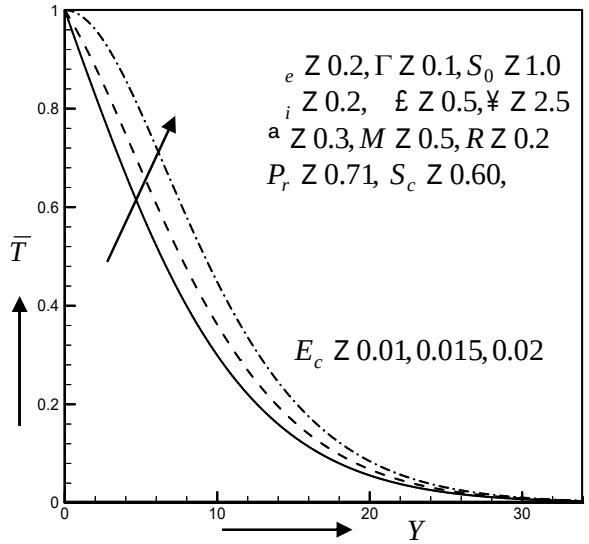

Fig. 5.1.17(a) Temperature profiles for different values of Eckert number E_c

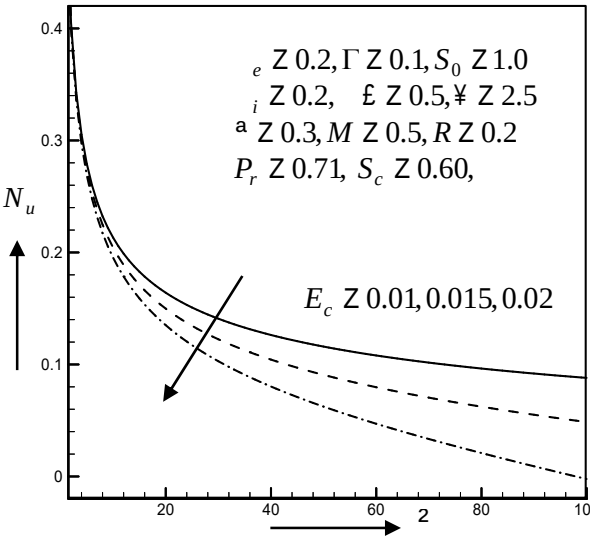

Fig. 5.1.17(b) Nusselt number profiles for different values of Eckert number E_c

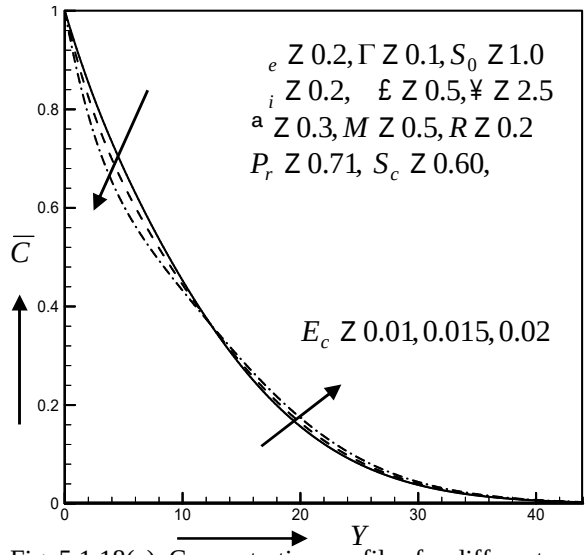

Fig. 5.1.18(a) Concentration profiles for different values of Eckert number E_c

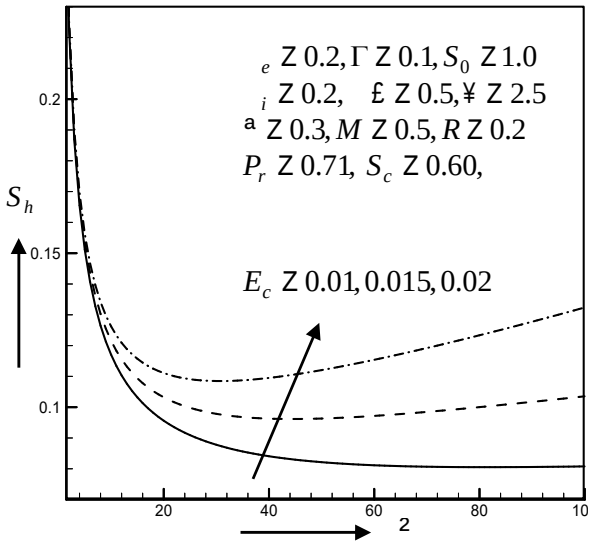

Fig. 5.1.18(b) Sherwood number profiles for different values of Eckert number E_c

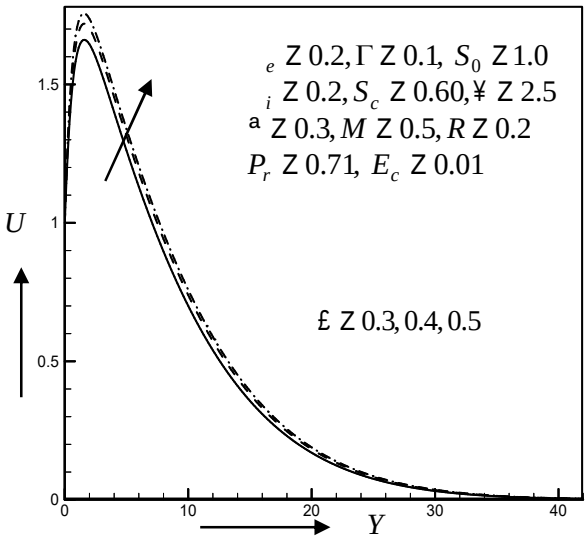

Fig. 5.1.19(a) Primary velocity profiles for different values of porosity parameter £

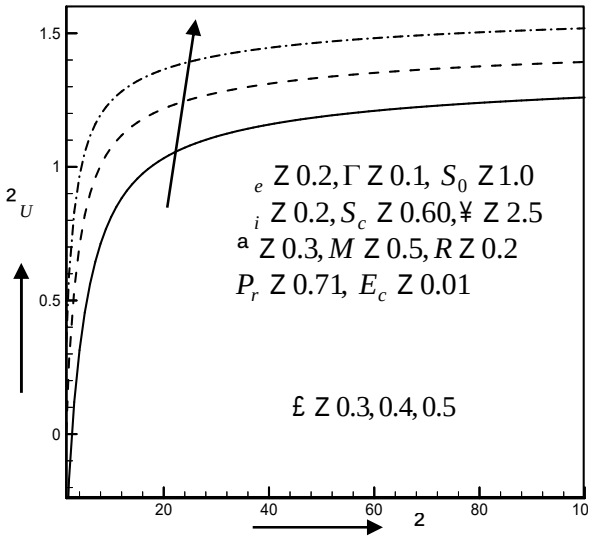

Fig. 5.1.19(b) Shear stress in x - axis for different values of porosity parameter £

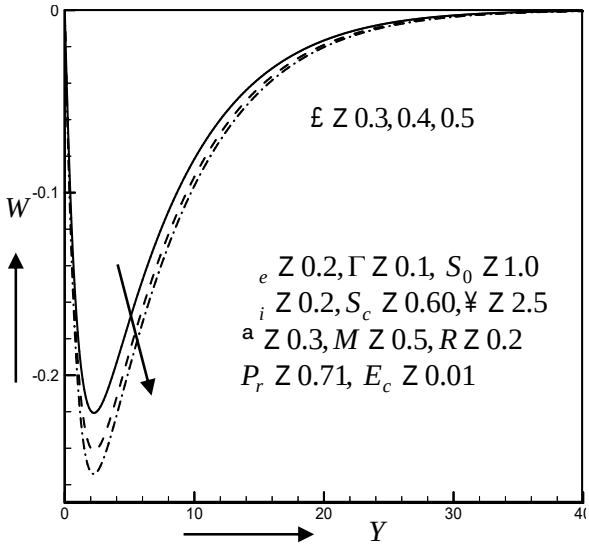

Fig. 5.1.20(a) Secondary velocity profiles for different values of porosity parameter £

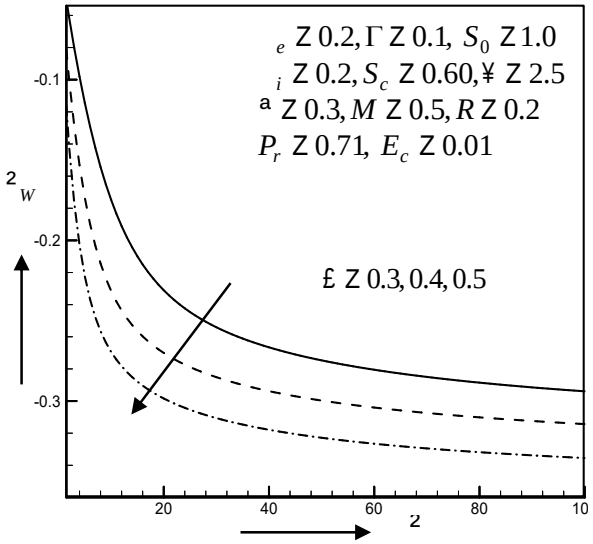

Fig. 5.1.20(b) Shear stress in z - axis for different values of porosity parameter £

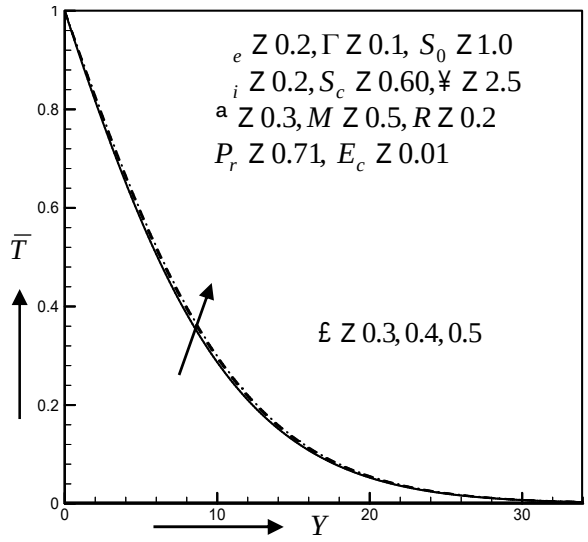

Fig. 5.1. 21(a) Temperature profiles for different values of porosity parameter £

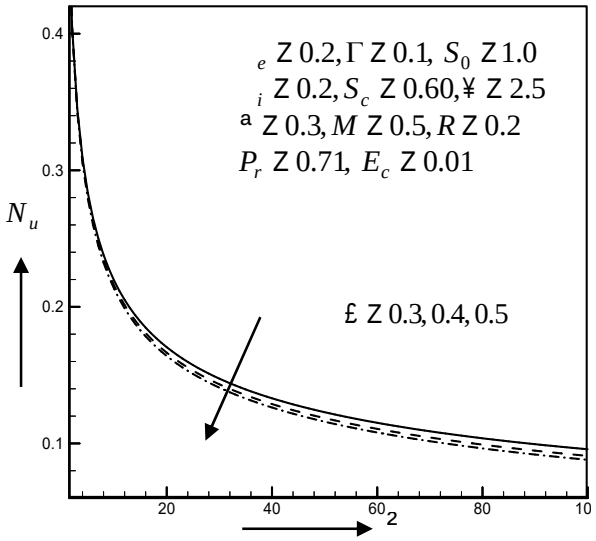

Fig. 5.1.21(b) Nusselt number profiles for different values of porosity parameter £

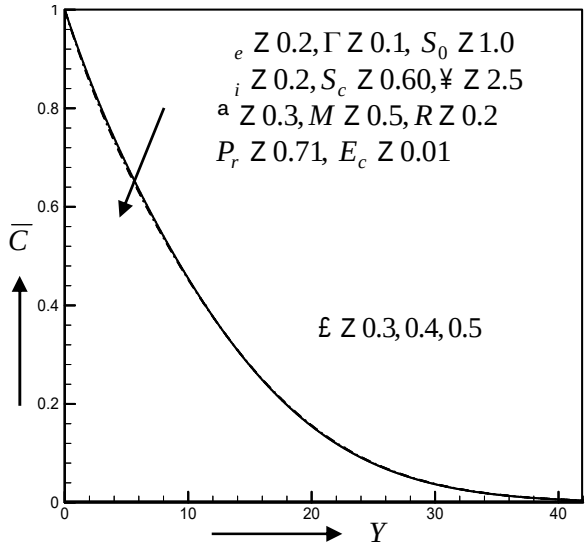

Fig. 5.1.22(a) Concentration profiles for different values of porosity parameter £

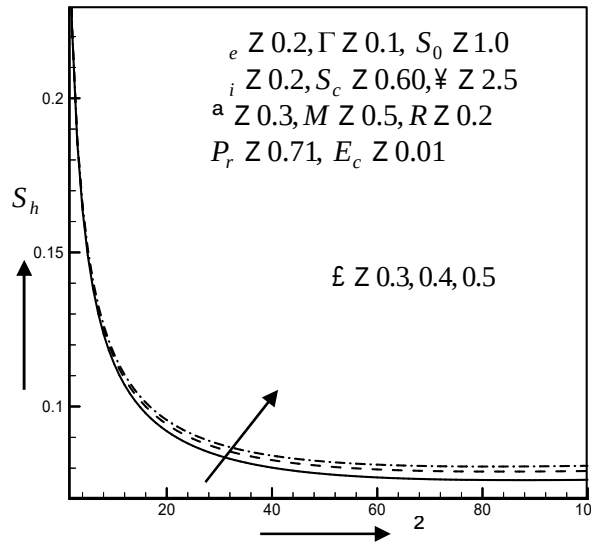

Fig. 5.1.22(b) Sherwood number profiles for different values of porosity parameter £

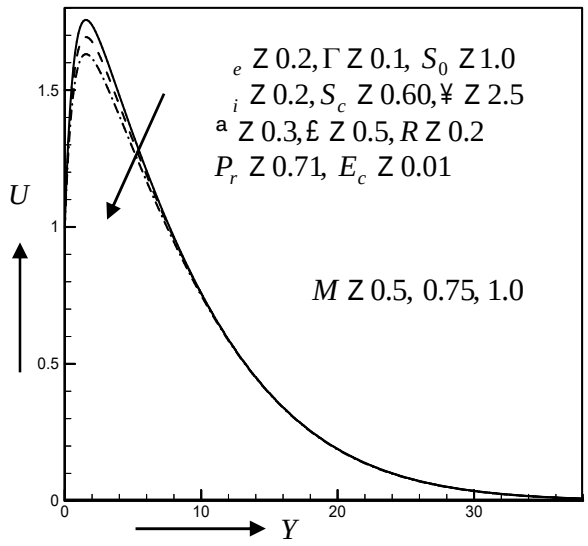

Fig. 5.1. 23(a) Primary velocity profiles for different values of magnetic parameter M

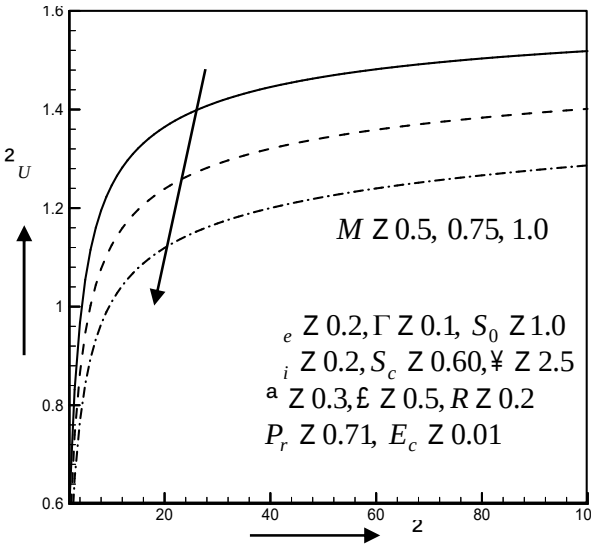

Fig. 5.1.23(b) Shear stress in x - axis for different values of magnetic parameter M

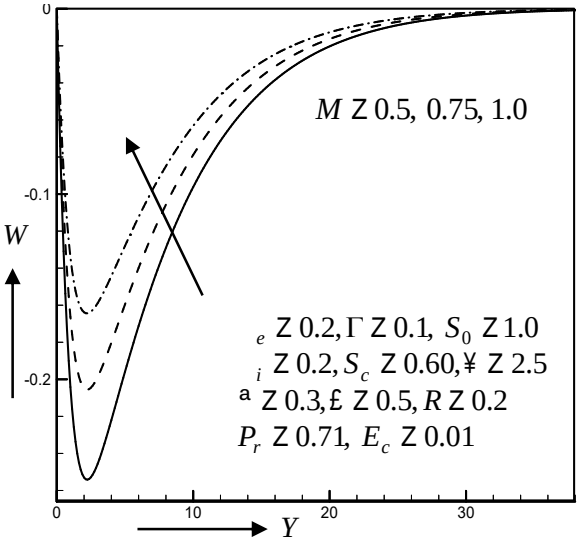

Fig. 5.1. 24(a) Secondary velocity profiles for different values of magnetic parameter M

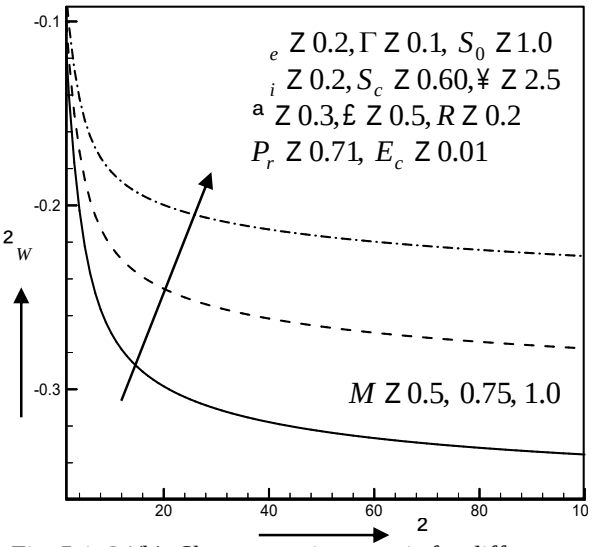

Fig. 5.1. 24(b) Shear stress in z - axis for different values of magnetic parameter M

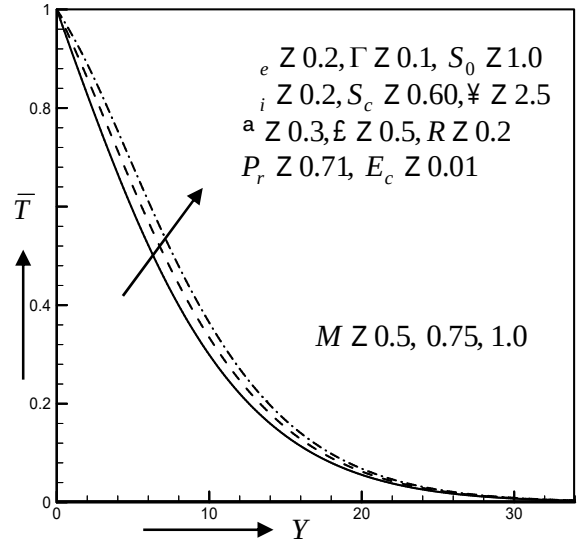

Fig. 5.1. 25(a) Temperature profiles for different values of magnetic parameter M

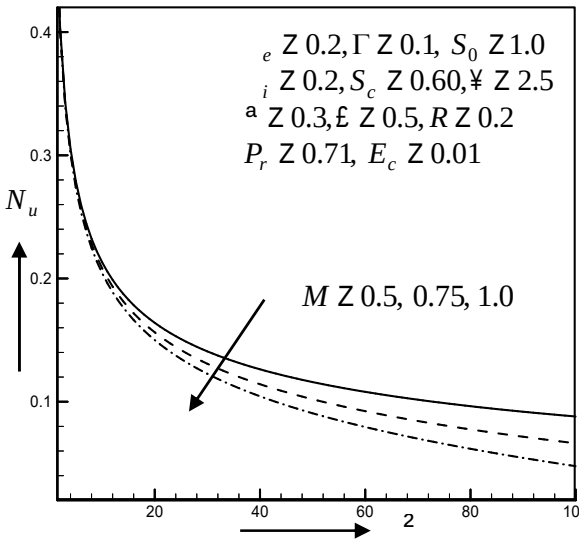

Fig. 5.1.25(b) Nusselt number profiles for different values of magnetic parameter M

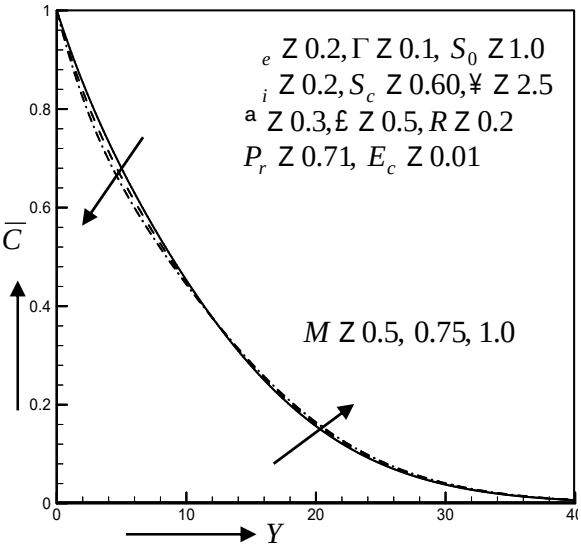

Fig. 5.1.26(a) Concentration profiles for different values of magnetic parameter M

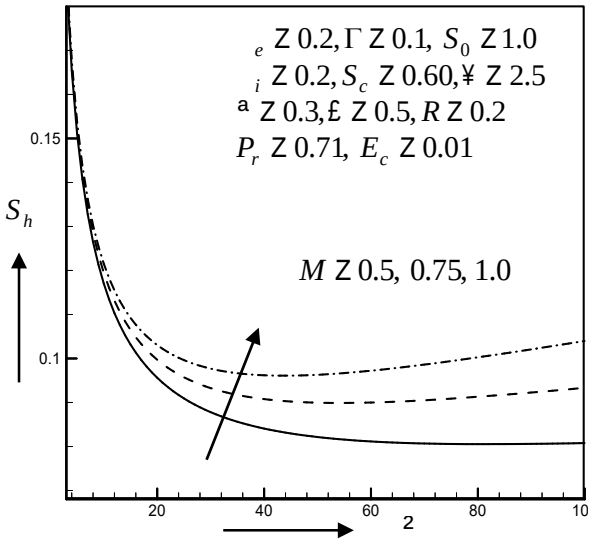

Fig. 5.1.26(b) Sherwood number profiles for different values of magnetic parameter M

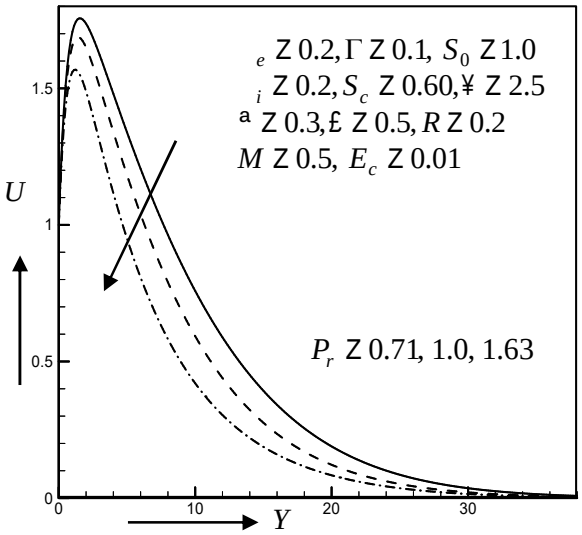

Fig. 5.1.27(a) Primary velocity profiles for different values of Prandtl number P_r

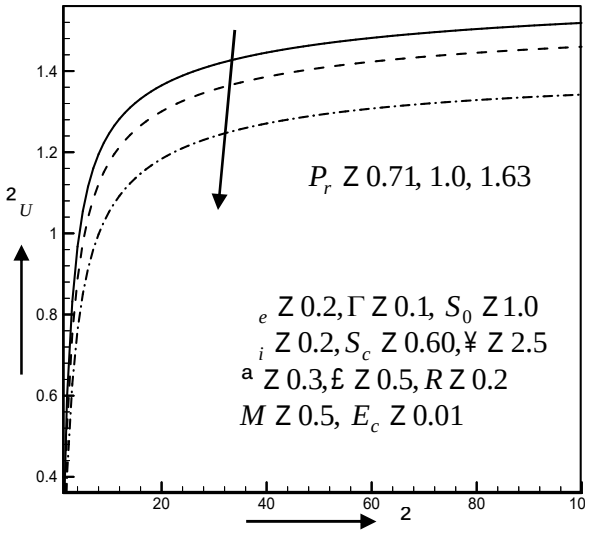

Fig. 5.1.27(b) Shear stress in x - axis for different values of Prandtl number P_r

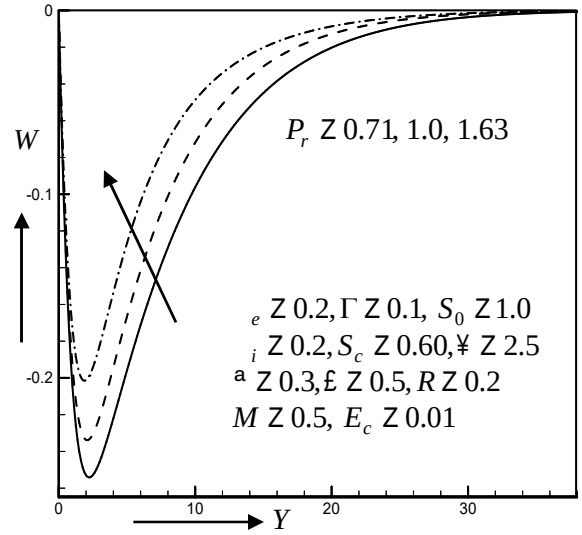

Fig. 5.1.28(a) Secondary velocity profiles for different values of Prandtl number P_r

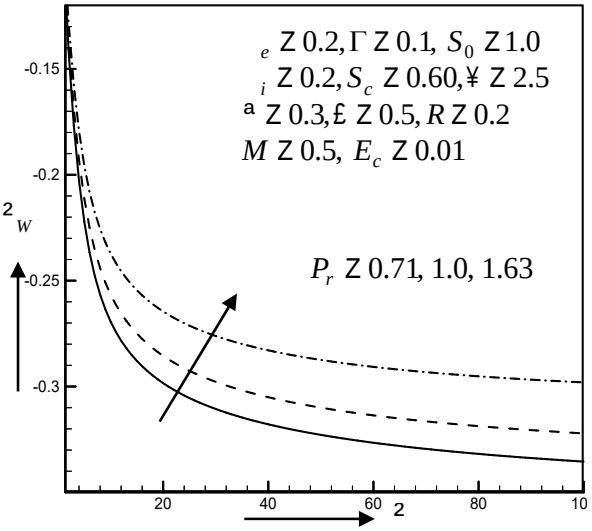

Fig. 5.1.28(b) Shear stress in z - axis for different values of Prandtl number P_r

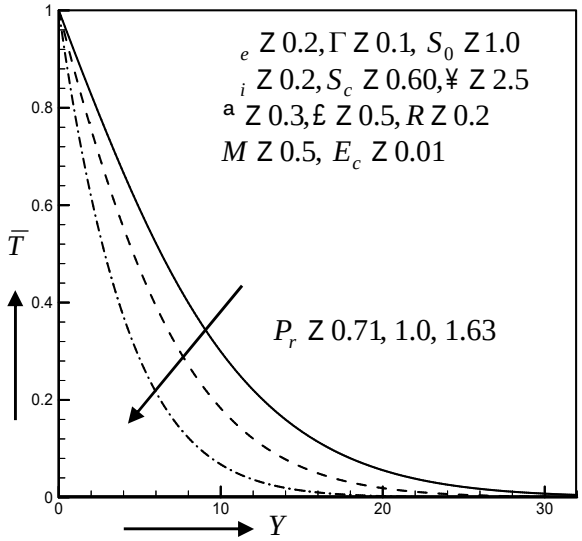

Fig. 5.1. 29(a) Temperature profiles for different values of Prandtl number P_r

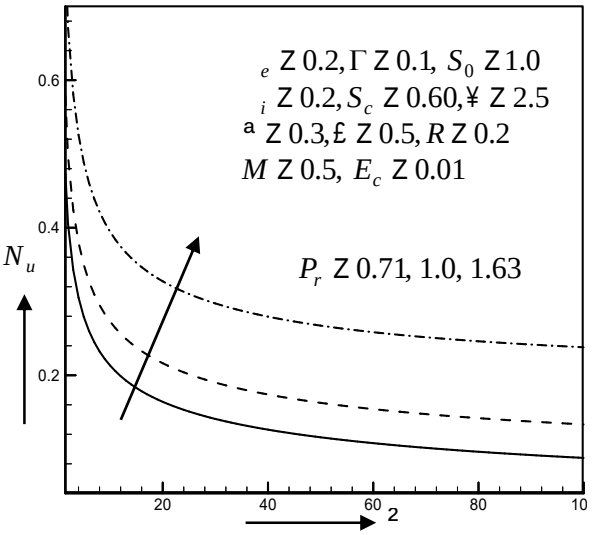

Fig. 5.1.29(a) Nusselt number profiles for different values of Prandtl number P_r

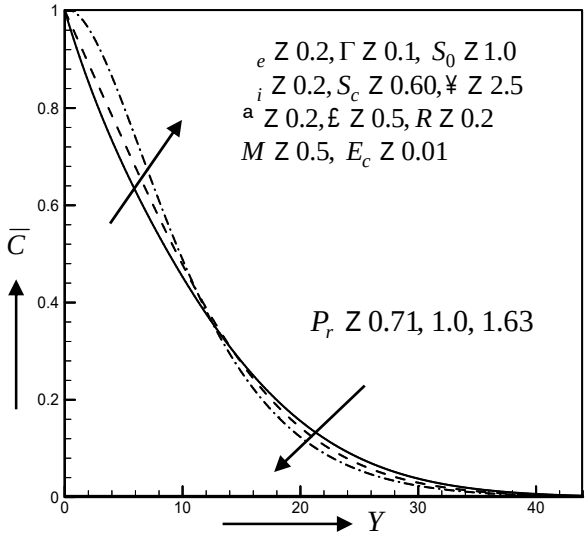

Fig. 5.1.30(a) Concentration profiles for different values of Prandtl number P_r

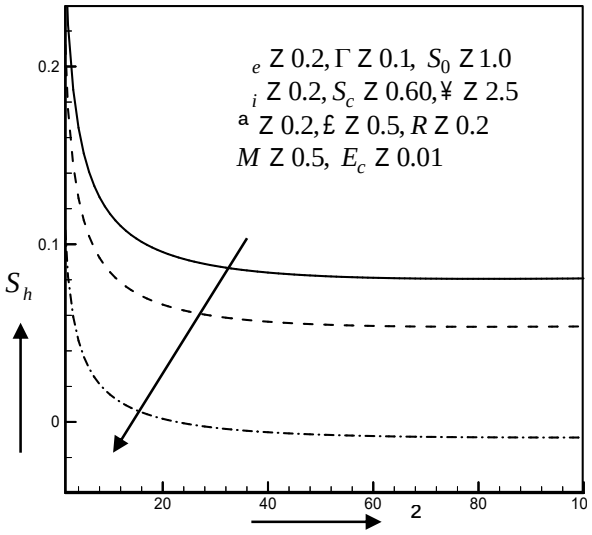

Fig. 5.1. 30(b) Sherwood number profiles for different values of Prandtl number P_r

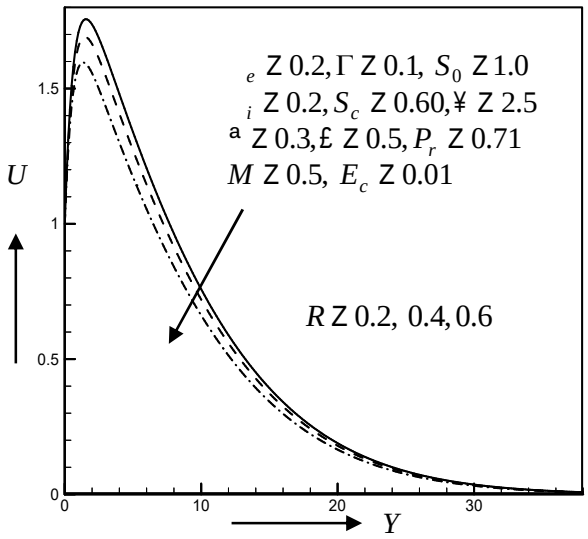

Fig. 5.1. 31(a) Primary velocity profiles for different values of rotation parameter R

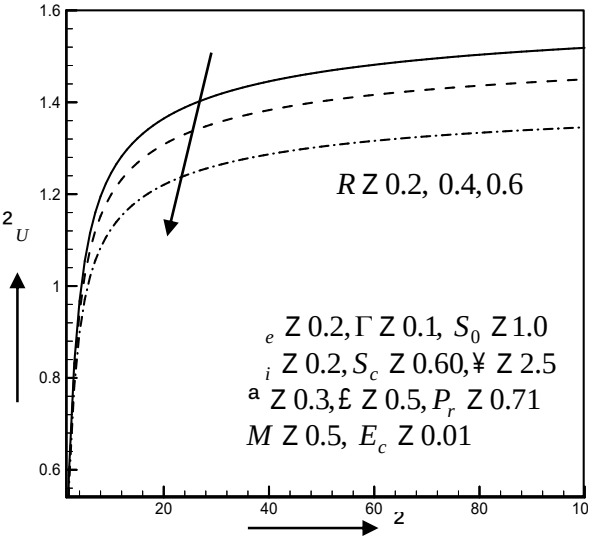

Fig. 5.1. 31(b) Shear stress in x - axis for different values of rotation parameter R

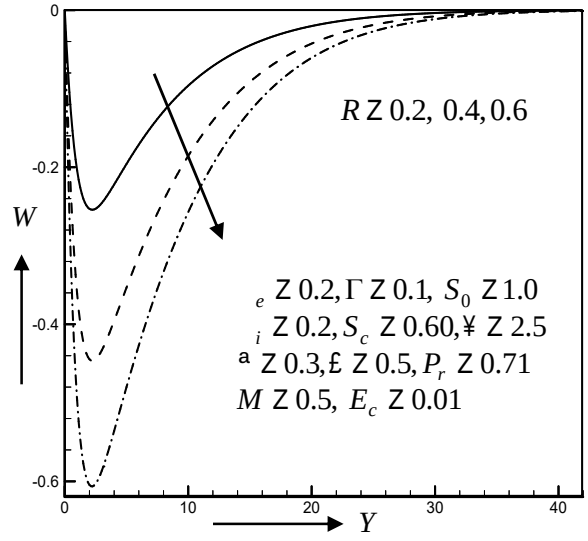

Fig. 5.1.32(a) Secondary velocity profiles for different values of rotation parameter R

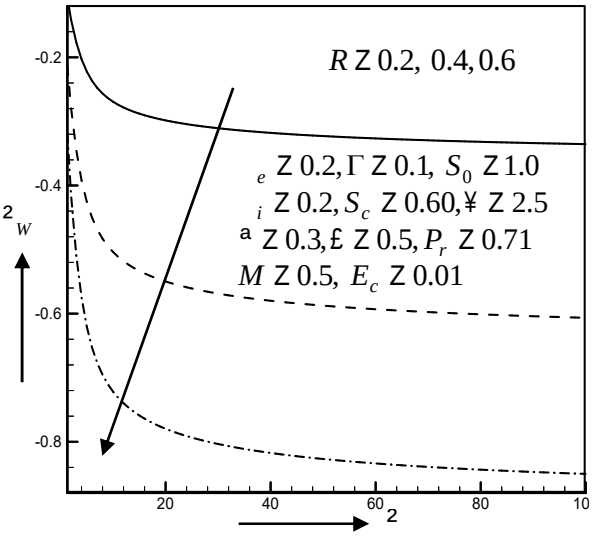

Fig. 5.1.32(b) Shear stress in z - axis for different values of rotation parameter R

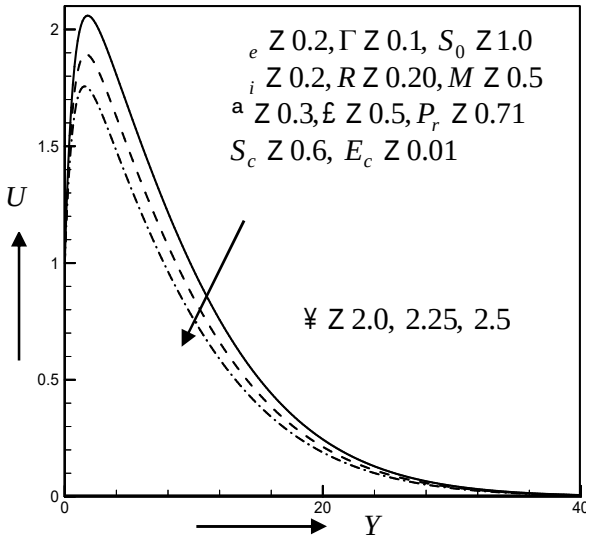

Fig. 5.1.33(a) Primary velocity profiles for different values of permeability parameter ¥

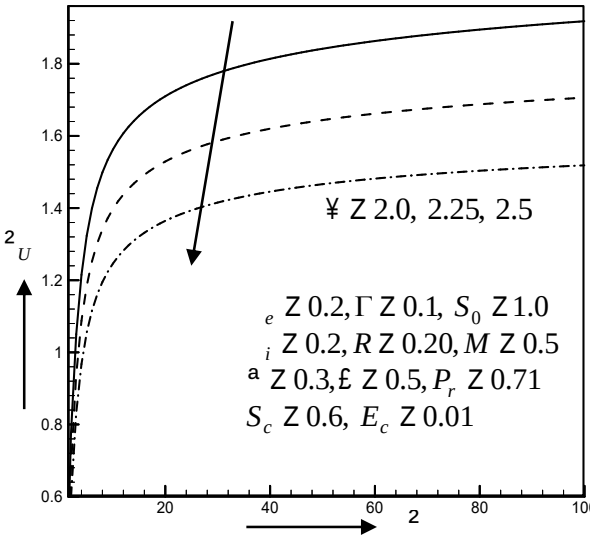

Fig. 5.1.33(b) Shear stress in x - axis for different values of permeability parameter¥

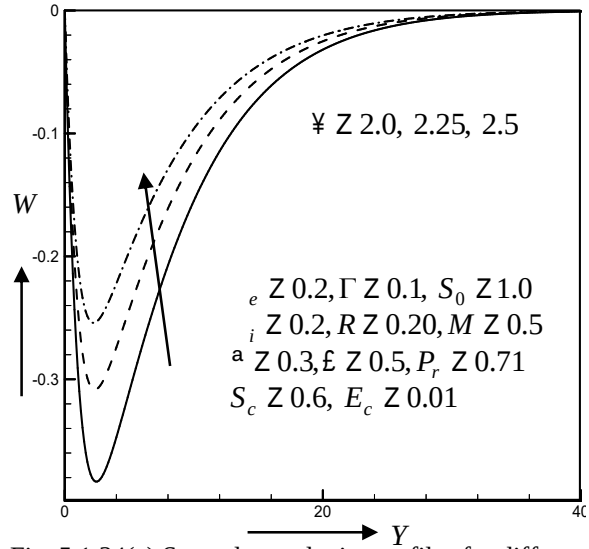

Fig. 5.1.34(a) Secondary velocity profiles for different values of permeability parameter ¥

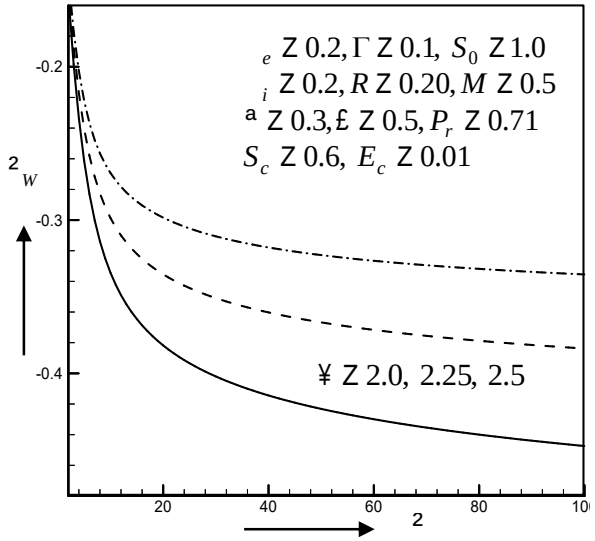

Fig. 5.1.34(b) Shear stress in z - axis for different values of permeability parameter¥

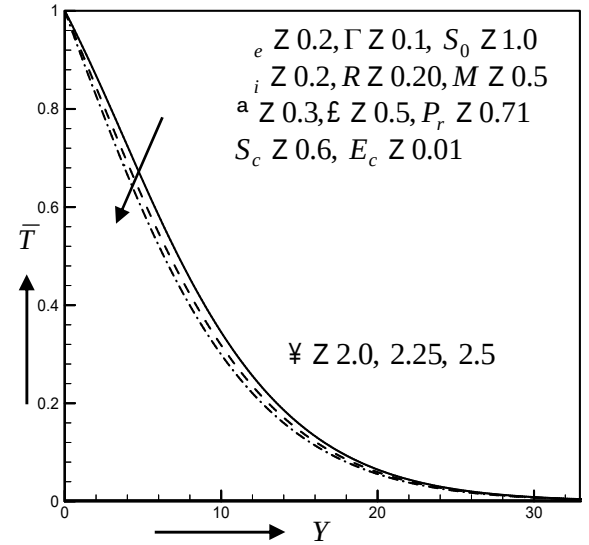

Fig. 5.1.35(a) Temperature profiles for different values of permeability parameter¥

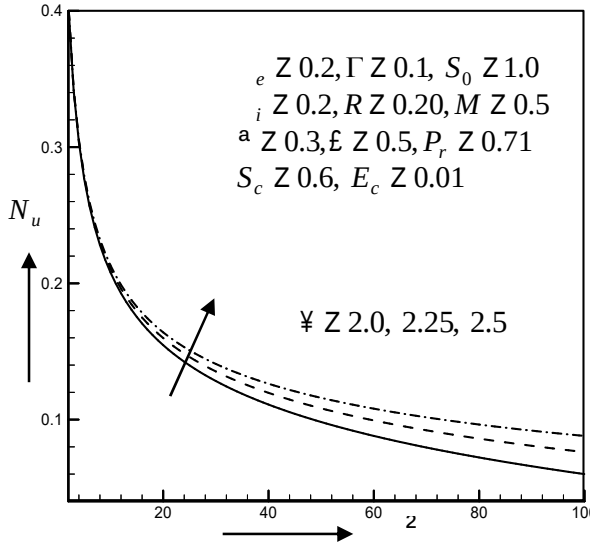

Fig. 5.1.35(b) Nusselt number profiles for different values of permeability parameter¥

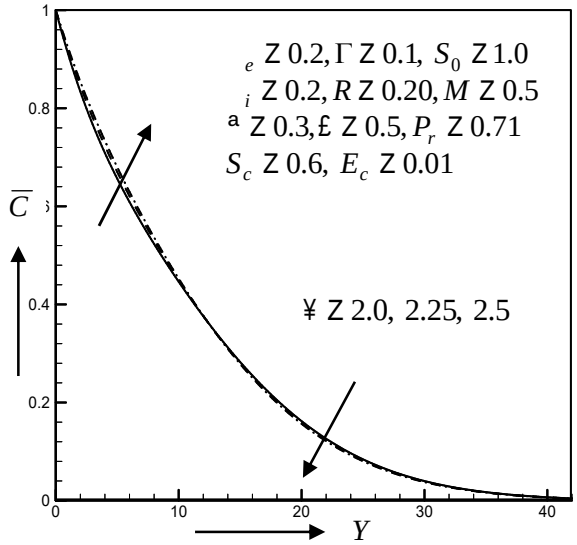

Fig. 5.1. 36(a) Concentration profiles for different values of permeability parameter¥

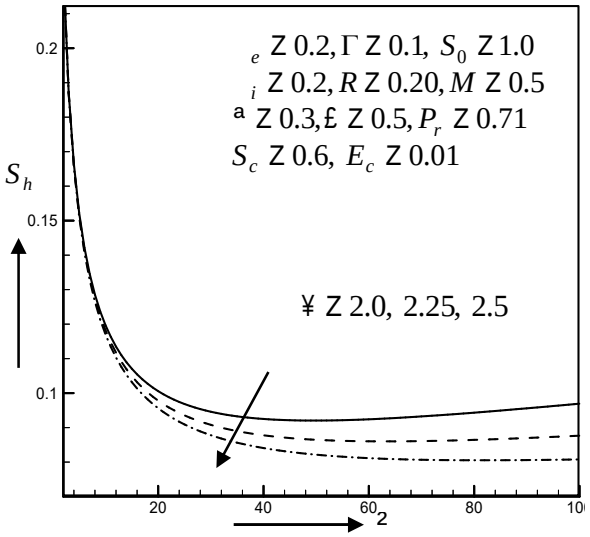

Fig. 5.1. 36(b) Sherwood number profiles for different values of permeability parameter¥

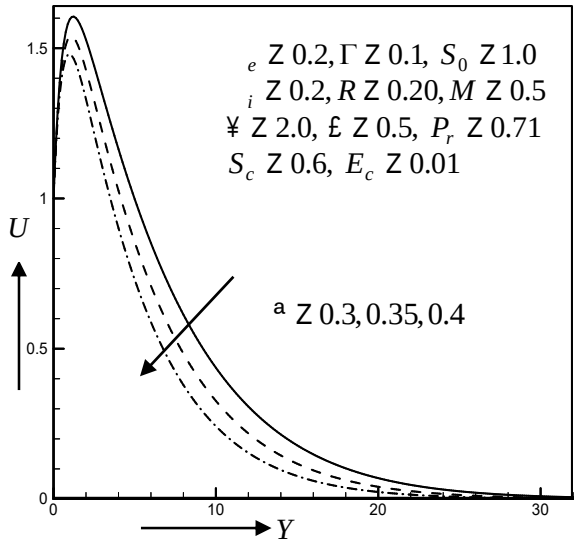

Fig. 5.1.37(a) Primary velocity profiles for different values of suction parameter ª

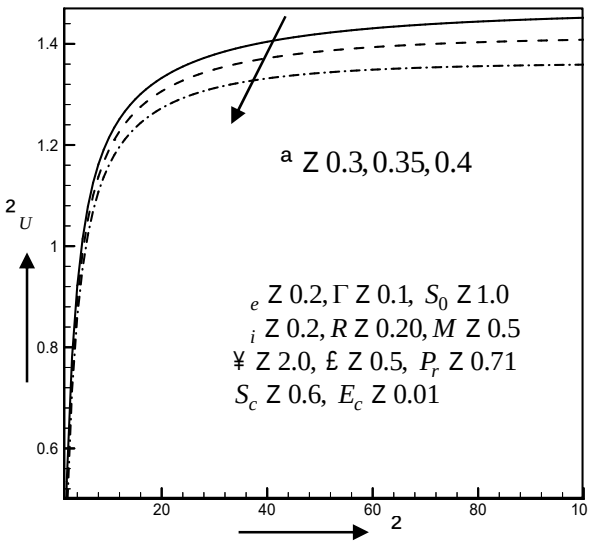

Fig. 5.1.37(b) Shear stress in x - axis for different values of suction parameter ª

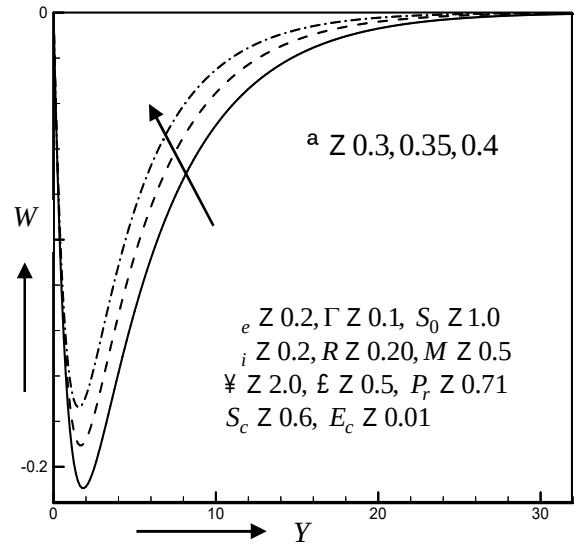

Fig. 5.1.38(a) Secondary velocity profiles for different values of suction parameter ª

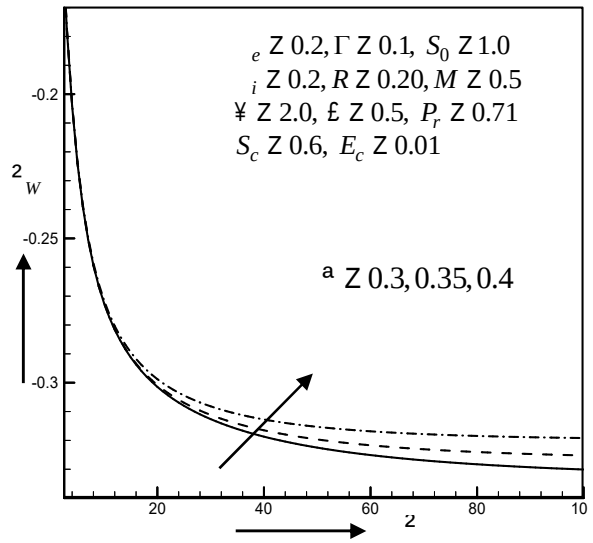

Fig. 5.1.38(b) Shear stress in z - axis for different values of suction parameter ª

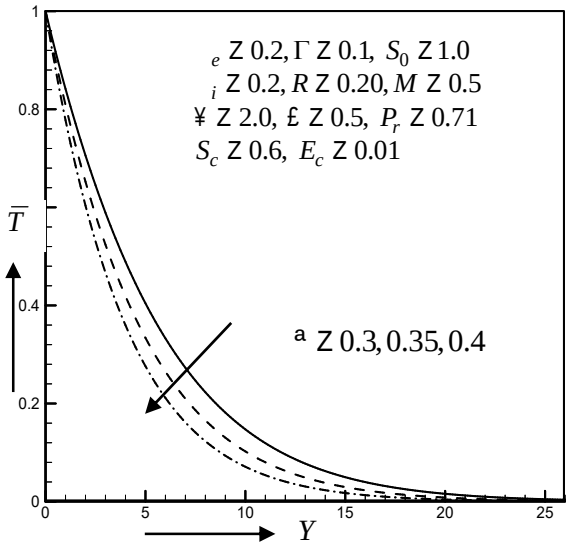

Fig. 5.1.39(a) Temperature profiles for different values of suction parameter ª

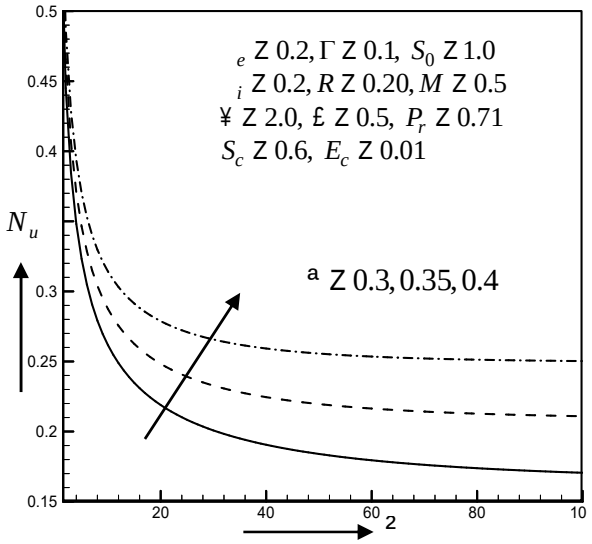

Fig. 5.1.39(b) Nusselt number profiles for different values of suction parameter ª

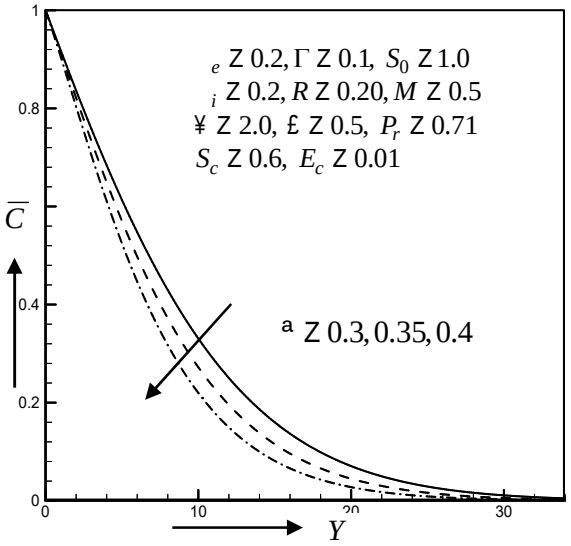

Fig. 5.1. 40(a) Concentration profiles for different values of suction parameter ª

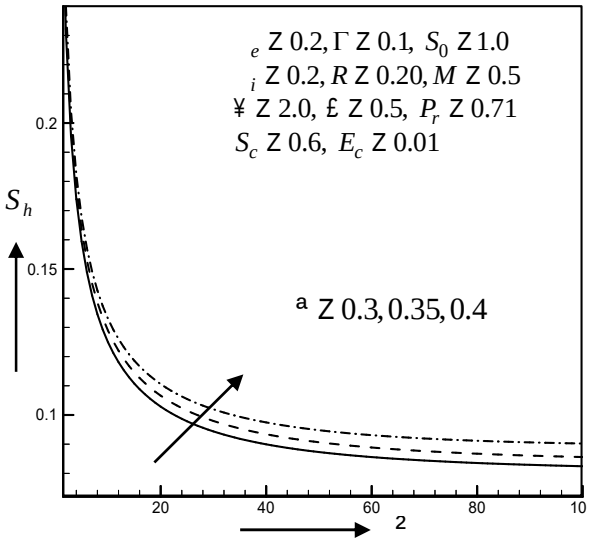

Fig. 5.1.40(b) Sherwood number profiles for different values of suction parameter ª

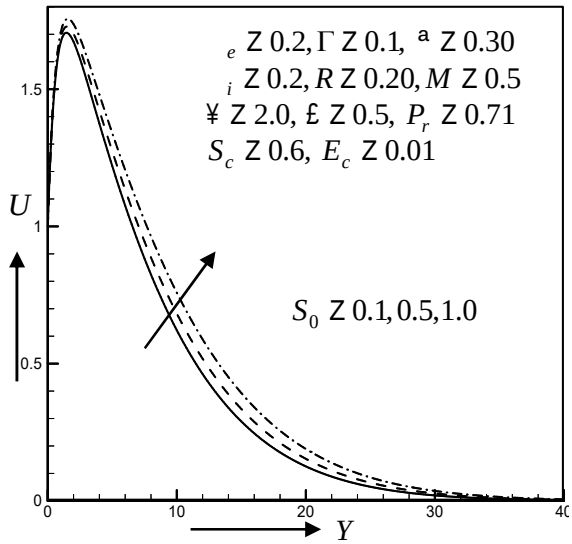

Fig. 5.1.41(a) Primary velocity profiles for different values of Soret number S_0

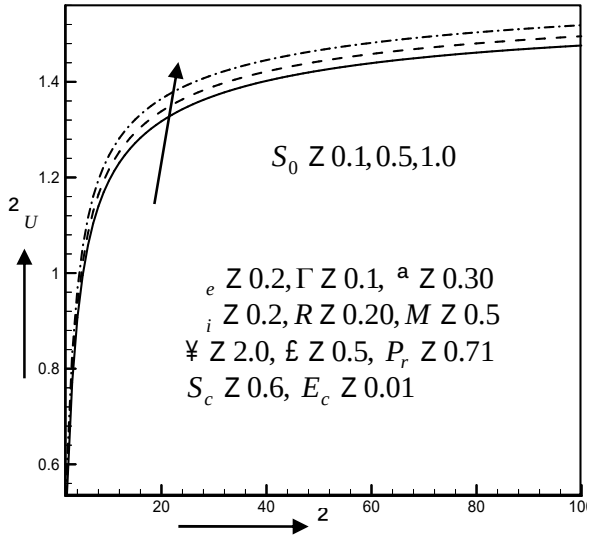

Fig. 5.1.41(b) Shear stress in x - axis for different values of Soret number S_0

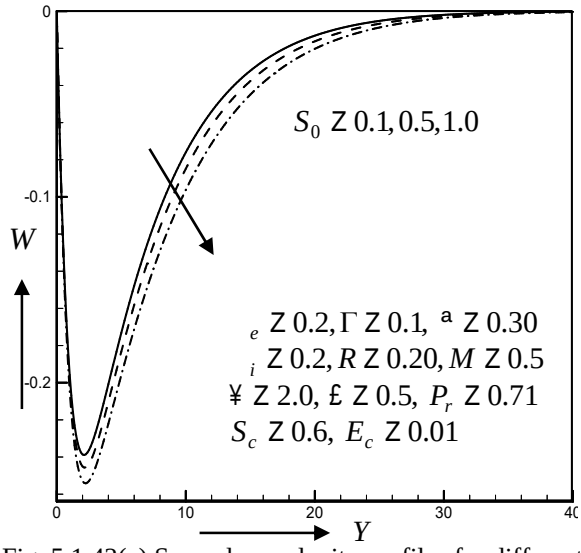

Fig. 5.1.42(a) Secondary velocity profiles for different values of Soret number S_0

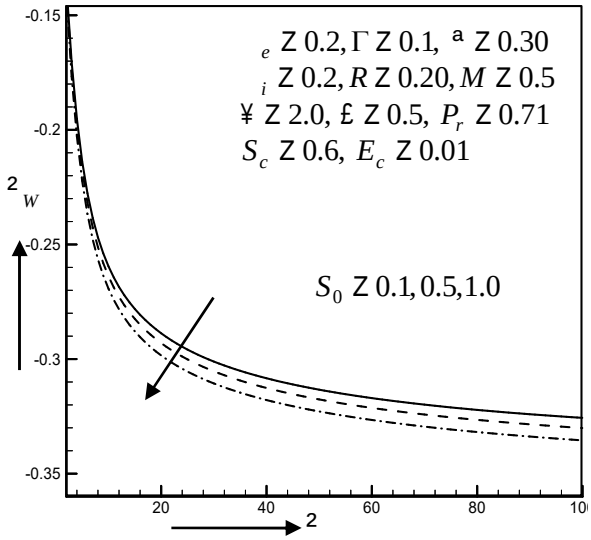

Fig. 5.1.42(b) Shear stress in z - axis for different values of Soret number S_0

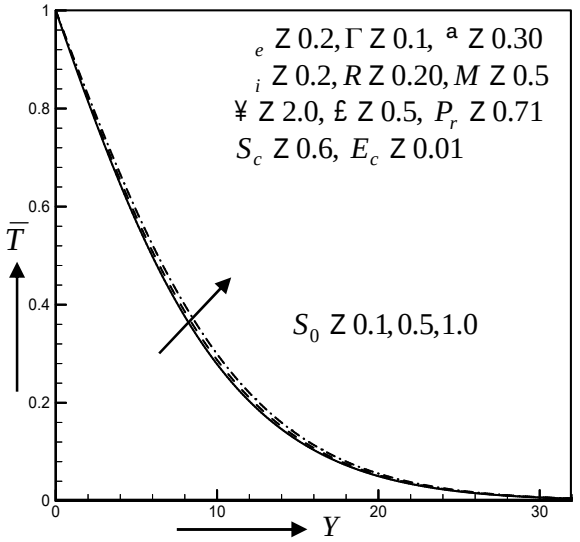

Fig. 5.1.43(a) Temperature velocity profiles for different values of Soret number S_0

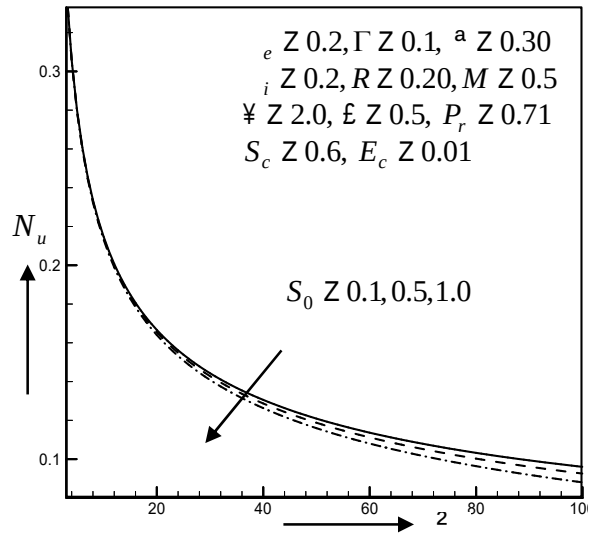

Fig. 5.1.43(b) Nusselt number profiles for different values of Soret number S_0

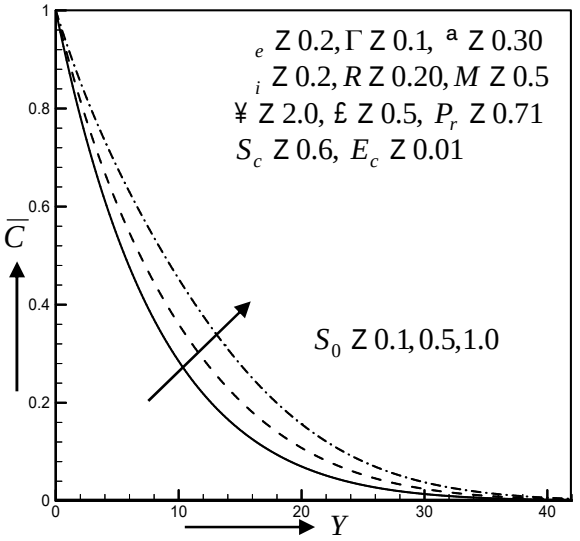

Fig. 5.1. 44(a) Concentration profiles for different values of Soret number S_0

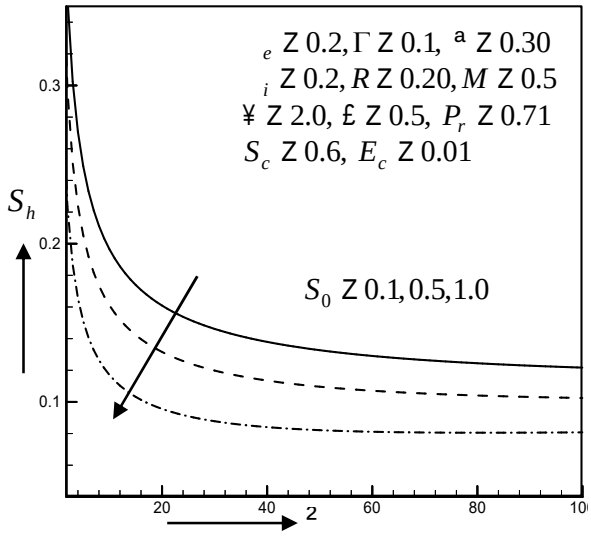

Fig. 5.1.44(b) Sherwood number profiles for different values of Soret number S_0

References

Ajay Kumar Singh, Rama Subba Reddy Gorla (2009), Free convection heat and mass transfer with Hall current, Joule heating and thermal diffusion, 'Heat and Mass Transfer', vol.**45**(11), p1341–1349.

Ali J. Chamkha, Harmindar S. Takhar and Girishwar Nath (2005), Natural convection flow in a rotating fluid over a vertical plate embedded in a thermally stratified high porosity medium, 'International Journal of fluid Mechanics Research', vol.**32**(5), p511-527.

Bhuvanavijaya, R. and Mallikarjuna, B. (2014), Effect of variable thermal conductivity on convective heat and mass transfer over a vertical plate in a rotating system with variable porosity regime, 'Journal of Naval Architecture and Marine Engineering', vol.**11**, p83-92.

Callahan, G. D. and Marner, W. J. (1976), Transient free convection flow with mass transfer on an isothermal vertical flat plate, 'International Journal of Heat and Mass Transfer', vol.**19**(2), p165-174.

Chen C.K., Hung C.I. and Horng H. C. (1987), Transient natural convection on a vertical flat plate embedded in a high porosity medium, 'ASME Journal of Energy Resources Technology', vol.**109**, p112-118.

Das, S., Sarkar, B. C. and Jana, R. N (2013), Hall effect on MHD free convection boundary layer flow past a vertical flat plate, 'Mecanica', vol.**48**(6), p1387-1394.

Farhad, A., Norzieha, M., Sharidan, S., Khan, I. and Samiulhaq (2012), Hydromagnetic rotating flow in a porous medium with slip condition and Hall current,'International Journal of Physical Sciences', vol.**7**(10), p1540-1548.

Ferdows, M., Koji Kaino and Chien-Hsin Chen (2010), Dufour, Soret and viscous dissipation effects on heat and mass transfer in porous media with high porosities, 'International Journal of Applied Engineering Research', vol.**5**(3), p477.

Foisal, A. A. and Alam, M. M. (2016), Unsteady free convection fluid flow over an inclined plate in the presence of a magnetic field with thermally stratified high porosity medium, 'Journal of Applied Fluid Mechanics', vol.**9**, No. 3, p1467-1475.

Gebhart, B. (1962*)*, Effects of viscous dissipation in natural convection, 'Journal of Fluid Mechanics', vol.**14**, p225-235

Hemant Poonia, Chaudhary, R. C.(2010), MHD free convection and mass transfer flow over an infinite vertical plate with viscous dissipation,'Journal Theoretical and applied Mechanics', vol.**37**, No.4, p263–287.

Jasem ,M., Al-Humud and Ali J. Chamkha (2006), Double diffusive convection of a rotating fluid over a surface embedded in a thermally stratified high porosity medium, 'Heat and Technology', vol.**24**, No 1, p51-59.

Khaled K. Jaber (2014), Effects of viscous dissipation and Joule heating on MHD flow of a fluid with variable properties past a stretching vertical plate, European Scientific Journal, vol.**10**, No.33, p383-393.

Mahender, D. and Srikanth Rao, P. (2015), Unsteady MHD free convection and mass transfer flow past a porous plate in presence of viscous dissipation,'Journal of Physics : Conference Series', vol.**662**, p012012.

Maleque, Kh. A. and Sattar, M. A. (2005), The effects of variable properties and Hall current on steady MHD laminar convective fluid due to a porous rotating disk, 'International Journal of Heat and Mass Transfer', vol.**48**, p4963-4972.

Rachna Khandelwal(2013),Unsteady MHD flow, heat and mass transfer along anaccelerated vertical porous plate in the influence of viscous dissipation, heat source and variable suction, 'International Journal of Mathematics and Computer Applications Research', vol. **3**(1), p229-236.

Sondalgekar, V. M. and Ganesan, P. (1980), Transient free convection flow past a semi-infinite vertical plate with mass transfer, 'Regional Journal of Energy, Heat and Mass Transfer', vol.**2**, p83-91.

Srinivas Reddy, D., Sreedhar sarma, G. and Govardhan, K. (2015), Effect of viscous dissipation, Soret and Dufour effect on free convection heat and mass transfer from vertical surface in a porous medium, 'Elsevier, Procedia Materials Science', vol.**10**, p563-571.

5.2 MHD free convection flow and mass transfer over a vertical plate with high porosity medium in presence of Hall and ion-slip currents in a rotating system

The natural convection flow on a vertical surface embedded in porous media occurs in many important engineering problems such as in the design of pebble-bed nuclear reactors, catalytic reactors and compact heat exchangers. Hall and ion-slip currents are important and they have a marked effect on the magnitude and direction of the current density and consequently on the magnetic force term. The rotating hydrodynamic flows of incompressible fluids in the presence of porous boundaries occur in MHD power generators, including magnetically such study is also useful in metallurgy. Study of the interaction of Coriolis force with electromagnetic force in porous media is important in some geophysical and astrophysical problems, since many astronomical bodies posses magnetic field and fluid interiors.

Soret and Dufour effects are interesting physical phenomenon in fluid mechanics, when heat and mass transfer occur simultaneously, the relations between the fluxes and the driving potentials are of a more intricate nature. The Soret effect has been utilized for isotope separation and in mixture between gases of very light molecular weight and of medium molecular weight. Viscous magnetohydrodynamic (MHD) flows arise in many applications in energy systems, chemical technology, astrophysics and flow control processes in the mechanical engineering industry. *Ferdows et al.* (2011) investigated the effects of Hall and ion-slip currents on free convective heat transfer flow past a vertical plate considering slip conditions. Steady motions of electrically conducting viscous fluids through a porous medium in presence of magnetic field, which are of interest in many scientific and engineering domains, have attracted considerable attention of many investigators like *Krishna et al.* (2002), *Geindreau and Auriault* (2002), *Chauhan and Jain* (2005) and *Dulal* (2008). *Sherman and Sutton* (1962) have considered the effect of Hall current on the efficiency of a MHD generator. *Anjali and Ganga* (2009) studied the effects of viscous and Joules dissipation on mhd flow, heat and mass transfer past a stretching porous surface embedded in a porous medium. *Singh and Rakesh*(2009) analyzed Soret and Hall current effects on heat and mass transfer in MHD flow of a viscous fluid through porous medium with variable suction. *Joaquin et al.* (2009) studied the numerical solutions for unsteady rotating high porosity medium channel couette flow hydrodynamics. *Koushik et al.* (2012) investigated MHD free convection and mass transfer flow from a vertical plate in the presence of Hall and ion-slip current. *Anwaret al.* (2012) investigated hydromagnetic viscous flow in a rotating annular high-porosity medium with nonliner Forchheimer drag effects. *Vidyasagar et al.* (2013) considered the effects of heat and mass transfer over a moving vertical porous plate. *Rajput and Mohammad* (2016) investigated rotation effect on unsteady MHD flow past an impulsively started vertical plate with variable temperature in porous medium. *Rao et al.* (2014) studied Soret and Dufour effects on MHD Boundary layer flow

over a Moving Vertical porous plate with suction. *Vijaya and Mallikarjuna* (2014) discussed the effect of variable thermal conductivity on convective heat and mass transfer over a vertical plate in a rotating system with variable porosity regime. *Das et al.*(2015) studied Hall effects on unsteady hydromagnetic flow past an accelerated porous plate in a rotating system. Diffusion-thermo effects on hydromagnetic free convection heat and mass transfer flow through high porous medium bounded by a vertical surface was studied by *Kiran et al.* (2015). *Abdullah and Mahmud* (2015) analyzed free convection fluid flow in the presence of a magnetic field with thermally stratified high porosity medium.

Hence our aim is to investigate the viscous dissipation, Joule heating and thermal diffusion effects on unsteady MHD free convective heat and mass transfer flow through a vertical infinite porous plate with porous medium under the action of transverse magnetic field taking into account Hall and ion-slip currents. The effects of various emerging parameters on the velocity, temperature and concentration field are discussed graphically in details.

5.2.1 Governing Equations

The two dimensional unsteady flow of an electrically conducting incompressible viscous fluid past an semi-infinite vertical porous plate has been considered. The flow is assumed to be in the $x-$axis which is taken along the plate in the upward direction and $y-$axis is normal to it. Initially the fluids as well as the plate are at rest but for time $t>0$ the whole system is allowed to rotate with a constant angular velocity Ω about the $y-$axis. Both the plate and the fluid are maintained initially at the same temperature. Also it is assumed that the temperature of the plate and spices concentration are raised to $T_w(>T_\infty)$ and $C_w(>C_\infty)$ respectively, which are there after maintained constant, where T_w, C_w are temperature and spices concentration at the wall and T_∞, C_∞ are the temperature and the concentration of the spices outside the boundary layer respectively. The physical configuration of the problem is shown in Fig.5.2.1. A strong magnetic field is applied in the y-direction. The uniform magnetic field strength B_0 can be taken as $\mathbf{B}=(0,\ B_0, 0)$. However, for such a fluid, the Hall and ion-slip currents will significantly affected the flow in presence of large magnetic fields. The induced magnetic field is neglected, since the magnetic Reynolds number of a partially-ionized fluid is very small. The equation of conservation of electric charge $\overline{\nabla}\bullet\mathbf{J}=0$ gives $J_y=$constant because the direction of propagation is considered only along y-axis and $\mathbf{J}$ does not have any variation along the y-axis. Since the plate is electrically non-conducting, the constant is zero i.e. $J_y=0$ at the plate and everywhere. The equations which govern the flow under the above consideration and Boussinesq's approximation are as follows:

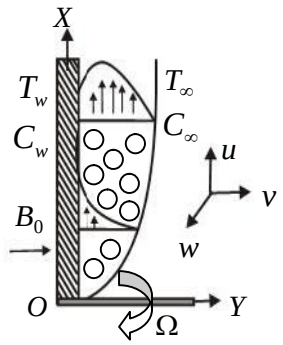

Fig.5.2.1 Physical configuration and coordinate system

The continuity equation; $$\frac{\partial u}{\partial x}+\frac{\partial v}{\partial y}=0 \tag{5.2.1}$$

Momentum equations;

$$\frac{1}{£^2}\left(\frac{\partial u}{\partial t}+u\frac{\partial u}{\partial x}+v\frac{\partial u}{\partial y}\right)=\frac{ł}{£}\frac{\partial^2 u}{\partial y^2}+g_0\ \ (T-T_\infty)+g_0\ \ ^*(C-C_\infty)+2\Omega w-\frac{ł}{k}u$$
$$-cu^2-\frac{±_e B_0^2}{°\left(~_e^2+\ \ _e^2\right)}\left(~_e u+\ \ _e w\right) \tag{5.2.2}$$

$$\frac{1}{£^2}\left(\frac{\partial w}{\partial t}+u\frac{\partial w}{\partial x}+v\frac{\partial w}{\partial y}\right)=\frac{ł}{£}\frac{\partial^2 w}{\partial y^2}-2\Omega u-\frac{ł}{k}w-cw^2+\frac{±_e B_0^2}{°\left(~_e^2+\ \ _e^2\right)}\left(\ \ _e u-~_e w\right) \tag{5.2.3}$$

Energy equation;

$$\frac{\partial T}{\partial t}+u\frac{\partial T}{\partial x}+v\frac{\partial T}{\partial y}=\frac{©}{°c_p}\frac{\partial^2 T}{\partial y^2}+\frac{ł}{c_p}\left[\left(\frac{\partial u}{\partial y}\right)^2+\left(\frac{\partial w}{\partial y}\right)^2\right]+\frac{±_e B_0^2}{°c_p\left(~_e^2+\ \ _e^2\right)}\left(u^2+w^2\right) \tag{5.2.4}$$

Concentration equation;

$$\frac{\partial C}{\partial t}+u\frac{\partial C}{\partial x}+v\frac{\partial C}{\partial y}=D_m\frac{\partial^2 C}{\partial y^2}+\frac{D_m k_T}{T_m}\frac{\partial^2 T}{\partial y^2} \tag{5.2.5}$$

where the variables and related quantities are defined in the Nomenclature.

The initial and boundary conditions for the problems are;

$$t\le 0,\ u=0,v=0,w=0,T=T_\infty,C=C_\infty \text{ everywhere} \tag{5.2.6}$$

$$t>0,\ \ u=0,v=0,w=0,T=T_\infty,C=C_\infty,\ \ at\ \ x=0$$
$$u=U_0,v=0,w=0,T=T_w,\ C=C_w \text{ at } y=0 \tag{5.2.7}$$
$$u=0,v=0,w=0,T=T_\infty,C=C_\infty \quad \text{as } y\to\infty$$

5.2.2 Mathematical Formulation

The problem is simplified by writing the equations in the non-dimensional form. Now introduce the following non-dimensional quantities

$$X=\frac{xU_0}{ł},Y=\frac{yU_0}{ł},U=\frac{u}{U_0},V=\frac{v}{U_0},W=\frac{w}{U_0},²=\frac{tU_0^2}{ł},\overline{T}=\frac{T-T_\infty}{T_w-T_\infty},\overline{C}=\frac{C-C_\infty}{C_w-C_\infty} \tag{5.2.8}$$

Then introducing the dimensionless quantities (5.2.8) in equations (5.2.1)-(5.2.5) respectively, the following dimensionless equations are as follows;

$$\frac{\partial U}{\partial X}+\frac{\partial V}{\partial Y}=0 \tag{5.2.9}$$

$$\frac{\partial U}{\partial ²}+U\frac{\partial U}{\partial X}+V\frac{\partial U}{\partial Y}=£\frac{\partial^2 U}{\partial Y^2}+£^2 G_r\overline{T}+£^2 G_m\overline{C}+2£^2 RW-£^2¥U-£^2\Gamma U^2$$
$$-\frac{£^2 M\left(~_e U+\ \ _e W\right)}{~_e^2+\ \ _e^2} \tag{5.2.10}$$

$$\frac{\partial W}{\partial ²}+U\frac{\partial W}{\partial X}+V\frac{\partial W}{\partial Y}=£\frac{\partial^2 W}{\partial Y^2}-2£^2 RU-£^2¥W-£^2\Gamma W^2+\frac{£^2 M\left(\ \ _e U-~_e W\right)}{~_e^2+\ \ _e^2} \tag{5.2.11}$$

$$\frac{\partial \bar{T}}{\partial ²}+U\frac{\partial \bar{T}}{\partial X}+V\frac{\partial \bar{T}}{\partial Y}=\frac{1}{P_r}\frac{\partial^2 \bar{T}}{\partial Y^2}+E_c\left[\left(\frac{\partial U}{\partial Y}\right)^2+\left(\frac{\partial W}{\partial Y}\right)^2\right]+\frac{ME_c}{\left(\sim_e^2+\ _e^2\right)}\left(U^2+W^2\right) \tag{5.2.12}$$

$$\frac{\partial \bar{C}}{\partial ²}+U\frac{\partial \bar{C}}{\partial X}+V\frac{\partial \bar{C}}{\partial Y}=\frac{1}{S_c}\frac{\partial^2 \bar{C}}{\partial Y^2}+S_0\frac{\partial^2 \bar{T}}{\partial Y^2} \tag{5.2.13}$$

The corresponding boundary conditions are as follows;

$$² \le 0,\ \ U=0, V=0, W=0,\ \bar{T}=0,\ \bar{C}=0 \quad \text{everywhere} \tag{5.2.14}$$

$$² > 0,\ \ U=0, V=0, W=0,\ \bar{T}=0,\ \bar{C}=0 \quad \text{at } X=0$$

$$U=1, V=0, W=0, \bar{T}=1,\ \bar{C}=1 \ \ at\ Y=0 \tag{5.2.15}$$

$$U=0,\ W=0,,\bar{T}=0,\bar{C}=0 \qquad \text{as } Y\to\infty$$

where $G_r\left(=\dfrac{g_0\ (T_w-T_\infty)^3}{U_0^3}\right)$, $G_m\left(=\dfrac{g_0\ ^*(C_w-C_\infty)^3}{U_0^3}\right), M\left(=\dfrac{\pm_e B_0^{2}3}{°U_0^2}\right)$, $P_r\left(=\dfrac{°^3 c_p}{©}\right)$,

$S_c\left(=\dfrac{^3}{D_m}\right)$, $S_0\left(=\dfrac{D_m k_T(T_w-T_\infty)}{^3 T_m(C_w-C_\infty)}\right)$, $R\left(=\dfrac{\Omega^3}{U_0^2}\right)$, $¥\left(=\dfrac{^3\ ^2}{kU_0^2}\right)$, $\Gamma\left(=\dfrac{c^3}{U_0}\right)$, $E_c\left(=\dfrac{U_0^2}{c_p(T_w-T_\infty)}\right)$.

5.2.3 Solution Technique

The governing second order non-linear coupled dimensionless partial differential equations have been solved numerically with the associated boundary conditions. The explicit finite difference method has been used to solve the coupled equations (5.2.9)-(5.2.13) with boundary conditions (5.2.14)- (5.2.15).To obtain the difference equations the region of the flow is divided into a grid or mesh of lines parallel to X and Y axes, where X –axis is taken along the plate and Y -axis is taken normal to the plate. Here the plate height $X_{\max}(80.0)$ is considered i.e. X varies form 0 to 80 and assumed $Y_{\max}(60.0)$ as corresponding $Y\to\infty$ i.e. Y varies from 0 to 60. There are m Z 300 and n Z 300 grid spacing in the X and Y directions respectively and taken as follows

ΔX Z 0.27(0 á X á 80) and ΔY Z 0.2(0 á Y á 60) with the smaller time step $\Delta²$ Z 0.005.

Let $U', V', W', \bar{T}'$ and $\bar{C}'$ denote the values of $U, V, W, \bar{T}$ and $\bar{C}$ at the end of a time-step. Then an appropriate set of finite difference equations corresponding to the equations (5.2.9)-(5.2.13) are as follows;

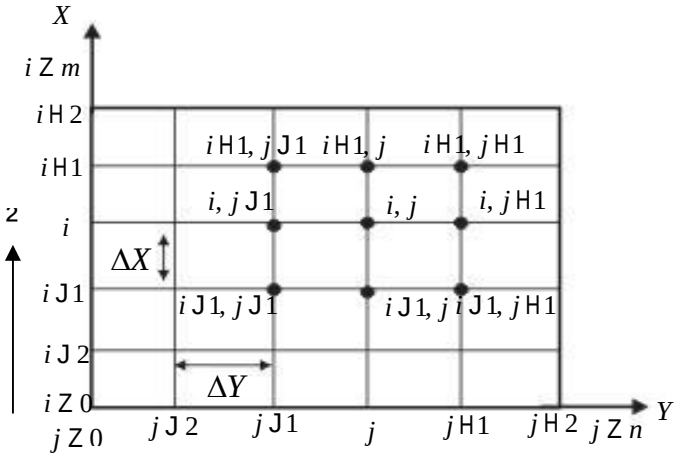

Fig.5.2.2 Finite difference grid space

$$\frac{U'_{i,j}-U'_{i-1,j}}{\Delta X}+\frac{V_{i,j}-V_{i,j-1}}{\Delta Y}=0 \tag{5.2.16}$$

$$\frac{U'_{i,j}-U_{i,j}}{\Delta^2}+U_{i,j}\frac{U_{i,j}-U_{i-1,j}}{\Delta X}+V_{i,j}\frac{U_{i,j+1}-U_{i,j}}{\Delta Y}=\pounds\frac{U_{i,j+1}-2U_{i,j}+U_{i,j-1}}{(\Delta Y)^2}+\pounds^2 G_r\overline{T}_{i,j}$$
$$+\pounds^2 G_m\overline{C}_{i,j}+2\pounds^2 RW_{i,j}-\pounds^2\text{¥}U_{i,j}-\pounds^2\Gamma U_{i,j}^2-\frac{M\pounds^2\left(\sim_e U_{i,j}+{}_e W_{i,j}\right)}{\sim_e^2+{}_e^2} \tag{5.2.17}$$

$$\frac{W'_{i,j}-W_{i,j}}{\Delta^2}+U_{i,j}\frac{W_{i,j}-W_{i-1,j}}{\Delta X}+V_{i,j}\frac{W_{i,j+1}-W_{i,j}}{\Delta Y}=\pounds\frac{W_{i,j+1}-2W_{i,j}+W_{i,j-1}}{(\Delta Y)^2}-2\pounds^2 RU_{i,j}$$
$$-\pounds^2\text{¥}W_{i,j}-\pounds^2\Gamma W_{i,j}^2+\frac{M\pounds^2\left({}_e U_{i,j}-\sim_e W_{i,j}\right)}{\sim_e^2+{}_e^2} \tag{5.2.18}$$

$$\frac{\overline{T}'_{i,j}-\overline{T}_{i,j}}{\Delta^2}+U_{i,j}\frac{\overline{T}_{i,j}-\overline{T}_{i-1,j}}{\Delta X}+V_{i,j}\frac{\overline{T}_{i,j+1}-\overline{T}_{i,j}}{\Delta Y}=\frac{1}{P_r}\frac{\overline{T}_{i,j+1}-2\overline{T}_{i,j}+\overline{T}_{i,j-1}}{(\Delta Y)^2}$$
$$+E_c\left[\left(\frac{U_{i,j+1}-U_{i,j}}{\Delta Y}\right)^2+\left(\frac{W_{i,j+1}-W_{i,j}}{\Delta Y}\right)^2\right]+\frac{ME_c}{\sim_e^2+{}_e^2}\left(U_{i,j}^2+W_{i,j}^2\right) \tag{5.2.19}$$

$$\frac{\overline{C}'_{i,j}-\overline{C}_{i,j}}{\Delta^2}+U_{i,j}\frac{\overline{C}_{i,j}-\overline{C}_{i-1,j}}{\Delta X}+V_{i,j}\frac{\overline{C}_{i,j+1}-\overline{C}_{i,j}}{\Delta Y}=\frac{1}{S_c}\frac{\overline{C}_{i,j+1}-2\overline{C}_{i,j}+\overline{C}_{i,j-1}}{(\Delta Y)^2}$$
$$+S_0\frac{\overline{T}_{i,j+1}-2\overline{T}_{i,j}+\overline{T}_{i,j-1}}{(\Delta Y)^2} \tag{5.2.20}$$

The initial and boundary conditions are obtained as follows;

$$U_{i,j}^0=0, V_{i,j}^0=0, W_{i,j}^0=0,\ \overline{T}_{i,j}^0=0,\ \overline{C}_{i,j}^0=0 \tag{5.2.21}$$

$$U_{0,j}^n=0, V_{0,j}^n=0, W_{0,j}^n=0,\ \overline{T}_{0,j}^n=0,\ \overline{C}_{0,j}^n=0$$

$$U_{i,0}^n=1, V_{i,0}^n=0, W_{i,0}^n=0, \overline{T}_{i,0}^n=1, \overline{C}_{i,0}^n=1 \tag{5.2.22}$$

$$U_{i,L}^n=0, V_{i,L}^n=0, W_{i,L}^n=0, \overline{T}_{i,L}^n=0, \overline{C}_{i,L}^n=0 \quad \text{where } L\to\infty$$

Here the subscripts i designate the grid points with X-coordinates and j designate the grid points with Y-coordinates and superscript n represents a value of time, $\text{²}=\overline{\overline{n}}\Delta\text{²}$ where $\overline{\overline{n}}=0,1,2,3,.....$From these conditions, the value of $\overline{T},\overline{C},U$ and W are known at $\text{²}=0$. During any one time step, the coefficients $U_{i,j}$ and $V_{i,j}$ appearing in equations (5.2.17)-(5.2.20) are treated constants. Then at the end of any time step $\Delta\text{²}$, the new temperature $\overline{T}'$, the new concentration $\overline{C}'$, the new primary velocity U', the new secondary velocity W' and V at any grid points may be obtained by successive applications of equations (5.2.17)-(5.2.20) respectively. This process is repeated in time and provided the time is sufficiently small, $U,V,W,\overline{T}$ and $\overline{C}$ should eventually converge to values which approximate the steady-state solutions of equations (5.2.9)-(5.2.13). These converged solutions are shown graphically in Figs. 5.2.5(a,b) - Figs. 5.2.48(a,b).

5.2.4 Stability and Convergence Analysis

The analysis will remain incomplete unless we discuss the stability and convergence of the finite difference scheme. For the constant mesh sizes, the stability criteria of the scheme can be established as follows. The general terms of the Fourier expansion for $U, W, \bar{T}$ and $\bar{C}$ at a time arbitrarily called $² = 0$ are $e^{i\sim X}, e^{i\ Y}$ apart from a constant, where $i = \sqrt{-1}$. At time $²$ latter, these terms will become

$$\begin{aligned} U &: \cdot\ (²)e^{i\sim X}e^{i\ Y} \\ W &: ¶(²)e^{i\sim X}e^{i\ Y} \\ \bar{T} &: \bar{\ }(²)e^{i\sim X}e^{i\ Y} \\ \bar{C} &: ¤(²)e^{i\sim X}e^{i\ Y} \end{aligned} \tag{5.2.23}$$

Substituting (5.2.23) into equations (5.2.17) to (5.2.20), regarding the coefficients U and V as constants, over any one time step and denoting the values after the time step by $\cdot\ ', ¶', \bar{\ }'$ and $¤'$ gives after simplifications

$$\cdot\ ' = A\cdot\ + B¶ + C\bar{\ }' + D¤' \tag{5.2.24}$$

$$¶' = E¶ + F\cdot \tag{5.2.25}$$

$$\bar{\ }' = G\bar{\ } + H\cdot\ + I¶ \tag{5.2.26}$$

$$¤' = J¤ + K\bar{\ } \tag{5.2.27}$$

where

$$A = 1 - \frac{\Delta²}{\Delta X}U\left(1 - e^{-i\sim\Delta X}\right) - \frac{\Delta²}{\Delta Y}V\left(e^{i\ \Delta Y} - 1\right) + \frac{2£\Delta²}{(\Delta Y)^2}\left(\cos\ \Delta Y - 1\right) - £^2\Delta²¥ - £^2\Delta²\Gamma U - \frac{\Delta² M£^2\sim_e}{\sim_e^2 + \ _e^2}$$

$$E = 1 - \frac{\Delta²}{\Delta X}U\left(1 - e^{-\sim i\Delta X}\right) - \frac{\Delta²}{\Delta Y}V\left(e^{i\ \Delta Y} - 1\right) + \frac{2£\Delta²}{(\Delta Y)^2}\left(\cos\Delta\ Y - 1\right) - \Delta²£^2¥ - \Delta²£^2\Gamma W + \frac{\Delta² M£^2\sim_e}{\sim_e^2 + \ _e^2}$$

$$G = 1 - \frac{\Delta²}{\Delta X}U\left(1 - e^{-i\sim\Delta X}\right) - \frac{\Delta²}{\Delta Y}V\left(e^{i\ \Delta Y} - 1\right) + \frac{1}{P_r}\frac{2\Delta²}{(\Delta Y)^2}\left(\cos\ \Delta Y - 1\right)$$

$$J = 1 - \frac{\Delta²}{\Delta X}U\left(1 - e^{-i\sim\Delta X}\right) - \frac{\Delta²}{\Delta Y}V\left(e^{i\ \Delta Y} - 1\right) + \frac{2}{S_c}\frac{\Delta²}{(\Delta Y)^2}\left(\cos\ \Delta Y - 1\right)$$

$$B = 2£^2R\Delta² - \frac{M£^2\ _e\Delta²}{\sim_e^2 + \ _e^2},\quad C = £^2G_r\Delta²,\quad D = £^2G_m\Delta²\ ,\ F = -2£^2R\Delta² + \frac{M£^2\ _e\Delta²}{\sim_e^2 + \ _e^2},$$

$$H = E_c\frac{\Delta²}{(\Delta Y)^2}U\left(e^{i\ \Delta Y} - 1\right)^2 + \frac{\Delta² ME_c}{\sim_e^2 + \ _e^2}U\ ,\ I = E_c\frac{\Delta²}{(\Delta Y)^2}W\left(e^{i\ \Delta Y} - 1\right)^2 + \frac{\Delta² ME_c}{\sim_e^2 + \ _e^2}W\ ,$$

$$K = \frac{2S_0\Delta²\left(\cos\ \Delta Y - 1\right)}{(\Delta Y)^2}$$

Equations (5.2.24)-(5.2.27) can be written as follows;

$$\cdot\ ' = A_1\cdot\ + B_1¶ + C_1\bar{\ } + D_1¤ \tag{5.2.28}$$

$$¶' = E¶ + F\cdot \tag{5.2.29}$$

$$\bar{\ }' = G\bar{\ } + H\cdot\ + I¶ \tag{5.2.30}$$

$$¤' = J¤ + K\bar{\ } \tag{5.2.31}$$

where $A_1 = A + CH,\ B_1 = B + CI, C_1 = CG + DK, D_1 = DJ$

Equation (5.2.28)- (5.2.31) can be expressed in the following matrix form

$$\begin{bmatrix} \cdot' \\ \P' \\ -' \\ ¤' \end{bmatrix} = \begin{bmatrix} A_1 & B_1 & C_1 & D_1 \\ F & E & 0 & 0 \\ H & I & G & 0 \\ 0 & 0 & K & J \end{bmatrix} \begin{bmatrix} \cdot \\ \P \\ - \\ ¤ \end{bmatrix}$$

i.e. $¦' = T¦$ where $¦$ is the column vector with element $\cdot, \P, -$ and $¤$. T

For stability, to find out eigenvalues of the amplification matrix T. But this study is very difficult since it is fourth order square matrix and all the elements of T are different. It is evident that, the elements of a diagonal matrix represent eigen values of a square matrix. For this purpose $B_1, C_1, D_1 F, H, I$ and K are assume to be very small that is tends to zero and the amplification matrix T can be written in the diagonal form as follows;

$$T \; Z \begin{bmatrix} A_1 & 0 & 0 & 0 \\ 0 & E & 0 & 0 \\ 0 & 0 & G & 0 \\ 0 & 0 & 0 & J \end{bmatrix}$$

For stability, the modulus of each eigenvalues of the amplification matrix T must not exceed unity. Assume that U is everywhere no-negative and V is everywhere non-positive, let

$$a = \frac{U\Delta^2}{\Delta X}, \quad b = \frac{|-V|\Delta^2}{\Delta Y}, \quad c = \frac{\Delta^2}{(\Delta Y)^2}.$$

Then

$$A_1 = 1 - a - b - 2£c + ae^{-i\sim\Delta X} + be^{i\sim\Delta Y} + 2c£\cos \quad \Delta Y$$

$$E = 1 - a - b - 2£c + ae^{-i\sim\Delta X} + be^{i\sim\Delta Y} + 2c£\cos \quad \Delta Y$$

$$G = 1 - a - b - \frac{2c}{P_r} + ae^{-i\sim\Delta X} + be^{i\sim\Delta Y} + \frac{2c}{P_r}\cos \quad \Delta Y$$

$$J = 1 - a - b - \frac{2c}{S_c} + ae^{-i\sim\Delta X} + be^{i\sim\Delta Y} + \frac{2c}{S_c}\cos \quad \Delta Y$$

The coefficients a, b and c are all real and nonnegative. Now demonstrate the maximum modulus of A_1, E, G and J occur when $\sim\Delta X = m®$ and $\Delta Y = n®$, where m and n are integer and hence A_1, E, G and J are real. For Δ^2 sufficiently large, the value of $|A_1|, |E|, |G|$ and $|J|$ are greater when both m and n are odd integer, in which case

$$A_1 = (1 - a - b - 2£c) + (-a - b - 2c£)$$

$$E = (1 - a - b - 2£c) + (-a - b - 2c£)$$

$$G = \left(1 - a - b - \frac{2c}{P_r}\right) + \left(-a - b - \frac{2c}{P_r}\right)$$

$$J = \left(1 - a - b - \frac{2c}{S_c}\right) + \left(-1 - b - \frac{2c}{S_c}\right)$$

To satisfy $|A_1| á 1, |E| á 1, |G| á 1$ and $|J| á 1$ the most negative allowable values are $A_1 = -1, E = -1, G = -1$ and $J = -1$. Hence the stability condition is

$$a+b+2£c \le 1$$
$$a+b+2£c \le 1$$
$$a+b+\frac{2c}{P_r} \le 1$$
$$a+b+\frac{2c}{S_c} \le 1$$

5.2.5 Shear Stress, Nusselt number and Sherwood number

The quantities of chief physical interest are shear stress, Nusselt number and Sherwood number. The shear stress is generally known as the Skin friction, the following equations represent the local and average shear stress at the plate. Local shear stress in x and z axes are as follows;

$²_{LU} = «\left(\frac{\partial u}{\partial y}\right)_{y=0}$ and $²_{LW} = «\left(\frac{\partial w}{\partial y}\right)_{y=0}$ which are proportional to $\left(\frac{\partial U}{\partial Y}\right)_{Y=0}$ and $\left(\frac{\partial W}{\partial Y}\right)_{Y=0}$.

The following equations define the x and z components of the average shear stress

$²_{AU} = «\int_0^{80}\left(\frac{\partial u}{\partial y}\right)_{y=0} dx$ and $²_{AW} = «\int_0^{80}\left(\frac{\partial w}{\partial y}\right)_{y=0} dx$ which are proportional to $\int_0^{80}\left(\frac{\partial U}{\partial Y}\right)_{Y=0} dX$

and $\int_0^{80}\left(\frac{\partial W}{\partial Y}\right)_{Y=0} dX$

The local and average Nusselt numbers are denoted by N_{uL}, N_{uA} which are proportional to

$-\left(\frac{\partial \overline{T}}{\partial Y}\right)_{Y=0}$ and $-\int_0^{80}\left(\frac{\partial \overline{T}}{\partial Y}\right)_{Y=0} dX$

respectively.

Similarly local and average Sherwood numbers are denoted by S_{hL}, S_{hA} are proportional to

$-\left(\frac{\partial C}{\partial Y}\right)_{Y=0}$ and $-\int_0^{80}\left(\frac{\partial \overline{C}}{\partial Y}\right)_{Y=0} dX$.

The values primary velocity $²_{LU}$, $²_{LW}$, N_{uL} and S_{hL} are evaluated by five point approximate formula for the derivatives and then the integral for $²_{AU}$, $²_{AW}$, N_{uA} and S_{hA} are evaluated by the use of the Simpson's $\frac{1}{3}$ integration formula. Values of $²_{LU}$, $²_{LW}$, N_{uL} and S_{hL} and $²_{AU}$, $²_{AW}$, N_{uA} and S_{hA} are shown graphically in Figs.5.2.5(c) -5.2.48(c) respectively for various parameters.

5.2.6. Results and Discussion

5.2.6.1 Justification of Grid Space

The code is converged with different grid space such as m, n = 250, 300, 400 . It is seen that there is a little change for the above mentioned grid points which are shown in Fig.5.2 3. For

save power and time, the results of velocity, temperature and concentration have been carried out for $m, n = 300$.

5.2.6.2 Steady-State Solution

The numerical solutions of the non-linear differential equation (5.2.10)-(5.2.13) under the boundary conditions (5.2.14)-(5.2.15) have been performed by applying explicit finite difference method. In order to verify the effects of time step size Δ², the programming code is conversed our model with different step sizes such as ² Z 20, 60, 70, 80, 90, 100, 110, 120. To get steady–state solutions, the computations have been carried out up to ² Z 120. It is observed that, the result of computations for $U, W, \bar{T}$ and $\bar{C}$, however show little changes after ² Z 100. Thus the solutions of all variables for ² Z 100 are essentially steady-state. Grid space and steady-state solutions are shown in Fig. 5.2.3 and Fig. 5.2.4 only for primary velocity for rotational parameter.

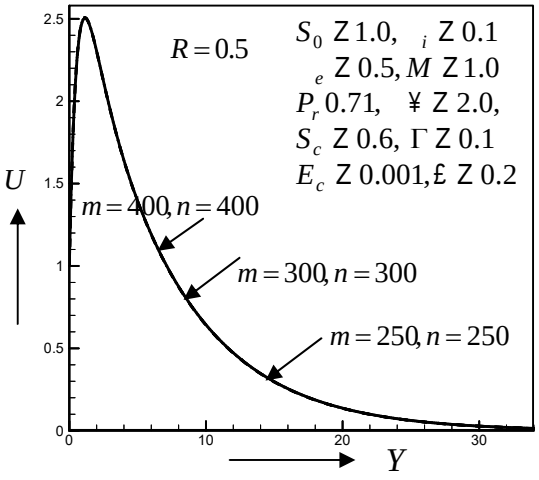

Fig.5.2.3 Primary velocity for different grid space of rotational parameter R

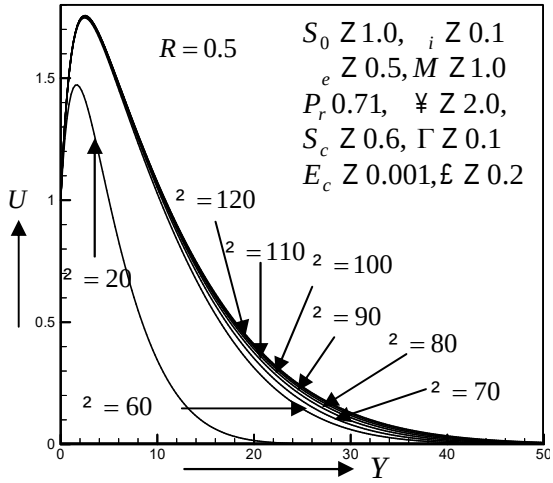

Fig.5.2.4 Primary velocity for different time step of rotation parameter R

In order to analyze the physical situation of the above model, the velocity profiles in x and z components are commonly known as the primary and secondary velocities. The numerical results has been carried out for dimensionless primary velocity (U), secondary velocity(W), temperature($\bar{T}$), species concentration ($\bar{C}$), local and average shear stresses in x-axis ($^2_{LU}$, $^2_{AU}$), local and average shear stresses in z-axis ($^2_{LW}$, $^2_{AW}$), local and average Nusselt numbers (N_{uL}, N_{uA}), local and average Sherwood numbers (S_{hL}, S_{hA}) for various values of the material parameters such as Hall parameter($_e$), ion-slip parameter($_i$), magnetic parameter(M), rotation parameter(R), Prandtl number(P_r), Schmidt number (S_c), Soret number(S_0), permeability parameter(¥), Eckert number (E_c), porosity parameter (£), iteration parameter (Γ). The values for the parameters are chosen arbitrarily in most cases. Some standard values for of the Prandtl number (P_r) is considered because of the physical importance. These are $P_r = 0.71$ corresponds to air, $P_r = 1.0$ corresponds to electrolyte solution such as salt water and $P_r = 1.63$ corresponds to glycerin at $50^0 C$ and Schmidt

number (S_c) the values $0.60, 1.0, 2.62$ are considered, which represent specific condition of flow (0.60 corresponds to water vapor, 1.0 correspond to carbonsioxid that represents the most common effect in air, 2.62 corresponds to propyl-benzene at $20^0 C$). The importance of cooling problem in nuclear engineering in connection with the cooling of reactors, the values of G_r and G_m are taken positive. Throughout the calculations the values of G_r and G_m are taken very large ($G_r = 5.0$ and $G_m = 2.0$).

Form Fig.5.2.5 (a-c) and Fig.5.2.9 (a-c) it has been seen that the primary velocity (U), local and average shear stresses in x-axis (τ_{LU}, τ_{AU}) increase with an increase of Hall and ion-slip parameter ($_e$ and $_i$). This is due to fact that the effective conductivity decreases, which reduces the magnetic resistive force affecting on the primary flow. But secondary velocity (W), local and average shear stresses in z-axis (τ_{LW}, τ_{AW}) have increasing effects with an increase of $_e$ which are found in Fig.6 (a-c). Since W is a result of the Hall Effect. Also secondary velocity (W), local and average shear stresses in z-axis (τ_{LW}, τ_{AW}) have decreasing effects with the increase of $_i$ which is found in Fig.10 (a-c). From this figure it is clear that ion-slip parameter $_i$ retards the flow which leads to reduction in boundary layer thickness. It is noted from Fig.5.2.7 (a) and Fig.5.2.11 (a) that the temperature ($\bar{T}$) decreases when $_e$ and $_i$ are increased and also thermal boundary layer thickness decreases. While local and average Nusselt numbers are increased which are found in Fig. 5.2.7(b,c) and Fig.5.2.11(b,c). Increases in the values of $_e$ have a tendency to increase the frictional effects and to augment the heat transfer at the wall. This is reflected in the increases in the local and average Nusselt numbers. Fig.5.2. 8(a) illustrates the concentration distribution for different values of Hall parameter ($_e$). It is seen that concentration distribution decreases with the increase of $_e$. But local and average Sherwood numbers increase with the increase of $_e$ which is seen in Fig.5.2.8 (b,c). The concentration ($\bar{C}$) distribution has minor increasing effects with an increased of $_i$ whereas local and average Sherwood numbers (S_{hL}, S_{hA}) have opposite behavior which have been shown in Fig.5.2.12 (a-c).

In Fig.5.2.13 (a), it has been illustrated that primary velocity (U) firstly decreases near the plate, then start to increase far away from the plate with an increase of inertia parameter (Γ). So there is cross flow at $Y \approx 11.0$ (approximately). The medium inertial (Γ) effects constitute resistance to flow. Thus the inertial parameter (Γ) increases, the resistance to the flow increases, causing the fluid flow in the porous medium to slow down. The local and average shear stresses in x-axis(τ_{LU}, τ_{AU}) decrease with the increase of Γ which is seen in Fig.5.2.13 (b,c). The secondary velocity (W), local and average shear stresses in z-axis (τ_{LW}, τ_{AW}) have decreasing effects which is found in Fig.14 (a-c). It is found that the temperature and concentration profiles increase whereas local and average Nusselt and Sherwood numbers are decreased with increasing Γ which are found in Fig. 5.2.15(a-c) and Fig. 5.2.16(a-c).

Analyzing the Fig.5.2.17 (a) it is clearly seen that the primary velocity (U) profiles firstly increases in the interval $(0 \le Y \le 21.0)$ and the minor decreasing effects $Y > 21.0$ with an

increase (E_c). A cross flow inside the boundary layer has been obtained. This is due to the heat energy stored in the liquid because of the frictional heating. The local and average shear stresses in *x*-axis (τ_{LU}, τ_{AU}) increases in Fig.5.2.17 (b,c). Also the secondary velocity (W) firstly decrease near the plate after then increases far away from the plate with an increase (E_c) in Fig.5.2.18(a). So there is cross flow at $Y \approx 20.0$ (approximately). The local and average shear stresses in z-axis (τ_{LW}, τ_{AW}) have decreasing effects which is found in Fig.5.2.18 (b,c). The effect of Eckert number E_c on the temperature is shown in Fig.5.2.19 (a). Eckert number is the ratio of the kinetic energy of the flow to the boundary layer enthalpy difference. The effect of viscous dissipation on flow field is to increase the energy, yielding a greater fluid temperature and as a consequence greater buoyancy force. The increase in the buoyancy force due to an increase in the dissipation parameter enhances the temperature. Local and average Nusselt numbers (N_{uL}, N_{uA}) have reverse effect which is shown in Fig.5.2.19 (b,c). Fig.5.2.20 (a) shows that E_c is increased, the concentration profile decreases whereas local and average Sherwood numbers (S_{hL}, S_{hA}) profiles increases which is found in Fig.5.2. 20(b,c).

Figures 5.2.21(a-c), 5.2.23(a) and 5.2.24(a) depict the effect of the porosity parameter on the primary velocity, local and average shear stresses in *x*-axis, temperature and concentration profiles of the flow. It is evident from this figure that an increase in the porosity parameter improves the primary velocity, local and average shear stresses profiles in *x*-axis while both temperature and concentration profiles have reverse effect. Increases in porosity parameter widen the porous layers of the flow which increases the velocity boundary layer thickness and decreases the thermal as well as concentration boundary layer thicknesses. Whereas secondary velocity(W), local and average shear stresses in z-axis (τ_{LW}, τ_{AW}) have decreasing effect which are found in Fig.5.2.22 (a-c). Local and average Nusselt and Sherwood numbers increase with increasing(£)which are shown in Figure 5.2.23(b,c) and Figure 5.2.24(b,c).

From Fig.5.2.25 (a) it is seen that, firstly the primary velocity (U) decreases up to $Y = 20.0$ but after that (U) increases with the increases of permeability parameter (¥). So there obtained a cross flow. An increase in ¥ will increase the resistance of the porous medium which will tend to decelerate the flow and reduce the velocity. Local and average shear stresses in x-axis (τ_{LU}, τ_{AU}) are decreased which are seen in Fig.5.2.25 (b,c). It is seen from Figs.5.2.26 (a-c), the secondary velocity (W), local, average shear stresses in z-axis (τ_{LW}, τ_{AW}) are increased with an increase of ¥ . From Fig.5.2.27 (a-c) and Fig.5.2.28 (a-c) it is observed that the temperature $\bar{T}$ and concentration ($\bar{C}$) distributions increase whereas local and average Nusselt (N_{uL}, N_{uA}) and Sherwood (S_{hL}, S_{hA}) numbers decrease with increasing ¥ . This is due to the fact that increasing the value of permeability parameter has tendency to increase the thermal boundary layer and concentration species.

From Fig.5.2.29 (a-c) and Fig.5.2.30 (a-c), it has been seen that the primary velocity (U), local and average shear stresses in x-axis (τ_{LU}, τ_{AU}) decrease whereas the secondary velocity (W), local and average shear stresses in z-axis (τ_{LW}, τ_{AW}) increase with an increase in

magnetic parameter (M). An increase in the value of the magnetic parameter (M) leads to increase in the magnitude of the Lorentz force which serves to retard the primary fluid velocity. The result of Fig.5.2.30 (a-c) indicates that the resulting Lorentzian body force will not act as a drag force as in conventional MHD flows, but as an aiding body force. This will serve to accelerate the secondary fluid velocity. Fig.5.2.31 (a-c) and Fig. 5.2.32(a-c) are illustrated that the temperature $(\bar{T})$ and concentration $(\bar{C})$ distributions increase whereas local and average Nusselt (N_{uL}, N_{uA}) and Sherwood numbers (S_{hL}, S_{hA}) decrease with increasing (M). The effects of a transverse magnetic field to an electrically conducting fluid gives rise to a resistive-type force called the Lorentz force. This force has the tendency to increase its temperature and concentration distributions.

From Fig.5.2.33 (a-c) it is seen that the primary velocity (U), local and average shear stresses in x-axis (τ_{LU}, τ_{AU}) decrease with an increases of Prandtl number(P_r). This is because in the free convection the plate velocity is higher than the adjacent fluid velocity and the momentum boundary layer thickness decreases. But opposite behavior is found for secondary velocity (W), local and average shear stresses in z-axis (τ_{LW}, τ_{AW}) which are shown in Fig.5.2.34 (a-c). From Fig. 5.2.35(a-c), it is observed that the temperature $(\bar{T})$ distribution decreases whereas local and average Nusselt numbers (N_{uL}, N_{uA}) have opposite behavior have been illustrate with an increases of Prandtl number (P_r). This is consistent with the well-known fact that the thermal boundary layer thickness decreases with increasing (P_r). Also the temperature decreased at a faster rate for higher values of (P_r). This shows that the rate of cooling is faster in the case of higher Prandtl number. In Fig.5.2.36 (a) the concentration distribution increases firstly, then starts to decrease with an increase (P_r). So there is a cross flow near $Y = 22.0$ (approximately). Because the concentration boundary layer thickness increases as (P_r) increases. But local and average Sherwood numbers (S_{hL}, S_{hA}) decrease in Fig.5.2.36 (b,c).

It is seen from Fig. 5.2.37(a), the primary velocity (U) profiles decreases firstly, then start to increase with the increase of rotational parameter (R). So there is a cross flow near $Y = 20.0$ (approximately). But local and average shear stresses in x-axis (τ_{LU}, τ_{AU}) decrease which are shown in Fig.5.2.37 (b-c). In fact rotation parameter defines the relative magnitude of the Coriolis force and the viscous force, thus rotation retards primary flow in the boundary layer. The secondary velocity (W), local and average shear stresses in z-axis (τ_{LW}, τ_{AW}) have decreasing effect in R are shown in Fig.5.2.38 (a-c).

From Fig.5.2.39(a-c) it is found that the primary velocity (U), local and average shear stresses in x-axis (τ_{LU}, τ_{AU}) profiles increase with an increase in Soret number(S_0). This is because either a decrease in concentration difference or an increase in temperature difference leads to an increase in the value of S_0. Hence, increasing the S_0 increases the velocity of the fluid. But opposite behavior are found on secondary velocity (W), local and average shear stresses in z-axis (τ_{LW}, τ_{AW}) which are shown in Fig.5.2.40 (a-c). It has been observed that the temperature $(\bar{T})$ has minor decreasing effects whereas local and average Nusselt numbers

(N_{uL} , N_{uA}) have reverse effects with an increase of S_0 which are found in Fig.5.2.41 (a-c). The concentration $(\overline{C})$ distribution increases while local and average Sherwood numbers (S_{hL} , S_{hA}) are decreased with an increase of S_0 .in Fig.5.2.42 (a-c). As the Soret parameter is increased, the concentration boundary layer thickness increases, thus decreasing the mass transfer rate at the wall.

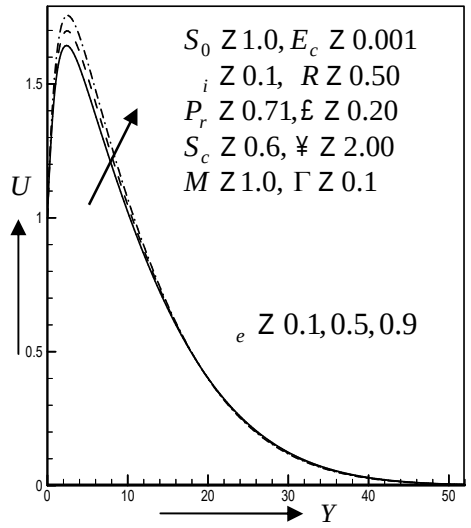

Fig.5.2.5(a) Primary velocity profiles for different values of $_e$

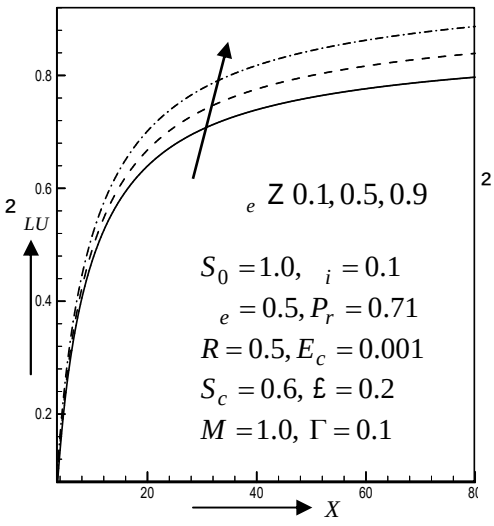

Fig.5.2.5 (b) Local Shear stress in x -axis for different values of $_e$

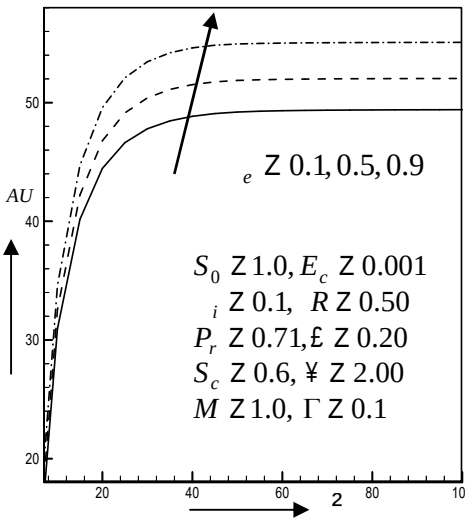

Fig.5.2.5(c) Average Shear stress in x -axis for different values of $_e$

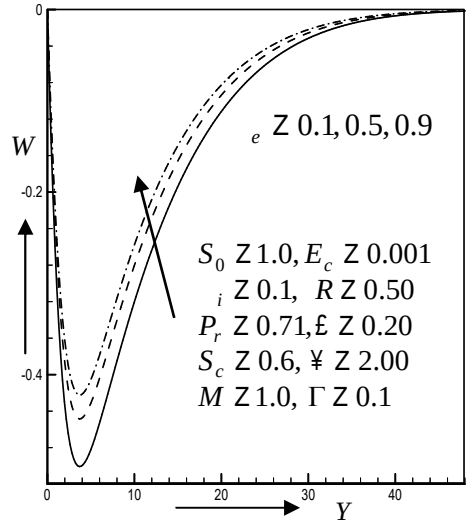

Fig.5.2.6(a) Secondary velocity profiles for different values of $_e$

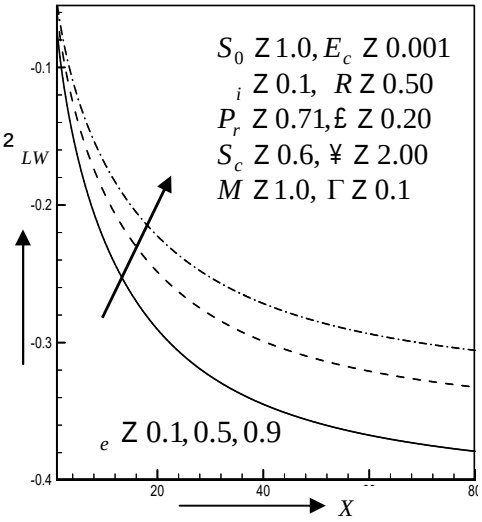

Fig.5.2.6(b) Local Shear stress in z -axis for different values of $_e$

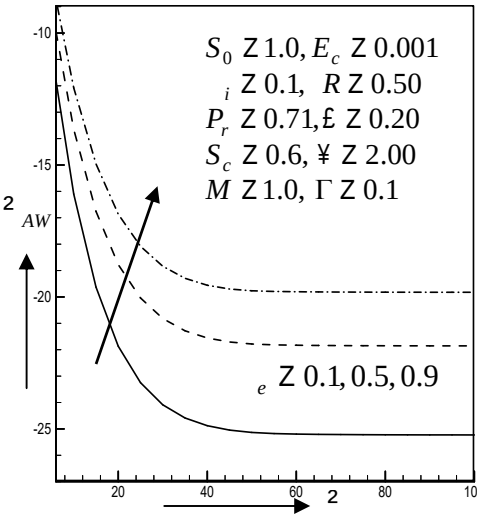

Fig.5.2.6(c) Average Shear stress in z -axis for different values of $_e$

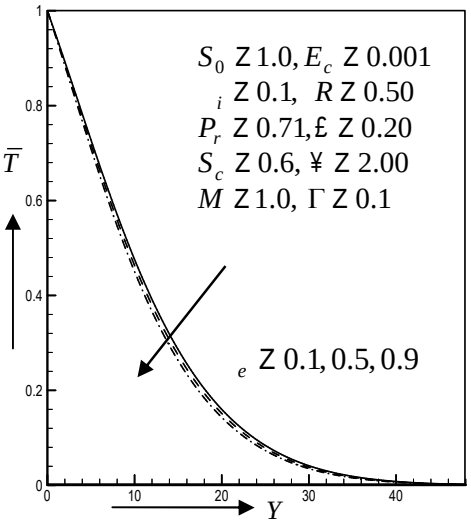

Fig.5.2.7(a) Temperature profiles for different values of $_e$

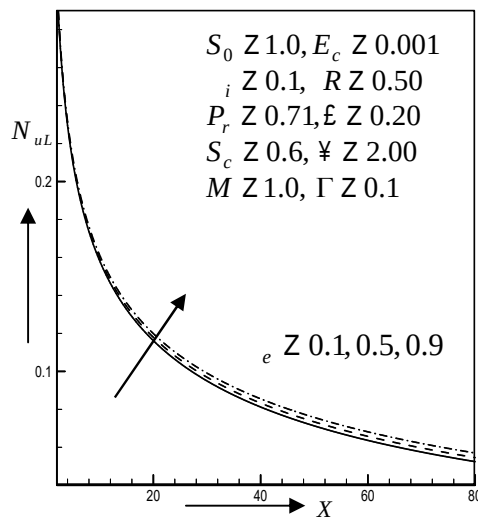

Fig.5.2.7(b) Local Nusselt number for different values of $_e$

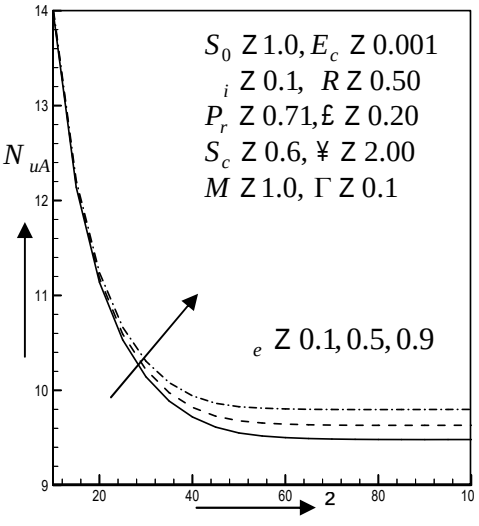

Fig.5.2.7(c) Average Nusselt number for different values of $_e$

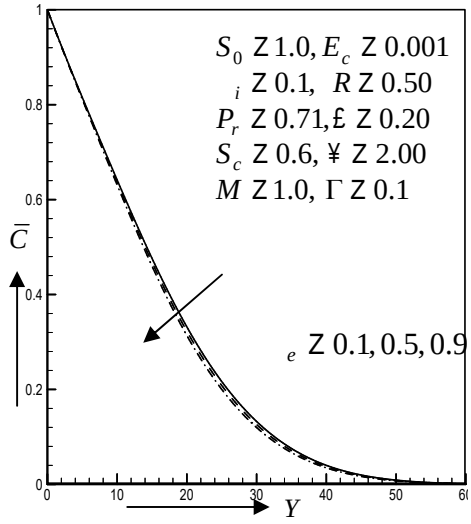

Fig.5.2.8(a) Concentration profiles for different values of $_e$

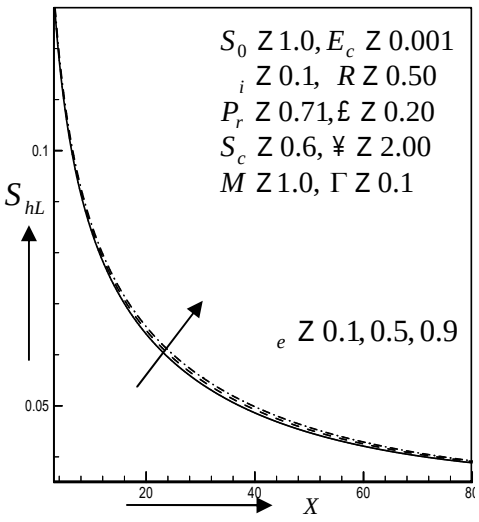

Fig.5.2.8(b) Local Sherwood number for different values of $_e$

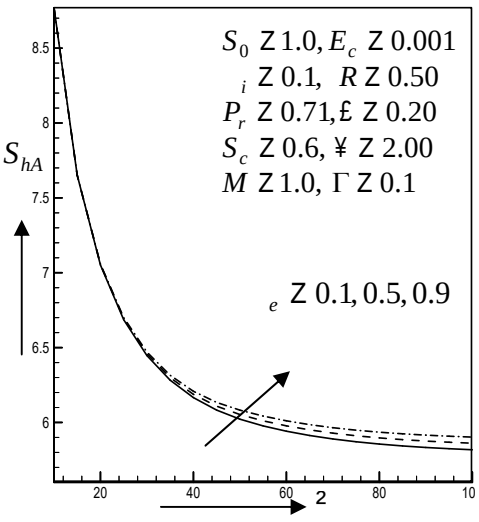

Fig.5.2.8(c) Average Sherwood number for different values of $_e$

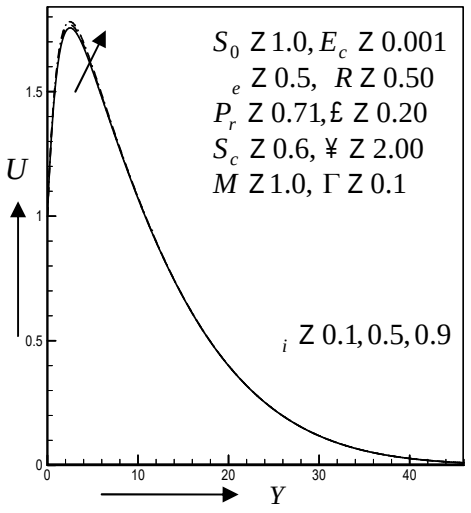

Fig.5.2.9(a) Primary velocity profiles for different values of $_i$

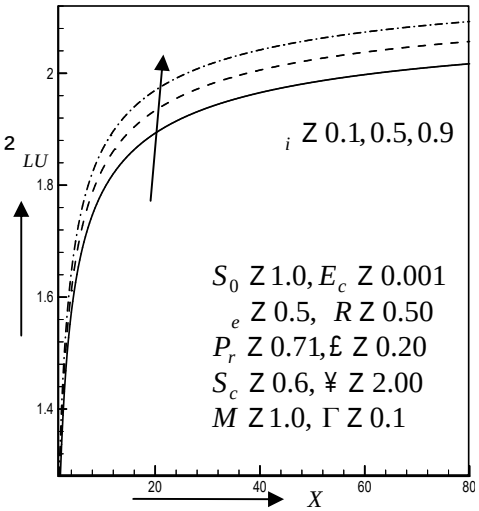

Fig.5.2.9(b) Local Shear stress in x -axis for different values of $_i$

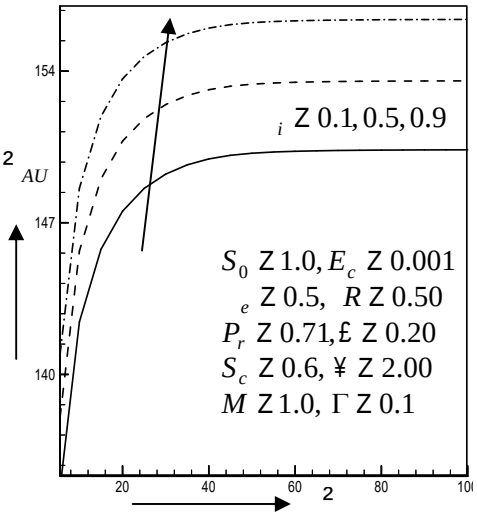

Fig.5.2.9(c) Average Shear stress in x -axis for different values of

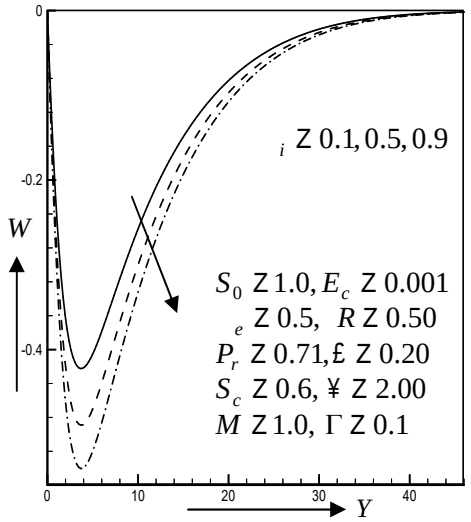

Fig.5.2.10(a) Secondary velocity profiles for different values of $_i$

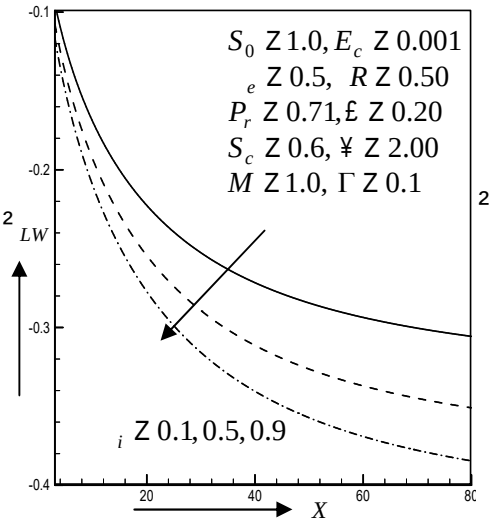

Fig.5.2.10(b) Local Shear stress in z -axis for different values of $_i$

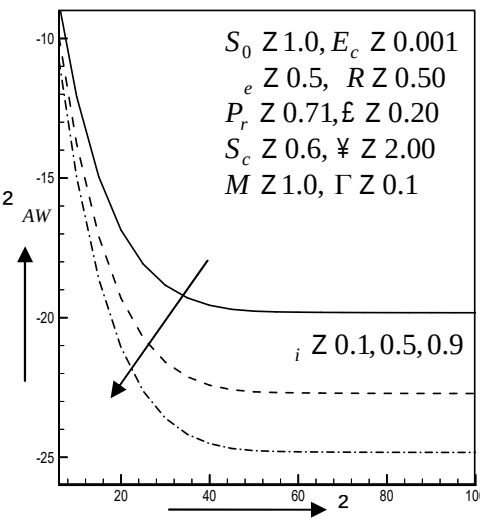

Fig.5.2.10(c) Average Shear stress in z -axis for different values of $_i$

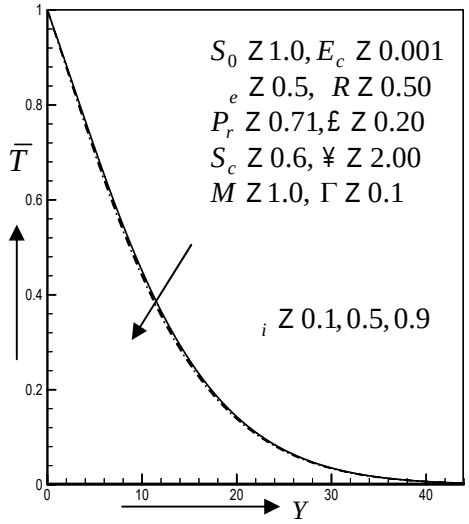

Fig.5.2.11(a) Temperature profiles for different values of $_i$

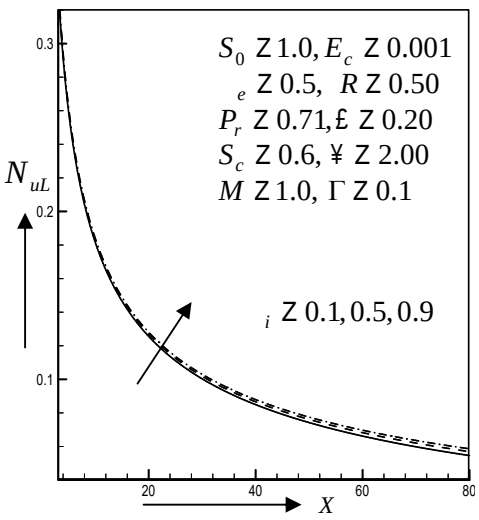

Fig.5.2.11(b) Local Nusselt number for different values of $_i$

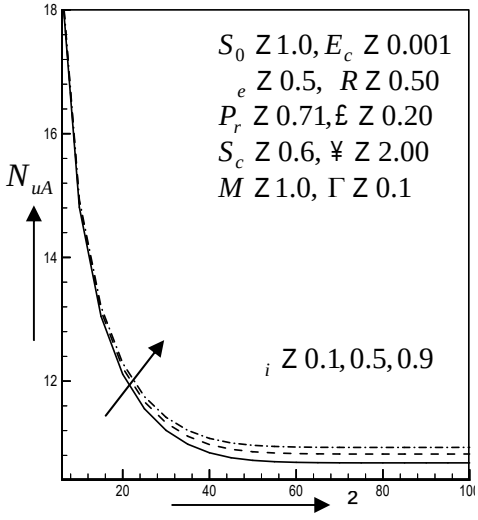

Fig.5.2.11(c) Average Nusselt number for different values of $_i$

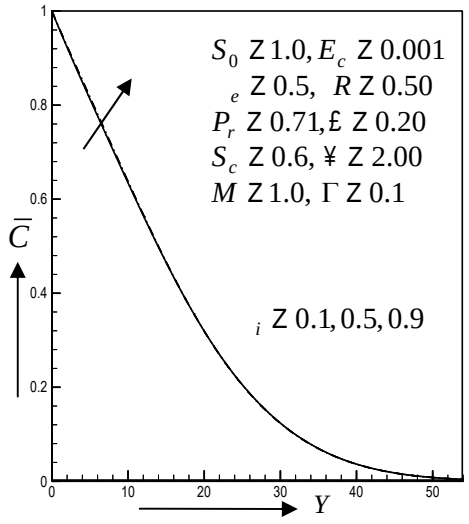

Fig.5.2.12(a) Concentration profiles for different values of $_i$

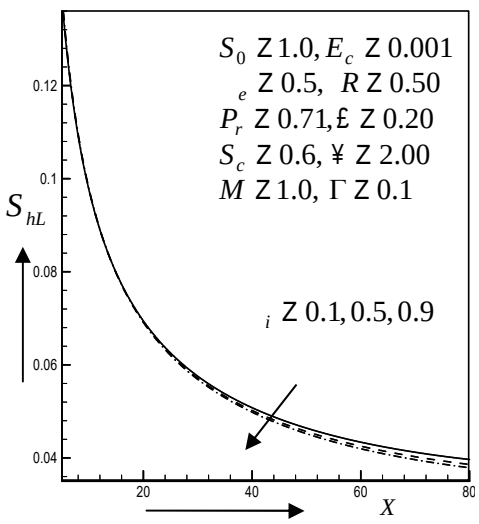

Fig.5.2.12(b) Local Sherwood number for different values of $_i$

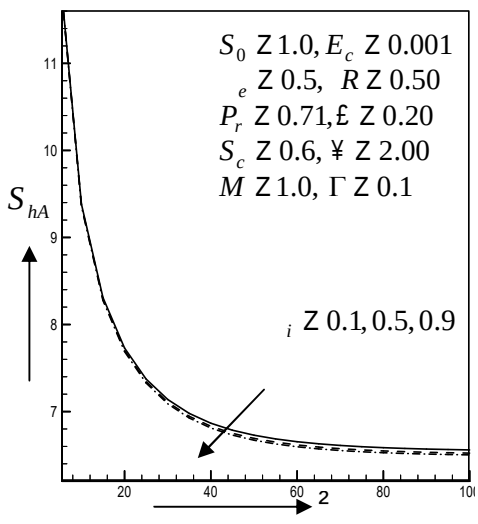

Fig.5.2.12(c) Average Sherwood number for different values of $_i$

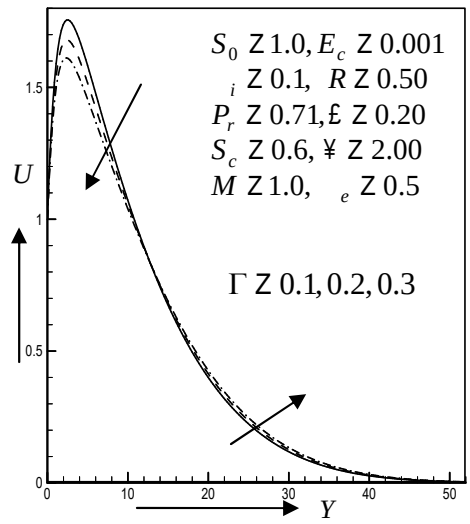

Fig.5.2.13(a) Primary velocity profiles for different values of Γ

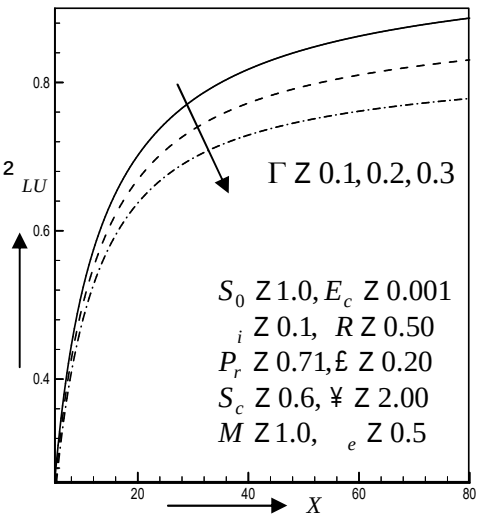

Fig.5.2.13(b) Local Shear stress in x-axis for different values of Γ

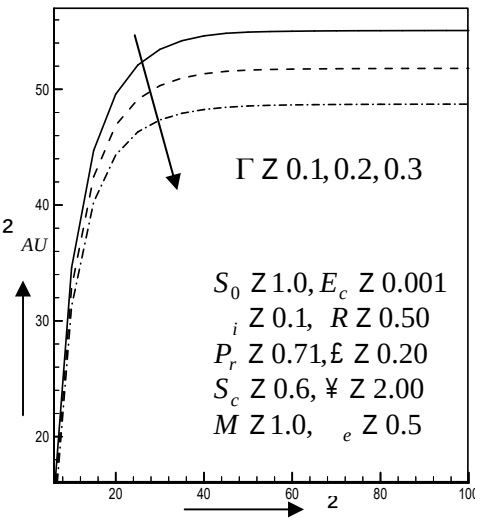

Fig.5.2.13(c) Average Shear stress in x-axis for different values of Γ

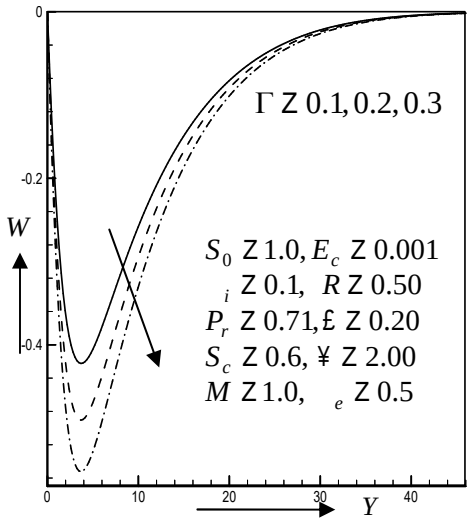

Fig.5.2.14(a) Secondary velocity profiles for different values of Γ

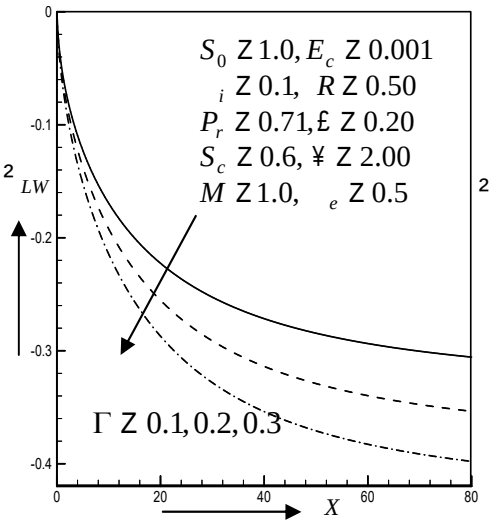

Fig.5.2.14(b) Local Shear stress in z - axis for different values of Γ

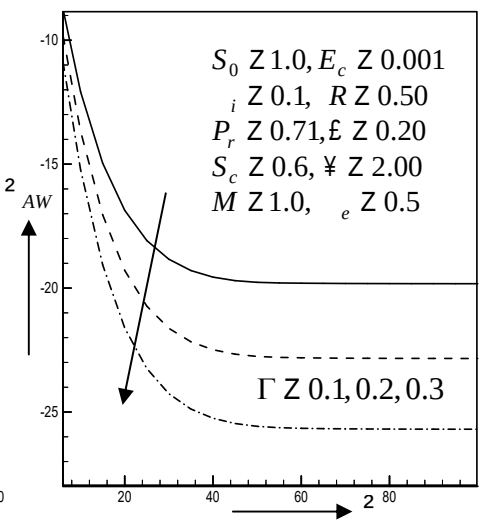

Fig.5.2.14(c) Average Shear stress in z - axis for different values of Γ

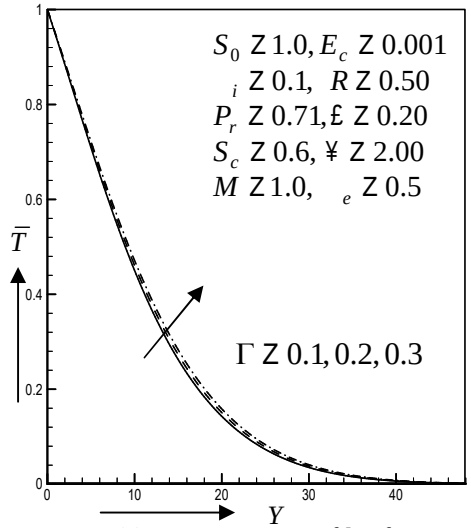

Fig.5.2.15(a) Temperature profiles for different values of Γ

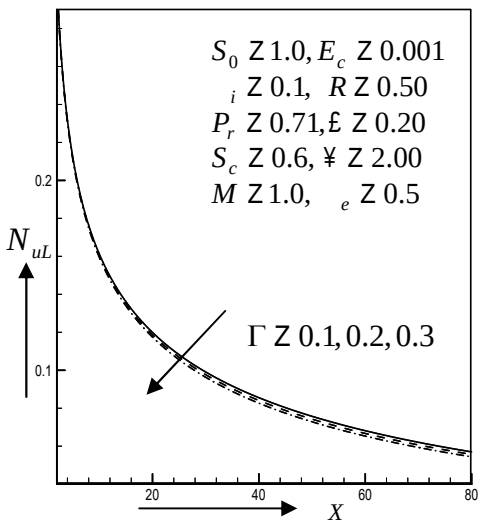

Fig.5.2.15(b) Local Nusselt number for different values of Γ

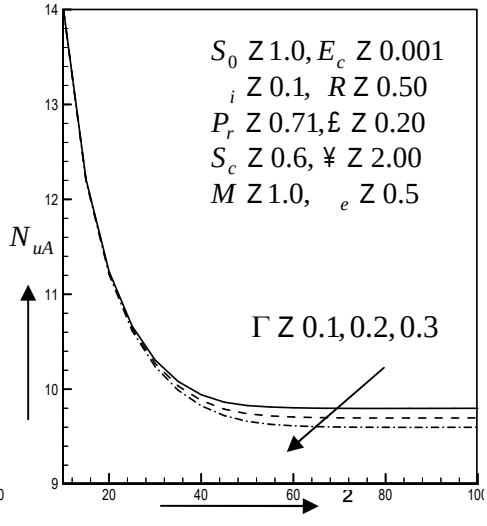

Fig.5.2.15(c) Average Nusselt number for different values of Γ

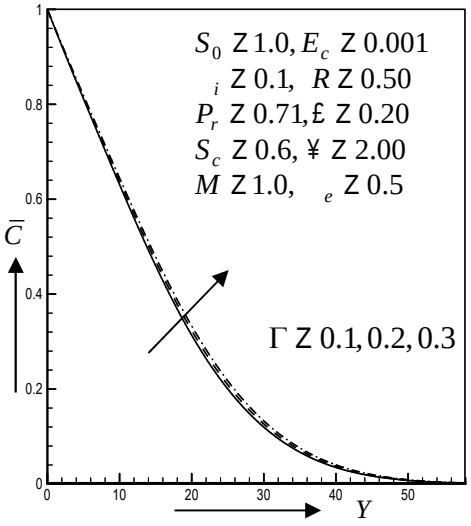

Fig.5.2.16(a) Concentration profiles for different values of Γ

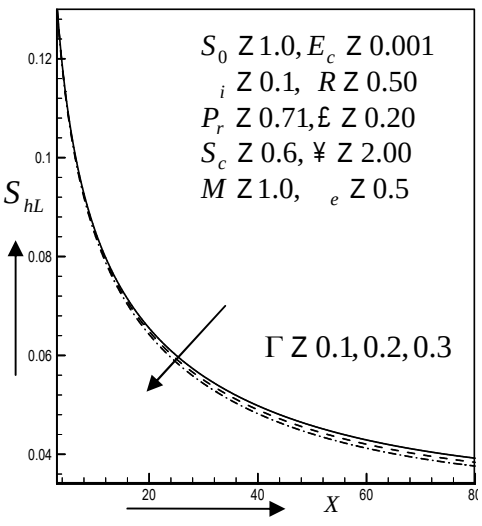

Fig.5.2.16(b) Local Sherwood number for different values of Γ

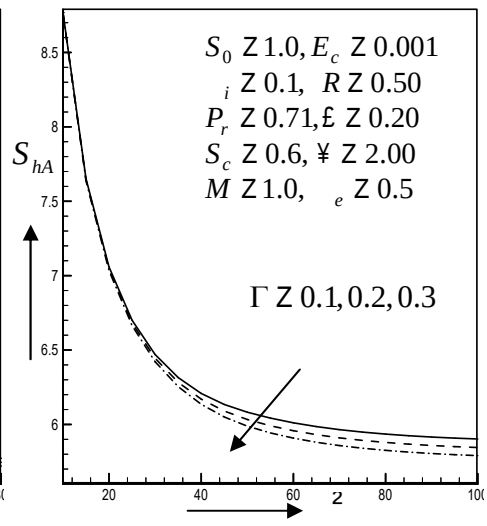

Fig.5.2.16(c) Average Sherwood number for different values of Γ

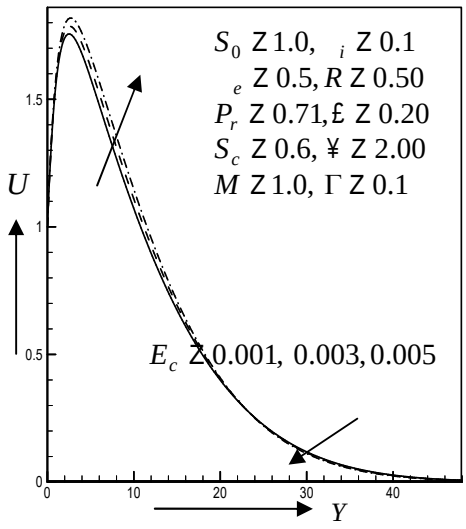

Fig.5.2.17(a) Primary velocity profiles for different values of E_c

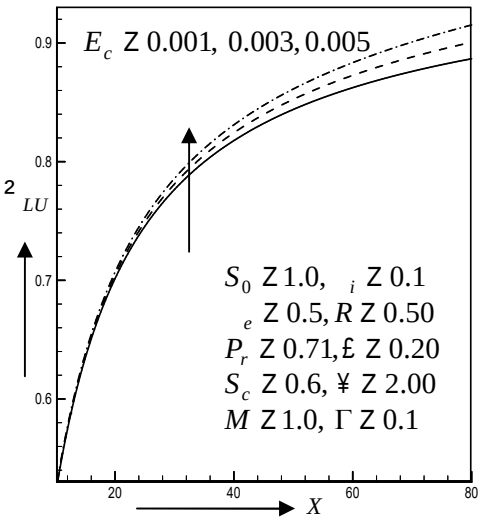

Fig.5.2.17(b) Local Shear stress in x-axis for different values of E_c

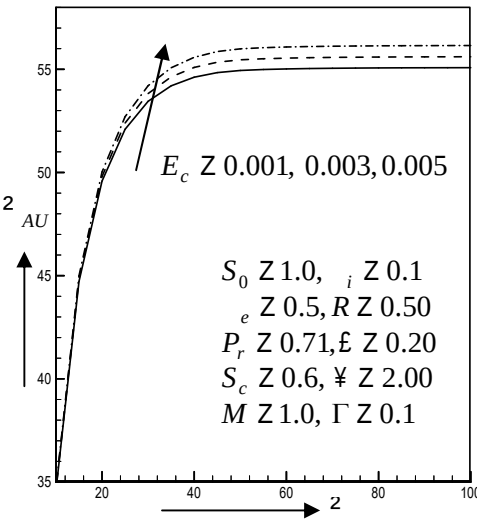

Fig.5.2.17(c) Average Shear stress in x-axis for different values of E_c

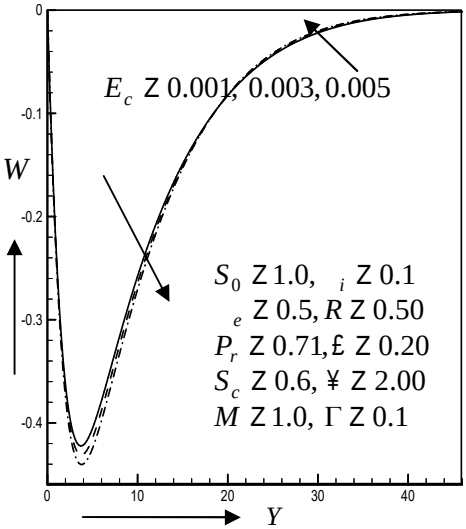

Fig.5.2.18(a) Secondary velocity profiles for different values of E_c

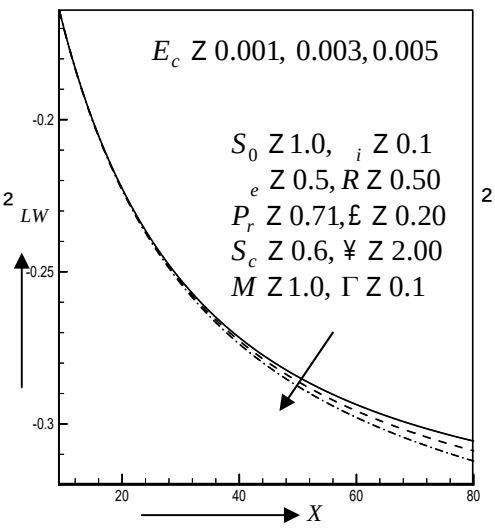

Fig.5.2.18(b) Local Shear stress in z-axis for different values of E_c

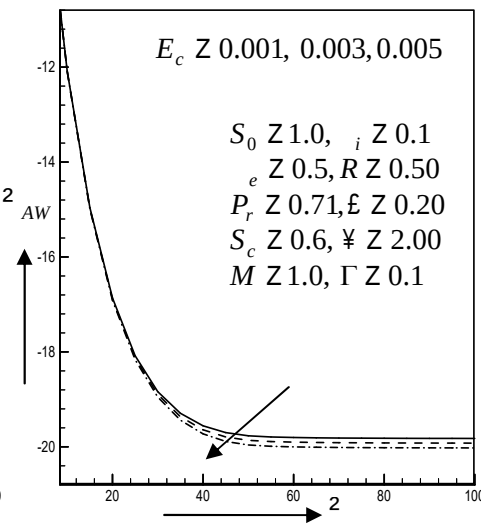

Fig.5.2.18(b) Average Shear stress in z-axis for different values of E_c

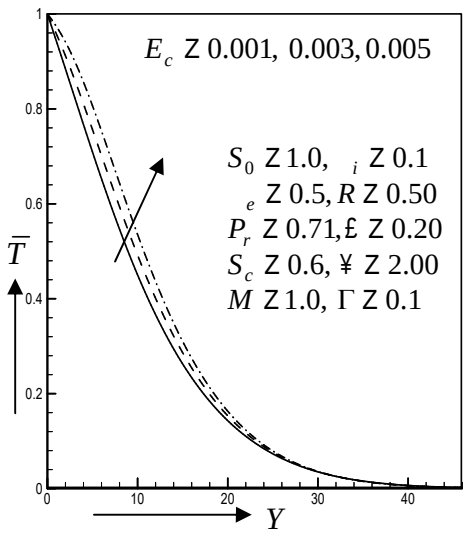

Fig.5.2.19(a) Temperature profiles for different values of E_c

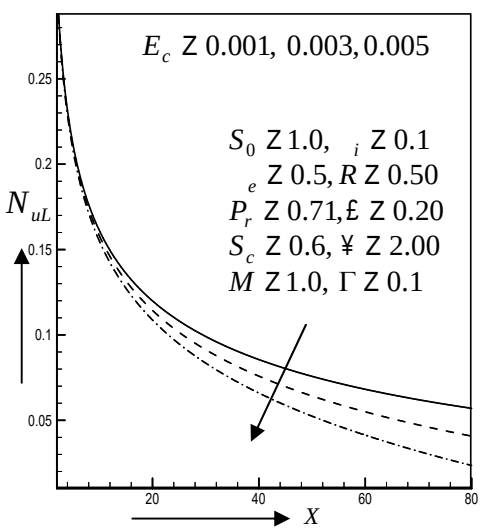

Fig.5.2.19(b) Local Nusselt number for different values of E_c

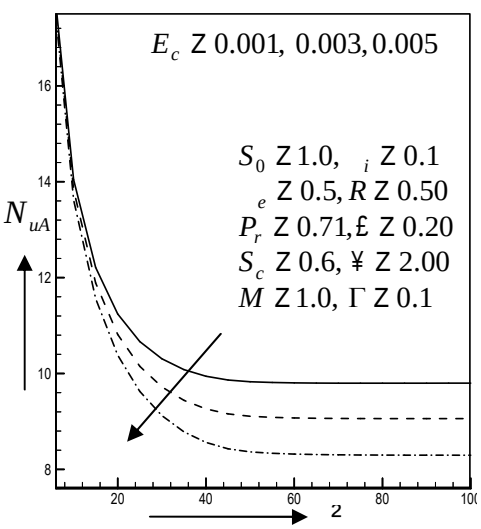

Fig.5.2.19(c) Average Nusselt number for different values of E_c

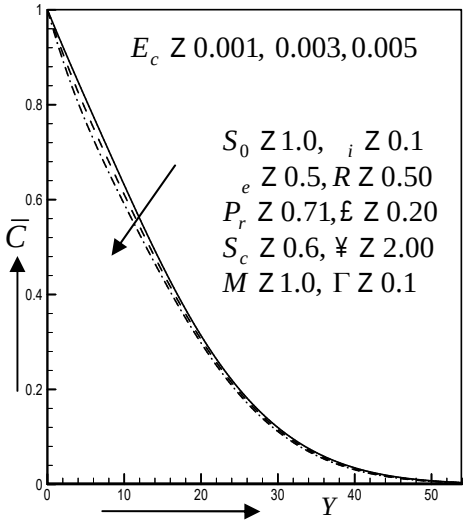

Fig.5.2.20(a) Concentration profiles for different values of E_c

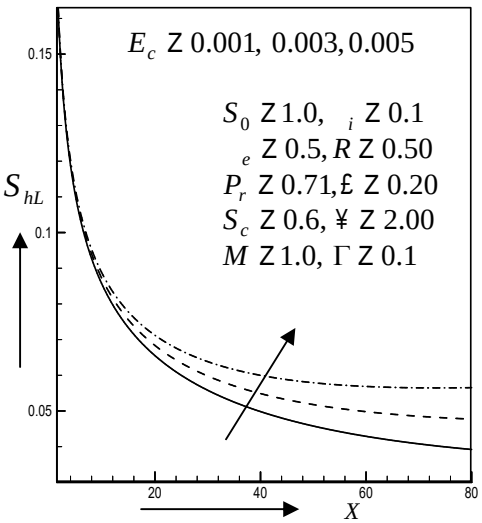

Fig.5.2.20(b) Local Sherwood number for different values of E_c

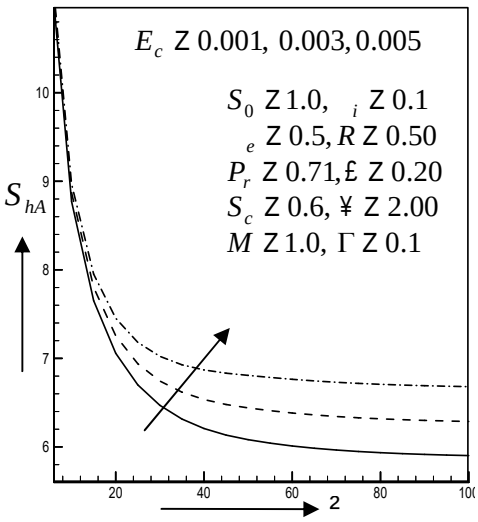

Fig.5.2.20(c) Average Sherwood number for different values of E_c

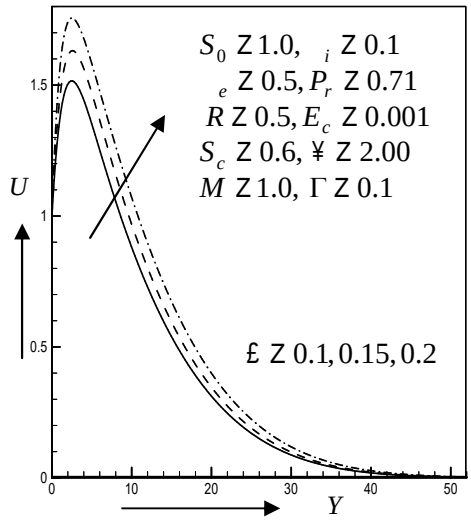

5.2.21(a) Primary velocity profiles for Fig. different values of £

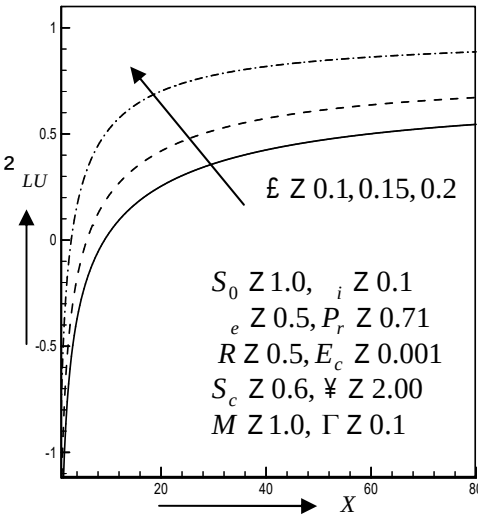

Fig.5.21(b) Local Shear stress in x -axis for different values of £

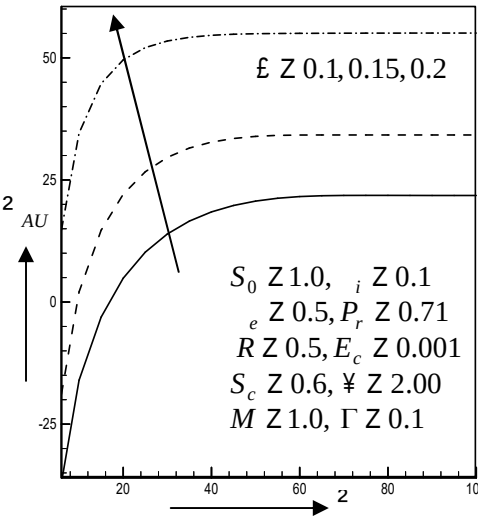

Fig.5.2.21(c) Average Shear stress in x -axis for different values of £

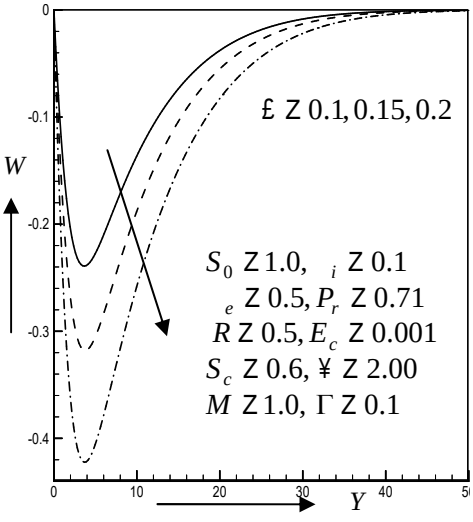

Fig.5.2.22(a) Secondary velocity profiles for different values of £

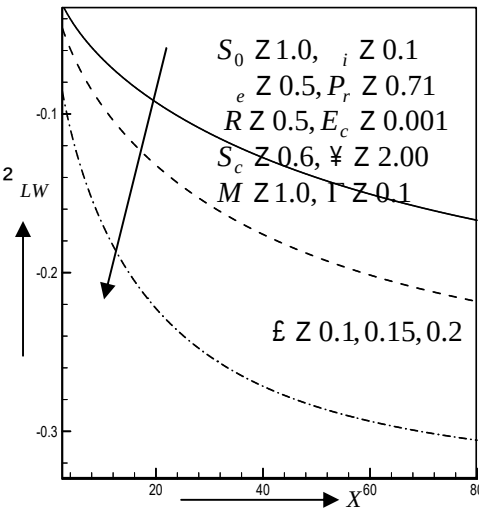

Fig.5.2.22(b) Local Shear stress in z -axis for different values of £

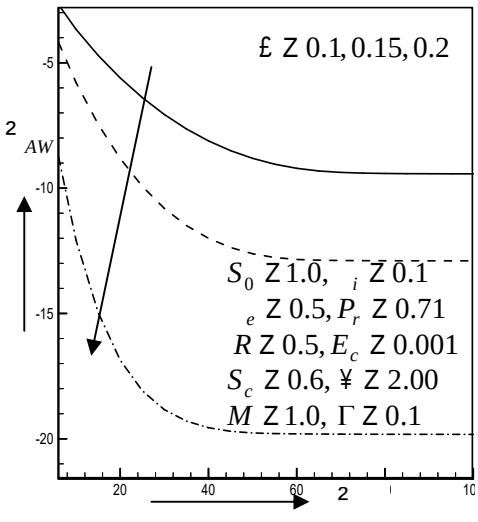

Fig.5.2.22(c) Average Shear stress in z -axis for different values of £

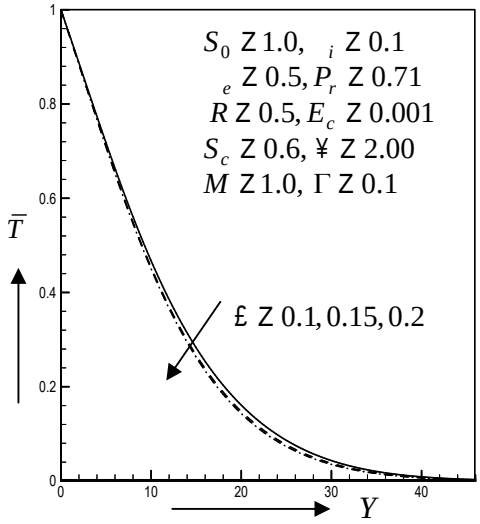

Fig.5.2.23(a) Temperature profiles for different values of £

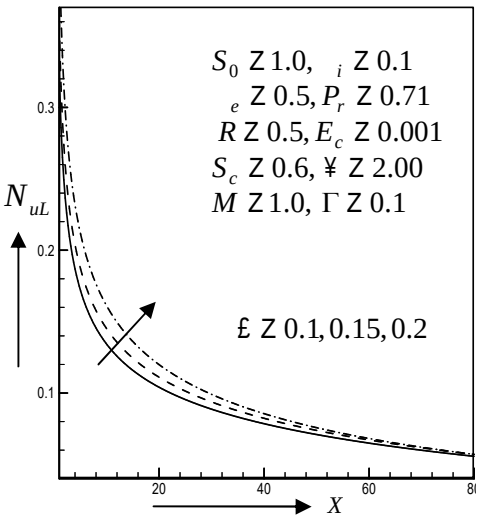

Fig.5.2.23(b) Local Nusselt number for different values of £

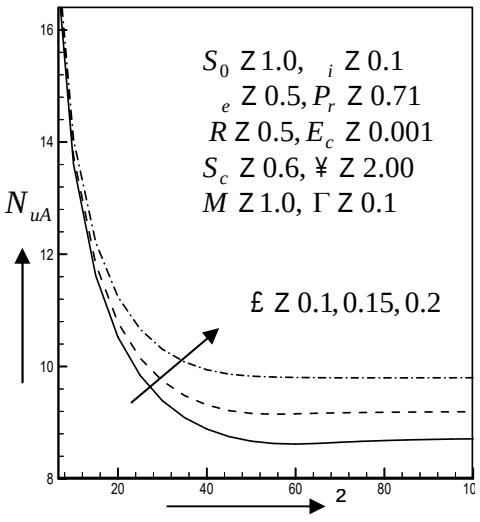

Fig.5.2.23(c) Average Nusselt number for different values of £

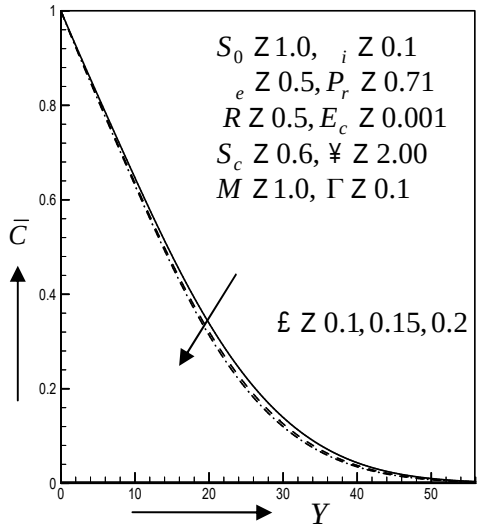

Fig.5.2.24(a) Concentration profiles for different values of £

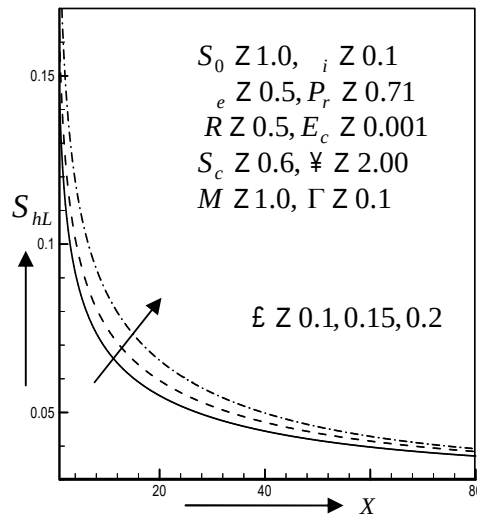

Fig.5.2.20(b) Local Sherwood number for different values of £

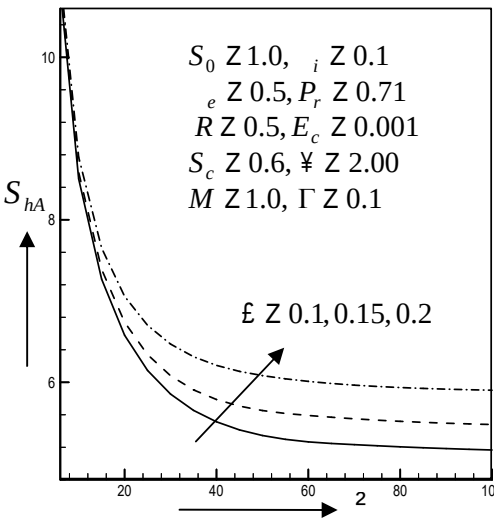

Fig.5.2.24(c) Average Sherwood number for different values of £

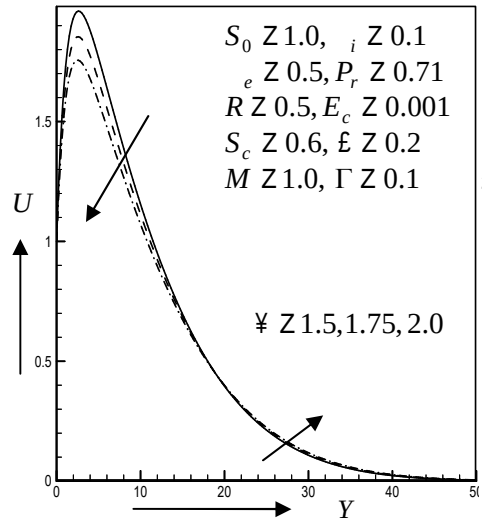

Fig.5.2.25(a) Primary velocity profiles for different values of ¥

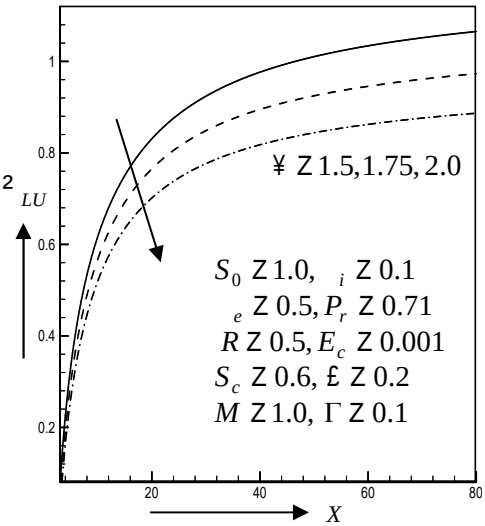

Fig.5.2.25(b) Local Shear stress in x - axis for different values of ¥

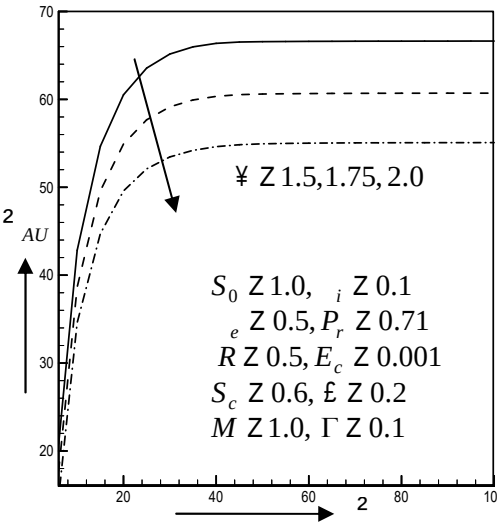

Fig.5.2.25(c)Average Shear stress in x - axis for different values of ¥

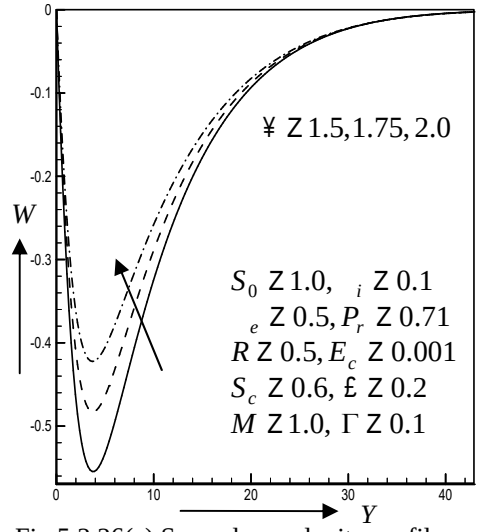

Fig.5.2.26(a) Secondary velocity profiles for different values of ¥

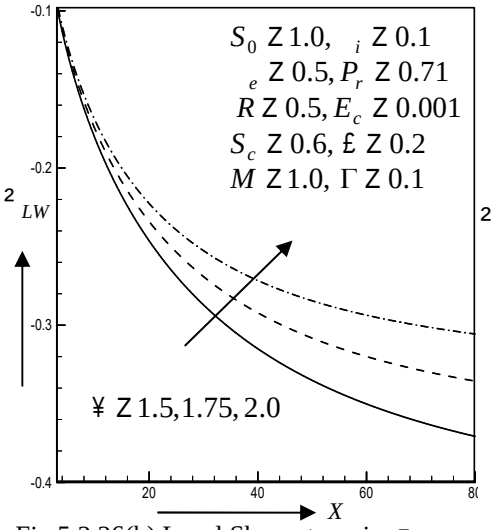

Fig.5.2.26(b) Local Shear stress in z - axis for different values of ¥

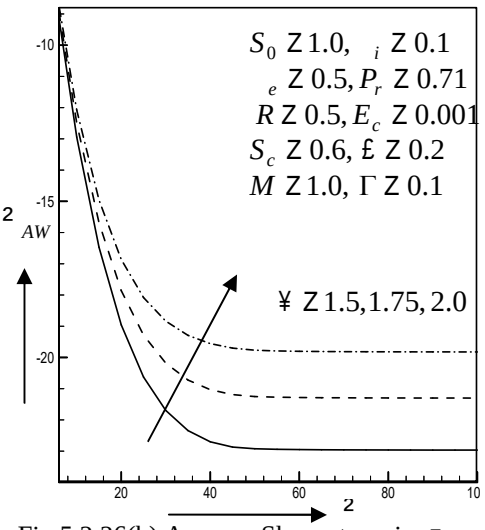

Fig.5.2.26(b) Average Shear stress in z - axis for different values of ¥

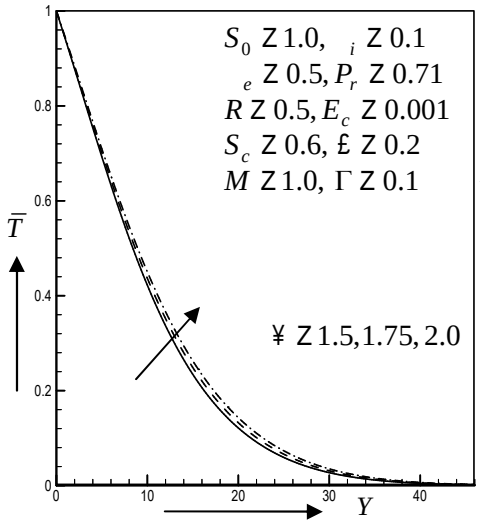

Fig.5.2.27(a)Temperature profiles for different values of ¥

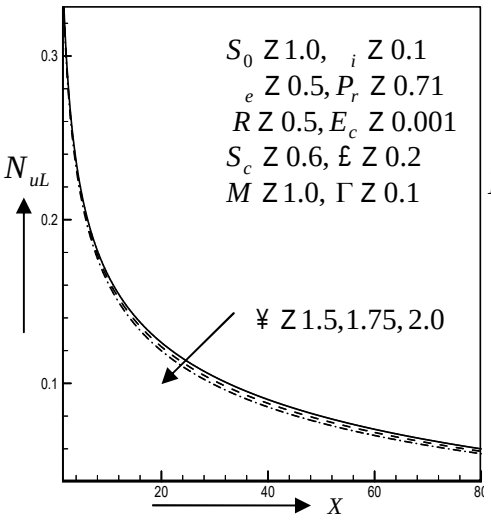

Fig.5.2.27(b) Local Nusselt number for different values of ¥

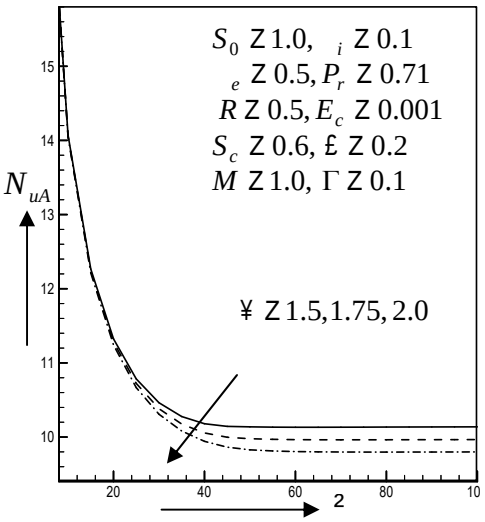

Fig.5.2.27(c)Average Nusselt number for different values of ¥

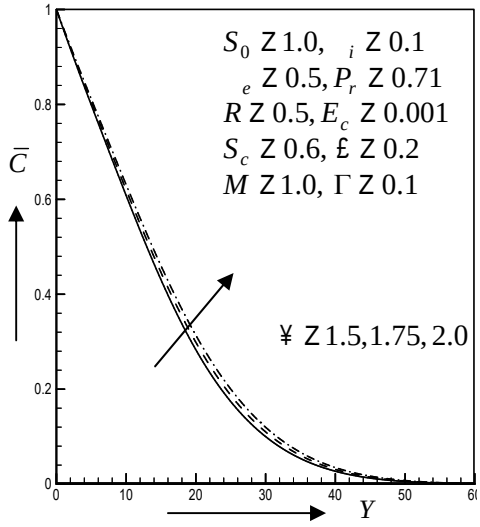

Fig.5.2.28(a) Concentration profiles for different values of ¥

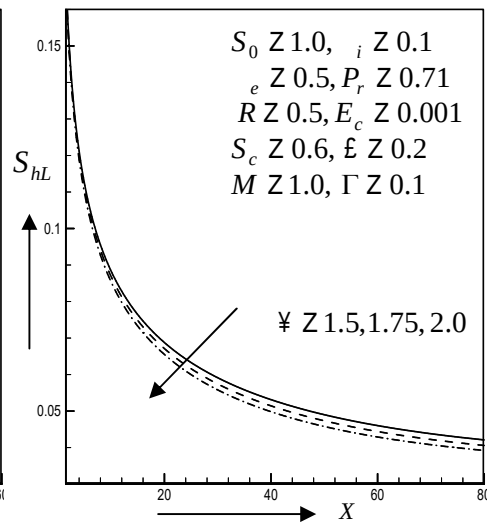

Fig.5.2.28(b) Local Sherwood number for different values of ¥

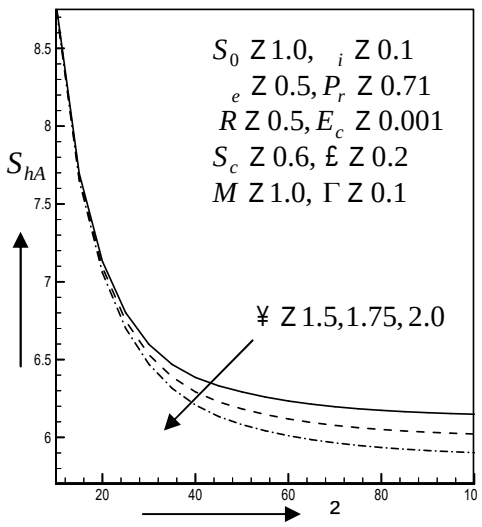

Fig.5.2.28(c) Average Sherwood number for different values of ¥

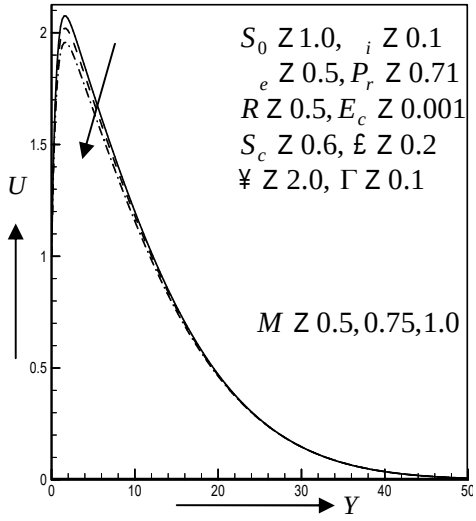

Fig.5.2.29(a) Primary velocity profiles for different values of M

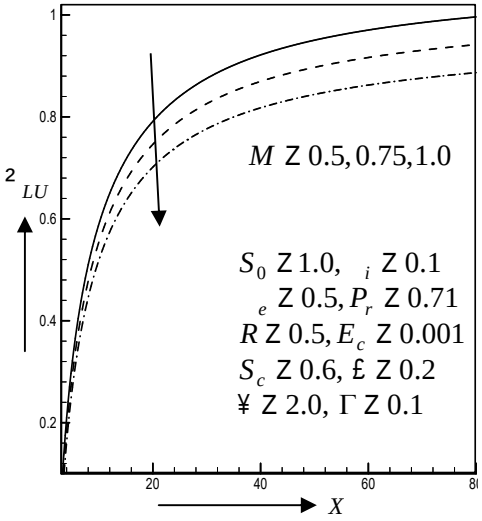

Fig.5.2.29(b) Local Shear stress in x - axis for different values of M

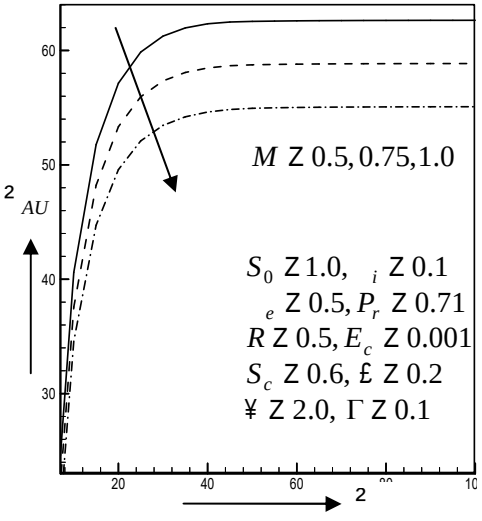

Fig.5.2.29(c) Average Shear stress in x - axis for different values of M

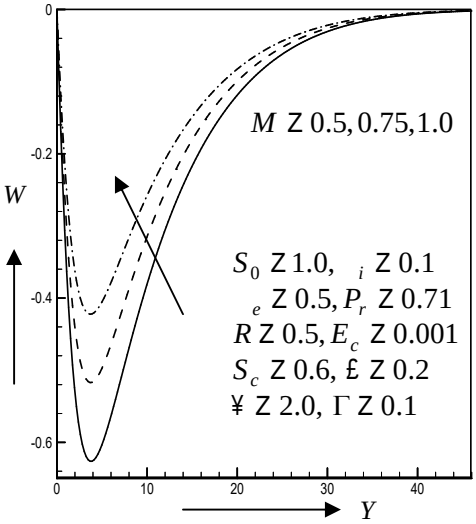

Fig.5.2.30(a) Secondary velocity profiles for different values of M

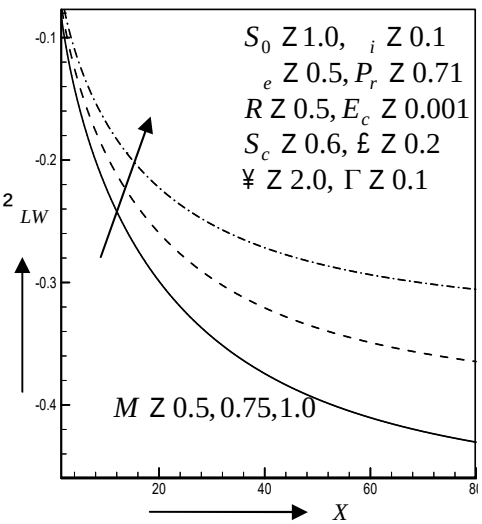

Fig.5.2.30(b) Local Shear stress in z - axis for different values of M

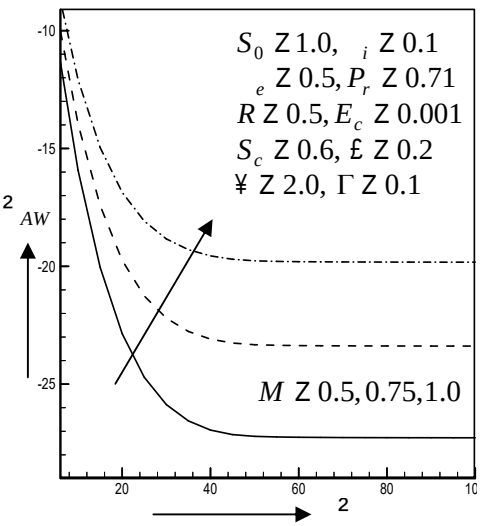

Fig.5.2.30(c) Average Shear stress in z - axis for different values of M

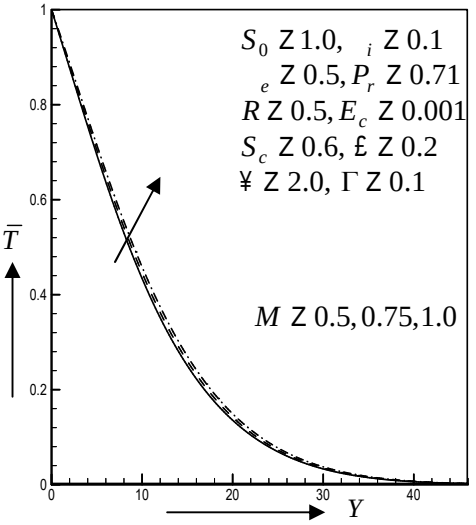

Fig.5.2.31(a) Temperature profiles for different values of M

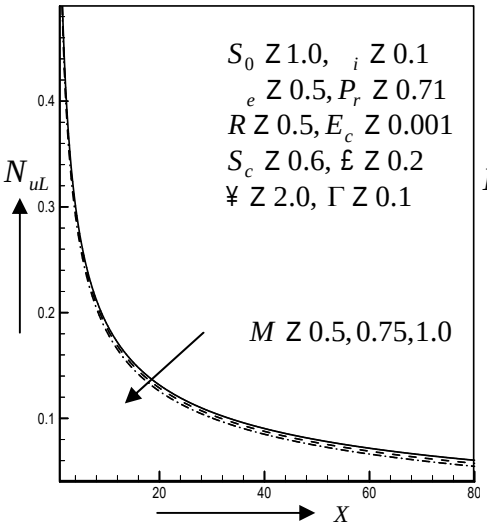

Fig.5.2.31(b) Local Nusselt number for different values of M

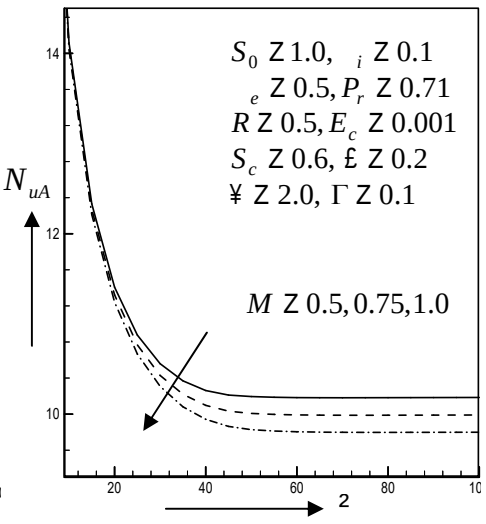

Fig.5.2.31(c) Average Nusselt number for different values of M

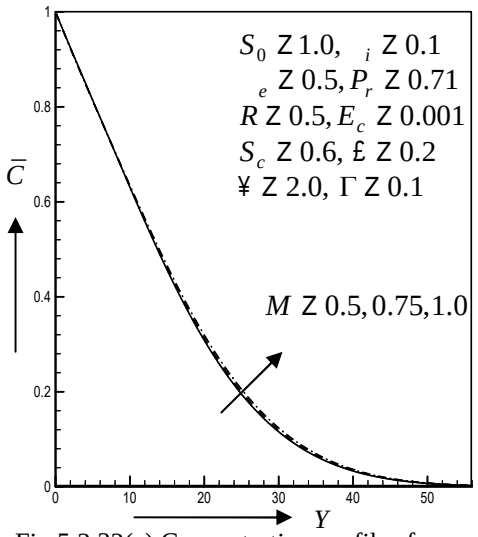

Fig.5.2.32(a) Concentration profiles for different values of M

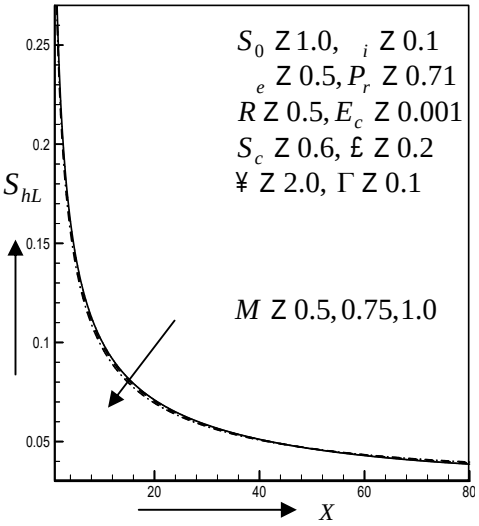

Fig.5.2.32(b) Local Sherwood number for different values of M

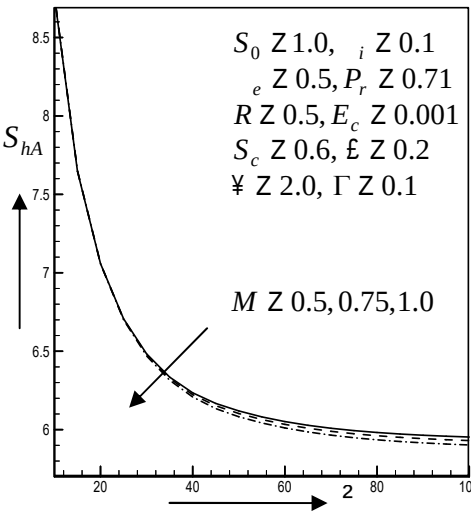

Fig.5.2.32(c) Average Sherwood number for different values of M

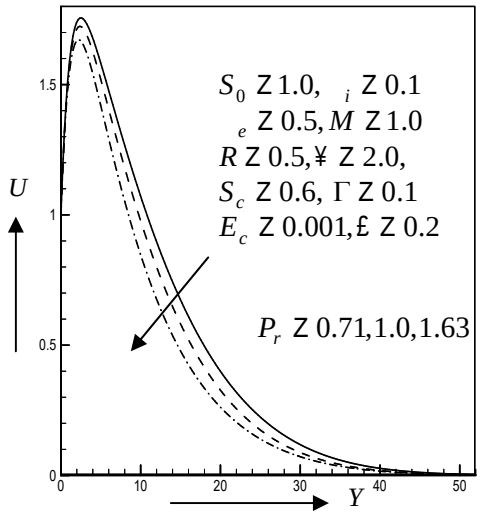

Fig.5.2.33(a) Primary velocity profiles for different values of P_r

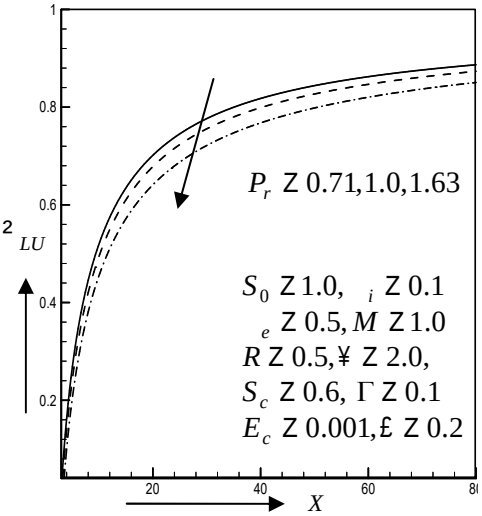

Fig.5.2.33(b) Local Shear stress in x -axis for different values of P_r

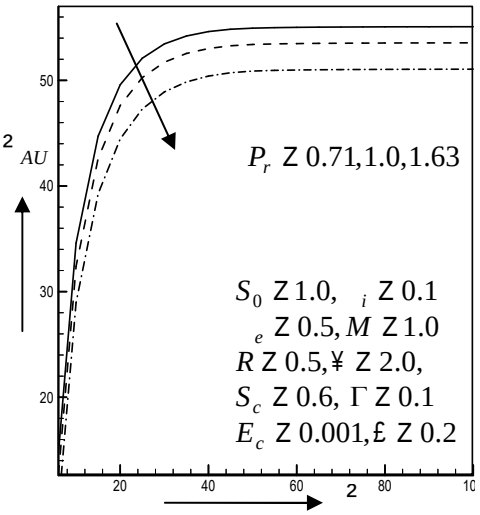

Fig.5.2.33(c) Average Shear stress in x -axis for different values of P_r

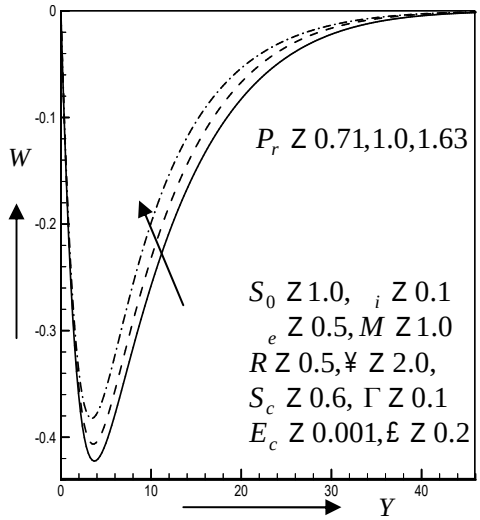

Fig.5.2.34(a) Secondary velocity profiles for different values of P_r

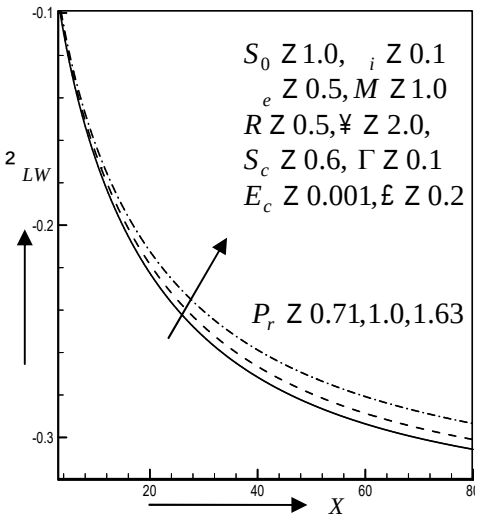

Fig.5.2.34(b) Local Shear stress in z -d for different values of P_r

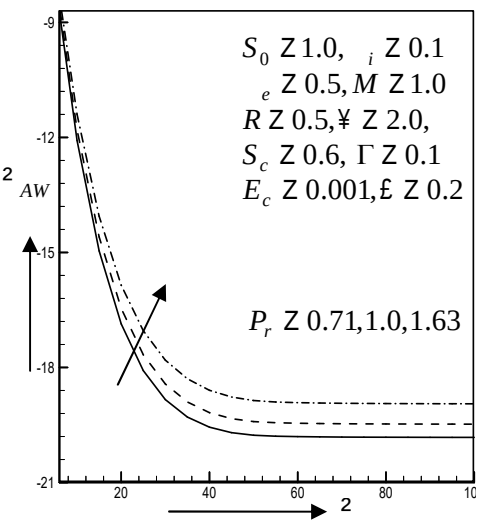

Fig.5.2.34(c) Average Shear stress in z -axis for different values of P_r

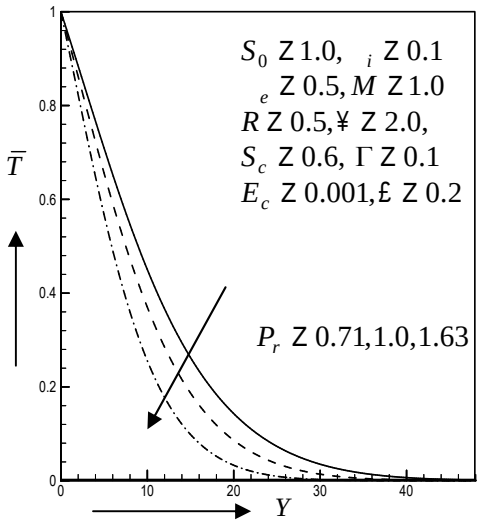

Fig.5.2.35(a) Temperature profiles for different values of P_r

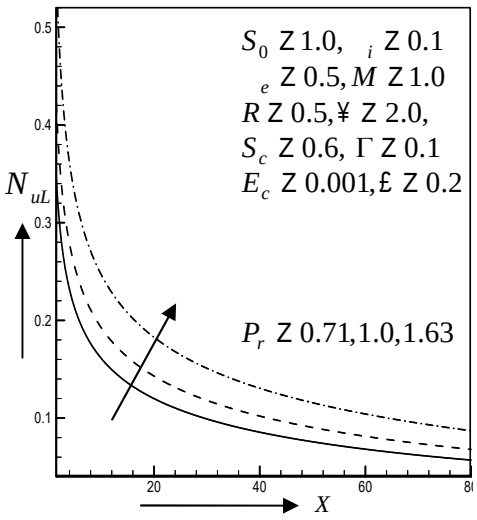

Fig.5.2.35(b) Local Nusselt number for different values of P_r

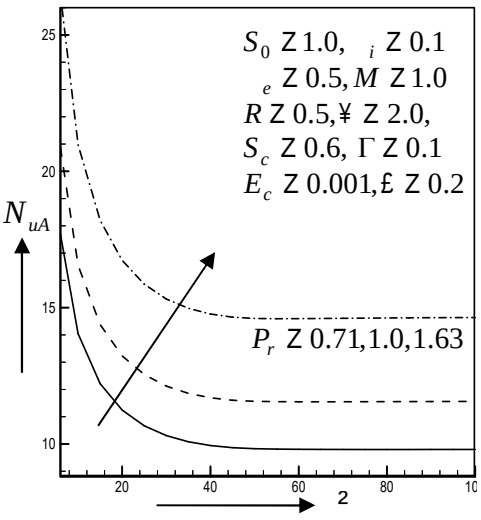

Fig.5.2.35(c) Average Nusselt number for different values of P_r

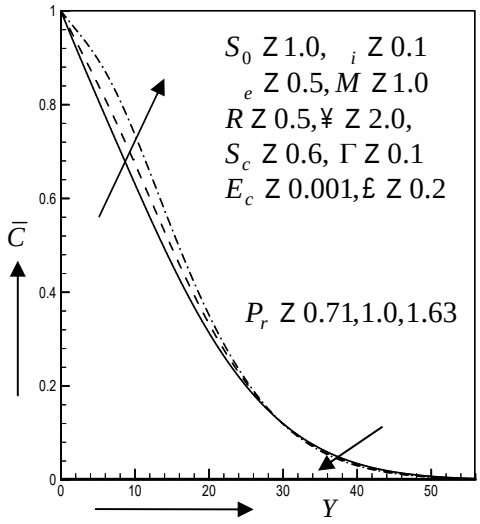

Fig.5.2.36(a) Concentration profiles for different values of P_r

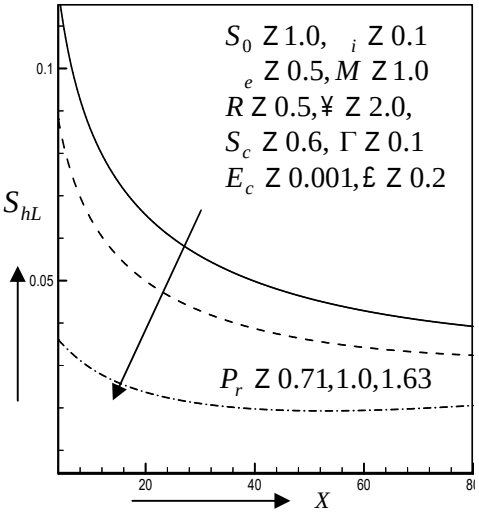

Fig.5.2.36(b) Local Sherwood number for different values of P_r

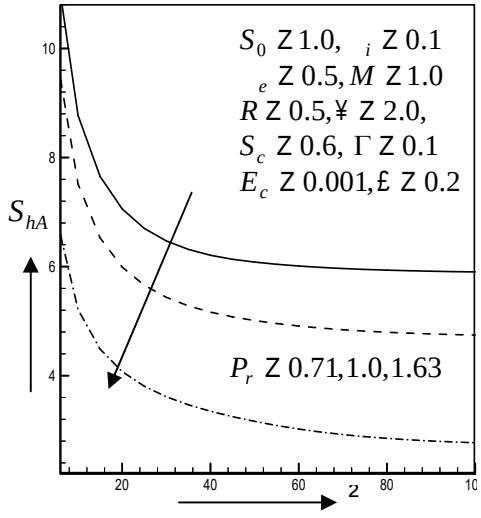

Fig.5.2.36(c) Average Sherwood number for different values of P_r

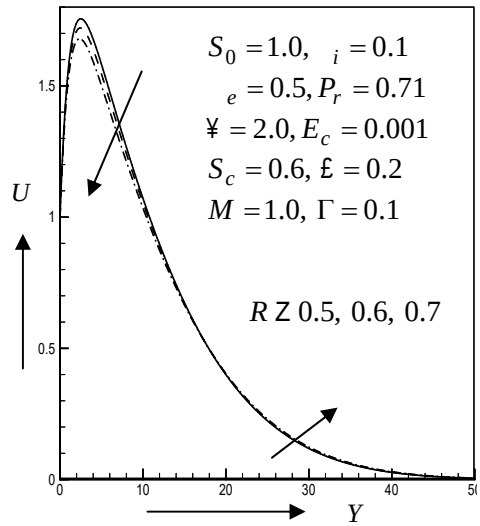

Fig.5.2.37(a) Primary velocity profiles for different values of R

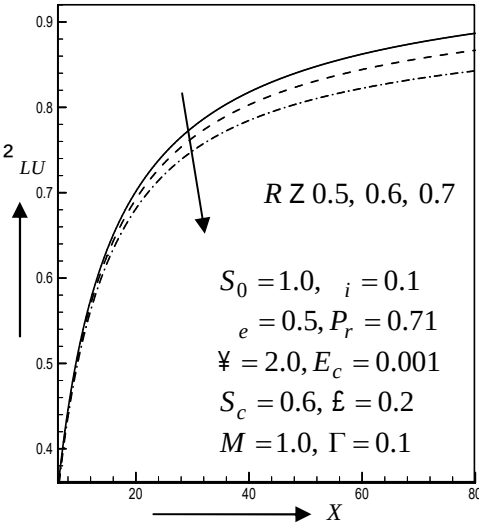

Fig.5.2.37(b) Local Shear stress in x - axis for different values of R

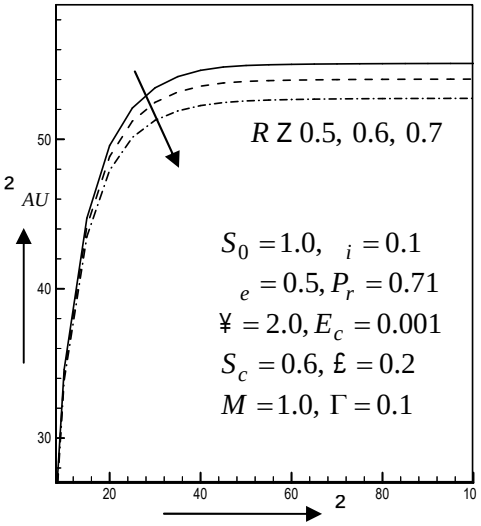

Fig.5.2.37(c) Average Shear stress in x - axis for different values of R

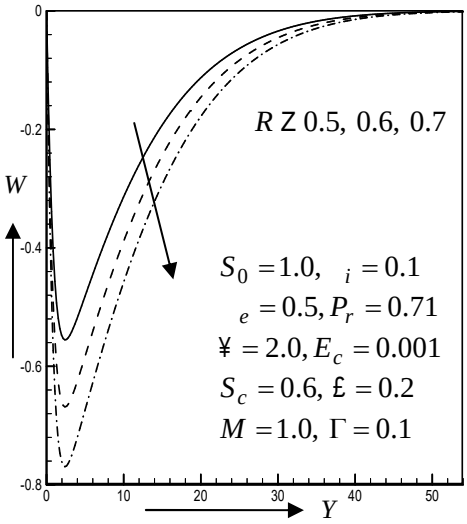

Fig.5.2.38(a) Secondary velocity profiles for different values of R

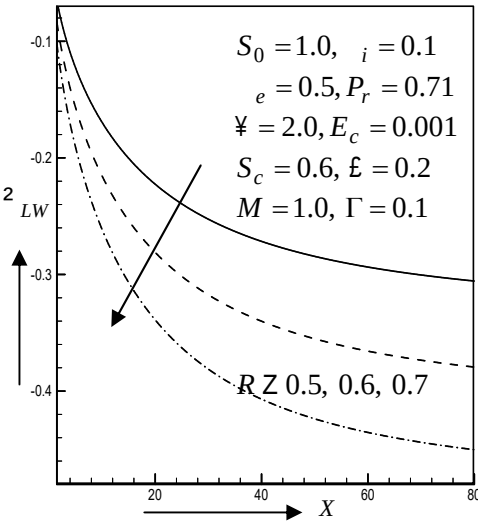

Fig.5.2.38(b) Local Shear stress in z - axis for different values of R

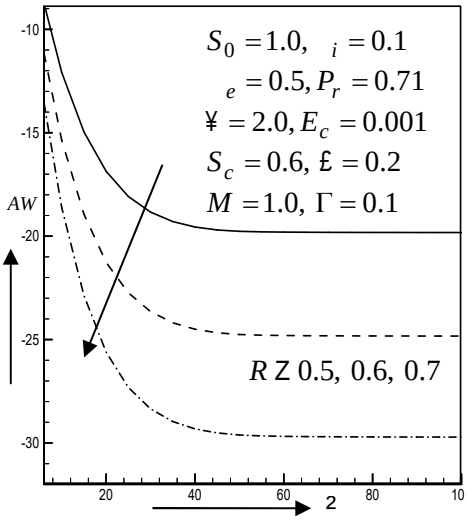

Fig.5.2.38(c)Average Shear stress in z - axis for different values of R

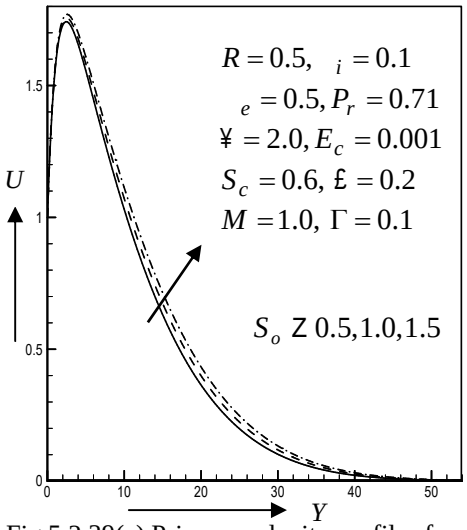

Fig.5.2.39(a) Primary velocity profiles for different values of S_0

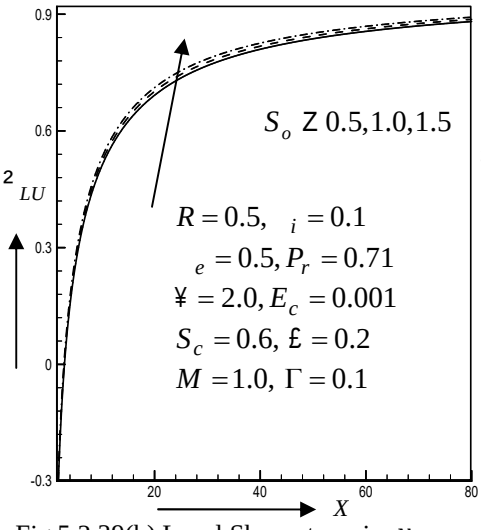

Fig.5.2.39(b) Local Shear stress in x - axis for different values of S_0

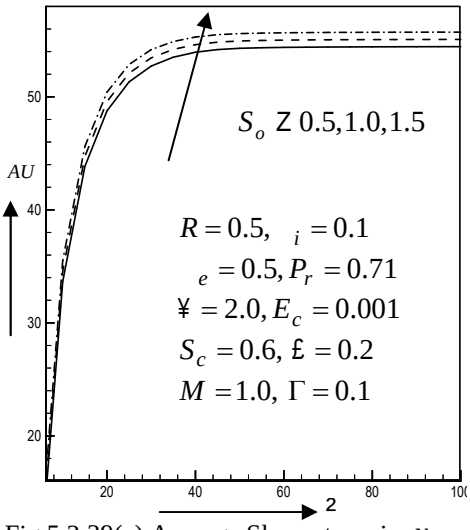

Fig.5.2.39(c) Average Shear stress in x - axis for different values of S_0

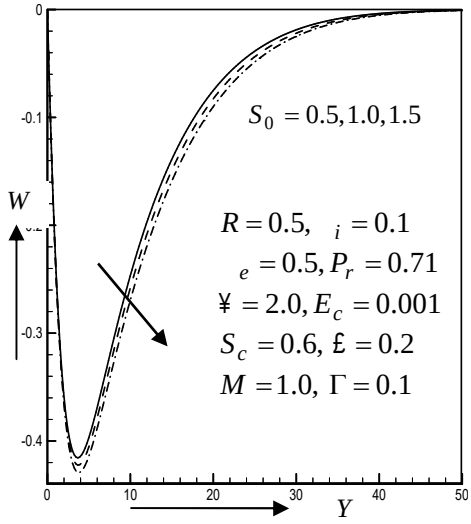

Fig.5.2.40(a) Secondary velocity profiles for different values of S_0

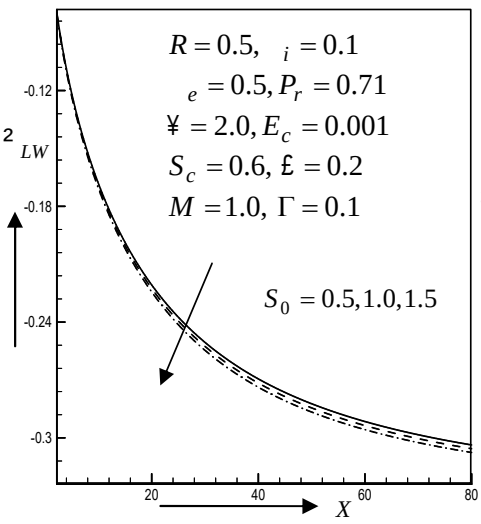

Fig.5.2.40(b) Local Shear stress in z - axis for different values of S_0

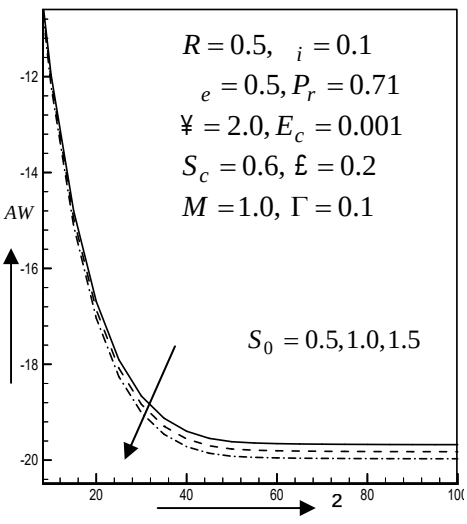

Fig.5.2.40(c) Average Shear stress in z - axis for different values of S_0

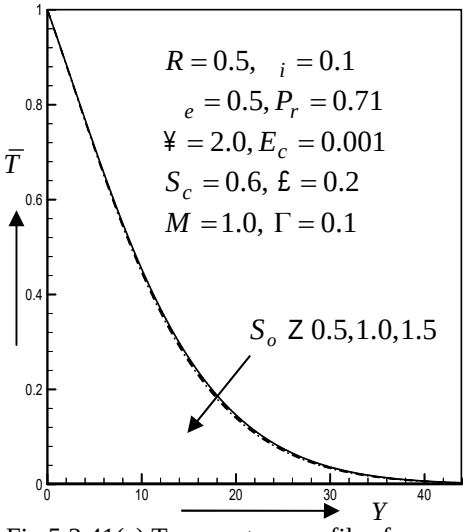

Fig.5.2.41(a) Temperature profiles for different values of S_0

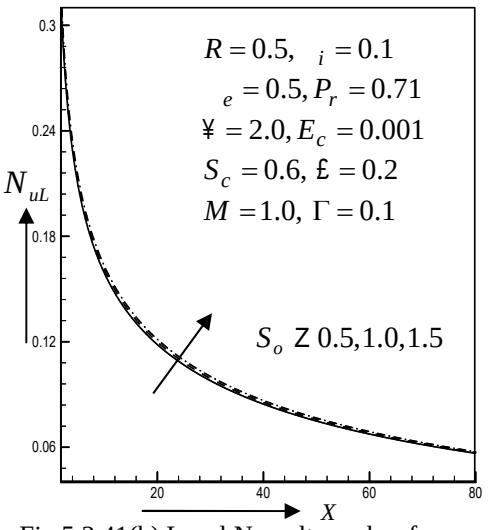

Fig.5.2.41(b) Local Nusselt number for different values of S_0

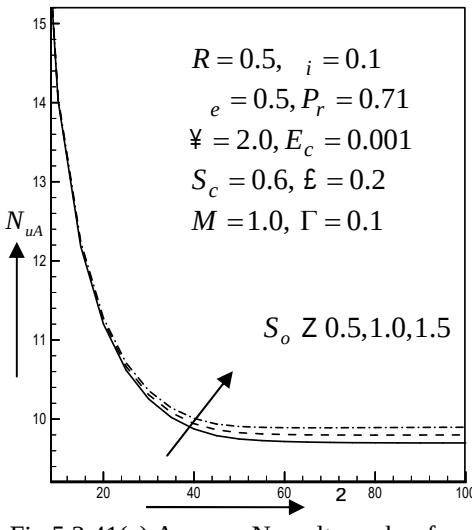

Fig.5.2.41(c) Average Nusselt number for different values of S_0

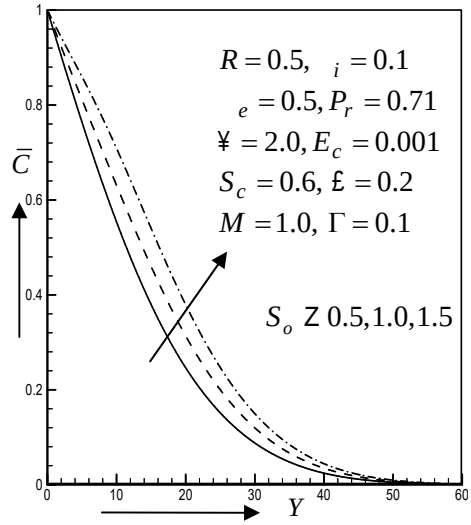

Fig.5.2.42(a) Concentration profiles for different values of S_0

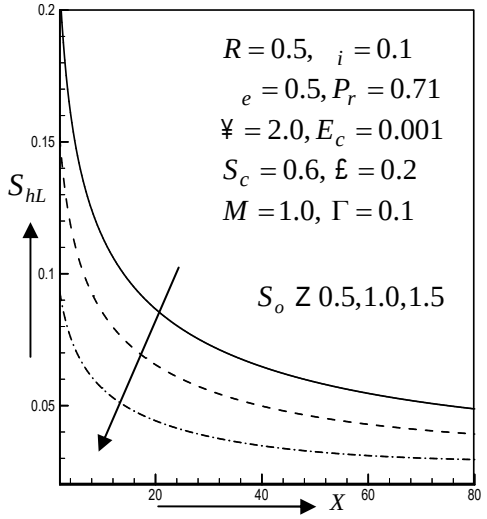

Fig.5.2.42(b) Local Sherwood number for different values of S_0

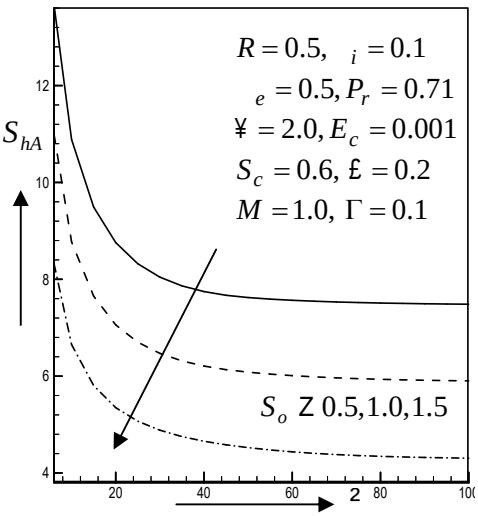

Fig.5.2.42(c)Average Sherwood number for different values of S_0

References

Abdullah Ahmed Foisal and Mahmud Alam(2015), Free convection fluid flow in the presence of a magnetic field with thermally stratified high porosity medium, 'Elsevier, Procedia Engineering', vol.**105**, p549-556.

Anajali Devi, S. P. and Ganga, B. (2009), Viscous dissipation effects on nonlinear MHD flow in a porous medium over a stretching porous surface, International Journal of Applied Mathematics and Mechanics, vol.**5**(7), p45-59.

Anwar Beg, O., Makinde, O. D., Zueco, J. and Ghosh, S. K. (2012), Hydromagnetic viscous flow in a rotating annular high-porosity medium with nonliner Forchheimer drag effects: numerical study, 'World Journal of Modelling and Simulation', vol.**8**, No. 2, p83-95.

Chauhan, D. S., Jain, R. (2005), Three dimensional steady flow of viscous incompressible fluid over a highly porous layer, 'Modeliing, Measurment and Control', vol.**74**(5), p19-34.

Das, S., Guchhait, S. K. and Jana, R. N. (2015), Hall effects on unsteady hydromagnetic flow past an accelerated porous plate in a rotating system, 'Journal of Applied Fluid Mechanics', vol. **8**, No. 3, p409- 417.

Dulal Pal (2008), MHD flow and heat transfer past a semi-infinite vertical plate embedded in a porous medium of variable permeability, 'International Journal of Fluid Mechanics Research', vol.**35**(6), p493-509.

Ferdows, M., Esrat Jahan, Hamad, M. M. and Masahiro OTA (2011), Effects of Hall and ion-slip currents on free convective heat transfer flow past a vertical plate considering slip conditions, 'Canadian Journal on Science and Engineering Mathematics', vol.**2**, No. 2, p70-76.

Geindreau, C., Auriault, J. L. (2002), Magnetohydrodynamic flows in porous media, 'Journal of Fluid Mechanics'. vol.**466,** p343-363.

Joaquin Zueco, Anwar Beg, O and Tasveer A Beg (2009), Numerical solutions for unsteady rotating high porosity medium channel couetee flow hydrodynamics, 'Physica Scripta', vol.**80**, No. 3, p5001.

Kiran Kumar, R. V. M. S. S, Sasikala, B., Raju, M. C. and Varma, S.V.K. (2015), Diffusion-thermo effects on hydromagnetic free convection heat and mass transfer flow through high porous medium bounded by a vertical surface, 'Chemical and Process Engineering Research', vol.**36**, p1-18.

Koushik Dash, Alam, M. and Wahiduzzaman, M. (2012), MHD free convection and mass transfer flow from a vertical plate in the presence of Hall and ion-slip current, 'Advances in Mechanical Engineering', vol.**2012**, Article ID 851957, 20 pages, doi:10.1155/2012/ 851957.

Krishna, D. V, Prasada, Rao D. R. V, Ramachandra Murththy, A.S. (2002), Hydromagnetic convection flow through a porous medium in a rotating channel, 'Journal of Engineering Physics and Thermophysics', vol.**75**(2), p281-291.

Rajput, U. S., Mohammad Shareef (2016), Rotation effect on unsteady MHD flow past an impulsively started vertical plate with variable temperature in porous medium, 'International Journal of Mathematical Archive', vol.**7**(2), p148-153.

Rao, G. S., Ramana, B., Reddy, B. R., Vidyasagar, G. (2014), Soret and Dufour effects on MHD boundary layer flow over a moving vertical porous plate with suction, 'International Journal of Emerging Trends in Engineering and Development', vol.**2**(4), p215-226.

Sherman, A, Sutton, G. W. (1962), Mgagnetohydrodynamic, 'North Western University Press', Evanston.

Singh, K, D and Rakesh kumar (2009), Soret and Hall current effects on heat and mass transfer in mhd flow of a viscous fluid through porous medium with variable suction, Proceedings Indian National Science Academy, vol.**75**, No.3,p119-126.

Vidyasagar, G., Ramana, B. and Bala, P. and Anki Reddy (2013), Heat and mass transfer effects on MHD boundary layer flow over a moving vertical porous plate, 'Journal of Global Research in Mathematical Archives', vol.**1**, No. 2, p49-62.

Vijaya, R. B. and Mallikarjuna, B. (2014), Effect of variable thermal conductivity on convective heat and mass transfer over a vertical plate in a rotating system with variable porosity regime, 'Journal of Naval Architecture and Marine Engineering', vol.**111**, No 1, p83-92.

Chapter 6

Effects of ion-slip current on MHD free convection flow with temperature stratified porous medium in a rotating system

Stratification effects are an important aspect in heat and mass transfer analyses. Stratification of fluid is a deposition/formation of layers and occurs due to temperature variations, concentration differences of fluid. Convective heat transfer in thermal stratified ambient fluid occurs in many industrial applications and is an important aspect in the study of heat transfer. If stratification occurs, the fluid temperature is function of distance and convection in such environment exists in lakes, oceans, nuclear reactors where coolant (generally liquid metals), thermal energy storage systems such as solar ponds and heat transfer from thermal sources such as the condensers of power plants is present in magnetic field etc. The dynamics of flow in a thermally stratified fluid is also important and arise in many contexts, ranging from industrial settings to the oceanic and atmospheric environments. Thermal stratification effects may arise when there is a continuous discharge of the thermal boundary layer into the medium. For example, a heated vertical surface embedded in a porous bed which is of limited extent in the direction of the plate. In such case, the thermal boundary layer eventually heats the ceiling and at that point it falls horizontally into the medium since it contains hotter fluid than the rest of the medium (hotter fluid is lighter than the colder fluid). The long time effect of this discharge activity is the stratification in the medium. *Gebhart et al.* (1988) has shown that stratification increases the local heat transfer coefficient and decreases the velocity and buoyancy levels. Another considerable effect of the stratification on the mean field is the formation of a region with the temperature deficit (i.e., a negative dimensionless temperature) and flow reversal in the outer part of the boundary layer. This phenomenon was first shown theoretically by *Prandtl* (1952) for an infinite wall and later by *Jaluria and Himasekhar* (1983) for semi infinite wall. Based on boundary- layer theory, *Lai et al.* (1990) has analyzed natural convection from a vertical flat plate immersed in a thermally stratified porous medium. *Angirasa and Peterson* (1997) discussed natural convection heat transfer from an isothermal vertical surface to a fluid saturated thermally stratified porous medium. *Iranian et al.* (2015) investigated an unsteady MHD natural convective flow over vertical plate in thermally stratified media with variable viscosity and thermal conductivity. *Angirasa and Srinivasan* (1989) have presented a numerical study of the natural convection flow on a vertical surface due to the combined effect of buoyancy forces caused by the heat and mass diffusion in a thermally stratified medium. *Ihsan and Basim* (2013) studied natural convection heat transfer from a plane wall to thermally stratified porous media. *Swati et al.* (2012) investigated the effects of thermal stratification on flow and heat transfer past a porous vertical stretching surface. *Singh and Sharma* (1990)

studied integral method to free convection in thermally stratified porous medium. *Chamkha* (1997) investigated MHD free convection from a vertical plate embedded
in a thermally stratified porous medium with Hall effects. Natural convection boundary layer flow of a double diffusive and rotating fluid past a vertical porous plate was investigated by *Rama et al.* (2016).

Convection in porous medium has important applications in many areas including thermal energy storage, flow through filtering devices, utilization of geothermal energy, oil extraction, high performance insulation for buildings, paper industry etc. Hence combined study may give some vital information which will surely be helpful in developing other relevant areas. Permeable porous plates are used in the filtration processes and also for a heated body to keep its temperature constant and to make the heat in solution of the surface more effective. Viscous dissipation effects are important in geophysical flows and also in certain industrial operations and are usually characterized by the Eckert number. Hall and ion-slip currents are important and they have a effect on the magnitude and direction of the current density and consequently on the magnetic force term. The problem of MHD free convection flow with Hall and ion-slip currents has many important engineering applications, e.g. in power generators, Hall accelerators and flows in channels and ducts. *Jha and Apere* (2010) studied combined effect of Hall and ion-slip currents on unsteatdy MHD couette flows in a rotating system. *Atul et al*. (2005) investigated Hydromagnetic free convection and mass transfer flow with Joule heating, thermal diffusion, heat source and Hall current. *Nirmal et al.*(2012) analyzed the effects of Hall current and ion-slip on unsteady MHD couette flow. MHD Natural Convection Flow of an incompressible electrically conducting viscous fluid through porous medium from a vertical flat plate was studied by *Prabhakara et al.* (2015).

The aim of the present work is to investigate the effects of thermal stratification, viscous dissipation and Joule heating on MHD unsteady free convection flow past an infinite vertical plate in porous medium in a rotating system with ion-slip current. The obtain nonlinear coupled ordinary differential equations have been solved numerically using sixth order Rung-Kutta method with shooting technique. The effects of different parameters on velocity and temperature distribution are illustrated graphically. The numerical values of shear stress and Nusselt number at the plate are discussed for various values of physical parameters and presented in tabular form.

6.1 Governing Equations

Consider the natural convection boundary layer flow past an infinite vertical plate embedded in a porous medium saturated with a stratified temperature. The plate is assumed to be electrically non-conducting. Choose the coordinate system such that x axis is along the vertical plate and y axis normal to the plate, while the origin of the reference system is considered at the leading edge of the vertical plate. The plate is maintained at a uniform and constant wall temperature T_w . The ambient medium is assumed to be stratified with respect to temperature in the form $T_\infty(t) = T_{\infty,t=0} + S\pm(t)$ where S is constant which is varied to alter

the intensity of stratification in the medium, $\pm(t)$ is the time dependent length schale. The value of T_w is assumed to be greater than the ambient temperature $T_{\infty,t=0}$ at any arbitrary reference point in the medium (inside the boundary layer). A uniform magnetic field of strength B_0 is applied in the y-direction normal to the plate surface. The fluid is assumed to be Newtonian, electrically conducting fluid. The induced magnetic field due to the motion of the electrically conducting fluid is negligible. This assumption is valid for small magnetic Reynolds number. The graphical model of the problem has been given along with flow configuration and coordinate system which is shown in Fig .6.1. The governing equations are as follows;

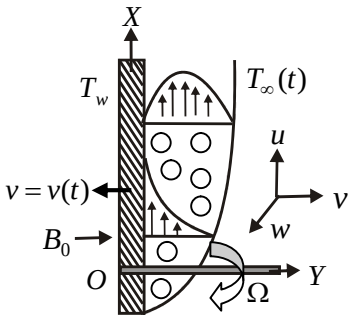

Fig. 6.1 Physical configuration and coordinate system

The continuity equation; $$\frac{\partial v}{\partial y} = 0 \tag{6.1}$$

Momentum equation;

$$\frac{\partial u}{\partial t} + v\frac{\partial u}{\partial y} - 2\Omega w = \nu \frac{\partial^2 u}{\partial y^2} + g_0 \quad (T - T_\infty(t)) - \frac{\nu}{k}u - \frac{\pm_e B_0^2}{\rho\left(\sim_e^2 + \ _e^2\right)}\left(\sim_e u + \ _e w\right) \tag{6.2}$$

$$\frac{\partial w}{\partial t} + v\frac{\partial w}{\partial y} + 2\Omega u = \nu \frac{\partial^2 w}{\partial y^2} - \frac{\nu}{k}w + \frac{\pm_e B_0^2}{\rho\left(\sim_e^2 + \ _e^2\right)}\left(\ _e u - \sim_e w\right) \tag{6.3}$$

Energy equation;

$$\frac{\partial T}{\partial t} + v\frac{\partial T}{\partial y} = \frac{\kappa}{\rho c_p}\frac{\partial^2 T}{\partial y^2} + \frac{\nu}{c_p}\left[\left(\frac{\partial u}{\partial y}\right)^2 + \left(\frac{\partial w}{\partial y}\right)^2\right] + \frac{\pm_e B_0^2}{\rho c_p\left(\sim_e^2 + \ _e^2\right)}\left(u^2 + w^2\right) \tag{6.4}$$

where all physical quantities are defined in the Nomenclature.

Boundary conditions are as follows:

$$u = 0 \quad v = v(t) \quad w = 0 \quad T = T_w \quad \text{at} \quad y = 0$$
$$u \to 0 \quad w \to 0 \quad T \to T_\infty(t) \quad \text{as} \quad y \to \infty \tag{6.5}$$
$$T_\infty(t) = T_{\infty,t=0} + S\pm(t),$$

$S = \frac{d}{dt}\{T_\infty(t)\} > 0$ is a stratification rate of the gradient of ambient temperature profiles.

6.2 Methematical Formulation

Now in order to obtain the similarity solutions of the problem, a similarity *Sattar and Alam* (1994) parameter $\pm$ is now introduced, $\pm$ is time dependent length scale as;

$$\pm = \pm(t) \tag{6.6}$$

In terms of this length scale, a convenient solution of the equation (6.1) is considered to be in the following form:

$$v = v(t) = -v_0\frac{\nu}{\pm} \tag{6.7}$$

where $v_0 > 0$ is the suction parameter.

The following dimensionless variables are now introduced;

$$\eta = \frac{y}{\pm}, \; u = U_0 f(\eta), \; g(\eta) = \frac{w}{U_0}, \; \theta(\eta) = \frac{T - T_\infty(t)}{T_w - T_{\infty,t=0}} \tag{6.8}$$

Then introducing the relations (6.6)–(6.8) into the equations (6.2)–(6.4) and obtained the following dimensionless ordinary coupled differential equations;

$$f''' + \eta\left(\frac{\pm(t)}{3}\frac{d\pm(t)}{dt}\right)f'' + v_0 f'' - \varphi f' - \frac{M\sim_e}{(\sim_e^2 + \;_e^2)} f' + G_r\theta + Rg - \frac{M\;_e}{(\sim_e^2 + \;_e^2)} g' = 0 \tag{6.9}$$

$$g''' + \eta\left(\frac{\pm(t)}{3}\frac{d\pm(t)}{dt}\right)g'' + v_0 g'' - \varphi g' - \frac{M\sim_e}{\sim_e^2 + \;_e^2} g' + \frac{M\;_e}{\sim_e^2 + \;_e^2} f' - Rf' = 0 \tag{6.10}$$

$$\theta'' + \eta\left(\frac{\pm(t)}{3}\frac{d\pm(t)}{dt}\right)P_r\theta' + v_0 P_r\theta' - 2P_r S_T + P_r E_c\left[f''^2 + g'^2\right] + \frac{P_r E_c M}{\sim_e^2 + \;_e^2}\left[f'^2 + g'^2\right] = 0 \tag{6.11}$$

where, $\varphi\left(= \frac{\pm^2(t)}{k}\right)$, $R\left(= \frac{2\Omega\pm^2(t)}{3}\right)$, $M\left(= \frac{\pm_e B_0^2 \pm^2(t)}{\circ 3}\right)$, $E_c\left(= \frac{U_0^2}{c_p(T_w - T_{\infty,t=0})}\right)$

$G_r\left(= \frac{\pm^2(t)}{3U_0} g_0 \;\; (T_w - T_{\infty,t=0})\right)$, $P_r\left(= \frac{\circ 3 c_p}{k}\right)$, $S_T\left(= \frac{S\pm(t)}{T_w - T_{\infty,t=0}}\right)$.

The equations (6.9)-(6.11) are similar except for the term $\frac{\pm(t)}{3}\frac{d\pm(t)}{dt}$ where time t appears explicitly. Thus the similarity condition requires that $\frac{\pm(t)}{3}\frac{d\pm(t)}{dt}$ in the equations (6.9)-(6.11) must be a constant quantity. Hence following the works *Sattar and Alam* (1994), *Sattar and Hossain* (1992), *Hasimoto* (1957) and *Sattar et al.* (2000) one can try a class of solutions of the equations (6.9)-(6.11) by assuming that

$$\frac{\pm(t)}{3}\frac{d\pm(t)}{dt} = c \text{ (Constant)} \tag{6.12}$$

Now integrating (12) one obtains

$$\pm(t) = \sqrt{2 3 ct} \tag{6.13}$$

where the constant of integration is determined through the condition that $\pm(t) = 0$ when $t = 0$. It thus appears from (6.1.13) that, by making a realistic choice of $c = 2$ in (6.1.12) the length scale $\pm(t)$ becomes equal to $\pm(t) = 2\sqrt{3t}$ which exactly corresponds to the usual scaling factor considered for various unsteady boundary layer flows. Since $\pm(t)$ is a scaling factor as well as a similarity parameter, any other value of c in (6.12) would not change the nature of the solution except that the scale would be different. Finally, introducing (6.12) with in equations (6.9)-(6.11), obtain the following dimensionless ordinary differential equations are as follows;

$$f''' + (2\eta + v_0)f'' - \varphi f' - \frac{M\sim_e}{(\sim_e^2 + \;_e^2)} f' + G_r\theta + Rg - \frac{M\;_e}{(\sim_e^2 + \;_e^2)} g' = 0 \tag{6.14}$$

$$g''' + (2\eta + v_0)g'' - \varphi g' - \frac{M\sim_e}{\sim_e^2 + \;_e^2} g' + \frac{M\;_e}{\sim_e^2 + \;_e^2} f' - Rf' = 0 \tag{6.15}$$

$$^{-}{}'' + (2\text{¦} + v_0)P_r^{-}{}' - 2P_r S_T + P_r E_c\left[f'^2 + g'^2\right] + \frac{P_r E_c M}{\sim_e^2 + {}_e^2}\left[f^2 + g^2\right] = 0 \qquad (6.16)$$

where primes denote differentiation with respect to ¦ .

The corresponding boundary conditions for t > 0 are obtained as:

$f = 0,\ g = 0,\ ^{-} = 1 - S'$ at ¦ Z 0

f Z 0, g Z 0, $^{-}$ Z 0 as ¦ $\to \infty$ (6.17)

6.3 Solutions Technique

The equations (6.14)-(6.16) constitute a set of ordinary differential equations, the solutions of which should unfold the characteristics of the problem under consideration. These equations under the boundary conditions (6.17) are solved numerically by using the *Nachtsheim-Swigert* (1965) shooting iteration technique together with a sixth-order Runge-Kutta integration scheme.

6.4 Shear Stress and Nusselt number

The parameters of engineering interest for the present problem are shear stress and Nusselt number. The shear stress is generally known as the Skin friction, the following equations represent the shear stress at the plate. Shear stress in x and z axes are as follows;

$^2{}_x = \ll\left(\frac{\partial u}{\partial y}\right)_{y=0}$ and $^2{}_z = \ll\left(\frac{\partial w}{\partial y}\right)_{y=0}$ which are proportional to $\left(\frac{\partial f}{\partial \text{¦}}\right)_{\text{¦}=0}$ and $\left(\frac{\partial g}{\partial \text{¦}}\right)_{\text{¦}=0}$.

The Nusselt number denoted by N_u which is proportional to $-\left(\frac{\partial ^{-}}{\partial \text{¦}}\right)_{\text{¦}=0}$.

6.5 Results and Discussion

The results of the numerical calculations are presented in the form of velocities (primary and secondary) and temperature distributions are shown graphically in Fig.6.2 to Fig. 6.23 for different values of thermal Stratification parameter (S_T), magnetic parameter(M), Hall parameter (${}_e$), ion-slip parameter(${}_i$), Eckert number(E_c), rotational parameter (R), permeability parameter (¥), suction parameter(v_0), Prandtl number(P_r). The effects of various parameters on shear stresses ($^2{}_x$ and $^2{}_z$) and Nusselt number (N_u) are shown in Table 1-Table 3. The discussion regarding the behavior of the parameters on the components of the shear stress and Nusselt number are self evident from the Tables. The values of the Prandtl number P_r are taken equal to 0.71, 1.0 ,1.38 which corresponds physically to air, salt water, ammonia. The values of Grashof number $(G_r = 10.0)$ is taken to be large positive value, since these values represent cooling of the plate.

The effects of suction parameter v_0 on the velocity field are shown in Fig.6.2. It is seen that the velocity profiles decrease with the increase of suction parameter. This is fact that suction

stabilizes the boundary layer growth. The secondary velocity has opposite behavior which is shown in Fig.6.3. It can be noted from Fig.6.4 that by increasing the value of suction parameter, the temperature distribution decreases in the fluid medium. As such thermal conduction is depressed and this reduces the temperature in the boundary layer.

The variation of the primary and secondary velocities, temperature distribution for different values of thermal stratification parameter (S_T) is illustrated in Fig. 6.5 - Fig. 6.7. It is observed from Fig.6.5 that the primary velocity decreases with increase in thermal stratified parameter, which is due to the layering effect of thermal stratification as it acts like a resistive force. The secondary velocity has opposite behavior which is shown in Fig. 6.6. From Fig. 6.7, it is clear that the temperature of the fluid decreases with the increase of thermal stratification parameter (S_T). This is because, when the thermal stratification is taken into consideration, the effective temperature difference between the plate and the ambient fluid will decrease, therefore the thermal boundary layer is thickened and the temperature is reduced.

The variation of the velocity (primary and secondary) profiles with magnetic parameter (M) is shown in Figs. 6.8 and Fig. 6.9. It can be observed from Fig. 6.8 that the primary velocity of the fluid is decreased with increase in the value of the magnetic parameter. This is due to the fact that the introduction of a transverse magnetic field, normal to the flow direction, has a tendency to create the drag known as the Lorentz force which tends to resist the flow. It is found from Fig.6.9, secondary velocity has opposite effects with the increase of magnetic parameter.

Fig.6.10 and Fig.6.11 depict the influence of Hall parameter ($_e$) on the primary and secondary velocity. It is evident from Figs.6.10 and Fig.6.11 that, primary and secondary velocities increase throughout the boundary layer region. This implies that, Hall current tends to accelerate primary and secondary velocities throughout the boundary layer region. This is due to the fact that Hall current induces secondary flow in the flow field.

Fig.6.12 shows that a slight increase in the primary velocity with an increase of ion-slip parameter ($_i$). This is due to the fact that $_i$ increases, the effective conductivity decreases, which in turn decrease the damping, force on velocity and hence primary velocity increases. The secondary velocity decreases with the increase of ion-slip parameter which is shown in Fig. 6.13. From this figure it is clear that ion-slip parameter $_i$ retards the flow which leads to reduction in boundary layer thickness.

Fig. 6.14 to Fig.6.16, show the influence of the Eckert number (E_c) on the primary velocity, secondary velocity and temperature distributions. It is clearly seen that the effect of Eckert number is to increase both the primary velocity and the temperature distributions in the flow region. This is due to the fact that the heat energy is stored in liquid due to the frictional heating. The secondary velocity has reverse effect which is shown in Fig. 6.15.

From Fig.6.17 and Fig.6.18 illustrated that primary and secondary velocities decrease with an increase the rotation parameter (R). In fact rotation parameter defines the relative magnitude of the Coriolis force and the viscous force, thus rotation retards primary and secondary velocities throughout the boundary layer region.

It is evident from Fig.6.19 that primary velocity decreases with an increases of permeability parameter (¥). This is due to the fact that increasing the value of permeability parameter has tendency to resist the flow causing to reduce the thickness of the boundary layer It is seen from Fig.6.20 that the secondary velocity has opposite behavior with an increase of (¥).

Fig. 6.21 illustrates the velocity component for different values of the Prandtl number(P_r). The primary velocity decreases with an increase of P_r . It is possible because fluids with high Prandtl number have high viscosity and hence move slowly. It is observed from Fig.6.22 that the secondary velocity has reverse effect with an increase of P_r . Fig. 6.23 represents the graph of temperature distribution for different values of Prandtl number (P_r). It is seen that the effect of increasing Prandtl number is to decrease temperature throughout the boundary layer which results in decrease in the thermal boundary layer thickness. The increase of Prandtl number means slow rate of thermal-diffusion.

Finally, the effects of various parameters on the components of the shear stresses ($²_x$, $²_z$) and the Nusselt number (N_u) are shown in Table 8.1-Table 8.3. Table 8.1 shows that the shear stress components $²_x$ decreases and $²_z$ increases with the increase of P_r, S_T, v_0 and ¥ . From this Table, it is observed that the Nusselt number increases with the increasing values of P_r, S_T, v_0 and ¥ .

From Table 8.2, it is seen that shear stress $²_x$ increases with the increase of $_e$ while decreases with the increasing values of R and M . Also the component of shear stress $²_z$ increases with the increasing values of $_e$ and M whereas decreases with the increase of R . The Nusselt number N_u increases with the increase R and M while decreases with the increase of $_e$.

It is observed from Table 8.3 that stress components $²_x$ increases and $²_z$ decreases with the increase of $_i$ and E_c . The Nusselt number N_u increases with the increase $_i$ while decreases with the increase of E_c .

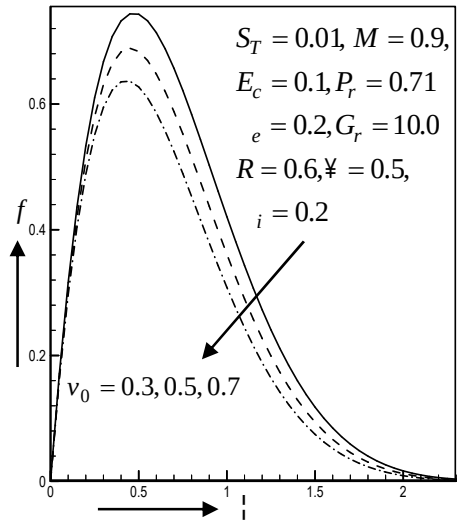

Fig.6.2 Primary velocity profiles for different values of suction parameter v_0

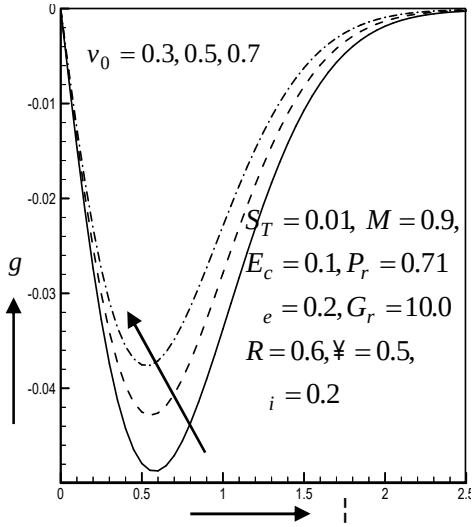

Fig.6.3 Secondary velocity profiles for different values of suction parameter v_0

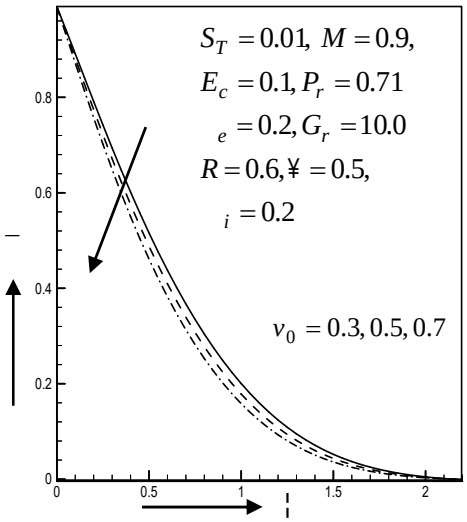

Fig.6.4 Temperature profiles for different values of suction parameter v_0

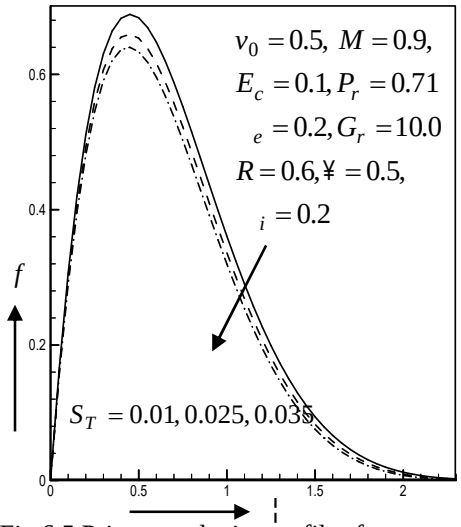

Fig.6.5 Primary velocity profiles for different values of stratification parameter S_T

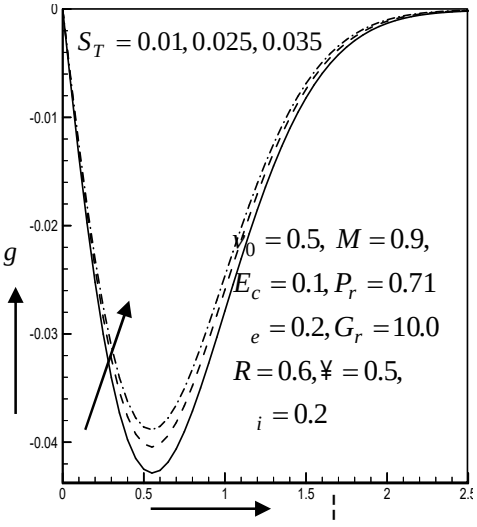

Fig.6.6 Secondary velocity profiles for different values of stratification parameter S_T

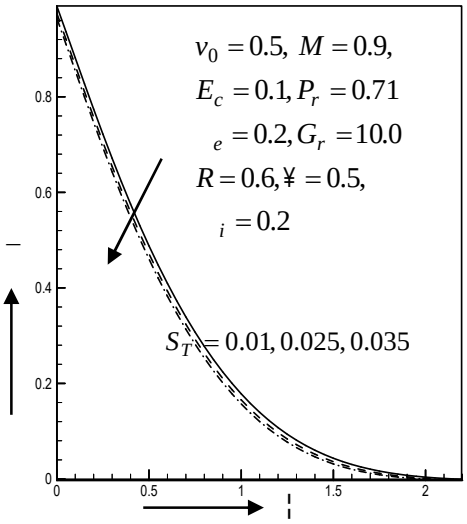

Fig.6.7 Temperature profiles for different values of stratification parameter S_T

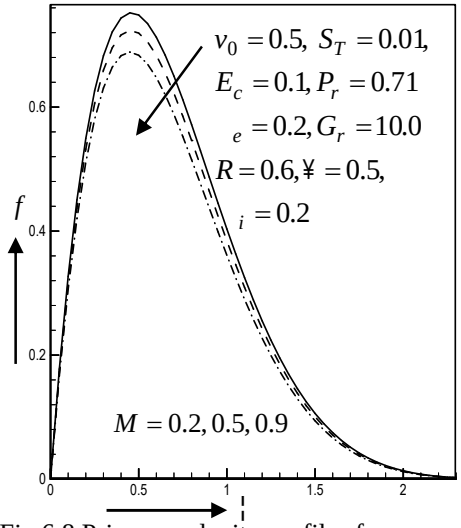

Fig.6.8 Primary velocity profiles for different values of magnetic parameter M

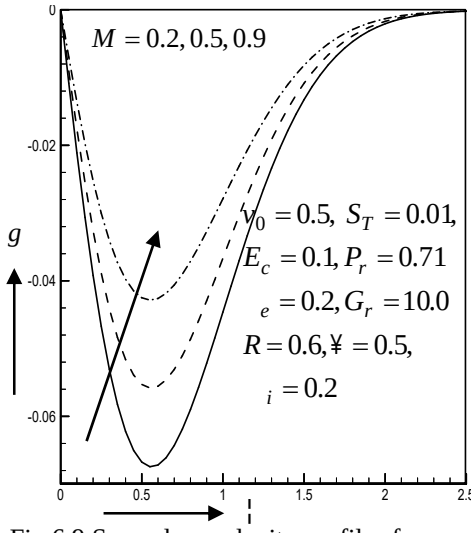

Fig.6.9 Secondary velocity profiles for different values of magnetic parameter M

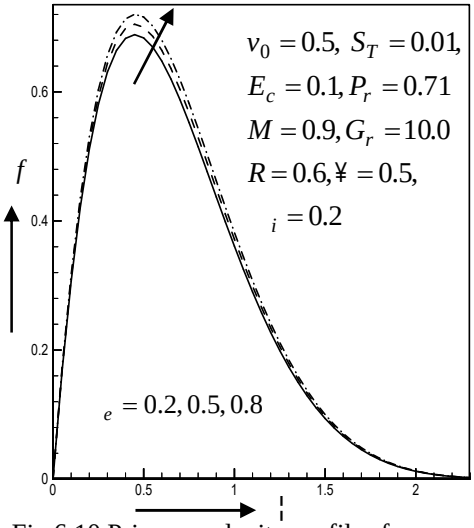

Fig.6.10 Primary velocity profiles for different values of Hall parameter $_e$

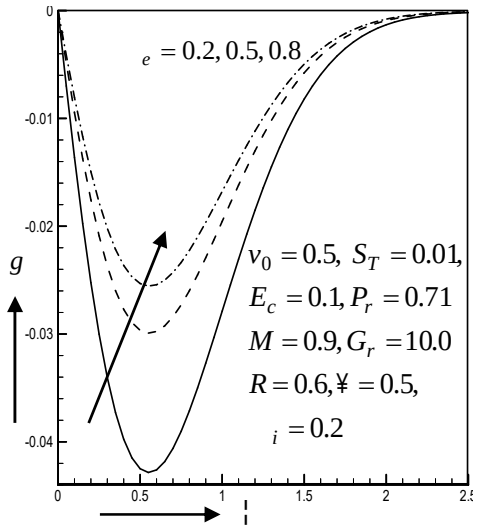

Fig.6.11 Secondary velocity profiles for different values of Hall parameter $_e$

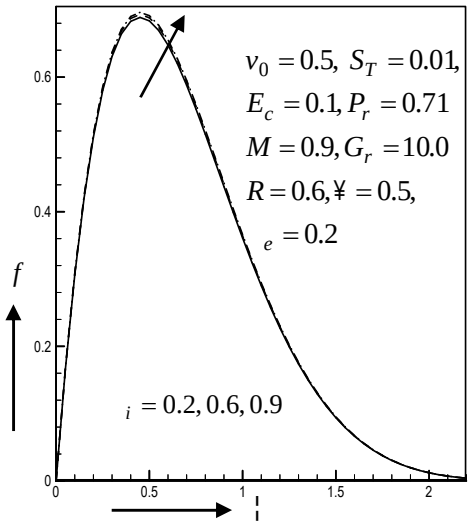

Fig.6.12 Primary velocity profiles for different values of ion-slip parameter $_i$

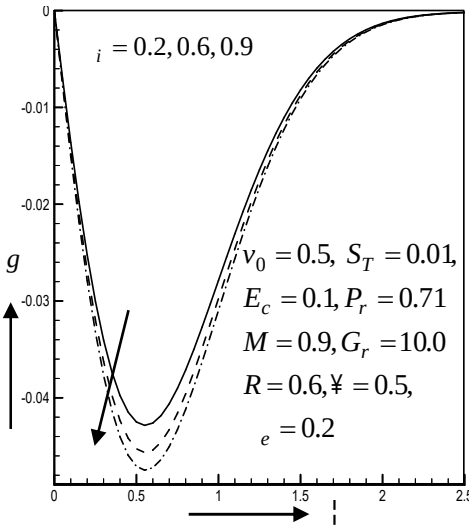

Fig.6.13 Secondary velocity profiles for different values of ion-slip parameter $_i$

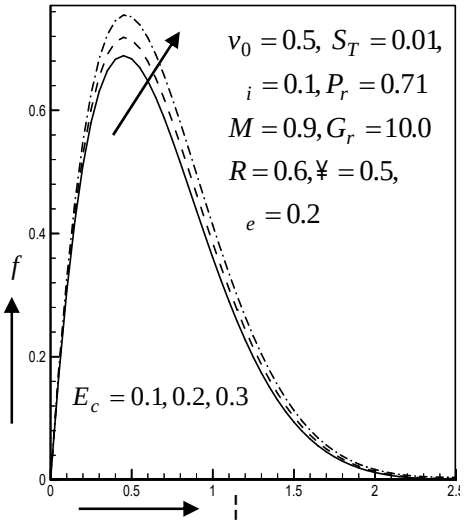

Fig.6.14 Primary velocity profiles for different values of Eckert number E_c

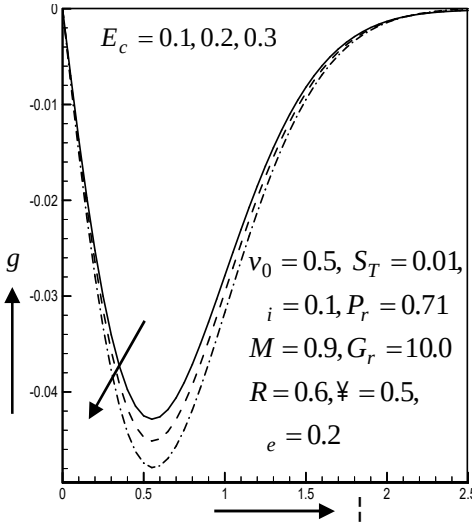

Fig.6.15 Secondary velocity profiles for different values of Eckert number E_c

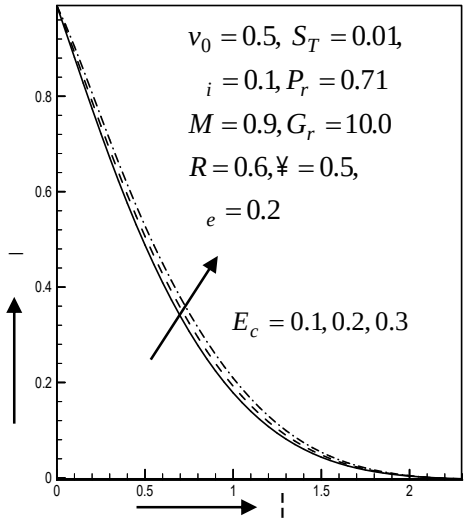

Fig.6.16 Temperature profiles for different values of Eckert number E_c

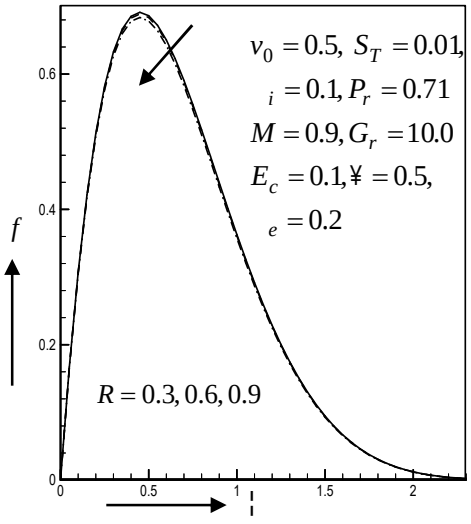

Fig.6.17 Primary velocity profiles for different values of rotation parameter R

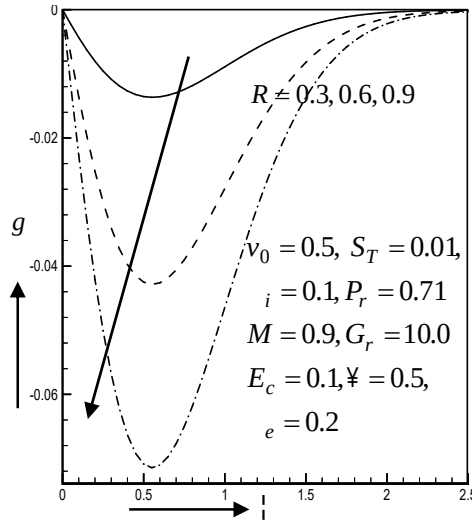

Fig.6.18 Secondary velocity profiles for different values of rotation parameter R

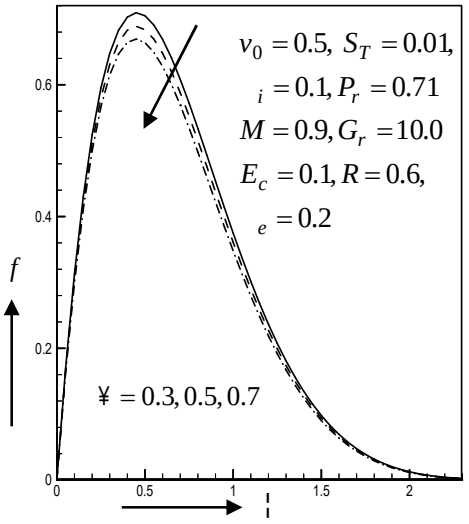

Fig.6.19 Primary velocity profiles for different values of permeability param. ¥

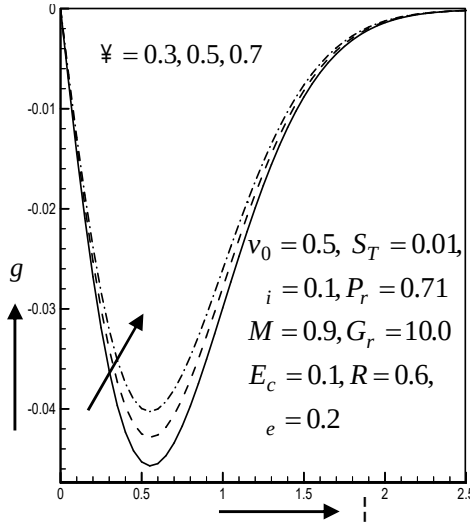

Fig.6.20 Secondary velocity profiles for different values of permeability parameter ¥

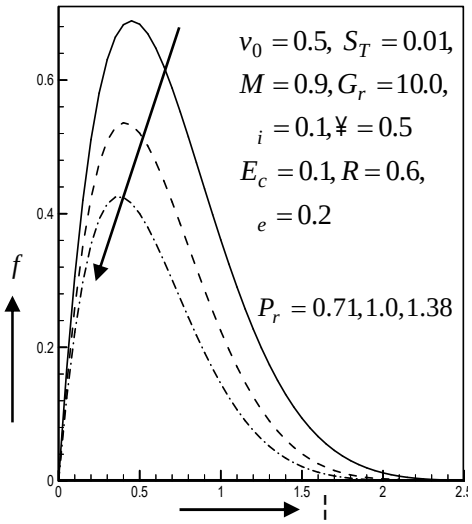

Fig.6.21 Primary velocity profiles for different values of Prandtl number P_r

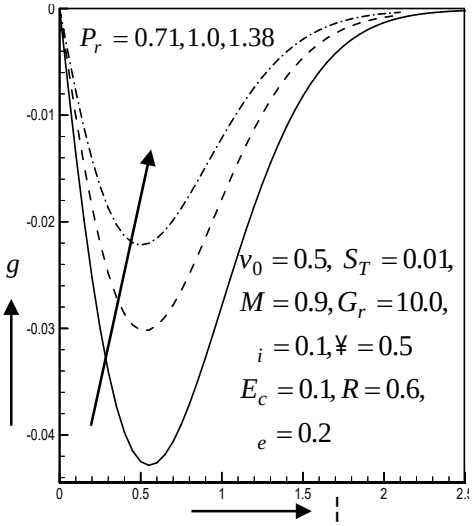

Fig.6.22 Secondary velocity profiles for different values of Prandtl number P_r

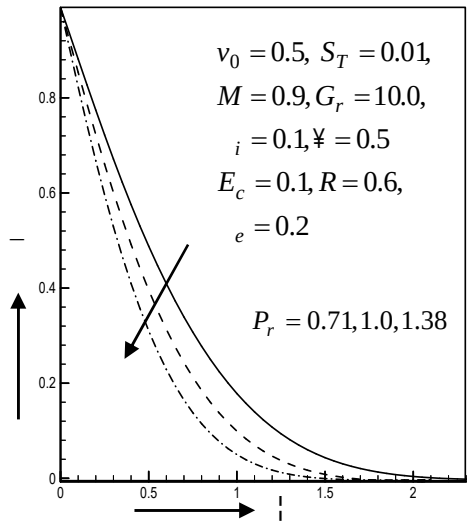

Fig.6.23 Temperature profiles for different values of Prandtl number P_r

Table 6.1

Numerical values of $²_x$, $²_z$ and N_u for $G_r = 10.0$, $_e = 0.2$, $_i = 0.2, M = 0.9, E_c = 0.1$, $R = 0.6$.

G_r	P_r	S_T	v_0	¥	$²_x$	$²_z$	N_u
+ve	0.71	0.01	0.5	0.5	3.6241715528	-0.1422943632	1.0683140011
	1.0	0.01	0.5	0.5	3.1433280098	-0.1059426549	1.363353855
	1.38	0.01	0.5	0.5	2.7557638641	-0.0813034334	1.696834592
	0.71	0.025	0.5	0.5	3.5130933222	-0.1352936363	1.084002649
	0.71	0.035	0.5	0.5	3.4392349293	-0.1306401579	1.094240637
	0.71	0.01	0.3	0.5	3.6893866697	-0.1509664447	0.959687995
	0.71	0.01	0.7	0.5	3.5541664941	-0.1335974968	1.179276909
	0.71	0.01	0.5	0.3	3.6949869259	-0.1509443392	1.061592986
	0.71	0.01	0.5	0.7	3.5576089923	-0.1344422180	1.074446263

Table 6.2

Numerical values of $²_x$, $²_z$ and N_u for $G_r = 10.0$, $_i = 0.2, E_c = 0.1, P_r = 0.71, S_T = 0.01$, $v_0 = 0.5$,¥ $= 0.5$.

G_r	$_e$	R	M	$²_x$	$²_z$	N_u
+ve	0.2	0.6	0.9	3.6241715528	-0.1422943632	1.0683140011
	0.5	0.6	0.9	3.6795556117	-0.0989259648	1.0663329579
	0.8	0.6	0.9	3.7326084715	-0.0841608228	1.0642041682
	0.2	0.3	0.9	3.6323547976	-0.0453463800	1.0678734897
	0.2	0.9	0.9	3.6077364616	-0.2375275581	1.0691981567
	0.2	0.6	0.2	3.8422364729	-0.2203550015	1.0583195026
	0.2	0.6	0.5	3.7446171929	-0.1836265251	1.0627714935

Table 6.3

Numerical values of $²_x$, $²_z$ and N_u for $G_r = 10.0$, $_e = 0.2, R = 0.6, P_r = 0.71, S_T = 0.01$, $v_0 = 0.5, M = 0.9$,¥ $= 0.5$.

G_r	$_i$	E_c	$²_x$	$²_z$	N_u
+ve	0.2	0.1	3.6241715528	-0.1422943632	1.068314001
	0.6	0.1	3.6397621835	-0.1514025690	1.068508835
	0.9	0.1	3.6504223692	-0.1573372206	1.068563060
	0.2	0.2	3.7247945542	-0.1489930874	0.919735419
	0.2	0.3	3.8468561780	-0.1571686104	0.744060366

References

Angirasa, D., Srinivasan, J. (1989), Natural convection flows due to the combined buoyancy of heat and mass transfer in a thermally stratified medium, 'ASME J. Heat Transfer', vol.**111**, p657-663.

Angirasa, D. and Peterson, G. P. (1997), Natural convection heat transfer from an isothermal vertical surface to a fluid saturated thermally stratified porous medium, 'International Journal of Heat and Mass transfer', vol.**40**(18), p4329-4335.

Atul Kumar Singh, Ajay Kumar Singh and Singh, N. P. (2005), Hydromagnetic free convection and mass transfer flow with Joule heating, thermal diffusion, heat source and Hall current, 'Bulleinof the Institute of Mathematics Academia Sinica', vol.**33**, p291–310.

Chamkha, A. J. (1997), MHD free convection from a vertical plate embedded in a thermally stratified porous medium with Hall effects, 'Applied Mathematical Modelling', vol.**21**, No. 10, p603-609.

Gebhart, B., Jaluria, Y., Mahajan, R. and Sammakia, B. (1988), Buoyancy induced flows and transport, 'Hemisphere', New York.

Hasimoto, H.(1957), Boundary layer growth on a flat plate with suction or injection, 'Journal of Physical Society of Japan', vol.**12**(1), p68-72.

Ihsan Y. Hussain and Basim K.Raheem (2013), Natural convection heat transfer from a plane wall to thermally stratified porous media, 'International Journal of Computer Applications', vol.**65**, No. 1, p42-49.

Iranian, D., Loganathan, P. and Ganesan, P.(2015), Unsteady MHD natural convective flow over vertical plate in thermally stratified media with variable viscosity and thermal conductivity, 'International Journal of Computer Applications', vol.**121**(3), p18-24.

Jha, B. K. and Apere, C.A. (2010), Combined effect of Hall and ion-slip currents on unsteady MHD couette flows in a rotating system, 'Journal of Physical Society of Japan', vol.**79**(10), p104401-9.

Jaluria, Y. and Himasekhar, K. (1983), Buoyancy induced two dimensional vertical flows in a thermally stratified environment, 'Comput. Fluids', vol.**11**, p39- 49.

Lai, F. C., Kulacki, F. A. and Pop, I. (1990), Natural convection from isothermal plates embedded in thermally stratified porous media. 'Journal of Thermophysics and Heat Transfer', vol.**4**, p533-535.

Nachtsheim, P. R. and Swigert, P. (1965), Satisfaction of the asymptotic boundary conditions in numerical solution of the system of non-linear equations of boundary layer type, 'NASA', TND-3004.

Nirmal Ghara, Sovan Lal Maji, Sanatan Das, Rabindranath Jana and Swapan Kumar Ghosh (2012). Effects of Hall current and ion-slip on unsteady MHD couette flow, Open Journal of Fluid Dynamics, vol.**2**, p1-13.

Prabhakara Rao, G. Dr., Naga sasikala, M. and Gayathri, P. Dr. (2015), MHD natural convection flow of an incompressible electrically conducting viscous fluid through porous medium from a vertical flat plate, 'International Journal of Engineering Research and Applications', vol.**5**(4), p44-49.

Prandtl, L. (1952), Essentials of fluid dynamics, 'Blackie', London.

Rama Mohan Reddy, L., Raju, M. C. and Raju, G. S. S. (2016), Natural convection boundary

layer flow of a double diffusive and rotating fluid past a vertical porous plate, 'International Journal Applied and Computational Mathematics', DOI 10.1007/s40819-016-0174-7.

Sattar, M. A., Hossain, M. M. (1992), Unsteady hydromagnetic free convection flow with Hall current and mass transfer along an accelerated porous plate with time-dependent temperature and concentration, Canadian Journal of Physics', vol.**70**, p369-374.

Sattar, M. A. Alam, M. M. (1994), Thermal diffusion as well as transpiration effects on MHD free convection and mass transfer flow past an accelerated vertical porous plate, 'Indian Journal of Pure and Applied Mathematics', vol.**25**, p679.

Sattar, M. A., Rahman, M. M. and Alam, M. M. (2000), Free convection flow and heat tansfer through a porous vertical flat plate immersed in a porous medium with variable suction, 'Journal of Energy, Heat and Mass Transfer', vol.**22**, p17-21.

Singh, P., Sharma, K. (1990), Integral method to free convection in thermally stratified porous medium, 'Acta Mechanica', vol.**83**, p157-163.

Swati Mukhopadhyay, Iswar Chandra Mondal and Rama Subba Reddy Gorla (2012), Effects of thermal stratification on flow and heat transfer past a porous vertical stretching surface, 'Heat Mass Transfer', vol.**48**, p915-921.

Chapter 7

Effects of stratification on MHD free convection flow past a vertical plate in a porous medium with Hall and ion-slip currents in a rotating system

Combined heat and mass transfer in fluid-saturated porous media finds applications in a variety of engineering processes such as heat exchanger devices, petroleum eservoirs, chemical catalytic reactors and processes, geothermal and geophysical engineering, moisture migration in a fibrous insulation and nuclear waste disposal and others. *Bejan and Khair* (1985) investigated the free convection boundary layer flow in a porous medium owing to combined heat and mass transfer. The exhaustive volume of work devoted to this area is documented by the most recent books by *Ingham and Pop* (1998), *Nield and Bejan* (1999), *Vafai* (2000), *Pop and Ingham* (2001), *Bejan and Kraus* (2003), *Ingham et al.* (2004), and *Bejan et al*. (2004). However, many problems which are important in applications, as well as in theory.

Many convection processes occur in environments with stratification. Stratification of fluid arises due to temperature variations, concentration differences, or the presence of different fluids. In practical situations where the heat and mass transfer mechanisms run parallel, it is interesting to analyze the effect of double stratification (stratification of medium with respect to thermal and concentration fields) on the convective transport in power-law fluid. Stratification of the medium may arise due to a temperature variation, which gives rise to a density variation in the medium. This is known as thermal stratification and usually arises due to thermal energy input into the medium from heated bodies and thermal sources. Thermally stratified flows are also of great interest in various buoyant flow systems including geothermal systems, geological transport, power plant condensation systems, lake thermohydraulics, and volcanic flows and also in industrial thermal treatment processes. Thermal stratification occurs in cooling ponds, lakes, solar ponds and in the atmosphere. Another situation of interest is the one in which stratification arises due to concentration differences. This is relevant in many natural processes such as transport processes in the sea where stratification exists due to salinity variation. The analysis of free convection in a doubly stratified medium (stratification of medium with respect to thermal and concentration fields) is a fundamentally interesting and important problem because of its

broad range of engineering applications. These applications include heat rejection into the environment such as lakes, rivers and seas, thermal energy storage systems such as solar ponds and heat transfer from thermal sources. Also, the analysis of thermal stratification is important for solar engineers because higher energy efficiency can be achieved with a better stratification. It has been shown by scientists that thermal stratification in energy store may considerably increase system performance. Due to the immense importance of stratification, authors have analyzed the influence of thermal stratification on the rate of heat and mass transfer. *Ganesan et al.* (2014) analyzed doubly stratified effects in a free convective flow over a vertical plate with heat and mass transfer. *Tak and Arti* (2007) studied the influence of double stratification on MHD free convection with Soret and Dufour effects in a Darcian porous media. *Murty et al.* (2004) studied the effect of double stratification on free convection in a Darcian porous medium. *A*li (1996) investigated MHD free convection from a vertical plate embedded in a thermally stratified porous medium. *Kaladhar et al.* (2016) investigated an analytical study for Soret, Hall, and Joule heating effects on natural convection flow saturated porous medium in a vertical channel. The effects of Soret and Dufour on an unsteady MHD free convection flow past a vertical porous plate in the presence of suction or injection was investigated by *Sarada and Shanker* (2013). *Lakshmi and Murthy* (2008) discussed Soret and Dufour effects on free convection heat and mass transfer from horizontal flat plate in a Darcy porous medium.

In recent years, considerable interest has been given to the theory of rotating fluids due to its application in cosmic and geophysical sciences. In an ionized gas where the density is low and/or the magnetic field is very strong, the effects of Hall and ion-slip currents play a significant role in the velocity distribution of the flow. The study of magnetohydrodynamic flows with Hall and ion-slip currents has important engineering applications in the problem of magnetohydrodynamic generators and of Hall accelerators as well as flight magnetohydrodynamics. *Ram and Takhar* (1993) dealt with MHD free convection from an impulsively moving infinite vertical plate in a rotating fluid with Hall and ion-slip currents. An investigation of the effect of Hall current and rotational parameter on dissipative fluid flow past a vertical semi-infinite plate was studied by *Abuga et al.* (2011). *Naroua* (2007) studied a computational solution of hydromagnetic free convective flow past a vertical plate in a rotating heat-generating fluid with Hall and ion-slip currents.

The heat and mass transfer simultaneously affecting each other that will cause cross-diffusion effect. These effects are very significant when the temperature and concentration gradient are very high. Thus Soret effect is referred to species differentiation developing in an initial homogenous mixture submitted to a thermal gradient and the Dufour effect referred to the heat flux produced by concentration gradient. *Nazmul and Alam* (2007) investigated Dufour and Soret effects on steady MHD free convection and mass transfer fluid flow through a porous medium in a rotating system. Soret and Dufour effects on steady MHD free

convection flow past a semi-infinite moving vertical plate in a porous medium with viscous dissipation were investigated by *Gnaneswara and Bhaskar* (2010). Dufour and Soret effects on unsteady MHD free convection and mass transfer flow past a vertical porous plate in a porous medium were analyzed by *Alam et al.* (2006). *RajaShekar* (2014) analyzed the effects of Dufour and Soret on unsteady MHD heat and mass transfer flow past a semi-infinite moving vertical plate in a porous medium with viscous dissipation. *Sreedhar et al.*(2013) studied numerical study of MHD free convection heat and mass transfer from vertical surfaces in porous media considering Soret and Dufour effects.

The aim of the present work is to investigate the effects of stratification on MHD free convection and mass transfer flow along a vertical plate in porous media saturated with viscous dissipation and Joule heating effects, Soret and Dufour effects, Hall and ion-slip currents in a rotating system. The obtained nonlinear coupled ordinary equations have been solved numerically using Nachtsheim-Swigert shooting iteration technique together with sixth order Rung-Kutta iteration scheme. The effects of different parameters on velocity, temperature and concentration are presented graphically. The numerical values of shear stress, Nusselt number and Sherwood number are discussed for various values of physical parameters and presented in tabular form.

7.1 Governing Equations

The system deals with a steady, laminar, incompressible, two-dimensional free convective heat and mass transfer flow along a semi-infinite vertical plate in porous media embedded in a doubly stratified, electrically conducting fluid. The viscous dissipation and Joule heating terms have been retained in the energy equation. A uniform magnetic field of magnitude B_0 is applied normal to the plate. The magnetic Reynolds number is assumed to be small so that the induced magnetic field can be neglected in comparison with the applied magnetic field. The x-coordinate is taken along the plate and y-coordinate is measured normal to the plate, while the origin of the reference system is considered at the leading edge of the vertical plate. The plate is maintained at uniform wall temperature and concentration T_w and C_w respectively. The values of T_w and C_w are assumed to be greater than the ambient temperature $T_{\infty,x=0}$ and $C_{\infty,x=0}$ at any arbitrary reference point in the medium (inside the boundary layer). At time $t > 0$, the plate is given an impulsive motion in its own plane with a uniform velocity U_0. The ambient medium is assumed to be vertically linearly stratified with respect to both temperature and concentration in the form $T_\infty(x) = T_{\infty,x=0} + S_1 x$ and $C_\infty(x) = C_{\infty,x=0} + S_2 x$ where S_1 and S_2 are constants which are varied to alter intensity of stratification in the medium and $T_{\infty,x=0}$ and $C_{\infty,x=0}$ are ambient temperature and concentration respectively.

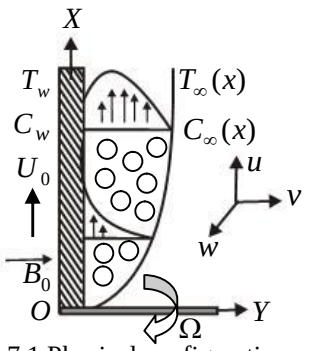

Fig.7.1 Physical configuration and coordinate system

Furthermore, only positive values of $S_1 = \frac{d}{dx}\{T_\infty(x)\}$ and $S_2 = \frac{d}{dx}\{C_\infty(x)\}$ are considered which imply a stable stratified ambient environment. The values of T_w and C_w are assumed to be greater than the ambient temperature $T_{\infty, x=0}$ and concentration $C_{\infty, x=0}$ at any arbitrary point in the medium (inside the boundary layer). The physical model and coordinate system which is shown in Fig.7.1. By employing boundary layer flow assumptions and the Boussinesq approximation, the governing equations are as follows;

The continuity equation;

$$\frac{\partial u}{\partial x} + \frac{\partial v}{\partial y} = 0 \tag{7.1}$$

Momentum equation;

$$\frac{1}{\pounds^2}\left(u\frac{\partial u}{\partial x} + v\frac{\partial u}{\partial y}\right) = \frac{\mathfrak{Z}}{\pounds}\frac{\partial^2 u}{\partial y^2} + g_0 \quad (T - T_\infty(x)) + g_0 \quad ^*(C - C_\infty(x)) + 2\Omega w - \frac{\mathfrak{Z}}{k}u - cu^2 - \frac{\pm_e B_0^2(\sim_e u + \quad_e w)}{\circ(\sim_e^2 + \quad_e^2)} \tag{7.2}$$

$$\frac{1}{\pounds^2}\left(u\frac{\partial w}{\partial x} + v\frac{\partial w}{\partial y}\right) = \frac{\mathfrak{Z}}{\pounds}\frac{\partial^2 w}{\partial y^2} - 2\Omega u - \frac{\mathfrak{Z}}{k}w - Cw^2 + \frac{\pm_e B_0^2(\quad_e u - \sim_e w)}{\circ(\sim_e^2 + \quad_e^2)} \tag{7.3}$$

Energy equation;

$$u\frac{\partial T}{\partial x} + v\frac{\partial T}{\partial y} = \frac{\copyright}{\circ c_p}\frac{\partial^2 T}{\partial y^2} + \frac{\mathfrak{Z}}{c_p}\left[\left(\frac{\partial u}{\partial y}\right)^2 + \left(\frac{\partial w}{\partial y}\right)^2\right] + \frac{\pm_e B_0^2(u^2 + w^2)}{\circ c_p(\sim_e^2 + \quad_e^2)} + \frac{D_m k_T}{c_s c_p}\frac{\partial^2 C}{\partial y^2} \tag{7.4}$$

Concentration equation;

$$u\frac{\partial C}{\partial x} + v\frac{\partial C}{\partial y} = D_m\frac{\partial^2 C}{\partial y^2} + \frac{D_m k_T}{T_m}\frac{\partial^2 T}{\partial y^2} \tag{7.5}$$

where all physical quantities are defined in the Nomenclature.

Boundary conditions are as follows;

$$\begin{aligned} &u = U_0,\ v = v_w(x), w = 0, T = T_W, C = C_W \quad t > 0 \quad at\ y = 0 \\ &u = 0,\ w = 0, T = T_\infty(x), C = C_\infty(x) \quad t > 0 \quad as\ y \to \infty \end{aligned} \tag{7.6}$$

where v_w is the uniform blowing/suction at the plate, the subscripts w, $(\infty, x = 0)$ and ∞ indicate the conditions at the wall, at some reference point in the medium and at the outer edge of the boundary layer respectively.

7.2 Mathematical Formulation

The continuity equation (7.1) is satisfied by introducing the stream function $\cdot$ such that

$$u = \frac{\partial \cdot}{\partial y},\ v = -\frac{\partial \cdot}{\partial x}$$

Introducing the following non dimensional variables:

$$\cdot = \sqrt{2U_0 {}^3 x}\, f(\dagger),\ \dagger = y\sqrt{\frac{U_0}{2{}^3 x}},\ u = \frac{\partial \cdot}{\partial y},\ v = -\frac{\partial \cdot}{\partial y},\ w = U_0 g(\dagger),\ {}^{-}(\dagger) = \frac{T - T_\infty(x)}{T_w - T_{\infty,x=0}}$$
$$\text{¤}(\dagger) = \frac{C - C_\infty(x)}{C_w - C_{\infty,x=0}} \tag{7.7}$$

Substituting equations (7.7) and in (7.2)-(7.5), then obtained the following equations are as follows:

$$f''' + \frac{1}{£} ff'' - £\left[¥ + \frac{M\sim_e}{\sim_e^2 + \ \ _e^2}\right] f' - £\Gamma f'^2 + £\left[R - \frac{M\ \ _e}{\sim_e^2 + \ \ _e^2}\right] g + £G_r{}^{-} + £G_m\text{¤} = 0 \tag{7.8}$$

$$g'' + \frac{1}{£} g'f - £\left[¥ + \frac{M\sim_e}{\sim_e^2 + \ \ _e^2}\right] g - £\Gamma g^2 - £\left[R - \frac{M\ \ _e}{\sim_e^2 + \ \ _e^2}\right] f' = 0 \tag{7.9}$$

$${}^{-}{}'' + P_r{}^{-}{}'f - S_T P_r f' + E_c P_r\left[f''^2 + g'^2\right] + \frac{ME_c P_r}{\sim_e^2 + \ \ _e^2}\left[f'^2 + g^2\right] + D_f P_r \text{¤}'' = 0 \tag{7.10}$$

$$\text{¤}'' + S_c \text{¤}'f - S_c S_T^* f' + S_0 S_c{}^{-}{}'' = 0 \tag{7.11}$$

where $G_r\left(= \frac{2xg_0\ \ (T_w - T_{\infty,x=0})}{U_0^2}\right)$, $G_m\left(= \frac{2xg_0\ \ ^*(C_w - C_{\infty,x=0})}{U_0^2}\right)$, $R\left(= \frac{4x\Omega}{U_0}\right)$, $¥\left(= \frac{2x{}^3}{U_0 k}\right)$,

$\Gamma(= 2xc), M\left(= \frac{2x\pm_e B_0^2}{\circ U_0}\right)$, $S_T\left(= \frac{2x}{(T_w - T_{\infty,x=0})}\frac{d}{dx}\{T_\infty(x)\}\right)$, $S_T^*\left(= \frac{2x}{(C_w - C_{\infty,x=0})}\frac{d}{dx}\{C_\infty(x)\}\right)$,

$P_r\left(= \frac{\circ {}^3 c_p}{©}\right)$, $E_c\left(= \frac{U_0^2}{c_p(T_w - T_{\infty,x=0})}\right)$, $S_0\left(= \frac{D_m k_T}{{}^3 T_m}\frac{T_w - T_{\infty,x=0}}{C_w - C_{\infty,x=0}}\right)$, $S_c\left(= \frac{D_m}{{}^3}\right)$

$D_f\left(= \frac{D_m k_T}{c_s c_p{}^3}\frac{(C_w - C_{\infty,x=0})}{(T_w - T_{\infty,x=0})}\right)$,

The transformed boundary conditions are as follows;

$$\begin{aligned} &f' = 1,\ f = f_w, g = 0, {}^{-} = 1 - \frac{1}{2}S_T, \text{¤} = 1 - \frac{1}{2}S_T^* \quad at\ \dagger = 0 \\ &f' = 0,, g = 0,\ {}^{-} = 0, \text{¤} = 0 \qquad\qquad as \dagger \to \infty \end{aligned} \tag{7.12}$$

where $f_w = -v_w(x)\sqrt{\frac{2x}{U_0{}^3}}$ is the suction parameter and primes denote differentiation with respect to similarity variable $\dagger$. Here $f_w > 0$ denotes the suction and $f_w < 0$ the injection.

7.3 Solution Technique

The set of non-linear and similar ordinary differential equations (7.8)–(7.11) with boundary conditions (7.12) have been solved numerically by sixth order Runge–Kutta method along with *Nachtsheim–Swigert* shooting iteration technique with prescribed parameters.

7.4 Shear Stress, Nusselt number and Sherwood number

The equation defining shear stress in x and z -axes are as follows;

$\tau_x = \mu\left(\frac{\partial u}{\partial y}\right)_{y=0}$ and $\tau_z = \mu\left(\frac{\partial w}{\partial y}\right)_{y=0}$ which are proportionally to $\left(\frac{\partial f}{\partial \eta}\right)_{\eta=0}$ and $\left(\frac{\partial g}{\partial \eta}\right)_{\eta=0}$.

The Nusselt number denoted by N_u is proportional to $-\left(\frac{\partial \theta}{\partial \eta}\right)_{\eta=0}$.

The Sherwood number denoted by S_h is proportional to $-\left(\frac{\partial \phi}{\partial \eta}\right)_{\eta=0}$.

7.5 Results and Discussion

The governing boundary layer equations (7.8)-(7.11) with boundary conditions (7.12) are coupled non-linear partial differential equations, which possess no similarity or closed form solution. Therefore, for numerical solution of the problem, the sixth-order Runge-Kutta method is needed. Numerical results which illustrate the effects of all involved physical parameters of the present problem. The values of P_r is taken to be $P_r = 0.71$ which corresponds to air at 20^0C, $P_r = 1.0$ correspond to salt water at 20^0C, $P_r = 1.38$ corresponds to ammonia, $S_c = 0.6$ corresponds to water vapor, $S_c = 0.78$ corresponds to ammonia, $S_c = 1.0$ corresponds to carbondioxide. For free convection and cooling plate positive large values of $G_r = 10.0$ and $G_m = 5.0$ are chosen. The values of Dufour number and Soret number are chosen in such a way that their product is constant provided that the mean temperature T_m is kept constant. However, the values of other physical parameters on the flow are chosen arbitrarily. The numerical results for the velocity, temperature and concentration distributions are displayed in Figs. 7.2-7.51.

From Fig.7.2, an increase in Hall parameter ($_e$) leads to an increase in the primary velocity profiles. When the Hall parameter is increased the induced current along x-axis increases and this translates to an increase in the primary velocity profiles. The secondary velocity has the same effect which is shown in Fig.7.3.

Fig.7.4 demonstrates the dimensionless primary velocity for different values of inertial parameter (Γ). It is clear that the primary velocity of the fluid decreases with the increase of Γ. Since Γ represents the initial drag, thus an increases Γ increases the resistance to the flow and so decrease in the primary velocity. The secondary velocity increases with the increase of Γ is seen in Fig.7.5.

Figs.7.6-7.9 display the non-dimensional velocity components (primary and secondary), temperature and concentration for different values of Dufour number(D_f). It is observed from Fig.7.6 that the primary velocity of the fluid increases with the increase of D_f while the secondary velocity has opposite behavior is seen in Fig.7.7. The dimensionless

temperature increases for different values of Dufour number is shown in Fig.7.8. The Dufour number signifies the contribution of the concentration gradients to the thermal energy flux in the flow. It is found that an increase in the Dufour number causes a rise in the temperature throughout the boundary layer i.e., the raise of Dufour number encourages heat transfer. In Fig.7.9, it is seen that the concentration distribution decreases with the increase of Dufour number. The Dufour effects reduce the concentration boundary layer in the fluid.

In Figs.7.10-7.13, the influence of Eckert number (E_c) on the dimensionless velocity (primary and secondary), temperature, concentration are presented. In Fig.7.10, an increase in Eckert number results to an increase in the primary velocity profiles. An increase in Eckert number means an increase in kinetic energy of the fluid particles and for this reason primary velocity increases. Whereas the secondary velocity has reverse effect is found in Fig.7.11. From Fig. 7.12, increase in Eckert number leads to an increase in the temperature profiles. Increasing the Eckert number causes the fluid to become warmer and therefore increase its temperature. In Fig.7.13, concentration profiles decreases with the increase of Eckert number.

Fig.7.14 illustrates the influence of porosity on the primary velocity. Increasing porosity clearly serves to enhance the flow velocity i.e. accelerates the flow. The secondary velocity decreases with increasing values of porosity parameter is shown in Fig.7.15. From Fig.7.16 it is observed that temperature distribution decreases with increasing porosity parameter. A reduction in the volume of solid particles in the medium implies a lower contribution via thermal conduction. This will serve to decrease temperature. In fig.7.17 a similar response for the concentration field is observed, as with the temperature distributions.

The numerical results for the velocity (primary and secondary), temperature and concentration distributions are displayed in Figs.7.18-7.21. The effects of suction parameter f_w on the velocity field are shown in Fig.7.18. It is seen from this figure that the velocity profiles decrease with the increase of suction parameter indicating the usual fact that suction stabilizes the boundary layer growth. The secondary velocity has reverse effects with increasing values of suction parameter is shown in Fig.7.19. The effect of suction parameter on the temperature and concentration field is displayed in Fig.7.20 and Fig.7.21 respectively. Both the temperature and concentration decreases with the increase of suction parameter. Sucking decelerated fluid particles through the porous wall reduce the growth of the fluid boundary layer as well as thermal and concentration boundary layers.

Figs.7.22-7.25 display results of velocity (primary and secondary), temperature and concentration distributions for various values of porous permeability parameter ¥. It is observed from Fig.7.22 that the velocity distribution decreases with increasing the porous permeability parameter because the presence of porous medium increases the resistance to the flow which causes the fluid velocity to decrease. The secondary velocity increases with increasing values of permeability parameter is shown in Fig.7.23. Fig.7.24 depicts the variations of temperature distributions for various values of porous permeability. It is found that increase in the value of ¥ increases the temperature because of increase in the thermal

boundary layer thickness due to the resistance offered to the fluid motion in the form of Darcy drag produced by the porous medium. It is seen from Fig.7.25 that the concentration distribution increases with increasing the value of porous permeability parameter due to increase in the concentration boundary layer thickness.

Fig.7.26 and Fig7.27 illustrated the primary velocity decrease and the secondary velocity increases with increasing values of magnetic parameter (M). An increase in the magnetic parameter leads to a decrease in the primary velocity and an increase in the secondary velocity profiles. Due the Lorentz force, there is a resistive force along the x-axis and this reduces the primary velocity but the secondary velocity profile increases since it is in the direction of the induced force. It is noticed from Fig.7.28 and Fig.7.29 that the temperature and concentration increases with increasing values of magnetic parameter. This is due to the fact that the transverse magnetic field gives rise to a resistive force known as the Lorentz force of an electrically conducting fluid. This force makes the fluid experience a resistance by increasing the friction between its layers and thus increases its temperature and concentration.

Fig.7.30 illustrates that the primary velocity (f') decreases with an increase in Prandtl number P_r. Physically, this is true because the increase in the Prandtl number is due to increase in the viscosity of the fluid which makes the fluid thick and hence causes a decrease in the velocity of the fluid. From Fig.7.31, it is observed that the secondary velocity has opposite behavior with increasing values of P_r. It is observed from Fig.7.32 that temperature of the fluid decreases with increasing the value of P_r. The reason underlying such a behavior is that P_r signifies the relative effects of viscosity to thermal conductivity and smaller values of P_r posses high thermal conductivity and therefore heat is able to diffuse away from the surface faster than at higher values of P_r. This results in the reduction of thermal boundary layer thickness. Fig.7.33 depicts the variation in the concentration distributions for different values of P_r. The concentration increases with increasing values of P_r.

It is seen from Fig.7.34 that there is a negligible effect of rotation parameter on the primary velocity. Fig.7.35 displays the influence of rotation parameter on the secondary velocity. The secondary velocity has decreasing effect with the increasing values of rotation parameter. This is due to the reason that Coriolis force is dominant in the region near to the axis of rotation.

Figs.7.36,7.39 are presented the primary velocity and concentration for various values of Schmidt number (S_c). It is seen that the primary velocity and concentration decreases with increasing S_c due to a decrease in the molecular diffusivity, which results in a decrease in the velocity and concentration boundary layer thickness. From Figs.7.37, it is seen that the secondary velocity increases with increasing values of S_c. Also the temperature distribution increases with increasing values of S_c in Fig.7.38. As Schmidt number increases the thermal

boundary layer thickness decreases due to a decrease in chemical species molecular diffusivity.

Figs.7.40,7.43 depict the primary velocity and concentration profiles for different values of the Soret number (S_0). The Soret number defines the effect of the temperature gradients inducing significant mass diffusion effects. It is noticed that an increase in the Soret number results in an increase in the velocity and concentration within the boundary layer. The secondary velocity decreases with increasing values of Soret number is shown in Fig.7.41. Fig.7.42 depicts the behavior of S_0 on temperature distribution. It is observed that as S_0 increases, there is a decrease in the temperature of the fluid.

The effect of thermal stratification parameter (S_T) on non-dimensional velocity (primary and secondary), temperature, concentration is shown in Figs.7.44-7.47. It is observed from Fig.7.44 that the primary velocity decreases with the increase of thermal stratification(S_T). Increase in thermal stratification parameter reduces the effective convective potential between the heated plate and the ambient fluid in the medium. This factor causes a decrease in the buoyancy force, which decelerates the velocity of the flow. It is seen from Fig.7.45, that there is an increasing effect of the secondary velocity profiles with increasing values of S_T. Influence of thermal stratification parameter S_T on the temperature and concentration distributions is shown in Fig.7.46 and Fig.4.47. Here the temperature and thermal boundary layer thickness is decreased while concentration and its related boundary layer thickness is increased when increase in thermal stratification parameter. When the thermal stratification effect is taken into account, the effective temperature difference between the surface and the ambient fluid is decreased while opposite behavior is observed for concentration profile.

In Figs. 7.48-7.51 the influence of mass stratification parameter S_T^* on the dimensionless velocity(primary and secondary), temperature and concentration are presented. From Fig. 7.48, it is observed that the primary velocity of the fluid decreases with the increase of mass stratification parameter. Increase in mass stratification parameter lessens the concentration gradient between the ambient and the surface. This declines the buoyancy force, which reduces the velocity of the flow. Influence of mass stratification parameter S_T^* on the temperature and concentration distributions are shown in Fig 7.50 and Fig.7.51. The temperature profile is enhanced while the concentration profile is reduced with an increase in mass stratification parameter.

Finally, the effects of various parameters on the components of the shear stress $^2{}_x$, $^2{}_z$, the Nusselt number N_u and Sherwood number S_h are shown in Table 7.1-Table 7.4. From Table 7.1, it is observed that the components of shear stress $^2{}_x$ increases with increasing values of $_e$ while decreases with the increasing values of R and Γ. Also the components $^2{}_z$ increases with increasing values of $_e$ and Γ whereas it decreases with increasing value of R.

Table 7.2 shows the components of the shear stress ² $_x$ increases and ² $_z$ decreases with the increase of D_f, E_c, S_0 and £. The Table also shows the Nusselt number increase with increase of £ and S_0 while decreases with the increase of D_f and E_c. Again from this Table, it is observed that the Sherwood number S_h increases with the increasing values of D_f, E_c, £ and decreases with the increasing values of S_0.

From Table 7.3, it is observed that the components of the shear stress ² $_x$ decreases and ² $_z$ increases with the increase of f_w, M, P_r and ¥. The Table also shows that the Nusselt number increases with increase of f_w and P_r while decreases with the increase of M and ¥. Again from this Table, it is observed that the Sherwood number S_h increases with the increasing values of f_w whereas decreases with the increasing values of M, P_r and ¥.

From Table 7.4, it is observed that the components of the shear stress ² $_x$ decreases and ² $_z$ increases with the increase of S_c, S_T and S_T^*. The Table also shows that the Nusselt number increases with increase of S_T while decreases with the increase of S_c and S_T^*. Again from this Table, it is observed that the Sherwood number S_h increases with the increasing values of S_c and S_T^* whereas decreases with the increasing values of S_T.

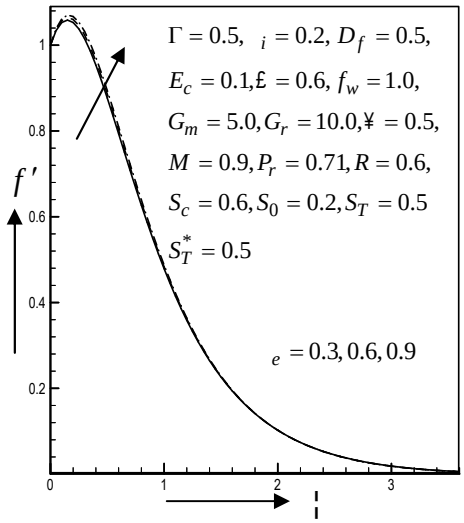

Fig. 7.2Primary velocity profiles for different values of Hall parameter $_e$

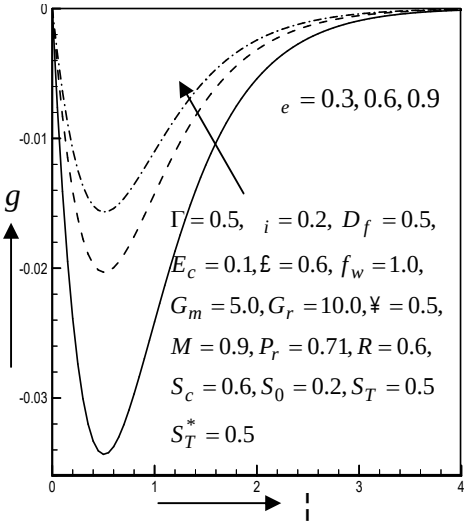

Fig. 7.3Secondary velocity profiles for different values of Hall parameter $_e$

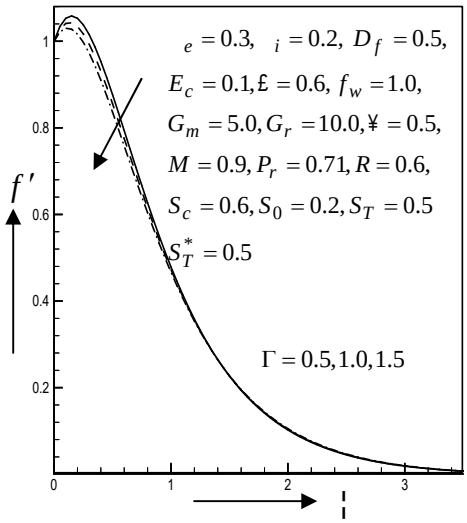

Fig. 7.4Primary velocity profiles for different values of inertial parameter Γ

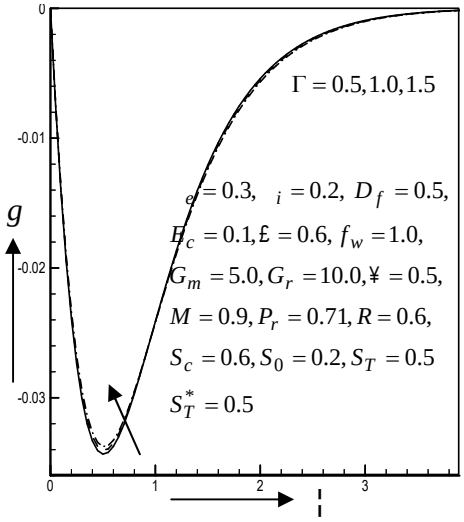

Fig. 7.5 Secondary velocity profiles for different values of inertial parameter Γ

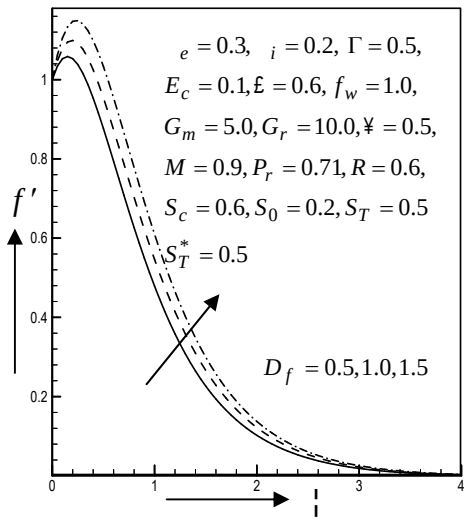

Fig. 7.6 Primary velocity profiles for different values of Dufour number D_f

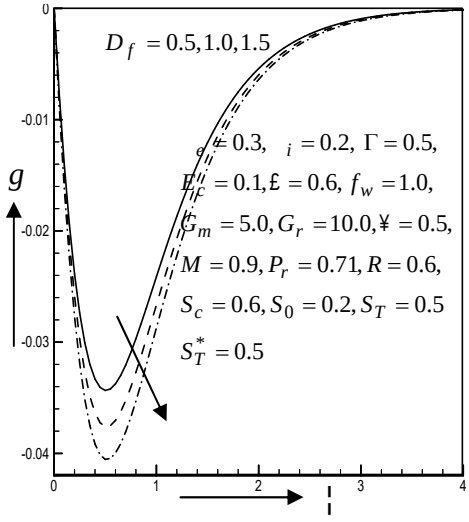

Fig. 7.7 Secondary velocity profiles for different values of Dufour number D_f

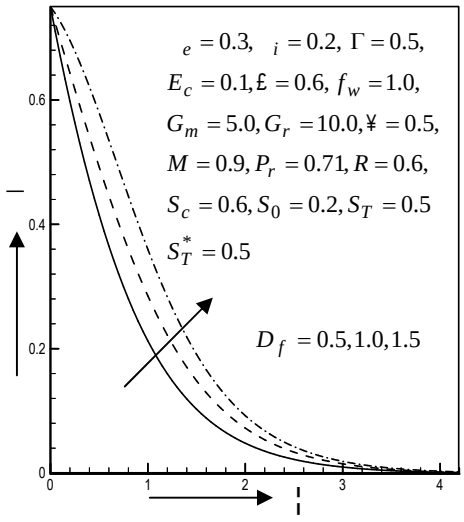

Fig. 7.8 Temperature distribution for different values of Dufour number D_f

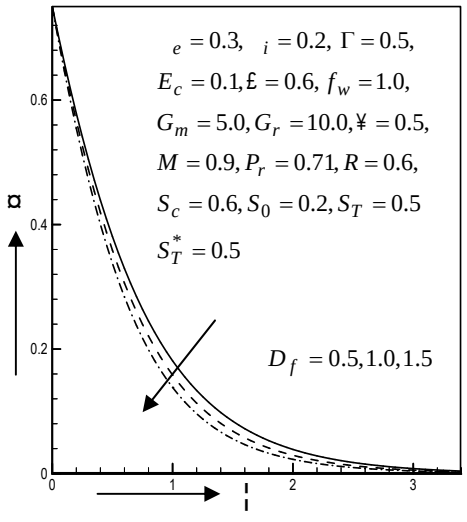

Fig. 7.9 Concentration distribution for different values of Dufour number D_f

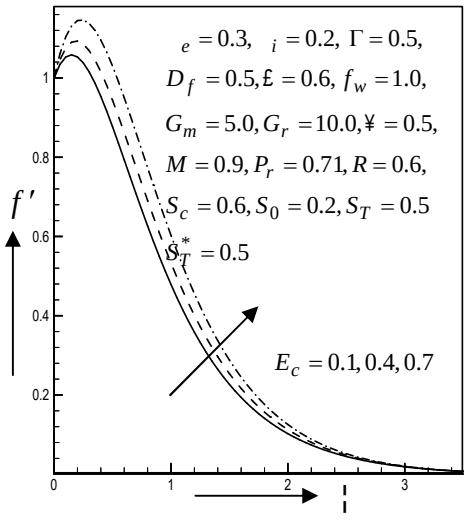

Fig. 7.10 Primary velocity profiles for different values of Eckert number E_c

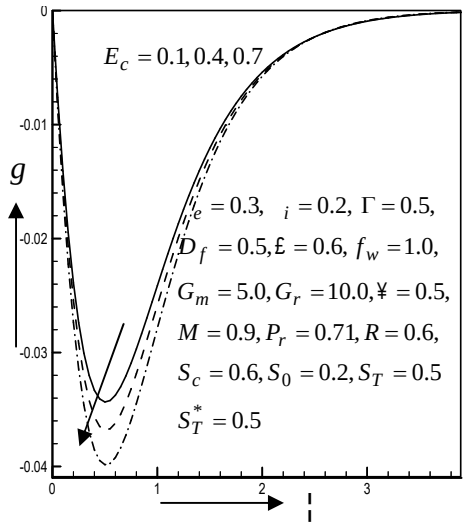

Fig. 7.11 Secondary velocity profiles for different values of Eckert number E_c

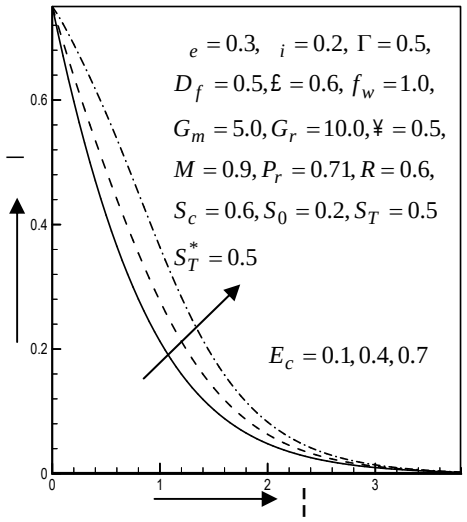

Fig. 7.12 Temperature distribution for different values of Eckert number E_c

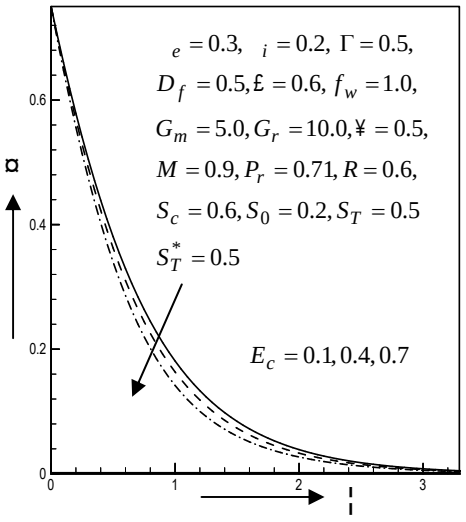

Fig. 7.13 Concentration distribution for different values of Eckert number E_c

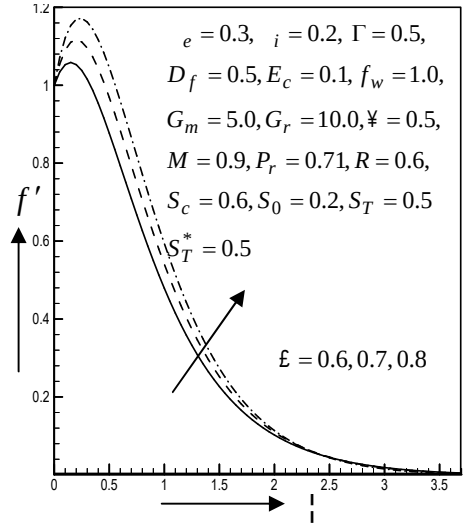

Fig. 7.14 Primary velocity profiles for different values of porosity parameter £

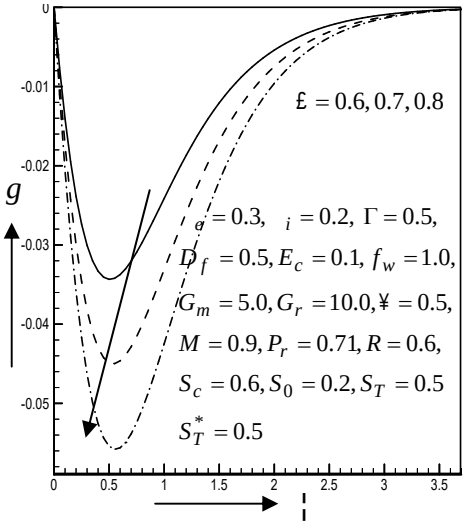

Fig. 7.15 Secondary velocity profiles for different values of porosity parameter £

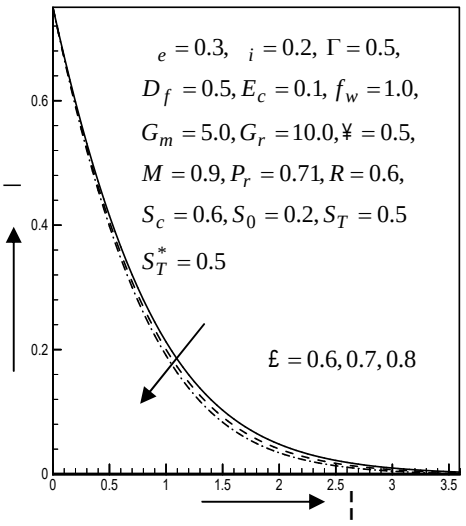

Fig. 7.16 Temperature distribution for different values of porosity parameter £

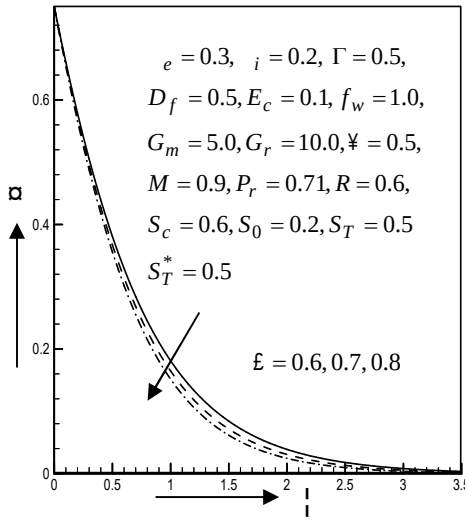

Fig. 7.17 Concentration distribution for different values of porosity parameter £

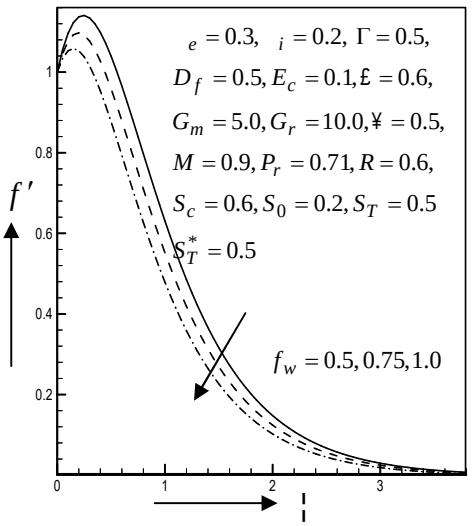

Fig. 7.18 Primary velocity profiles for different values of suction parameter f_w

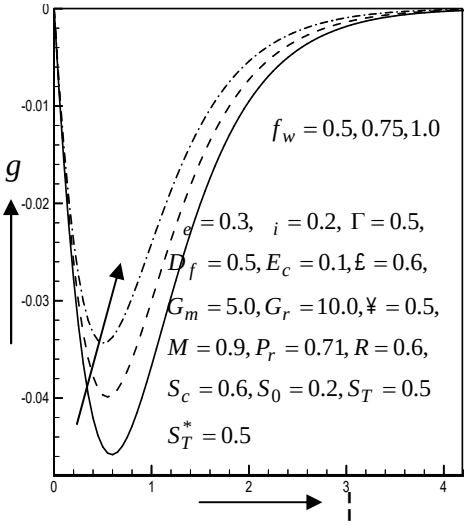

Fig. 7.19 Secondary velocity profiles for different values of suction parameter f_w

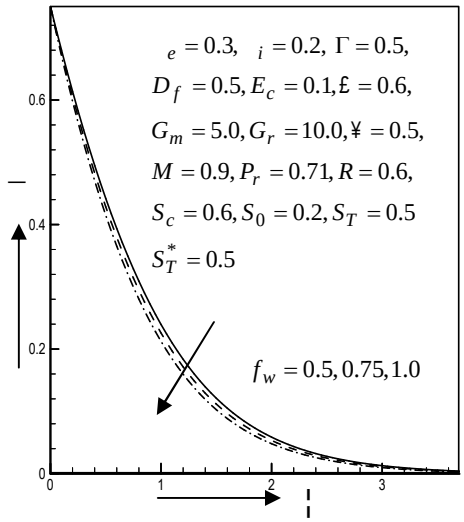

Fig. 7.20 Temperature distribution for different values of suction parameter f_w

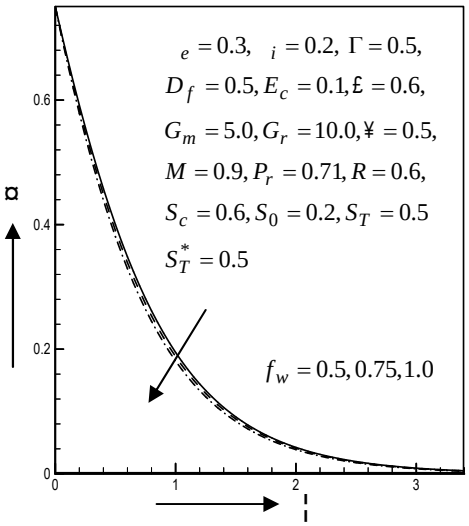

Fig. 7.21 Concentration distribution for different values of suction parameter f_w

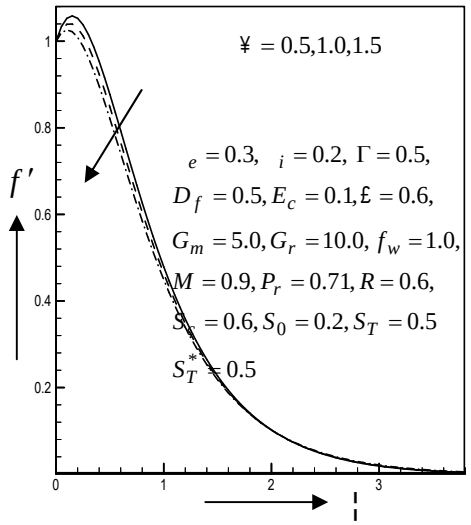

Fig. 7.22 Primary velocity profiles for different values of permeability parameter ¥

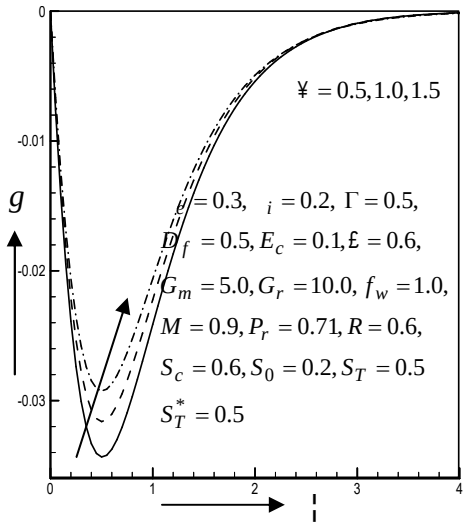

Fig. 7.23 Secondary velocity profiles for different values of permeability parameter ¥

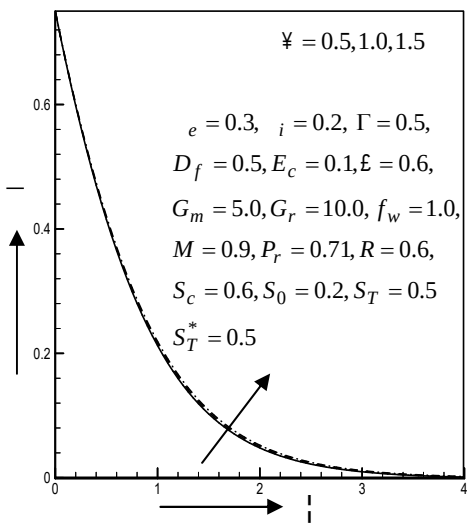

Fig. 7.24 Temperature distribution for different values of permeability parameter ¥

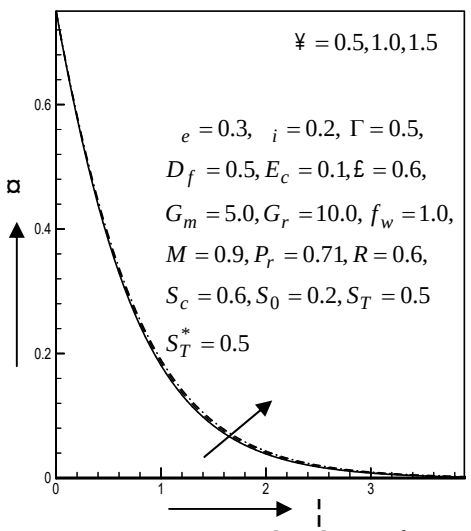

Fig. 7.25 Concentration distribution for different values of permeability parameter ¥

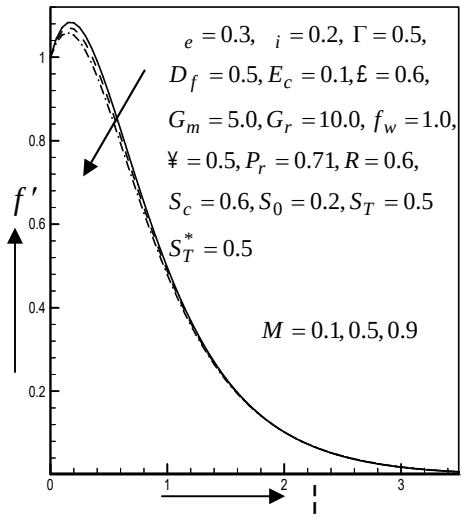

Fig. 7.26 Primary velocity profiles for different values of magnetic parameter M

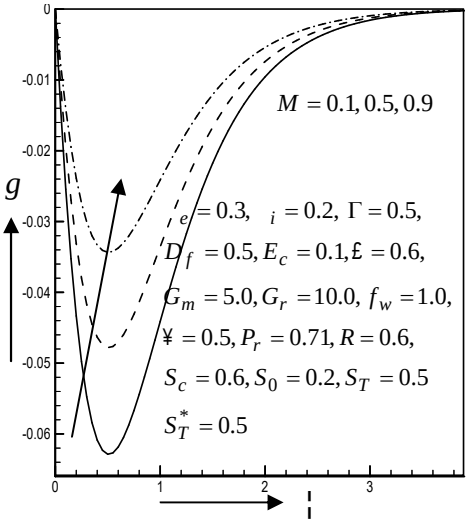

Fig. 7.27 Secondary velocity profiles for different values of magnetic parameter M

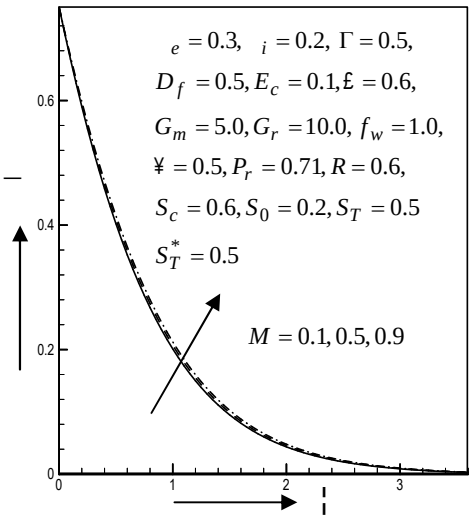

Fig. 7.28 Temperature distribution for different values of magnetic parameter M

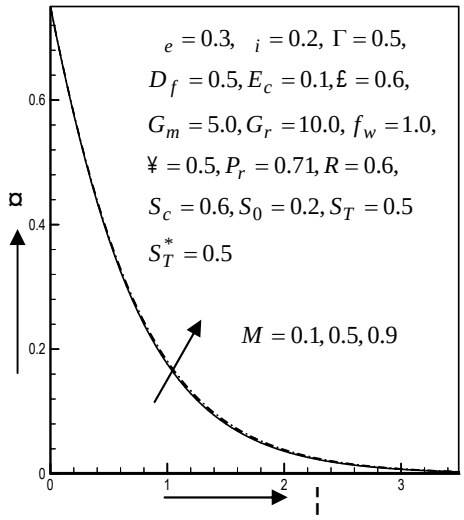

Fig. 7.29 Concentration distribution for different values of magnetic parameter M

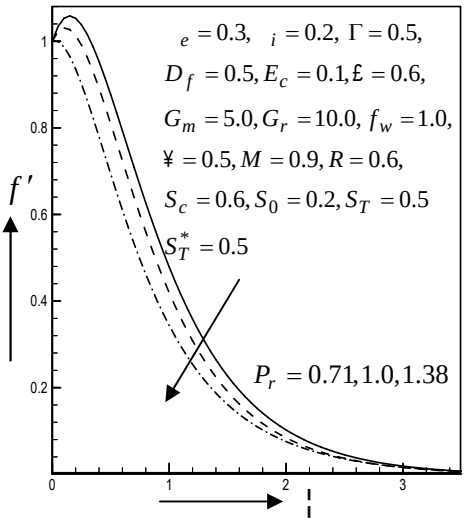

Fig. 7.30 Primary velocity profiles for different values of Prandtl number P_r

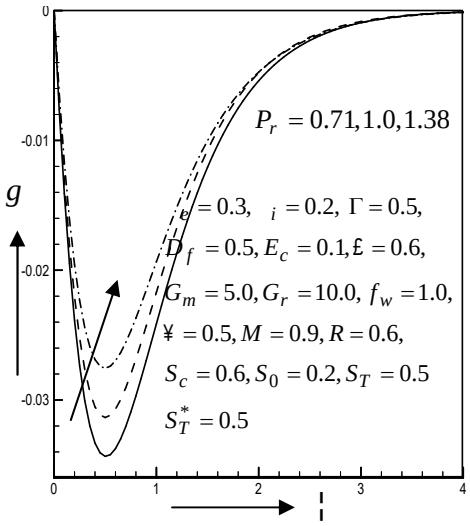

Fig. 7.31 Secondary velocity profiles for different values of Prandtl number P_r

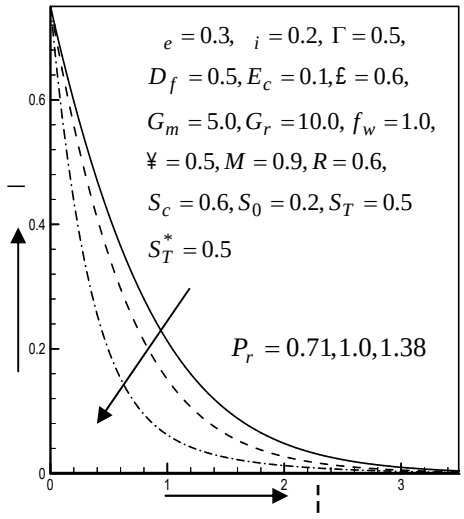

Fig. 7.32 Temperature distribution for different values of Prandtl number P_r

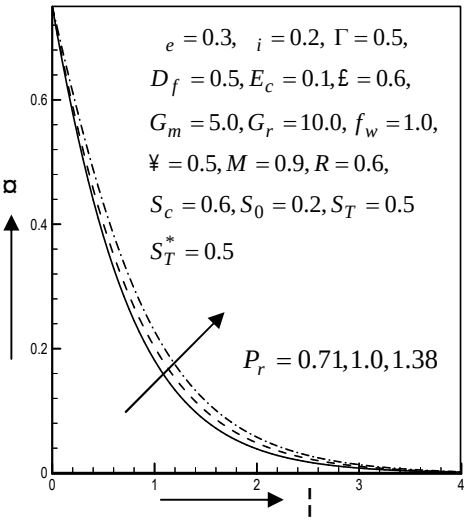

Fig. 7.33Concentration distribution for different values of Prandtl number P_r

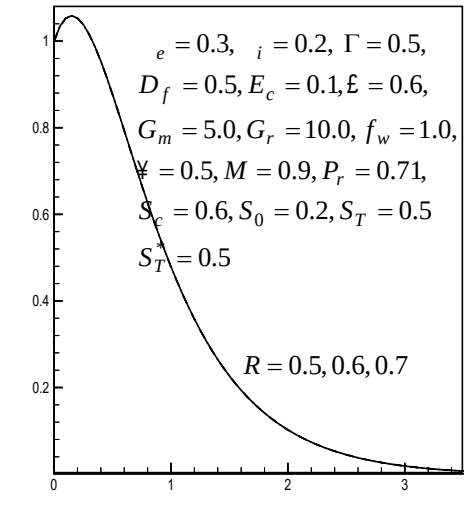

Fig. 7.34 Primary velocity profiles for different values of rotation parameter R

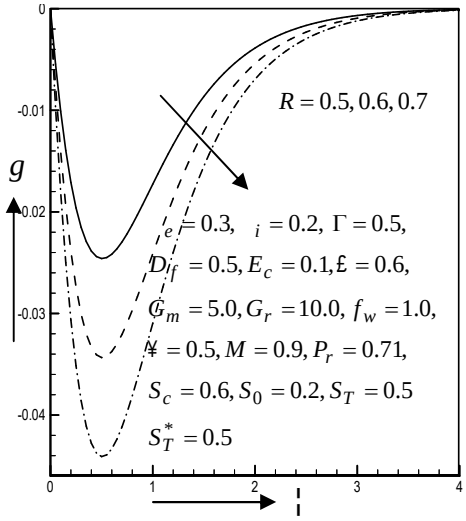

Fig. 7.35 Secondary velocity profiles for different values of rotation parameter R

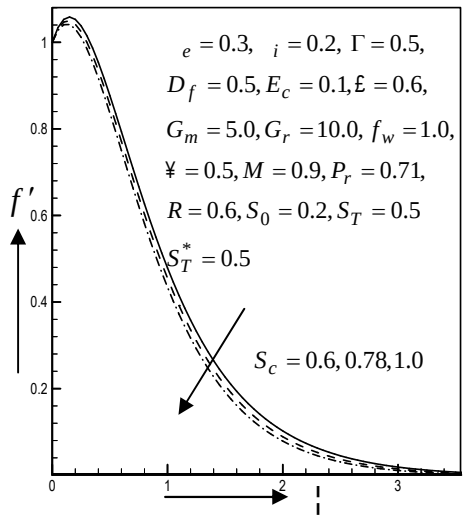

Fig. 7.36 Primary velocity profiles for different values of Schmidt number S_c

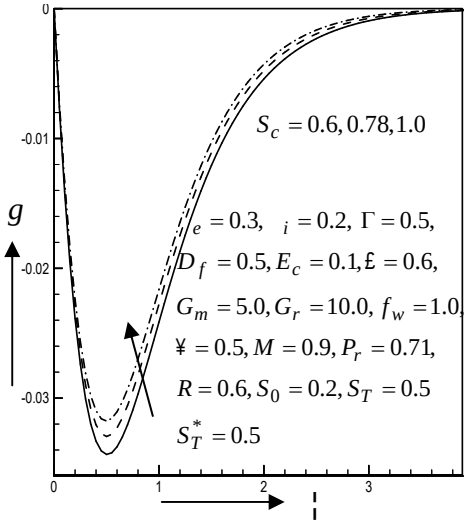

Fig. 7.37 Secondary velocity profiles for different values of Schmidt number S_c

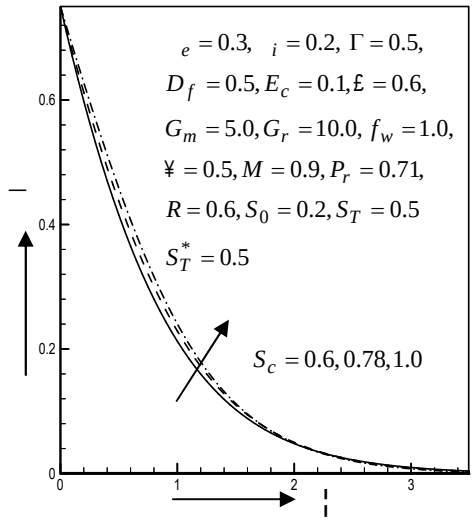

Fig. 7.38 Temperature distribution for different values of Schmidt number S_c

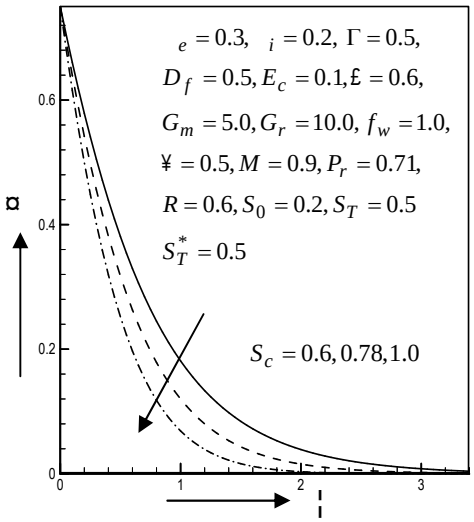

Fig. 7.39 Concentration distribution for different values of Schmidt number S_c

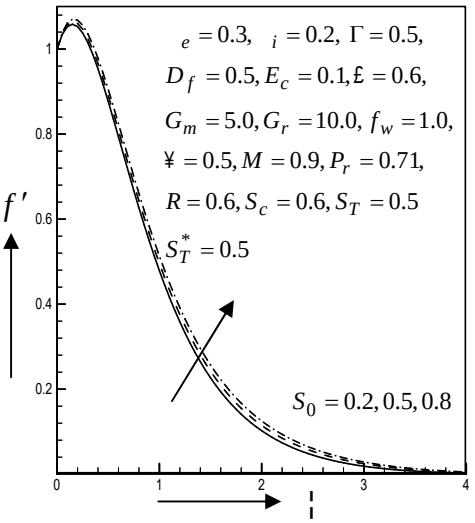

Fig. 7.40 Primary velocity profiles for different values of Soret number S_0

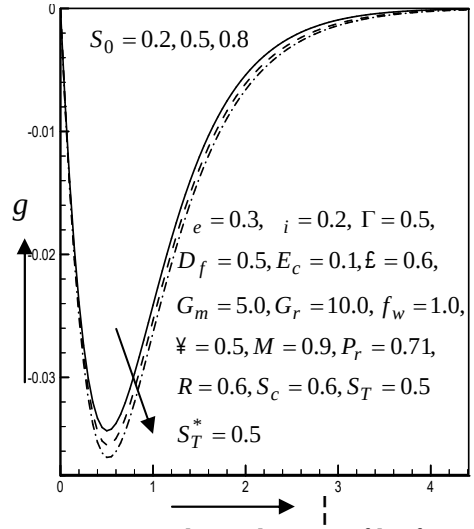

Fig. 7.41 Secondary velocity profiles for different values of Soret number S_0

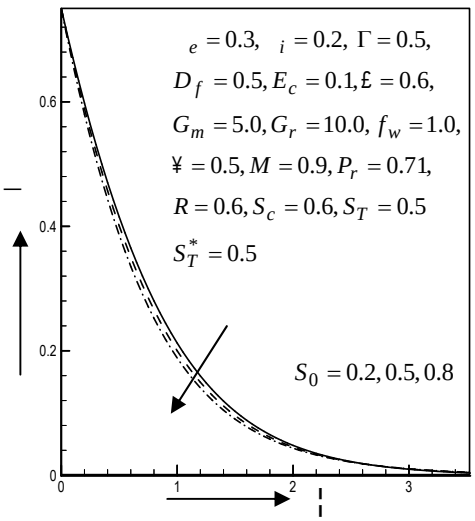

Fig. 7.42 Temperature distribution for different values of Soret number S_0

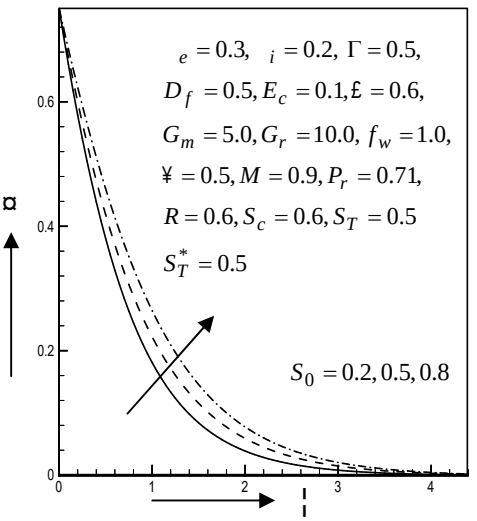

Fig. 7.43 Concentration distribution for different values of Soret number S_0

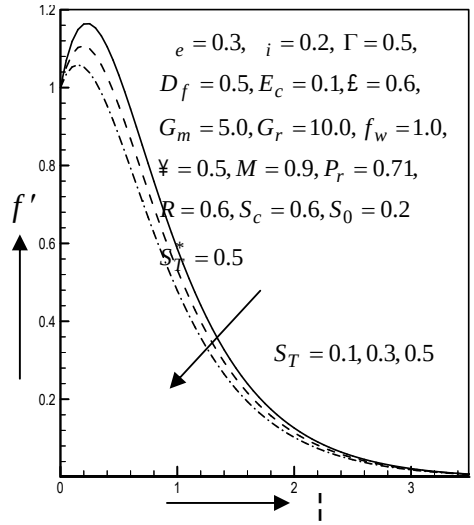

Fig. 7.44 Primary velocity profiles for different values of thermal stratified parameter S_T

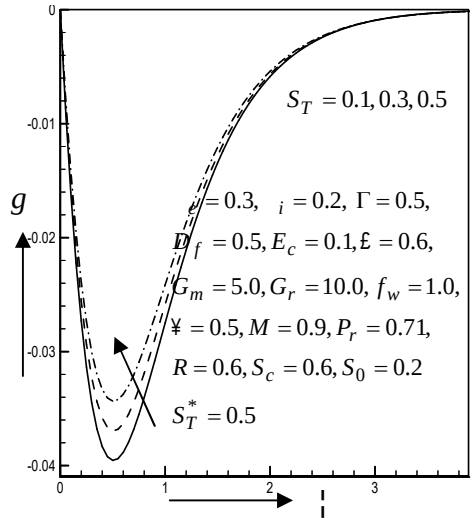

Fig. 7.45 Secondary velocity profiles for different values of thermal stratified parameter S_T

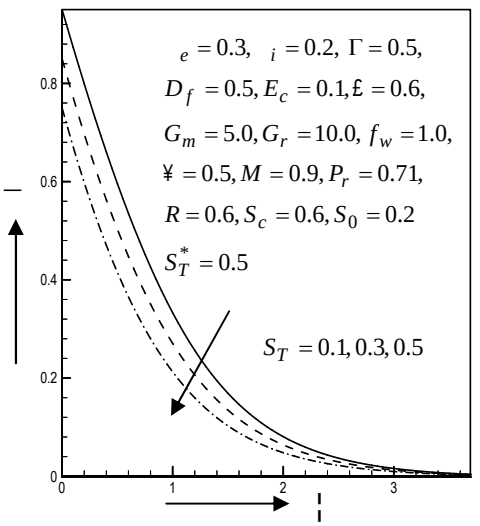

Fig. 7.46 Temperature distribution for different values of thermal stratified parameter S_T

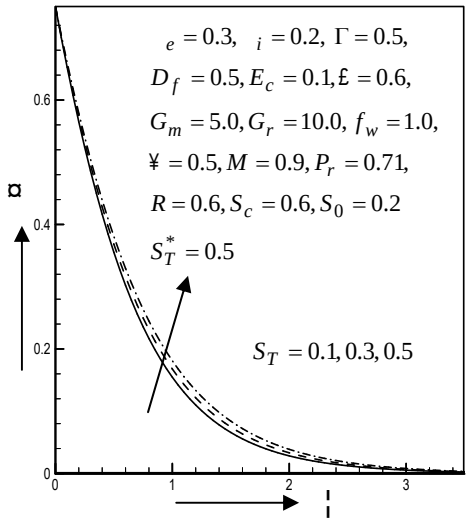

Fig. 7.47 Concentration distribution for different values of thermal stratified parameter S_T

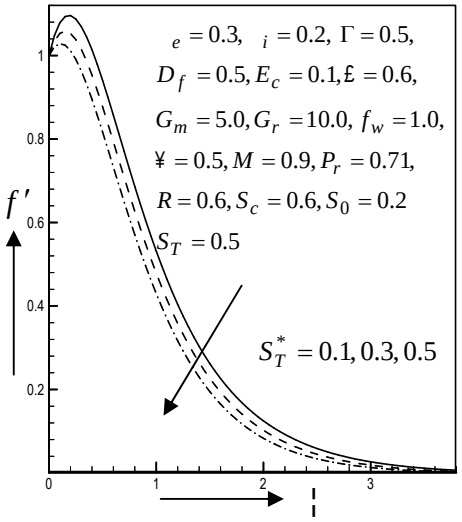

Fig. 7.48 Primary velocity profiles for different values of mass stratified parameter S_T^*

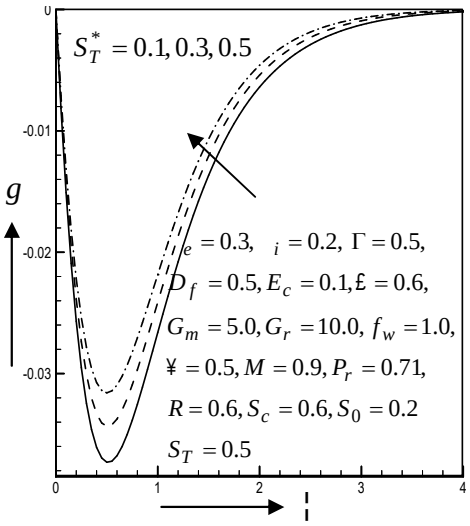

Fig. 7.49 Secondary velocity profiles for different values of mass stratified parameter S_T^*

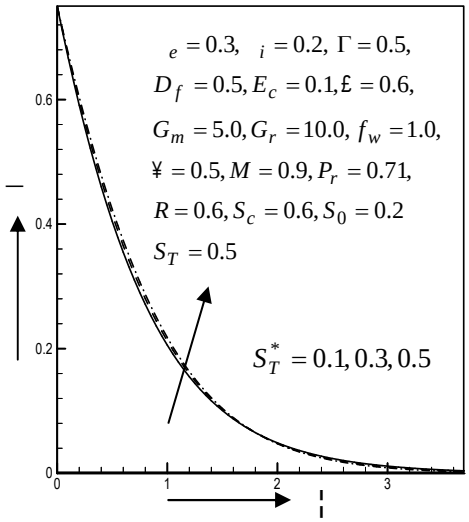

Fig. 7.50 Temperature distribution for different values of mass stratified parameter S_T^*

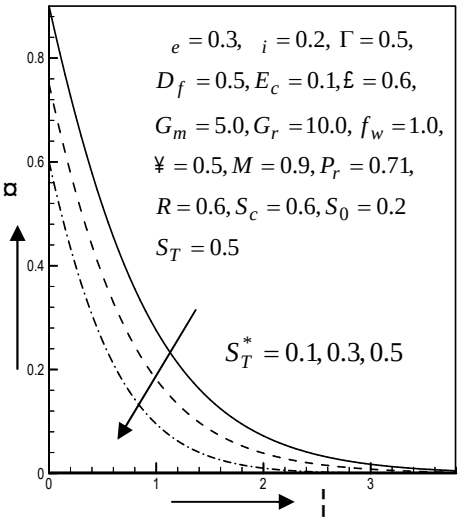

Fig. 7.51 Concentration distribution for different values of mass stratified parameter S_T^*

Table 7.1

Numerical values of $²_x$ and $²_z$ for $G_r = 10.0, G_m = 5.0, S_c = 0.6, S_T = 0.5, M = 0.9, £ = 0.6$ $D_f = 0.5, P_r = 0.71, S_T^* = 0.5, f_w = 1.0, ¥ = 0.5, S_0 = 0.2, \ _i = 0.2, E_c = 0.1.$

$G_r \& G_m$	R	$_e$	Γ	$²_x$	$²_z$
+ve	0.5	0.3	0.5	0.8540158	-0.1176121
	0.6	0.3	0.5	0.8523298	-0.1642355
	0.7	0.3	0.5	0.8500862	-0.2108412
	0.6	0.6	0.5	0.9043732	-0.0966837
	0.6	0.9	0.5	0.9553969	-0.0742697
	0.6	0.3	1.0	0.7077584	-0.1624380
	0.6	0.3	1.5	0.5720807	-0.1607554

Table 7.2

Numerical values of $²_x$, $²_z$, N_u and S_h for $G_r = 10.0, G_m = 5.0, S_c = 0.6, S_T = 0.5, \Gamma = 0.5,$ $P_r = 0.71, S_T^* = 0.5, R = 0.6, \ _e = 0.3, \ _i = 0.2, M = 0.9, f_w = 1.0, ¥ = 0.5$

$G_r \& G_m$	D_f	E_c	S_0	£	$²_x$	$²_z$	N_u	S_h
+ve	0.5	0.1	0.2	0.6	0.8523298	-0.1642355	0.8194647	0.9376818
	1.0	0.1	0.2	0.6	1.1329476	-0.1764397	0.5359260	1.0094275
	1.5	0.1	0.2	0.6	1.4283914	-0.1878266	0.2024831	1.0834770
	0.5	0.4	0.2	0.6	1.0973506	-0.1737405	0.5660066	0.9975611
	0.5	0.7	0.2	0.6	1.4126295	-0.1856003	0.2283047	1.0742673
	0.5	0.1	0.5	0.6	0.8961587	-0.1680962	0.8733375	0.8115556
	0.5	0.1	0.8	0.6	0.9421728	-0.1715598	0.9334194	0.6648544
	0.5	0.1	0.2	0.7	1.2930466	-0.2001934	0.8392247	0.9749975
	0.5	0.1	0.2	0.8	1.6603251	-0.2349740	0.8521140	1.0058803

Table 7.3

Numerical values of $²_x$, $²_z$ N_u and S_h for $G_r = 10.0, G_m = 5.0, S_c = 0.6, S_T = 0.5, \Gamma = 0.5,$ $S_T^* = 0.5, R = 0.6, \ _e = 0.3, \ _i = 0.2, D_f = 0.5, £ = 0.6, E_c = 0.1, S_0 = 0.2$

$G_r \& G_m$	f_w	M	P_r	¥	$²_x$	$²_z$	N_u	S_h
+ve	1.0	0.9	0.71	0.5	0.8523298	-0.1642355	0.8194647	0.9376818
	0.5	0.9	0.71	0.5	1.2784448	-0.1747568	0.7136184	0.8460865
	0.75	0.9	0.71	0.5	1.0877677	-0.1707482	0.7657946	0.8907201
	1.0	0.1	0.71	0.5	1.0724093	-0.2949641	0.8654834	0.9464273
	1.0	0.5	0.71	0.5	0.9615540	-0.2264331	0.8420795	0.9420856
	1.0	0.9	1.0	0.5	0.6092746	-0.1531513	1.0695553	0.8729027
	1.0	0.9	1.38	0.5	0.1255028	-0.1378504	1.9933580	0.7135160
	1.0	0.9	0.71	1.0	0.6868804	-0.1533763	0.8135879	0.9266327
	1.0	0.9	0.71	1.5	0.5301094	-0.1439224	0.8073987	0.9163717

Table 7.4

Numerical values of $²_x$, $²_z$ N_u and S_h for $G_r = 10.0, G_m = 5.0, E_c = 0.1, P_r = 0.71, \Gamma = 0.5,$ ¥ $= 0.5, M = 0.9, S_0 = 0.2, R = 0.6,$ $_e = 0.3, f_w = 1.0,$ $_i = 0.2, D_f = 0.5,$£ $= 0.6,$

G_r & G_m	S_c	S_T	S_T^*	$²_x$	$²_z$	N_u	S_h
+ve	0.60	0.5	0.5	0.8523298	-0.1642355	0.8194647	0.9376818
	0.78	0.5	0.5	0.7855988	-0.1594663	0.7269293	1.1659213
	1.00	0.5	0.5	0.7195395	-0.1553044	0.6207048	1.4421991
	0.60	0.1	0.5	1.6270881	-0.1855449	0.7702318	1.0172652
	0.60	0.3	0.5	1.2332185	-0.1748621	0.8042110	0.9763110
	0.60	0.5	0.1	1.2514272	-0.1790109	0.8782022	0.9188355
	0.60	0.5	0.3	1.0505220	-0.1717407	0.8476198	0.9330703

References

Abuga, J. G., Kinyanjui, M. and Sigey, J. K. (2011). An investigation of the effect of Hall current and rotational parameter on dissipative fluid flow past a vertical semi-infinite plate, Journal of Engineering and Technology Research, vol.**3**(11), p314-320.

Alam, M. S., Rahman, M. M. and Samad, M. A. (2006). Dufour and Soret effects on unsteady MHD free convection and mass transfer flow past a vertical porous plate in a porous medium, Nonlinear Analysis: Modelling and Control, vol.**11**, No. 3, p217–226.

Ali Chamkha (1996).MHD free convection from a vertical plate embedded in a thermally stratified porous medium, Fluid/Partile Separation Journal, vol.**9**, No. 3, p194-206.

Mahmud Alam, Md. Delowar Hossain, M. and Arif Hossain, M. (2011). Viscous dissipation and Joule heating effects on steady MHD combined heat and mass transfer flow through a porous medium in a rotating system, Journal of Naval Architecture and Marine Engineering, vol.**2**, p105-120.

Bejan, A. and Khair, K. R. (1985). Mass transfer to natural convection boundary layer flow driven by heat transfer, American Society of Mechanical Engineers Journal of Heat Transfer, vol.**107**, p1979-1981.

Bejan, A. and Kraus, A. D. (2003). Heat Transfer Handbook, Wiley, New York.

Bejan, A., Dincer, I., Lorente, S., Miguel, A. F. and Reis, A. H. (2004). Porous and complex flow structures in modern technologies, Springer, New York.

Gnaneswara Reddy, M. and Bhaskar Reddy, N. (2010). Soret and Dufour effects on steady MHD free convection flow past a semi-infinite moving vertical plate in a porous medium with viscous dissipation, International Journal of Applied Mathematics and Mechanics, vol.**6**(1), p1-12.

Ganesan Periyanagounder , Suganthi Renugopal Kanniappan and Loganathan Parasuraman (2014). Doubly stratified effects in a free convective flow over a vertical plate with heat and mass transfer, Thermal Science, vol.**18**, No. 2, p365-376.

Ingham, D.B., Bejan, A., Mamut,E. and Pop, I.(2004). Emerging technologies and techniques

in porous media, Kluwer, Dordrecht.

Ingham, D. B. and Pop, I. (1998). Transport Phenomena in Porous Media, **II 2002,** Pergamon, Oxford.

Kaladhar, K., RamReddy, Ch., Srinivasacharya, D. and Pradeepa, T. (2016). Analytical study for Soret, Hall, and Joule heating effects on natural convection flow saturated porous medium in a vertical channel, Math Sci, DOI 10.1007/s40096-016-0188-7.

Lakshmi, P. A. and Murthy, P.V.S.N (2008). Soret and Dufour effets on free conve-ction heat and mass transfer from horizontal flat plate in a Darcy porous medium, Journal Heat Transfer, vol.**130**(10), 104504-8.

Naroua, H. (2007). A computational solution of hydromagnetic free convective flow past a vertical plate in a rotating heat-generating fluid with Hall and ion-slip currents, International Journal for Numerical Methods in Fluids, vol.**53**, p1647-1658

Nazmul Islam, M. and Alam, M. M. (2007). Dufour and Soret effects on steady MHD free convection and mass transfer fluid flow through a porous medium in a rotating system, Journal of Naval Architecture and Marin Engineering, vol.**4**, 43-55.

Nield D. A . and Bejan A. (1999). Convection in Porous Media, 2nd edition, Springer, New York.

Murthy, P.V.S.N., Srinivasacharya, D. and Krishna, P.V.S.S.S.R. (2004). Effect of double stratification on free convection in a Darcian porous medium, Journal of Heat Transfer, vol.**126**(2), p297-300.

Pop, I. and Ingham, D. B. (2001). Convective heat transfer mathematical and computational modelling of viscous fluids and porous media, Elsevier Science and Technology Books, Pergaman, UK.

RajaShekar, M. N. (2014). Effects of Dufour and Soret on unsteady MHD heat and mass transfer flow past a semi-infinite moving vertical plate in a porous medium with viscous dissipation, International Journal of Applied Physics and Mathematics, vol.**4**, No. 2, p130-134.

Ram, P. C. and Takhar, H. S. (1993). MHD free convection from an infinite vertical flate plate in a rotating fluid with Hall and ion-slip currents, Fluid Dynamics Research., vol.**11**, p99-105.

Sarada, K. and Shanker, B. (2013). The effects of Sore t and Dufour on an unsteady MHD free convection flow past a vertical porous plate in the presence of suction or injection, International Journal Of Engineering And Science, vol.**2**(7), p13-25.

Sreedhar Sarma, G., Sreenivasu, D., Govardhan, K. and Ramakrishna Prasad, K. (2013). Numerical study of MHD free convection heat and mass transfer from vertical surfaces in porous media considering Soret and Dufour effects, Advances in Applied Science Research, vol.**4**(1), p300-307.

Tak, S. S. and Arti Lodha (2007). Influence of double stratification on MHD free convection with Soret and Dufour effects in a Darcian porous media , PAMM · Proc. Applied Mathematics and Mechanics, vol.**7**, p2100089–2100090.

Vafai, K. (2000). Handbook of Porous Media, Marcel Dekker, New York.

Chapter 8

Effect of Hall and ion-slip currents on MHD boundary layer flow past along a vertical plate in porous medium with power-law variation wall temperature in a rotating system

The magnetohydrodynamic (MHD) flow has attracted a great interest to many researchers during the last several decades owing to the effect of magnetic field on the boundary layer flow control and applications in many engineering and physical aspects such as MHD generators, plasma studies, nuclear reactors, geothermal energy extractions, purification of molten metals from non-metalic inclusion, geothermal energy extractions etc. A transformation of the boundary layer equation for free convection flow past a vertical flat plate with arbitrary and wall temperature variation, was studied by *Vedhanayagam* (1980). *Soundalgekar and Ramana* (1980) investigated the constant surface velocity case with a power-law temperature variation. The effect of viscous dissipation and Joule heating on MHD free convection flow past a semi-infinite vertical flat plate in the presence of the combined effect of Hall and non-slip currents for the case of power-law variation of the wall temperature is analyzed by *Emad and Mohamed* (2005). *Chen* (2004) considered the heat and mass transfer in MHD flow by natural convection from a permeable, inclined surface with variable wall temperature and concentration. *Satish and Pradhan* (2015) studied the problem numerical solution of boundary layer equation with viscous dissipation effect along a flat plate with variable temperature. Natural convection heat and mass transfer in MHD fluid flow past a moving vertical plate with variable surface temperature and concentration in a porous medium were investigated by *Javaherdeh et al.* (2015).

Hall and ion-slip currents trend for the application of magnetohydrodynamic is towards a strong magnetic field, so that the influence of the electromagnetic force is noticeable. The problem of MHD free convection flow with Hall and ion-slip currents has many important engineering applications e.g. in power generators, Hall accelerators and flows in channels and ducts. *Ahmed and Sarmah* (2011) analyzed MHD transient flow past an impulsively started infinite horizontal porous plate in a rotating system with Hall current. *Odelu and Naresh* (2013) studied numerical study of MHD flow and heat transfer through porous medium between two parallel plates with Hall and ion slip effects.

The rotating flow of an electrical conducting fluid in the presence of magnetic field is encountered in geophysical and comical fluid dynamics. Study of the interaction of Coriolis force with electromagnetic force in porous media is important in some geophysical and astrophysical problems. *Dileep and Priyanka* (2012) investigated the Hall effects on MHD slip flow and heat transfer through a porous medium over an accelerated plate in a rotating

system. Hall effects on MHD flow in a rotating system with heat transfer characteristics was studied by *Ghosh et al.* (2009).

Viscous dissipation effects play an important role in natural convection in various devices which are subjected to large variations of gravitational force or which operate at high speeds. *Brinkman* (1951) appears to be the first theoretical work dealing viscous dissipation. *Anjali et al.* (2012) investigated Hall effect on unsteady MHD free convection flow past an impulsively started porous plate with viscous and Joule's dissipation. *Palanisamy and Muthamperumal* (2011) investigated viscous dissipation effect on steady free convection and mass transfer flow past a semi-infinite flat plate. *Khaled* (2016) studied Joule heating and viscous dissipation on effects on MHD flow over a stretching porous sheet subjected to power law heat flux in presence of heat source. *Hossain* (1992) studied the effect of viscous and Joule heating on the flow of an electrically conducting, viscous, incompressible fluid past a semi-infinite plate with surface temperature varying linearly with the distance from the leading edge in the presence of a uniform transverse magnetic field.

The aim of the present work is to study the viscous dissipation, Joule heating effect in two dimensional MHD free convection flow past along a vertical plate in presence of Hall and ion-slip currents, power-law variation wall temperature in a rotating system as well as uniform magnetic field which is normal to the vertical porous plate. The nonlinear governing partial differential equations are transformed into ordinary differential equations using usual similarity transformations. This system is solved numerically by applying Nachtsheim-Swigert shooting iteration technique together with Runge-Kutta sixth order integration scheme. Representative results are presented graphically for the velocity and temperature distributions. The numerical values of the shear stress components and the Nusselt number have been calculated for various values of physical parameters and presented in tabular form.

8.1 Governing Equations

Consider a steady laminar, incompressible viscous electrically conducting fluid of temperature T past along a semi-infinite vertical porous plate in presence of power-law wall temperature under the influence of a transversely applied magnetic field. The wall temperature varies with the distance along the plate according to a power-law model and they are always greater than their uniform ambient values existing far from the plate. Fluid suction or blowing is imposed at the plate surface. The wall temperature is assumed to have power-law variation form as shown in the follow equation $T_w(x) = T_\infty + Ax^a$, where A is constant, T_∞ is ambient temperature and a is the power index of the wall temperature. The x-axis is assumed to be taken along the plate and the y-axis normal to the plate. The physical configuration and coordinate system is shown in Fig.8.1. An external strong

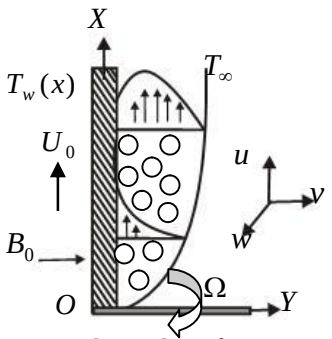

Fig.8.1 Physical configuration and coordinate system

magnetic field $\mathbf{B}=(0,B_0,0)$ where magnetic field of uniform strength B_0 is imposed along the y-direction. For an electrically conducting fluid, the Hall and ion-slip currents significantly affected the flow in the presence of large magnetic field. The induced magnetic field is neglected, since the magnetic Reynolds number is assumed to be very small. The effects of Hall current give rise to a force in the z-direction, which induces a cross flow in that direction and hence the flow becomes three dimensional. The equation of conservation of electric charge $\nabla.\vec{j}=0$ gives $j_y=$constant, where $\vec{j}=\left(j_x,j_y,j_z\right)$. This constant is assumed to be zero since $j_y=0$ everywhere in the flow. The governing boundary layer equations may be written as;

Continuity equation; $$\frac{\partial u}{\partial x}+\frac{\partial v}{\partial y}=0 \tag{8.1}$$

Momentum equations;

$$u\frac{\partial u}{\partial x}+v\frac{\partial u}{\partial y}=\nu\frac{\partial^2 u}{\partial y^2}+g_0\left(T-T_\infty\right)+2\Omega w-\frac{\nu}{k}u-\frac{\sigma_e B_0^2}{\rho\left(\sim_e^2+\ _e^2\right)}\left(\sim_e u+\ _e w\right) \tag{8.2}$$

$$u\frac{\partial w}{\partial x}+v\frac{\partial w}{\partial y}=\nu\frac{\partial^2 w}{\partial y^2}-2\Omega u-\frac{\nu}{k}w+\frac{\sigma_e B_0^2}{\rho\left(\sim_e^2+\ _e^2\right)}\left(\ _e u-\sim_e w\right) \tag{8.3}$$

Energy equation;

$$u\frac{\partial T}{\partial x}+v\frac{\partial T}{\partial y}=\frac{\kappa}{\rho c_p}\frac{\partial^2 T}{\partial y^2}+\frac{\nu}{c_p}\left[\left(\frac{\partial u}{\partial y}\right)^2+\left(\frac{\partial w}{\partial y}\right)^2\right]+\frac{\sigma_e B_0^2}{\rho c_p\left(\sim_e^2+\ _e^2\right)}\left(u^2+w^2\right) \tag{8.4}$$

where all physical quantities are defined in the Nomenclature.

Boundary conditions are as follows;

$$\left.\begin{array}{ll} u=U_0,\ v=-v_w(x),\ w=0,\ T=T_w(x) & at\ \ y=0 \\ u=0,\ w=0,\ T=T_\infty & as\ \ y\to\infty \end{array}\right\} \tag{8.5}$$

where A is constant and a is the power index of the wall temperature.

8.2 Mathematical formulation

Introducing the similarity variables are as follows;

$$\eta=\sqrt{\frac{U_0}{2\nu x}}y,\ \ \psi=\sqrt{2U_0\nu x}\,f(\eta),\ \theta(\eta)=\frac{T-T_\infty}{T_w-T_\infty},\ u=\frac{\partial\psi}{\partial y},\ v=\frac{\partial\psi}{\partial x},\ w=U_0 g(\eta)$$

Now equation (8.2)-(8.4) become

$$f'''+ff''-\left[\varphi+\frac{M\sim_e}{\sim_e^2+\ _e^2}\right]f'+\left[R-\frac{M\ _e}{\sim_e^2+\ _e^2}\right]g+G_r\theta=0 \tag{8.6}$$

$$g''+fg'-\left[\varphi+\frac{M\sim_e}{\sim_e^2+\ _e^2}\right]g-\left[R-\frac{M\ _e}{\sim_e^2+\ _e^2}\right]f'=0 \tag{8.7}$$

$$\theta''+P_r f\theta'-2aP_r f'\theta+P_r E_c\left[f''^2+g'^2\right]+\frac{P_r E_c M}{\sim_e^2+\ _e^2}\left[f'^2+g^2\right]=0 \tag{8.8}$$

where primes denote differentiation with respect to similarity variable ¦ .

The corresponding boundary conditions are as follows;

$$\left.\begin{aligned} f' = 1.0,\ f = f_w,\ g = 0.0,\ \bar{} = 1.0 \quad at\ \ ¦ = 0 \\ f' = 0.0,\quad g = 0.0,\ \bar{} = 0.0 \quad as\ \ ¦ \to \infty \end{aligned}\right\} \tag{8.9}$$

where $G_r\left(= \dfrac{2xg_0\ (T_w - T_\infty)}{U_0^2}\right)$, $R\left(= \dfrac{4x\Omega}{U_o^2}\right)$, $¥\left(= \dfrac{2x^3}{kU_0}\right)$, $M\left(= \dfrac{2x±_e B_0^2}{°U_0}\right)$, $P_r\left(= \dfrac{°^3 c_p}{©}\right)$,

$E_c\left(= \dfrac{U_0^2}{c_p(T_w - T_\infty)}\right)$, $f_w = \sqrt{\dfrac{2x}{U_0{}^3}}\, v_w$.

8.3 Solutions Technique

The system of non-linear ordinary differential equations (8.6)–(8.8) together with the boundary conditions (8.9) are solved numerically using Nachtsheim-Swigert shooting iteration technique (guessing the missing value) along with sixth order Runge-Kutta initial value solver.

In a shooting method, the missing (unspecified) initial condition at the initial point of the interval is assumed, and the differential equation is then integrated numerically as an initial value problem to the terminal point. The accuracy of the assumed missing initial condition is then checked by comparing the calculated value of the dependent variable at the terminal point with its given value there. If a difference exists, another value of the missing initial condition must be assumed and the process is repeated. This process is continued until the agreement between the calculated and the given condition at the terminal point is within the specified degree of accuracy.

The Nachtsheim-Swigert iteration technique thus needs to be discussed elaborately. The boundary conditions (8.9) associated with the non-linear ordinary differential equations (8.6)–(8.8) are the two-point asymptotic class. Two-point boundary conditions have values of the dependent variable specified at two different values of independent variable. Specification of an asymptotic boundary condition implies that the first derivative (and higher derivatives of the boundary layer equations, if exist) of the dependent variable approaches zero as the outer specified value of the independent variable is approached.

The method of numerically integrating a two-point asymptotic boundary-value problem of the boundary-layer type, the initial-value method is similar to an initial-value problem. The governing differential equations are then integrated with these assumed surface boundary conditions. If the required outer boundary condition is satisfied, a solution has been achieved. Hence, a method must be devised to estimate logically the new surface boundary conditions for the next trial integration. Asymptotic boundary value problems such as those governing the boundary-layer equations are further complicated by the fact that the outer boundary condition is specified at infinity. In the trial integration, infinity is numerically approximated by some large value of the independent variable. There is no a

priori general method of estimating these values. Selecting too small a maximum value for the independent variable may not allow the solution to asymptotically converge to the required accuracy. Selecting large a value may result in divergence of the trial integration or in slow convergence of surface boundary conditions. Selecting too large a value of the independent variable is expensive in terms of computer time.

Nachtsheim-Swigert (1965) developed an iteration method to overcome these difficulties. Extension of the Nachtsheim-Swigert iteration scheme to the system of equations (8.6)-(8.8) and the boundary conditions (8.9) is straightforward. In equation (8.9) there are three asymptotic boundary conditions and hence three unknown surface conditions $f''(0), g'(0)$ and $\theta'(0)$.

Within the context of the initial-value method and Nachtsheim-Swigert iteration technique the outer boundary conditions may be functionally represented as follows;

$$\alpha_j(\eta_{\max}) = \alpha_j\left(f''(0), g'(0), \theta'(0)\right) = \beta_j,\ j = 1,2,.....,6 \tag{8.10}$$

where $\alpha_1 = f', \alpha_2 = g, \alpha_3 = \theta, \alpha_4 = f'', \alpha_5 = g', \alpha_6 = \theta'$. The last three of these represents asymptotic convergence criteria.

Choosing $f'' = g_1, g' = g_2, \theta' = g_3$ and expanding in a first-order Taylor's series after using equation (8.10) yield

$$\alpha_j(\eta_{\max}) = \alpha_{j,C}(\eta_{\max}) + \sum_{i=1}^{3} \frac{\partial \alpha_j}{\partial g_i} \Delta g_i = \beta_j,\ j = 1,2,.....,6 \tag{8.11}$$

where subscript 'C ' indicates the value of the function at $\eta_{\max}$ determined from the trial integration.

Solution of these equations in a least-square sense requires determining the minimum value of

$$E = \sum_{j=1}^{6} \beta_j^{\,2} \tag{8.12}$$

with respect to $g_i (i = 1,2,3)$.

Now differentiating E with respect to g_i, then obtain then obtain the following equations

$$\sum_{j=1}^{6} \beta_j \frac{\partial \beta_j}{\partial g_i} = 0 \tag{8.13}$$

Substituting equation (8.11) into (8.13) after some algebra, then obtain the following equation

$$\sum_{k=1}^{3} a_{ik} \Delta g_k = b_i \quad (i = 1,2,3) \tag{8.14}$$

where

$$a_{i,k} = \sum_{j=1}^{6} \frac{\partial \alpha_j}{\partial g_i} \frac{\partial \alpha_j}{\partial g_k},\ b_i = \sum_{j=1}^{6} \alpha_{j,C} \frac{\partial \alpha_j}{\partial g_i} \qquad (i,k = 1,2,3) \tag{8.15}$$

Now solving the system of linear equation (8.14) using Cramer's rule we obtain the missing (unspecified) values of g_i as

$$g_i = g_i + \Delta g_i \tag{8.16}$$

Thus adopting the numerical technique aforementioned, the solution of the nonlinear ordinary differential equations (8.6)–(8.8) with boundary conditions (8.9) is obtained together with sixth-order Runge-Kutta initial value solver and determine the velocity and temperature as a function of the coordinate ¦ .

8.4 Shear Stress and Nusselt number

The quantities of physical interest are the shear stress and the Nusselt number. Shear stress due to the primary and secondary velocities are given by

$^2_x = «\left(\frac{\partial u}{\partial y}\right)_{y=0}$, $^2_z = «\left(\frac{\partial w}{\partial y}\right)_{y=0}$ which are proportional to $\left(\frac{\partial f}{\partial ¦}\right)_{¦=0}$ and $\left(\frac{\partial g}{\partial ¦}\right)_{¦=0}$.

The Nusselt number denoted by $N_u = \left(\frac{\partial T}{\partial y}\right)_{y=0}$ which is proportional to $-\left(\frac{\partial ¯}{\partial ¦}\right)_{¦=0}$.

8.5 Results and Discussion

In order to get a clear insight of the physical problem, numerical results are displayed with the help of tables and graphs. The numerical results are presented in Figs. 8.2-Fig.8.21and Tables 8.1-8.2 to illustrate the influence of several non-dimensional parameters. The transformed ordinary differential equations with the corresponding boundary conditions are solved numerically using the Rung-Kutta sixth order using shooting iteration technique by giving appropriate initial guess values of $f''(0), g'(0), ¯'(0)$ to match the values with corresponding boundary conditions at $f'(\infty), g(\infty), ¯(\infty)$ respectively. The numerical results of velocity components $f'(0), g(0)$, temperature $¯(0)$ distributions have been obtained for value of the power-law index "a" taking values 1.0. The values of Grashof number G_r are taken to be positive, since these values represent respectively, cooling of the plate. For brevity negligible effects on velocity and temperature distributions are not shown.

From Fig.8.2, it is observed that an increase in the Hall parameter ($_e$) causes negligible effect on the primary velocity profiles. Fig.8.3 shows that the Hall parameter has a strong increasing effect on secondary flow velocity. The secondary velocity is induced by the component of the Lorentz force in the z-axis which arises solely due to the Hall current. This means that the magnitude of the component of the Lorentz force in the z-axis increases as $_e$ increases the secondary velocity is increased.

The effect of the viscous dissipation parameter i.e., the Eckert number (E_c) on the dimensionless primary velocity component (f') and temperature ($¯$) is shown in Figs. 8.4, 8.6 respectively. The greater viscous dissipative causes a rise in the velocity as well as the temperature, which is evident from Figs. 8.4 and 8.6. The secondary velocity (g) decreases with the increase of Eckert number which is shown in Fig. 8.5.

Figs.8.7-8.9 illustrate the velocity (primary and secondary) and temperature distributions for different values of suction parameter (f_w). From Fig.8.7 it can be seen that for cooling of the plate ($G_r > 0$), the velocity profiles decrease with the increase of suction parameter(f_w) indicating the usual fact that suction stabilizes the boundary layer growth. The secondary velocity increases with the increase of f_w which is shown in Fig.8.8. Also from Fig. 8.9 it is observed that increase in suction parameter leads to a decrease in the temperature distributions. Suction stabilizes the thermal boundary layers growth.

Increase in rotation parameter (R) has minor effect on the primary velocity profiles which is shown in Fig. 8.10. The secondary velocity decreases with the increase of rotation parameter which is found in Fig.8.11. This is due to the fact that rotation parameter defines the relative magnitude of the Coriolis force and viscous force, thus rotation retards the secondary flow in the boundary layer.

Fig.8.12 display results of primary velocity for various values of permeability parameter (¥). It is observed that the primary velocity profiles decrease with increasing ¥ because the presence of porous medium increases the resistance to the flow which causes the fluid velocity decrease. Whereas the secondary velocity has opposite behavior which is shown in Fig.8.13.

Fig.8.14 and Fig.8.15 show the dimensionless primary and secondary velocity profiles for different values of magnetic parameter (M). An increase in the Magnetic parameter, the primary velocity decreases. Due the Lorentz force, there is a resistive force along the x -axis and this reduces the primary velocity. The secondary velocity has reverse effect with the increase of M .

Figs. 8.16-8.18 illustrate the velocity (primary and secondary) and temperature profiles for different values of Prandtl number (P_r). The numerical results show that the effect of increasing values of Prandtl number results in a decreasing velocity. The secondary velocity has reverse effect which is shown in Fig. 8.17. The temperature distribution decreases with the increases of P_r which is illustrated in Fig. 8.18. It is seen that the effect of increasing Prandtl number P_r is to decrease temperature throughout the boundary layer which results in decrease in the thermal boundary layer thickness.

Figs. 8.19 -8.21 show the effects of wall temperature power index "a" on the velocity (primary and secondary) and temperature distributions within the boundary layer. Fig.8.19 shows that the primary velocity decreases as "a" increases. But the secondary velocity has reverse effect which is found in Fig.8.210. From Fig. 8.21, it is seen that the temperature distribution decreases with increases of "a".

Finally, the effects of various parameters on the components of the shear stress $²_x, ²_z$ and the Nusselt number N_u are shown in Table 8.1-Table 8.2. From Table 8.1, it is seen that the component of shear stress $²_x$ increases with increasing values of $_e$ while it decreases with increasing values of $¥, M$ and R. Also the component $²_z$ increases with the increase of $_e, ¥, M$ whereas decreases with the increase of R.

From Table 8.2, it is observed that the components of the shear stress $^{2}_{x}$ decreases and $^{2}_{z}$ increases with the increase of f_w, P_r and a. Further from this Table, it is seen $^{2}_{x}$ increases and $^{2}_{z}$ decreases with the increase of E_c. This Table also shows that the Nusselt number increase with increase of f_w, P_r and a while decreases with the increase of E_c.

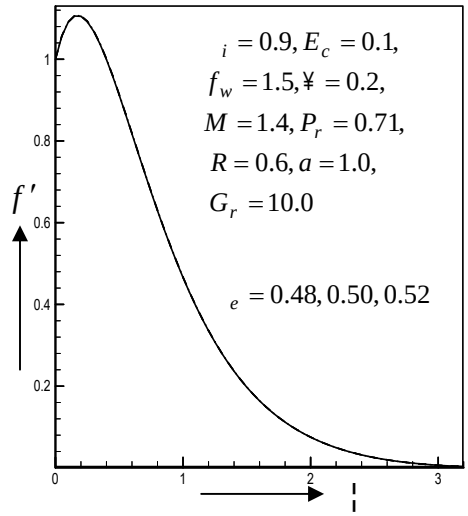

Fig. 8.2 Primary velocity profiles for different values of Hall parameter $_e$

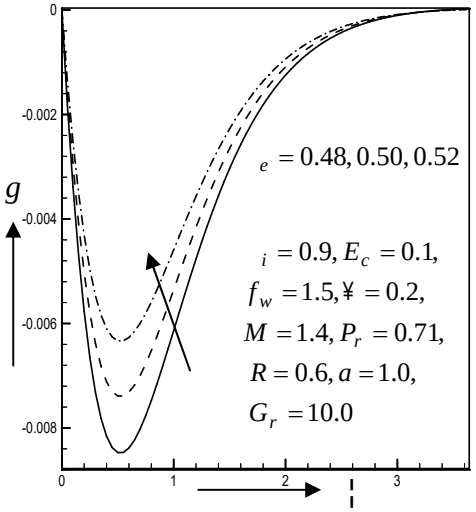

Fig. 8.3 Secondary velocity profiles for different values of Hall parameter $_e$

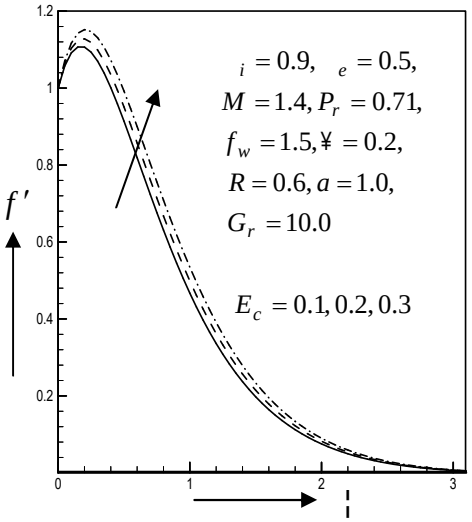

Fig. 8.4 Primary velocity profiles for different values of Eckert number E_c

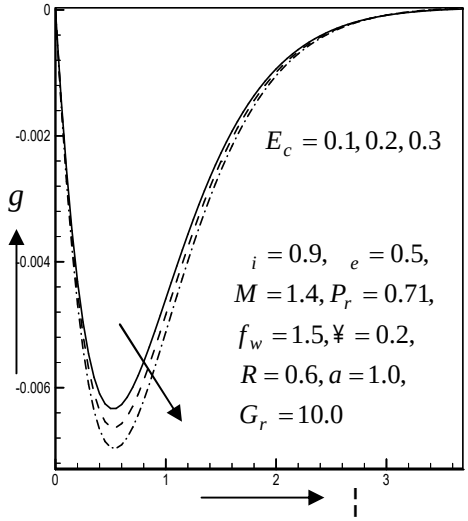

Fig. 8.5 Secondary velocity profiles for different values of Eckert number E_c

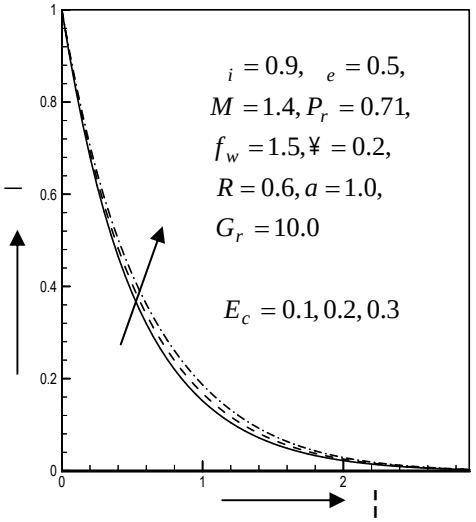

Fig. 8.6 Temperature distribution for different values of Eckert number E_c

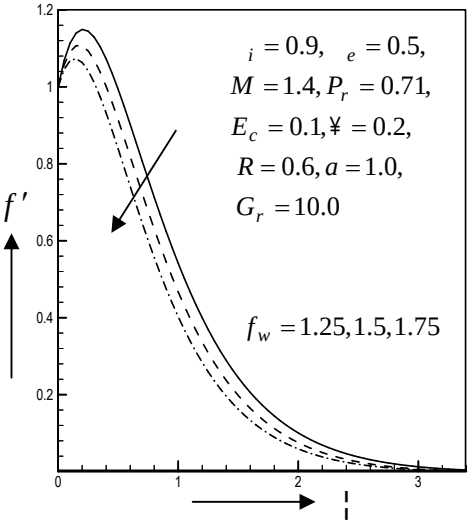

Fig. 8.7 Primary velocity profiles for different values of suction parameter f_w

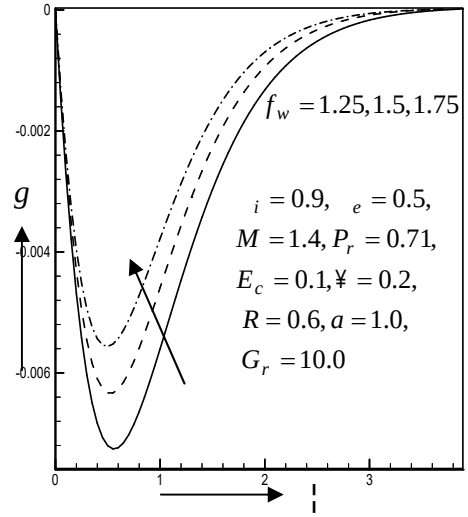

Fig. 8.8 Secondary velocity profiles for different values of suction parameter f_w

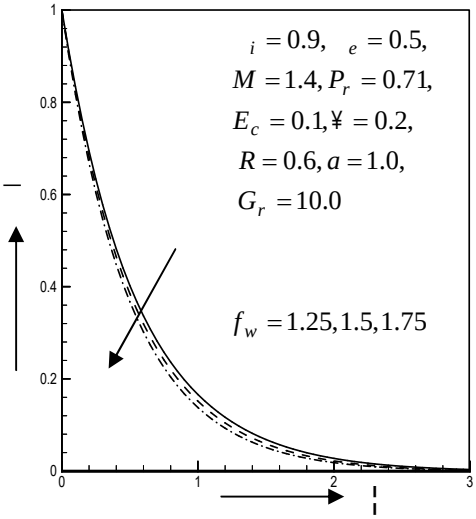

Fig. 8.9 Temperature distribution for different values of suction parameter f_w

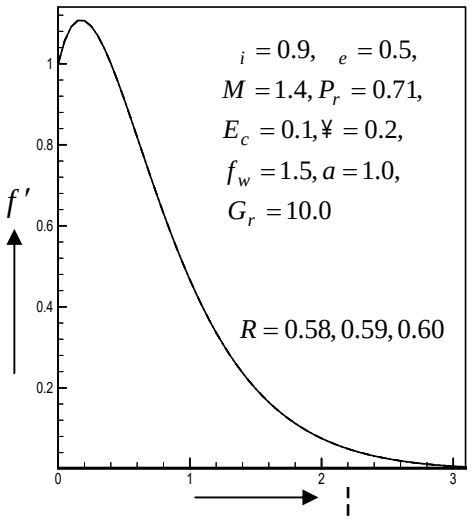

Fig. 8.10 Primary velocity profiles for different values of rotation parameter R

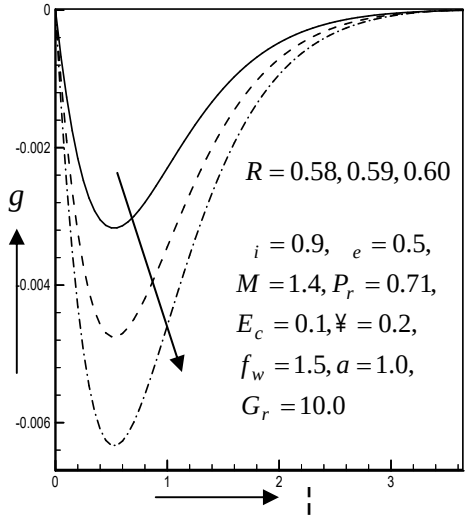

Fig. 8.11 Secondary velocity profiles for different values of rotation parameter R

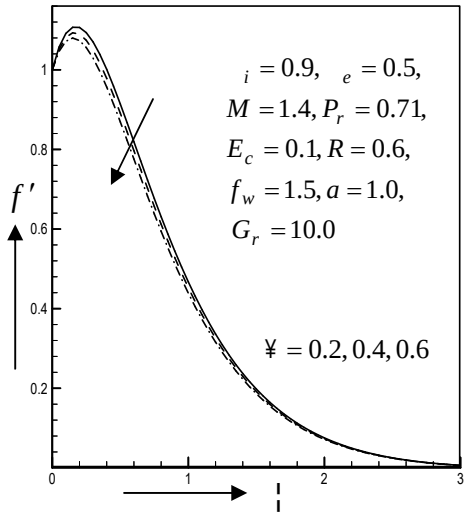

Fig. 8.12 Primary velocity profiles for different values of permeability parameter ¥

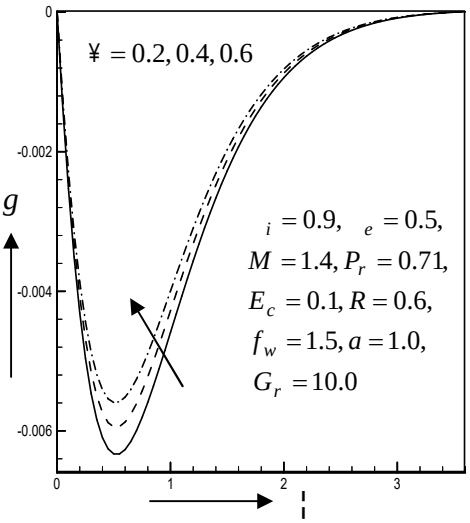

Fig. 8.13 Secondary velocity profiles for different values of permeability parameter ¥

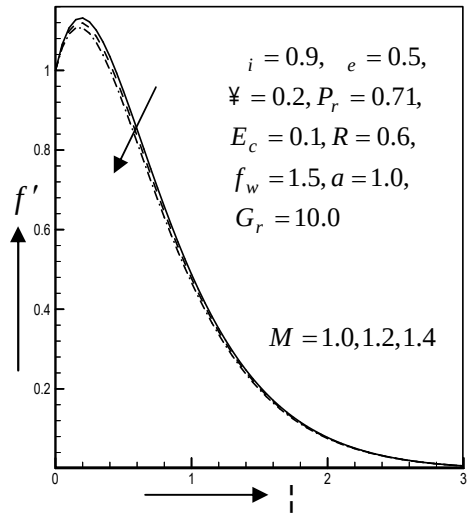

Fig. 8.14 Primary velocity profiles for different values of magnetic parameter M

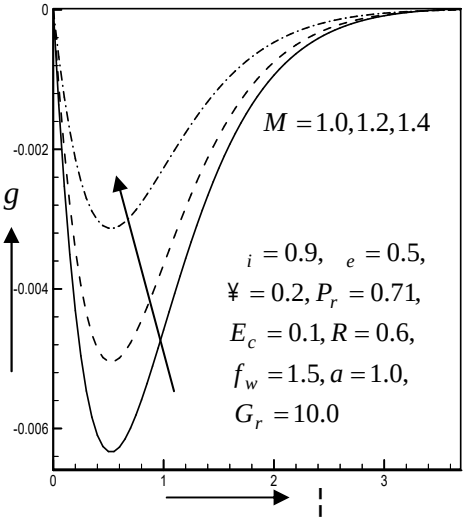

Fig. 8.15 Secondary velocity profiles for different values of magnetic parameter M

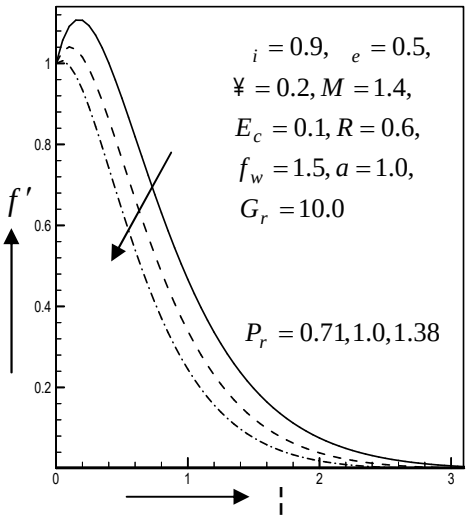

Fig. 8.16 Primary velocity profiles for different values of Prandtl number P_r

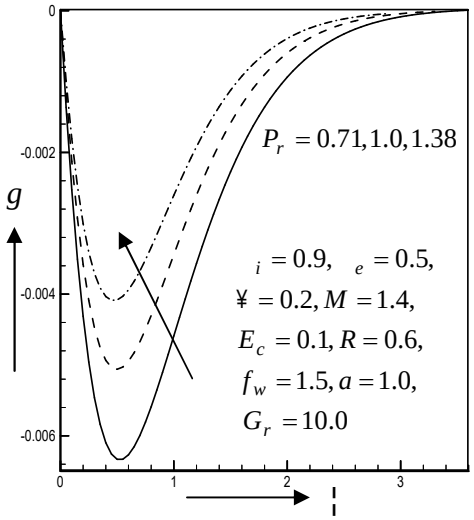

Fig. 8.17 Secondary velocity profiles for different values of Prandtl number P_r

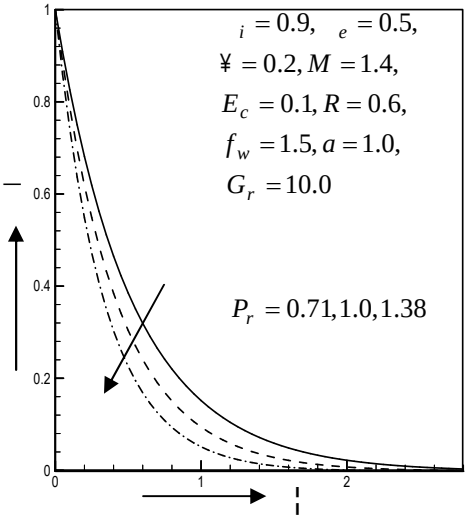

Fig. 8.18 Temperature distribution for different values of Prandtl number P_r

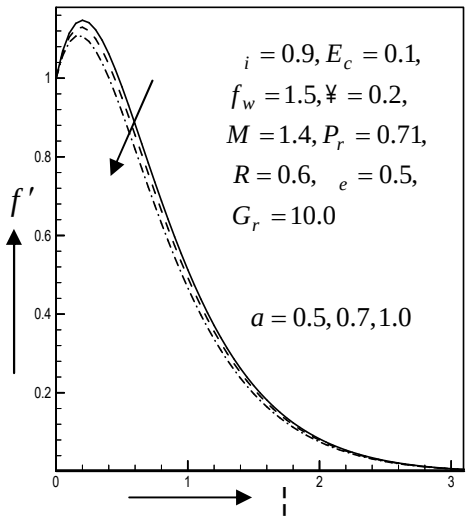

Fig. 8.19 Primary velocity profiles for different values of wall temperature power index a

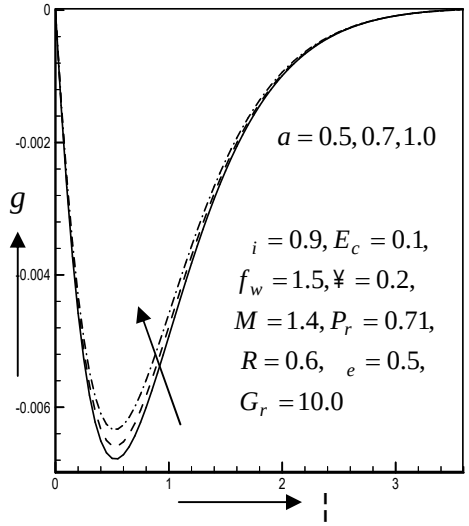

Fig. 8.20 Secondary velocity profiles for different values of wall temperature power index a

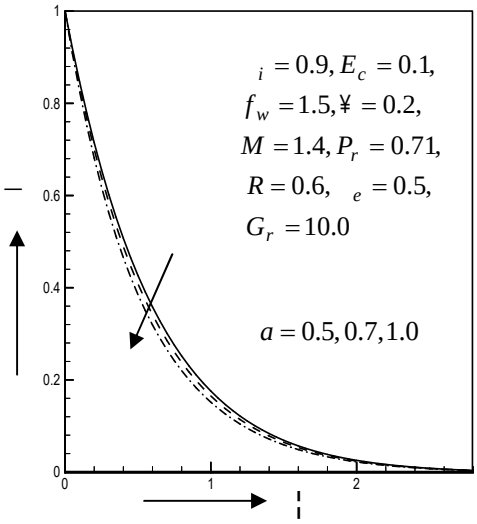

Fig. 8.21 Temperature distribution for different values of wall temperature power index a

Table 8.1

Numerical values of ² $_x$ and ² $_z$ for $G_r = 10.0, E_c = 0.1, P_r = 0.71, a = 1.0,$ $f_w = 1.5,$ $_i = 0.9$

G_r	$_e$	¥	M	R	² $_x$	² $_z$
+ve	0.48	0.20	1.40	0.60	1.3887127	-0.0393246
	0.50	0.20	1.40	0.60	1.3987249	-0.0293501
	0.52	0.20	1.40	0.60	1.4088152	-0.0198665
	0.50	0.40	1.40	0.60	1.2799888	-0.0279403
	0.50	0.60	1.40	0.60	1.1660146	-0.0266577
	0.50	0.20	1.00	0.60	1.5782452	-0.1584064
	0.50	0.20	1.20	0.60	1.4878745	-0.0914259
	0.50	0.20	1.40	0.58	1.3988209	-0.0146801
	0.50	0.20	1.40	0.59	1.3987808	-0.0220164

Table 8.2

Numerical values of ² $_x$, ² $_z$ and N_u for $M = 1.4, G_r = 10.0, R = 0.6,$ $_e = 0.5,$ $_i = 0.9,$ ¥ $= 0.2$

G_r	P_r	a	f_w	E_c	² $_x$	² $_z$	N_u
+ve	0.71	0.50	1.50	0.1	1.6491914	-0.0309601	1.6443798
	0.71	0.75	1.50	0.1	1.5404890	-0.0302626	1.7527704
	0.71	1.00	1.50	0.1	1.3987249	-0.0293501	1.9001984
	1.00	1.00	1.50	0.1	0.8457370	-0.0249719	2.3915810
	1.38	1.00	1.50	0.1	0.3463293	-0.0215169	3.0059706
	0.71	1.00	1.25	0.1	1.6247840	-0.0309125	1.7978870
	0.71	1.00	1.75	0.1	1.1577353	-0.0278433	2.0068689
	0.71	1.00	1.50	0.2	1.5276628	-0.0303697	1.8194304
	0.71	1.00	1.50	0.3	1.6712756	-0.0315034	1.7282861

References

Anjali Devi, S. P., Shailendhra, K. and Ramesan, C. V. (2012), Hall Effect on unsteady MHD free convection flow past an impulsively started porous plate with viscous and Joule's dissipation, 'International Journal of Science and Engineering Investigations', vol.**1**(6), p64-71.

Ahmed,N. and Sarmah, H. K. (2011), MHD transient flow past an impulsively started infinite horizontal porous plate in a rotating system with Hall current, 'International Journal of Applied Mathematics and Mechanics'. vol.**7** (2), p1-15.

Brinkman, H. C. (1951), Heat Effects in Capillary Flow I, 'Applied Scientific Research', vol.**2**, p120-124.

Chen, C.-H. (2004), Heat and mass transfer in MHD flow by natural convection from a perm-eable, inclined surface with variable wall temperature and concentration, 'Acta Mechanica', vol. **172**, p219–235.

Dileep Singh Chauhan and Priyanka Rastogi (2012), Hall effects on MHD slip flow and heat transfer through a porous medium over an accelerated plate in a rotating system, 'International Journal of Nonlinear Science', vol.**14**, No.2, p228-236.

Emad M. Abo-Eldahab, Mohamed A. El Aziz (2005), Viscous dissipation and Joule heating effects on MHD free-convection from a vertical plate with power-law variation in surface temperature in the presence Hall and ion-slip currents, 'Applied mathematical modeling', vol.**29**. p579-695.

Ghosh, S.K., Anwar Beg, O. and Narahari, M.(2009), Hall effects on MHD flow in a rotating system with heat transfer characteristics, 'Mecanica', vol.**44**, p.741.

Hossain, M. A. (1992), Viscous and Joule heating effects on MHD free convection flow with variable plate temperature, 'International Journal Heat Mass Transfer', vol.**35**(12), p3485-3487.

Javaherdeh, K., Mehrzad Mirzaei Nejad and Moslemi, M. (2015), Natural convection heat and mass transfer in MHD fluid flow past a moving vertical plate with variable surface temperature and concentration in a porous medium, 'Engineering Science and Technology: An International Journal', vol.**18**, p423-431.

Khaled K. Jaber (2016), Joule heating and viscous dissipation on effects on MHD flow over a stretching porous sheet subjected to power law heat flux in presence of heat source, 'Open Journal of Fluid Dynamics', vol.**6**, p156-165.

Odelu Ojjela and Naresh Kumar, N. (2013), MHD flow and heat transfer through porous medium between two parallel plates with Hall and ion slip effects. Proceedings of the 2013 International Conference on Mechanics, 'Fluids, Heat, Elasticity and Electromagnetic Fields', p161-162.

Palanisamy Geetha and Muthamperumal Bhavathikannu Krishna Moorthy (2011), Viscous dissipation effect on steady free convection and mass transfer flow past a semi-infinite flat plate,' Journal of Computer Science', vol.**7 (7)**, p1113-1118.

Satish, Desale and Pradhan, V. H. (2015), Numerical solution of boundary layer equation with viscous dissipation effect along a flat plate with variable temperature, 'Elsevier, Science Direct, Procedia engineering', vol.**127**, p846-853.

Soundalgekar, V. M. and Ramana Murthy, T. V. (1980), Heat transfer in the flow past a continuous moving plate with variable temperature, 'Warme-rund-Stoffubertragung', vol.**14,** p91-93.

Vedhanayagam, M., Altenkirch, R. A. and Eichhorn, R. (1980), A transformation of the boundary layer equation for free convection flow past a vertical flat plate with arbitrary and wall temperature variation, 'International Journal of Heat mass transfer', vol.**23**, p1286-1288.

Chapter 9

General Discussion

Considering some physical viability of the flows model studies on various aspects of the magnetohydrodynamics (MHD) free convection and mass transfer flow has been made. In natural processes or in engineering problems, the types of flow that arise are of similar nature to the model studies made herein. The well recognized and widely used mathematical approaches, analytical and numerical techniques have been adopted to analyze the construct equations separately.

The model flows, were considered into two parts, one comparatively simple one dimensional model flows, the second one is a relatively difficult two-dimensional model flows. In the first case all model problems were considered to be unsteady while in the second case both the steady. As for the unsteady one dimensional model, the solution has been obtained by implicit finite difference method while as for the unsteady two dimensional model, the solution has been obtained by explicit finite difference method which are considered in **chapter 4 and chapter 5**. Also for the unsteady one dimensional and steady two dimensional problems, the solution has been obtained by Nachtsheim-Swigert iteration technique which is considered in **chapter 6, chapter 7 and chapter 8**.

In many industrial applications, porosity of materials is an intrinsic aspect of the engineering process and in geophysical systems and as the porosity of soil can exert a considerable influence on flow and temperature distributions, include suction with the problem which are considered in **chapter 5**.

In **chapter 6**, effect of ion-slip current on MHD free convection flow in a temperature stratified porous medium in a rotating system is considered. The unsteady one dimensional model, similarity solutions have been obtained by introducing a similarity parameter $\pm(t)$, the functional value of which has been obtained during the process of analyses. This functional value was found to correspond exactly with the usual similarity length scale considered prior to the analyses adopted in various unsteady problems. The advantage of taking this similarity parameter $\pm(t)$ is that one can easily obtain the similarity equation of governing equations as has been found in **chapter 6**.

Since viscous dissipation and Joule heating effects are also important in a high speed fluid flow, one may include these effects with the problems are considered in **chapter 5-8**.

Influence of stratification is an important aspect in heat and mass transfer analysis. The formation or deposition of the layers is known as the stratification. This phenomenon occurs due to the change in temperature or concentration, or variations in both, or presence of various fluids or different densities. It is important to control the temperature stratification and concentration differences of hydrogen and oxygen in such environments such as they may directly affect the growth of all cultured species. The ambient temperature is

assumed to be an increasing function with the distance along the plate. Effects of stratification on MHD free convection flow past a vertical plate in a porous medium with Hall and ion-slip currents in a rotating system has been considered in **chapter 7**.

In **chapter 8**, effect of Hall and ion-slip currents on MHD boundary layer flow past a vertical plate in porous medium with power-law variation wall temperature in a rotating system has been considered.

The magnetohydrodynamic heat and mass transfer flow with rotation or with Hall and ion-slip currents or with viscous and Joule dissipation or with thermal diffusion and diffusion thermo or stratifications or with all those phenomena together in fact results in a very complicated structure physically as well as mathematically.

References

Abdullah Ahmed Foisal and Mahmud Alam (2015), Free convection fluid flow in the presence of a magnetic field with thermally stratified high porosity medium, 'Science Direct Procedia Engineering', vol.**105**, p549-556.

Abo-Eldahab, E.M. and Aziz, M. A. (2000), Hall and ion-slip effects on MHD free convective heat generating flow past a semi-infinite vertical plate flat plate, 'Physica Scripta', vol.**61**, p344-348.

Abuga, J. G., Kinyanjui, M. and Sigey, J. K. (2011), An investigation of the effect of Hall current and rotational parameter on dissipative fluid flow past a vertical semi-infinite plate, 'Journal of Engineering and Technology Research', vol.**3**(11), p314-320.

Ahmed S and Khatun H. (2013), Magnetohydrodynamic oscillatory flow in a planer porous channel with suction and injection. 'Internal Journal of Engineering and Technology', vol.**2013**(11), p1024–9.

Ahmed, A. A. (2009), Similarity solution in MHD: Effects of thermal-diffusion and diffusion-thermo on free convective heat and mass transfer over a stretching surface considering suction or injection, 'Communication in Nonlinear Science and Numerical Simulation', vol.**14**, p2202-2214.

Ahmed, N., Kalita, H. and Barua, D. P. (2010), Unsteady MHD free convective flow past a vertical porous plate immersed in a porous medium with Hall current, thermal diffusion and heat source, 'International Journal of Engineering, Science and Technology', vol.**2**, No. 6, p59-74.

Ahmed, N. and Sarmah, H.K. (2011), MHD transient flow past an impulsively started infinite horizontal porous plate in a rotating system with Hall current, 'International Journal Applied Mathematics and Mechanics', vol.**7(2)**, p1-15.

Ahmmed,S.F., Das, M.K., Ali,L.E.(2015), Analytical study on unsteady MHD free convection and mass transfer flow past a vertical porous plate, 'American Journal of Applied Mathematics', vol.**3(2)**, p64-74.

Ajay Kumar Sing and Rama Subba Reddy Gorla (2009), Free convection heat and mass transfer with Hall current, Joule heating and thermal diffusion, 'Heat and Mass Transfer', vol.**45**(11), p1341-1349.

Akira Nakayama and Hitoshi Koyama(1987), Effect of thermal stratification on free convection within a porous medium. 'Journal of thermophysics and heat transfer', vol.**1**, p282-285.

Alam, M. M. and Sattar, M. A. (2000), Unsteady free convection and mass transfer flow in a rotaing system with Hall currents, viscous dissipation and joule heating, 'Journal of Energy Heat and Mass transfer', vol.**22**, p31-39.

Alam, M. S., Rahman, M. M. and Samad, M. A. (2006), Dufour and Soret effects on unsteady MHD free convection and mass transfer flow past a vertical porous plate in a porous medium, 'Nonlinear Analysis: Modelling and Control', vol.**11**, No. 3, p217-226.

Alam, M. S., Haque, M. M. and Uddin, M. J. (2014), Unsteady MHD free convective heat transfer flow along a vertical porous flat plate with internal heat generation, International 'Journal of Advances in Applied Mathematics and Mechanics', vol.**2**(2), p52-61.

Alfven, H. (1942), On the existence of electromagnetic waves, 'Arkiv for Matematik, Astronomi Och Fysik', Bd. vol.**295**. No. 2.

Ambethkar, V. (2009), Numerical solutions of heat and mass transfer effects of an unsteady MHD free convective flow past an infinite vertical plate with constant suction and heat source or sink, 'International Journal of Applied Mathematics and Mechanics', vol.**5(3)**, p96-115.

Al-Humoud, J. and Chamkha, A. J. (2006), Double diffusive convection of a rotating fluid over a surface embedded in a thermally stratified high-porosity medium, 'International Journal of Heat and Technology', vol.**24**, p51-60.

Ali Chamkha (1996), MHD free convection from a vertical plate embedded in a thermal stratified porous medium, 'Fluid/Particle Separation Journal', vol.**9**, No. 3, p195-206.

Ali J. Chamkha (1997), MHD-free convection from a vertical plate embedded in a thermally stratified porous medium with Hall effects, 'Applied Mathematical Modelling', vol.**21**, p603-609.

Ali J. Chamkha, Harmindar S., Takhar and Girishwar Nath (2005), Natural convection flow in a rotating fluid over a vertical plate embedded in a thermally stratified high porosity medium, 'International Journal of fluid Mechanics Research', vol.**32**(5), p511-527.

Alizadeh, R., Farahmand, M. and Rahmdel, K. (2015), MHD free convection and mass transfer flow of a dissipative fluid over a vertical plate with time-dependent plate velocity and constant heat flux, 'Applied Mathematics and Computational Intelligence', vol.**4** (1), p293-308.

Ambethkar, V. (2009), Numerical solutions of heat and mass transfer effects of an unsteady MHD free convective flow past an infinite vertical plate with constant suction and heat source or sink, 'International Journal of Applied Mathematics and Mechanics', vol.**5**(3), p96-115.

Angirasa, D and Srinivasan, J. (1989), Natural convection flows due to the combined buoyancy of heat and mass transfer in a thermally stratified medium, 'ASME Journal of Heat Transfer', vol.**111**, p657-663.

Angirasa, D. and Peterson, G. P. (1997), Natural convection heat transfer from an isothermal ertical surface to a fluid saturated thermally stratified porous medium, 'International Journal of Heat and Mass transfer', vol.**40**(18), p4329-4335.

Anajali Devi, S. P. and Ganga, B. (2009), Viscous dissipation effects on nonlinear MHD flow in a porous medium over a stretching porous surface, 'International Journal of Applied Mathematics and Mechanics', vol.**5**(7) , p45-59

Anjali Devi, S. P. and Wilfred Samuel R, J. (2011), Thermo-diffusion effects on unsteady hydromagnetic free convection flow with heat and mass transfer past a moving vertical plate with time dependent suction and heat source in a slip flow regime, 'International Journal of Applied Mathematics and Mechanics', vol. **21**(7), p20-51.

Anjali Devi, S. P., Shailendhra, K. and Ramesan, C. V. (2012), Hall Effect on unsteady MHD free convection flow past an impulsively started porous plate with viscous and Joule's dissipation, 'International Journal of Science and Engineering Investigations', vol.**1**(6), p64-71.

Anwar Beg, O., Takhar, H. S., Tasveer A. Beg, Chamkha, A. J., Nath, G. and Rui Majeed (2005), Modelling convection heat transfer in a rotating fluid in a thermally-stratified high-porosity medium: numerical finite difference solutions, 'International Journal of Fluid Mechanics Research', vol.**32**, No. 4, p383-401.

Anwar Beg, O., Makinde, O. D., Zueco, J. and Ghosh, S. K. (2012), Hydromagnetic viscous

flow in a rotating annular high-porosity medium with nonliner forchheimer drag effects: numerical study, 'World Journal of Modelling and Simulation', vol.**8**, No. 2, p83-95.

Asek Kumar Singh and Benu Madhab (2013), MHD free convective heat and mass transfer of fluid flow past a moving variable surface in porous media, 'International Journal of Engineering Trends and Technology', vol.**4**(4), p1151-1157.

Attia, H. A.(2005), Unsteady couette flow with heat transfer considering ion-slip, 'Turkish Journal of Physics', vol.**29**, p379-388.

Attia, H. A. (2006), Time varying hydromagnetic flow of Dusty fluid between parallel porous plates considering the ion-slip, 'Journal of Technical Physics', vol.**47**(3), p131-147.

Attia, H. A. (2009), Ion-slip effect of unsteady couette flow with heat transfer under exponential decaying pressure gradient, 'Tamkang Journal of Science and Engineering', vol.**12**(2), p209-214.

Atul Kumar Singh, Ajay Kumar Singh and Singh, N.P.(2005), Hydromagnetic free convection and mass transfer flow with Joule heating, thermal diffusion, heat source and Hall current, 'Bulletin of the Institute of Mathematics Academia Sinica', vol.**33**, p291-310.

Basant K Jha and Clement A Apere (2010), Combined effects of Hall and ion-slip currents on unsteady MHD couette flows in rotating system, 'Journal of the Physic al society of Japan', vol.**79,** No. 10. p1-9.

Bejan, A. and Khair, K. R. (1985), Mass transfer to natural convection boundary layer flow driven by heat transfer, 'American Society of Mechanical Engineers Journal of Heat Transfer', vol.**107**, p1979-1981.

Bejan, A. (1994), Convection Heat Transfer, 'John Wiley', New York, NY, USA.

Bejan, A. and Kraus, A. D. (2003), Heat Transfer Handbook, 'Wiley', New York.

Bejan, A., Dincer, I., Lorente, S., Miguel, A. F. and Reis, A. H. (2004), Porous and complex flow structures in modern technologies, 'Springer', New York.

Bhavana, M , Chenna Kesavaiah, D. and Sudhakaraiah, A. (2013), The soret effect on free convective unsteady MHD flow over a vertical plate with heat source, 'International Journal of Innovative Research in Science', Engineering and Technology', vol.**2(5)**, p1617-1628.

Bhuvanavijaya, R. and Mallikarjuna, B. (2014), Effect of variable thermal conductivity on convective heat and mass transfer over a vertical plate in a rotating system with variable porosity regime, 'Journal of Naval Architecture and Marine Engineering', vol.**11**, p83-92.

Bishwa Ram Sharma and Animesh Aich (2016), Soret and Dufour effects on steady MHD flow in presence of heat source through a porous medium over a non-isothermal stretching sheet, 'IOSR Journal of Mathematics', vo.**12**(1), p53-60.

Brinkman, H. C. (1951), Heat Effects in Capillary Flow I. 'Applied Scientific Research', vol. **2**, p120-124.

Callahan, G. D. and Marner, W. J. (1976), Transient free convection flow with mass transfer on an isothermal vertical flat plate, 'International Journal of Heat and Mass Transfer', vol.**19**(2), p165-174.

Caldwell,D.R.(1974), Experimental studies on the onset of thermohaline convection, 'Journal of Fluid Mechanics', vol.**64**(2), p347-367.

Chamkha A.J. (1997), Hydromagnetic natural convection from an isothermal inclined surface adjacent to a thermally stratified porous medium, 'International Journal of Engineering Sciences', vol.**35**, p975-986.

Chamkha, A. J. (1997), MHD-free convection from a vertical plate embedded in a thermally stratified porous medium with Hall effects, 'Applied Mathematical Modelling', vol.**21**, No. 10, p603-609.

Chapman, S. and, Cowling, T. ,G. (1952), The Mathematical theory of non-uniform gases, 'Cambridge University Press', Cambridge, UK.

Chauhan, D. S., Jain, R. (2005), Three dimensional steady flow of viscous incompressible fluid over a highly porous layer, 'Modeliing, Measurment and Control', vol.**74**(5), p19-34.

Chaudhary R. C., Arpita Jain (2007), Combined heat and mass transfer effects on MHD free convection flow past an oscillating plate embedded in porous medium, 'Romanian Journal of Physics', vol.**52**, Nos. 5-7, p505-524.

Chen, C. C., Eichhorn, R. (1976), Natural convection from a vertical surface to a thermally stratified fluid, 'Journal of Heat Transfer', vol.**98**, p446-451.

Chen C. K., Hung C. I., Horng H. C. (1987), Transient natural convection on a vertical flat plate embedded in a high porosity medium, 'ASME Journal of Energy Resources Technology', vol.**109**, p112-118.

Chen, C.-H. (2004), Heat and mass transfer in MHD flow by natural convection from a permeable, inclined surface with variable wall temperature and concentration, 'Acta Mechanica', vol.**172**, p219-235.

Cowling, T. G. (1957), Magnetohydrodynamics, 'Interscinces publication', Inc. New York.

Cramer, K. R. and Pai, S. I. (1973), Magneto fluid Dynamics for Engineers and applied Physicists, 'McGraw Hill', New York.

Das, S., Jana, M., Guria, M. and Jana, R. N. (2008), Unsteady viscous incompressible flow due to an oscillating plate in a rotating fluid,'Journal of Physical Sciences',vol.**12**, p51-64.

Das, S. S. (2009), Effect of suction and injection on MHD three dimensional couette flow and heat transfer through a porous medium, 'Journal of Naval Architecture and Marine Engineering', p41-51, DOI: 10.3329/jname.v6i1.2570.

Das,K. and Jana,S. (2010), Heat and mass transfer effects on unsteady MHD free convection flow near a moving vertical plate in porous medium, 'Bulletin of Society of Mathematicians Banja Luka', vol.**17**, p15-32.

Das, S. S., Mishra, L. K. and Mishra, P. K . (2011), Effect of heat source on MHD free convection flow past an oscillating porous plate in the slip regime, 'International Journal of Energy and environment', vol.**2(5)**, p945-951.

Das, S., Sarkar, B. C. and Jana, R. N. (2013), Hall effect on MHD free convection boundary layer flow past a vertical flat plate, 'Mecanica', vol.**48**(6), p1387-1394.

Das, S., Guchhait, S. K. and Jana, R. N. (2015), Hall effects on unsteady hydromagnetic flow past an accelerated porous plate in a rotating system, 'Journal of Applied Fluid Mechanics', vol.**8**, No. 3, p409-417.

Dileep Singh Chauhan and Priyanka Rastogi (2012), Heat transfer effects on rotating MHD couette flow in a channel partially filled by a porous medium with hall current, 'Journal of Applied Science and Engineering', vol.**15**(3), p281-290.

Dileep Singh Chauhan and Priyanka Rastogi (2012), Hall effects on MHD slip flow and heat transfer through a porous medium over an accelerated plate in a rotating system, 'International Journal of Nonlinear Science', vol.**14**, No.2, p228-236.

Dulal Pal (2008), MHD flow and heat transfer past a semi-infinite vertical plate embedded in a porous medium of variable permeability, 'International Journal of Fluid Mechanics Research', vol.**35**(6), p493-509.

Dursunkaya, Z. and Worek, W. M. (1992), Diffusion-thermo and thermal-diffusion effects in transient and steady natural convection from a vertical surface, 'Internal Journal of Heat Mass Transfer', vol.**35**, p2060-2065.

Eckert, E. R.G. and Drake, R.M. (1972), Analysis of Heat and Mass Transfer, 'McGraw-Hill Book Co.', New York.

Emad M Abo-Eldahab and Mohaned A ElAziz. (2000), Hall and ion-slip effects on MHD free convective heat generating flow past a semi-infinite vertical flat plate, 'Physica Scripta', vol.**61**, No. 3, p344.

Emad M. Aboeldahab and Elsayed M.E. Elbarbary (2001), Hall current effect on magnetohydrodynamic free convection flow past a semi infinite vertical plate with mass transfer, 'International Journal of Engineering Science', vol.**39**, p1641-1652.

Emad M. Abo-Eldahab, Mamdouh M. El-Kady and Ali A. Hallool (2011), Effects of Heat and Mass Transfer on MHD Flow Over a Vertical Stretching Surface with Free Convection and Joule-Heating, 'International Journal of Applied Mathematics and Physics', vol.**3**(2), p249-258.

Emad M. Abo-Eldahab, Mohamed A. El Aziz (2005), Viscous dissipation and Joule heating effects on MHD free-convection from a vertical plate with power-law variation in surface temperature in the presence Hall and ion-slip currents, 'Applied mathematical modeling', vol.**29**. p579-695.

Emmanuel Osalusi, Jonathan Side, Robert Haris (2008), Thermal-diffusion and diffusion thermo effects on combined heat and mass transfer of a steady MHD convective and slip flow due to a rotating disk with viscous dissipation and Ohmic heating, 'International Communications in Heat and Mass Transfer', vol.**35**, p908-915.

Faraday, M. (1832), Experimental researches in electricity, 'Philosophical Transactions of Royal Socity', vol.**1**, p125-162.

Farhad, A., Norzieha, M., Sharidan, S., Khan, I. and Samiulhaq (2012), Hydromagnetic rotating flow in a porous medium with slip condition and Hall current, 'International Journal of Physical Sciences', vol.**7**(10), p1540-1548.

Farhad Ali, Ilyas Khan, Sharidan Shafie, and Norzieha Musthapa (2013), Heat and mass transfer with free convection MHD flow past a vertical plate embedded in a porous medium, 'Hindawi Publishing Corporation Mathematical Problems in Engineering', vol.**2013**, p1-13.

Ferdows, M., Esrat Jahan, Hamad, M. M. and Masahiro Ota (2011), Effects of Hall and ion-slip currents on free convective heat transfer flow past a vertical plate considering slip conditions, 'Canadian Journal on Science and Engineering Mathematics', vol.**2**, No. 2, 70-76.

Ferdows, M., Koji Kaino and Chien-Hsin Chen (2010), Dufour, Soret and viscous dissipation effects on heat and mass transfer in porous media with high porosities, 'International Journal of Applied Engineering Research', vol.**5**(3), p477.

Foisal, A. A. and Alam, M. M. (2016), Unsteady free convection fluid flow over an inclined plate in the presence of a magnetic field with thermally stratified high porosity medium, 'Journal of Applied Fluid Mechanics', vol.**9**, No. 3, p1467-1475.

Ganapathy, R. (1994), A note on oscillatory couette flow in a rotating system, ASME Journal of Applied Mechanics', vol.**61**, p208-209.

Ganesan Periyanagounder , Suganthi Renugopal Kanniappan and Loganathan Parasuraman (2014), Doubly stratified effects in a free convective flow over a vertical plate with heat and mass transfer', 'Thermal Science', vol.**18**, No. 2, p365-376.

Gebhart B.(1962), Effects of viscous dissipation in natural convection, 'Journal of Fluid Mechanics', vol.**14**, p225-235.

Gebhart, B., Jaluria, Y., Mahajan, R. and Sammakia, B. (1988), Buoyancy induced flows and transport, 'Hemisphere', New York.

Geindreau, C., Auriault, J.L. (2002), Magnetohydrodynamic flows in porous media, 'Journal of Fluid Mechanics', vol.**466,** p343-363.

Georgantopoulos,G.A.,Nanousis,N.D. and Goudas, C. L. (1979), Effects of mass transfer transfer on the free convective flow in the Stokes' problem for an infinite vertical limiting surface, 'Astrophysics and Space Sciences', vol.**66**(1), p13-21.

Georgantopolous, G. A. and Nanousis, N. D. (1980), Effects of mass transfer on the hydromagnetic free convective flow in the Stoke's problem, 'Astrophysics and Space Science', vol.**67**(1), p229.

Ghara, N., Guria, M. and Jana, R. N. (2012), Hall Effect on oscillating flow due to eccentrically rotating porous disk and a fluid at infinity, 'Meccanica', vol.**47**, p557-571.

Gnaneswara Reddy, M. and Bhaskar Reddy, N. (2010), Soret and Dufour effects on steady MHD free convection flow past a semi-infinite moving vertical plate in a porous medium with viscous dissipation, 'International Journal of Applied Mathematics and Mechanics'. vol.**6**(1), p1-12.

Ghosh, S.K., Anwar Beg,O. and Narahari, M. (2009), Hall effects on MHD flow in a rotation system with heat transfer characteristics, 'Mecanica', vol.**44**, p741.

Gosman,A.D., Pun,W.M., Runchal, A.K., Spalding, D.B. and Wollfshtein, M.(1969), Heat and mass transfer in recirculating flows, 'Academic Press', London.

Govardhan, K., Balaswamy, B. and Kishan, N. (2012), Effect of internal heat generation, Soret and Dufour on MHD free convection heat and mass transfer in a doubly stratified darcy porous medium with viscous dissipation, 'Emirates Journal for Engineering Research', vol.**17**(2), p29-42.

Griith, A. A. and Meredith, F. W. (1936), The possible improvement in Aircrat performance due to use of boundary layer suction, 'Tech. Rep. 2315, Aeronautical Research Council, London', UK.

Groots, S. R. T. and Mozur, P.(1962), Non-equilibrium thermodynamics, 'North Holland, Amsterdam.

Hadey F. M., Mohamed R. A., Mahdy A. (2006), MHD f ree convection flow along a vertical wavy surface with heat generation or absorption effect, 'International Communications in Heat and Mass Transfer', vol.**33**, No. 10, p1253-1263.

Hannington Situma, Johana K. Sigey, Jeconiah A. Okello, James M. Okwoyo and David

Theuri. (2015), Effect of Hall current and rotation on MHD free convection flow past a vertical infinite plate under a variable transverse magnetic field, 'The SIJ Transactions on Computer Networks & Communication Engineering', vol.**3**, No. 5, p59-65.

Hartmann, J. and Lazarus, F. (1937), The influence of transverse uniform magnetic field on the flow of a conducting fluid between two infinite parallel, stationary and insulated plates, 'Danske Videnskab, Selskab, Matematisk-Fysiske Meddelelser', vol.**15**, p346-369.

Hashimoto,H.(1957), Boundary layer growth on a flat plate with suction or injection, 'Journal of the Physical Society of Japan', vol.**12**(1), p68-72.

Hayat, T. and Abbas, Z. (2007), Effects of Hall current and heat transfer on the flow in a porous medium with slip condition, 'Journal of Porous Media', vol. **10**, No. 1, p35-50.

Hemant Poonia, Chaudhary, R. C. (2010), MHD free convection and mass transfer flow over an infinite vertical plate with viscous dissipation, 'Journal Theoretical and applied Mechanics', vol.**37**, No.4, p263-287.

Hirshfelder, J. O., Curtis, C. F. and Bird, R. B. (1954), Molecular theory of gases and liquids , 'Weley', NewYork.

Hossain, M.A. (1992), Viscous and Joule heating effects on MHD-free convection flow with variable plate temperature, 'International Journal Heat Mass Transfer', vol.**35**(12), p3485-3487.

Hughes, W. F.and Young, F.J.(1966), The electromagnetodynamics of fluids, 'Jhon Wiley', New York.

Hurle, D. T. J. and Jakeman, E. (1971), Soret-driven thermosulutal convection, 'Journal of Fluid Mechanics', vol.**47**(2), p667-687.

Ihsan Y. Hussain and Basim K. Raheem (2013), Natural convection heat transfer from a plane wall to thermally stratified porous media, 'International Journal of Computer Applications', vol.**65**, No. 1, p42-49.

Inger, G. R. and Swearn, T. F. (1975), Vectoret injection into laminar boundary layers with heat transfer, 'AIAA Journal', vol.**13**(5), p616-622.

Ingham, D. B. and Pop, I.(1998), Transport Phenomena in Porous Media II, vol.**2002,** 'Perga-mon', Oxford.

Ingham, D. B., Bejan, A., Mamut, E. and Pop, I. (2004), Emerging Technologies and Techniques in Porous Media, 'Kluwer', Dordrecht.

Iranian, D., Loganathan, P. and Ganesan, P. (2015), Unsteady MHD natural convective flow over vertical plate in thermally stratified media with variable viscosity and thermal conductivity, 'International Journal of Computer Applications', vol.**121**(3), p18-24.

Jaluria, Y. (1980), Natural convection heat and mass transfer, vol.**5**, 'Pergamon Press', Oxford, UK.

Jaluria, Y. and Himasekhar, K. (1983), Buoyancy induced two dimensional vertical flows in a thermally stratified environment, 'Computers and Fluids', vol.**11**, p39- 49.

Javaherdeh, K., Mehrzad Mirzaei Nejad and Moslemi, M. (2015), Natural convection heat and mass transfer in MHD fluid flow past a moving vertical plate with variable surface temperature and concentration in a porous medium, 'Engineering Science and Technology: An International Journal', vol.**18**, p423-431.

Jha, B.K. and Apere, C.A. (2010), Combined effect of Hall and ion-slip currents on unsteady

MHD couette flows in a rotating system, 'Journal of Physical Society of Japan', vol.**79**(10), p10441-104401-9.

Jha, B. K. and Apere, C. A. (2012), Time-dependent MHD couette flow of rotating fluid with hall and ion-slip currents, 'Applied Mathematics and Mechanics. -Engl. Ed.', vol.**33**(4), p399–410.

Joaquin Zueco, Anwar Beg, O and Tasveer A Beg (2009), Numerical solutions for unsteady rotating high porosity medium channel couetee flow hydrodynamics, 'Physica Scripta', vol.**80**, No. 3, p5001.

Joaquin Zueco, Luis Ma Lopez-Ochoa, Pablo Eguia and Joaquin Collazo (2011), Combined heat and mass transfer by natural convection from a semi-infinite plate submitted to a magnetic field with hall currents, 'Engineering Applications of Computational Fluid Mechanics', vol.**5**, No. 2, p188-200.

Jsaem M., Al-Humud and Ali J. Chamkha (2006), Double diffusive convection of a rotating fluid over a surface embedded in a thermally stratified high porosity medium, 'Heat and Technology', vol.**24**, No 1, p51-59.

Julius Hartman (1937), Theory of laminar flow of an electrically conductive liquid in a homogeneous magnetic field , 'Danke Videnskab. Selskab. Matematisk-Fysiske Meddelelser', vol.**15**, No. 6, p1-28.

Kafoussias,N.G. (1992), MHD thermal-diffusion effects on free-convective and mass transfer flow over an infinite vertical moving plate, 'Astrophysics and Space Science', vol.**192**, p11-19.

Kaladhar, K., RamReddy, Ch., Srinivasacharya, D. and Pradeepa, T. (2016), Analytical study for Soret, Hall and Joule heating effects on natural convection flow saturated porous medium in a vertical channel, 'Mathematical Science', p1-10.

Katsurai, M.(1972), Studies on the MHD rotating machine, 'Electrical Engineering in Japan, vol.**92**, p31- 43.

Khaled K. Jaber (2014), Effects of viscous dissipation and joule heating on MHD flow of a fluid with variable properties past a stretching vertical plate, 'European Scientific Journal', vol.**10**, No.33, p383-393.

Khaled K. Jaber (2015), Influence of Hall current and viscous dissipation on MHD convective heat and mass transfer in a rotating porous channel with Joule heating, 'American Journal of Mathematics and Statistics', vol.**5(5)**, p272-284.

Khaled K. Jaber (2016), Joule heating and viscous dissipation on effects on MHD flow over a stretching porous sheet subjected to power law heat flux in presence of heat source, 'Open Journal of Fluid Dynamics', vol.**6**, p156-165.

Khaled K. Jaber (2016), Effect of viscous dissipation on flow over a stretching porous sheet subjected to power law heat flux in presence of heat source, 'International Journal of Modern Mathematical Sciences', vol.**14**(3), p212-220.

Kiran Kumar, R.V. M. S. S, Sasikala, B., Raju, M. C. and Varma, S. V. K. (2015), Diffusion-thermo effects on hydromagnetic free convection heat and mass transfer flow through high porous medium bounded by a vertical surface, 'Chemical and Process Engineering Research', vol.**36**, p1-18.

Kirimi Jacob , Musundi Sammy Wabomba , Anthony Muthondu Kinyanjui , Murwayi Alice Lunani (2012), Magnetic field and Hall current effect on MHD free convection flow past a vertical rotating flat plate, 'Asian Journal of Current Engineering and Maths' vol.**6**, p346 – 354.

Kolesnichenko, A. F. (1990), Electromagnetic processes in liquid material in the USSR and eastern european countries, 'Iron and steel Institute of Japan', vol.**30**, No. 1, p8-26.

Koushik Dash, Alam, M. and Wahiduzzaman, M. (2012), MHD free convection and mass transfer flow from a vertical plate in the presence of Hall and ion-slip current, 'Advances in Mechanical Engineering', vol.**2012**, 20 pages.

Krishna, D. V, Prasada, Rao D. R. V, Ramachandra Murththy, A. S. (2002), Hydromagnetic convection flow through a porous medium in a rotating channel, 'Journal of Engineering Physics and Thermophysics', vol.**75**(2), p281-291.

Labroopulu F, Dorrepael J. M., Chandna O. P. (1996), Oblique flow impinging on a wall with suction or blowing, 'Acta Mechanica', vol.**115**, p15–25.

Lai, F. C., Kulacki, F. A. and Pop, I. (1990), Natural convection from isothermal plates embedded in thermally stratified porous media, 'Journal of Thermophysics and Heat Transfer', vol.**4**, p533-535.

Lakshmi, P. A. and Murthy, P. V. S. N (2008), Soret and Dufour effets on free convection convection heat and mass transfer from horizontal flat plate in a Darcy porous medium, 'Journal Heat Transfer', vol.**130**(10), p104504-8.

Maji, S.L., Kanch, A.K., Guria, M., Jana, R.N. (2009), Hall effects on hydromagnetic flow on an oscillating porous plate, 'Applied Mathematics and Mechanics, –Engl. Ed', vol.**30**(4), p503-512.

Makinde, O. D. and Chinyoka, T. (2013), Numerical investigation of buoyancy efects on hydromagnetic unsteady low through a porous channel with suction/injection, 'Journal of Mechanical Science and Technology', vol.**27**, No. 5, p1557-1568.

Mahender, D. and Srikanth Rao, P. (2015), Unsteady MHD free convection and mass transfer flow past a porous plate in presence of viscous dissipation, 'Journal of Physics: Conference Series', vol.**662**, p012012.

Maleque, Kh. A. and Sattar, M. A. (2005), The effects of variable properties and Hall current on steady MHD laminar convective fluid due to a porous rotating disk, 'International Journal of Heat and Mass Transfer', vol.**48**, p.4963-4972.

Mangathai, P., Ramana Reddy, G.V. and Rami Reddy, B. (2015), Heat and mass transfer effects on MHD free convection flow over an inclined plate embedded in a porous medium, 'International Journal of Advanced Computer and Mathematical Science', vol.**7(1)**, p1-12.

Mark O. Okongo, Gichohi P. Nderitu and James M. Mugambi (2014), Hall current effects on a flow in a variable magnetic field past an infinite vertical, porous flat plate, 'International Journal of Recent Research and Applied Studies', vol.**19**(1), p96-113.

Michiyoshi, I. and Numano, M. (1967), Performance characteristics of a vortex-type MHD power generator – II, 'Plasma Physics', vol.**9**, p549- 555.

Mital, M. L. and Bhat, A. N. (1980), Heat transfer in a MHD channel with uniform wall heat flux effects of Hall and ion-slip currents, 'International Journal of Heat and Mass Transfer', vol.**23**, p919-926.

Murali Gundagani (2015), Unsteady MHD free convection viscous dissipative flow past an

infinite vertical plate with constant suction and heat source/sink, 'Journal of Science and Arts', No. 1(30), p89-98.

Murthy,P. V. S. N., Srinivasacharya,D. and Krishna, P. V. S. S. S. R. (2004), Effect of double double stratification on free convection in a Darcian porous medium, 'Journal of Heat Transfer', vol.**126**(2), p297-300.

Muthucumaraswamy, R. and Vijayalakshmi, A. (2008), Effects of heat and mass transfer on flow past an oscillating vertical plate with variable temperature, 'International Journal of Applied Mathematics and Mechanics', vol.**4**(1), p59-65.

Mutua, N. M., Musyoki, I. N .M , Kinyanjui, M . N , Kwanza, J. K. (2013), Magnetohydrodynamic free convection flow of a heat generating fluid past a semi-infinite vertical porous plate with variable suction, 'International Journal of Applied Mathematical Research', vol.**2**(3), p356-371.

Nachtsheim, P. R. and Swigert, P. (1965), Satisfaction of the asymptotic boundary conditions in numerical solution of the system of non-linear equations of boundary layer type, 'NASA' TND-3004.

Nanousis, N. (1992), Thermal-diffusion effects on MHD free convective and mass transfer flow past a moving infinite vertical plate in a rotating fluid, 'Astrophysics and Space Science', vol.**191**(2), p313-322.

Narayana, P. A. L. and Murthy,P. V. S. N. (2006), Free convective heat and mass tansfer in a doubly stratified non-darcy porous medium. 'Transactions of the ASME, Journal of Heat Transfer', vol.**128**, p1204-1212.

Naroua, H. (2007), A computational solution of hydromagnetic free convective flow past a vertical plate in a rotating heat-generating fluid with Hall and ion-slip currents, 'International Journal for Numerical Methods in Fluids', vol.**53**, p1647-1658.

Nazibuddin Ahmed and Sujit Talukdar (2012), MHD couette flow with heat transfer in presence of constant heat source,'International Journal of Engineering Science and Technology', vol.**4**, No.06, p2887-2897.

Nazmul Islam, M. and Alam, M. M. (2007), Dufour and Soret effects on steady MHD free convection and mass transfer fluid flow through a porous medium in a rotating system, 'Journal of Naval Architecture and Marin Engineering', vol.**4**, p43-55.

Nield, D. A. and Bejan A.(1999), Convection in Porous Media, 2nd edition, 'Springer', New York.

Nield, D. A. and Bejan, A.(2013), Convection in Porous Media, 'Springer', New York, NY, USA, 4th edition.

Nirmal Ghara, Sovan Lal Maji, Sanatan Das, Rabindranath Jana and Swapan Kumar Ghosh (2012), Effects of Hall current and ion-slip on unsteady MHD couette flow, 'Open Journal of Fluid Dynamics', vol.**2**, p1-13.

Odelu Ojjela and Naresh Kumar, N. (2013), Numerical study of MHD flow and heat transfer through porous medium between two parallel plates with Hall and ion slip effects. 'Proceedings of the 2013 International Conference on Mechanics, Fluids, Heat, Elasticity and Electromagnetic Fields', p161-167.

Okedoye, A. M. (2013), Heat and Hall effect of an oscillating plate in a porous medium, 'Advances in Agriculture, Sciences and Engineering Research', vol.**3**(7), p972-983.

Oliver, D. A. (1974), Time dependent magnetohydrodynamic generator, 'MIT gas turbine laboratory report, mechanical engineering, Massachusetts Institute of Technology', USA.

Pai, S. I. (1962), Magnetogasdynamics and Plasma dynamics, 'Springier Verlag', New York.

Panneerselvi, R. and Kowsalya, J. (2015), Ion- Slip and Dufour effect on unsteady free convection flow past an infinite vertical plate with oscillatory suction velocity and variable permeability, 'International Journal of Science and Research', vol.**4**(12), p2079-2090.

Patankar, S. V., and Spalding, D. B. (1970), Heat and Mass Transfer in Boundary Layers, 2nd Edu. 'Intertex Book', London.

Palanisamy Geetha and Muthamperumal Bhavathikannu Krishna Moorthy (2011), Viscous dissipation effect on steady free convection and mass transfer flow past a semi-infinite flat plate, 'Journal of Computer Science', vol.**7**(7), p1113-1118.

Prabhakara Rao, G. Dr., Naga sasikala, M. and Gayathri, P. Dr. (2015), MHD Natural convection Flow of an incompressible electrically conducting viscous fluid through porous medium from a vertical flat plate, 'International Journal of Engineering Research and Applications', vol. **5**(4), p44-49.

Praveen Saraswat, Rudraman Singh (2014), MHD unsteady free convection of heat and mass transfer flow through porous medium with time dependent suction and constant heat source/sink, 'International Journal of Mathematical, Computational, Physical, Electrical and Computer engineering', vol **8**, No. 3, p619-624.

Pop, I. and Ingham, D. B. (2001), Convective heat transfer mathematical and computational modelling of viscous fluids and porous media, 'Elsevier Science and Technology' Books, Pergaman, UK.

Pop, I. and Watanabe, T. (1994), The effect of viscous dissipation and stress work on MHD flow over an isothermal flat plate in the presence of a transverse magnetic field, 'Acta Mechanic',. vol.**105**, p233.

Prandtl, L. (1952), Essentials of fluid dynamics, 'Blackie', London.

Prandtl, L.(1904),Uber Flussigkeits bewegung beisehr kleiner reibung, 'Proceedings Third International Mathematics Congress', Heidelberg.

Prasanna Lakshmi, M., Bhaskar Reddy, N. and Poornima, T. (2012), MHD boundary layer flow of heat and mass transfer over a moving vertical plate in a porous medium with suction and viscous dissipation, 'International Journal of Engineering Research and Applications', vol.**2**(5), p149-159.

Rachna Khandelwal(2013),Unsteady MHD flow, heat and mass transfer along an accelerated vertical porous plate in the influence of viscous dissipation, heat source and variable suction, 'International Journal of Mathematics and Computer Applications Research', vol.**3**(1), p229-236.

RajaShekar, M. N. (2014), Effects of Dufour and Soret on unsteady MHD heat and mass transfer flow past a semi-infinite moving vertical plate in a porous medium with viscous dissipation, 'International Journal of Applied Physics and Mathematics', vol.**4**, No. 2, p130-134.

Rajput, U. S., Mohammad Shareef (2016), Rotation effect on unsteady MHD flow past an impulsively started vertical plate with variable temperature in porous medium, 'International Journal of Mathematical Archive', vol.**7**(2), p148-153.

Rajput, U. S. and Gaurav Kumar (2016), Soret effect on unsteady MHD flow through porous medium past an oscillating inclined plate with variable wall temperature and mass diffusion, 'International Research Journal of Engineering and Technology', vol.**3**(5)**,** p2353-2358.

Ram, P.C.(1991), MHD convective flow in a rotating fluid with Hall and ion-slip current , 'Wfirme- und Stofffibertragung', vol.**26**, p203-205.

Ram, P. C. and Takhar, H. S. (1993), MHD free convection from an infinite vertical flate plate in a rotating fluid with Hall and ion-slip currents, 'Fluid Dynamics Research, vol.**11**, p99-105.

Ram, P. C. (1995), Effects Hall and ion-slip currents on free convective heat generating flow in a rotating fluid, 'International Journal of Energy Research', vol.**19**, p371-376.

Rama Mohan Reddy, L., Raju, M. C. and Raju, G. S. S. (2016), Natural convection boundary layer flow of a double diffusive and rotating fluid past a vertical porous plate, 'International Journal Applied and Computational Mathematics', DOI 10.1007/s40819-016-0174-7.

Ramana Reddy, G. V., Ramana Murthy, Ch. V. and Bhaskar Reddy, N. (2011), Unsteady MHD free convective mass transfer flow past an infinite vertical porous plate with variable suction and soret effect, 'International Journal of Applied Mathematics and Mechanics', vol.**7(21)**, p70-84.

Rao, G. S., Ramana, B., Reddy, B. R., Vidyasagar, G. (2014), Soret and Dufour effects on MHD boundary layer flow over a moving vertical porous plate with suction, 'International Journal of Emerging Trends in Engineering and Development', vol.**2**(4), p215-226.

Reddy, T. S., O. Reddy, O. S. P., Raju, M. C. and Varma, S. V. K. (2012), MHD free convect-ion heat and mass transfer flow through a porous medium bounded by a vertical surface in presence of Hall current, 'Advances in Applied Science Research', vol.**3**(6), p3482-3490.

Reddy, G.V.R. (2016), Soret and Dufour effects on MHD free convective flow past a vertical porous plate in the presence of heat generation, 'International Journal of Applied Mechanics and Engineering', vol.**21**, No.3, p649-665.

Revankar S. T. (2000), Free convection effect on flow past an impulsively started or oscillat-ing infinite vertical plate, 'Mechanics Research Communications', vol.**27**, p241-246.

Richard Rosa R. J. (1959), Magnetohydrodynamic Energy Conversion, 'Hemisphere Publishing', Washington, D.C.

Rohsenow, W.M. et al. (1998), Handbook of Heat transfer, 3rd edition, 'McGraw-Hill', New York.

Rossow, V.J. (1957), On flow of electrically conducting fluids over a flat plate in the ptrsence of transverse magnetic field, 'NACATN' , vol.**3971**, p1-54.

Satish, Desale and Pradhan, V.H.(2015), Numerical solution of boundary layer equation with viscous dissipation effect along a flat plate with variable temperature, 'Elsevier, Science Direct, Procedia engineering', vol.**127**, p846-853.

Sarada, K. and Shanker, B. (2013), The effects of Soret and Dufour on an unsteady mhd free convection flow past a vertical porous plate in the presence of suction or injection, 'International Journal of Engineering and Science', vol.**2**(7), p13-25.

Sattar, M. A., Hossain, M. M. (1992), Unsteady hydromagnetic free convection flow with

Hall current and mass transfer along an accelerated porous plate with time-dependent temperature and concentration, 'Canadian Journal of Physics', vol.**70**, p369-374.

Sattar, M. A. and Alam, M. M. (1994), Thermal diffusion as well as transpiration effects on MHD free convection and mass transfer flow past an accelerated vertical porous plate, 'Indian Journal of Pure and Applied Mathematics', vol.**25**(6), p679-688.

Sattar, M.A., Rahman,M. M. and Alam, M. M. (2000), Free convection flow and heat transfer through a porous vertical flat plate immersed in a porous medium with variable suction, 'Journal of Energy, Heat and Mass Transfer', vol.**22**, p17-21.

Schilichting, H. (1968), Boundary layer theory, 'McGraw-Hill', New York.

Sreedhar Sarma, G., Sreenivasu, D., Govardhan, K. and Ramakrishna Prasad, K. (2013), Numerical study of MHD free convection heat and mass transfer from vertical surfaces in porous media considering Soret and Dufour effects, 'Advances in Applied Science Research', vol.**4**(1), p300-307.

Seth, G. S., Nandkeolyar, R. and Ansari, M. S. (2011), Effect of rotation on unsteady hydromagnetic natural convection flow past an impulsively moving vertical plate with ramped temperature in a porous medium with thermal diffusion and heat absorption, 'International Journal of Applied Mathematics and Mechanics', vol.**7**(21), p52-69.

Seth, G.S., Nandkeolyar, R. and Ansari, Md. S. (2012), Effects of Hall current and rotation on unsteady MHD couette flow in the presence of an inclined magnetic field, 'Journal of Applied Fluid Mechanics', vol.**5**, No. 2, p67-74.

Sharma, P. R., Manisha Sharma and Yadav, R. S. (2014), Viscous dissipation and mass transfer effects on unsteady MHD free convective flow along a moving vertical porous plate in the presence of internal heat generation and variable suction, 'International Journal of Scientific and Research Publications', vol.**4**(9), p1-9.

Sherman, A, Sutton, G. W. (1962), Mgagnetohydrodynamic, 'North Western Uni. Press'. Evanston.

Shercliff, J. A.(1965), A text book of magnetohydrodynamics, 'Pergamon Press', New York, USA.

Shojaefard, M. H., Noorpoor, A. R., Avanesians, A. and Ghafapour, M. (2005), Numerical investigation of low control by suction and injection on a subsonic airfoil, 'The American Journal of Applied Sciences', vol.**20**, p1474-1480.

Siegel, R. (1958), Transient free convection from a vertical flat plate, 'Transactions of the American Society of Mechanical Engineers', vol.**80**, p347-359.

Singh, P., S harma, K. (1990), Integral method to free convection in thermally stratified porous medium. 'Acta Mechanica', vol.**83**, p157-163.

Singh, K D and Rakesh kumar (2009), Soret and Hall current effects on heat and mass transfer in MHD flow of a viscous fluid through porous medium with variable suction, 'Proceedings Indian National Science Academy', vol.**75**, No.3, p119-126.

Singh, J. K., Ghousia Begum, S. and Naveen Joshi (2016), Effect of Hall current and ion-slip on unsteady hydromagnetic generalized couette flow in a rotating channel, 'Journal of Mathematical Modeling', vol.**3**(2), p145-167.

Smita Sharma, Jitendra Singh and Singh, B. B. (2015), Effects of Hall current on transient

convective mhd flow through porous medium past an infinite vertical oscillating plate with temperature gradient dependent heat source, 'IOSR Journal of Mathematics', vol.**11**(4), p42-47.

Soundalgekar, V. M. and Ramana Murthy, T. V. (1980), Heat transfer in the flow past a continuous moving plate with variable temperature, 'Warme-rund-Stoffubertragung', vol.**14,** p91-93.

Sondalgekar, V. M., Vighnesam, N. V. and Takhar, H. S. (1979), Hall and ion-slip effects in MHD couette flow with heat transfer, 'IEEE Transactions on Plasma Science', vol.**7**(3), p178-182.

Sondalgekar, V. M., and Ganesan, P. (1980), Transient free convection flow past a semi-infinite vertical plate with mass transfer, 'Regional Journal of Energy, Heat and Mass Transfer', vol.**2**, p83-91.

Sparrow, E. M. and Cess, R. D. (1961), The effect of a magnetic field on free convection heat transfer, 'International Journal Heat and Mass Transfer', vol.**19**, p267-279.

Sparrow, E. M. and Cess, R. D. (1961), The effect of magnetic field on free convection heat transfer, 'International Journal Heat and Mass Transfer', vol.**19**, p267-279.

Sporn,P.and Kantrouitz, A. (1959), Magnetohydrodynamics: Future power process, vol.**103**, No. 11, p62-65.

Srinivas Reddy, D., Sreedhar sarma, G. and Govardhan, K. (2015), Effect of viscous dissipation, Soret and Dufour effect on free convection heat and mass transfer from vertical surface in a porous medium, 'Elsevier, Procedia Materials Science', vol.**10**, p563-571.

Srinivas Maripala and Kishan, N. (2014), Dufour and Soret effects on convective heat and mass transfer in non-darcy doubly stratified porous media, 'International Journal of Engineering Research and Applications', vol.**4**(9), p17-26.

Srinivasa Rao, G., Ramana, B., Rami Reddy, B. and Vidyasagar, G. (2014), Soret and Dufour effects on MHD boundary layer flow over a moving vertical porous plate with suction, 'International Journal of Emerging Trends in Engineering and Development', vol.**2**(4), p215-226.

Steg, L. and Sutton, G. W.(1960), Prospects of MHD power Generation,'Astronautics',vol.**5**, p22- 25.

Stokes G. (1851), On the effect of the internal friction of fluid on the motion of pendulum, 'Transactions Cambridge Philosophical Society', vol.**IX**, 8– 106.

Sutton, G. W. and Gloersen, P. (1961), 2nd Symposium on the Engineering Aspects of magn-etohydrodynamics, 'Physics Today', vol.**14**(9), p18.

Sutton, G.W. and Sherman, A. (1965), Engineering magnetohydrodynamics, 'McGraw-hill', New York.

Swati Mukhopadhyay, Iswar Chandra Mondal and Rama Subba Reddy Gorla (2012), Effects of thermal stratification on flow and heat transfer past a porous vertical stretching surface, 'Heat Mass Transfer', vol.**48**(6), p915-921.

Tak, S. S. and Arti Lodha (2007), Influence of double stratification on MHD free convection with Soret and Dufour effects in a Darcian porous media, 'PAMM. Proc. Applied Mathematics and Mechanics', vol.**7**, p2100089-2100090.

Takhar, H. S., Chamkha, A. J. and Nath, G. (2003), Effects of non-uniform wall temperature or mass transfer in finite sections of an inclined plate on the MHD natural convection flow in a temperature stratified high-porosity medium, 'International Journal of Thermal Sciences', vol.**42**, p829-836.

Thamizhsudar, M. and Pandurangan, J. (2015), Hall effects and rotation effects on MHD flow past an exponentially accelerated vertical plate with combined heat and mass transfer effects, 'International Journal of Applied Mechanics and Engineering', vol.**20**, No.3, p605-616.

Tani, I.(1962), Steady flow of conducting fluids in channels under transverse magnetic fields, with consideration of Hall effect. Aerospace Science, vol.**29**, p.297-305.

Turbatu S., Bühler, K. and Zierep, J. (1998), New solutions of the II Stokes problem for an oscillating flat plate, 'Acta Mechanica', vol.**129**, p25–30.

Tavva. Sudhakar Reddy, O. Siva Prasad Reddy, M. C. Raju an S.V. K. Varma (2012), MHD free convection heat and mass transfer flow through a porous medium bounded by a vertical surface in presence of Hall current, 'Advances in Applied Science Research', vol.**3**(6), p3482-1390.

Vafai, K. (2000), Handbook of Porous Media, 'Marcel Dekker', New York.

Veera Krishna, M., Neeraja, E. and Siddesh Babu, G. (2013), Hall effects on MHD convection flow through a medium in a rotating parallel plate channel, 'Asian Journal of Current Engineering and Maths', vol.**2**(3), p181-189.

Vedhanayagam, M., Altenkirch, R. A. and Eichhorn, R. (1980), A transformation of the boundary layer equation for free convection flow past a vertical flat plate with arbitrary and wall temperature variation, 'International Journal of Heat mass transfer', vol.**23**, p1286-1288.

Venkata Madhu, J., Raja Shekar, M. N. and Saritha, K. (2014), Dufour and Soret effect on unsteady MHD free convection flow past a semi-infinite moving vertical plate in a porous medium with viscous dissipation, 'International Journal of Mathematics and Engineering', vol.**251,** p2465-2477.

Vidyasagar, G., Ramana, B. and Bala, P. and Anki Reddy (2013), Heat and mass transfer effects on MHD boundary layer flow over a moving vertical porous plate, 'Journal of Global Research in Mathematical Archives', vol.**1**, No. 2, p49-62.

Vijaya, R. B. and Mallikarjuna, B. (2014), Effect of variable thermal conductivity on convective heat and mass transfer over a vertical plate in a rotating system with variable porosity regime, 'Journal of Naval Architecture and Marine Engineering', vol.**111**, No 1, p83-92.

Yantovskiy, Y. I. and Tolmach, I. M. (1963), On the theory of an asynchronous magnetohydrodynamic generator with a rotating field. 'Technical Report, Wright- Patterson Air Force Base', Ohio, USA.